

AD A092175

## FEDD DOCUMENT

Note that this document bears the label "FEDD," an acronym for "FOR EARLY DOMESTIC DISSEMINATION." The FEDD label is affixed to documents that may contain information having high commercial potential.

The FEDD concept was developed as a result of the desire to maintain U.S. leadership in world trade markets and encourage a favorable balance of trade. Since the availability of tax-supported U.S. technology to foreign business interests could represent an unearned benefit, research results that may have high commercial potential are being distributed to U.S. industry in advance of general release.

The recipient of this report must treat the information it contains according to the conditions of the FEDD label on the front cover.

Accession For	
NTIS GPOAI	<input checked="checked" type="checkbox"/>
DTIC TAB	<input type="checkbox"/>
Unannounced	<input type="checkbox"/>
Justification	
By	
Distribution/	
Availability Codes	
Distribution for	
Dist	Special
A	

18  
6 NASA Contractor Report 3251

17 CR-324 I-VOL-1

# PAN AIR—A Computer Program for Predicting Subsonic or Supersonic Linear Potential Flows About Arbitrary Configurations Using a Higher Order Panel Method.

## Volume I—Theory Document (Version 1.0).

10  
Alfred E. Magnus Michael A. Epton  
Boeing Military Airplane Company  
Seattle, Washington

Prepared for  
Ames Research Center  
and  
Langley Research Center  
under Contract NAS2-9830

and for the  
Air Force Aeronautical Systems Division  
Air Force Wright Aeronautical Laboratories  
Naval Coastal Systems Center

14 D180-24910-3-VOL-1

12 598

Because of its significant early commercial potential, this information, which has been developed under a U.S. Government program, is being disseminated within the United States in advance of general publication. This information may be duplicated and used by the recipient with the express limitation that it not be published. Release of this information to other domestic parties by the recipient shall be made subject to these limitations. Foreign release may be made only with prior NASA approval and appropriate export licenses. This legend shall be marked on any reproduction of this information in whole or in part. Date for general release August, 1982.

9 Contract rept.  
Jan 78-Apr 80

# NASA

National Aeronautics and  
Space Administration

Ames Research Center  
Moffett Field, California 94035



411593

JW

1. Report No. NASA CR-3251		2. Government Accession No. <b>AD-A092175</b>		3. Recipient's Catalog No.	
4. Title and Subtitle PAN AIR - A computer program for predicting subsonic or supersonic linear potential flows about arbitrary configurations using a higher order panel method Volume I - Theory Document (Version 1.0)				5. Report Date April 15, 1980	
				6. Performing Organization Code	
7. Author(s) Alfred E. Magnus and Michael A. Epton				8. Performing Organization Report No. D180-24910-3 ✓	
				10. Work Unit No.	
9. Performing Organization Name and Address Boeing Military Airplane Company ✓ P. O. Box 3707 Seattle, Washington 98124				11. Contract or Grant No. NAS2-5830	
				13. Type of Report and Period Covered Contractor Report January 1978-April 1980	
12. Sponsoring Agency Name and Address o NASA, Washington D.C. 20546 o AFWAL and ASD, Wright-Patterson AFB, Ohio 45433 o NCSC, Panama City, Florida 32407				14. Sponsoring Agency Code	
15. Supplementary Notes Technical Monitors: NASA-Ames: Larry L. Erickson, Ralph L. Carmichael, Alan D. Levin NASA-Langley: David S. Miller, James L. Thomas ASD: James R. Snyder AFWAL: Capt. Jay DeJongh, William A. Sotomayer NCSC: Neill S. Smith					
16. Abstract:  An outline of the derivation of the differential equation governing linear subsonic and supersonic potential flow is given. The use of Green's Theorem to obtain an integral equation over the boundary surface is discussed. The engineering techniques incorporated in the PAN AIR (Panel Aerodynamics) program (a discretization method which solves the integral equation for arbitrary first order boundary conditions) are then discussed in detail.  Items discussed include the construction of the compressibility transformation, splining techniques, imposition of the boundary conditions, influence coefficient computation (including the concept of the finite part of an integral), computation of pressure coefficients, and computation of forces and moments.					
17. Key Words (Suggested by Author(s)) aerodynamics, linear potential flow, panel methods, Prandtl-Glauert equation, splines, influence coefficients, discretization			18. Distribution Statement  FEDD Distribution: STAR Category 02		
19. Security Classif. (of this report) unclassified		20. Security Classif. (of this page) unclassified		21. No. of Pages 693	
				22. Price \$16.50	

\*For sale by the National Technical Information Service, Springfield, Virginia 22161

NASA-Langley, 1980

**411593** *GM*



## Contents

	Page
List of Figures	xi
1.0 Introduction	1.0-1
2.0 Fundamental Fluid Mechanics	2.0-1
2.1 The Navier-Stokes Equations	2.1-1
2.2 Euler's Equation	2.2-1
2.3 The Unsteady Potential Equation	2.3-1
2.4 The Steady Non-Linear Potential Equation	2.4-1
2.5 The Prandtl-Glauert Equation	2.5-1
3.0 Panel Method Theory	3.0-1
3.1 Coordinate Scaling	3.1-1
3.2 Green's Theorems	3.2-1
3.3 Discretization	3.3-1
4.0 An Overview of PAN AIR	4.0-1
4.1 Historical Development of Panel Methods	4.0-1
4.2 Summary of PAN AIR Technology	4.2-1
4.2.1 Basis Function Computation	4.2-2
4.2.1.1 Subpanel Splines	4.2-2
4.2.1.2 Outer Splines	4.2-3
4.2.2 Panel Influence Coefficients	4.2-4
4.2.2.1 Near Field PIC's	4.2-5
4.2.2.2 Far Field PIC's	4.2-6
4.2.3 Potential and Velocity Influence Coefficient Assembly	4.2-6
4.2.4 Aerodynamic Influence Coefficient Matrix Construction	4.2-7
5.0 Elaboration on the Technology in PAN AIR	5.1-1
5.1 Networks and Panels	5.1-1
5.2 Coordinate Transformations	5.2-1
5.3 Network Edge Matching	5.3-1
5.4 Control Points and Boundary Conditions	5.4-1
5.4.1 Control Point Location	5.4-1
5.4.2 Boundary Conditions	5.4-1
5.4.2.1 Impermeability Boundary Conditions	5.4-2
5.4.2.2 Thin Surfaces	5.4-4
5.4.2.3 Thick Configurations	5.4-5
5.4.2.4 Superinclined Surfaces	5.4-7
5.4.2.5 The General Boundary Condition	5.4-8
5.5 Singularity Splines	5.5-1
5.5.1 The Matrices $B^S$ and $B^D$	5.5-1
5.5.2 The Definition of SPSPL	5.5-3
5.5.3 Construction of the Matrices $B$	5.5-4
5.5.4 Construction of SPSPL	5.5-6

5.6	Influence Coefficients	5.6-1
5.6.1	Computation of Potential and Velocity	5.6-1
5.6.2	Reformulation of the Doublet Velocity Integral	5.6-4
5.6.3	The Far Field Expansion	5.6-6
5.7	The Aerodynamic Influence Coefficient Matrix	5.7-1
5.7.1	Non-Standard Boundary Conditions	5.7-2
5.7.2	Symmetry	5.7-3
5.7.3	Known Singularity Parameters	5.7-6
5.7.4	Multiple Right Hand Side	5.7-8
5.7.5	Updatability	5.7-9
5.8	Solution of the System of Equations	5.8-1
5.9	Post-Solution Features	5.9-1
5.9.1	Computation of Potential and Velocity	5.9-1
5.9.2	Pressure Computation	5.9-2
5.9.3	Velocity Corrections	5.9-2
5.9.4	Force and Moment Computation	5.9-4
6.0	A Guide to the Appendices	6.0-1
7.0	References	7.0-1
8.0	List of Symbols	8.0-1
9.0	Engineering Glossary	9.0-1
Appendices		
A.0	Fundamental Fluid Mechanics	A.0-1
A.1	The Small Perturbation Assumptions	A.1-1
B.0	The Prandtl-Glauert Equation	B.0-1
B.1	Existence and Uniqueness	B.1-1
B.2	Wakes and Modeling	B.2-1
B.3	Removal of Line Vortex Terms	B.3-1
B.4	Linear Sources and Quadratic Doublets	B.4-1
C.0	The Design Problem	C.0-1
C.1	Linearized Design	C.1-1
C.2	Sequential Design	C.2-1
C.3	Iterative Design	C.3-1
C.4	Stability	C.4-1
D.0	Geometry of Networks and Panels	D.0-1
D.1	Networks	D.1-1
D.1.1	Network Types	D.1-1
D.2.1	Wake Networks and the Kutta Condition	D.1-1
D.1.3	Indexing	D.1-2
D.1.4	Collapsing of Network Edges	D.1-2
D.1.5	Additional Network Processing	D.1-3
D.2	Basic Panel Geometry	D.2-1
E.0	Matrices and Coordinates	E.0-1
E.1	Vectors and Dual Vectors	E.1-1
E.2	Metric Matrices, Dual Matrices, and Inner Products	E.2-1
E.3	Coordinate Transformations	E.3-1

F.0	Edge Matching	F.0-1
F.1	Continuity Requirements	F.1-1
F.2	Network Abutments	F.2-1
F.3	Automatic Abutment Searches	F.3-1
F.4	Doublet Matching Along Abutments	F.4-1
F.5	Abutment Intersections	F.5-1
F.6	Gap-Filling Panels	F.6-1
G.0	Control Point Locations	G.0-1
H.0	Boundary Conditions and Onset Flows	H.0-1
H.1	Reduction of User Specified Boundary Conditions to Standard Formulation	H.1-1
H.2	Program Overrides of User Boundary Condition Specifications	H.2-1
H.2.1	Superinclined Panel Override	H.2-1
H.2.2	Nullification of User-Input Boundary Conditions	H.2-2
H.2.3	Source and Doublet Matching Boundary Conditions	H.2-2
H.2.4	Closure Boundary Conditions	H.2-3
H.2.5	The Boundary Condition Hierarchy	H.2-5
H.3	Onset Flows	H.3-1
I.0	Singularity Splines	I.0-1
I.1	Outer Splines	I.1-1
I.1.1	Source Spline Vectors for Analysis Vectors	I.1-1
I.1.1.1	Neighboring Singularity Parameters	I.1-2
I.1.1.2	Computation of a Local Coordinate System	I.1-2
I.1.1.3	The Bilinear Fit at Panel Corner Points	I.1-3
I.1.2	Doublet Spline Vectors for Analysis Networks	I.1-5
I.1.2.1	The Quadratic Least Squares Fit for Panel Corners or Panel Edge Midpoints	I.1-6
I.1.2.2	Neighboring Points for Least Squares Fit	I.1-8
I.1.2.3	Construction of a Local Coordinate System	I.1-9
I.1.2.4	Weights for the Least Squares Fit	I.1-10
I.1.2.5	Edge Splines for Non-Smooth Abutments	I.1-11
I.1.2.6	Edge Splines for Smooth Abutments	I.1-15
I.1.3	Doublet Spline Vectors for Wake Networks	I.1-17
I.1.4	Source Splines for Design Networks	I.1-17
I.1.5	Doublet Splines for Design Networks	I.1-17
I.2	Subpanel Splines	I.2-1
I.2.1	Source Subpanel Splines	I.2-1
I.2.1.1	Preliminaries	I.2-1
I.2.1.2	Inversion of the Matrix of Coordinates	I.2-2
I.2.1.3	The Extension Matrix	I.2-5
I.2.2	Doublet Subpanel Splines	I.2-6
I.2.2.1	Continuity Requirements	I.2-6
I.2.2.2	Definition of Kappa Quantities	I.2-7
I.2.2.3	Computation of Kappa Quantities	I.2-8
I.2.2.4	The Doublet Extension Matrix	I.2-12
I.2.2.5	The Matrix of Coordinates $G^D$	I.2-12
I.2.2.6	Inversion of $G^D$	I.2-14

I.3	Full Panel and Half Panel Splines	I.3-1
I.3.1	Full Panel Spline Matrices	I.3-1
I.3.2	Half Panel Spline Matrices (Background Material)	I.3-3
I.3.2.1	Requirements for the Source Half Panel Spline Matrix	I.3-3
I.3.2.2	Computation of $D^S$	I.3-5
I.3.2.3	The Extension Matrix $XH^S$	I.3-7
I.3.2.4	Requirements for the Doublet Half Panel Spline Matrix	I.3-8
I.3.2.5	Computation of $D^D$	I.3-9
I.3.2.6	The Extension Matrix $XH^D$	I.3-12
I.4	Far Field Moments	I.4-1
I.4.1	The Defining Equations	I.4-1
I.4.1.1	Source Far Field Moments	I.4-1
I.4.1.2	Symmetrization	I.4-2
I.4.1.3	Doublet Far Field Moments	I.4-3
I.4.1.4	Doublet Velocity Far Field Moments	I.4-4
I.4.2	Construction of the Far Field Moments	I.4-4
I.4.2.1	Preliminaries	I.4-4
I.4.2.2	$FFM_S^1$	I.4-5
I.4.2.3	$FFM_S^2$	I.4-7
I.4.2.4	$FFM_S^3$	I.4-10
I.4.2.5	$FFM_D^0$	I.4-12
I.4.2.6	$FFM_D^1$	I.4-13
I.4.2.7	$FFM_{D,0}^2$ and $FFM_{D,0}^3$	I.4-13
I.4.2.8	$FFM_D^4$	I.4-14
I.4.2.9	$FFM_D^5$	I.4-16
I.4.2.10	$FFM_{D,0}^6$	I.4-18

I.4.3 Basic Far Field Moments	I.4-19
I.4.3.1 Reduction to Line Integrals	I.4-20
I.4.3.2 Computation of the Line Integrals	I.4-22
I.5 Constrained Least Squares	I.5-1
I.5.1 Definition of the Problem	I.5-1
I.5.2 Elimination of the Weights	I.5-1
I.5.3 The Case of No Exact Constraints	I.5-2
I.5.4 Reduction of the General Case	I.5-2
J.0 Panel Influence Coefficient Calculation	J.1-1
J.1 Introduction and Notation	J.1-1
J.1.1 Definitions	J.1-1
J.1.2 Summary	J.1-2
J.1.2.1 Near Field Versus Far Field	J.1-2
J.1.2.2 The Domain of Dependence	J.1-3
J.1.2.3 Near Field and Intermediate Field PIC Calculation	J.1-3
J.1.2.4 Far Field PIC's	J.1-6
J.1.3 Integration Techniques	J.1-7
J.1.4 Notation	J.1-8
J.2 The Distance Algorithm	J.2-1
J.2.1 The Far Field Criterion	J.2-1
J.2.2 The Intermediate Field Criterion	J.2-3
J.3 Supersonic Influence Test	J.3-1
J.3.1 Definition of $D_p$	J.3-1
J.3.2 A Zero Influence Test	J.3-1
J.3.3 Panel Wholly Within the Mach Cone	J.3-4
J.3.4 The Influence Test For a Subpanel	J.3-4
J.3.4.1 The Point of Closest Approach	J.3-5
J.3.4.2 The Winding Number Test	J.3-7
J.3.4.3 Half Panels and Projected Panels	J.3-8
J.4 Cylindrical Coordinates	J.4-1
J.4.1 Fundamental Results	J.4-1
J.4.2 The Mach Disk	J.4-2
J.4.3 The Case of the Mach Disk Lying Within the Panel	J.4-2
J.4.4 Arbitrary Intersection of the Mach Disk With the Panel	J.4-3
J.4.4.1 Corner Points	J.4-4
J.4.4.2 The Phase Function	J.4-4
J.4.4.3 Edges and the Mach Disk	J.4-7
J.4.4.4 Edge Tangents and Normals	J.4-7
J.4.4.5 The Function $P(\phi)$	J.4-10
J.5 Hyperbolic Coordinates	J.5-1
J.5.1 Fundamental Results	J.5-1
J.5.2 Subsonic Edges	J.5-8
J.5.3 Supersonic Edges	J.5-12
J.5.4 Computation of the Integrals	J.5-16
J.6 The Panel Integral Matrices	J.6-1
J.6.1 Preliminaries	J.6-2
J.6.1.1 Transformation Rules	J.6-2
J.6.1.2 Transformation of the Integrals	J.6-3
J.6.1.3 Singularity Strength Coefficients	J.6-5
J.6.1.4 Uniform Formulas for Local Variables	J.6-6
J.6.1.5 Differentiation Formulas	J.6-9

J.6.2	Source Potential and Velocity	J.6-10
J.6.2.1	Source Potential	J.6-10
J.6.2.2	Tangential Source Velocity	J.6-12
J.6.2.3	Normal Source Velocity	J.6-13
J.6.3	Doublet Potential and Velocity	J.6-15
J.6.3.1	Doublet Potential	J.6-15
J.6.3.2	Tangential Doublet Velocity	J.6-16
J.6.3.3	Normal Doublet Velocity	J.6-18
J.6.4	Reduction to Fundamental Integrals	J.6-19
J.6.4.1	Definition of the Integrals	J.6-19
J.6.4.2	Source Potential and Velocity	J.6-20
J.6.4.3	Doublet Potential and Velocity	J.6-23
J.6.5	The Fundamental Integral in Terms of Panel and Edge Functions	J.6-25
J.6.5.1	Computation of $a$	J.6-25
J.6.5.2	Computation of $b$	J.6-27
J.6.5.3	Computation of $\bar{a}$	J.6-28
J.6.5.4	Computation of $\bar{b}$	J.6-28
J.6.5.5	Computation of $B$	J.6-30
J.6.5.6	Computation of $F$	J.6-33
J.6.5.7	Computation of $H$	J.6-33
J.6.6	The Origin Shift	J.6-35
J.6.7	Finite Parts of Singular Integrals	J.6-41
J.6.7.1	Definition of a Finite Part	J.6-41
J.6.7.2	Properties of a Finite Part	J.6-41
J.6.7.3	Finite Parts and the Integral Equation	J.6-42
J.6.7.4	Finite Parts and PIC Computation	J.6-42
J.6.7.5	Summary of Finite Part Integrals	J.6-43
J.7	Edge and Panel Functions	J.7-1
J.7.1	Expressions For Edge and Panel Functions	J.7-1
J.7.1.1	Subsonic Flow	J.7-1
J.7.1.2	Subsonic Edges of Subinclined Panels in Supersonic Flow	J.7-2
J.7.1.3	Supersonic Edges of Subinclined Panels	J.7-3
J.7.1.4	Superinclined Panels	J.7-3
J.7.1.5	Uniform Formulas	J.7-4
J.7.2	Computation of Edge and Panel Function Arguments in Reference Coordinates	J.7-4
J.7.2.1	Computation of $h$	J.7-5
J.7.2.2	Computation of $v$	J.7-5
J.7.2.3	Computation of $a$	J.7-7
J.7.2.4	Computation of $g$	J.7-8
J.8	Rationalization Formulas	J.8-1
J.8.1	Edge Functions	J.8-1
J.8.1.1	Non-Sonic Edges	J.8-2
J.8.1.2	Nearly Sonic Edges	J.8-6
J.8.1.3	Essentially Sonic Edges	J.8-10
J.8.2	Panel Function Computation	J.8-12
J.8.2.1	The Standard Rationalization	J.8-12
J.8.2.2	A Special Rationalization	J.8-18

J.9	Far Field PIC's	J.9-1
J.9.1	The Basic Principle	J.9-1
J.9.2	Computation of the Gradient	J.9-4
J.9.3	Source Velocity	J.9-5
J.9.4	Doublet Potential	J.9-6
J.9.5	Doublet Velocity	J.9-7
J.9.6	Symmetrization	J.9-8
J.9.6.1	Source Potential	J.9-9
J.9.6.2	Source Velocity	J.9-9
J.9.6.3	Doublet Potential	J.9-10
J.9.6.4	Doublet Velocity	J.9-10
J.10	Line Vortex PIC's	J.10-1
J.10.1	Computation of $\vec{v}_D^*$	J.10-1
J.11	Singular Behavior of Integrals	J.11-1
J.11.1	Discontinuous Source Strength	J.11-1
J.11.2	Discontinuous Doublet Strength	J.11-5
J.11.2.1	Doublet Potential	J.11-5
J.11.2.2	Doublet Velocity	J.11-5
J.11.3	Discontinuities in Doublet Gradient	J.11-6
J.11.4	Singularities of the Panel Function	J.11-8
J.11.4.1	The Plane $h = 0$	J.11-8
J.11.4.2	Discontinuities Due to $C_0$	J.11-10
J.11.4.3	Discontinuities in $J_k(\psi)$	J.11-12
J.11.4.4	Summary of Panel Function Behavior	J.11-14
J.11.5	Singularities of the Edge Function	J.11-15
J.11.5.1	Supersonic Edges	J.11-15
J.11.5.2	Subsonic Edges	J.11-16
J.11.5.3	Subsonic Nearly Sonic Edges	J.11-17
J.11.5.4	Supersonic Nearly Sonic Edges	J.11-19
J.11.5.5	Essentially Sonic Edges	J.11-19
J.11.6	Singularities in Subsonic Flow	J.11-19
J.11.6.1	Discontinuous Source Strength	J.11-19
J.11.6.2	Discontinuous Doublet Gradient	J.11-20
J.11.6.3	Discontinuous Doublet Gradient	J.11-22
J.11.7	Discontinuous Source Strength in Supersonic Flow	J.11-22
J.11.7.1	Source Potential	J.11-22
J.11.7.2	Source Velocity	J.11-23
J.11.8	Discontinuous Doublet Strength in Supersonic Flow	J.11-23
J.11.9	Discontinuous Doublet Gradient in Supersonic Flow	J.11-24
K.0	Matrix Assembly	K.0-1
K.1	Symmetry Planes	K.1-1
K.1.1	One Plane of Geometric Symmetry	K.1-1
K.1.2	Two Planes of Symmetry	K.1-4
K.1.3	Networks Lying on a Plane of Symmetry	K.1-6
K.1.4	Networks Lying on a Plane of Symmetry	K.1-8
K.2	Known Singularity Parameters	K.2-1

K.3	Aerodynamic Boundary Conditions	K.3-1
K.3.1	Combining for Symmetry	K.3-1
K.3.2	Computing Influence on Image Panels	K.3-1
K.3.3	Partial Rows	K.3-3
K.3.4	Data Manipulation Problem	K.3-3
K.3.5	Imposition of the Boundary Conditions	K.3-4
K.4	Closure	K.4-1
K.5	Matching	K.5-1
K.6	The Update Capability	K.6-1
L.0	The Constraint Matrix	L.0-1
M.0	Computation of the Minimal Data Set	M.0-1
M.1	Recovery of the Singularity Parameters	M.1-1
M.2	Singularity Strength Calculation	M.2-1
M.3	Computation of Potential and Normal Mass Flux	M.3-1
N.0	Surface and Wake Flow Properties	N.0-1
N.1	Velocity Computation	N.1-1
N.2	Pressure Formulas	N.2-1
N.2.1	Preliminary Results	N.2-1
N.2.2	Constant Density Flow	N.2-2
N.2.3	Compressible Flow	N.2-3
N.2.4	Limitation of the Formula	N.2-4
N.2.4.1	The Vacuum Pressure Coefficient	N.2-5
N.2.4.2	The Critical Speed	N.2-5
N.2.4.3	The Pressure Coefficient at the Critical Speed	N.2-7
N.2.5	The Isentropic Formula Under Simplifying Assumptions	N.2-7
N.2.5.1	Second Order Theory	N.2-8
N.2.5.2	The Second Order Theory Under Additional Assumptions	N.2-10
N.3	Velocity Corrections	N.3-1
N.3.1	The First Velocity Correction	N.3-1
N.3.2	The Second Velocity Correction	N.3-2
N.4	Onset Flow Calculations	N.4-1
N.4.1	Bernoulli's Equation	N.4-1
N.4.2	Pressure Formulas	N.4-2
N.4.3	Simplifying Assumptions	N.4-4
N.5	Associated Data	N.5-1
O.0	Forces and Moments	O.0-1
O.1	Basic Formulas	O.1-1
O.2	Integration Procedure	O.2-1
O.3	Leading and Side Edge Force	O.3-1
O.3.1	Thin Airfoil Theory	O.3-1
O.3.2	Linearized Three-Dimensional Theory	O.3-1
O.3.3	Application in PAN AIR	O.3-3
O.4	Coordinate Transformations	O.4-1



## List of Figures

Figures are placed at the end of each numbered section or appendix.

Page

### Section 3

3.1	Region $V$ of space with boundary $S$	3.4-1
3.2	A surface $S$ dividing regions $V_1$ and $V_2$	3.4-1
3.3	A surface $S$ which does not divide space into 2 separate regions	3.4-2
3.4	Basis function for constant strength panels	3.4-2

### Section 4

4.1	Historical overview of panel methods	4.3-1
4.2	Division of panel into subpanels	4.3-2
4.3	Panel and far field control point	4.3-2

### Section 5

5.1	Network geometry	5.10-1
5.2	Decomposition of panel into 5 planar regions	5.10-1
5.3	Definition of compressibility directions in terms of angles of attack and sideslip	5.10-2
5.4	Superinclined surface, $r = 1$	5.10-2
5.5	Subinclined and Mach-inclined surfaces	5.10-3
5.6	Gap between leading edge of wing and body	5.10-3
5.7	Example of abutment intersection	5.10-4
5.8	Control point locations	5.10-4
5.9	Thin wing boundary conditions	5.10-5
5.10	Two solutions for potential in enclosed volume	5.10-5
5.11	Thick wing boundary conditions	5.10-6
5.12	Boundary conditions on superinclined surfaces	5.10-6
5.13	Singularity parameter locations	5.10-7
5.14	Singularity parameters in the neighborhood of the panel	5.10-8
5.15	Neighboring source parameters for a panel corner point	5.10-9
5.16	Neighboring doublet parameters for a panel corner point	5.10-9
5.17	Neighboring doublet parameters for a panel edge midpoint	5.10-10
5.18	Panel points and midpoints	5.10-10
5.19	Opposite orientations of adjacent networks	5.10-11
5.20	Configuration and image	5.10-11
5.21	Pressure coefficient rules	5.10-12
5.22	Surfaces of integration for leading edge force	5.10-12

### Appendix A

A.1	Thin wing at small angle of attack	A.2-1
A.2	Blunt object at small Mach number	A.2-1
A.3	Small perturbation "engine-on" case	A.2-2

### Appendix B

B.1	An exterior boundary value problem	B.5-1
B.2	A region of finite volume	B.5-1

B.3	Specification of normal flow on both sides of a surface	B.5-2
B.4	A superinclined surface	B.5-2
B.5	A boundary value problem with no unique solution	B.5-3
B.6	The domain of dependence	B.5-3
B.7	A permeable surface inclined to the freestream	B.5-4
B.8	A region which fails to be simply connected	B.5-4
B.9	Airplane and wake	B.5-5
B.10	Leading edge vortices from a highly swept wing	B.5-6
B.11	Panel edge on a network edge	B.5-7
B.12	Two adjacent panel edges	B.5-7
B.13	Three adjacent panels	B.5-8
B.14	Intersection of 3 surfaces (cross-section)	B.5-8
B.15	Region of integration in neighborhood of P	B.5-9

#### Appendix C

C.1	Design boundary conditions on a thin configuration	C.5-1
C.2	Indexing of network points	C.5-1
C.3	A panel	C.5-2
C.4	Design boundary conditions for a thick wing	C.5-2
C.5	A constant doublet strength spline	C.5-3
C.6	Stability for constant doublet spline	C.5-3
C.7	Quadratically varying doublet spline	C.5-4
C.8	A single interval	C.5-4
C.9	Stability for a quadratic doublet spline	C.5-5
C.10	Instability of analysis spline with boundary conditions	C.5-6
C.11	A doublet spline for design problems	C.5-7
C.12	Stability for design boundary conditions	C.5-7

#### Appendix D

D.1	Locations of source singularity parameters	D.3-1
D.2	Doublet analysis and design singularity parameter locations	D.3-2
D.3	Doublet wake singularity parameter locations	D.3-3
D.4	Network and panel indexing	D.3-4
D.5	Network with an edge to be collapsed by the program	D.3-4
D.6	Network with revised geometry	D.3-5
D.7	Paneling of data wing	D.3-5
D.8	A panel	D.3-6
D.9	A subpanel	D.3-7
D.10	Definition of skewness parameters	D.3-8
D.11	impermissible network (two adjacent collapsed edges)	D.3-9

#### Appendix E

E.1	Surface S in compressibility and scaled coordinates	E.4-1
E.2	Illustration of the transformation law for $\hat{n} \cdot dS$	E.4-2
E.3	Definition of the compressibility vector $\hat{c}_0$ in terms of $\alpha_c$ and $\beta_c$	E.4-2

## Appendix F

F.1	Impermissible network intersection (in cross-section)	F.7-1
F.2	Leading edge vortex (in cross-section)	F.7-1
F.3	Simulation of a vortex core by a line vortex	F.7-2
F.4	Multiple pairwise abutments involving the same edges	F.7-2
F.5	Each network edge is a refinement of the other	F.7-3
F.6	Edge 1 is a refinement of edge 2	F.7-3
F.7	Control points on a supersonic leading edge are used for doublet matching	F.7-4
F.8a	Six network wing with wakes	F.7-5
F.8b	Doublet distribution arising from specification of $\mu$ at trailing edge	F.7-5
F.9	One edge is not precisely a refinement of the other	F.7-6
F.10	An abutment intersection with 4 abutments	F.7-6
F.11	An abutment intersection with 6 abutments	F.7-7
F.12	Another abutment intersection with 4 abutments	F.7-8
F.13	Line segment and point diagrams corresponding to three abutment intersections	F.7-9
F.14	Gap-filling panel	F.7-10
F.15	Gap-filling panels on an abutment with 3 network edges	F.7-10

## Appendix G

G.1	Control point locations	G.1-1
G.2	Division of network edge into two abutments	G.1-1
G.3	Control point recession vectors	G.1-2
G.4	Recession of corner control points when subpanel is triangular or nearly triangular	G.1-2
G.5	Subpanel 1, projected	G.1-3
G.6	Abutment with 3 network edges (cross-section)	G.1-3
G.7	Hypothetical locations of a control point	G.1-4

## Appendix H

H.1	Boundary condition locations for source networks	H.4-1
H.2	Boundary condition locations for doublet networks	H.4-2
H.3	Columns of panels illustrated by cross-hatching	H.4-4
H.4	Design of upper surface of thick wing	H.4-4
H.5	Pattern of streamlines on imposition of a closure boundary condition	H.4-5
H.6	Boundary condition categories	H.4-5
H.7	Total internal stagnation	H.4-6
H.8	Onset flow, not parallel to compressibility direction	H.4-6
H.9	Propeller slipstream	H.4-7
H.10	Airplane undergoing small rolling motion	H.4-7

## Appendix I

I.1a	Panel source parameter locations	I.6-1
I.1b	Panel doublet parameter locations	I.6-1
I.1c	Panel singularity parameter locations for a nine-panel network	I.6-2
I.2	Neighboring source parameters for analysis network	I.6-3
I.3	Thin wing with curved planform	I.6-3
I.4a	Neighboring singularity parameters ( $P_0$ away from network edge)	I.6-4
I.4b	Neighboring points for least squares fit ( $P_0$ near network edge)	I.6-4

1.4c	Neighboring points for least squares fit ( $P_0$ near a smooth abutment)	1.6-5
1.5	Basis vectors for local coordinate system for spline vector construction	1.6-6
1.6	Projections to tangent plane of points on curved surface	1.6-6
1.7a	Unequal spacing in a non-smooth abutment (second edge is a refinement of the first)	1.6-7
1.7b	Identification of points on a network edge	1.6-7
1.8	Differentiable 2-D quadratic spline	1.6-8
1.9a	Neighboring singularity parameters for points $P_0$ on a smooth abutment	1.6-9
1.9b	Parameterization of an abutment	1.6-10
1.9c	Panel edge on coarse network	1.6-10
1.10a	Neighboring point for least square fit ( $P_0$ on a doublet design network)	1.6-11
1.10b	Edge of a doublet design network	1.6-11
1.11	Adjacent panels	1.6-12
1.12	Panel defining points and subpanel local coordinate systems	1.6-12
1.13	Subpanel local coordinates	1.6-13
1.14	Triangular coordinates	1.6-13
1.15	Values of differentiable doublet distribution on a square panel	1.6-14
1.16	Values of doublet distribution on square panel with Pan Air spline	1.6-14
1.17	An interval with midpoint	1.6-15
1.18	Quadratic doublet distribution on a subpanel	1.6-15
1.19	Division on panel into half panels	1.6-16
1.20	Diagram of half panel i	1.6-16
1.21	Standard half panel	1.6-17
1.22	Computation of basic far field moments	1.6-17

#### Appendix J

J.1	Domain of dependence	J.12-1
J.2	Superinclined panel partially within $D_p$ without corners in $D_p$	J.12-1
J.3	Notation used frequently in Appendix J	J.12-2
J.4	Two region approximations to panel	J.12-3
J.5	Region in which intermediate field PIC is not performed	J.12-4
J.6	Splitting a panel into half panels	J.12-4
J.7	$(\bar{X}, \bar{Y})$ coordinate system	J.12-5
J.8	Subsonic and supersonic edges	J.12-5
J.9	Point of closest approach	J.12-6
J.10	Subinclined and superinclined panel	J.12-6
J.11	$P_*$ lies in the interior of the subpanel	J.12-7
J.12	Region of integration, $\Sigma' \cap C_h$ for a typical subpanel	J.12-7
J.13	$P_{k*}, Q_{k*}$ when $C_h \subset \Sigma'$	J.12-8
J.14	Edge numbering for various panel configurations	J.12-8
J.15	Phase angle $\phi'$ exceeds $\pi$	J.12-9
J.16	Coordinate systems in the $(\xi', \eta')$ plane	J.12-9
J.17	Determining if an edge of $\Sigma'$ is an edge of $\Sigma' \cap C_h$	J.12-10
J.18	Definition of $\rho(\phi)$ , the upper limit of integration for $\rho$	J.12-11
J.19	Region of integration for superinclined panel	J.12-12
J.20	Transformation to $(s, t)$ variables and region of integration	J.12-13
J.21	Numbering of edges of $\Sigma' \cap H_h$	J.12-13
J.22	A region $\Sigma'$ with edge $E$ , oriented tangent $\vec{t}$ and outward edge normal $\vec{n}$	J.12-14
J.23	An edge $E$ and its image $E'$ in the $s - t$ coordinate system (subsonic edge)	J.12-14

J.24	An edge E and its image E' in the s - t coordinate system (supersonic edge)	J.12-15
J.25a	Region of integration for subinclined panel	J.12-16
J.25b	Region of integration for subinclined panel	J.12-17
J.26	Polygon $\Sigma'_c$ approximating $\Sigma'ND_p$	J.12-18
J.27	Illustration of supersonic, nearly sonic edges on which v changes sign	J.12-19
J.28	An example of a superinclined panel with $g^2 = n^2 - a^2 \approx 0$	J.12-19
J.29	Evaluating v on the boundary of $D_p$ : the various special cases	J.12-20
J.30	The value of $J'$ for some special configurations	J.12-21
J.31	Region with nearly sonic edge	J.12-22
J.32	Potential lines of discontinuity in $J^+$	J.12-22
J.33	Panel corners on Mach lines	J.12-23
J.34	A point lies on the extension of an edge (subsonic flow)	J.12-24
J.35	A point lies on the extension of an edge (supersonic flow)	J.12-24
J.36	Edge barely intersects $D_p$	J.12-25
J.37a	The Mach wedge in cross-section	J.12-25
J.37b	Mach wedge behind supersonic panel edge	J.12-26
J.38	Subsonic nearly sonic edge	J.12-27
J.39	The distances h, v, a, g, and R in subsonic flow	J.12-28

#### Appendix K

K.1	Reflection of point or velocity vector in plane of symmetry	K.7-1
K.2	Reflection of point in 2 planes of symmetry	K.7-1
K.3	Vertical tail on a plane of symmetry	K.7-2
K.4	Reflections of abutments at and away from a plane of symmetry	K.7-2
K.5	Abutment on two planes of symmetry	K.7-3
K.6	Extra singularity parameter and control point dependent on existence of updateable network	K.7-3

#### Appendix M

M.1	Neighboring control points for potential spline computation	M.4-1
-----	---	-------

#### Appendix O

O.1	Effect of leading edge force	O.5-1
O.2	Vectors associated with leading edge force	O.5-1

## 1.0 Introduction

PAN AIR (an abbreviation for "panel aerodynamics") is a system of computer programs designed to analyze subsonic and supersonic inviscid flows about arbitrary configurations. It is one of a sequence of computer programs developed over the past two decades which fall in the category of "panel methods." Generally speaking, a panel method is a program which solves a linear partial differential equation numerically by approximating the configuration surface by a set of panels on which unknown "singularity strengths" are defined, imposing boundary conditions at a discrete set of points, such as panel centers, and thereby generating a system of linear equations relating the unknown singularity strengths. The equations are then solved for the singularity strengths, which, once known, provide information about the properties of the flow.

PAN AIR differs from earlier panel methods in two significant respects. First, it is a "higher order" panel method; that is, the singularity strengths are not constant on each panel. This is necessitated by the more stringent requirements of supersonic flow problems. Numerical solution of the differential equation relevant to supersonic flow, namely, the wave equation, is far more sensitive to numerical panel method idiosyncracies than solution of Laplace's equation, which governs subsonic flow. The potential for numerical error is greatly reduced by requiring the singularity strength to be continuous.

It is this "higher order" attribute which, in turn, allows PAN AIR to be used to analyze flow about arbitrary configurations. The A-230 program (Reference 1.1), for instance, can only analyze flow about thick objects such as bodies and thick wings, while the Woodward program (Reference 1.2) can only deal with "linearized" configurations, in which a wing is represented by its

mean surface. So, PAN AIR can handle the simple configurations considered in preliminary design, and at the same time serve as an "analytical wind tunnel" which can analyze the flow about detailed, complex configurations.

Second, PAN AIR includes advanced software technology as well as advanced engineering technology. It has been developed in accordance with Systematic Software Development Methodology, an approach that emphasizes modular, structured software. The separate "modules" communicate with each other only through a "data base" of information residing on a disk. Thus, changes in one module affect other modules in a clearly identifiable manner.

The basic Version 1.0 PAN AIR capabilities include:

- (a) the ability to handle, within the limitations of linear potential flow theory, completely arbitrary configurations, using either exact or linearized boundary conditions,
- (b) the ability to handle asymmetric configurations as well as those with one or two planes of symmetry,
- (c) the ability to handle symmetric configurations in either symmetric or asymmetric flow,
- (d) the ability to superimpose an incremental velocity on the freestream, either locally or globally, in order to simulate effects such as a rotational motion, differing angles of attack for different portions of a configuration, or a propeller slipstream,
- (e) the ability to calculate pressures, forces and moments using a variety of pressure formulas (such as isentropic, linear, etc), including the forces and moments due to flow through the surface,
- (f) the ability to calculate leading edge and side edge thrust forces and moments for thin configurations, and

- (g) the ability to perform non-iterative design of a configuration, a process in which a desired pressure or tangential velocity distribution is specified. The program then determines the "residual" normal flow through the surface required to obtain the desired pressure distribution.

This document has been structured to provide an overview of the theory of potential flow in general and PAN AIR in particular, with detailed mathematical formulations reserved for the appendices. Section 2 contains a brief discussion of fluid dynamics, outlining without proofs the steps from the Navier-Stokes equations to the linear differential equation solved by PAN AIR. Section 3 discusses the general theory of panel methods without discussing PAN AIR in particular. Section 4 is an overview of PAN AIR as it compares to older panel methods. Section 5 is devoted specifically to PAN AIR.

A complete discussion of the theory of potential flow and PAN AIR will be given in the appendices.

This document is not intended to be a textbook on fluid dynamics, and thus detailed derivations which are available in standard texts will not be repeated here; rather, the appropriate reference will be given. The standard fluid mechanics references we will use are the works of Kellogg (1.3), Liepmann and Roshko (1.4) and Ward (1.5). Those appendices dealing with items of theory unique to PAN AIR will be more thorough, however, referring to outside sources only when questions of abstract linear algebra are involved. There will be a correspondence between appendices and portions of the actual computer code, with each appendix either supplying background information or discussing the theory behind a module or part of a module of PAN AIR.



A glossary containing the definition of all technical terms is contained in this document. When a term first appears, it will be given in quotes, and briefly defined. The glossary will give a more detailed definition if necessary.

The authors wish to thank Kathleen Crites, Michele Sorensen, and Valerie Spura for their efforts in typing this document and Forrester Johnson for his assistance in its preparation.

## 2.0 Fundamental Fluid Dynamics

In this section, we will outline the process by which one arrives at a second order linear partial differential equation, called the Prandtl-Glauert equation, which describes steady, irrotational, inviscid flow in a perfect fluid. Our starting point is the Navier-Stokes equations, which describe flow in a fluid under very general circumstances. The assumption that viscosity can be neglected permits the Navier-Stokes equations to be replaced by a simpler system of equations including a "continuity equation", a "momentum equation," two "energy equations," and "Euler's equation." The further assumptions of "irrotationality" and "isentropic flow" lead to the "unsteady potential equation." The assumption of steady flow leads to the "steady non-linear potential equation." Finally, the "small perturbation assumption" leads to the "Prandtl-Glauert equation." The remainder of this document will deal with the numerical solution of the latter equation.

## 2.1 The Navier-Stokes Equations

The basic equations describing the flow of a viscous compressible, heat-conducting fluid are the Navier-Stokes equations. These are:

(a) The equation of continuity,

$$\frac{\partial \rho}{\partial t} + \sum_{i=1}^3 \frac{\partial (\rho v_i)}{\partial x_i} = 0 \quad (2.1.1)$$

where  $\vec{\nabla} = \left( \frac{\partial}{\partial x_1}, \frac{\partial}{\partial x_2}, \frac{\partial}{\partial x_3} \right)$  is the gradient operator with respect to the location vector  $\vec{x} = (x_1, x_2, x_3)$ , and where we have used the convenient index notation as an alternate to  $\vec{x} = (x, y, z)$ .

Also,  $t$  is time,  $\rho(\vec{x}, t)$  is the density, and  $\vec{V}(\vec{x}, t)$  is the total velocity, with  $\vec{V} = (V_1, V_2, V_3)$ .

(b) The momentum equation

$$\begin{aligned} & \frac{\partial}{\partial t} (\rho v_j) + \sum_{i=1}^3 \frac{\partial}{\partial x_i} (\rho v_i v_j) \\ &= -\frac{\partial p}{\partial x_j} + \sum_{i=1}^3 \frac{\partial}{\partial x_i} \tau_{ji} + \rho f_j \end{aligned} \quad (2.1.2)$$

$$j = 1, 2, 3$$

where  $\tau$  is the portion of the "stress tensor" which vanishes for a frictionless fluid,  $\vec{f}(\vec{x}, t)$  is an external body force per unit mass exerted on the fluid, and  $p(\vec{x}, t)$  is the pressure.

(c) The energy equation

$$\begin{aligned} & \frac{\partial}{\partial t} \left( \rho e + \frac{1}{2} \rho |\vec{V}|^2 + p \right) + \sum_{i=1}^3 \frac{\partial}{\partial x_i} \left[ \left( \rho e + \frac{1}{2} \rho |\vec{V}|^2 + p \right) v_i \right] \\ &= \frac{\partial p}{\partial t} + \sum_{i,m} \frac{\partial}{\partial x_i} \left( \tau_{im} v_m + k \frac{\partial \tau}{\partial x_i} \right) + \rho \sum_i f_i v_i \end{aligned} \quad (2.1.3)$$

where  $e(\vec{x}, t)$  is the "internal energy" of the fluid,  $k$  is the coefficient of heat conductivity for the fluid, and  $T(\vec{x}, t)$  is the temperature.

(d) The equation of state

$$f(\rho, p, T) = 0 \quad (2.1.4)$$

where the function  $f$  depends on the type of fluid. For a perfect gas, (2.1.4) can be written as

$$p = \rho RT \quad (2.1.5)$$

where  $R$  is a constant.

The equations in this section are derived in Liepmann and Roshko (1.4), section 13.13.

## 2.2 Euler's Equation

The Navier-Stokes equations can be simplified by the neglect of viscosity, which is equivalent to setting the tensor  $\tau_{ij} = 0$ . Combining the momentum and continuity equations, we obtain

$$\rho \frac{dv_j}{dt} = - \frac{\partial p}{\partial x_j} \quad j = 1, 2, 3 \quad (2.2.1)$$

where

$$\frac{d}{dt} = \frac{\partial}{\partial t} + \sum_i v_i \frac{\partial}{\partial x_i}$$

Equation (2.2.1) is called Euler's equation. We can obtain a full system of equations including (2.2.1) (see Liepmann and Roshko (1.4), p. 188, for details) as follows.

The continuity and energy equations can be reduced to two energy equations:

$$\rho \frac{d}{dt} \left( \frac{1}{2} |\vec{v}|^2 \right) = -\vec{v} \cdot \vec{\nabla} p + \rho \vec{v} \cdot \vec{f} \quad (2.2.2)$$

and

$$\frac{d\rho}{dt} + \rho \frac{d}{dt} \frac{1}{\rho} = q \quad (2.2.3)$$

where  $q$  is the amount of heat added to the fluid per unit mass.

In addition, it follows from (2.1.5) and (2.2.3) that a perfect gas obeys the equation

$$\frac{\partial e}{\partial t} = c_v \frac{\partial T}{\partial t} \quad (2.2.4)$$

where  $C_v$  is the specific heat of the gas at constant volume.

### 2.3 The Unsteady Potential Equation

The equations of section 2.2 can be reduced to a single equation (see Landahl, section 1.2, for details) if four further assumptions are made. First we assume "isentropic flow" so that no heat is added to the fluid, and thus

$$q = 0 \quad (2.3.1)$$

Second, we assume irrotationality, that is,

$$\vec{\nabla} \times \vec{V} = 0 \quad (2.3.2)$$

which is shown in Liepmann and Roshko (p. 196) to be equivalent to the existence of a "potential" function  $\phi(\vec{x}, t)$  such that

$$\vec{\nabla} \phi = \vec{V} \quad (2.3.3)$$

Third, we assume the existence of a freestream potential  $\phi_\infty$ , whose gradient is the uniform velocity  $\vec{V}_\infty$  attained at points sufficiently distant from the disturbance being analyzed, and thus write

$$\phi = \phi - \phi_\infty \quad (2.3.4)$$

and

$$\vec{V} = (u, v, w) = \vec{\nabla} \phi \quad (2.3.5)$$

The quantities  $\phi$  and  $\vec{V}$  are called the perturbation potential and velocity, respectively. For convenience, we assume the freestream  $\vec{V}_\infty$  is aligned in the x direction and has magnitude 1.

Fourth, we assume that

$$\vec{v} \ll a_{\infty} \quad (2.3.6)$$

everywhere, where  $a_{\infty}$  is the freestream speed of sound. Equation (2.3.6) is generally called a small perturbation assumption, but the reader is warned that other "small perturbation" assumptions exist in the literature and in this document.

Based on these four assumptions, one can obtain (denoting differentiation by subscripts) the unsteady potential equation (writing  $M_{\infty}$  for  $|\vec{V}_{\infty}|/a_{\infty}$ ):

$$\begin{aligned} & (1-M_{\infty}^2) \phi_{xx} + \phi_{yy} + \phi_{zz} - 2M_{\infty}^2 \phi_{xt} - M_{\infty}^2 \phi_{tt} \\ & = M_{\infty}^2 \left[ \frac{1}{2} (\gamma - 1) (2u + 2\phi_t + |\vec{v}|^2) \nabla^2 \phi \right. \\ & \quad + (2u + u^2) \phi_{xx} + v^2 \phi_{yy} + 2vw \phi_{yz} + w^2 \phi_{zz} \\ & \quad \left. + 2(1+u) (v \phi_{xy} + w \phi_{xy}) + 2(uu_t + vv_t + ww_t) \right] \quad (2.3.7) \end{aligned}$$

#### 2.4 The Steady Non-Linear Potential Equation

If we assume the flow conditions do not change with time, we can eliminate the time derivative terms in (2.3.7), obtaining (see Landahl, (2.1))

$$\begin{aligned}
 & (1 - M_{\infty}^2) \phi_{xx} + \phi_{xx} + \phi_{zz} \\
 & = M_{\infty}^2 \left[ \frac{1}{2} (\gamma - 1) (2u + |\vec{v}|^2) \nabla^2 \phi \right. \\
 & \quad + (2u + u^2) \phi_{xx} + v^2 \phi_{yy} + 2vw \phi_{yz} + w^2 \phi_{zz} \\
 & \quad \left. + 2(1 + u)(v\phi_{xy} + w\phi_{xz}) \right] \quad (2.4.1)
 \end{aligned}$$

where  $\gamma$  is the ratio of specific heats.

Equation (2.4.1) is often called the "small perturbation transonic equation" because it holds at transonic speeds (that is, for  $M \approx 1$ ) under the assumption (2.3.6). Of course, the assumptions of steady, inviscid, irrotational, and isentropic flow must also hold.



## 2.5 The Prandtl-Glauert Equation

So far, each reduction of the Navier-Stokes equations to a simpler form has been based on precisely defined assumptions. But the conditions under which (2.4.1) reduces to a linear differential equation are not so precisely defined.

If  $M_\infty = 0$ , (2.4.1) reduces to

$$\nabla^2 \phi = 0 \quad (2.5.1),$$

a linear partial differential equation known as Laplace's equation. But (2.4.1) reduces to a linear differential equation even if  $M_\infty \neq 0$ .

Suppose

$$M_\infty^2 |\vec{V}| \ll |1 - M_\infty^2| \quad (2.5.2)$$

and

$$M_\infty^2 |\vec{V}| \ll 1 \quad (2.5.3)$$

which, like (2.3.6), are called small perturbation assumptions. Under those assumptions, the steady non-linear potential equation reduces (see Appendix A) to the Prandtl-Glauert equation:

$$(1 - M_\infty^2) \phi_{xx} + \phi_{yy} + \phi_{zz} = 0 \quad (2.5.4)$$

Equations (2.5.2) and (2.5.3) should be considered carefully by any user of PAN AIR, since they best indicate when PAN AIR will provide a reasonable analysis of the flow about a configuration. Equation (2.5.2) clearly cannot

be satisfied for  $M_\infty \approx 1$ , and thus the Prandtl-Glauert equation does not describe "transonic" flow. Equation (2.5.3) does not hold for  $M_\infty \gg 1$ , and so (2.5.4) does not describe "hypersonic" flow.

But there is no precise answer to the question: for what range of Mach numbers does (2.5.4) describe the flow? For a thick configuration, or one at a high angle of attack, the perturbation quantities  $u$ ,  $v$ , and  $w$  tend to be large, and thus (2.5.2) and (2.5.3) only hold for a narrow range of Mach numbers. For a very slender configuration, at a small angle of attack, (2.5.3) and (2.5.4) hold for a much wider range of Mach numbers. But deciding whether (2.5.4) is a "reasonable" approximation for a particular configuration and a particular Mach number may be very difficult, and depend greatly on one's definition of "reasonable."

The remainder of this document will deal with the solution of the Prandtl-Glauert equation. Using Green's Theorem, (2.5.4) is converted to an integral equation over the configuration surface. The integral equation is then solved by a "discretization" process: the configuration surface is divided into panels, "boundary conditions" are imposed at a discrete set of points, and a system of linear equations is generated. The system of equations is solved, and data of aerodynamic interest is calculated from the solution.

### 3.0 Panel Method Theory

In this section, we outline the process by which the Prandtl-Glauert equation

$$(1 - M_{\infty}^2) \phi_{xx} + \phi_{yy} + \phi_{zz} = 0 \quad (3.0.1)$$

is converted to an integral equation, and the way in which a general panel method solves that integral equation.

### 3.1 Coordinate Scaling

Equation (3.0.1) is further simplified by performing a scaling of the coordinate system. If

$$s = \text{sign} (1 - M_{\infty}^2) \quad (3.1.1)$$

and

$$\beta = \sqrt{s (1 - M_{\infty}^2)} \quad (3.1.2)$$

then we define

$$\begin{aligned} \bar{x} &= x \\ \bar{y} &= \beta y \\ \bar{z} &= \beta z \end{aligned} \quad (3.1.3)$$

In this new, scaled coordinate system, (3.0.1) can be written

$$s \phi_{\bar{x}\bar{x}} + \phi_{\bar{y}\bar{y}} + \phi_{\bar{z}\bar{z}} = 0 \quad (3.1.4)$$

But equation (3.1.4) is just the same as (3.0.1) with  $M_{\infty} = 0$  or  $M_{\infty} = \sqrt{2}$ . Thus, the subsonic case reduces to the  $M_{\infty} = 0$  case while the supersonic case reduces to the  $M_{\infty} = \sqrt{2}$  case. Equation (3.1.4) is called Laplace's equation if  $s = 1$ , and the wave equation if  $s = -1$ . These equations occur in other branches of physics (for instance, Laplace's equation occurs in electrostatics), and thus PAN AIR potentially has applications in fields other than fluid mechanics.

For the rest of section 3, we will assume  $M_{\infty} = 0$  (note, incidentally, that this does not mean  $|\vec{V}_{\infty}| = 0$ ; rather,  $|\vec{V}_{\infty}| = 1$  and the freestream speed of

sound  $a_\infty$  is infinite). A similar discussion, for the case  $M_\infty = \sqrt{2}$ , is given in Ward (1.5). The integral equation (3.2.7) which results may be generalized to arbitrary subsonic and supersonic Mach numbers, as discussed by Ward in sections 2.8 and 2.10.

### 3.2 Green's Theorems

There are a number of theorems, all of them slightly different formulations of the same result, known as Green's theorem or theorems. It is one of these results, often known as Green's third identity (see Kellogg, p. 219) which allows us to convert Laplace's equation to an integral equation. The most fundamental version of these theorems is also known as the "divergence theorem", or Gauss' Theorem, which states that if  $F(x)$  is a "well-behaved" function (that is, continuously differentiable) on a "nice" region  $V$  in space with boundary  $S$  (see figure 3.1), then

$$\iiint_V \vec{\nabla} \cdot \vec{F} \, dV = \iint_S \hat{n} \cdot \vec{F} \, dS \quad (3.2.1)$$

where  $\hat{n}(\vec{x})$  is an outward-pointing unit normal to the surface. This theorem is discussed on p. 39 of Kellogg.

Green's third identity follows from (3.2.1). We need some notation to state this result, however. Let  $U$  be a twice continuously differentiable function in a region  $V$  of space. Let  $P$  be a point in  $V$ ,  $S$  the boundary of  $V$ ,  $Q$  an arbitrary point of integration on  $S$ , and  $R = |\vec{P} - \vec{Q}|$ . Then

$$\begin{aligned} U(P) = & -\frac{1}{4\pi} \iiint_V \frac{\nabla^2 U}{R} \, dV \\ & -\frac{1}{4\pi} \iint_S \frac{\hat{n} \cdot \vec{\nabla} U}{R} \, dS \\ & +\frac{1}{4\pi} \iint_S U \hat{n} \cdot \vec{\nabla} \left( \frac{1}{R} \right) \, dS \end{aligned} \quad (3.2.2)$$

This result is derived in Chapter VIII of Kellogg, where minus signs appear because the normal points inward. Also,

$$\nabla^2 = \vec{\nabla} \cdot \vec{\nabla} = \sum_{i=1}^3 \frac{\partial^2}{\partial x_i^2} \quad (3.2.2a)$$

A number of results follow by substituting into (3.2.2) a function  $\phi$  satisfying Laplace's equation

$$\nabla^2 \phi = 0 \quad (3.2.3)$$

First, letting  $P$  approach  $S$  we find that  $\phi$  is finite as we approach  $S$ . Thus,  $\phi$  is an integrable function over  $S$ . Next, let  $V$  be a region consisting of all of space except for a surface  $S$ , which is thus the boundary of  $V$ . We illustrate two such cases. In figure 3.2,  $S$  is a closed surface, and thus  $V$  is divided into two regions:  $V_1$ , the "interior" of  $S$ , and  $V_2$ , the "exterior". In figure 3.3,  $S$  is not closed, and thus  $V$  consists of a single region. Let us define the "upper" surface of  $S$  as the surface bounding that portion of  $V$  into which  $\hat{n}$  points, where  $\hat{n}$  is the outward-pointing normal for a closed surface, and may be chosen arbitrarily otherwise. Let us write  $\phi_U$  and  $\phi_L$  to denote the limiting values of  $\phi$  at a point on  $S$ , approaching from above and below. Then (see p. 221 of Kellogg)

$$\begin{aligned} \phi(P) = & -\frac{1}{4\pi} \iint_S \left[ \frac{\hat{n} \cdot (\vec{\nabla} \phi_U - \vec{\nabla} \phi_L)}{R} \right. \\ & \left. - (\phi_U - \phi_L) \hat{n} \cdot \vec{\nabla} \left( \frac{1}{R} \right) \right] dS \end{aligned} \quad (3.2.4)$$

Equation (3.2.4) is the fundamental integral equation which a panel method solves. Two quantities are generally introduced because of their importance in the numerical solution of (3.2.4). These are functions on  $S$ . The first is the "source strength", defined as

$$\sigma(Q) = \hat{n} \cdot (\vec{\nabla} \phi_U(Q) - \vec{\nabla} \phi_L(Q)) \quad (3.2.5)$$

and the second is the "doublet strength", defined as

$$\mu(Q) = \phi_U(Q) - \phi_L(Q) \quad (3.2.6)$$

These quantities are often called "singularity strengths", because they measure the singular behavior of  $\phi$  on  $S$ . Now, (3.2.4) becomes

$$\phi(P) = -\frac{1}{4\pi} \iint_S \left[ \frac{\sigma}{R} - \mu \hat{n} \cdot \vec{\nabla} \left( \frac{1}{R} \right) \right] dS \quad (3.2.7)$$

Equation (3.2.4) has infinitely many solutions, however, until "boundary conditions" are specified. Boundary conditions are equations relating  $\phi$  or its derivatives on  $S$ . The specification of boundary conditions in conjunction with (3.2.7) is called a "boundary value problem," and this problem in turn is called "well-posed" if it has a unique solution, and "ill-posed" otherwise. A typical example of a boundary condition might be (see figure 3.2)

$$\phi_L = 0 \quad (3.2.8)$$



$$\text{or } \vec{\nabla} \phi_U \cdot \hat{n} = b \quad (3.2.9)$$

It can be shown (see Appendix B) that the combination of (3.2.7) with the specification of the boundary conditions (3.2.8) and (3.2.9) on the configuration in figure 3.2 is a well-posed boundary value problem. We will discuss ill-posed and well-posed boundary value problems further in section 4 and Appendix B.

### 3.3 Discretization

We will now outline the discretization process by which a panel method solves a boundary value problem consisting of (3.2.7) and a set of boundary conditions. First, the configuration surface  $S$  is approximated by "panels." Next, a discrete set of points (for example, all panel centers) is chosen, and the values of source and doublet strength at these points are identified as unknown "singularity parameters". Next, a source and doublet distribution is defined over each panel, in terms of the unknown singularity parameters.

That is, for each singularity parameter  $\lambda_i$ , we implicitly define a "basis function"  $b_i$  on  $S$ , where  $b_i$  is the source or doublet distribution that would occur if  $\lambda_i = 1$ , and all  $\lambda_j, j \neq i$  were zero (see section 4.2.1 for further discussion). In the simplest case of "constant strength" panels this basis function  $b_i$  is identically equal to 1 on the panel containing  $\lambda_i$  and identically zero on all other panels. We illustrate such a basis function in figure 3.4.

Next, a discrete set of points, called control points, at which the boundary conditions are imposed, is chosen. The imposition of each boundary condition results in a linear equation in the unknown singularity parameters. We illustrate this in the following example.

Let us assume the boundary condition  $\phi_L = 0$  is imposed at a control point  $P$ . Then we use equation (3.2.7) to obtain a row vector, whose length  $N$  is the total number of singularity parameters and whose  $i$ th entry is the dependence of  $\phi_L(P)$  on  $\lambda_i$ . We define the row vector  $\underline{AIC}(P)$  ("AIC" stands for "aerodynamic influence coefficient") by

$$\Lambda_{i,j}^{AIC(P)} = -\frac{1}{4\pi} \iint_S \frac{b_i}{R} dS \quad \text{if } \lambda_i \text{ is a source parameter} \quad (3.3.1)$$

$$\text{or} = \frac{1}{4\pi} \iint_S b_i \hat{n} \cdot \vec{\nabla} \left( \frac{1}{R} \right) dS \quad \text{if } \lambda_i \text{ is a doublet parameter} \quad (3.3.2)$$

The most complex portion of a panel method is the computation of the integrals in (3.3.1) and (3.3.2).

Now, by the definition of the basis function  $b_i$ , for a point  $Q$  on the surface  $S$  (see figure 3.1)

$$\sigma(Q) = \sum_{i=1}^N b_i(Q) \delta_{i,S} \lambda_i \quad (3.3.3)$$

$$\mu(Q) = \sum_{i=1}^N b_i(Q) \delta_{i,D} \lambda_i \quad (3.3.4)$$

where  $\delta_{i,S} = 0$  if  $\lambda_i$  is a doublet parameter, 1 if it is a source parameter. Similarly,  $\delta_{i,D} = 0$  or 1 depending on whether  $\lambda_i$  is a doublet parameter. Substituting (3.3.3) and (3.3.4) into (3.2.7), we obtain,

for each control point  $P$ ,

$$\begin{aligned} \Lambda_{i,j}^{AIC(P)} &= -\frac{1}{4\pi} \iint_S \frac{1}{R} \sum_{i=1}^N b_i(Q) \delta_{i,S} \lambda_i dS \\ &\quad + \frac{1}{4\pi} \iint_S \sum_{i=1}^N b_i(Q) \delta_{i,D} \lambda_i \hat{n} \cdot \vec{\nabla} \left( \frac{1}{R} \right) dS \\ &= (\text{by definition}) \sum_{i=1}^N \Lambda_{i,j}^{AIC(P)} \lambda_i \end{aligned} \quad (3.3.5)$$

$\Lambda_{i,j}^{AIC(P)} \vec{\lambda}$   
where  $\vec{\lambda}$  is the vector of source and doublet singularity parameters whose  $i$ th entry is  $\lambda_i$ .

Thus the imposition at P of the boundary condition

$$\phi_L = 0 \quad (3.3.6)$$

leads to the equation in the N variables  $\lambda_1, \dots, \lambda_N$

$$[AIC(P)] \vec{\lambda} = 0 \quad (3.3.7)$$

Now we impose boundary conditions (which are not necessarily the same form as equation (3.3.6)) at all the control points in the configuration, obtaining as many boundary conditions as there are singularity parameters. Each boundary condition generates one linear equation, and thus we have a system of N equations in the N variables  $\lambda_1, \dots, \lambda_N$ :

$$[AIC] \vec{\lambda} = \vec{b} \quad (3.3.8)$$

where  $\vec{b}$  is a vector of "constraints" (the entry of  $\vec{b}$  corresponding to the boundary condition equation (3.3.7) is zero). The elements of  $\vec{b}$  are not to be confused with the basis functions  $b_i$  appearing in equations (3.3.2) to (3.3.5). Each row of the square matrix  $[AIC]$  is a row vector of the form  $[AIC(P)]$  for some control point P.

Next, equation (3.3.8) is solved by standard linear algebra techniques for the values  $\lambda_i$ . Once these values are known, the previously computed AIC matrix can be used to determine aerodynamic properties at control points. For instance, we can obtain  $\phi(P)$  by substituting the vector  $\vec{\lambda}$ , whose entries are now known, in (3.3.5). The velocity at a point can be obtained by evaluating the gradient of (3.2.7), and the pressure at a point can be

obtained from the velocity by using standard formulas. We will discuss all the steps in the discretization process in more detail in section 4, in which we consider PAN AIR exclusively.

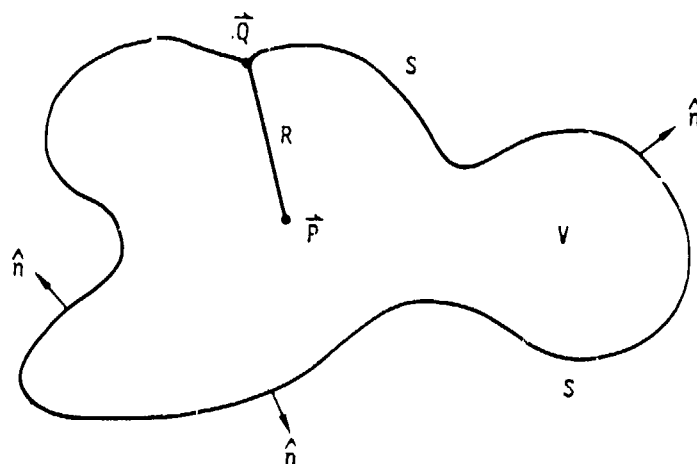


Figure 3.1 - Region  $V$  of space with boundary  $S$

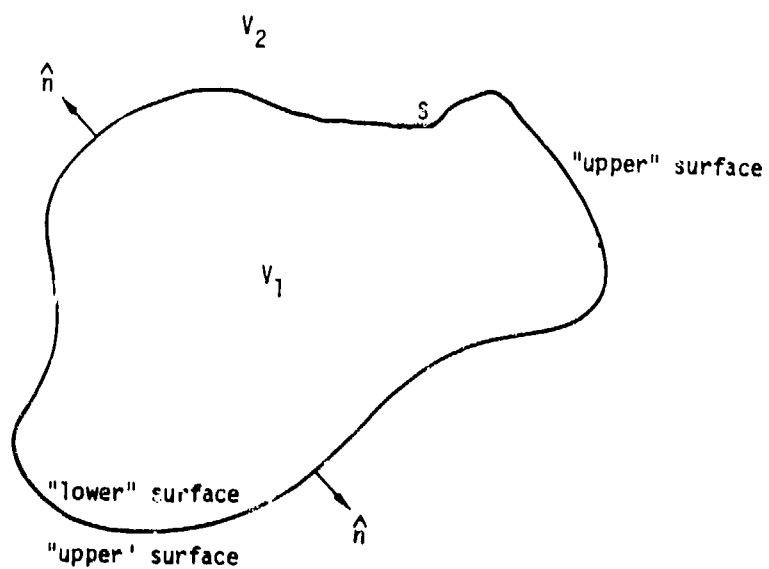


Figure 3.2 - A surface  $S$  dividing regions  $V_1$  and  $V_2$

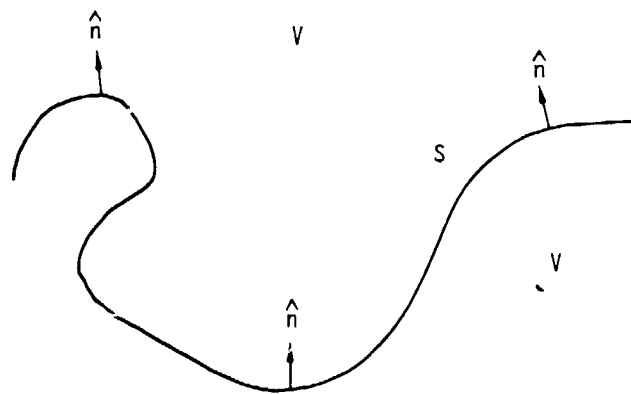


Figure 3.3 - A surface  $S$  which does not divide space into 2 separate regions



Figure 3.4 - Basic function for constant strength panels

#### 4.0 An Overview of PAN AIR

##### 4.1 Historical Development of Panel Methods

In this section, we will discuss the features which distinguish PAN AIR from earlier, less complex, panel methods. These features are (a) "continuous geometry," (b) linear source and quadratic doublet variation, and (c) continuity of singularity strength. We will explain how these features make PAN AIR more accurate and reliable than previous methods, and discuss briefly the manner in which these items are implemented in PAN AIR.

Virtually every panel method approximates the configuration geometry with panels whose planform is a quadrilateral. Thus, if the panels themselves are planar, only a small class of configurations (such as cylinders and flat wings) can be described without gaps being left between panels. These gaps tend to be very small, except for highly twisted surfaces. In subsonic flow, the gaps cause little if any numerical error, but in supersonic flow the cumulative effect of the gaps is serious, not because of "leakage" of flow through the gaps, but because the doublet strength jumps abruptly from a non-zero value to zero at a panel edge which does not exactly meet the adjacent edge. In PAN AIR, gaps are closed by means of "piecewise flat" panels, that is, panels which are comprised of several planar regions.

Some panel methods use "curved" panels, generally paraboloidal in shape. These approximate the configuration surface far more accurately in regions of high curvature such as the leading edge of a wing, but necessarily have gaps, even though small ones. Thus they are excellent for the analysis of subsonic flow, but not for supersonic flow.



As we stated earlier, PAN AIR employs a linear source variation and a quadratic doublet variation. That is, the basis function  $b_i$  corresponding to a source parameter is locally linear, while the basis function corresponding to a doublet parameter is locally quadratic. This contrasts with earlier, simpler programs in which the doublet and source variations were locally constant.

The reasons behind the "higher order" singularity distributions in PAN AIR are discussed in detail in Appendix B.4. Briefly, they are as follows. Consider a control point on a panel, and assume the source and doublet distributions in the immediate neighborhood of the control point are polynomials. Then we show in Appendix B.4 that a source distribution locally of the form

$$\sigma(\xi, \eta) = \sum_{N=1}^{\infty} \sum_{i=0}^{2N} a_{iN}^S \xi^i \eta^{2N-i} \quad (4.1.1)$$

or a doublet distribution

$$\mu(\xi, \eta) = \sum_{N=1}^{\infty} \sum_{i=0}^{2N+1} a_{iN}^D \xi^i \eta^{2N+1-i} \quad (4.1.2)$$

does not induce any perturbation velocity locally. That is, even terms in the polynomial source distribution and odd terms in the doublet distribution do not generate a local perturbation velocity. So, since we have concluded that constant source and doublet strengths are insufficient, the next reasonable higher order approximation to use is linear source strength and quadratic doublet strength.

Another reason for using a higher order doublet distribution is to provide a continuous doublet distribution, that is, each of the basis functions is constructed so that its value is continuous everywhere (obviously, a locally constant function can not be continuous). A continuous doublet strength, once again, is much more important in supersonic than in subsonic flow. That is due to the failure of disturbances caused by doublet discontinuities to diminish with distance in supersonic flow as they do in subsonic flow. A detailed description of the behavior of these distributions is given in Appendix J.12.

In addition, experimental evidence (references (4.9) to (4.12)) indicates that exact surface analysis is not feasible in supersonic flow without doublet continuity. The requirement of doublet continuity results in the spline complexity discussed in section 5.

In figure 4.1, we compare some panel methods of the last two decades. The list is by no means complete, with inclusion in the list generally reserved for methods containing innovations, whether or not the method enjoyed any great success.

Of the other panel methods described in figure 4.1, the one which most closely resembles PAN AIR is that of Ehlers et al. That program was written to demonstrate the technological feasibility of a panel code which was capable of analyzing arbitrary configurations in supersonic flow. The development of that program took place with the intention of eventually constructing production software (that is, PAN AIR) based on the same principles, and thus that program is generally referred to as the PAN AIR "pilot code."

#### 4.2 Summary of PAN AIR Technology

We now outline the method by which PAN AIR computes a row of the aerodynamic influence coefficient matrix. There are four basic steps. First, the basis functions must be computed. That is, the exact locally linear or locally quadratic variation on every panel must be defined for each basis function (see section 4.2.1). Next, for each panel, the perturbation that the panel induces on the potential and velocity at each control point, in terms of the singularity parameters, must be computed (see section 4.2.2 for details). Next (see section 4.2.3) these perturbation influences must be summed over all panels, to give a "potential influence coefficient" row vector ( $\Phi_{IC}(P)_j$ ) and a "velocity influence coefficient" matrix  $[VIC(P)]$  with the properties

$$\Phi_A(P)_i = \sum_{j=1}^N \Phi_{IC}(P)_j \lambda_j = \Phi_{IC}(P)_j \vec{\lambda} \quad (4.2.1)$$

$$\vec{v}_A(P)_i = \sum_{j=1}^N [VIC(P)]_{ij} \lambda_j = ([VIC(P)] \vec{\lambda})_i \quad (4.2.2)$$

$i = 1, 2, 3$

That is, the  $j$ th columns of  $\Phi_{IC}(P)_j$  and  $[VIC(P)]$  give the dependence of the potential and velocity at  $P$  on the  $j$ th singularity parameter. The subscript  $A$  indicates that the average of upper and lower surface potential and velocity are under consideration. Note that upper and lower surface potential and velocity are different, their difference being defined by the source and doublet strength (cf. (3.2.5-6)).

Finally, an arbitrary boundary condition of the form

$$(\hat{a}\vec{n} + \vec{t}) \cdot \vec{v} + c\phi = h \quad (4.2.3)$$

(where  $\vec{t}$  is a user-defined tangent vector and generally only one coefficient is

nonzero) leads to a row

$\underline{AIC(P)}$  of  $[AIC]$  as follows:

$$\underline{AIC(P)} = c \underline{IC(P)} + \left\{ \hat{a}\hat{n} + \vec{t} \right\}^T [\underline{VIC(P)}]$$

(4.2.4)

#### 4.2.1 Basis Function Computation

The computation of the basis functions is one of the more complex portions of PAN AIR. To be precise, we do not directly compute basis functions, but rather, for each region on which the source and doublet strengths are defined by a single polynomial, we compute matrices which describe the coefficients of these polynomial distributions as linear combinations of the singularity parameters in the neighborhood of the panel. A column of such a matrix defines the coefficients of a basis function on a subpanel.

These matrices are called "spline" matrices, and are computed in two steps as follows.

##### 4.2.1.1 Subpanel Splines

The first step is the computation of a "sub-panel spline" (SPSPL) matrix. Each panel is divided into eight triangular regions called "subpanels", as indicated in figure 4.2. The source subpanel spline matrices are  $3 \times 5$  matrices  $SPSPL^S$  giving the three coefficients  $\sigma_0, \sigma_\xi, \sigma_\eta$  of a linearly varying source strength (a linear function in two variables has three coefficients) in terms of five "panel source parameters",  $\sigma_1, \dots, \sigma_4, \sigma_9$  that is, the values of source strength at five points on the panel:

$$\begin{Bmatrix} \sigma_0 \\ \sigma_\xi \\ \sigma_\eta \end{Bmatrix} = [\text{SPSPL}^S] \begin{Bmatrix} \sigma_1 \\ \vdots \\ \sigma_4 \\ \sigma_9 \end{Bmatrix} \quad (4.2.5a)$$

where  $\sigma$  is defined in terms of local coordinates by

$$\sigma(\xi, \eta) = \sigma_0 + \sigma_\xi \xi + \sigma_\eta \eta \quad (4.2.5b)$$

Similarly, the (6x9) doublet subpanel spline matrices give the six coefficients of a quadratically varying doublet strength on the region in terms of nine "panel doublet parameters:"

$$\begin{Bmatrix} \mu_0 \\ \vdots \\ \mu_{\eta\eta} \end{Bmatrix} = [\text{SPSP}^D] \begin{Bmatrix} \mu_1 \\ \vdots \\ \mu_9 \end{Bmatrix} \quad (4.2.6)$$

where

$$\mu(\xi, \eta) = \mu_0 + \mu_\xi \xi + \mu_\eta \eta + \frac{1}{2} \mu_{\xi\xi} \xi^2 + \mu_{\xi\eta} \xi \eta + \frac{1}{2} \mu_{\eta\eta} \eta^2 \quad (4.2.7)$$

#### 4.2.1.2 Outer Splines

Next, the five panel source parameters and nine panel doublet parameters are described, as linear combinations of singularity parameters in the neighborhood of the panel, by "outer spline" matrices  $B^S$  ( $5 \times k_S$ ) and  $B^D$  ( $9 \times k_D$ ) where  $k_S$  and  $k_D$  are the number of source and doublet singularity parameters in the neighborhood of the panel for which the dependence is non-zero:

$$\begin{Bmatrix} \sigma_1 \\ \vdots \\ \sigma_4 \\ \sigma_9 \end{Bmatrix} = [B^S] \begin{Bmatrix} \lambda_1^S \\ \vdots \\ \lambda_{k_S}^S \end{Bmatrix} \quad (4.2.8)$$

$$\begin{Bmatrix} \mu_1 \\ \vdots \\ \mu_9 \end{Bmatrix} = [B^D] \begin{Bmatrix} \lambda_1^D \\ \vdots \\ \lambda_{k_D}^D \end{Bmatrix} \quad (4.2.9)$$

The values  $k_S$  and  $k_D$  depend on the location of a panel in a network (networks are discussed in section 5.1). In general,  $k_S$  is 9 and  $k_D$  is 21. In all cases,  $k_S + k_D \leq 31$ .

#### 4.2.2 Panel Influence Coefficients

The perturbations that a source and doublet distribution on a panel induce at a control point are described by "panel influence coefficient" (PIC) matrices. These matrices are a 4x5 matrix  $PIC^S$  and a 4x9 matrix  $PIC^D$  which give the potential and velocity at the control point, induced by the panel, in terms of the five panel source parameters and nine panel doublet parameters. That is,

$$\begin{Bmatrix} \phi(P) \\ v(P) \end{Bmatrix}_{\text{perturbation induced by panel}} = [PIC^S] \begin{Bmatrix} \sigma_1 \\ \vdots \\ \sigma_4 \\ \sigma_9 \end{Bmatrix} + [PIC^D] \begin{Bmatrix} \mu_1 \\ \vdots \\ \mu_9 \end{Bmatrix} \quad (4.2.10)$$

where  $\sigma_1$  through  $\sigma_4$ ,  $\sigma_9$  and  $\mu_1$  through  $\mu_9$  are the panel source and doublet parameters.

The method by which the PIC matrices are calculated depends on the distance from the panel to the control point.

#### 4.2.2.1 Near Field PIC's

If the distance is small compared to panel size, a "near field" method is used, and the PIC matrices are computed as a sum of integrals over the eight subpanels. For instance,

$$\begin{aligned} & \text{PIC}^S \text{ POTENTIAL} \quad 1 \times 5 \\ & = -\frac{1}{4\pi} \sum_{i=1}^8 \iint_{\Delta_i} \frac{1}{R} \begin{bmatrix} 1 & \xi & \eta \end{bmatrix} d\xi d\eta \begin{bmatrix} \text{SPSPL}_i^S \end{bmatrix} \quad 3 \times 5 \quad (4.2.11) \end{aligned}$$

Here,  $(\xi, \eta)$  are the local coordinates on the  $i$ th subpanel,  $\Delta_i$ , and  $\text{SPSPL}_i^S$  is the  $3 \times 5$  source subpanel spline matrix. Note that, for a point  $Q = (\xi, \eta)$ , using (4.2.5a) and (4.2.5b),

$$\sigma(Q) = \begin{bmatrix} 1 & \xi & \eta \end{bmatrix} \begin{bmatrix} \text{SPSPL}_i^S \end{bmatrix} \begin{Bmatrix} \sigma_1 \\ \vdots \\ \sigma_4 \\ \sigma_9 \end{Bmatrix} \quad (4.2.12)$$

and thus (4.2.11) follows from (3.2.7) and (4.2.10). The integrals in (4.2.11) are evaluated analytically, and can be expressed as logarithms and arc tangents of quantities which are determined by the geometric relation between the panel and the control point. In equation (4.2.11) the entries of  $\begin{bmatrix} \text{SPSPL}_i^S \end{bmatrix}$  are constants and may be removed from the integral. The application of (3.2.7) and an equation similar to (4.2.12) leads to a similar equation for the row of  $\text{PIC}^0$  corresponding to the potential. The rows of the PIC matrices corresponding to velocity are computed by using a differentiated version of (3.2.7). The entire subject of PIC computation is discussed in more detail in section 5.6 and Appendix J.

#### 4.2.2.2 Far Field PIC's

If the distance from the panel to the control point is large compared to panel size, a "far field" approximation is used in computing the influence of the panel. This is done by approximating the expression  $(1/R)$  by a power series

$$\frac{1}{R} = \frac{1}{R_0} \left( 1 + a_1 \frac{\Delta R}{R_0} + a_2 \left( \frac{\Delta R}{R_0} \right)^2 \right) \quad (4.2.13)$$

where  $R_0$  and  $\Delta R$  are illustrated in figure 4.3. This far field evaluation requires considerably less computer time than the near field method (see section 5.6 for further details). To further save computer time, an "intermediate field" method described in section 5.6 is used when the near field method is not necessary and the far field method is inadequate.

#### 4.2.3 Potential and Velocity Influence Coefficient Assembly

The influence of each panel is accumulated to determine the influence of the entire configuration on the control point. Combining equations (4.2.8-10), we see that the products

$$[PIC^S \cdot B^S] \quad \text{and} \quad [PIC^D \cdot B^D]$$

give us the potential and velocity induced by a panel, in terms of the singularity parameters in the neighborhood of the panel. These matrices are then "added" together; that is, entries of distinct PIC matrices which correspond to the same singularity parameter are accumulated, so that the "sum" of expanded PIC matrices (none of which has more than 31 non-zero columns) is the 4XN matrix



$$\begin{bmatrix} \phi IC(P) \\ -VIC(P) \end{bmatrix}$$

Here, N is the total number of singularity parameters.

#### 4.2.4 Aerodynamic Influence Coefficient Matrix Construction

Once the matrices  $\phi IC(P)$  and  $[VIC(P)]$  have been constructed, the vector  $[AIC(P)]$  is easily constructed using (4.2.4). The entire process is performed for all the control points in the configuration, and the result is the square matrix  $[AIC]$ . Additional details are given in section 5.7.

From here on, the basic structure of PAN AIR is similar to that of other panel methods. The system of linear equations is solved, "post-multiplication" (multiplying  $\phi IC$  and  $[VIC]$  by the vector  $\vec{\lambda}$ ) is performed, and the resulting velocities are used to compute pressures.

ORIGINATOR AND METHOD NAME (IF ANY)	YEAR	REF #	PANEL GEOMETRY	SOURCE TYPE	DOUBLET TYPE	BOUNDARY CONDITIONS	RESTRICTIONS	COMMENTS
HESS AND SMITH (DOUGLAS)	1962	4.1	FLAT	CONSTANT	NONE	SPECIFICATION OF NORMAL FLOW	NON-LIFTING WINGS AND BODIES ONLY	
RUBBERT (VORTEX LATTICE)	1964	4.2	FLAT	NONE	CONSTANT	NORMAL FLOW	PLANAR WINGS ONLY	
RUBBERT AND SAARIS (A-230)	1968	1.1	FLAT	CONSTANT	CONSTANT	NORMAL FLOW	NEARLY CONSTANT PANEL DENSITY	
WOODWARD	1968	1.2	FLAT	CONSTANT	LINEAR	NORMAL FLOW	WINGS MUST BE PLANAR	
HESS	1972	4.3	FLAT	CONSTANT	LINEAR	NORMAL FLOW	WINGS AND BODIES ONLY	
ROBERTS AND RUNDLE	1973	4.4	PARABOLOIDAL	QUADRATIC	QUADRATIC	NORMAL FLOW		NUMERICAL INTEGRATION - VERY EXPENSIVE
MERCER, WEBER AND LESFORD	1973	4.5	FLAT	NONE	SMOOTH, CUBIC/QUADRATIC	NORMAL FLOW IN LEAST SQUARES SENSE	PLANAR WINGS	SUBSONIC AND SUPERSONIC CUBIC SPANWISE, QUADRATIC CHORDWISE
MARINO AND KUO	1974	4.6	CONTINUOUS, HYPERBOLOIDAL	CONSTANT	CONSTANT	POTENTIAL	NO THIN CONFIGURATIONS	
JOHNSON AND RUBBERT	1975	4.7	PARABOLOIDAL	LINEAR	QUADRATIC	NORMAL FLOW		
EHLERS AND RUBBERT (MACH LINE PANELING)	1976	4.8	FLAT	LINEAR	CONTINUOUS QUADRATIC	NORMAL FLOW	PLANAR WINGS, SPECIAL PANELING	SUPERSONIC FLOW
EHLERS ET AL ("PILOT CODE")	1977	4.9	CONTINUOUS, PIECEWISE FLAT	LINEAR	CONTINUOUS QUADRATIC	ARBITRARY IN $\phi$ , $\nabla\phi$		SUBSONIC AND SUPERSONIC
PAN AIR	1980		CONTINUOUS, PIECEWISE FLAT	CONTINUOUS LINEAR	CONTINUOUS, QUADRATIC	ARBITRARY IN $\phi$ , $\nabla\phi$		SUBSONIC AND SUPERSONIC

Figure 4.1 - Historical Overview of Panel Methods

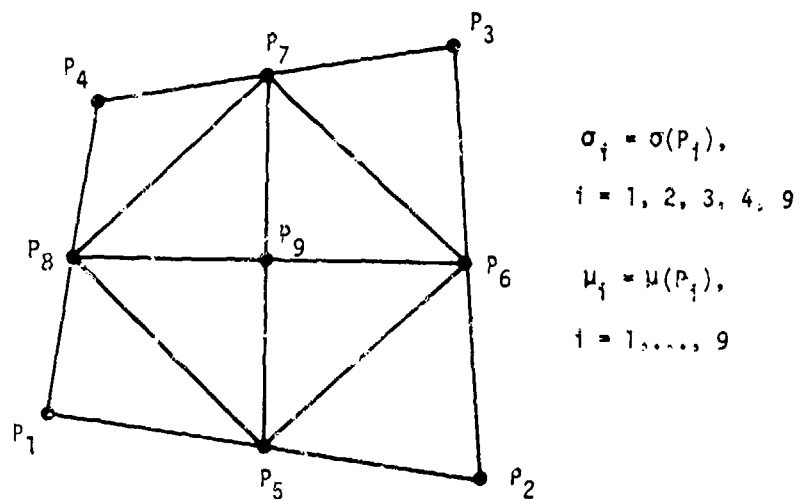


Figure 4.2 - Division of panel into subpanels

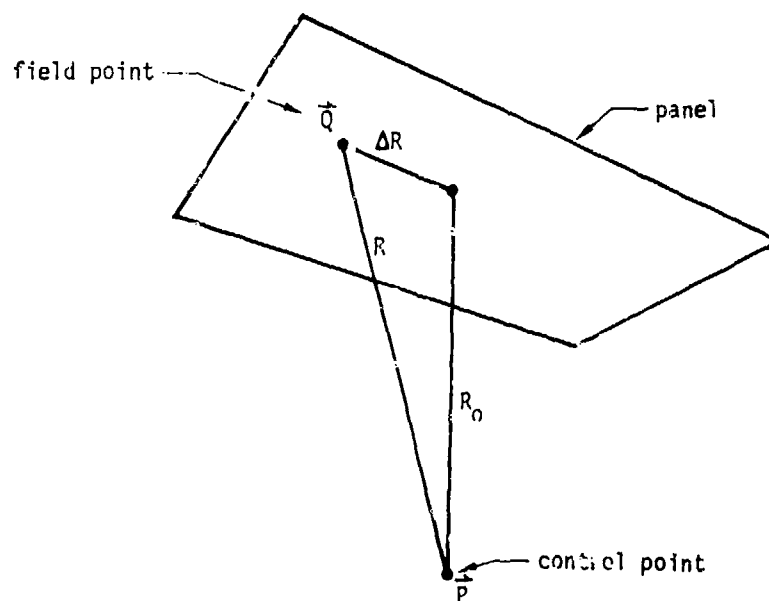


Figure 4.3 - Panel and far field control point

## 5.0 Elaboration on the Technology in PAN AIR

In this section, we discuss PAN AIR in greater detail than in section 4.

### 5.1 Networks and Panels

The configuration on which boundary conditions are to be imposed is described by a collection of networks of points. Each network consists of (say)  $N$  columns of points lying on the configuration surface, where each column has the same number ( $M$ , say) of points. By a point, we mean its  $(x, y, z)$  coordinates, with each point's coordinates given in the same arbitrary coordinate system. Thus, each network consists of an  $M \times N$  grid of points in space (see figure 5.1). This grid need not lie in a plane, but it should be sufficiently regular to define a surface which does not intersect itself.

Each network is assigned two "singularity types," describing the manner in which the source and doublet distributions are defined on the portion of the surface defined by the network. A network source type may be "null", "analysis", or "design", while its doublet type may be "null", "analysis", "design", or "wake." The singularity type "null" means that the corresponding singularity distribution is identically zero over the whole network. The singularity type "analysis" is used when the corresponding boundary conditions are the standard ones of zero normal flow, while the singularity type "design" is used when the boundary conditions correspond to specifying a desired pressure distribution on the surface. The doublet type of "wake" is generally used with a source type of null to model a wake surface. A wake is a surface across which a discontinuity in potential exists, while normal flow is continuous; generally a wake is attached to the trailing edge of a lifting surface. The positioning of wakes can be a complicated problem, and is discussed in more detail in the PAN AIR Users' and Case Manuals.

Note that, unless the source or doublet type is null, all networks are composite networks, that is, both the network's source distribution and its doublet distribution are non-zero. This is in contrast to most earlier panel methods, which required source networks and doublet networks to be entered separately. Generally speaking, all non-wake networks in PAN AIR will be composite networks which directly describe the impermeable object about which one is analyzing the flow. In particular, the "internal lifting system" doublet networks required by the Boeing A-230 program (Ref. 1.1) are not required in PAN AIR. These composite networks allow two boundary conditions, such as the standard boundary conditions of (5.4.28), to be imposed on a surface.

Each network of  $M$  rows and  $N$  columns of points defines  $(M-1)$  rows and  $(N-1)$  columns of panels, where a panel is a quadrilateral defined by four network points all lying in two adjacent rows and two adjacent columns of a network. Figure 5.1 illustrates the subdivision of a network into panels. In the example of Figure 5.1, there are five rows and columns of points and four rows and columns of panels.

Now, each panel is defined by its four corner points, but these four points need not lie on a plane. Previous programs using flat panels on arbitrary surfaces have handled this problem by projecting the four corner points onto an "average plane", thus forming a planar quadrilateral panel. The formation of such panels leaves gaps between panel edges, however, since the panels do not in fact go through their corner points.

This discontinuity in geometry is avoided by constructing piecewise flat panels which do in fact contain all four corner points and, in fact, all four panel edges (a panel edge is a line segment connecting adjacent corner points). The decomposition of a panel into five planar regions is illustrated in figure 5.2. It will be shown in Appendix D that the four edge midpoints, which define the vertices of the interior quadrilateral, do in fact lie on a plane. In section 5.5., the interior quadrilateral will be divided into four triangular regions for the purpose of defining source and doublet distributions. Thus the panel will be divided into 8 "subpanels" there, but at least four of them will lie in one plane.

## 5.2 Coordinate Transformations

Recall (see (3.2.7)) that for  $M_\infty = 0$ , we wrote the fundamental integral equation as

$$\phi(P) = \frac{1}{4\pi} \iint_S \left[ -\frac{\sigma}{R} + \mu \hat{n} \cdot \nabla \left( \frac{1}{R} \right) \right] dS \quad (5.2.1)$$

We can easily generalize this equation to arbitrary Mach number. For details, see Ward (Ref. 1.5). Let  $P = (x, y, z)$ , and the point of integration  $Q = (\xi, \eta, \zeta)$ . Recall

$$s = \text{sign}(1 - M_\infty^2)$$

$$\beta = \sqrt{s(1 - M_\infty^2)} \quad (5.2.2)$$

Now, generalizing the definition for  $M_\infty = 0$ , let

$$R = \sqrt{(\xi - x)^2 + s\beta^2(\eta - y)^2 + s\beta^2(\zeta - z)^2} \quad (5.2.3)$$

when the item under the square root is non-negative. Let  $R$  be zero otherwise.

For subsonic flow, let  $D_P$ , the "domain of dependence" on the point  $P$ , be all of space, while for supersonic flow let it be the set of points  $Q$  such that  $\xi \leq x$ , and the expression under the square root is non-negative. Let  $\kappa = 2\pi$  if  $s = -1$ ,  $\kappa = 4\pi$  if  $s = 1$ . Let us define the compressible gradient operator

$$\vec{\nabla} = (s\beta^2 \frac{\partial}{\partial \xi}, \frac{\partial}{\partial \eta}, \frac{\partial}{\partial \zeta}) = [B_o] \vec{\nabla} \quad (5.2.4)$$

where

$$[B_o] = \begin{bmatrix} s\beta^2 & 0 & 0 \\ 0 & 1 & 0 \\ 0 & 0 & 1 \end{bmatrix} \quad (5.2.5)$$

$$\text{Let } \vec{n} = [B_o] \hat{n} \quad (5.2.6)$$

(a vector generally called the "conormal")

$$\text{and} \quad \sigma = \vec{\nabla} (\Phi_U - \Phi_L) \cdot \vec{n} \quad (5.2.7)$$

a generalization of our previous definition of source strength to arbitrary Mach number. Then we can rewrite (5.2.1) for arbitrary  $M_\infty$  as

$$\Phi(P) = \frac{1}{k} \iint_{S \cap D_p} \left[ -\frac{\sigma}{R} + \mu \hat{n} \cdot \vec{\nabla} \frac{1}{R} \right] dS \quad (5.2.8)$$

Here, " $S \cap D_p$ " means the set of points common to both regions.

Now, in order to obtain "panel influence coefficient" matrices, we must perform integrations of the form of (4.2.11). This task is somewhat obscured by the multiplicity of coordinate systems with which we deal. We will now discuss these coordinate systems and describe the transformations among them.

The coordinate system with which this document primarily deals is the "compressibility coordinate system." This is the system in which equation (2.5.4)



$$(1 - M_{\infty}^2) \phi_{xx} + \phi_{yy} + \phi_{zz} = 0 \quad (5.2.9)$$

is valid.

For  $M_{\infty} \neq 0$ , (5.2.9) requires a preferred direction, called the "compressibility direction," which is the direction of  $\vec{V}_{\infty}$ . We have assumed so far that this is the x-direction.

A program user, however, may not want to describe the configuration geometry such that the compressibility direction is the x-direction. PAN AIR permits the user to specify an arbitrary compressibility direction by specifying angles  $\alpha_c$  and  $\beta_c$ , angles of attack and sideslip, which describe the compressibility direction with respect to the input (or reference) coordinate system.

If the coordinates of a point are  $(x, y, z)$  in the compressibility axis system, and  $(x_0, y_0, z_0)$  in the reference axis system, then

$$\begin{Bmatrix} x \\ y \\ z \end{Bmatrix} = [T_c] \begin{Bmatrix} x_0 \\ y_0 \\ z_0 \end{Bmatrix} \quad (5.2.10)$$

where  $T_c$  is the coordinate transformation matrix

$$\Gamma_c = \begin{Bmatrix} \cos \alpha_c & \cos \beta_c & -\sin \beta_c & \cos \beta_c & \sin \alpha_c \\ \sin \beta_c & \cos \alpha_c & \cos \beta_c & \sin \alpha_c & \sin \beta_c \\ -\sin \alpha_c & 0 & 0 & \cos \alpha_c & 0 \end{Bmatrix} \quad (5.2.11)$$

We show how  $\Gamma_c$  is obtained as a product of a rotation by an angle  $\alpha_c$  about the y-axis and a rotation by an angle  $\beta_c$  about the modified z-axis in Appendix E.3. It should be noted that the above sequence of coordinate rotations is equivalent to the opposite sequence of basis vector transformations. That is, the configuration is first rotated about its z-axis by an angle  $\beta_c$ , then about its y-axis by an angle  $\alpha_c$ . This transformation is discussed further in the Users' Document.

Now, the unit vector (written in reference coordinates) in the compressibility direction is

$$\hat{c}_0 = [\Gamma_c]^{-1} \begin{Bmatrix} 1 \\ 0 \\ 0 \end{Bmatrix} \quad (5.2.12)$$

Since  $\Gamma_c$  is an orthogonal matrix,

$$\hat{c}_0 = [\Gamma_c]^T \begin{Bmatrix} 1 \\ 0 \\ 0 \end{Bmatrix} = \begin{Bmatrix} \cos \alpha_c & \cos \beta_c \\ -\sin \beta_c \\ \sin \alpha_c & \cos \beta_c \end{Bmatrix} \quad (5.2.13)$$

The relationship of  $\hat{c}_0$  to the reference coordinate system is shown in figure 5.3.

A third coordinate system of importance in PAN AIR is the "local" coordinate system (see Glossary). We want to compute the surface integrals required for PIC calculation as integrals in two variables, and thus we construct a local coordinate system  $(x', y', z')$  for each subpanel, in which the subpanel lies in the  $x'-y'$  plane.

The transformation from reference to local coordinates is not orthogonal, however, but includes a scaling transformation so that the factor  $\beta$  does not appear in the expression for  $R$ . This simplifies the influence coefficient integrals, such as (5.6.9), which must be calculated.

Recall from (5.2.3) that in compressibility coordinates, for a control point  $P = (x, y, z)$  and field point  $(\xi, \eta, \zeta)$ , we have

$$R^2 = (\xi - x)^2 + s\beta^2 (\eta - y)^2 + s\beta^2 (\zeta - z)^2 \quad (5.2.14)$$

where  $R$  is the denominator of the integrand of (5.2.8). In order to describe the appearance of  $R$  in local coordinates, we need to introduce

$$\begin{aligned} r &= \text{sign} (\hat{n} \cdot \hat{n}) \\ &= (\text{by (5.2.6)}) \text{sign} (\hat{n}^T [B_0] \hat{n}) \\ &= \text{sign} \left\{ \hat{n}, \hat{n} \right\} \end{aligned} \quad (5.2.15)$$

where we define  $\left\{ \begin{matrix} \vec{X} \\ \vec{Y} \end{matrix} \right\}$  by saying that for any two vectors  $\vec{X}$  and  $\vec{Y}$ ,

$$\left\{ \vec{x}, \vec{y} \right\} = \vec{x}^T [B_0] \vec{y} \quad (5.2.16)$$

The meaning of  $r$  can be understood if we work in compressibility coordinates.

Then by (5.2.5) and (5.2.6),

$$r = \text{sign} ( s \beta^2 n_x^2 + n_y^2 + n_z^2 ) \quad (5.2.17)$$

If  $s = 1$  (that is, for subsonic flow), we see that the expression in (5.2.17) is positive, and so  $r = 1$ . If  $s = -1$  (supersonic flow), and  $\beta = 1$  ( $M_\infty = \sqrt{2}$ ), we see that

$$\begin{aligned} r &= -1 \quad \text{if} \quad n_x^2 > n_y^2 + n_z^2 \\ r &= +1 \quad \text{if} \quad n_x^2 < n_y^2 + n_z^2 \end{aligned} \quad (5.2.18)$$

Recall from section 4.2.1.1 that the PAN AIR panels are comprised of eight triangular subpanels. Each of these flat subpanel surfaces has a unit surface normal  $\hat{n}$  of fixed direction. If  $\hat{n}$  is such that  $r = -1$  in equation (5.2.18), the surface normal is inclined at more than  $45^\circ$  to the freestream. But this  $45^\circ$  angle is also that of the "Mach cone" emanating forward from a point  $P$  on the subpanel, as illustrated in figure 5.5, and defines the "domain of dependence" of  $P$ . In other words, point  $P$  is affected only by disturbances (such as those produced by the source and doublet distributions) that originate within this forward Mach cone.

Thus we see that if  $r = -1$ , no point on the subpanel surface lies in the domain of dependence of any other point on the subpanel, and we call such a surface "superinclined." If  $r = +1$ , the more upstream points on the subpanel do lie in the domain of dependence of the more downstream points, and such a surface is called subinclined. If  $\hat{n} \cdot \tilde{n} = 0$ , the more upstream points lie exactly on the boundary of, but never in the interior of, the domain of dependence of more downstream points. Such a surface is called Mach-inclined. We will see shortly that no portion of the paneled configuration is permitted to be Mach-inclined. The above definitions, illustrated in figures 5.4 and 5.5, are equally valid at all supersonic Mach numbers.

Now, for ease of integration, we want the local coordinate system  $(x', y', z')$  defined on each subpanel to have the property that if  $P = (x', y', z')$ ,  $Q = (\xi', \eta', \zeta')$  then

$$R^2 = r(\xi' - x')^2 + s(\eta' - y')^2 + rs(\zeta' - z')^2 \quad (5.2.19)$$

In this manner, we reduce the denominator of (5.2.8) to one of three standard forms:

(a) Subsonic flow

$$R = \sqrt{(\xi' - x')^2 + (\eta' - y')^2 + (\zeta' - z')^2} \quad (5.2.20)$$

(b) Supersonic flow, subinclined panels

$$R = \sqrt{(\xi' - x')^2 - (\eta' - y')^2 - (\zeta' - z')^2} \quad (5.2.21)$$

(c) Supersonic flow, superinclined panels

$$R = \sqrt{(\zeta' - z')^2 - (\xi' - x')^2 - (\eta' - y')^2} \quad (5.2.22)$$

So, if we can find a local coordinate system in which (5.2.19) holds, we will have succeeded in removing the factors of  $\beta$  from the integrand of (5.2.8). Further, the subpanel always lies in the  $(\xi', \eta')$  plane, with the flow oriented in the  $\xi'$ -direction in case (b), and in the  $\zeta'$ -direction in case (c).

We will compute the reference to local coordinate transformation A, such that

$$[A] \begin{Bmatrix} x_0 \\ y_0 \\ z_0 \end{Bmatrix} = \begin{Bmatrix} x' \\ y' \\ z' \end{Bmatrix} \quad (5.2.23)$$

in Appendix E.3.

We now describe the result computed there. Let  $\hat{v}_0$  be a unit vector perpendicular to  $\hat{c}_0$  and  $\hat{n}_0$ , the unit normal to the subpanel. Let  $\hat{u}_0 = \hat{v}_0 \times \hat{n}_0$ . Let

$$[C_0] = s\beta^2 [I] + (1 - s\beta^2) [\hat{c}_0 \hat{c}_0^T] \quad (5.2.24)$$

$$[B_0] = [I] + (s\beta^2 - 1) [\hat{c}_0 \hat{c}_0^T] \quad (5.2.25)$$

Note that the definition (5.2.5) of  $[B_0]$  in the compressibility coordinate system is consistent with (5.2.25) since in that coordinate system

$$\begin{bmatrix} \hat{c}_0 & \hat{c}_0^T \end{bmatrix} = \begin{bmatrix} 1 & 0 & 0 \\ 0 & 0 & 0 \\ 0 & 0 & 0 \end{bmatrix} \quad (5.2.26)$$

Recalling the definition (5.2.16) of  $\{ \cdot, \cdot \}$

$$A = \left[ \frac{1}{|\{\hat{n}_0, \hat{n}_0\}|^{1/2}} [c_0] \hat{u}_0 \mid \frac{rs}{\beta} [c_0] \hat{v}_0 \mid \frac{\beta}{|\{\hat{n}_0, \hat{n}_0\}|^{1/2}} \hat{n}_0 \right]^T \quad (5.2.27)$$

Several remarks may be made here. First, if  $M_\infty = 0$ ,  $\hat{c}_0$  is meaningless, but is given a default value by PAN AIR just so that no special formula is needed to replace (5.2.27). Since all occurrences of  $\hat{c}_0$  are multiplied by  $(1 - s\beta^2) = M_\infty^2$  any value for  $\hat{c}_0$  is equally valid if  $M_\infty = 0$ .

Next, (5.2.27) blows up if  $\beta = 0$  or  $\{\hat{n}_0, \hat{n}_0\} = 0$ . But the former case corresponds to  $M_\infty = 1$ , and is impermissible, while the latter case corresponds to a Mach-inclined panel, and is also impermissible.

### 5.3 Network Edge Matching

The splines which are discussed in section 5.5 insure that the source and doublet strength on the configuration are continuous within a network, but do nothing to insure continuity across network edges. The contribution of continuous doublet splines to the goal of increased program reliability would be wasted if the doublet strength were discontinuous at network boundaries.

One solution to the problem of matching doublet strength at network edges (hence called the edge matching problem) is to impose the boundary condition of zero normal flow along the edge. As shown in Appendix J.11, a discontinuity in doublet strength along an edge induces an infinite velocity there. Thus, the requirement that the flow be finite causes the doublet strength to be continuous across the edge. This method has worked successfully in the earlier versions of the "pilot code", for instance) in many cases. Unfortunately, the method requires that the geometric fit among networks be exact; if there is a gap, say, where networks meet, the boundary condition of zero normal flow will force the doublet strength along the edge to zero.

The requirement that network edges match exactly in a geometric sense is a severe burden on the user of a panel code. Figure 5.6 illustrates the type of panelling frequently used by aerodynamicists at the intersection of the leading edge of a wing and the body of an airplane. The aerodynamicist is usually more interested in detailed wing pressures than detailed body pressures; further, the high curvature of the wing leading edge requires dense panelling for accurate definition. But accurate definition of the leading edge of the wing is incompatible with coarse definition of the body, unless a gap is left between network edges. In figure 5.6, the shaded area represents the gap between the body and the wing.



The most complex portion of the edge matching problem is the determination of those pairs (or larger collections) of network edges along which the doublet strength is to be matched. This determination is performed in two ways: (1) For each network edge, the program searches for other network edges which lie within a user-input tolerance distance of the first network edge. (2) For edges which lie far from each other (compared to the tolerance), but which ideally would be identical, such as those of figure 5.6, there is an option which permits the user to directly specify that doublet matching should occur along the edges.

PAN AIR incorporates two features to insure the matching of doublet strength across network edges. The first feature is that the matching of doublet strength is done directly rather than indirectly. That is, in construction of the AIC matrix, the boundary condition  $\mu_1 - \mu_2 = 0$  (assuming  $\mu_1$  and  $\mu_2$  are the doublet strengths at two opposing points where networks meet) is imposed exactly (rather than approximately by the requirement of zero normal flow). The second feature is that "gap-filling" panels are introduced whenever there are gaps between network edges which do not actually represent gaps in the physical configuration. A doublet distribution is defined on these gap-filling panels in such a manner that continuity of doublet strength is produced everywhere.

Imposing doublet matching exactly, rather than indirectly, requires considerable care. The doublet matching boundary conditions must never be redundant. Redundancy is permissible in the case of zero normal flow boundary conditions, because of the rather inexact manner in which these boundary conditions perform doublet matching (experimentation has shown that the partial redundancy of zero normal flow boundary conditions may lead to

ill-conditioned matrices). But if the matching of doublet strength is imposed exactly, any redundancy leads to a singular AIC matrix.

Preventing redundancy along a curve where two or more network edges meet (such a curve is called an abutment) is fairly straightforward. The only difficult problem occurs at "abutment intersections," that is, points where several abutments meet (see figure 5.7). The details concerning the imposition of edge matching, and concerning gap-filling panels, are given in Appendix F.

## 5.4 Control Points and Boundary Conditions

### 5.4.1 Control Point Location

Control points are points at which boundary conditions are imposed. Such points are either (1) in the vicinity of a panel center (the point whose coordinates are the average of the panel corner coordinates), (2) in the vicinity of the midpoint of a panel edge which also lies on a network edge, or (3) in the vicinity of a panel corner which lies on a network edge. These points are called center, edge, and corner control points respectively. "Extra" corner control points are located at panel corners which belong to "abutment intersections." Figure 5.7 illustrates a situation which would cause the construction of an extra control point. There,  $N_1$ ,  $N_2$ , and  $N_3$  are three separate networks.

In figure 5.8 we illustrate the control point locations on a network with no extra control points. Note that control points are always receded slightly from a panel edge. This is done because the velocity induced by the doublet distribution on a panel causes an infinite velocity at the panel edge. Thus, for numerical reasons the control point is withdrawn approximately 1/10 of the way toward the center of the panel. The precise method by which control points are receded is described in Appendix G.

### 5.4.2 Boundary Conditions

Boundary conditions are imposed at every control point. Recall that a boundary condition is a linear equation in  $\phi$  and its derivatives. Since  $\phi$  or its gradient may be discontinuous on the configuration surface, upper and lower surface potential and velocity are different, and so the boundary condition equation may involve "upper surface" and/or "lower surface" terms.

The number of boundary conditions imposed at a control point is between zero and two (inclusive), and is determined by the basic principle that the number of boundary conditions must equal the number of singularity parameters. For analysis networks, there are two boundary conditions imposed at every panel center control point, but, since only doublet parameters (and not source parameters) are located on network edges, there is only one boundary condition imposed at panel edge and corner control points.

#### 5.4.2.1 Impermeability Boundary Conditions

For most cases, the boundary condition the user wishes to impose is that there is no flow through the configuration surface. At Mach zero, this is achieved by setting

$$\vec{V} \cdot \hat{n} = 0 \quad (5.4.1)$$

or equivalently,

$$\vec{\nabla} \phi \cdot \hat{n} = \vec{v} \cdot \hat{n} = -\vec{V}_{\infty} \cdot \hat{n} \quad (5.4.2)$$

Equation (5.4.2) does not generalize in that form to arbitrary Mach number however. In Appendix H, we see that the appropriate boundary condition for non-linear potential flow (that is, flow satisfying the non-linear potential equation (2.4.1)) is

$$\rho \vec{V} \cdot \hat{n} = 0 \quad (5.4.3)$$

where  $\rho$  is the density of the fluid.

In section 1.11 of Ward (1.5), it is shown that, neglecting terms of the same order as those neglected in reducing equation (2.4.1) to the Prandtl-Glauert equation, we have

$$\rho \vec{V} = \rho_{\infty} (\tilde{\nabla} \phi + \vec{V}_{\infty}) \quad (5.4.4)$$

where  $\rho_{\infty}$  is the density at infinity. Note that  $\tilde{\nabla} \phi$  rather than  $\vec{\nabla} \phi$  occurs in (5.4.4). Thus the appropriate boundary condition to impose is

$$\rho_{\infty} (\tilde{\nabla} \phi + \vec{V}_{\infty}) \cdot \hat{n} = 0 \quad (5.4.5)$$

$$\text{or} \quad \tilde{\nabla} \phi \cdot \hat{n} = -\vec{V}_{\infty} \cdot \hat{n} \quad (5.4.6)$$

The validity of (5.4.4) can be justified intuitively by recalling that the continuity equation (2.1.1), neglecting the unsteady flow term, is

$$\vec{\nabla} \cdot (\rho \vec{V}) = 0 \quad (5.4.7)$$

while the Prandtl-Glauert equation

$$s R^2 \phi_{xx} + \phi_{yy} + \phi_{zz} = 0 \quad (5.4.8)$$

can be rewritten as

$$\vec{\nabla} \cdot (\rho_{\infty} \vec{V}_{\infty} + \rho_{\infty} \tilde{\nabla} \phi) = 0 \quad (5.4.9)$$

since  $\rho_{\infty}$  is a constant and

$$\vec{\nabla} \cdot \vec{V}_{\infty} = 0 \quad (5.4.10)$$

So, we see that both the left and right hand sides of (5.4.4) are vector fields whose divergence is zero, that is, they are "conserved quantities."

The expression  $(\rho/\rho_{\infty}) \vec{V}$  is called the mass flux,  $\tilde{\nabla} \phi + \vec{V}_{\infty}$  is called the total linearized mass flux, and  $\tilde{\nabla} \phi$  is called the linearized perturbation mass flux. We will never consider the non-linear mass flux in section 5, and thus will drop the modifier "linearized." We will denote the

perturbation and total mass flux by  $\vec{w}$  and  $\vec{W}$  respectively, and call  $\vec{w} \cdot \hat{n}$  and  $\vec{W} \cdot \hat{n}$  the perturbation and total normal mass flux.

Now, the combination of (5.4.3) and (5.4.4) indicates that to specify impermeability of a surface, we set total normal mass flux equal to zero. This can be done directly or indirectly, as illustrated by the following examples.

#### 5.4.2.2 Thin Surfaces

In the case of the thin wing illustrated in figure 5.9, we clearly require both the upper and lower surfaces to be impermeable, and thus specify

$$\begin{aligned}\vec{w}_U \cdot \hat{n} &= -\vec{V}_\infty \cdot \hat{n} \\ \vec{w}_L \cdot \hat{n} &= -\vec{V}_\infty \cdot \hat{n}\end{aligned}\quad (5.4.11)$$

But recall from section 5.2 that

$$\sigma = \vec{\nabla}(\phi_U - \phi_L) \cdot \hat{n} = \vec{\nabla}(\phi_U - \phi_L) \cdot \{[B_0] \hat{n}\} \quad (5.4.12)$$

$$= \{\vec{\nabla}(\phi_U - \phi_L)\}^T \{[B_0] \hat{n}\} = \{[B_0] \vec{\nabla}(\phi_U - \phi_L)\}^T \hat{n} \quad (5.4.13)$$

$$= \{\vec{\nabla}(\phi_U - \phi_L)\} \cdot \hat{n} = \vec{w}_U \cdot \hat{n} - \vec{w}_L \cdot \hat{n} \quad (5.4.14)$$

Note that these equations reveal

$$\hat{n} \cdot \vec{\nabla} = \hat{n} \cdot \vec{w} \quad (5.4.15)$$

This relation will be used later.

Thus, (5.4.11) implies

$$\sigma = 0 \quad (5.4.16)$$

so we can impose the boundary conditions

$$\vec{w}_U \cdot \hat{n} = -\vec{v}_\infty \cdot \hat{n} \quad (5.4.17)$$

$$\sigma = 0$$

on the thin wing.

Note that we show a wake trailing behind the wing in figure 5.9. A wake is a surface across which a potential jump occurs, even though the surface does not correspond to a solid, physical object. Deciding where to position the wake for a particular configuration is an extremely difficult problem. For many problems, however, any wake position roughly parallel to the freestream and extending downstream from the object being analyzed is adequate. A detailed study of wake positioning is not part of this document.

#### 5.4.2.3 Thick Configurations

For a "thick" wing, that is, a wing for which we panel both the upper and lower surfaces, we can not simply impose the boundary conditions (5.4.17). This is because imposition of zero normal flow on the interior of a closed surface is an ill-posed boundary value problem since there is no unique solution: if a particular function  $\phi$  satisfies the Prandtl-Glauert equation and the boundary conditions, then adding any constant to  $\phi$  in the interior of the closed surface yields another solution. We illustrate the two possible solutions in figure 5.10.

So, we must specify zero normal flow on the interior of a closed surface in some other manner. There are many possibilities, some of which will be discussed in Appendix H. The method illustrated in figure 5.11 has been experimentally shown to be reliable in a wide variety of circumstances. There, the boundary condition  $\phi_L = 0$  on the configuration surface insures (assuming a sufficient density of control points) that  $\phi$  is identically zero in the entire interior region. Such a condition is called "perturbation stagnation" (it is not really stagnation, since the total potential is not constant), since  $\vec{\nabla}\phi$ , the perturbation velocity, is everywhere zero.

Thus we impose the boundary conditions

$$\begin{aligned}\phi_L &= 0 \\ \vec{w}_U \cdot \hat{n} &= -\vec{V}_\infty \cdot \hat{n}\end{aligned}\tag{5.4.18}$$

But  $\vec{w}_L = \vec{\nabla}\phi_L = 0$ , so we can replace  $\vec{w}_U \cdot \hat{n}$  by  $(\vec{w}_U - \vec{w}_L) \cdot \hat{n} = \sigma$ , and thus we obtain

$$\begin{aligned}\phi_L &= 0 \\ \sigma &= -\vec{V}_\infty \cdot \hat{n}\end{aligned}\tag{5.4.19}$$

The boundary conditions (5.4.19) for a thick wing, or (5.4.17) for a thin wing are preferable to their equivalents (5.4.18) and (5.4.11) because they directly specify the source strength. This allows the source parameters to be removed from the system of linear equations, thus considerably lowering the cost of solving the equations.



#### 5.4.2.4 Superinclined Surfaces

A final example of the imposition of boundary conditions is shown in figure 5.12. The surface shown perpendicular to the freestream is a superinclined surface; recall from section 5.2 that a surface is superinclined whenever

$$\hat{n} \cdot \tilde{n} < 0$$

(5.4.20)

An important result, which we discuss further in Appendix B, is that boundary conditions of zero normal mass flux must never be placed on the upstream side of a superinclined surface, or else the boundary value problem is ill-posed. This is not really too surprising, since the flow about any impermeable object so blunt as to be superinclined certainly violates the "small perturbation" assumption.

The need for permeable superinclined surfaces does occur, however, nacelle faces being the prime example. The example in figure 5.12 shows the use of boundary conditions on the lower (that is, downstream) surface to induce perturbation stagnation in the interior of the configuration.

#### 5.4.2.5 The General Boundary Condition

The previous three examples do not exhaust the generality of boundary conditions which a PAN AIR user may impose. But we must warn that, while an arbitrary condition on  $\phi$  and its derivatives is permitted, the boundary condition may not yield a well-posed problem. The arbitrary boundary condition can be written

$$\begin{aligned} a_A \vec{w}_A \cdot \hat{n} + c_A \phi_A + \vec{t}_A \cdot \vec{\nabla}_A \phi_A \\ + a_D \sigma + c_D \mu + \vec{t}_D \cdot \vec{\nabla} \mu = b \end{aligned} \quad (5.4.21)$$

where the subscripts A and D stand for "average" and "difference," that is,

$$\phi_A = \frac{\phi_U + \phi_L}{2} \quad (5.4.22)$$

$$\phi_D = \phi_U - \phi_L = \mu \quad (5.4.23)$$

Comparing to equation (3.2.6), we see that the definition of doublet strength is the same for all Mach numbers. The constants a and c may be arbitrary, while the vectors  $\vec{t}$  are tangent to the surface at the control point (as opposed to  $\hat{n}$ , which is normal to the surface).

To see that (5.4.21) permits an arbitrary combination of upper or lower surface conditions, we solve (5.4.22-23) for  $\phi_U$  and  $\phi_L$ , obtaining,

$$\phi_U = \phi_A + \frac{1}{2} \phi_D = \phi_A + \frac{1}{2} \mu \quad (5.4.24)$$

$$\phi_L = \phi_A - \frac{1}{2} \mu$$

Similarly,

$$\vec{w}_A \cdot \hat{n} = \frac{1}{2} (\vec{w}_U \cdot \hat{n} + \vec{w}_L \cdot \hat{n}) \quad (5.4.25)$$

$$\sigma = \vec{w}_D \cdot \hat{n} = \vec{w}_U \cdot \hat{n} - \vec{w}_L \cdot \hat{n}$$

and, solving,

$$\vec{w}_U \cdot \hat{n} = \vec{w}_A \cdot \hat{n} + \frac{1}{2} \sigma \quad (5.4.26)$$

$$\vec{w}_L \cdot \hat{n} = \vec{w}_A \cdot \hat{n} - \frac{1}{2} \sigma$$

Thus the boundary condition pair

$$\phi_L = 0 \quad (5.4.27)$$

$$\vec{w}_U \cdot \hat{n} = -\vec{V}_\infty \cdot \hat{n}$$

can be written as

$$\phi_A - \frac{1}{2} \mu = 0 \quad (5.4.28)$$

$$\vec{w}_A \cdot \hat{n} + \frac{1}{2} \sigma = -\vec{V}_\infty \cdot \hat{n}$$

Thus, the first equation in (5.4.28) is equivalent to (5.4.21) with

$$c_A = 1$$

$$c_D = -\frac{1}{2}$$

(5.4.29)

$$a_A = a_D = 0$$

$$\vec{t}_A = \vec{t}_D = 0$$

$$b = 0$$

while the second equation corresponds to

$$a_A = 1$$

$$a_D = \frac{1}{2}$$

$$c_A = c_D = 0$$

(5.4.30)

$$\vec{t}_A = \vec{t}_D = 0$$

$$b = -\vec{V}_\infty \cdot \hat{n}$$

For the remainder of this document, we will generally use the boundary condition formulation (5.4.21) since it is used internally in PAN AIR. It should be noted, however, that the program user need not be concerned with this formulation, but may express boundary conditions in the upper and lower form if he wishes. The average and difference formulation is used in PAN AIR in order to separate out the singularity strength (or difference) contribution to the boundary condition, which is computed from the splines. The average potential and velocity at a point on the surface, in turn, do not depend on the singularity strength at the point. For more details on the computation of the average quantities see Appendix J.6.

There is one type of user-specified boundary condition, called a closure boundary condition, which is not of the form (5.4.21). This is used in design problems to specify the integral of the normal mass flux over a surface. A detailed description of the use and implementation of closure boundary conditions will be given in Appendix H.4.

### 5.5 Singularity Splines

In this section we will discuss without details the construction of spline matrices for analysis and wake networks. The technical details of the spline construction, and all discussion of splines for design networks, will be reserved for Appendix I. In figure 5.13, we illustrate the locations of source parameters on a source analysis network, and the locations of doublet parameters on a doublet analysis or wake network.

Source parameters on analysis networks are located at panel centers only. Doublet parameters on analysis networks are located at panel centers and in addition along network edges as illustrated. The "extra" doublet parameters occur at those points at which an "extra" corner control point was stationed because of edge matching considerations (see figure 5.7). Doublet parameters are required on network edges (while source parameters are not) because of the quadratic variation of the approximation to the doublet strength. A quadratic variation causes rapid changes in doublet strength which make extrapolation of the doublet values from the interior of the network to the edges ill-advised. The source strength approximation is only linear, however. Finally, doublet parameters are only located on the upstream edge of a wake network. The doublet strength on a wake network is defined to be constant in the streamwise direction, and thus doublet parameters are only required on one edge in order to define the doublet strength on the entire network.

#### 5.5.1 The Matrices $B^S$ and $B^D$ .

The value of a source parameter is always the value of source strength at the parameter location, and similarly for doublet parameters located at panel centers. The value of a doublet parameter on a network edge involves the value and gradient of the doublet strength at a panel corner on the edge.

Recall from section 4.2.1 that a spline defines the manner in which an approximation to the singularity distribution on a network is determined in terms of the singularity parameters located on the network. The manner in which this occurs is defined by matrices, called source (and doublet) "outer" and subpanel spline matrices respectively. The outer spline matrices (one source matrix  $B^S$  and one doublet matrix  $B^D$  for each panel) define the source strength and doublet strength at certain points on the panel as linear combinations of source and doublet parameters located in the neighborhood of the panel. The subpanel spline matrices (one source matrix  $SPSPL^S$  and one doublet matrix  $SPSPL^D$  for each of the eight triangular regions composing the panel) each define the coefficients of the polynomial distribution of singularity strength on the triangular region as a linear combination of the singularity strengths at the certain panel points previously mentioned.

To be precise, consider the panel and network in figure 5.14. The matrix  $B^S$  is a  $5 \times 9$  matrix which gives the value of source strength at  $P_1, P_2, P_3, P_4$ , and  $P_9$  in terms of the source parameters  $\{\lambda_i^S, i=1, \dots, 9\}$  located at the nine panel centers marked by a circle. The matrix  $B^D$  is a  $9 \times 21$  matrix giving the values of doublet strength at  $P_1, \dots, P_9$  in terms of the doublet parameters  $\{\lambda_i^D, i=1, \dots, 21\}$  located at the 21 panel centers marked by an x. Because  $\mu$  is a continuous locally quadratic function where  $\sigma$  is only a continuous locally linear function,  $\mu$  must be defined at 9 points on a panel by  $B^D$  while  $\sigma$  is only defined by 5 points by  $B^S$ . The values of  $\sigma$  at the 5 points are called "panel source parameters," while the values of  $\mu$  at the 9 points are called "panel doublet parameters."

### 5.5.2 Definition of SPSP

Next, on each triangular region, source and doublet strengths  $\sigma(\xi', \eta')$  and  $\mu(\xi', \eta')$  are defined in terms of local coordinates  $(\xi', \eta')$

$$\begin{aligned}\sigma(\xi', \eta') &= \sigma_0 + \sigma_\xi \xi' + \sigma_\eta \eta' \\ \mu(\xi', \eta') &= \mu_0 + \mu_\xi \xi' + \mu_\eta \eta' \\ &\quad + \frac{1}{2} \mu_{\xi\xi} \xi'^2 + \mu_{\xi\eta} \eta' \xi' + \frac{1}{2} \mu_{\eta\eta} \eta'^2\end{aligned}\tag{5.5.1}$$

where the constants  $\sigma_0, \sigma_\xi, \sigma_\eta, \mu_0, \dots, \mu_{\eta\eta}$  are defined by the subpanel spline matrices:

$$\begin{Bmatrix} \sigma_0 \\ \sigma_\xi \\ \sigma_\eta \end{Bmatrix} = \begin{bmatrix} \text{SPSP}^S \end{bmatrix} \begin{Bmatrix} \sigma(P_1) \\ \sigma(P_2) \\ \sigma(P_3) \\ \sigma(P_4) \\ \sigma(P_9) \end{Bmatrix}\tag{5.5.2}$$

and

$$\begin{Bmatrix} \mu_0 \\ \mu_\xi \\ \mu_\eta \\ \mu_{\xi\xi} \\ \mu_{\xi\eta} \\ \mu_{\eta\eta} \end{Bmatrix} = \begin{bmatrix} \text{SPSP}^D \end{bmatrix} \begin{Bmatrix} \mu(P_1) \\ \cdot \\ \cdot \\ \cdot \\ \mu(P_9) \end{Bmatrix}\tag{5.5.3}$$



### 5.5.3 Construction of the Matrices B.

The B matrices are constructed one row at a time. Each row defines the singularity strength at a panel corner, edge midpoint, or panel center in terms of surrounding singularity parameters. This identical row vector then becomes part of the B matrix of each panel which shares the particular grid point. This insures that the value of the singularity strength is identical as one approaches the grid point from the interior of any of the panels sharing it.

The source strength at a panel corner is obtained from the source singularity parameters located at the centers of the four panels sharing that corner, as illustrated in figure 5.15. The dependence of  $\sigma$  on  $\lambda_1, \dots, \lambda_4$  is determined by a bilinear fit procedure described in Appendix I.1. Essentially, this procedure determines what "bilinear" function (a bilinear function in two variables  $(\xi, \eta)$  is a quadratic function which reduces to a linear function for constant  $\xi$  and  $\eta$ )

$$f(\xi, \eta) = a + b\xi + c\eta + d\xi\eta \quad (5.5.4)$$

is determined by the four values  $\lambda_i$ , and then sets  $\sigma_1$  to be the "value" the function takes at that point. By "value", we mean a row vector  $(a_1, a_2, a_3, a_4)$ , so that

$$\sigma_1 = [a_1 \ a_2 \ a_3 \ a_4] \begin{Bmatrix} \lambda_1 \\ \lambda_2 \\ \lambda_3 \\ \lambda_4 \end{Bmatrix} \quad (5.5.5)$$

regardless of the values of the  $\lambda_i$ 's.

Now, finding the row vector that describes the source strength at a panel center is very simple, since a source parameter is located there. To obtain a matrix  $B^S$  for a panel, we assemble the row vectors corresponding to the 5 grid points. Each row vector has length 4, but by adding zeros each row vector expands to length 9. Thus each row vector has one entry from each of the 9 source parameters in the neighborhood of the panel. While only four parameters lie in the neighborhood of a particular corner point, (cf., figure 5.14) nine parameters lie in the neighborhood of at least one of the panel corners. Collecting the five row vectors, we have the  $5 \times 9$  matrix  $B^S$ , which was first introduced by equation (4.2.3).

Thus for the panel in figure 5.14,

$$\begin{bmatrix} B^S \end{bmatrix} = \begin{bmatrix} 0 & * & * & 0 & * & * & 0 & 0 & 0 \\ * & * & 0 & * & * & 0 & 0 & 0 & 0 \\ 0 & 0 & 0 & * & * & 0 & * & * & 0 \\ 0 & 0 & 0 & 0 & * & * & 0 & * & * \\ 0 & 0 & 0 & 0 & * & 0 & 0 & 0 & 0 \end{bmatrix} \quad (5.5.6)$$

where the columns of  $B^S$  are arranged according to the integer labels given to the source parameters in figure 5.14. Here, an asterisk denotes some generally non-zero entry.

The outer doublet spline matrix  $B^D$ , introduced in equation (4.2.9), is similarly constructed row by row. To obtain the row vector describing  $\mu$  at a panel corner, a least squares fit is used. As shown in figure 5.16,

$\mu(P)$  is obtained by finding the quadratic function  $\mu(\xi, \eta)$  which best goes through the 12 values  $\lambda_i^D$  at the 12 doublet parameter locations in the neighborhood of  $P$  in a weighted least squares sense (a quadratic function in two variables certainly can not go through 12 values exactly). The

computation of the weights is discussed in Appendix I.1.2.4. The quadratic function thus obtained (its 6 coefficients are each row vectors of length 12, since they depend on the  $\lambda_i^D$ ) is evaluated at P to obtain  $\mu(P)$ . This weighted least squares procedure will be described in detail in Appendix I.5.

To obtain a row vector defining  $\mu$  at a panel edge midpoint, we again use a weighted least squares fit, though this time we only fit to 8 neighboring singularity parameters, as illustrated in figure 5.17. If the grid point lies near the network edge, a special treatment (which is described in Appendix I.1) is used.

#### 5.5.4 Construction of SPSPL

Next, let us consider the method by which the subpanel spline matrices define singularity distributions within a panel. In referring to the panel illustrated in figure 5.18, we will write  $\sigma_i$  for  $\sigma(P_i)$  and  $\mu_i$  for  $\mu(P_i)$ .

Recall that  $\sigma_1, \sigma_2, \sigma_3, \sigma_4$  and  $\sigma_9$  are defined in terms of neighboring source singularity parameters by the matrix  $B^S$ . We then define  $\sigma_5 = \frac{1}{2}(\sigma_1 + \sigma_2)$ ,  $\sigma_6 = \frac{1}{2}(\sigma_2 + \sigma_3)$ ,  $\sigma_7 = \frac{1}{2}(\sigma_3 + \sigma_4)$ , and  $\sigma_8 = \frac{1}{2}(\sigma_4 + \sigma_1)$ . We have now defined  $\sigma_i$  at all vertices of all 8 triangular regions, and we now define a linear distribution  $\sigma(\xi', \eta')_i$ ,  $i = 1, \dots, 9$  on each triangular region by specifying it to be the unique linear distribution to attain the appropriate values at the 3 vertices of the triangle.

Note that this construction forces  $\sigma$  to vary linearly along the edge of a triangular region, and thus the value of  $\sigma$  at any point along the edge is determined by the values of  $\sigma$  at the two endpoints of the edge. Thus  $\sigma$  is continuous within the panel. Further, since  $\sigma$  at a panel edge midpoint  $M$  is the average of the values at the adjacent corners,  $\sigma$  varies as a single linear function on an entire panel edge. Thus  $\sigma$  on a panel edge is determined by its values at the two endpoints, and so, within a network,  $\sigma$  is continuous across panel edges. At network edges,  $\sigma$  is not continuous across the network edge.

To determine the doublet distribution on each of the 8 regions, we note first that a quadratic distribution on a triangular region is uniquely defined by its value at the three vertices and the three edge midpoints of the triangle. Thus the doublet distribution on each triangle is determined once we know  $\mu$  at  $P_1, \dots, P_9$ , and  $M_1, \dots, M_{16}$ . Now  $\mu$  at  $P_1, \dots, P_9$  is defined by  $B^D$ . We define  $\mu$  at  $M_1, \dots, M_8$ , and  $M_{13}, \dots, M_{16}$  by requiring that  $\mu$  be described by a single quadratic function in one variable on the line segments  $P_1P_5P_2$ ,  $P_2P_6P_3$ ,  $P_3P_7P_4$ ,  $P_4P_8P_1$ ,  $P_5P_9P_7$ , and  $P_7P_9P_8$ . Note that a quadratic function on a line is uniquely determined by its values at 3 distinct points. Finally,  $\mu$  is defined at  $M_9, M_{10}, M_{11}, M_{12}$  in such a manner as to minimize the discontinuities in doublet gradient at  $P_5, P_6, P_7, P_8$ .

By defining  $\mu$  at  $M_i$ ,  $i = 1, \dots, 16$ , in this manner, we insure that, within a network, the doublet strength is continuous across triangle boundaries. (Doublet strength matching at network edges is discussed in section 5.3.) In addition, the doublet gradient is continuous at  $P_9$ . Also, the doublet strength is continuous across panel edges because the values of  $\mu$  at the endpoints and midpoint of an edge define the value on the whole segment.

Summarizing, for each triangular region we obtain subpanel spline matrices  $\text{SPSPL}^S$  and  $\text{SPSPL}^D$  such that

$$\begin{aligned} \begin{Bmatrix} \sigma_0 \\ \sigma_\xi \\ \sigma_\eta \end{Bmatrix} &= [\text{SPSPL}^S] \begin{Bmatrix} \sigma \\ \cdot \\ \cdot \\ \sigma_4 \\ \sigma_9 \end{Bmatrix} \\ \begin{Bmatrix} \mu_0 \\ \cdot \\ \cdot \\ \mu_{nn} \end{Bmatrix} &= [\text{SPSPL}^D] \begin{Bmatrix} \mu_1 \\ \cdot \\ \cdot \\ \mu_9 \end{Bmatrix} \end{aligned} \quad (5.5.7)$$

and matrices  $B^S$  and  $B^D$  such that

$$\begin{Bmatrix} \sigma_1 \\ \cdot \\ \cdot \\ \sigma_4 \\ \sigma_9 \end{Bmatrix} = [B^S] \begin{Bmatrix} \lambda_1^S \\ \cdot \\ \cdot \\ \cdot \\ \lambda_9^S \end{Bmatrix} \quad (5.5.3a)$$

and

$$\begin{Bmatrix} \mu_1 \\ \cdot \\ \cdot \\ \cdot \\ \mu_9 \end{Bmatrix} = [B^D] \begin{Bmatrix} \lambda_1^D \\ \cdot \\ \cdot \\ \cdot \\ \lambda_{21}^D \end{Bmatrix} \quad (5.5.8b)$$

Combining (5.5.7) and (5.5.8a-b), we obtain the source and doublet distributions on a triangular region, in terms of source and doublet parameters, by

$$\begin{Bmatrix} \sigma \\ \sigma_{\xi} \\ \sigma_{\eta} \end{Bmatrix} = \begin{bmatrix} \text{SPSPL}^S \end{bmatrix} \begin{bmatrix} B^S \end{bmatrix} \begin{Bmatrix} \lambda_1^S \\ \vdots \\ \lambda_9^S \end{Bmatrix} \quad (5.5.9)$$

$$\begin{Bmatrix} \mu_0 \\ \vdots \\ \mu_{\eta\eta} \end{Bmatrix} = \begin{bmatrix} \text{SPSPL}^D \end{bmatrix} \begin{bmatrix} B^D \end{bmatrix} \begin{Bmatrix} \lambda_1^D \\ \vdots \\ \lambda_{21}^D \end{Bmatrix} \quad (5.5.10)$$

## 5.6 Influence Coefficients

In order to impose the arbitrary boundary condition given by equation (5.4.21), viz.,

$$\begin{aligned} a_A \vec{w}_A \cdot \hat{n} + c_A \Phi_A + \vec{t}_A \cdot \vec{v}_A \\ + a_D \sigma + c_D \mu + \vec{t}_D \cdot \vec{\nabla} \mu = b \end{aligned} \quad (5.6.1)$$

at a control point, it is necessary to evaluate the left hand side expression as a linear combination of the singularity parameters  $\{\lambda_i\}$ . To evaluate  $\sigma$  and  $\mu$  at the control point, we use the subpanel spline and outer spline matrices. For example, if a control point P has local coordinates  $(\xi', \eta')$ , we find, using equations (5.5.1), (5.5.7) and (5.5.8),

$$\sigma(P) = [1 \ \xi' \ \eta'] [SPSPL^S] [B^S] \begin{Bmatrix} \lambda_1^S \\ \vdots \\ \lambda_9^S \end{Bmatrix} \quad (5.6.2)$$

and thus the row vector describing  $\sigma(P)$  in terms of all the  $\lambda_i^S$  is the expansion of the  $1 \times 9$  matrix

$$[1 \ \xi' \ \eta'] [SPSPL^S] [B^S]$$

into the corresponding  $1 \times N$  matrix (where all but 9 values are zero), with an entry for each of the N singularity parameters in the entire configuration. We obtain the row vector describing  $\mu(P)$  similarly.

### 5.6.1 Computation of Potential and Velocity

Next we wish to evaluate  $\Phi_A$  and  $\vec{v}_A$  at a control point, as a linear combination of all the singularity parameters in the configuration. The row vectors which describe these quantities at a control point are called the potential influence coefficient and velocity influence coefficient matrices,

or  $\Phi$ IC and VIC respectively. The matrices  $\Phi$ IC and VIC should not be confused with the panel influence coefficient (PIC) matrices, introduced in section 4.2.2, which define the perturbation potential and velocity induced by a panel on a control point. The  $\Phi$ IC and VIC matrices are evaluated by using the basic integral equation (5.2.8)

$$\phi(x, y, z) = -\frac{1}{\kappa} \iint_{S'} \frac{\sigma(\eta)}{R} dS + \frac{1}{\kappa} \iint_{S'} \mu(\eta) \hat{n} \cdot \vec{\nabla} \left( \frac{1}{R} \right) dS \quad (5.6.3)$$

(where  $S' = S \cap D_p$  is the intersection of the domain of dependence on  $P$  with the surface of integration  $S$ ) and its gradient

$$\begin{aligned} \vec{v}(x, y, z) = & -\frac{1}{\kappa} \vec{\nabla}_p \iint_{S'} \frac{\sigma(\eta)}{R} dS \\ & + \frac{1}{\kappa} \vec{\nabla}_p \iint_{S'} \mu(\eta) \hat{n} \cdot \vec{\nabla} \left( \frac{1}{R} \right) dS \end{aligned} \quad (5.6.4)$$

where  $P' = (x, y, z)$ ,  $Q = (\xi, \eta, \zeta)$  is a point on  $S$ ,

$$\vec{\nabla} = \begin{Bmatrix} sB^2 \partial/\partial \xi \\ \partial/\partial \eta \\ \partial/\partial \zeta \end{Bmatrix} \quad \vec{\nabla} = \begin{Bmatrix} \partial/\partial x \\ \partial/\partial y \\ \partial/\partial z \end{Bmatrix} \quad (5.6.5)$$

and

$$R^2 = (\xi - x)^2 + sB^2 (\eta - y)^2 + sB^2 (\zeta - z)^2 \quad (5.6.6)$$

We perform the integration one triangular region at a time; thus, denoting a subpanel by  $\Delta$ , with local coordinates  $(\xi', \eta')$ , we have



$$\Phi(x,y,z) = \sum_{\Delta} \left\{ -\frac{1}{\kappa} \iint_{\Delta \cap D_p} \frac{\sigma(\xi', \eta')}{R} dS + \frac{1}{\kappa} \iint_{\Delta \cap D_p} \mu(\xi', \eta') \hat{n} \cdot \vec{\nabla} \left( \frac{1}{R} \right) dS \right\} \quad (5.6.7)$$

and a corresponding expression for  $\vec{V}(x,y,z)$ . Here we substitute for the exact (and unknown) values of  $\sigma$  and  $\mu$  the row vector in (5.6.2) and a similar row vector for  $\mu$ .

In practice, the sum of all triangular regions is taken as a sum over all panels, and the integral over a panel is taken as a sum over the 8 triangular regions in the panel. The integral over a single panel describes the perturbation potential and velocity induced at the control point (which does not necessarily lie near the panel) by the panel. Since the singularity distribution on the panel depends on the 5 panel source parameters and the 9 panel doublet parameters, the perturbation potential and velocity induced by the panel can be defined by two "panel influence coefficient" (PIC) matrices, one a 4x5 source matrix,  $PIC^S$ , the other a 4x9 doublet matrix  $PIC^D$ .

That is,

$$\begin{Bmatrix} \Phi(x,y,z) \\ \partial\Phi/\partial x(x,y,z) \\ \partial\Phi/\partial y(x,y,z) \\ \partial\Phi/\partial z(x,y,z) \end{Bmatrix} = [PIC^S] \begin{Bmatrix} \sigma_1 \\ \sigma_2 \\ \sigma_3 \\ \sigma_4 \\ \sigma_9 \end{Bmatrix} + [PIC^D] \begin{Bmatrix} \mu_1 \\ \mu_2 \\ \mu_3 \\ \mu_4 \\ \mu_5 \\ \mu_6 \\ \mu_7 \\ \mu_8 \\ \mu_9 \end{Bmatrix} \quad (5.6.8)$$

Substitution of (5.6.2) into (5.6.7) shows that  $PIC^S =$

$$\sum_{\substack{3 \text{ sub-} \\ \text{panels}}} = \frac{1}{\kappa} \iint_{\Delta_i \cap D_p} \begin{Bmatrix} 1/R \\ \partial/\partial x (1/R) \\ \partial/\partial y (1/R) \\ \partial/\partial z (1/R) \end{Bmatrix}^{4 \times 1} \begin{bmatrix} 1 & \xi' & \eta' \end{bmatrix}^{1 \times 3} [SPSPL_i^S]^{3 \times 5} d\xi' d\eta'$$

(5.6.9)

Similarly,  $PIC^D =$

$$\sum_{i=1}^8 \frac{1}{\kappa} \iint_{\Delta_i \cap D_p} \begin{Bmatrix} \hat{n} \cdot \tilde{\nabla} (1/R) \\ \partial/\partial x \hat{n} \cdot \tilde{\nabla} (1/R) \\ \partial/\partial y \hat{n} \cdot \tilde{\nabla} (1/R) \\ \partial/\partial z \hat{n} \cdot \tilde{\nabla} (1/R) \end{Bmatrix}^{4 \times 1}$$

$$\begin{bmatrix} 1 & \xi' & \eta' & \frac{1}{2} \xi'^2 & \xi' \eta' & \frac{1}{2} \eta'^2 \end{bmatrix}^{1 \times 6} [SPSPL_i^D]^{6 \times 9} d\xi' d\eta' \quad (5.6.10)$$

#### 5.6.2 Reformulation of the Doublet Velocity Integral

In Appendix J, we describe the method by which we calculate the matrix  $PIC^S$ . The doublet integral, however, is evaluated by making use of the continuity of  $\mu$ . We show in Appendix B.3 that the velocity due to the doublets can be written as

$$\begin{aligned} \vec{v}(P) &= \frac{1}{\kappa} \vec{\nabla}_p \iint_{S \cap D_p} \mu(Q) \hat{n} \cdot \tilde{\nabla} \frac{1}{R} dS \\ &= \frac{1}{\kappa} \iint_{S \cap D_p} (\hat{n} \times \vec{\nabla}_Q \mu) \times (\tilde{\nabla} \frac{1}{R}) dS + \frac{1}{\kappa} \int_{\partial S \cap D_p} \mu \tilde{\nabla} \frac{1}{R} \times d\vec{l} \end{aligned} \quad (5.6.11)$$

Here,  $\partial S$  is the boundary of the surface  $S$ . The first integral is called the regular part of the doublet velocity, and the second integral is called the line vortex term. Now, in general,  $\mu = 0$  on the boundary of an isolated network edge because the doublet matching boundary conditions in PAN AIR force this to be the case. Further, where two networks meet along a common line, the doublet strengths in PAN AIR are made equal; thus, if the integration is performed one network at a time, the integral of the line vortex term over the edge of the first network cancels with the corresponding integral over the edge of the second network (see figure 5.19). The integrals similarly cancel when three or more networks meet because of the doublet matching boundary conditions which are imposed (see Appendices G and J).

Similarly, when we divide  $S$  up into subpanels (triangular regions), the line vortex integrals cancel on the subpanel boundaries because the doublet strength is continuous. Thus every contribution to the second integral in (5.6.11) is canceled by an equal and opposite contribution, provided  $\mu$  is everywhere continuous. So, if  $\mu$  is continuous, we see that the doublet velocity may be defined by an integral in the quantity  $\hat{n} \times \vec{\nabla} \mu$ , which is generally known as the surface vorticity. For a discussion of surface vorticity, see section 2.8 of Ward.

The assumption that  $\mu$  is continuous everywhere is in fact violated in only one instance in PAN AIR, namely, on the trailing edge of a wake. The doublet strength there is non-zero, but this edge is so far from the control points at which boundary conditions are imposed that neglect of the line vortex term for this edge results in a negligible error.

There are two reasons for evaluating the regular part of (5.6.11) rather than the complete integral. First, if the boundary of a subpanel (triangular) region of integration contains points  $Q = (\xi', \eta', \zeta')$  for which  $R = 0$ , the line vortex term may become infinite (or, in practice, very large), where this infinite quantity is cancelled out by an identical infinite integral in the opposite direction. This is very poor numerically; even if infinite quantities are avoided, the cancellation of large numbers of opposite sign tends to be inexact, and the final answer may lose many digits of accuracy. In evaluating the regular part of the integral, however, large numbers are generated, with a few exceptions, only when the final answers are large. The singular behavior of these integrals will be discussed further in Appendix J.12.

#### 5.6.2 The Far Field Expansion

The second reason for evaluating only the regular integral is efficiency. When  $R$  is small compared to panel size, the integral in (5.6.11) must be evaluated exactly in terms of transcendental functions (logarithms and arc tangents) whose arguments are complicated expressions depending on the geometric relationship of the control point and the panel. To evaluate the first form of equation (5.6.11), that is, the complete integral, requires the computation of a greater number of these expressions than is required by the regular part of (5.6.11), and thus takes longer. Further, if  $R$  is large compared to panel size, the integrand can be replaced by a power series in

$$\Delta \vec{Q} = \vec{Q} - \vec{Q}_0 = \sqrt{(\xi' - \xi'_0)^2 + (\eta' - \eta'_0)^2 + (\zeta' - \zeta'_0)^2} \quad (5.6.12)$$

where  $\vec{Q}_0 = (\xi_0, \eta_0, \zeta_0)$  is the panel center. This power series has coefficients which only depend on  $\vec{Q}_0$  and the control point  $P$ , while the terms of the power

series only depend on the panel. Then (see Appendix J.10 for details) the coefficients can be taken out from under the integral, while the integral itself now depends only on the panel and thus need only be evaluated once in the course of the problem, rather than once for every pair of panel and control point. The approximation of the integrand by a power series in  $\Delta \vec{Q}$  is called a far field expansion.

Now, applying a gradient operator to  $1/R$  yields terms of order  $R^{-3}$ , and applying a gradient operator to those terms yields ones of order  $R^{-5}$ . Thus the left hand expression in (5.6.11) contains terms of order  $R^{-5}$ , while the regular part only contains terms of order  $R^{-3}$ . Now, for a fixed value of  $R$ ,  $R^{-3}$  is more accurately expressible as a power series in  $\Delta \vec{Q}$  of fixed length than  $R^{-5}$  (see below for a justification), and so a far field expansion can be used for smaller values of  $R$  if only the regular part of (5.6.11) is evaluated. This is important since the far field expansion is considerably less time-consuming than the exact evaluation of the integral. In practice, PAN AIR will use the far field expansion if  $R$  is large compared to the panel diameter for all points  $\vec{Q}$  on the panel. For details, see section J.3.

To justify this procedure, consider a quantity  $\epsilon \ll 1$ . By the binomial theorem

$$\begin{aligned} (1 + \epsilon)^r &= 1 + r\epsilon + \frac{r(r-1)}{2} \epsilon^2 + \dots \\ &= 1 + \sum_{i=1}^{\infty} \frac{r(r-1)\dots(r-i)}{(i+1)!} \epsilon^{i+1} \end{aligned} \quad (5.6.13)$$

That is,

$$(1 + \epsilon)^{-3/2} = 1 - \frac{3}{2} \epsilon + \frac{15}{8} \epsilon^2 - \frac{135}{48} \epsilon^3 + \dots$$

$$(1 + \epsilon)^{-5/2} = 1 - \frac{5}{2} \epsilon + \frac{35}{8} \epsilon^2 - \frac{315}{48} \epsilon^3 + \dots \quad (5.6.14)$$

So if we want to approximate  $(1+\epsilon)^{-5/2}$  by a power series with 3 terms (that is, a quadratic expression), the first neglected term has a coefficient of  $315/48$ , which is more than twice the size of the first neglected coefficient if we approximate  $(1+\epsilon)^{-3/2}$ . Thus, for a particular value of  $\epsilon$  our quadratic approximation to  $(1+\epsilon)^{-3/2}$  is better than our quadratic approximation to  $(1+\epsilon)^{-5/2}$ .

Once the  $1 \times N$  matrix  $\Phi IC$  and the  $3 \times N$  matrix  $VIC$  ( $N$  the total number of singularity parameters in the configuration) have been computed for a control point, it is quite straightforward to impose the boundary condition (5.6.1). The left hand side of (5.6.1) then gives a row of the  $[AIC]$  matrix (see equations (4.2.4) and (3.3.8))

In arriving at this result, equation (5.6.2) was used for  $\sigma$  (a similar equation for  $\mu$ ), and we have used the fact that  $\tilde{n} \cdot \vec{v} = \hat{n} \cdot \vec{w}$  (see equation (5.4.15)). The control point P has local coordinates  $(\xi', \eta')$ , A is the transformation from reference to local coordinates and  $\overline{B^S}$  and  $\overline{B^U}$  are the outer spline matrices, the overbar signifying that they have been expanded to N columns, with one column of zeros for every singularity parameter on which the panel source or doublet distribution does not depend. We will show in Appendix K that the last term of (5.7.1) is equivalent to  $\vec{t}_n \cdot \vec{\nabla} \mu$ ; the

remaining terms have been discussed previously. Thus, a row of the AIC matrix (corresponding to a boundary condition) can be generated in a completely straightforward manner. Several considerations make the process somewhat less straightforward, however. These are: imposition of boundary conditions which are not of the form (5.6.1), utilization of the existence of one or two planes of configuration symmetry in order to reduce the size of the problem, and elimination of singularity parameters whose values are directly specified by a boundary condition ("known" singularity parameters) from the system of equations.

#### 5.7.1 Non-Standard Boundary Conditions

There are two types of boundary conditions which are not of the form (5.6.1). The first type is the doublet matching boundary condition (see section 5.3, or Appendix K.5 for full details). The second type is a closure boundary condition, described in full detail in Appendix K.4. Briefly, a program user may specify a desired pressure distribution on a design network by imposing boundary conditions of the form

$$\vec{t}_U \cdot \vec{v}_U + \vec{t}_L \cdot \vec{v}_L = b \quad (5.7.2)$$

a panel center control points. When a tangential component of the flow is thus specified over a surface, there are no boundary conditions remaining at panel centers to also require that the normal flow to the surface be zero; but the boundary conditions at a network edge may not yet have been used. At these control points one may specify



$$\int \int_{\left( \begin{array}{l} \text{column or} \\ \text{row of panels} \end{array} \right)} a_U \vec{w}_U \cdot \hat{n} + a_L \vec{w}_L \cdot \hat{n} = b \quad (5.7.3)$$

For  $a_L = 0 = b$ , for instance, equation (5.7.3) requires that the integral of the normal flow over a column (or row) of panels be zero. When the program user then updates the network geometry to approximately impose impermeability of the surface, the position of the trailing edge of the network will not be changed.

This alternate iteration of a potential flow solution with an update of the surface geometry is a method of solving the design problem, in which a user wishes to obtain an impermeable surface with a specified pressure distribution. The closure boundary condition is used, for example, in designing a thick wing, in order to insure that the trailing edge of the wing remain closed. The Design problem is discussed further in Appendix C.

#### 5.7.2 Symmetry

When a configuration contains a plane of symmetry, there are separate entries of the AIC matrix which are identical. This allows one to split the system of linear equations into two systems, each of which has only half the number of unknown singularity parameters. In addition, each entry in the AIC

matrix occurs twice, and thus only half of the AIC matrix must be constructed to obtain all of it.

In figure 5.20, we illustrate a symmetric configuration. We call half of the configuration the real half, and the other half the image. The basic result which permits us to make use of symmetry is that if the freestream flow is approximately parallel to the plane of symmetry (unless  $M_\infty = 0$ , in which case it may be in any direction), the perturbation influence of a real panel on a boundary condition quantity such as potential or normal mass flux at a control point equals the perturbation influence of the image panel on the symmetric image of the control point.

We discuss symmetry in detail in Appendix K.1. Briefly, if we order the singularity parameters  $\lambda_1, \dots, \lambda_N, \lambda'_1, \dots, \lambda'_N$ , and order the boundary conditions so that those applied on the real half come first, followed by their counterparts for the image half, then the basic system of linear equation

$$[AIC]^{2N \times 2N} \vec{\lambda}^{2N \times 1} = \vec{b}^{2N \times 1} \quad (5.7.4)$$

can be written

$$\begin{bmatrix} AIC_1 & AIC_2 \\ AIC_2 & AIC_1 \end{bmatrix}^{2N \times 2N} \begin{Bmatrix} \lambda_1 \\ \vdots \\ \lambda_N \\ \lambda'_1 \\ \vdots \\ \lambda'_N \end{Bmatrix}^{2N \times 1} = \begin{Bmatrix} b_1 \\ \vdots \\ b_N \\ b'_1 \\ \vdots \\ b'_N \end{Bmatrix}^{2N \times 1} \quad (5.7.5)$$

$$\text{or} \quad [AIC_1] \vec{\lambda} + [AIC_2] \vec{\lambda}' = \vec{b} \quad (5.7.6)$$

$$[AIC_2] \vec{\lambda} + [AIC_1] \vec{\lambda}' = \vec{b}'$$

Adding these two equations, we get

$$[AIC_1 + AIC_2]^{N \times N} \{ \vec{\lambda} + \vec{\lambda}' \}^{N \times 1} = \{ \vec{b} + \vec{b}' \}^{N \times 1} \quad (5.7.7)$$

Subtracting, we obtain

$$[AIC_1 - AIC_2]^{N \times N} \{ \vec{\lambda} - \vec{\lambda}' \}^{N \times 1} = \{ \vec{b} - \vec{b}' \}^{N \times 1} \quad (5.7.8)$$

Thus we obtain two systems of equations, in the new variables  $\{ \vec{\lambda}_1 + \vec{\lambda}_1' \}$  and  $\{ \vec{\lambda}_1 - \vec{\lambda}_1' \}$ . Since the cost of solving  $N$  equations in  $N$  variables is proportional to  $N^3$ , the systems (5.7.7) and (5.7.8) together cost only one fourth as much to solve as (5.7.4). Further, as we see from the partitioning of  $[AIC]$  in (5.7.5), we may save half the cost of the construction of the AIC matrix by making use of the plane of symmetry.

If the flow is exactly symmetric, we will have

$$\vec{b} = \vec{b}' \quad (5.7.9)$$

and thus

$$\vec{\lambda} - \vec{\lambda}' = 0 \quad (5.7.10)$$

In this case, we do not even have to solve (5.7.8).

Finally, PAN AIR will also permit a case with two planes of configuration symmetry. See Appendix K.1 for details.

### 5.7.3 Known Singularity Parameters

In a variety of cases, the value of a singularity parameter is directly specified. The most common example occurs with potential conditions on a thick configuration (equation (5.4.19)), in which case a source parameter is specified directly as

$$\sigma = -\vec{V}_\infty \cdot \hat{n} \quad (5.7.11)$$

If, of the  $N$  singularity parameters in the whole configuration,  $p$  are directly specified and  $q$  are not, we can reorder them so that  $(\lambda_1, \dots, \lambda_p)$  are specified, and thus (assuming no planes of symmetry) the basic system of linear equations can be written as

$$\left( \begin{array}{c|c} [DI]^{p \times p} & 0^{p \times q} \\ \hline [AIC_{KP}]^{q \times p} & [AIC_{UP}]^{q \times q} \end{array} \right) \begin{Bmatrix} \lambda_1 \\ \vdots \\ \lambda_q \\ \lambda_{p+1} \\ \vdots \\ \lambda_N \end{Bmatrix} = \begin{Bmatrix} b_1 \\ \vdots \\ b_p \\ b_{p+1} \\ \vdots \\ b_N \end{Bmatrix} \quad (5.7.12)$$

Here, the matrix  $DI$  is a diagonal matrix whose entries are the coefficients  $a_D$  or  $c_D$  of an equation

$$\begin{aligned} \text{or} \quad a_D \sigma &= b \\ c_D \sigma &= b \end{aligned} \quad (5.7.13)$$

which specifies the value of a singularity parameter.

The matrix  $AIC_{KP}$  (KP stands for known parameters, UP for unknown parameters) gives the dependence of the boundary condition expressions

$$a_A \vec{w}_A \cdot \vec{n} + c_A \phi_A + \vec{t}_A \cdot \vec{v}_A \quad (5.7.14)$$

$$+ a_D \sigma + c_D \mu + \vec{t}_D \cdot \vec{\nabla} \mu$$

on the set of known parameters, while  $AIC_{UP}$  gives the dependence of the expressions (5.7.14) on the set of unknown parameters.

As a specific example, consider the case where all the source singularity parameters are specified according to equation (5.7.11). Then,  $\lambda_{p+1}, \dots, \lambda_N$  are the unknown doublet singularity parameters,  $\lambda_j = \sigma(P_j)$  and  $b_j = -\vec{V}_\infty \cdot \hat{n}_j$  for  $1 \leq j \leq p$ ,  $[DI] = [I]$ , and  $[AIC_{KP}]$  gives the effect of the known source strength singularity parameters on the expression (5.7.14), which, in our example, becomes lower surface potential.

Now, the first  $p$  lines of (5.7.12) express the system of equations

$$[DI] \begin{Bmatrix} \lambda_1 \\ \vdots \\ \lambda_p \end{Bmatrix} = \begin{Bmatrix} b_1 \\ \vdots \\ b_p \end{Bmatrix} \quad (5.7.15a)$$

or

$$\begin{Bmatrix} \lambda_1 \\ \vdots \\ \lambda_p \end{Bmatrix} = [DI]^{-1} \begin{Bmatrix} b_1 \\ \vdots \\ b_p \end{Bmatrix} \quad (5.7.15b)$$

where  $[DI]^{-1}$  is readily computable since  $[DI]$  is a diagonal matrix.  
The remainder of (5.7.12) is

$$[AIC_{KP}] \begin{Bmatrix} \lambda_1 \\ \vdots \\ \lambda_p \end{Bmatrix} + [AIC_{UP}] \begin{Bmatrix} \lambda_{p+1} \\ \vdots \\ \lambda_N \end{Bmatrix} = \begin{Bmatrix} b_{p+1} \\ \vdots \\ b_N \end{Bmatrix} \quad (5.7.16)$$

Substituting (5.7.15b) into (5.7.16), we obtain

$$[AIC_{UP}]^{q \times q} \begin{Bmatrix} \lambda_{p+1} \\ \vdots \\ \lambda_N \end{Bmatrix}^{q \times 1} = \begin{Bmatrix} b_{p+1} \\ \vdots \\ b_N \end{Bmatrix}^{q \times 1} - [AIC_{KP}]^{q \times p} [DI^{-1}]^{p \times p} \begin{Bmatrix} b_1 \\ \vdots \\ b_p \end{Bmatrix}^{p \times 1} \quad (5.7.17)$$

We have thus reduced (5.7.12), a system of equations in the  $N$  parameters  $\lambda_1, \dots, \lambda_N$  to a system of equations in the  $q$  unknown parameters  $\lambda_{p+1}, \dots, \lambda_N$ .

#### 5.7.4 Multiple Right Hand Sides

So far, we have always considered a system or systems of equations of the general form

$$[AIC]^{n \times n} \vec{\lambda}^{n \times 1} = \vec{b}^{n \times 1} \quad (5.7.18)$$

But if the AIC matrix does not change, it is very economical to solve (5.7.18)

for a sequence of distinct vectors  $\vec{b}_i$ , obtaining a sequence of solution vectors  $\vec{\lambda}_i$ .

The ability to solve (5.7.18) for multiple vectors  $\vec{b}$  can be very useful. The uses include analyzing the flow about a configuration at multiple angles of attack or sideslip, evaluating stability derivatives, or analyzing a variety of quasi-steady flows in which the configuration is undergoing a pitching, rolling, or yawing motion. This is especially useful when  $M_\infty = 0$ , and the small perturbation assumption is not necessary for the Prandtl-Glauert equation to hold. For a further discussion of "right hand side" or "constraint" vectors  $\vec{b}$ , see Appendix L.

So, in its most general form, (5.7.18) can be written

$$[AIC]^{n \times n} [\Lambda]^{n \times m} = [B]^{n \times m} \quad (5.7.19)$$

where each of the  $m$  columns of  $B$  is a constraint vector  $\vec{b}_i$ , and each column of  $\Lambda$  is a solution vector  $\vec{\lambda}_i$ .

#### 5.7.5 Updatability

One final feature of PAN AIR is that of "updatability." That is, a program user may identify certain networks as being subject to modification. The program then segregates boundary conditions and singularity parameters corresponding to these networks, so that the AIC matrix in (5.7.7), (5.7.8) or (5.7.18) can be partitioned as:

$$[AIC] = \begin{bmatrix} AIC_{NU} & AIC_{U,1} \\ AIC_{U,2} & AIC_{U,3} \end{bmatrix} \quad (5.7.20)$$

Here, the subscripts U and NU stand for updatable and non-updatable.

Now, the matrix  $AIC_{NU}$  is stored, and when the program user makes a second run in which updatable networks are modified, the program need only recalculate  $AIC_{U,i}$ ,  $i = 1, 2, 3$ , rather than the whole AIC matrix. Here, "modification" may consist of the alteration of the network geometry, or the alteration of the left hand side boundary condition expressions (5.7.14). It is easy to see that  $AIC_{NU}$  remains unchanged under a modification of an "updatable" network. For a full discussion, see Appendix K.6.



## 5.8 Solution of the System of Equations

As we see from (5.7.7), (5.7.8), (5.7.13), and (5.7.19) the program sets up a system or systems of linear equations of the general form

$$[A]^{n \times m} [X]^{n \times m} = [B]^{n \times m} \quad (5.8.1)$$

Generally speaking, the matrix A is too large to store in the central memory of a computer at one time. Thus the matrices are stored in block format on a disk, and (5.8.1) is solved with no more than a small number of these blocks in core at once.

Generally, the matrix A is decomposed as a product of lower triangular and upper triangular matrices

$$[A]^{n \times n} = [L]^{n \times n} [U]^{n \times n} \quad (5.8.2)$$

This process frequently involves "in-core pivoting", that is, the interchange of columns within one of the blocks composing A. It is possible, though not proven, that a boundary value problem of aerodynamic interest may result in one of the blocks of A which lies on the diagonal being singular, in which case a decomposition of the form (5.8.2) is not possible. Such a case requires the interchange of columns lying in different blocks, a process called "out-of-core pivoting." The out-of-core pivoting process decreases the efficiency of the solution process since additional data must be transferred between disk and core. This process is described in the Maintenance Document.

After the decomposition (5.8.2) the next step is "forward substitution", that is, the system of equations

$$\begin{bmatrix} L \end{bmatrix}^{n \times n} \begin{bmatrix} Y \end{bmatrix}^{n \times m} = \begin{bmatrix} B \end{bmatrix}^{n \times m} \quad (5.8.3)$$

is solved for the matrix Y. The final step is "back substitution", in which the system

$$\begin{bmatrix} U \end{bmatrix}^{n \times n} \begin{bmatrix} X \end{bmatrix}^{n \times m} = \begin{bmatrix} Y \end{bmatrix}^{n \times m} \quad (5.8.4)$$

is solved for the matrix X.

The equation solution procedure has two distinct "updatability" features. First, suppose A is an AIC matrix partitioned as in (5.7.20). Then the factorization (5.8.2) is performed on AIC<sub>NU</sub> first, after which A is factored in its entirety. The factorization of AIC<sub>NU</sub> is stored, and in a later run in which AIC<sub>U,i</sub>, i = 1, 2, 3, are changed, the factorization continues from that point. This may result in a significant saving of time.

The other "updatability" feature is that a program user may request the entire factorization (5.8.2) to be stored, and then at a later time submit additional constraint vectors  $\vec{b}$ . Thus, a user may find that the results for one angle of attack are useful, and thereupon obtain results for additional angles of attack, angles of sideslip, or for stability derivatives, at small additional cost.

## 5.9 Post-Solution Features

### 5.9.1 Computation of Potential and Velocity

Once the system or systems of linear equations (5.7.19) have been solved for one or more solution vectors, it remains to translate the vector(s) into quantities of aerodynamic or hydrodynamic interest. The first step is to obtain the values of  $\phi_A$  and  $\vec{v}_A$  at control points. Clearly,

$$\begin{aligned}\phi_A &= [\phi_{IC}] \quad 1 \times N \quad \vec{\lambda} \quad N \times 1 \\ \vec{v}_A &= [V_{IC}] \quad 3 \times N \quad \vec{\lambda} \quad N \times 1\end{aligned}\tag{5.9.1}$$

but obtaining  $\phi_A$  and  $\vec{v}_A$  this way requires the storage of  $4N$  words of data for each control point. Often it is possible to obtain  $\phi_A$  from a boundary condition. For example (recalling  $\phi_L = \frac{1}{2}(\phi_U + \phi_L) - \frac{1}{2}(\phi_U - \phi_L) = \phi_A - \frac{1}{2}\mu$ ), the boundary condition

$$\phi_L = \phi_A - \frac{1}{2}\mu = 0\tag{5.9.2}$$

is often imposed at control points. Thus,

$$\phi_A = \frac{1}{2}\mu\tag{5.9.3}$$

Since  $\mu$  at the control point is already available (it is one of the unknown parameters), we can obtain  $\phi_A$  without storing the  $\phi_{IC}$  matrix.

Once  $\phi_A$  has been found at every control point, we may make use of the doublet spline matrices to obtain a distribution of  $\phi_A$  on the whole surface. This quadratic distribution may then be differentiated to obtain tangential velocities on the surface. The conormal component of

velocity,  $\vec{v}_A \cdot \hat{n} = \vec{w}_A \cdot \hat{n}$ , can often be obtained from a boundary condition of the form

$$\vec{w}_A \cdot \hat{n} = -\vec{v}_\infty \cdot \hat{n} \quad (5.9.4)$$

Then, all three components of velocity may be obtained from the tangential and conormal components. The details of how we can use boundary conditions and splines to obtain velocities at control points or grid points (panel corner points, centers, or edge midpoints) are given in Appendix M.

The velocities are calculated at control points or grid points in a user-selected reference coordinate system  $(x_0, y_0, z_0)$ . The formulas for calculating pressures are most easily written in the compressibility coordinate system  $(x, y, z)$ , in which the freestream direction is the x-direction, so we will describe them in that system, in which we write  $\vec{v} = (u, v, w)$  and  $\vec{V}$  (the total velocity) =  $(V_\infty + u, v, w)$ .

#### 5.9.2 Pressure Computation

PAN AIR will calculate the pressure at a point from the velocity according to any of five different pressure coefficient rules. These pressure rules will be derived in Appendix N. We assume we are dealing with a gas or an incompressible liquid. Let  $\gamma$  be the ratio of specific heats. Subject to certain constraints on the range of velocities for which the pressure coefficient rules hold, they are listed in figure 5.21. For an incompressible liquid, the isentropic formula does not apply.

#### 5.9.3 Velocity Corrections

In addition, PAN AIR will calculate two semi-empirical velocity correction

formulas. The first is often used in practice in areas such as inlets where the component of the velocity in the freestream direction is less than the freestream. If  $u < 0$ , we solve

$$s \beta^2 u = u' \left[ 1 + \frac{\gamma-1}{2} M_\infty^2 (1 - |\vec{V}'|^2) \right]^{\frac{1}{\gamma-1}} \quad (5.9.5)$$

$$= \frac{\rho_\infty}{\rho} \vec{w}_x$$

for  $u'$ , where  $\rho_\infty$  is the freestream density,  $\rho$  is the density at the point in question, and  $\vec{w}_x = s \beta^2 u$  is the x-component of the mass flux. Here the corrected total velocity is

$$\vec{V}' = \vec{V}_\infty + \vec{V}' = \vec{V}_\infty + \begin{Bmatrix} u' \\ v \\ w \end{Bmatrix} \quad (5.9.6)$$

This velocity correction is closely related to the Lieblein-Stockman formula (cf., Reference 5.1).

The second velocity correction formula is often used in regions of near-stagnation such as the leading edge of a wing. If  $u \geq 0$ , we set

$$\vec{V}' = \frac{|\vec{V}|}{|\vec{W}|} \vec{W} \quad (5.9.7)$$

If  $u < 0$ , we set

$$\vec{V}' = \frac{\vec{W}}{1 - M_\infty^2 u} \quad (5.9.8)$$

where the denominator is a first order approximation to  $\rho/\rho_\infty$ .

These two correction formulas are essentially empirical. The first has been used successfully only in subsonic flow, while the second has been used successfully in both subsonic and supersonic flow. An example of a successful application of the second velocity correction is given in figure 36 of Ehlers et al., Reference 5.2.

#### 5.9.4 Force and Moment Computation

PAN AIR will also integrate pressures on a surface to obtain coefficients of force. The formula we use for the force is

$$\vec{F} = - \iint_S \left\{ \frac{\rho \vec{V} \cdot \hat{n}}{|\vec{V}_\infty|^2} \vec{V} + p \hat{n} \right\} dS \quad (5.9.9)$$

where  $p$  is the pressure and  $\rho$  is the density.

The first term in the integrand is, of course, zero for an impermeable surface, but does in fact contribute to the force on a porous surface. The evaluation of this integral is discussed in Appendix O.

PAN AIR also evaluates the moment  $\vec{M}$  about a point. If  $R_0$  is the point in question, and  $Q$  is a point on the surface,

$$\vec{M} = - \iint_S \left\{ (\vec{Q} - \vec{R}_0) \times \left( \frac{\rho \vec{V} \cdot \hat{n}}{|\vec{V}_\infty|^2} \vec{V} \right) + p (\vec{Q} - \vec{R}_0) \times \hat{n} \right\} dS \quad (5.9.10)$$

The derivation of (5.9.9) and (5.9.10) is given in Ashley and Landahl (reference 5.3), section 1-6.

Equation (5.9.9) ignores a contribution to the total force, called the edge force, which occurs for thin configurations. To obtain the force on the configuration illustrated in figure 5.22, we should integrate the expression

in (5.9.9) over the combined surface  $S = S_1 \cup S_2$ , while in fact we only integrate the expression over  $S_1$ . The integral over  $S_2$  is the leading edge force. Because the velocity is infinite at a subsonic leading edge for a flow that satisfies the Prandtl-Glauert equation, the integral over  $S_2$  is non-zero even as  $\epsilon \rightarrow 0$ . It can be shown that, for planar wings,

$$|\vec{v}| = \frac{G}{\beta} (\Delta x)^{-\frac{1}{2}} \quad (5.9.11)$$

where  $\Delta x$  is the distance between the point in question and the point on the leading edge. Here  $G$  is a constant whose value depends on the local geometry of the wing, and  $\beta = \sqrt{1 - M_\infty^2}$ .

PAN AIR uses an extrapolation procedure to evaluate  $G$  from the values of  $\vec{v}$  at points in the interior of the network. Once  $G$  is known, the integral in (5.9.9) can readily be evaluated over  $S_2$ . This procedure is discussed in Appendix O.

PRECEDING PAGE BLANK-NOT FILMED

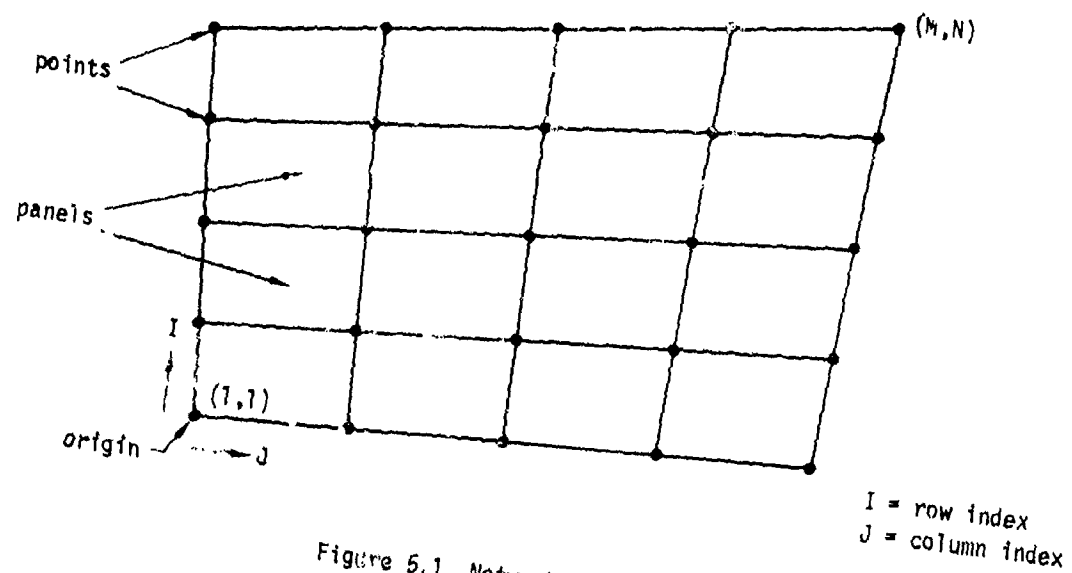


Figure 5.1 Network geometry

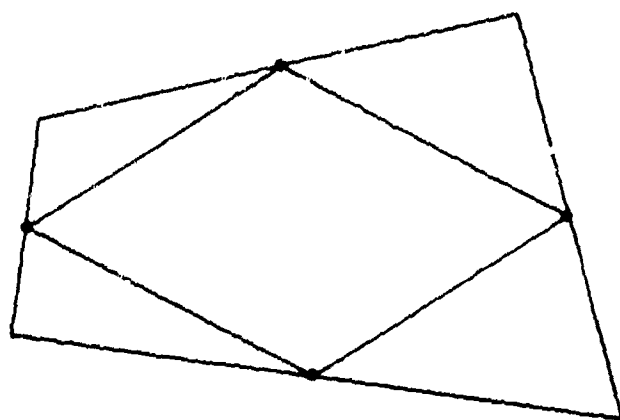


Figure 5.2 Decomposition of panel into 5 planar regions



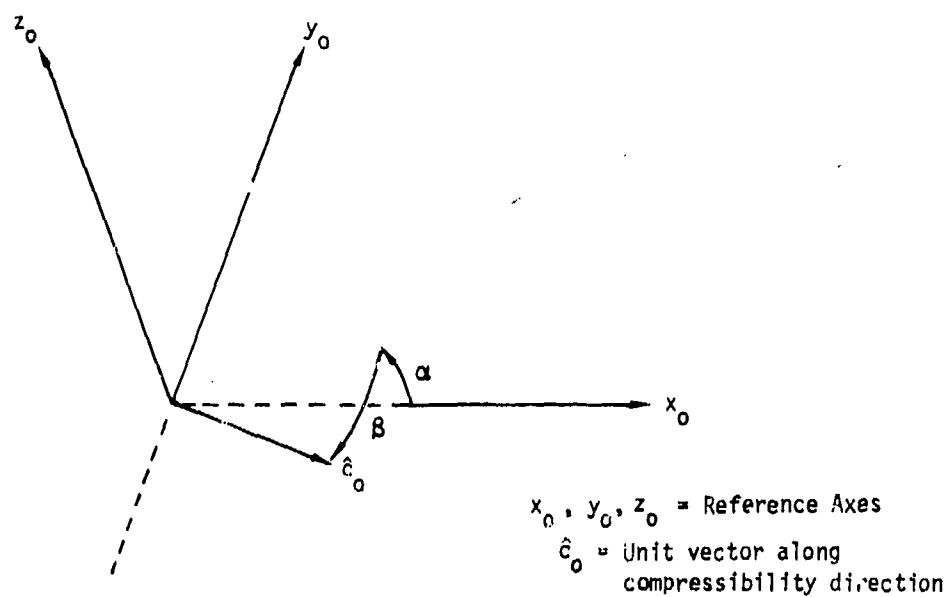


Figure 5.3 - Definition of compressibility directions in terms of angles of attack and sideslip

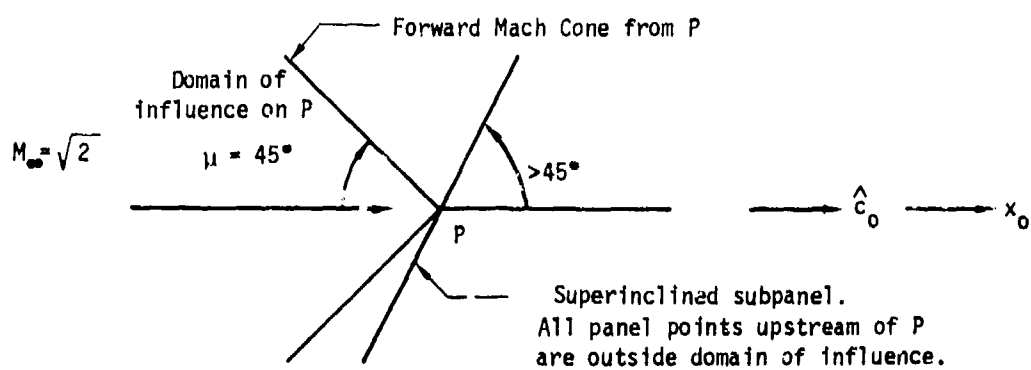
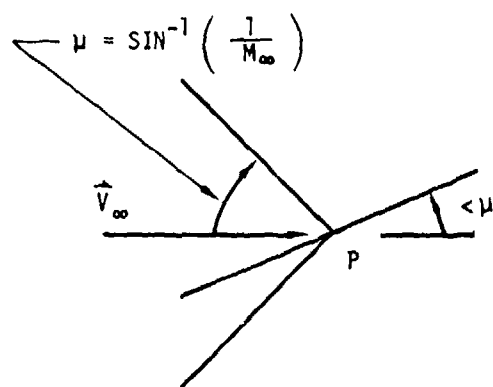
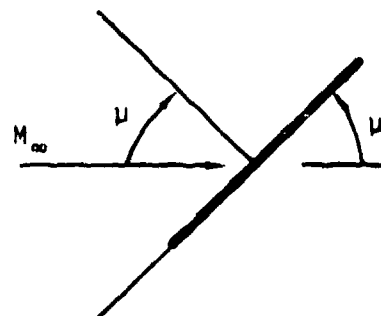


Figure 5.4 - Superinclined Surface,  $r = -1$



a - Subinclined,  $r = +1$



b - Mach-inclined,  $\hat{n} \cdot \tilde{n} = 0$ .

Figure 5.5 - Subinclined and Mach-inclined surfaces

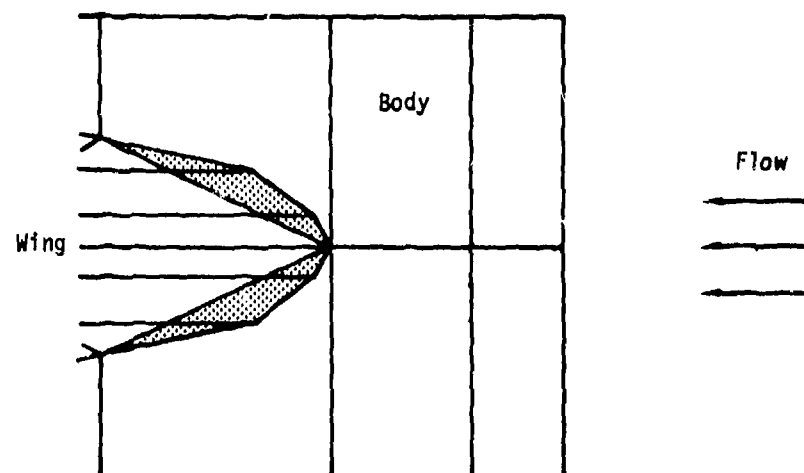


Figure 5.6 - Gap between leading edge of wing and body

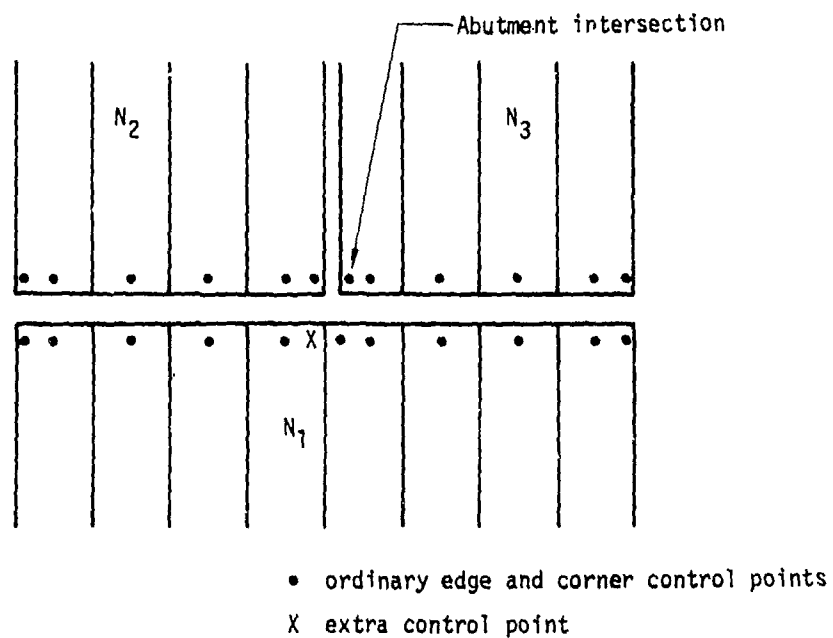


Figure 5.7 - Example of abutment intersection

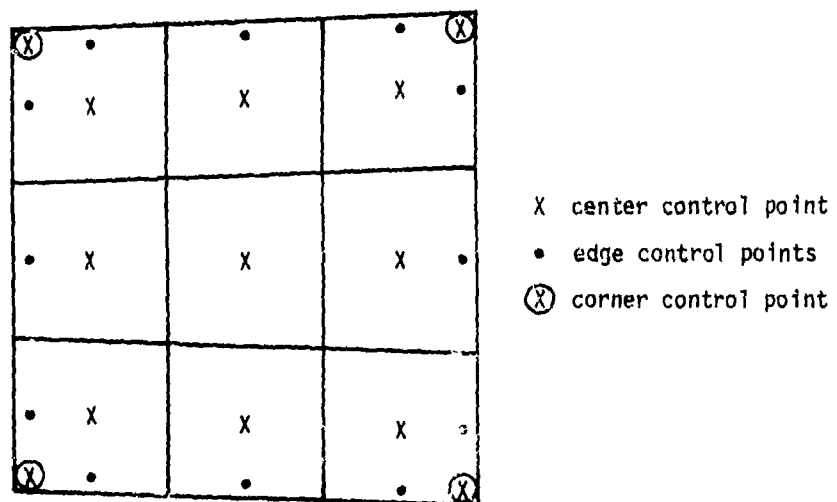


Figure 5.8 - Control point locations

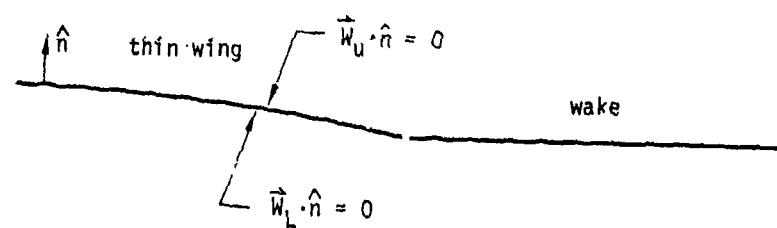


Figure 5.9 - Thin wing boundary conditions

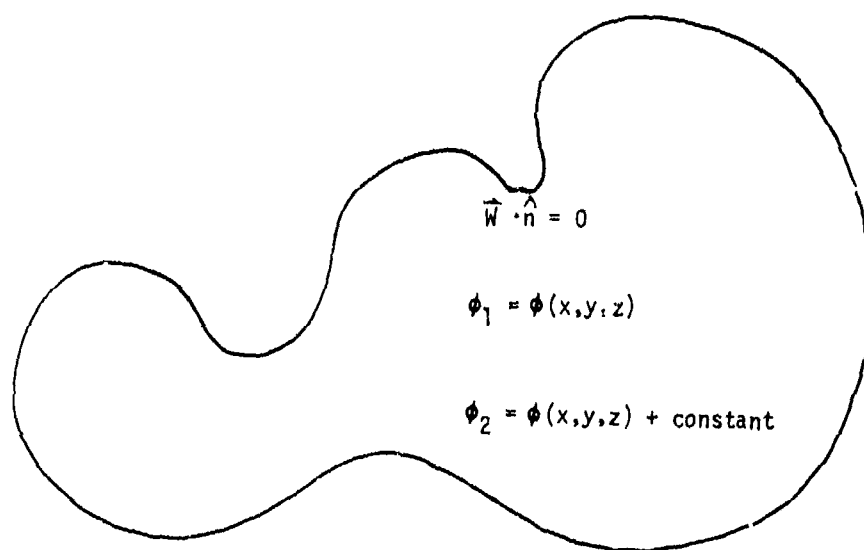


Figure 5.10 - Two solutions for potential in enclosed volume



Figure 5.11 - Thick wing boundary conditions

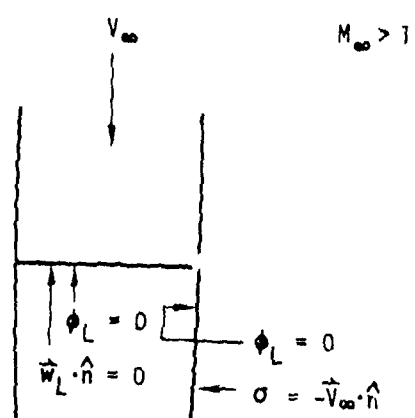
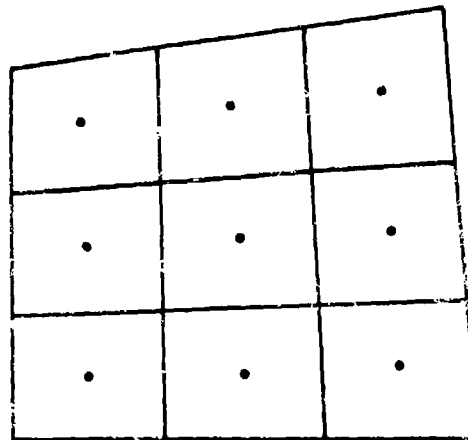


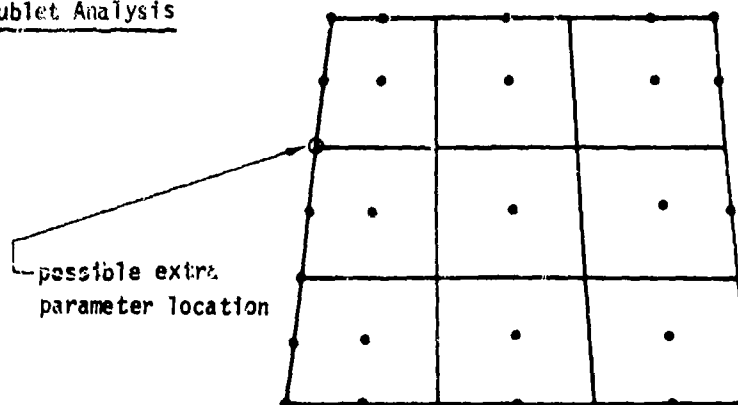
Figure 5.12 - Boundary conditions on superinclined surfaces

Source Analysis



• source parameter locations

Doublet Analysis



• doublet parameter locations

Doublet Wake

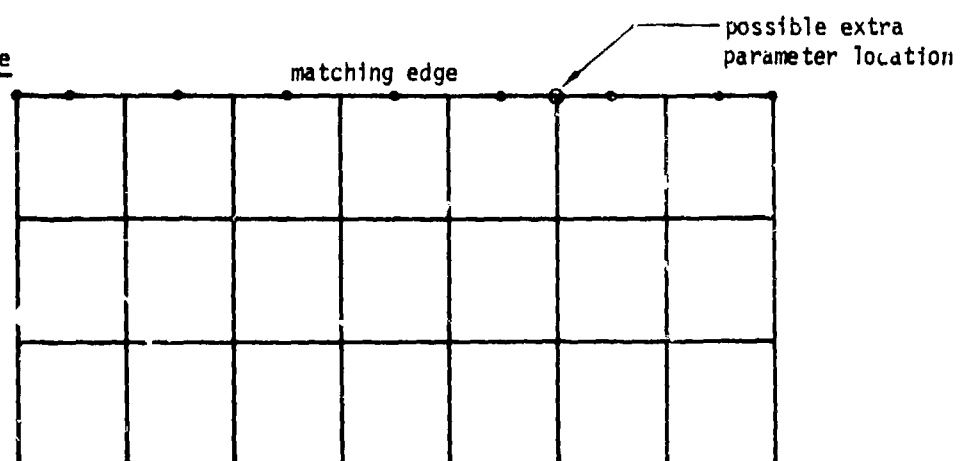
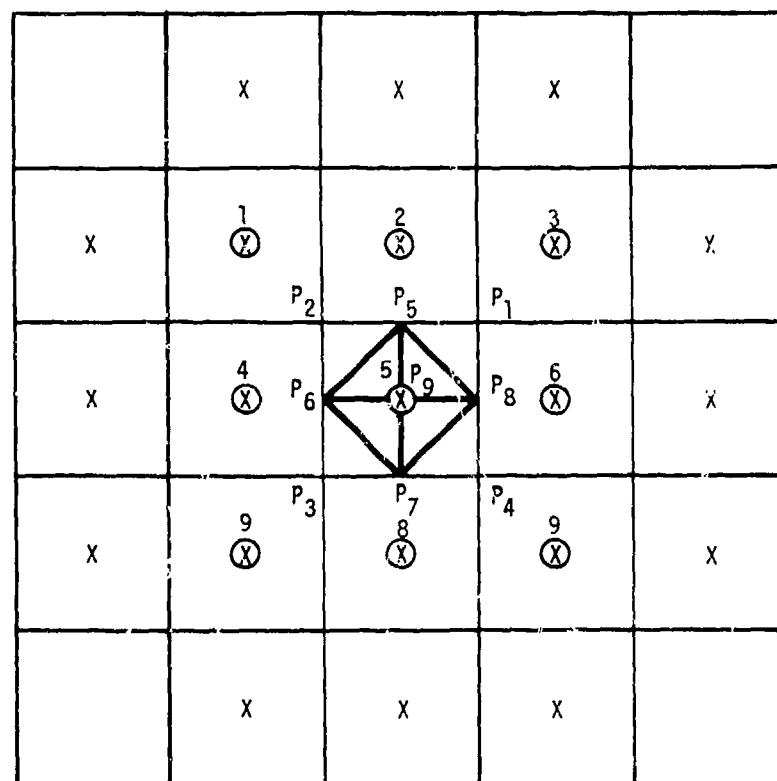
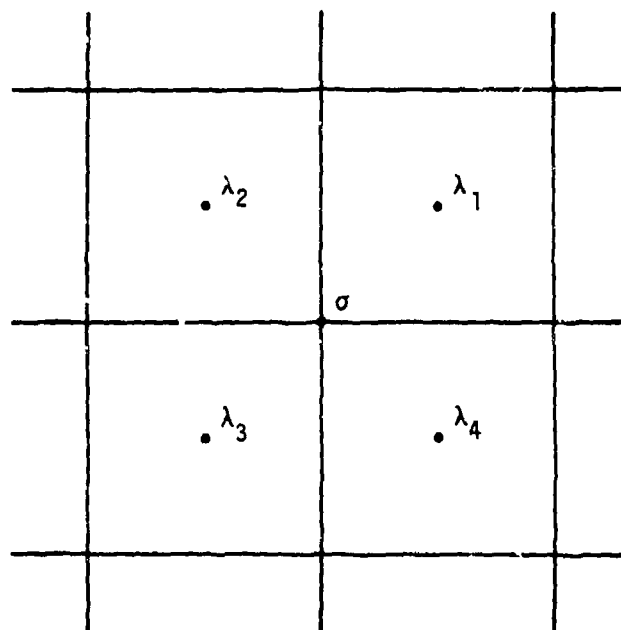


Figure 5.13 - Singularity parameter locations



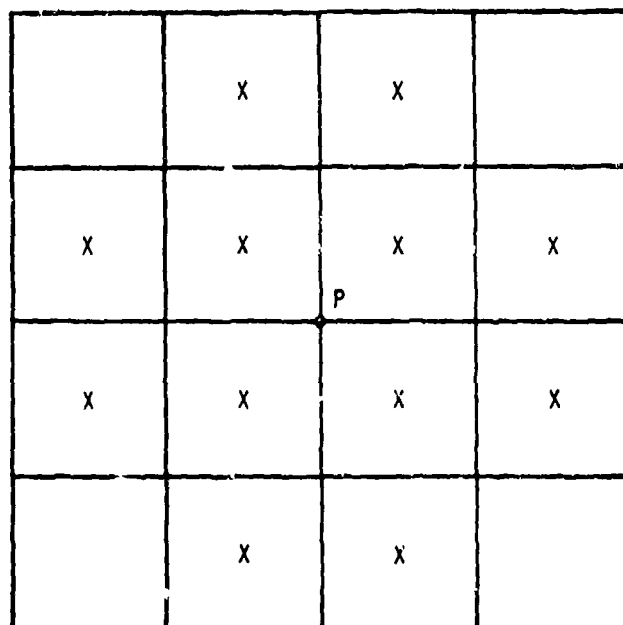
X doublet parameters in the neighborhood of the panel  
 ⊙ source parameters in the neighborhood of the panel

Figure 5.14 - Singularity parameters in the neighborhood of the panel



• neighboring source parameters

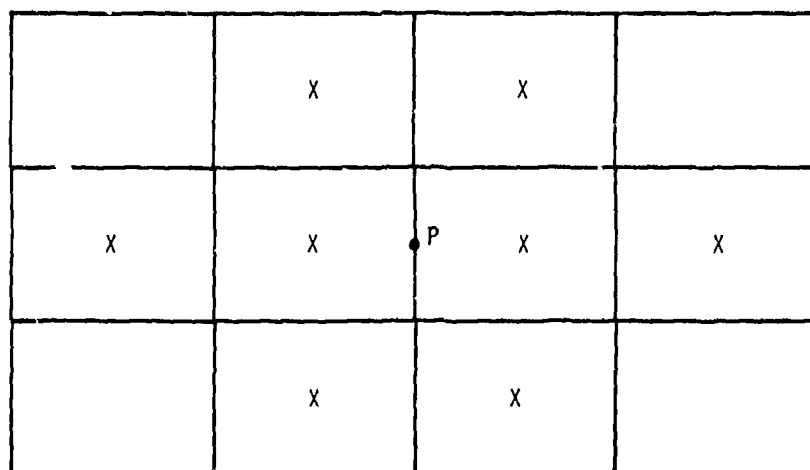
Figure 5.15 - Neighboring source parameters for a panel corner point



X neighboring doublet parameters

Figure 5.16 - Neighboring doublet parameters for a panel corner point





X neighboring doublet parameters

Figure 5.17 - Neighboring doublet parameters for a panel edge midpoint

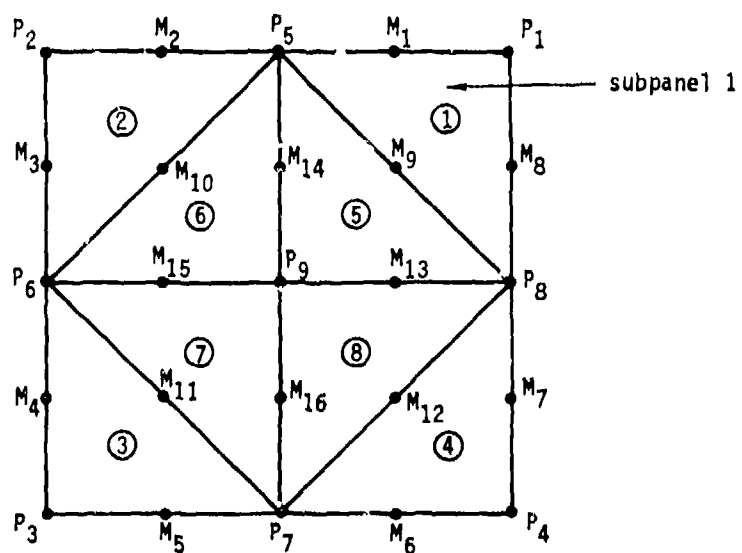


Figure 5.18 - Panel points and midpoints

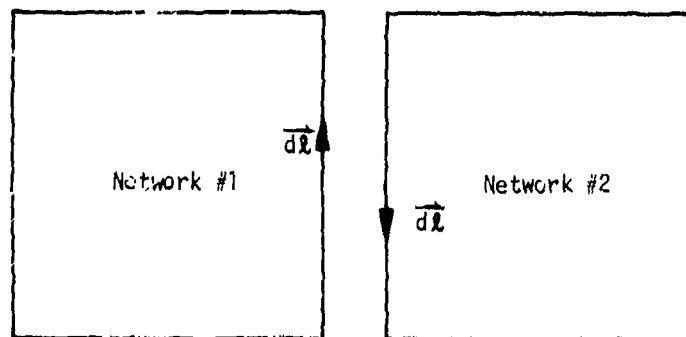


Figure 5.19 - Opposite orientations of adjacent networks

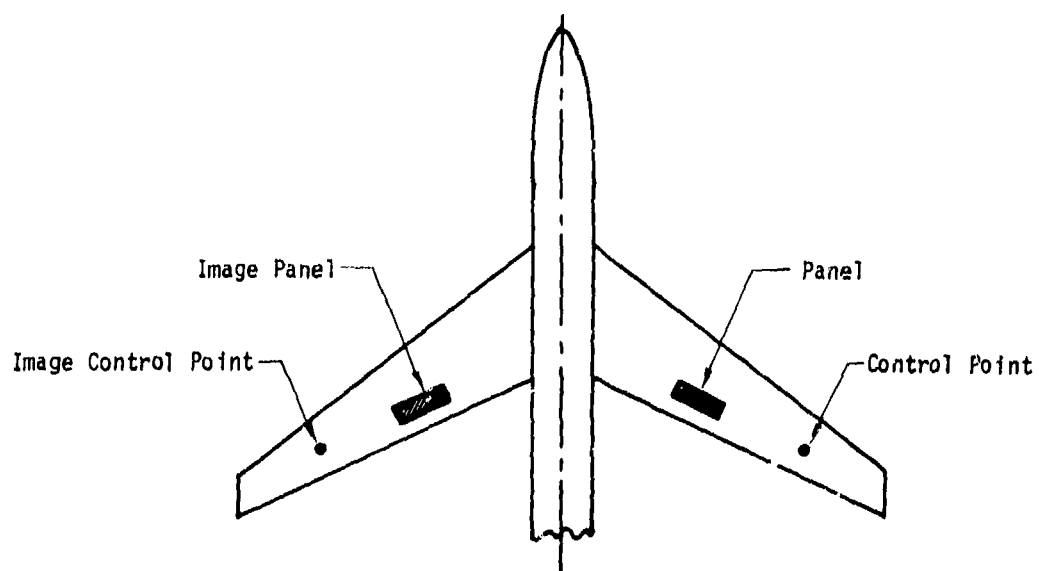


Figure 5.20 - Configuration and image

<u>RULE</u>	<u>C<sub>p</sub></u>
Isentropic	$\frac{-2}{\gamma M_\infty^2} \left\{ \left[ 1 + \frac{\gamma-1}{2} M_\infty^2 (1 -  \vec{V} ^2) \right]^{\frac{\gamma}{\gamma-1}} \right\}$ used if $M_\infty > .01$
Incompressible	$1 -  \vec{V} ^2$ used if $M_\infty \leq .01$
Second Order	$1 -  \vec{V} ^2 + M_\infty^2 u$
Slender Body	$-(2u + v^2 + w^2)$
Linear	$-2u$
Reduced Second Order	$1 -  \vec{V} ^2$

Figure 5.21 - Pressure coefficient rules

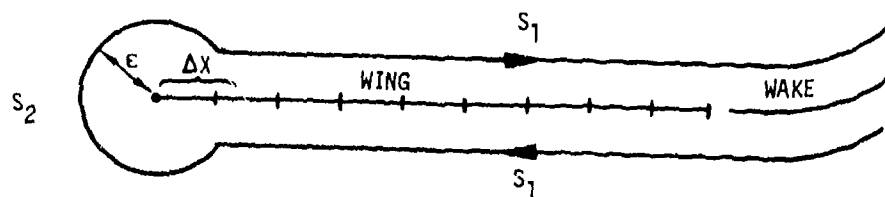


Figure 5.22 - Surfaces of integration for leading edge force

## 6.0 A Guide to the Appendices

The purpose of the appendices is three-fold:

- (a) they give background material, not reflected in the computer code, but explaining why the computer program performs the functions it does,
- (b) they describe in considerable detail the functions performed by the program, and
- (c) they describe the equations which are actually implemented in the code.

Appendices A through C cover background material exclusively. The remaining appendices are predominantly devoted to the PAN AIR program, but often derivations are supplied to prove or justify the validity of an equation.

Often a conflict may occur between organizing the material according to the structure of the program or organizing it according to subject matter (for instance splines, panels, networks, pressures, etc.) or capability (for instance symmetry, updatability, multiple right hand sides, etc.). This conflict will almost invariably be resolved in favor of organization according to subject matter or capability.

This document will generally discuss only engineering functions within PAN AIR. Specifically, the functions of the Data Input Processor (DIP), which reads and echoes user-input data, and the Print Plot Processor, which prepares files of output data for processing by plotting programs, will be ignored. Also, input/output and other data manipulation functions which are necessary due to core limitations, will, with few exceptions, be ignored. For example, a detailed discussion of matrix solution procedures will be contained in the Maintenance Document rather than the Theory Document, since the complexity of these procedures is largely due to data manipulation problems. Finally, there

will be no discussion of the "Scientific Data Management System" (SDMS) used by PAN AIR to transfer data between core and disk.

## 7.0 References

### PAN AIR Documents

PAN AIR - A Computer Program for Predicting Subsonic or Supersonic Linear Potential Flows about Arbitrary Configurations Using a Higher Order Panel Method.

Volume II, User's Manual (Version 1.0), by K. Sidwell, P. K. Baruah, and J. E. Bussoletti, NASA CR-3252, 1980.

Volume IV, Maintenance Document (Version 1.0), by P. K. Baruah, et. al., NASA CR-3254, 1980.

### Other References

- 1.1 Rubbert, P. E., and Saaris, G. R.: "Review and Evaluation of Three Dimensional Lifting Potential Flow Analysis Method for Arbitrary Configurations," AIAA paper 72-188, January 1972.
- 1.2a Woodward, F. A.: "Analysis and Design of Wing-Body Combinations at Subsonic and Supersonic Speeds," Journal of Aircraft, Vol. 5, No. 6, Nov.-Dec. 1968, pp. 528-534.
- 1.2b Woodward, F. A.: "An Improved Method for the Aerodynamic Analysis of Wing-Body-Tail Configurations in Subsonic and Supersonic Flow, Part I - Theory and Application," NASA CR-2228, Part I (1973).
- 1.3 Kellogg, O. D.: Foundations of Potential Theory, New York, Dover Publishing Company, 1953.
- 1.4 Liepmann, H. W., and Roshko, A.: Elements of Gasdynamics, New York, John Wiley and Sons, 1957.
- 1.5 Ward, G. N.: Linearized Theory of Steady High-Speed Flow, Cambridge University Press, 1955.
- 2.1 Landahl, M. T.: Unsteady Transonic Flow, Pergamon Press, 1961.
- 4.1 Hess, J. L., and Smith, A. M. O.: Calculation of Nonlifting Potential Flow About Arbitrary Three-Dimensional Bodies, ES40622, Douglas Aircraft Company, 1962.
- 4.2 Rubbert, P. E.: Theoretical Characteristics of Arbitrary Wings by a Nonplanar Vortex Lattice Method, D6-9244, The Boeing Company, 1964.
- 4.3 Hess, J. L.: Calculation of Potential Flow About Arbitrary 3-D Lifting Bodies, Douglas Report MDC-J5679-01, October 1972.
- 4.4 Roberts, A., and Rundle, K.: Computation of First Order Compressible Flow About Wing-Body Configurations, AERO MA No. 20, British Aircraft Corporation, February 1973.
- 4.5 Mercer, J. E., Weber, J. A., and Lesferd, E. P.: Aerodynamic Influence Coefficient Method Using Singularity Splines, NASA CR-2423, May 1974.

- 4.6 Morino, L. and Kuo, Ching-Chiang: "Subsonic Potential Aerodynamics for Complex Configurations: A General Theory," AIAA Journal, Vol. 12, No. 2, pp. 191-197, February 1974.
- 4.7 Johnson, F.T., and Rubbert, P. E.: "Advanced Panel-Type Influence Coefficient Methods Applied to Subsonic Flow," AIAA Paper 75-50, January 1975.
- 4.8 Ehlers, F. E., and Rubbert, P. E.: A Mach Line Panel Method for Computing the Linearized Supersonic Flow Over Planar Wings, NASA CR-152123, 1979.
- 4.9 Ehlers, F. E., Epton, M. A., Johnson, F. T., Magnus, A. E., and Rubbert, P. E.: A Higher Order Panel Method for Linearized Supersonic Flow, NASA CR-3062, 1979.
- 5.1 Lieblein, S. and Stockman, N. O.: "Compressibility Corrections for Internal Flow Calculations," Journal of Aircraft, Vol. 9, No. 4, pp. 312-313, April 1972.
- B.1 Butter, D. J., Compressibility Corrections Used in Panel Methods, HSA-MAE-R-FDM-0039, British Aircraft Corporation, November, 1978.
- B.2 Johnson, F. T., Lu, P., Tinoco, E. N., and Epton, M. A.: An Improved Panel Method for the Solution of Three-Dimensional Leading Edge Vortex Flows, NASA CR-159173, 1979.
- B.3 Lass, H.: Vector and Tensor Analysis, New York, McGraw-Gill, 1950.
- F.1 Jones, R. T., and Cohen, D., "Aerodynamics of Wings at High Speeds," in Aerodynamic Components of Aircraft at High Speeds, A. F. Donovan and H. R. Lawrence, editors, Princeton University Press, pp. 3-243, 1957.
- J.1 Johnson, F. T.: A General Panel Method for the Analysis and Design of Arbitrary Configurations in Subsonic Flows, NASA CR-3079, 1979.
- J.2 Handbook of Mathematical Functions, M. Abramowitz and I. A. Stegun, editors, National Bureau of Standards, 1964.
- J.3 Robinson, A. "On Source and Vortex Distributions in the Linearized Theory of Steady Supersonic Flow," Quart. J. Mech. Appl. Math., I, pp. 408-432, 1948.
- I.1 Faddeeva, V. N.: Computational Methods in Linear Algebra, New York, Dover Publications.
- O.1 Ashley H. and Landahl, M.: Aerodynamics of Wings and Bodies, Addison - Wesley, 1965.
- O.2 Sears, W. R.: General Theory of High Speed Aerodynamics, Princeton University Press, 1954.

## 8.0

## List of Symbols

$a$	speed of sound, m/sec
$a$	coefficient of normal mass flux in boundary condition equation
$a$	distance from projection of control point to edge of $\Sigma ND_p$
$a$	one of the fundamental integrals in PIC computation
$\vec{a}$	one of the fundamental integrals in PIC computation
$a$	freestream speed of sound, m/sec
$A$	endpoint of an edge
$A$	area
$A_i$	$i$ th abutment in an abutment intersection
$[A]$	reference to local transformation, defined in sections 5.2 and E.3
$[A_i]$	$4 \times 4$ matrix containing reference to local transformation for $i$ th subpanel as a subset
$[AIC]$	aerodynamic influence coefficient matrix
$b$	constraint in a boundary condition equation
$b$	vector of constraints in a system of equations
$b_i$	basis function corresponding to $i$ th singularity parameter
$b$	one of the fundamental integrals in PIC computation
$\vec{b}$	one of the fundamental integrals in PIC computation
$B$	endpoint of an edge
$[B]$	one of the fundamental integrals in PIC computation
$[B]$	outer spline matrix
$[B]$	a matrix of constraint vectors
$[B]$	dual compressible metric matrix in compressibility coordinates
$[B_0]$	dual compressible metric matrix in reference coordinates
$c$	coefficient of potential in boundary condition equation
$c_v$	specific heat of a gas at constant volume
$c_0$	unit vector in compressibility direction



$C_p$	pressure coefficient
$\Delta C_p$	difference of upper surface and lower surface pressure coefficient
$\vec{C}_F$	force coefficient vector
$\vec{C}_M$	moment coefficient vector
$C_{pp}$	preliminary pressure coefficient
$C_{ps}$	specified pressure coefficient
$C_i$	$i$ th corner point in an abutment intersection
$[C]$	Compressible metric matrix in compressibility coordinates
$[C_0]$	Compressible metric matrix in reference coordinates
$C_{ij}$	Panel skewness parameters defined in section D.2, $i = 1, 2$ , $j = 1, \dots, 4$
$C_h$	Mach disk
$C_{MN}^i$	basic far field moments for $i$ th subpanel
$C_0$	= 0 or 1, defined by equation (J.4.30)
$d$	distance between two points, or between a point and a set of points
$[D]$	doublet integral matrix (section J.6.4.3)
$[D_0]$	doublet integral matrix with origin shift included
$[D]$	inverse of reference to local transformation in section E.3
$[D]$	intermediate matrix in half panel spline computation
$\det$	determinant
$[DI]$	Diagonal matrix of coefficient specifying known singularity parameters
$D_p$	Domain of dependence corresponding to point P
$e$	internal energy density, joules/kg
$e$	coefficient of velocity in boundary condition equation
$\Delta E$	energy added by incremental onset flow
$E_i$	$i$ th network edge in an abutment

$\vec{f}$	external body force, newtons
$F_j$	linear combination of skewness parameters defined by equation (F.2.50)
$\vec{F}$	force due to fluid, newtons
[F]	one of the fundamental integrals in PIC computation
FFM	Far field moment tensor (see section 1.4.1)
$g$	distance from control point to edge of $\Sigma D_p$
$\vec{G}_0$	$= \vec{\nabla}_Q (1/R)$
[G]	matrix depending on panel geometry defined by equation (I.2.4) and (I.2.62)
[G]	local compressible scaling matrix defining pseudo-inner product
$h$	height of the control point above the plane containing the panel
$H_i$	$i$ th hypothetical location of a control point
$H$	one of the fundamental integrals in PIC computation
[HPINT]	half panel integral matrix
[HPSPL]	Half panel spline matrix
$I$	row index
$I$	edge function
[I]	identity matrix
$I(\psi), I(x)$	basic integrals in PIC computation
$J$	column index
$J$	panel function
$J_i$	Jacobian factor for subpanel $i$
$J(\psi), J(x)$	basic integrals in PIC computation
$k$	coefficient of heat conductivity, $m^2/sec$
$k_D$	number of doublet singularity parameters in the neighborhood of a panel
$k_S$	number of source singularity parameters in the neighborhood of a panel

[L]	Lower triangular matrix
$L_i$	triangular coordinate functions, $i = 1, 2, 3$
[LSQ]	least squares matrix defined in section I.5
[LINV]	matrix giving line vortex contribution to PIC
M	number of rows of panels corner points in a network
$\vec{M}$	moment vector, newton-meters
$M_\infty$	freestream Mach number
$M_l$	local Mach number
$M_i$	midpoint of $i$ th panel edge on a network edge
[M]	matrix of coefficients giving quadratic component of doublet variation
mod	$i(\text{mod } j)$ is the remainder obtained when the integer $i$ is divided by the integer $j$
$M$	tensor of coefficients giving cubic component of doublet variation
$\hat{n}$	outward-pointing unit vector normal to a surface
$\tilde{n}$	conormal vector
$\vec{n}$	edge normal, normalized by pseudo-inner product
N	number of columns of panel corner points in a network
NCPM	normal cross product moment matrix
p	pressure, newtons/m <sup>2</sup>
$p_\infty$	pressure in the freestream, newtons/m <sup>2</sup>
ph	phase function
phh	hyperbolic phase function (see section (J.5))
$P(\phi)$	limit of integration in polar coordinates
P	point in space or control point
$P_i$	panel defining point, $1 \leq i \leq 2$
$\vec{P}$	vector whose entries are the coordinates of P
[PIC]	panel influence matrix
q	amount of heat added to fluid per unit mass, joules/kg
8.0-4	

$q$	edge indicator, = -1 for supersonic edges, + 1 for subsonic edges
$Q$	arbitrary point on panel, or point on integration surface, or field point
$\vec{Q}$	vector whose entries are the coordinates of $Q$
$Q$	modified integration point, defined by equation (J.9.4)
$r$	$\text{sign}(\hat{n} \cdot \tilde{n}) = +1$ for subsonic flow and subinclined panels, -1 for superinclined panels
$R$	gas constant, joules/kg - degree Kelvin
$R$	compressible distance from point in space to point of integration
$R$	control point recession vector
$R_0$	compressible distance from control point to panel center
$s$	$\text{sign}(1 - M_\infty^2)$
$s_i$	= + 1, sign corresponding to network edge in an abutment
$ds$	differential of arc length
$S$	surface in space, surface of integration
$\partial S$	boundary of $S$
$\{SP\}$	spline vector
$[SPSPL_i]$	subpanel spline matrix for $i$ th subpanel, $1 \leq i \leq 8$
$S$	source integral matrix (section J.6.4.2)
$S_0$	source integral matrix with origin shift included
$SPFFM$	subpanel far field moment matrix or tensor
$[SPINT]$	subpanel integral matrix
$t$	time, sec
$t$	parameter value under abutment parametrization for point on network edge
$\vec{t}$	coefficient of tangential velocity in boundary condition equation
$\vec{t}$	vector tangent to surface
$\hat{t}$	unit vector tangent to edge

$\hat{t}$	edge tangent, normalized by pseudo-inner product
$T$	temperature, degrees Kelvin
$(u,v,w)$	components of perturbation velocity in coordinate system whose x-axis is aligned with the freestream or the uniform onset flow
$\hat{u}_0$	unit vector perpendicular to panel normal and compressibility direction
$[U]$	Upper triangular matrix
$\vec{U}_\infty$	uniform onset flow
$\vec{U}_0$	total onset flow
$\Delta \vec{U}$	incremental onset flow
$v$	local edge coordinate
$\vec{v}$	perturbation velocity
$\hat{v}_0$	unit vector perpendicular to $U_0$ and $n$
$v_\xi, v_\eta, v_\zeta$	basis vectors used to define local coordinate system for spline vector computation
$\vec{v}_D$	line vortex contribution to velocity
$V$	region of space
$\vec{V}$	velocity
$\vec{V}_\infty$	freestream velocity
$V_c$	critical speed
$[VIC]$	velocity influence coefficient matrix
$\vec{w}$	linearized perturbation mass flux
$\vec{W}$	total linearized mass flux
$\vec{v}_D$	regular term of doublet velocity
$\vec{x}$	position vector
$(x_0, y_0, z_0)$	reference coordinates
$(x, y, z)$	scaled coordinates
$(x', y', z')$	local coordinates; several local coordinate systems are used in Appendix I
$[XT]$	extension matrix

$[XH]$	half panel extension matrix
$X$	arbitrary boundary condition coefficient
$X$	compressibility coordinate system
$X_0$	reference coordinate system
$\bar{x}$	scaled coordinate system
$x'$	local coordinate system

# Greek Symbols

$\alpha$	angle of attack, rad
$\alpha_c$	angle of attack used for computing compressibility direction, rad
$\beta$	$=  1 - M_\infty^2 ^{1/2}$
$\beta$	angle of sideslip, rad
$\beta_c$	angle of sideslip used for computing compressibility direction, rad
$\gamma$	ratio of specific heats of a gas
$\Gamma$	rotation matrix
$\Gamma_c$	transformation matrix from reference to compressibility coordinates
$\delta_{ij}$	Kronecker delta
$\Delta_i$	$i$ th subpanel, $i = 1, \dots, 8$
$\epsilon$	user-defined tolerance distance for edge matching
$\epsilon$	small quantity whose higher powers may be neglected
$\epsilon_{ijk}$	permutation symbol defined in section B.3
$\kappa$	$= 4\pi$ if subsonic flow, $2\pi$ if supersonic flow
$\kappa$	quantity associated with quadratic function on an edge segment, defined by equation (I.2.27)
$\vec{\lambda}$	vector of singularity parameters
$\lambda_i$	$i$ th singularity parameter
$[A]$	matrix of vectors of unknown singularity parameters
$\mu$	doublet strength at a point on a surface or distribution of doublet strength on a surface
$\mu_i$	panel doublet parameters, $i = 1, \dots, 9$
$\mu_i$	doublet strength at point on the $i$ th network edge of an abutment
$\mu_0$	coefficient defining constant component of doublet variation
$\mu_\epsilon, \mu_\eta$	coefficient defining linear component of doublet variation
$\mu_\epsilon, \mu_\eta, \mu_{\eta\eta}$	coefficient defining quadratic component of doublet variation

$\mu_{EEE}, \mu_{EEn},$	coefficient defining cubic component of doublet variation
$\mu_{Enn}, \mu_{nnn}$	
$\vec{\mu}$	vector of coefficients giving linear component of doublet variation
$\hat{v}$	unit vector normal to plane of symmetry
$\vec{v}$	edge conormal
$(E, n, \zeta)$	local coordinates, panel or subpanel coordinates
$\rho$	density of fluid, kg/m <sup>3</sup>
$\rho_\infty$	density of fluid in freestream, kg/m <sup>3</sup>
$\vec{r}$	vector from control point to corner of $\Sigma ND_p$
$\sigma$	source strength at a point on a surface, or distribution of source strength
$\sigma_i$	panel source singularity parameter, $i = 1, \dots, 5$ , or $i = 1, \dots, 4, 9$
$\sigma_0$	coefficient defining constant component of source variation
$\sigma_E, \sigma_n$	coefficient defining linear component of source variation
$\sigma_{EE}, \sigma_{nn}, \sigma_{En}$	coefficient defining quadratic component of source variation
$\vec{\sigma}$	vector of coefficients giving linear component of source variation
$\Sigma$	denotes summation
$\Sigma$	a panel
$[\Sigma]$	matrix of coefficients giving quadratic components of source variation
$\tau$	stress tensor
$\tau$	compressible inner product of unit edge tangent with itself
$\vec{\tau}$	edge cotangent
$\phi$	perturbation potential
$\phi$	phase or hyperbolic phase, radians
$\Phi$	total potential
$[\Phi IC]$	potential influence coefficient matrix



$\chi$	hyperbolic angle
$\psi$	$1/R$
$\vec{\omega}$	vector describing strength and direction of rotational onset flow

#### Subscripts

A	average of upper and lower
c	denotes compressibility
D	difference of upper and lower
KP	corresponding to known parameters
L	lower
NU	non-updateable
U	upper
U	updateable
UP	corresponding to unknown parameters
0	denotes reference coordinates
1,2,3,4	denotes images of real configuration (first image = input) used to define matrix or vector which is a subset of a higher order tensor (see section 1.4.1.1)

### Superscripts

D	doublet, pertaining to doublet strength
(i)	pertaining to ith symmetrized matrix or vector, $i = 1, 2, 3, 4$
I	input, that is, defined by the user
S	source, pertaining to source strength
T	matrix transpose
-T	inverse of transpose (same as transpose of inverse)
0	unsymmetrized matrix
-	denotes scaled coordinate system
->	denotes a vector
'	denotes local coordinate system
'	image value
*	finite part of integral
~	denotes vector modified by application of metric matrix

# Other Symbols

$\partial$	denotes partial differentiation
$\partial$	boundary of a region
$\nabla$	gradient operator
$\tilde{\nabla}$	compressible gradient operator, see section B.1
$\nabla^2$	$= \tilde{\nabla} \cdot \tilde{\nabla} =$ Laplace operator
$( , )$	Euclidean inner product
$\{ \}$	denotes a column vector or a three-index tensor
$\{ , \}$	dual compressible inner product, see equation (E.2.8)
$L$	denotes a row vector
$[ \ ]$	denotes a matrix
$[ \ ]_{i, \cdot}$	a vector defined by equation (I.4.70)
$[ \ ]_{\cdot, i}$	a vector defined by equation (I.4.71)
$[ \ ]_{ij}$	(i,j) entry of the matrix
$[ \ , \ ]$	compressible inner product, see equation (E.2.4)
$[ \ , \ ]_p$	positive definite compressible inner product, see equation (J.2.7)
$\langle \ , \ \rangle$	pseudo-inner product, see equation (J.6.44)
$\cup$	union of sets of points
$\cap$	intersection of sets of points
$\int$	line integral
$\int \int$	surface integral
$\ll$	very much less than
$\hat{\nabla}_p$	gradient with respect to location of (control point) P
$\hat{\nabla}_q$	gradient with respect to location of (integration point) Q
$\hat{\nabla}_2$	gradient operator in two dimensions
$\hat{\nabla}_x$	curl operator
$\times$	vector cross product operation
$:$	denotes contraction of two matrices, defined by equation (I.6.37)

## 9.0 PAN AIR Engineering Glossary

This glossary defines the most commonly used engineering terms in the PAN AIR Theory and User's Documents. In general, all specialized terms (that is, terms whose meaning in the context of PAN AIR is different from their meaning in common usage) are included, as are standard engineering terms which are used in the PAN AIR engineering documents. Terms which relate to the computing aspects of PAN AIR are defined in a separate glossary, the PAN AIR computing glossary, which is contained in the maintenance document.

The format of the glossary is the following: Each term is followed by a list of principal references and a definition. The references give the section number where the item is discussed, preceded by a T for Theory Document, a U for User's Document, and an S for Summary Document.

<u>ITEM</u>	<u>DEFINITION</u>	<u>REFERENCES</u>
Abutment	A curve where two or more network edges (exactly or approximately) meet.	T-5.3, U-B.3.5
Abutment, empty space	An abutment involving only one network edge, which is thus a free edge.	T-F.2
Abutment intersection	A point where several abutments meet.	T-5.3, T-F.5
Abutments, overlapping	Two distinct user-defined abutments which involve the same portion of some network edge.	Program printout only
Abutments, pairwise	Abutments involving pairs of network edges. They are generated by the program whenever the distance between network edges is less than the tolerance distance.	T-F.2
Abutment parameterization	The assignment of a real number between zero and one to each panel corner or panel edge midpoint in an abutment. Zero is assigned to the starting point, one to the end point.	T-F.6
Abutment, program generated	An abutment generated by the program rather than defined by the user, involving any number of network edges, computed by analyzing pairwise abutments.	T-F.2
Abutment search, automatic	The process by which the program determines the set of all pairwise abutments.	T-F.3
Abutments, user-defined	Any abutment which the program user identifies.	T-F.2
Angle of attack, $\alpha$	The angle of coordinate rotation about the y-axis; this appears in the coordinate transformation (rotation) matrices.	T-5.2, U-B.2.2
Angle of sideslip, $\beta$	The angle of coordinate rotation about the modified z-axis; this appears in coordinate transformation (rotation) matrices.  Note: The effect of the orientation of the flow due to the specification of an angle of attack $\alpha$ and an angle of sideslip $\beta$ corresponds to effect of rotating the configuration through the sideslip angle $\beta$ , followed by a rotation through the angle of attack $\alpha$ .	T-5.2, U-B.2.2

<u>ITEM</u>	<u>DEFINITION</u>	<u>REFERENCES</u>
Area, reference	A user-defined scaling factor for the force and moment coefficient computation.	T-0.1, U-8.4.3
Axis system	A coordinate system in which the force and moment coefficients are expressed.	U-2.1.7, U-8.2.1
Axis system, body	An arbitrary user-defined coordinate system specified by means of Euler angles.	U-2.1.7, U-8.2.1
Axis system, reference	The reference coordinate system (that system in which user defines the configuration geometry).	U-2.1.7, U-8.2.1
Axis system, stability	The coordinate system conventionally used by stability and control engineers.	U-2.1.7, U-8.2.1
Axis system, wind	The coordinate system whose x-axis is aligned with uniform onset flow.	U-2.1.7, U-8.2.1

<u>ITEM</u>	<u>DEFINITION</u>	<u>REFERENCES</u>
Basis function	A function (of surface coordinates) which expresses the distribution due to a unit value of a single singularity parameter.	T-3.3, T-4.2.1
Boundary condition	A linear equation imposed at points on the configuration. This equation specifies some combination of the velocity potential and its derivatives.	T-2.5, T-3.2, T-3.3, T-4.2, T-5.4, T-H
Boundary surface	A surface, defined by the user, on which boundary conditions are imposed.	U-A.3
Boundary condition, aerodynamic	The specific form of boundary conditions for the aerodynamic problem in PAN AIR.	T-K.3
Boundary condition classes	The result of grouping the boundary conditions into five separate categories.	U-B.3.1
Boundary condition, closure	An equation specifying the total normal mass flux passing through a surface.	U-B.3.5, T-5.4, T-5.7.1, T-K.4
Boundary condition coefficient, average, ( ) <sub>A</sub>	The average of upper and lower coefficients.	T-5.4, U-B.3.1
Boundary condition coefficient, difference, ( ) <sub>D</sub>	The difference of upper and lower coefficients.	T-5.4, U-B.3.1
Boundary condition coefficients, upper (lower), ( ) <sub>U</sub> , ( ) <sub>L</sub>	Coefficients in the boundary condition equations corresponding to the upper (lower) side of the configuration.	T-5.4, U-B.3.1
Boundary condition, doublet (or edge) matching	A boundary condition specifying continuity of doublet strength across network edges.	T-5.3, T-5.7.1, I-F
Boundary condition hierarchy	An ordering of all admissible boundary conditions defined by the program. When two user-input boundary conditions are supplied and only one needs to be imposed, the program imposes that boundary condition which is higher on the hierarchy.	T-H.2.5

<u>ITEM</u>	<u>DEFINITION</u>	<u>REFERENCES</u>
Boundary condition, non-standard	Either a closure or a doublet matching boundary condition.	T-5.7.1, U-8.3.5
Boundary condition, right-hand-side	The specified value of the linear combination of the potential and its derivatives given by the boundary condition.	T-5.7.4
Boundary value problem	The combination of a partial differential (or integral) equation and boundary condition equations on a surface.	T-3.2, U-A.3
Boundary value problem, analysis	A boundary value problem with boundary conditions specifying the normal component of the velocity or mass flux.	U-3.3, U-8.3.2
Boundary value problem, design	A boundary value problem in which the boundary conditions specify the values of a tangential component of the velocity on a surface.	T-C, U-8.3.3
Boundary value problem, ill-posed	A boundary value problem which does not have a unique solution, or has no solution.	T-5.4, T-8.1, U-A.3
Boundary value problem, well-posed	A boundary value problem which has a unique solution.	U-A.3, T-3.2, T-5.4, T-8.1



<u>ITEM</u>	<u>DEFINITION</u>	<u>REFERENCES</u>
Column index	An integer which, in conjunction with the row index, describes the indicial location of a panel or a panel corner point. When panel corner points are defined by a user, all the points whose column indices are identical are input consecutively.	U-8.1.1, T-5.1
Compressibility direction	The direction of freestream flow in the Prandtl-Glauert equation. It is defined by the input terms "CALPHA" and "CBETA".	T-5.2, U-8.2.1
Compressibility vector	A unit vector in the compressibility direction.	T-5.2
Configuration	The surface (including possible wakes) on which flow boundary conditions are applied or the potential or velocity is discontinuous.	T-5.1
Configuration, image part	That part of a symmetric configuration which is not input by the user.	T-5.7.2, U-2.1.2
Configuration modeling	The process of representing an object, the flow field about which is of physical interest, as a collection of networks of panels on which boundary conditions are applied.	U-3.1, U-8.1, T-8.2, S-2.2
Configuration modeling, exact	The representation of a physical surface with networks of panels describing the exact physical location of the surface.	U-2.1.4, S-3.1.4
Configuration modeling, linearized	The representation of thickness or deflection of a physical surface by means of a mean surface paneling combined with the specification of boundary conditions which simulate the perturbation of the true surface geometry from the paneled surface.	U-2.1.4, S-3.1.4
Configuration, real part	The user-defined (that is, input) part of a symmetric configuration.	T-5.7.2, U-2.1.2
Configuration symmetry	Existence of one or two (perpendicular) planes through which the real part of configuration may be reflected to obtain the complete configuration.	T-5.7.2, U-2.1.2, U-8.2.3, S-3.1.2

<u>ITEM</u>	<u>DEFINITION</u>	<u>REFERENCES</u>
Configuration, thick	A configuration model in which one surface of a network is exposed to a flow field of interest, while the other surface is exposed to a flow field of no physical interest.	U-2.1.2, T-5.4.2.3, S-3.1.3
Configuration, thin	A configuration model in which both sides of a network are exposed to the flow field of interest. An example arises from the modeling of a wing as a single paneled surface.	U-2.1.2, T-5.4.2.2 S-3.1.3
Conormal vector, $\tilde{n}$	The vector obtained by a Mach number - dependent transformation of a unit surface normal vector. In compressibility coordinates, $\tilde{n} = (sg^2 n_x, n_y, n_z)$ .	T-5.2, T-E.2
Constraint matrix	The right-hand-side term in a multiple system of boundary condition equations, that is, a system of equations with more than one right-hand-side vector.	T-5.7.4, T-L
Constraint number	The right-hand-side term of a single boundary condition equation.	T-3.2
Constraint vector	The right-hand-side term in a system of boundary condition equations with only one right-hand-side vector.	T-3.3, T-5.7.2
Continuity of doublet strength	The condition that a certain alternating sum of doublet strengths along an abutment is zero. This reduces to equality of doublet strengths if two network edges are involved. It permits the elimination of the line vortex term from the integral equation.	T-F
Continuity equation	The equation expressing conservation of mass in a small fluid element.	T-2.1
Control points	The points on a configuration surface at which up to two boundary conditions are applied.	T-3.3, T-5.4, T-G
Control point, center	A control point whose location is recessed slightly from a panel center point.	T-G, U-B.3.4
Control point, corner	A control point whose location is recessed slightly from a panel corner point at the end of an abutment.	T-G, U-B.3.4

<u>ITEM</u>	<u>DEFINITION</u>	<u>REFERENCES</u>
Control point, edge	A control point whose location is receded slightly from a panel edge midpoint on a network edge.	T-G, U-B.3.4
Control points, extra	Control points introduced by the subdivision of a network edge into more than one abutment.	T-5.4, T-G
Control point recession vector	A vector which defines the difference between the location of the control point and the location of the point from which it is receded.	T-G
Compressible gradient operator,	The gradient operator whose component in the freestream direction has been multiplied by $(1-M^2)$ , where $M$ is the freestream Mach number.	T-5.2
Coordinate system, compressibility, $(x, y, z)$	The coordinate system in which the preferred direction of the Prandtl-Glauert equation is the $x$ -direction.	T-5.2, U-B.2.1
Coordinate system, local, $(x', y', z')$	A generally non-orthogonal coordinate system used to compute surface integrals for each subpanel, and generally distinct for each subpanel.	T-5.2
Coordinate system, reference, $(x_0, y_0, z_0)$	An arbitrary rectangular Cartesian coordinate system in which the program user defines the configuration geometry.	T-5.2, U-B.2.1
Coordinate system, scaled, $(x, y, z)$	The non-orthogonal coordinate system in which the Prandtl-Glauert equation transforms to either Laplace's equation or the wave equation.	T-3.1
Coordinate transformation	A linear transformation, defined by a matrix, which transforms point coordinates from one system to another.	T-E, U-B.2.1
Corrections, velocity	Optional semi-empirical corrections applied to the computed velocity.	U-B.4.1, T-5.9.3, T-N.3
Critical speed	The speed of sound at a particular point in the flow field.	U-B.4.2, T-N.2.4.2

<u>ITEM</u>	<u>DEFINITION</u>	<u>REFERENCES</u>
Data check	A run of PAN AIR in which the validity of the configuration geometry and boundary conditions is checked without a potential flow solution being attempted.	U-2.3.1
Differentiated influence coefficients	Matrices which define the derivative with respect to panel or control point location of the potential and velocity induced by a panel on a control point. (Not currently used in PAN AIR.)	T-C.3
Dirichlet problem	A boundary value problem consisting of the specification of potential on the boundary of a region of finite volume.	U-A.3
Discretization	A numerical method for solving an integral equation by replacing continuous quantities with discrete ones.	T-2.5, T-3.3
Displacement modeling	The representation of viscous effects such as a boundary layer by a perturbation of the boundary conditions (through the definition of a specified flow) or the surface paneling.	U-2.1.4
Design capability	The ability to specify a desired pressure distribution on a surface whose shape is only known approximately, and obtain a relofted surface which more nearly yields the desired pressure distribution.	U-2.2, T-C, S-1.0
Design, iterative	A multi-step design procedure in which the relofting algorithm makes use of "differentiated influence coefficients".	T-C.3
Design, linearized	A one-step design procedure in which a first order approximation to the desired surface is sufficient.	T-C.1
Design, sequential	A multi-step design procedure in which the relofting algorithm makes use of the normal mass flux which the program computes on the paneled surface.	T-C.2
Domain of dependence	The spatial domain in which disturbances are felt at a particular point P. It consists of all of space in subsonic flow and the upstream Mach cone from P in supersonic flow.	T-5.2

<u>ITEM</u>	<u>DEFINITION</u>	<u>REFERENCES</u>
Domain of influence	The domain in which disturbances at a point P are felt. It consists of all of space in subsonic flow, and the downstream Mach cone from P in supersonic flow.	T-Figure 5.4
Doublet distribution	One of the two unknown quantities in the fundamental integral equation.	T-3.2, U-A.2
Doublet matching	See boundary condition, doublet matching.	
Doublet parameters	Unknown quantities on which the doublet distribution on the configuration depends.	U-B.3.5 T-5.5
Doublet strength	The value of the doublet distribution at a particular point. It is equal to the size of the jump in velocity potential across the surface.	T-3.1, U-A.2
Drag	The x-component of the force on the configuration in the wind axis system. PAN AIR computes drag on an impermeable surface by integrating the pressure distribution on the surface. The drag computed by PAN AIR does not include viscous effects.	U-2.1.7
Dual vector	A real-valued linear function on a vector space. Dual vectors transform according to equation (E.1.8e) of the Theory Document. Typical dual vectors are the gradient operator and the surface normal. A dual vector is also known as a covariant vector.	T-E.1
Dual vector, almost	A vector transforming according to equation (E.1.12) of the Theory Document.	T-E.1

ITEM	DEFINITION	REFERENCES
Edge conormal	A vector lying in the plane of the panel or subpanel whose "pseudo-inner product" with the edge tangent is zero.	T-J.5.1
Edge function	One of the two basic components (along with the panel function) of the entries of a PIC matrix. It is defined by an integral along a panel or subpanel edge.	T-J.7
Edge force computation	A special computation of forces on the edge of a thin surface, where the small perturbation assumptions may not be valid.	T-5.9.4, T-0.3, U-8.4.3
Edge matching	The problem of imposing appropriate conditions on singularity strength variation across network edges.	T-2.2, U-8.3.5
Edge, nearly sonic	A subpanel or panel edge for which the pseudo-inner product of the edge tangent with itself is approximately zero. Such an edge can only occur in supersonic flow, and is inclined to the flow at approximately the same angle as a Mach cone.	T-J.5.1
Edge, network	That collection of panel edges lying on one extreme of a network and thus not shared by two adjoining panels.	T-D.1, U-8.1.1
Edge normal	A vector lying in the plane of the panel or subpanel and perpendicular to the edge.	T-J.5.1
Edge, panel	A line segment connecting two panel corner points.	T-D.1
Edge, subsonic	A subpanel or panel edge for which the "pseudo-inner product" of the edge tangent with itself is positive.	T-J.5.1
Edge, supersonic	A subpanel or panel edge for which the pseudo-inner product of the edge tangent with itself is negative. Such an edge can only occur in supersonic flow, and is inclined to the flow at a greater angle than the Mach cone.	T-J.5.1
Edge tangent	A unit vector parallel to a panel or subpanel edge.	T-J.5.1

<u>ITEM</u>	<u>DEFINITION</u>	<u>REFERENCES</u>
Energy equation	An equation expressing conservation of energy in a small fluid element.	T-2.1
Entrainment	The phenomenon in which an efflux from a propulsion source absorbs fluid from the surrounding flow as the distance from the configuration increases.	U-2.1.4
Equation of state	An equation relating the pressure, density, and temperature of a fluid.	T-2.1
Euler's equation	A differential equation relating density, velocity, and pressure in a fluid (momentum equation for inviscid fluid without body forces).	T-2.2
Existence of a solution	The problem of determining whether a boundary value problem has at least one solution.	T-B.1, U-A.3
Extension matrix, doublet	A matrix which gives the values of doublet strength at the corners of a subpanel and the "kappa quantities" for its edges in terms of the panel doublet parameters.	T-I.2.2.4
Extension matrix, source	A matrix which gives the values of source strength at the corners of a subpanel in terms of panel source parameters.	T-I.2.1.3

ITEM	DEFINITION	REFERENCES
Far field method	An approximation for the computation of panel influence based upon the distance of the control point from the panel being much greater than distances within panel.	T-4.2.2, T-5.6, T-J.9
Far field moment, subpanel	A matrix or tensor which describes the dependence of a particular integral over a panel on the panel source or doublet parameters.	T-I.4.2.1
Far field moment, basic	Scalars giving the values of certain integrals of polynomial functions over a subpanel.	T-I.4.3
Far field moment, subpanel	A matrix or tensor which describes the dependence of the same integral over a subpanel on the panel singularity parameters.	T-I.4.2.1
Flow symmetry	The existence of one or two (orthogonal) planes of symmetry for the flow field.	T-5.7.2, U-2.1.2, U-8.2.1
Force	For impermeable surfaces, the force is the integral over the surface of the pressure times the surface normal vector. For permeable surfaces, an additional "momentum transfer" term contributes to the force.	U-2.1.7, T-0
Force coefficient	A normalized form of the force vector which removes the force due to the freestream flow and allows for a scaling factor introduced by the user. The force coefficient on an impermeable surface is the integral of the pressure coefficient times the normal vector divided by a user-supplied reference area.	T-0.1, U-8.4.3
Force, edge	See edge force computation.	
Freestream, $\vec{U}_\infty$	The uniform flow which is perturbed by the introduction of a configuration on which boundary conditions are imposed. See also onset flow, uniform, and velocity perturbation.	T-2.3



<u>ITEM</u>	<u>DEFINITION</u>	<u>REFERENCES</u>
Global data	Information (such as symmetry plane locations and the compressibility direction) supplied by the PAN AIR user to describe the configurations as a whole.	U-7
Gradient operator, $\vec{\nabla}$	A vector whose entries are the partial differentiation operation with respect to the coordinate functions.	T-8.1
Grid points	Panel corner points.	T-5.1, U-8.1.1
Grid points, fine or enriched	Rectangular array of points which are corner points, edge midpoints, or center points of quadrilateral (or triangular) panels of a network.	T-5.1, U-8.1.1
Green's theorems	Several relations between spatial integrals and surface integrals. These relations are used to derive the integral equation (8.0.1) of the Theory Document, which PAN AIR solves numerically.	T-3.2

<u>ITEM</u>	<u>DEFINITION</u>	<u>REFERENCES</u>
Influence coefficient	A matrix giving one or more field flow properties as a linear combination of the array of singularity parameters.	T-5.6
Influence coefficient, aerodynamic, AIC	Combination of potential and velocity influence coefficient matrices giving left-hand-side of boundary condition equation as a linear combination of singularity parameters.	T-3.3, T-4.2, T-5.7
Influence coefficient, panel, PIC	Matrix giving perturbations that a source or doublet distribution on a panel induces at a control point.	T-4.2.2, T-5.6, T-J
Influence coefficient, potential, PIC	Matrix giving the perturbation velocity potential at network control points as a linear combination of singularity parameters.	T-4.2, T-5.6
Influence coefficient, velocity, VIC	Same for perturbation velocity.	T-4.2, T-5.6
Intermediate field method	Approximation for computation of panel influence; intermediate between near field and far field methods.	T-5.6, T-J.9
Irrotational flow	Property that the curl of the velocity field is zero; assure existence of velocity potential.	V-2.3

<u>ITEM</u>	<u>DEFINITION</u>	<u>REFERENCES</u>
Jet efflux	A flow emanating from the propulsion unit. A jet efflux may be modeled in PAN AIR by paneling the jet efflux with a wake network.	U-2.1.1
Jet efflux tube	The cylindrical surface surrounding the jet efflux, extending from the configuration to infinity.	U-2.1.1

ITEM

Kappa quantity,  $\kappa$

DEFINITION

A quantity defined for a line segment (generally a panel or subpanel edge) on which a quadratic function is defined. The value of the quantity is the value of the function at an endpoint of the segment plus half the gradient of the function dotted into the difference vector between the positions of the two endpoints.

Kutta condition

The boundary condition imposed at the trailing edge of a lifting surface such as a wing, specifying that the jump in pressure coefficient be zero there.

REFERENCES

T-I.2.2.2

U-A.2, T-B.2

<u>ITEM</u>	<u>DEFINITION</u>	<u>REFERENCES</u>
Laplace's equation	Fundamental partial differential equation saying that divergence of gradient of a scalar is zero.	T-3.2, U-2
Least squares fit, constrained	The process of fitting a function as well as possible to a set of values at a point on a plane. The values need not be known in advance; the result of the process is a matrix giving the defining coefficients of the function in terms of the unknown values.	T-I.1.2.1, T-I.5.1
Length, reference	A user-input length for the scaling of moment coefficients computed by the program.	T-0.1, U-8.4.3
Line vortex term	The line integral in the expression for velocity at a point in space. This integral vanishes if doublet continuity is maintained everywhere.	T-5.6, T-8.3, U-A.2
Lofting	The revision of the geometry of a surface to more nearly attain a pressure distribution specified in a design run.	T-C.2

ITEM	DEFINITION	REFERENCES
M-direction	The direction of increasing panel row index.	U-7.4, U-8.1.1
Mach angle	The angle formed between the freestream direction and a Mach line.	T-J
Mach cone, upstream	A right circular cone located upstream of a field point, containing domain of dependence of that point, in supersonic flow.	T-5.2
Mach disk	The interior of the circle resulting from the intersection of a Mach cone with a plane perpendicular to its axis.	T-J.4.2
Mach - inclined surface	A surface whose normal is perpendicular to its conormal ( $\hat{n} \cdot \tilde{n} = 0$ ). Such a surface is tangent to a Mach cone.	T-5.2, U-8.1.3
Mach line	A straight line generator of the Mach cone. One of the lines of intersection of the Mach cone with a plane containing the origin point of the cone.	T-J
Mach number	The ratio of the speed of the fluid to the speed of sound.	T-2.3
Mach wedge	The set of all point affected by a disturbance on a supersonic edge. The Mach wedge emanates downstream from the edge. A point Q lies in the Mach wedge if some point P on the edge lies in the domain of dependence of Q.	T-J.11
Mass flux, linearized perturbation, $\vec{w}$	The vector obtained by applying the compressible gradient operator to the velocity potential, or by scaling the freestream component of the perturbation velocity by $(1-M_\infty^2)$ . In compressibility coordinates $\vec{w} = (sg^2 u, v, w) = \nabla \phi$ .	T-5.4
Mass flux, total, $\vec{W}$	Produce of local density (normalized by freestream density) and velocity of fluid, $\vec{W} = (\rho/\rho_\infty) \vec{V} = \vec{V} + \vec{w}$ .	T-4.5
Matrix decomposition	Expression of a square matrix as product of lower and upper triangular matrices.	T-5.8

<u>ITEM</u>	<u>DEFINITION</u>	<u>REFERENCES</u>
Metric matrices	Matrices which account for compressibility effects. The first metric matrix (denoted B) multiplies the freestream component of a vector by $(1-M_\infty^2)$ , while the second metric matrix (denoted C) multiplies the component of the vector perpendicular to the freestream by $(1-M_\infty^2)$ .	T-E.2
Minimal data set	A small amount of data (potential, normal mass flux, source and doublet strength) stored for each solution and each control or grid point in anticipation of post-processing.	T-M, U-2.1.1
Modified data set	A small amount of data (potential, normal mass flux, source and doublet strength) stored for each solution and each control or grid point in anticipation of post-processing.	T-M, U-2.3.4
Modeling	See configuration modeling.	
Modified dual vector	A dual vector whose component in the freestream direction has been scaled by $(1-M_\infty^2)$ . A modified dual vector is obtained from a dual vector by the application of the first metric matrix.	T-E.2
Modified vector	A vector whose component perpendicular to the freestream has been scaled $(1-M_\infty^2)$ . A modified vector is obtained from a vector by the application of the second metric matrix.	T-E.2
Moment coefficient, $C_m$	An angular momentum analog of the force coefficient. The moment coefficient contains a user-supplied scaling factor, and is defined by equation (0.1.3) of the Theory Document.	T-0.1, U-8.4.3
Momentum equation	Equation expressing conservation of linear momentum in a small fluid element.	T-2.1
Multiply connected	A region of space is multiply connected if a closed path can be drawn in the region which cannot be shrunk to a point. See also "simply connected."	T-B.1, U-A.3

<u>ITEM</u>	<u>DEFINITION</u>	<u>REFERENCES</u>
N-direction	The direction of increasing panel column index.	U-7.4, U-8.1.1
Navier - Stokes equation	Combination of continuity, momentum, and energy equation for a fluid.	T-2.1
Near field method	Computation of a panel influence coefficient matrix by summing over all eight subpanels the influence of each subpanel.	T-3.1
Network	An indicially rectangular array of panels corner points; basic unit for defining the geometry of the configuration.	T-5.1, U-8.1.1, T-8.1
Network, analysis	Network with singularity parameter locations as required for analysis boundary conditions.	T-5.1
Network, composite	Network having both source and doublet distributions.	T-5.1
Network, design	Network with singularity parameter locations as required for design boundary conditions.	T-5.1
Network, doublet	Network having a (locally quadratic) doublet distribution.	T-5.1
Network gaps	Gaps due to non-coincidence of network edges.	T-4.1, T-5.3
Network, wake	See wake network.	
Network, source	Network having a (locally linear) source distribution.	T-5.1
Network type, doublet	A description of the function performed by the doublet distribution on the network. Doublet types existing are analysis, design, wake, and null; (zero doublet distribution).	T-5.1, T-8
Network type, source	Same for source distribution. Types are analysis, design, and null.	T-5.1, T-8
Network, wake	Network used to model wake surfaces: has continuous normal flow, may have discontinuity in potential across network.	T-5.1, U-8.1.1
Normal vector, unit	See unit normal vector.	



<u>ITEM</u>	<u>DEFINITION</u>	<u>REFERENCES</u>
Onset flow, $\vec{U}$	The user-defined flow field in which the configuration is analyzed. In the simplest case, this is just the uniform freestream flow $\vec{U}_\infty$ .	U-8.2, T-H.3, S-3.1.5
Onset flow, local incremental, $\frac{\Delta \vec{U}}{\Delta t}$	A supplementary term added to the onset flow at individual control points to simulate the superposition of a non-uniform effect (such as a slipstream) onto the freestream.	U-8.2, T-H.3
Onset flow, rotational	A supplementary term added to simulate a rolling or pitching motion.	U-8.2, T-H.3
Onset flow, total, $\vec{U}_0$	The sum of all terms in the onset flow.	U-3.2.1
Onset flow, uniform, $\vec{U}_\infty$	An onset flow which is constant over the entire flow field, and is used to simulate a uniform freestream. The uniform onset flow need not be parallel to the freestream direction $\vec{U}_\infty$ on which compressibility effects are based.	U-8.2, T-H.3

<u>ITEM</u>	<u>DEFINITION</u>	<u>REFERENCES</u>
Panel	Part of a network surface, defined by four network defining points which are indicially adjacent.	T-3.3, T-4.1, T-5.1, T-D.1
Panel, almost non-convex	A panel with an interior angle of nearly 180°.	U-B.1.3, T-D.2
Panel aspect ratio	The ratio of the length of a panel to its width.	U-B.1.3, T-D.2
Panel center point	The point whose coordinates are the average of the coordinates of the four panel corner points.	T-D.1
Panel column	A sequence of panels with the same column index. See column index.	U-B.1.1, T-5.1
Panel corner point	One of the grid of points which defines a network. Four of these points (appropriately adjacent in an indicial sense) are sufficient to construct a panel's geometry.	T-D.1
Panel defining points	The corner points, edge midpoints, and center point of a panel.	T-D.2
Panel diameter	Twice the panel radius.	T-D.2
Panel edge midpoint	The midpoint of a segment connecting adjacent panel corner points.	T-D.1
Panel function	One of the two basic components (along with the edge function) of the entries of a PIC matrix. Defines as an integral over a panel or subpanel.	T-J.7
Panel integral matrix	Matrix giving the velocity and/or potential induced at a control point by a panel or subpanel, in terms of the coefficients of the polynomial describing the source or doublet strength on the region.	T-J.6
Panel method	Method for solving potential flow problems, using panel model of surface to reduce integral equation to a system of linear equations.	T-1.0, T-4.1 U-A.2

<u>ITEM</u>	<u>DEFINITION</u>	<u>REFERENCES</u>
Panel, non-convex	A panel containing interior angles exceeding 180°.	U-8.1.3, T-D.2
Panel radius	The distance.	T-D.2
Panel skewness parameters	Real numbers whose magnitude describe the extent to which a panel fails to be a parallelogram.	T-D.2
Panel, subinclined, superinclined, or Mach-inclined	See subinclined, superinclined, or Mach-inclined surface.	
Panel, triangular	A panel two of whose corner points coincide.	U-8.1.1
Parameterization	See abutment parameterization.	T-J.4.4.2
Perturbation	Change to undisturbed flow field or geometry.	T-2.3, T-A.1
Phase function	Function with two arguments equivalent to the FORTRAN function ATAN2 with arguments reversed. Phase $(x,y) = \arg(x+iy)$ , where $\arg$ is the argument of a complex number.	T-J.4.4.2
Post-processing	The computation of pressures, or forces and moments from the minimal data set.	U-2
Potential	See velocity potential.	
Potential flow	Fluid flow characterized by the existence of a velocity potential function, satisfying a particular partial differential equation, whose gradient at a point is the velocity there.	T-2, T-A
Prandtl-Glauert equation	Partial differential equation for compressible flow: divergence of compressible gradient of perturbation velocity potential is zero.	T-2.5, T-A, S-2.0, U-A.1

ITEM	DEFINITION	REFERENCES
Preferred directic	In the solution of the potential flow problem (that is, the construction and solution of the system of linear equation), it is the compressibility direction. In post-processing, it is the user-specified x-direction in which velocity = (u,v,w) for the computation of the pressure coefficient.	T-N.3, U-B.2.1
Pressure, P	Force per unit area.	T-N.1, U-B.4.2
Pressure coefficient, Cp	A normalized expression for pressure which removes the contribution of the freestream flow to the pressure.	T-N.2.1, U-B.4.2
Pressure coefficient, isentropic	A formula for pressure coefficient resulting from certain basic assumptions about the character of the fluid flow.	T-N.2.1, U-B.4.2
Pressure coefficient, linear	A formula for pressure coefficient resulting from the additional assumption that second order terms in perturbation quantities are negligible.	T-N.2.5, U-B.4.2
Pressure coefficient, reduced second order	A formula for pressure coefficient based on the second order assumption and the additional assumption that terms containing the Mach number squared are negligible.	T-N.2.5, U-B.4.2
Pressure coefficient, second order	A formula for the pressure coefficient resulting from the additional assumption that third powers of perturbation quantities are negligible.	T-N.2.4, U-B.4.2
Pressure coefficient, slender body	A formula for pressure coefficient based on the second order assumption and the additional assumption that second order terms in the component of velocity parallel to the freestream are negligible.	T-N.2.5, U-B.4.2
Pressure coefficient, vacuum	The most negative value the isentropic pressure coefficient can attain.	U-B.4.2, T-N.2.4.1
Pseudo-inner product	Modified inner product, one of whose terms is scaled to account for compressibility.	T-J.5.1

<u>ITEM</u>	<u>DEFINITION</u>	<u>REFERENCES</u>
Recession vector	See control point recession vector.	
Refinement of paneling	The paneling along one network edge is a refinement of the paneling along a second network edge on the same abutment if the first edge has a panel corner point wherever the second edge has a panel corner point.	T-1.1.2.5
Region, exterior	Spatial region outside a finite surface.	T-3.2
Region, interior	Spatial region inside a finite surface.	T-3.2
Right-hand-side	See boundary condition, right-hand-side.	
Row index	An integer which, in conjunction with the column index, describes the indicial location of a panel or panel corner point. When the panel corner points are input by the user all points with the same column index are input consecutively. For each column of points input by the user, the row index runs consecutively from 1 to the maximum row index.	T-5.1, U-8.1.1

<u>ITEM</u>	<u>DEFINITION</u>	<u>REFERENCES</u>
Shear layer	A surface in the flow field on which the velocity tangential to the surface is discontinuous. A shear layer is modeled in PAN AIR by means of a wake network.	U-2
Simply connected	A region of space in which any path may be shrunk to a point. See also "multiply connected" and Figure B.8 of the Theory Document.	T-B.1, U-A.3
Singularity parameters	Unknown in system of linear equations constructed by a panel method.	T-3.3
Singularity parameters, unknown	Singularity parameters specified by a single boundary condition equation.	T-5.7.2, T-5.7.3, T-K.2
Singularity parameter, panel	The value of source strength at one of five panel points (corners or center) or the value of doublet strength at the nine panel defining points.	T-1.1, T-1.2
Singularity type	The source of doublet type of network. This may be analysis, design, wake 1 or wake 2 (for doublets only), or null.	U-A.2
Slipstream	The flow field induced by a rotating propeller.	T-H.3
Small perturbation assumptions	Assumptions that certain quantities are small enough that their higher powers may be ignored. The Prandtl-Glauert equation holds for irrotation, isentropic, inviscid flow in which certain small perturbation assumptions have been satisfied.	T-A.1
Solution list	A list of different constraints under which the system of linear equations is to be solved. Typically, a list of solutions might consist of several angles of attack and/or sideslip.	U-7
Solution vector	The vector of unknowns in the system of linear equations.	T-5.7.4
Source distribution	One of two unknown quantities in the fundamental integral equation.	T-3.2, U-A.2

<u>ITEM</u>	<u>DEFINITION</u>	<u>REFERENCES</u>
Source parameters	Known or unknown quantities on which the source distribution on the configuration depends.	T-5.5
Source strength, $\sigma$	The value of the source distribution at a particular point. It is equal to the size of its jump in normal mass flux across the surface.	T-3.2, U-A.2
Specified flow, $b$	The right-hand side term in a boundary equation. That is, some combination of potential and velocity is specified by the equation to equal $b$ .	U-B.3
Spline	The method by which a function on a surface is obtained from the specification of values of the function at a discrete set of points on the surface.	T-I
Spline, edge	The method by which doublet spline vectors are constructed for five grid points on the edge of a network.	T-1.1.2
Spline matrix, outer	A matrix giving values of (five source or nine doublet) panel singularity parameters values in terms of surrounding singularity parameters.	T-1.1
Spline matrix, subpanel (or panel or half panel)	A matrix giving the singularity distribution on subpanel (or panel or half panel) in terms of panel singularity parameters.	T-4.2.1.1, T-5.5, T-1.2, T-1.3.1, T-1.3.2
Spline, two-dimensional	The method by which a function on a line segment is obtained from the specification of values of the function at a discrete set of points on the line segment.	T-C.4
Spline vector	A row vector giving source or doublet strength at a fine grid point in terms of surrounding singularity parameters.	T-I.1
Stability	The property of a spline, in conjunction with a set of boundary conditions, that a perturbation in the boundary conditions at one point causes a disturbance in the solution which decreases rapidly with distance from the point.	T-C.4

<u>ITEM</u>	<u>DEFINITION</u>	<u>REFERENCES</u>
Stagnation to ambient	Flow which is no faster than freestream (ambient) flow, yet not highly perturbed as to have a negative component in the freestream direction. Such a flow may be corrected using the semi-empirical "velocity corrections".	U-8.4.1
Stagnation, perturbation	A point at which the perturbation velocity is zero.	T-5.4.2.3
Stagnation, total	A point at which the total velocity is zero.	T-5.4.2.3
Subinclined surface	A surface for which the inner product of normal and conormal is positive. All surfaces are subinclined in subsonic flow.	U-8.1.1, T-5.2
Subpanel	A flat triangular surface which is the basic unit of the panel analysis in PAN AIR (a panel consists of eight subpanels).	T-4.2.1.1, T-5.1
Subpanel, subinclined, superinclined, or Mach-inclined	See subinclined, superinclined, or Mach-inclined surface.	
Subsonic flow	Flow for which the Mach number is less than one.	T-3.1, U-2.0, S-1.0
Superinclined surface	A surface for which the inner product of normal and conormal is negative. Such a surface is inclined to the freestream at more than the Mach angle.	U-8.1.1, T-5.2
Supersonic flow	Flow for which the Mach number is greater than one.	T-3.1, U-2.0, S-1.0
Surface, lower	The side opposite to the upper surface.	T-5.4, U-A.3.1
Surface, upper	The side of the surface bounding the region into which the unit normal points. An exception is that for post-processing only, upper and lower surfaces are switched by means of the "reverse" option.	T-5.4, U-A.3.1
Symmetry, plane of	A plane such that either the flow or the configuration geometry is left unchanged if reflected in this plane.	U-2.1.2, U-8.2.3, T-K.1



<u>ITEM</u>	<u>DEFINITION</u>	<u>REFERENCES</u>
Tangent vector	A vector perpendicular to the surface normal.	T-5.4
Thick body	See configuration, thick.	
Thin body	See configuration, thin.	
Tolerance distance	A distance supplied by the user. The program searches for network edges which lie closer together than the tolerance distance, and forms pairwise abutments for these edges.	T-F.2, U-3
Total	The sum of a freestream quantity and a perturbation quantity.	U-A.1
Transformation, orthogonal	A length-preserving coordinate transformation.	T-E.3

<u>ITEM</u>	<u>DEFINITION</u>	<u>REFERENCES</u>
Update, 1C	The capability allowing reuse of AIC's for some networks when modifying other networks.	T-5.7.5, T-K.6, S-3.3.3, U-2.3.2
Update, solution	Capability of storing AIC's and reusing them later in a new problem in which only the boundary condition constraints have been changed.	U-2.3.2, T-L, T-5.8, S-3.3.2
Unit normal vector, $\hat{n} = (n_x, n_y, n_z)$	A vector of length 1 which is perpendicular to a surface. Its direction is defined as the direction of increasing column index cross the direction of increasing row index.	T-D.2

<u>ITEM</u>	<u>DEFINITION</u>	<u>REFERENCES</u>
Velocity, $\vec{v}$	The time rate of position change of fluid particles.	T-2.1, U-A.1
Velocity computation method	One of two methods of computing the velocity at a point from the minimal data set. The boundary condition method attempts to obtain data from boundary conditions and spline it, while the VIC method obtains the velocity from the product of a velocity influence coefficient matrix with the vector of singularity parameters.	U-2.1.6
Velocity, perturbation, $\vec{v}$	The difference between total velocity and that of the undisturbed fluid.	T-2.3, U-A.1
Velocity potential, $\phi, \Phi$	The function whose gradient is the velocity, $\vec{v} = \vec{\nabla}\phi$ , $\vec{v} = \vec{\nabla}\Phi$ .	T-2.3, U-A.1
Vorticity, surface, $\vec{\gamma}$	The cross product of surface normal vector and doublet gradient, $\vec{\gamma} = \vec{n} \times \vec{\nabla}\phi$ .	U-A.2, T-5.6.2

<u>ITEM</u>	<u>DEFINITION</u>	<u>REFERENCES</u>
Wake, physical	A sheet of vorticity shed from the physical configuration.	T-5.1, T-8.2
Wake network	A network used by PAN AIR to model a physical wake. The normal mass flux is continuous on such a network, while the potential and tangential velocity may be discontinuous.	T-5.1, T-8.2
Wave equation	A particular hyperbolic partial differential equation. PAN AIR solves this equation when the Mach number is $\sqrt{2}$ .	T-3.1
Wetted surface	A surface is wetted by a region of space of it borders on that region.	U-A.3

## A.0 Fundamental Fluid Mechanics

To repeat our warning in section 1, this document is not meant to be a text in basic fluid mechanics (several basic references are listed in section 1). We will not discuss the derivations of the equations which lead to the Prandtl-Glauert equation, nor will we discuss the assumptions of irrotational, inviscid, steady, and isentropic flow which lead to the Prandtl-Glauert equation. We will, however, briefly discuss the "small perturbation" assumptions, since these assumptions pervade both the theory and usage of panel methods, and hence determine the application and validity of the methods to particular problems.

## A.1 The Small Perturbation Assumptions

Recall from section 2.3 that we assumed

$$|\vec{v}| \ll |\vec{V}| \ll a_\infty \quad (\text{A.1.1})$$

To be precise, the transonic small perturbation equation is obtained by assuming (in addition to irrotational, inviscid, isentropic flow) that terms of order  $|\vec{v}|^2/a^2$  can be ignored. Recall that  $\vec{v}(x,y,z)$  is the perturbation of the local velocity from a uniform freestream  $\vec{V}_\infty$ . Assumption (A.1.1) holds under a wide variety of cases, including

- a thin wing at small angle of attack (shown in figure A.1) at any Mach number other than approximately 1,
- a blunt object at small Mach number (see figure A.2)
- a static airplane configuration with engines on, sucking in air, with local velocities in the inlet duct which are small compared to the speed of sound:

$$|\vec{v}| = |\vec{V}| \lesssim .2a_\infty \quad (\text{A.1.2})$$

(see figure A.3).

In case (a), both  $|\vec{v}|/|\vec{V}|$  and  $|\vec{v}|/a_\infty$  are small. In case (b),  $|\vec{v}|$  is of the same order as  $|\vec{V}_\infty|$ , and so we are ignoring terms of size

$$|\vec{v}|^2/a^2 \approx (.1)^2 = .01 \quad (\text{A.1.3})$$

Similarly, in case (c), we ignore terms of size

$$|\vec{v}|^2/a^2 \approx (.2)^2 = .04 \quad (\text{A.1.4})$$

which is still small with respect to one.

But now, let us reconsider case (c), with

$$|\vec{v}|/a_\infty = .7 \quad (\text{A.1.5})$$

In that case, assumption (A.1.1) no longer holds, since we are ignoring terms of order  $.7^2 = .49$ , which are not small compared to 1.

Thus, the "engine-on" problem does not satisfy the small perturbation transonic equation, let alone the Prandtl-Glauert equation, if the "local Mach number" ( $|\vec{v}|/a$ ) is too large. This does not mean that PAN AIR has no use for such a problem. Its use, however, is restricted to predicting qualitative trends, rather than detailed pressure distributions. Note that as the forward speed of the airplane increases, the perturbation velocity within the duct decreases, and equation (A.1.1) is more nearly satisfied.

Now, let us examine the small perturbation steady transonic equation (assuming  $M_\infty = 1$ ):

$$\begin{aligned} (1-M_\infty^2) \phi_{xx} + \phi_{yy} + \phi_{zz} = M_\infty^2 [1/2 (\gamma-1) (2u + |\vec{V}|^2) \nabla^2 \phi + \\ (2u + u^2) \phi_{xx} + v^2 \phi_{xy} + 2vw \phi_{yz} + w^2 + w^2 \phi_{zz} \\ + 2(1+u)(v \phi_{xy} + w \phi_{xz})] \end{aligned} \quad (A.1.6)$$

Since  $|\vec{V}|^2 = u^2 + v^2 + w^2$ , all the terms on the right side of (A.1.6) are quadratic or cubic expressions in the first or second derivatives of  $\phi$ , while the terms on the left hand side are linear expressions in the derivatives of  $\phi$ . So, formally, it is justifiable to drop all the terms on the right, and say that to first order, the Prandtl-Glauert equation

$$(1-M_\infty^2) \phi_{xx} + \phi_{yy} + \phi_{zz} = 0 \quad (A.1.7)$$

holds (where the freestream direction is the x-direction).

But a formal elimination of all quadratic and cubic terms only has meaning if the terms being ignored are in fact small, compared to the terms which are being retained.

We can rewrite (A.1.6) as

$$\begin{aligned} [(1-M_\infty^2) + A] \phi_{xx} + B \phi_{xy} + C \phi_{xz} \\ + (1+D) \phi_{yy} + E \phi_{yz} + (1+F) \phi_{zz} = 0 \end{aligned} \quad (A.1.8)$$

where

$$\begin{aligned} A &= -M_\infty^2 [1/2(\gamma-1) (2u + |\vec{V}|^2) + (2u + u^2)] \\ B &= -2M_\infty^2 (1+u)v \\ C &= -2M_\infty^2 (1+u)w \\ D &= -M_\infty^2 [1/2(\gamma-1) (2u + |\vec{V}|^2) + v^2] \\ E &= -2M_\infty^2 v w \\ F &= -M_\infty^2 [1/2(\gamma-1) (2u + |\vec{V}|^2) + w^2] \end{aligned} \quad (A.1.9)$$

Now, (A.1.7) holds if the sum of all the ignored terms is small compared to each of the retained terms, that is, if

$$\begin{aligned} A \ll 1-M_\infty^2 \\ S = A + B + C + D + E + F \ll 1 \end{aligned} \quad (A.1.10)$$

Adding the terms in (A.1.9)

$$\begin{aligned} S \leq M_\infty^2 & [3/2(\gamma-1)(2|u| + |\vec{v}|^2 \\ & + 2v + u^2 + 2|1+u|(|v| + |w|) \\ & + v^2 + 2|vw| + w^2)] \end{aligned} \quad (\text{A.1.11})$$

Now, since the absolute value of a sum is at most the sum of the absolute values,

$$\begin{aligned} S \leq M_\infty^2 & [3(\gamma-1)|u| + 3/2(\gamma-1)|\vec{v}|^2 + 2|u| + u^2 \\ & + 2|\vec{v}| + 2|w| + 2|uv| + 2|vw| + v^2 + 2|vw| + w^2] \end{aligned} \quad (\text{A.1.12})$$

Now, since  $|u|$ ,  $|v|$ , and  $|w|$  are  $\leq |\vec{v}|$  and all products of these are  $\leq |\vec{v}|^2$ , we obtain

$$\begin{aligned} S \leq M_\infty^2 & [(3(\gamma-1)+2+2+2)|\vec{v}| + \\ & (3/2(\gamma-1)+1+2+2+1+2+1)|\vec{v}|^2] \end{aligned} \quad (\text{A.1.13})$$

$$\text{or} \quad S \leq M_\infty^2 [(3+3\gamma)|v| + 15/2 + 3/2\gamma)|\vec{v}|^2] \quad (\text{A.1.14})$$

$$\text{or} \quad S \leq M_\infty^2 k(\gamma)[|\vec{v}| + |\vec{v}|^2] \quad (\text{A.1.15})$$

$$\text{where} \quad k(\gamma) = \max(3+3\gamma, 15/2 + 3/2\gamma) \quad (\text{A.1.16})$$

depends only on the gas. For diatomic gases,  $\gamma = 7/5$ , and thus  $k(\gamma) = 9.6$ .

Thus, we see that (A.1.10) holds if

$$M_\infty^2 k(\gamma)[|\vec{v}| + |\vec{v}|^2] \ll 1 \quad (\text{A.1.17})$$

$$\text{and} \quad M_\infty^2 k(\gamma)[|\vec{v}| + |\vec{v}|^2] \ll 1 - M_\infty^2 \quad (\text{A.1.18})$$

(since  $|A| \leq |S|$ ).

Recall from section 2.3 that  $|\vec{v}_\infty| = 1$ ; thus  $|\vec{v}|$  is the size of the perturbation velocity divided by the freestream speed.

For Mach numbers  $< \sqrt{2}$ , (A.1.18) is the more restrictive equation, while for  $M_\infty > \sqrt{2}$ , (A.1.17) is more restrictive. Equations (2.5.2) and (2.5.3) are simplifications of (A.1.17) and (A.1.18), based on a scaling by a factor of  $2k(\gamma)$  of what we mean by "very much less than", and based on the assumption

$$|\vec{v}|^2 \leq |\vec{v}| \quad (\text{A.1.19})$$



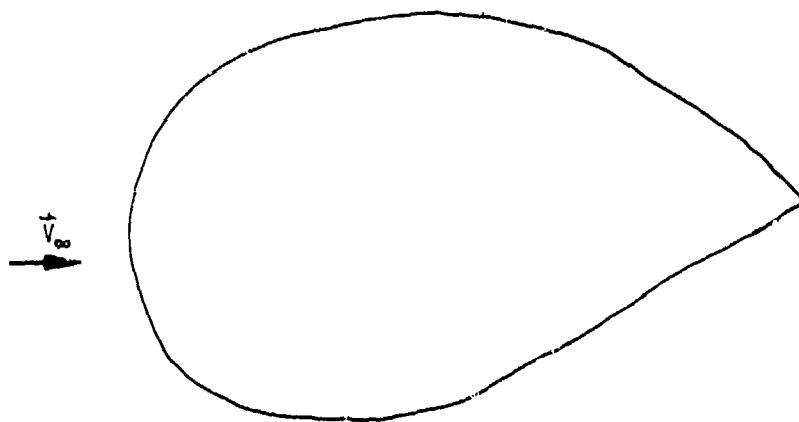
Equation (A.1.19) holds in virtually all cases of aerodynamic interest, since we have assumed that  $|\vec{V}_\infty| = 1$ , that is, we are not dealing with the "engine-on" case, in which  $|\vec{V}_\infty| = M_\infty = 0$ .

From (A.1.17) and (A.1.18), we derive the principle that the more nearly transonic or the more hypersonic the flow becomes, the smaller the perturbations to the free stream must be. Small perturbations, in turn, mean slender objects and small angles of attack. This does not mean, however, that PAN AIR is of no use if the restrictions (A.1.17) or (A.1.18) are violated locally. Experimentation has shown that, for instance, wings with rounded leading edges can be successfully analyzed at Mach numbers such as .7, at which (A.1.17) is thoroughly violated. This is true because the Prandtl-Glauert equation is only violated in a small region of space, and the quality of the solution in other areas is not affected. Further, semi-empirical velocity correction formulas (see section 5.9) are available. Pressures calculated from the correction velocity agree more accurately with those determined by experiments. Thus a fairly accurate approximation to the true flow properties can be obtained in this case despite the violation of the assumptions behind the Prandtl-Glauert equation.



$M_\infty = .1$   
 or  $M_\infty = .9$   
 or  $M_\infty = 3$

Figure A.1 - Thin Wing at small angle of attack



$M_\infty = .1$

Figure A.2 - Blunt object at small mach number

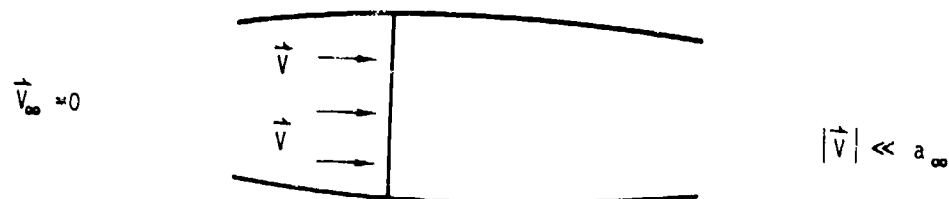


Figure A.3 - Small perturbation "engine-on" case

## B.0 The Prandtl-Glauert Equation

In this appendix, we discuss some basic results concerning solutions of the Prandtl-Glauert equation. We make no effort to prove results which are proved in any of the standard references, but we will supply derivations of results which are not available elsewhere.

The basic step in analyzing solutions  $\phi(x,y,z)$  of the Prandtl-Glauert equation is to convert it to the integral equation

$$\phi(x,y,z) = \frac{1}{K} \iint_{S \cap D_p} \left[ \frac{-\sigma(Q)}{R} + u(Q) \hat{n} \cdot \nabla \left( \frac{1}{R} \right) \right] dS \quad (B.0.1)$$

where  $S \cap D_p$  is the intersection of the configuration surface  $S$  with the domain of dependence  $D_p$  on the point  $P=(x,y,z)$ ,

$$\begin{aligned} \sigma &= \nabla(\phi_U - \phi_L) \cdot \hat{n} \\ \hat{n} &= \text{unit surface normal} \\ u &= \phi_U - \phi_L \\ Q &= (\xi, \eta, \zeta) \\ R^2 &= (\xi - x)^2 + s\beta^2(\eta - y)^2 + s\beta^2(\zeta - z)^2 \\ s &= \text{sign}(1 - M_\infty^2) \\ \beta^2 &= 1 - M_\infty^2 \\ K &= \begin{cases} 2\pi & \text{if } s = -1 \\ 4\pi & \text{if } s = +1 \end{cases} \quad \text{and} \\ \nabla_Q &= \begin{Bmatrix} s\beta^2 \partial/\partial\xi \\ \partial/\partial\eta \\ \partial/\partial\zeta \end{Bmatrix} \end{aligned} \quad (B.0.2)$$

The asterisk refers to the fact that for supersonic flow we only take the "finite part" of the integral, a concept defined in section 3.4 of Ward (1.5), and in section J.6.7 of this document.

Equation (B.0.1) is derived for subsonic flow in Ward, Chapter 2, and for supersonic flow in Chapter 3. A more thorough derivation is given for  $M_\infty = 0$  in Kellogg (1.3), p. 221, and for  $M_\infty > 1$  in Ehlers, et al. (4.8), sections 3.5 and 3.7.

In this appendix, we discuss the concept of a boundary value problem, that is, the combination of (B.0.1) with a set of boundary conditions. In section B.1, we discuss boundary value problems for which existence and uniqueness of a solution have been proved or disproved. In B.2, we discuss the role of wakes in the formulation of a boundary value problem. And finally, in B.3, we show that the gradient of (B.0.1), defining  $v(x,y,z)$ , can be replaced by a different expression which is more readily computable. All of the material in this appendix is "background" material; none of it is reflected in the actual PAN AIR computer code.

We emphasize that Pan Air actually solves the integral equation (B.0.1), with boundary conditions imposed on the true configuration geometry (cf., (3.1.3)) while other panel methods solve the integral equation corresponding to Laplace's equation with zero normal velocity boundary conditions applied on the scaled geometry. These methods can be demonstrated to be equivalent in subsonic flow (cf., Butter, reference B.1), and go under the general name "Gothert's rule".

We note that the two versions of Gothert's rule are equivalent only in subsonic flow. This is because the scaling (3.1.3) in subsonic flow yields an "equivalent incompressible geometry", and at zero Mach number mass flux is identical to velocity. In supersonic flow, on the other hand, application of (3.1.3) yields an "equivalent geometry" corresponding to a Mach number of  $\sqrt{2}$ . But at this Mach number, velocity and mass flux are not identical; rather, the freestream components of perturbation velocity and mass flux have opposite sign. Thus normal mass flux and normal velocity boundary conditions are inherently different in supersonic flow.

In addition, some European panel methods use yet another method, referred to as Gothert Rule 2, to account for compressibility effects in subsonic flow. In this method, the Prandtl-Glauert equation is solved, with boundary conditions of normal velocity (rather than normal mass flux) applied on the true configuration. This method is not equivalent to either of the two equivalent versions of Gothert's rule described above.

## B.1 Existence and Uniqueness

In this section, we give four examples of boundary value problems which are well-posed (that is, for which there exists a unique solution), and two examples of ill-posed boundary value problems. Finally, we discuss two boundary value problems for which excellent numerical results have been obtained, without any actual proof that the problem is well-posed.

The first well-posed problem is the subsonic exterior Neumann problem. A Neumann problem is the specification of normal mass flux on the boundary of a region  $R$ . If  $R$  is an infinite region with finite boundary as illustrated in figure B.1 or figure B.3, the boundary value problem is called "exterior" since the boundary of  $R$  is the "outer" surface of  $S$ . The precise formulation of the result (see p. 311 of Kellogg, 1.3) is: The specification of a continuous distribution of  $\hat{n} \cdot \nabla \phi$  on the boundary  $S$  of an infinite region  $R$  yields a unique distribution of potential  $\phi$ , whose value approaches zero at infinity on  $R$ , satisfying the Prandtl-Glauert equation, for  $M_\infty < 1$ . Kellogg only proves this result for  $M_\infty = 0$ , but the coordinate scaling (3.1.3) (which reduces the Prandtl-Glauert equation to Laplace's equation in the scaled coordinates) allows one to prove the result for arbitrary subsonic Mach numbers.

The second well-posed boundary value problem is the interior subsonic Dirichlet problem (a Dirichlet problem is the specification of  $\phi$  on a surface). Again, this is shown to be well posed (see Kellogg, p. 311) for  $M_\infty = 0$ , and is formulated precisely as follows: Let  $R$  be a region of finite volume (see figure B.2). Then the specification of a continuous distribution of  $\phi$  on the boundary  $S$  of  $R$  is a well-posed boundary value problem. Further, if the specification of  $\phi$  is a constant  $b$ , then  $\phi$  is identically equal to  $b$  in all of  $R$ .

The third well posed boundary value problem is discussed in Ward, 1.5, section 4.13, and is formulated as follows. Let  $S$  be a finite smooth surface (see figure B.3) which is everywhere inclined behind the Mach angle (such a surface has  $\hat{n} \cdot \hat{n} > 0$ , and is called subinclined). The specification of a continuous distribution of  $\hat{w} \cdot \hat{n}$  on both sides of  $S$  defines a unique value of  $\phi$  in all of space for  $M_\infty \neq 1$ . For  $M_\infty < 1$ , this is just a special case of the first boundary value problem discussed above.

The fourth well-posed boundary value problem is illustrated in figure B.4. There,  $S$  is a smooth superinclined surface ( $\hat{n} \cdot \hat{n} < 0$ , which automatically implies  $M_\infty > 1$ ). Then, the specification of continuous distributions of both  $w_n$  and  $\phi$  on the downstream side of  $S$  is a well posed boundary value problem, and once again is discussed by Ward in section 3.2.

Now let us consider two ill-posed boundary value problems. The first is the interior Neumann boundary value problem, that is, the specification of  $w_n$  on the boundary of a region  $R$  of finite volume, as illustrated in figure B.5. The proof that no unique solution exists is simple. Suppose a certain function  $\phi(x,y)$  were a solution. Then, for any constant  $\phi_0$ ,  $\phi(x,y,z) = \phi_0$  is also a solution, since  $\nabla \phi_0 = 0$  and thus the normal mass flux ( $\hat{n} \cdot \hat{n} = \hat{\nabla} \phi \cdot \hat{n}$ ) is unchanged. Thus, there cannot exist a unique solution  $\phi$ , and so the problem is ill-posed.

A second example of an ill-posed boundary value problem is the specification of  $\phi$  or  $\vec{w} \cdot \hat{n}$  on the upstream side of a superinclined surface. Consider, for instance, the point P in figure B.4. According to the integral equation (B.0.1),  $\phi(P)$  is an integral over  $S \cap D_P$ . But the intersection of S with  $D_P$ , the domain of dependence of the point P, is empty. That is, there is no point on S which influences P, since the domain of dependence consists of the interior of a cone pointing upstream from P, as illustrated in figure B.6.

So,  $\phi(P) = 0$ , regardless of the source or doublet distribution on S. Further, this holds for all points P on the upstream side of S. So, specifying  $\phi = b$  or  $\vec{w} \cdot \hat{n} = b$  on the upstream surface of S results in infinitely many solutions if  $b = 0$ , and no solutions if  $b \neq 0$ . Thus, no matter what our choice of  $b$ , upstream specification is an ill-posed boundary value problem.

This discussion of ill-posed and well-posed boundary value problems is of some interest to the user of PAN AIR because of a basic principle. This principle is that the use of a panel method to solve an ill-posed boundary value problem invariably leads to a system of linear equations whose matrix is singular. Even if the system of equations has infinitely many solutions, the numerical equation solving techniques used by panel methods break down, and none of the solutions can be found.

On the other hand, the lack of a proof that a particular boundary value problem is well-posed should not be an impediment to attempting to find a numerical solution. The prime examples of this are the successes achieved by the "pilot code" in solving the exterior Neumann problem and interior Dirichlet problem for subinclined surfaces in supersonic flow (see figures B.1 and B.2). Specific cases are described in Ehlers, et al., (4.9). A second example is the specification of design boundary conditions, a subject which will be discussed in more detail in Appendix C.

Summarizing, for a thick closed configuration such as that of figure B.2, one is fairly safe (assuming that the surface is subinclined when  $M > 1$ ) in imposing the boundary conditions

$$\phi_L = 0 \quad (B.1.1)$$

$$\vec{w}_U \cdot \hat{n} = 0$$

which, as pointed out in section 5.4, is equivalent to

$$\begin{aligned} \phi_L &= 0 \\ \sigma &= -\vec{v}_\infty \cdot \hat{n} \end{aligned} \quad (B.1.2)$$

Here, the subscripts U and L refer to upper and lower surfaces. For thin configurations such as that in figure B.3, the boundary conditions should be (assuming the surface is subinclined again)

$$\begin{aligned} \vec{w}_U \cdot \hat{n} &= 0 \\ \vec{w}_L \cdot \hat{n} &= 0 \end{aligned} \quad (B.1.3)$$

or, equivalently

$$\begin{aligned}\vec{W}_U \cdot \hat{n} &= 0 \\ \sigma &= 0\end{aligned}\tag{B.1.4}$$

For a permeable surface inclined to the freestream, as shown in figure B.7, the boundary conditions for subsonic flow should be

$$\begin{aligned}\phi_L &= 0 \\ \vec{W}_U \cdot \hat{n} &= b\end{aligned}\tag{B.1.5}$$

or equivalently

$$\begin{aligned}\phi_L &= 0 \\ \sigma &= -\vec{V}_\infty \cdot \hat{n} + b\end{aligned}\tag{B.1.6}$$

while for supersonic flow they should be

$$\begin{aligned}\phi_L &= 0 \\ \vec{W}_L \cdot \hat{n} &= b\end{aligned}\tag{B.1.7}$$



## B.2 Wakes and Modeling

Up to this point, we have implicitly assumed that the surface  $S$  on which non-zero source or doublet distributions are given represents a real physical object. But for a wide variety of problems of physical interest, it does not suffice to impose boundary conditions of impermeability on the physically existing configuration. The general problem of determining the surface  $S$ , and what boundary conditions should be imposed there, is called the modeling problem, and will be discussed here briefly.

The first case of a non-physical surface  $S$  arises from one of the hypotheses of Green's Theorem which we ignored when discussing the subject in section 3.2. This hypothesis requires that the region  $V$  on which  $\phi$  is defined be "simply connected". That is, there must not be any closed path in  $V$  which cannot be shrunk to a point within  $V$ . In figure B.8, we illustrate in cross section a region  $V$ , whose boundary  $S$  is the surface of a nacelle, which fails to be simply connected. The imposition of boundary conditions of impermeability on  $S$  once again results in an ill-posed boundary value problem.

The boundary value problem can be made well-posed by the addition of a surface  $S'$  which "blocks off" the inlet. The surface  $S'$  is not impermeable, however; so the user specifies the total normal mass flux  $b$  flowing through the surface. The boundary conditions illustrated in figure B.7 only apply to subsonic flow, though. For supersonic flow, upper surface normal mass flux must not be specified on the superinclined surface  $S'$ ; instead, the boundary condition

$$\begin{aligned}\vec{W}_L \cdot \hat{n} &= b \\ \phi_L &= 0\end{aligned}\tag{B.2.1}$$

should be imposed.

The second case in which the surface  $S$  includes non-physical surfaces arises not from theoretical but from empirical considerations. These considerations arise from the fact that the assumption of zero viscosity is invalid near the trailing edge of a wing. No matter how small the viscosity of the fluid, the conditions at the trailing edge are considerably different from those of the zero viscosity case. The difference is the following: at zero viscosity, the velocity at the trailing edge of a wing becomes infinite, while at any non-zero viscosity, the velocity is bounded by a fixed number which depends mostly on the wing geometry and Mach number, and is only weakly dependent on the viscosity.

In order to reproduce this effect while using a program which ignores viscous effects, the concept of a wake is introduced. A wake is a surface across which the normal mass flux is continuous, while the potential and the tangential velocity are not. Thus, source strength is zero on a wake, while doublet strength  $\mu$  is non-zero, and the jump in tangential velocity is  $\nabla\mu$ . The actual physical situation, namely that the tangential velocity varies very rapidly in a small region of space, is modeled quite well by this type of surface.

In modeling a configuration, wakes are generally inserted in a roughly streamwise direction emanating from the trailing edges of all "lifting surfaces" such as wings, fins, etc. The exact location of the wake generally is not very important. The boundary conditions imposed on the wake, reflecting the physical situation, are generally (though not in PAN AIR):

$$\sigma = 0$$

$$\vec{w}_U \cdot \hat{n} = 0$$

(B.2.2)

The flow about lifting surfaces in subsonic flow is known to satisfy a condition called the "Kutta condition", that is, the pressure jump across the surface is zero along the trailing edge. The successful modeling of a potential flow problem generally requires that the Kutta condition be satisfied. In section D.1.1, we describe the boundary conditions that PAN AIR imposes on wake networks. We also outline a justification that these boundary conditions results in the Kutta condition being satisfied.

An illustration of the wake location for a typical wing-body configuration is given in figure B.9. Note that no trailing edge of the wake is shown. In true physics, the wake is dissipated by viscous effects. In terms of solving the Prandtl-Glauert equation, the effect of the far regions of the wake on the configuration is negligible, and thus the wake can be terminated at any finite point which is reasonably far from the physical configuration. The division of the wake into "wake 1" and "wake 2" networks will be discussed in section D.1.2.

Several major exceptions exist to the assertions that a wake should generally be positioned in a streamwise direction from the trailing edge of a lifting surface, and that the exact position of the wake is generally not important. One is the case of a "leading edge vortex", a phenomenon that occurs at the leading edge of a highly swept wing at large angles of attack as illustrated in figure B.10. In that case, the wake tends to roll up (trailing wakes also roll up, but at so much greater distance from the airplane as to be ignored) as shown, and the exact position of the wake is important in determining the aerodynamic behavior of the configuration. The use of a potential flow program to analyze such a case involves an iterative determination of the wake position, a problem similar to the design problem discussed in Appendix C. Some success in obtaining numerical solutions of this problem has been obtained by the program of Johnson, et al., (B.2).

Another case in which wake positioning is important is the case where the wake from a wing passes near the tail of the airplane. Generally speaking, whenever the flow leaving the trailing edge of a lifting surface passes near another portion of the configuration (or the ground, if ground effect is being studied), the location of the wake is important in analyzing the flow.

### B.3 Removal of Line Vortex Terms

In order to impose boundary conditions involving  $\phi$  (such as  $w n = v r = b$ ), we must evaluate the perturbation velocity at an arbitrary point. Differentiating (B.0.1), we obtain

$$\vec{v}(x,y,z) = \vec{\nabla}\phi = \frac{1}{\kappa} \vec{\nabla} \iint_{SND_p}^* \left[ \frac{-\sigma(Q)}{R} + u(Q)\hat{n} \cdot \vec{\nabla}\left(\frac{1}{R}\right) \right] dS \quad (B.3.1)$$

Putting the gradient within the integral, and writing it as  $\vec{\nabla}_p$  to emphasize that we are differentiating in  $(x,y,z)$  coordinates:

$$\vec{v} = \frac{1}{\kappa} \iint_{SND_p}^* \left[ -\sigma(Q) \vec{\nabla}_p\left(\frac{1}{R}\right) + u(Q) \vec{\nabla}_p\left(\vec{\nabla}_Q\left(\frac{1}{R}\right) \cdot \hat{n}\right) \right] dS \quad (B.3.2)$$

$$\text{Recalling } \vec{\nabla}_p = \begin{Bmatrix} \partial/\partial x \\ \partial/\partial y \\ \partial/\partial z \end{Bmatrix} \quad \vec{\nabla}_Q = \begin{Bmatrix} sB^2 \partial/\partial \xi \\ \partial/\partial \eta \\ \partial/\partial \zeta \end{Bmatrix}$$

$$\text{and } R^2 = (\xi - x)^2 + sB^2 (\eta - y)^2 + sB^2 (\zeta - z)^2 \quad (B.3.3)$$

we have

$$\vec{\nabla}_Q(R) = \left( \frac{sB^2(\xi-x)}{R}, \frac{sB^2(\eta-y)}{R}, \frac{sB^2(\zeta-z)}{R} \right) = \frac{sB^2}{R} (\xi-x, \eta-y, \zeta-z) \quad (B.3.4)$$

and similarly

$$\vec{\nabla}_p(R) = - \frac{(\xi-x, sB^2(\eta-y), sB^2(\zeta-z))}{R} \quad (B.3.5)$$

Further, by the chain rule,

$$\vec{\nabla}_Q(R^n) = nR^{n-1} \vec{\nabla}_Q(R) \quad (B.3.6)$$

$$= sB^2 n (\xi-x, \eta-y, \zeta-z) R^{n-2} \quad (B.3.7)$$

and similarly

$$\vec{\nabla}_p(R^n) = -n (\xi-x, sB^2(\eta-y), sB^2(\zeta-z)) R^{n-2} \quad (B.3.8)$$

Thus,  $\nabla_p \nabla_Q (1/R)$  contains a term with  $R^{-5}$  as a factor. This  $R^{-5}$  term, which only exists in the doublet velocity integral, not occurring in the source velocity integral or the source or doublet potential integrals, is a serious source of numerical difficulties. One difficulty is that if the boundary of  $S$  contains a point at which  $R=0$  (as may easily happen in supersonic flow), the integral in (B.3.1) becomes infinite. This is especially serious since the integration over  $S$  is performed one "panel" at a time. Thus, a very large value of the integral may be computed over one panel, which is then theoretically cancelled by the integral over the neighboring panel. In practice, however, computing limitations will prevent exact cancellation and thereby introduce numerical error.

In addition, when  $P$  lies far from the panel over which integration is performed, a "far field" method, involving the approximation of  $1/R$  by a power series, is used. But  $R^{-5}$  is less accurately approximated by a power series of given length than  $R^{-3}$ , so the use of the far field method in evaluating potential and velocity is somewhat restricted by its poor accuracy in evaluating the velocity induced by the doublet distribution (see section 5.6, equations (5.6.14-15), for a discussion of this).

Thus we wish to transform equation (B.3.2) through an integration by parts in order that the resulting integrands contain no powers of  $1/R$  greater than 3. Reducing the exponent of  $1/R$  in the doublet potential or source velocity terms is certainly of far less priority. It is also extremely difficult, and thus, since it is not incorporated in PAN AIR, will not be discussed here.

Now, at the end of this section, we will show that

$$\vec{v}(x,y,z) = -\frac{1}{\kappa} \iint_{S \cap D_p}^* \sigma(Q) \vec{\nabla}_p \left( \frac{1}{R} \right) dS + \frac{1}{\kappa} \iint_{S \cap D_p}^* (\hat{n} \times \vec{\nabla}_Q \mu) \times \vec{\nabla}_Q \left( \frac{1}{R} \right) dS \quad (B.3.9)$$

$$+ \frac{1}{\kappa} \int_{\partial S}^* \mu \vec{\nabla}_Q \left( \frac{1}{R} \right) \times d\vec{l}$$

where  $\partial S$  is the boundary of the surface  $S$ .

We will also shortly show why the line integral (the last term of (B.3.9)) can be ignored. Under this assumption, we have succeeded in our goal of removing integrands more singular than  $R^{-3}$ . As a matter of terminology, the second term of (B.3.9) is called the regular term of the doublet velocity, while the third term is called the line vortex term. The latter term also has an integrand of order  $R^{-3}$ , but since the integral is only a line integral, it is more singular.

Now, we perform the integrations in (B.3.9) one panel at a time. Let us consider what is required for the line integrals to vanish. First, consider a panel edge with no adjoining panel edge next to it, for instance, the edge AB in figure B.11. Clearly, if  $\mu$  identically equals zero on  $\Delta_{AB}$ , the line integral along AB vanishes. Second, consider two adjacent panels as shown in figure B.12. As a convention, we define  $d\vec{l}$  as being in the counterclockwise

direction when looking from "above". That is,  $d\vec{l} \times \hat{n}$  lies in the plane of the panel and points outward. Then if the doublet strength on the panel  $\Sigma_1$ , is  $\mu_1(x,y,z)$ , and on  $\Sigma_2$  it is  $\mu_2(x,y,z)$ , and if  $\mu_1 = \mu_2$  at every point on the edge AB, we have

$$\int_{\Sigma_1 \cap AB \cap D_P}^* \mu \vec{\nabla}_Q (1/R) \times d\vec{l} + \int_{\Sigma_2 \cap AB \cap D_P}^* \mu \vec{\nabla}_Q (1/R) \times d\vec{l} = 0 \quad (B.3.10)$$

since the integrands have identical values with opposite sign due to the opposite directions  $d\vec{l}$ . Here, again, the symbol " $\cap$ " indicates the intersection of regions in space.

We can generalize (B.3.10) to the case where arbitrarily many panel edges meet (see figure B.13 for an illustration of 3 panels meeting). Let

$$s_i = \text{sign} (d\vec{l}_i \cdot (\vec{B} - \vec{A})) \quad (B.3.11)$$

where  $d\vec{l}_i$  is the counterclockwise direction on  $\Sigma_i$ .

Then if  $n$  = number of panels, and

$$\sum_{i=1}^n s_i \mu_i = 0 \quad (B.3.12)$$

on the entire edge AB,

$$\sum_{i=1}^n \int_{\Sigma_i \cap AB \cap D_P}^* \left\{ \mu_i \vec{\nabla}_Q (1/R) \times d\vec{l} \right\}_i = 0 \quad (B.3.13)$$

Equation (B.3.13) follows from

$$\sum_{i=1}^n \mu_i d\vec{l}_i = 0 \quad (B.3.14)$$

at all points on AB, which in turn follows from (B.3.11) and (B.3.12). It should be noted that if  $n=1$  or  $2$ , (B.3.12) reduces to our previous assumptions.

So, if (B.3.12) is satisfied along a particular intersection of panel edges, the line integral in (B.3.9) can be ignored along that edge.

But now we must justify that (B.3.12) is physically reasonable. Consider the three surfaces in figure B.13, illustrated in cross section in figure B.14. Let  $P_1$ ,  $P_2$ , and  $P_3$  be points a small distance apart, as illustrated in figure B.14. Let us assume (and this is not a completely trivial assumption) that  $\phi$  is continuous in each of the regions  $V_1$ ,  $V_2$ , and  $V_3$ , and bounded by some fixed value in the general vicinity of the intersection line. Writing  $\phi_i$  for  $\phi(P_i)$ , it is then true that  $\phi_i$  does not change much if  $P_i$  is moved slightly. Thus, we can let  $P_i$  approach one of the surfaces  $\Sigma_j$  without changing  $\phi_i$  much. In particular, letting  $P_1$

and  $P_2$  approach  $\Sigma_i$ , we see that  $\phi_1 - \phi_2 \approx u_1$ . In fact, in the limit as  $P_1$  and  $P_2$  approach the intersection line,

$$\phi_1 - \phi_2 = u_1 \quad (\text{B.3.15})$$

Similarly, in the limit as the  $P_i$  approach the intersection,

$$\phi_3 - \phi_2 = u_2 \quad (\text{B.3.16})$$

$$\phi_1 - \phi_3 = u_3 \quad (\text{B.3.17})$$

Subtracting (B.3.15) from the sum of (B.3.16) and (B.3.17), we obtain

$$0 = -u_1 + u_2 + u_3 \quad (\text{B.3.18})$$

which is equivalent to equation (B.3.12).

The previous argument is generalizeable to an intersection of  $n$  surfaces. The assumption that  $\phi$  is continuous off the surfaces is valid (and is in fact required for the basic integral equation to hold), but the requirement that  $\phi$  be bounded in a neighborhood of the surface is not necessarily valid. It is, however, physically reasonable, since an unbounded potential produces an infinite velocity. So, we will make the assumption within PAN AIR. The mechanism by which (B.3.12) is applied is described in Appendix F. As a result of this assumption, the line vortex term in (B.3.9) may be ignored.

It now remains to derive (B.3.9). Much of the derivation may be found in texts (for instance, (B.3.41) is found in Lass, Vector and Tensor Analysis, reference B.3, p. 112). First we will introduce a non-standard form of Stokes' theorem as follows: Let  $S$  be a surface,  $H$  a vector valued function on  $S$ . Then

$$\int_{\partial S} \{ \vec{H} \times d\vec{l} \}_i = \sum_{k=1}^3 \iint_S \left\{ \frac{\partial H_k}{\partial x_k} \hat{n}_i - \frac{\partial H_k}{\partial x_i} \hat{n}_k \right\} dS \quad (\text{B.3.19})$$

To derive (B.3.19), consider the more standard form of Stokes' theorem (see Kellogg, p. 73): let  $G$  be a vector valued function on  $S$ , then

$$\int_{\partial S} \vec{G} \cdot d\vec{l} = \iint_S \hat{n} \cdot (\vec{\nabla} \times \vec{G}) dS \quad (\text{B.3.20})$$

Writing  $d\vec{l} = (dx_1, dx_2, dx_3)$ , and recalling that for vectors  $A$  and  $B$ , by definition,

$$(A \times B)_k = \sum_{i,j} \epsilon_{ijk} A_i B_j \quad (\text{B.3.21})$$

where  $\epsilon_{ijk} = 1$  if  $(ijk)$  occur in cyclic order (123), (231), or (312),  $-1$  if

they occur in reverse cyclic order, and 0 if any two of  $i, j, k$  are equal, we can rewrite (B.3.20) as

$$\sum_j \int_{\partial S} G_j dx_j = \sum_{ijk} \iint_S \hat{n}_k \epsilon_{ijk} \frac{\partial G_j}{\partial x_i} dS \quad (B.3.22)$$

Now, for a fixed value of  $l = 1, 2$ , or  $3$ , let

$$G_j = \sum_{m=1}^3 \epsilon_{lmj} H_m \quad (B.3.23)$$

Substituting in (B.3.22), we obtain

$$\sum_{j,m} \int_{\partial S} \epsilon_{lmj} H_m dx_j = \sum_{j,m} \iint_S \hat{n}_k \epsilon_{ijk} \left( \frac{\partial}{\partial x_i} \right) (\epsilon_{lmj} H_m) dS \quad (B.3.24)$$

But now consider

$$\left\{ (\hat{n} \times \vec{\nabla}) \times \vec{H} \right\}_l = \sum_{j,m} \epsilon_{jml} (\hat{n} \times \vec{\nabla})_j H_m \quad (B.3.25a)$$

while

$$(\hat{n} \times \vec{\nabla})_j = \sum_{k,i} \epsilon_{kij} \hat{n}_k \frac{\partial}{\partial x_i} \quad (B.3.25b)$$

and thus  $\left\{ (\hat{n} \times \vec{\nabla}) \times \vec{H} \right\}_l =$

$$\sum_{k,i,j,m} \epsilon_{jml} \epsilon_{kij} \hat{n}_k \frac{\partial}{\partial x_i} (H_m) \quad (B.3.26)$$

Now,

$$\epsilon_{jml} = -\epsilon_{lmj}$$

$$\epsilon_{kij} = \epsilon_{ijk} \quad (B.3.27)$$

and thus, substituting (B.3.26) in (B.3.24),

$$\sum_{k,m} \int_{\partial S} \epsilon_{mj1} H_m dx_j = - \iint_S ((\hat{n} \times \vec{\nabla}) \times \vec{H})_1 dS \quad (B.3.28)$$

$$\text{But } ((\vec{H} \times d\vec{l}))_1 = \sum_{j,m} \epsilon_{mj1} H_m dx_j \quad (B.3.29)$$

and thus we can write (B.3.28) as

$$\int_{\partial S} \vec{H} \times d\vec{l} = - \iint_S ((\hat{n} \times \vec{\nabla}) \times \vec{H}) dS \quad (B.3.30)$$

Now, we claim that for any 3 vectors A, B, C,

$$((\vec{A} \times \vec{B}) \times \vec{C})_i = (\vec{A} \cdot \vec{C}) B_i - (\vec{B} \cdot \vec{C}) A_i = \sum_k (A_k B_i C_k - A_i B_k C_k) \quad (\text{B.3.31})$$

For,  $(\vec{A} \times \vec{B}) \times \vec{C}$  is perpendicular to  $\vec{A} \times \vec{B}$ , and thus lies in the plane spanned by  $\vec{A}$  and  $\vec{B}$ .

So,

$$(\vec{A} \times \vec{B}) \times \vec{C} = a_1 \vec{A} + a_2 \vec{B} \quad (\text{B.3.32})$$

$$\text{Further, } [(\vec{A} \times \vec{B}) \times \vec{C}] \cdot \vec{C} = 0 \quad (\text{B.3.33})$$

$$\text{or } a_1 (\vec{A} \cdot \vec{C}) + a_2 (\vec{B} \cdot \vec{C}) = 0 \quad (\text{B.3.34})$$

$$\text{Thus, } a_1 = k(\vec{B} \cdot \vec{C}) \quad (\text{B.3.35})$$

$$a_2 = k(\vec{A} \cdot \vec{C})$$

where k is some constant, and so

$$(\vec{A} \times \vec{B}) \times \vec{C} = k [(\vec{B} \cdot \vec{C}) \vec{A} - (\vec{A} \cdot \vec{C}) \vec{B}] \quad (\text{B.3.36})$$

But both the left and right hand sides are homogenous polynomials (that is, they have no lower order terms) of cubic order in the 9 variables  $A_i, B_i, C_i, i = 1, 2, 3$ . Thus the real number k is a constant which is independent of A, B, and C, and so we can determine k by picking arbitrary vectors A, B, C. Picking

$$A = \begin{pmatrix} 1 \\ 0 \\ 0 \end{pmatrix}, B = \begin{pmatrix} 0 \\ 1 \\ 0 \end{pmatrix}, C = \begin{pmatrix} 1 \\ 0 \\ 0 \end{pmatrix} \quad (\text{B.3.37})$$

$$\text{we find } \vec{A} \times \vec{B} = \begin{pmatrix} 0 \\ 0 \\ 1 \end{pmatrix}, (\vec{A} \times \vec{B}) \times \vec{C} = \begin{pmatrix} 0 \\ 1 \\ 0 \end{pmatrix} \quad (\text{B.3.38})$$

$$\begin{aligned} \vec{B} \cdot \vec{C} &= 0 \\ \vec{A} \cdot \vec{C} &= 1 \end{aligned} \quad (\text{B.3.39})$$



and thus  $k = -1$ . So, (B.3.31) holds.

Substituting  $\hat{n}$  for  $\vec{A}$ ,  $\vec{\nabla}$  for  $\vec{B}$ , and  $\vec{H}$  for  $\vec{C}$ , in (B.3.31),

$$((\hat{n} \times \vec{\nabla}) \times \vec{H})_i = \sum_k \hat{n}_k \left( \frac{\partial}{\partial x_i} H_k - \hat{n}_i \frac{\partial}{\partial x_k} H_k \right) \quad (\text{B.3.40})$$

Substituting the above into (B.3.30),

$$\int_{\partial S} (\vec{H} \times d\vec{l})_i = - \iint_S \left( \sum_k \hat{n}_k \frac{\partial}{\partial x_i} H_k - \hat{n}_i \frac{\partial}{\partial x_k} H_k \right) dS \quad (\text{B.3.41})$$

which is identical to (B.3.19), the alternate form of Stokes' Theorem we were trying to prove.

Now, we substitute  $\vec{H} = \mu \vec{\nabla} (1/R)$  in (B.3.19), obtaining

$$\int_{\partial S} \left\{ \mu \vec{\nabla} \left( \frac{1}{R} \right) \times d\vec{l} \right\}_i = \sum_k \iint_S \left[ \left( \frac{\partial}{\partial x_k} \left[ \mu \frac{\partial}{\partial x_k} \left( \frac{1}{R} \right) \right] \right) \hat{n}_i - \left( \frac{\partial}{\partial x_i} \left[ \mu \frac{\partial}{\partial x_k} \left( \frac{1}{R} \right) \right] \right) \hat{n}_k \right] dS \quad (\text{B.3.42})$$

Now, by the product rule for differentiation

$$\sum_k \frac{\partial}{\partial x_k} \left[ \mu \frac{\partial}{\partial x_k} \left( \frac{1}{R} \right) \right] = \sum_k \frac{\partial \mu}{\partial x_k} \frac{\partial}{\partial x_k} \left( \frac{1}{R} \right) + \mu \frac{\partial^2}{\partial x_k \partial x_k} \left( \frac{1}{R} \right) \quad (\text{B.3.43})$$

and

$$\frac{\partial}{\partial x_i} \left[ \mu \frac{\partial}{\partial x_k} \left( \frac{1}{R} \right) \right] = \frac{\partial \mu}{\partial x_i} \frac{\partial}{\partial x_k} \left( \frac{1}{R} \right) + \mu \frac{\partial}{\partial x_k} \frac{\partial}{\partial x_i} \left( \frac{1}{R} \right) \quad (\text{B.3.44})$$

Now,

$$\sum_k \frac{\partial^2}{\partial x_k \partial x_k} \left( \frac{1}{R} \right) =$$

$$\left( \begin{array}{l} s\beta^2 \frac{\partial^2}{\partial \xi^2} \\ + \frac{\partial^2}{\partial n^2} \\ + \frac{\partial^2}{\partial z^2} \end{array} \right) [(\xi - x)^2 + (n - y)^2 + (\zeta - z)^2]^{-1/2} \quad (\text{B.3.45})$$

$$\text{Now, } \frac{\partial^2}{\partial \xi^2} \left( \frac{1}{R} \right) = \frac{-\partial}{\partial \xi} \frac{-x}{R^3} = -\frac{[R^3 - 3(\xi - x)(\xi - x)R]}{R^6} = \frac{R^2}{R^5} - \frac{3(\xi - x)^2}{R^5} \quad (\text{B.3.46})$$

$$(\text{B.3.47})$$

Obtaining similar expressions for the  $n$  and  $z$  derivatives,

$$\sum_k \frac{\partial^2}{\partial x_k \partial x_k} \left( \frac{1}{R} \right) = s\beta^2 \frac{3R^2 - 3(\xi - x)^2 - 3s\beta^2(n - y)^2 - 3s\beta^2(\zeta - z)^2}{R^5} = 0 \quad (\text{B.3.48})$$

Note that this proves that  $1/R$  satisfies the Prandtl-Glauert equation.

So, (B.3.42) becomes

$$\int_{\partial S} (\mu \vec{\nabla} \left(\frac{1}{R}\right) \times d\vec{l})_i = \iint_S ((\vec{\nabla} \mu \cdot \vec{\nabla} \frac{1}{R}) \hat{n}_i - \sum_k \mu \frac{\partial^2}{\partial x_i \partial x_k} \left(\frac{1}{R}\right) \hat{n}_k) dS \quad (B.3.49)$$

$$- \sum_k \frac{\partial \mu}{\partial x_i} \frac{\partial}{\partial x_k} \left(\frac{1}{R}\right) \hat{n}_k$$

$$= \iint_S \left\{ (\vec{\nabla} \mu \cdot \vec{\nabla} \frac{1}{R}) \hat{n}_i - (\vec{\nabla} \frac{1}{R} \cdot \hat{n}) (\vec{\nabla} \mu)_i - \mu \frac{\partial}{\partial x_i} (\hat{n} \cdot \vec{\nabla} \frac{1}{R}) \right\} dS \quad (B.3.50)$$

Applying (B.3.31) in (B.3.50), with  $\vec{A} = \vec{\nabla} \mu$ ,  $\vec{B} = \hat{n}$ ,  $\vec{C} = \vec{\nabla}(1/R)$ , we obtain

$$\int_{\partial S} \mu \vec{\nabla} \left(\frac{1}{R}\right) \times d\vec{l} = \iint_S ((\vec{\nabla} \mu \times \hat{n}) \times \vec{\nabla} \frac{1}{R} - \mu \vec{\nabla} (\hat{n} \cdot \vec{\nabla} \frac{1}{R})) dS \quad (B.3.51)$$

$$\text{Or } \iint_S \mu \vec{\nabla} Q (\hat{n} \cdot \vec{\nabla} \left(\frac{1}{R}\right)) dS = \iint_S \left\{ ((\vec{\nabla} \mu \times \hat{n}) \times \vec{\nabla} \frac{1}{R}) \right\} dS - \int_{\partial S} \mu \vec{\nabla} \left(\frac{1}{R}\right) \times d\vec{l} \quad (B.3.52)$$

$$\text{Now,} \quad \vec{\nabla} p \left(\frac{1}{R}\right) = - \vec{\nabla} Q \left(\frac{1}{R}\right) \quad (B.3.53)$$

$$\text{and} \quad (\hat{n} \times \vec{\nabla} \mu) = -(\vec{\nabla} \mu \times \hat{n}) \quad (B.3.54)$$

and thus, substituting (B.3.52) in (B.3.1), we obtain

$$\begin{aligned} \vec{v}(x,y,z) &= \frac{1}{\kappa} \iint_{S \cap D_p} \left( - \vec{\nabla} p \frac{\sigma(Q)}{R} + (\hat{n} \times \vec{\nabla} Q \mu) \times \vec{\nabla} \frac{1}{R} \right) dS \\ &+ \int_{\partial S} \mu \vec{\nabla} Q \left(\frac{1}{R}\right) \times d\vec{l} \end{aligned} \quad (B.3.55)$$

Equation (B.3.55) is identical to (B.3.9), the result we were attempting to prove.

#### B.4 Linear Sources and Quadratic Doublets

In this section we outline a justification for the use of a linear source strength approximation and a quadratic doublet approximation. For simplicity, we assume  $M_\infty = 0$ , though the proof is readily extendable to all subsonic Mach numbers. These results cannot be readily generalized to supersonic Mach numbers, however.

Nevertheless, for both supersonic and subsonic flow, we can show that a doublet distribution whose order is one higher than that of the source distribution is reasonable. We do this by considering the jump  $\vec{v}_D$  in velocity occurring on a surface. In section N.1, we find

$$\vec{v}_D = \vec{\nabla} u + \frac{\sigma}{R \cdot \vec{n}} \hat{n} \quad (B.4.1)$$

Thus the discontinuity in velocity has the same direct dependence on doublet gradient as on source strength. In addition, we will see in section J.11 that a discontinuity in doublet gradient induces the same singularities in potential and velocity as a singularity in source strength.

For these reasons we conclude that the doublet gradient is the same order of singularity as the source strength. It is thus reasonable to approximate the source strength and the components of the doublet same order of polynomial. Thus the doublet strength should be approximated by a polynomial of one degree higher than the source strength.

We now consider the case of zero Mach number. We consider the perturbation velocity resulting at a point  $P = 0$  due to a source distribution

$$\sigma(\xi, n) = \sum_{i+j \leq n} \sigma_{ij} \xi^i n^j, \quad i \geq 0, j \geq 0 \quad (B.4.2a)$$

or a doublet distribution

$$u(\xi, n) = \sum_{i+j \leq n} u_{ij} \xi^i n^j \quad (B.4.2b)$$

on the square region  $S$  of size  $2\epsilon \times 2\epsilon$  about  $P$ , illustrated in figure B.15.

Let us first consider the source distribution. By (B.3.1),

$$\vec{v}^S(x, y, z) = \frac{1}{4\pi} \vec{\nabla} P \iint_S \frac{-\sigma(\xi, n)}{(\xi-x)^2 + (n-y)^2 + (\zeta-z)^2} d\xi dn \quad (B.4.3)$$

$$\text{Thus,} \quad \vec{v}_x(P) = \frac{1}{4\pi} \iint_{-\epsilon-\epsilon}^{\epsilon\epsilon} \frac{-\sigma_{ij} \xi^{i+1} n^j}{(\xi^2 + n^2)^{3/2}} d\xi dn \quad (B.4.4)$$

$$v_y(P) = \frac{1}{4\pi} \int_{-\epsilon}^{\epsilon} \int_{-\epsilon}^{\epsilon} \frac{-\sigma_{ij} \xi^i \eta^{j+i}}{(\xi^2 + \eta^2)^{3/2}} d\xi d\eta \quad (B.4.5)$$

and

$$v_z(P) = \lim_{z \rightarrow 0} \frac{1}{4\pi} \int_{-\epsilon}^{\epsilon} \int_{-\epsilon}^{\epsilon} \frac{-\sigma_{ij} \xi^i \eta^j (-z)}{(\xi^2 + \eta^2 + z^2)^{3/2}} d\xi d\eta \quad (B.4.6)$$

Now, let us consider (B.4.4) one term at a time; that is, we assume

$$\sigma(\xi, \eta) = \sigma_{ij} \xi^i \eta^j \quad (B.4.7)$$

If  $(i+j)$  is even, the integrand in (B.4.4) is an "odd" function in  $\xi$  or  $\eta$ ; that is, its value at  $(\xi, \eta)$  is minus its value at  $(-\xi, \eta)$ , or minus its value at  $(\xi, -\eta)$ , and thus the integral over  $S$  is zero. Similarly, if  $(i+j)$  is even, the integral (B.4.5) corresponding to that term is zero. Finally, let us consider the integral (B.4.6) for a single term.

We have

$$v_z(P) = \lim_{z \rightarrow 0} \frac{\sigma_{ij} z}{4\pi} \int_{-\epsilon}^{\epsilon} \int_{-\epsilon}^{\epsilon} \frac{\xi^i \eta^j}{(\xi^2 + \eta^2 + z^2)^{3/2}} d\xi d\eta \quad (B.4.8)$$

$$\text{Now,} \quad \int_0^{\epsilon} \frac{\xi}{(\xi^2 + \eta^2 + z^2)^{3/2}} d\xi = \quad (B.4.9)$$

(substituting  $u = \xi^2 + \eta^2 + z^2$ )

$$\begin{aligned} \int_{\eta^2 + z^2}^{\epsilon^2 + \eta^2 + z^2} (u^{-3/2})^{1/2} du &= [-u^{-1/2}] \Big|_{\eta^2 + z^2}^{\epsilon^2 + \eta^2 + z^2} \\ &= \frac{1}{(\eta^2 + z^2)^{1/2}} - \frac{1}{(\epsilon^2 + \eta^2 + z^2)^{1/2}} \end{aligned} \quad (B.4.10)$$

When this function is integrated over  $\eta$ , the result is  $f(\epsilon, z) - \log |z|$  where  $f(\epsilon, z)$  is bounded as  $z \rightarrow 0$ . Thus the limit in (B.4.8) is zero, provided  $i = 1$ . Since  $\epsilon$  is small,  $\xi^i \eta^j < |\xi|$  so the limit in (B.4.8) is zero whenever  $i \geq 1$ . Similarly, it is zero whenever  $j \geq 1$ , so we see that

$$\lim_{z \rightarrow 0} \frac{z \xi^i \eta^j}{(\xi^2 + \eta^2 + z^2)^{3/2}} d\xi d\eta = 0 \quad (B.4.11)$$

if  $i+j \leq 1$ , and in particular, whenever  $i+j$  is even and greater than zero.

So, writing

$$\vec{v}^S(P)_{ij} = \frac{1}{4\pi} \vec{\nabla} P \iint_S \frac{\sigma_{ij} \xi^i \eta^j d\xi d\eta}{((\xi-x)^2 + (\eta-y)^2 + (\zeta-z)^2)^{3/2}} \quad (B.4.12)$$

$$\text{we have } \vec{v}^S(P)_{ij} = 0 \quad (B.4.13)$$

if  $i+j$  is even, and  $i+j > 0$ .

Let us now consider the velocity

$$\vec{v}^D(P)_{ij} = \frac{1}{4\pi} \vec{\nabla} P \iint_S u_{ij} \xi^i \eta^j \hat{n} \cdot \vec{\nabla}_Q \frac{1}{[(\xi-x)^2 + (\eta-y)^2 + (\zeta-z)^2]^{3/2}} d\xi d\eta \quad (B.4.14)$$

induced by a polynomial doublet distribution

$$u(\xi, \eta) = u_{ij} \xi^i \eta^j \quad (B.4.15)$$

on the region in figure B.15.

Now,

$$\hat{n} = \begin{pmatrix} 0 \\ 0 \\ 1 \end{pmatrix} \quad (B.4.16)$$

and so

$$\hat{n} \cdot \vec{\nabla}_Q = \partial / \partial \zeta \quad (B.4.17)$$

Now,

$$\frac{\partial}{\partial \xi} \frac{1}{[(\xi-x)^2 + (\eta-y)^2 + (\zeta-z)^2]^{3/2}} = \frac{-(\zeta-z)}{[(\xi-x)^2 + (\eta-y)^2 + (\zeta-z)^2]^{5/2}} \quad (B.4.18)$$

and since  $\xi = 0, x=y=0$

$$\begin{aligned} \vec{v}^D(P)_{ij} &= \lim_{z \rightarrow 0} \frac{1}{4\pi} u_{ij} \iint_S \frac{3z \xi^i \eta^j}{[\xi^2 + \eta^2 + z^2]^{3/2}} \begin{pmatrix} +\xi \\ +\eta \\ -z \end{pmatrix} d\xi d\eta \\ &+ \iint_S \frac{\xi^i \eta^j}{[\xi^2 + \eta^2 + z^2]^{3/2}} \begin{pmatrix} 0 \\ 0 \\ 1 \end{pmatrix} d\xi d\eta \end{aligned} \quad (B.4.19)$$

For the x and y components of  $\vec{v}^D(P)_{ij}$  we see that if  $i+j$  is even then the integrand is an odd function, so the integrals are zero. If  $i+j$  is odd and greater than 1, then performing an integration similar to (B.4.5) shows that the integrals in (B.4.19) are of the form  $f(\epsilon, z) - \log z$  where  $f(\epsilon, z)$  is bounded as  $z \rightarrow 0$ . Multiplying by  $z$  and taking the limit as  $z \rightarrow 0$  we conclude that

$$\vec{v}_x^D(P)_{ij} = \vec{v}_y^D(P)_{ij} = 0 \quad (\text{B.4.20})$$

if  $i+j > 1$ .

The z component of  $\vec{v}^D(P)_{ij}$  behaves somewhat differently, due to the presence of the second term. Both terms vanish if at least one of  $i$  or  $j$  is odd, by the usual odd function argument. In addition, the first term is zero if  $i+j \geq 3$  by the same reasoning as the last paragraph. The second term,

$$\lim_{z \rightarrow 0} \frac{\mu_{ij}}{4\pi} \iint_S \frac{\xi^i \eta^j}{(2 + \eta^2 + z^2)^{3/2}} d\xi d\eta, \quad (\text{B.4.21})$$

does not necessarily vanish if both  $i$  and  $j$  are even. But it is of order  $\epsilon^2$  if  $i+j \geq 4$ , and since it vanishes for  $i+j = 3$ , it seems reasonable to approximate the local doublet distribution by a polynomial with  $i+j \leq 2$ .

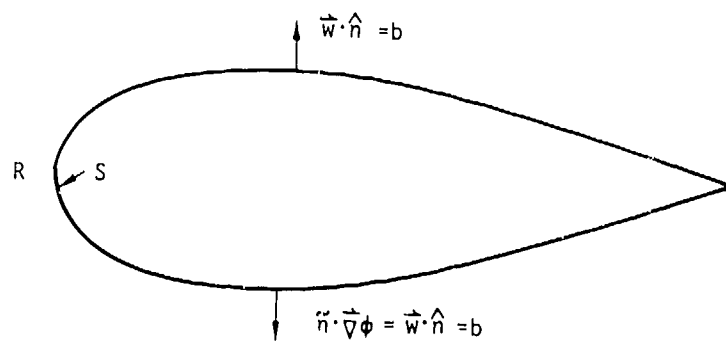


Figure B.1 - An exterior boundary value problem

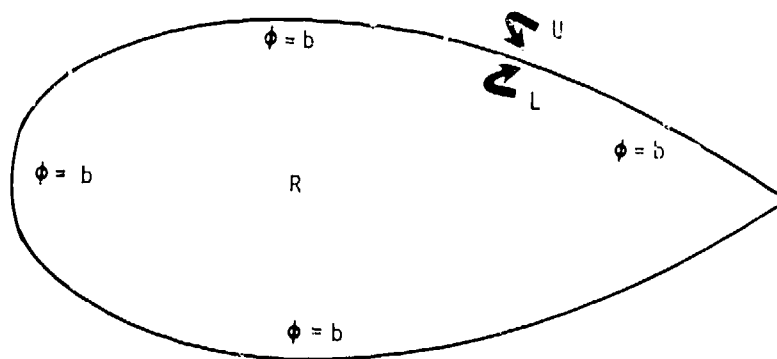


Figure B.2 - A region of finite volume

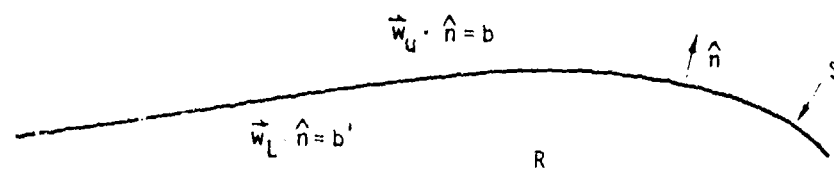


Figure B.3 - Specification of normal flow on both sides of a surface

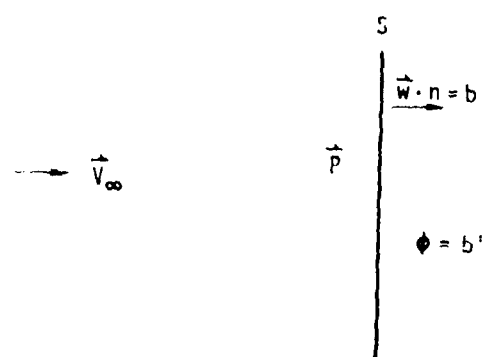


Figure B.4 - A superinclined surface



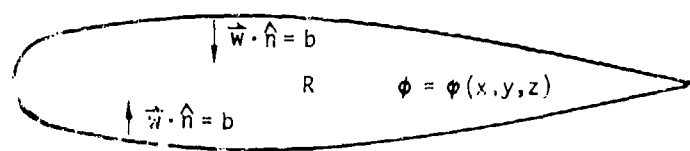


Figure B.5 - A boundary value problem with no unique solution

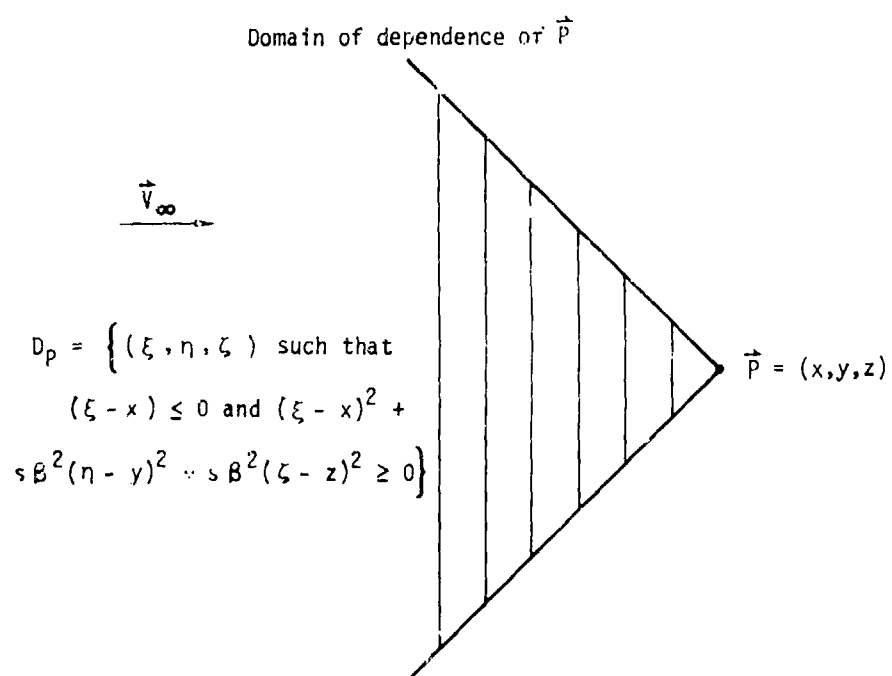


Figure B.5 - The Domain of Dependence

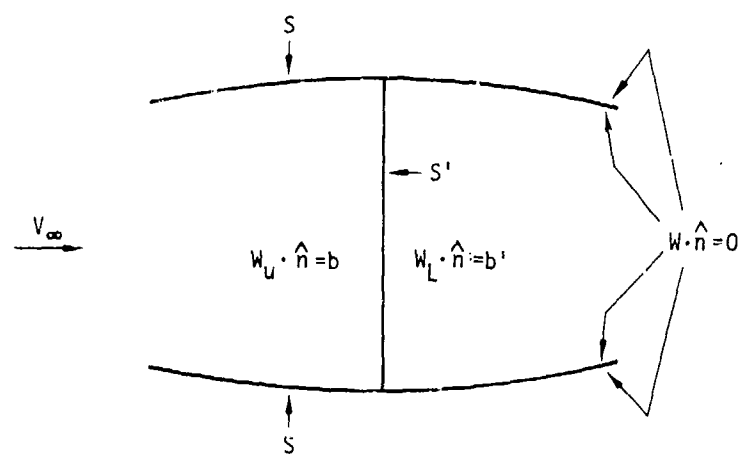


Figure B.7 - A permeable surface inclined to the freestream

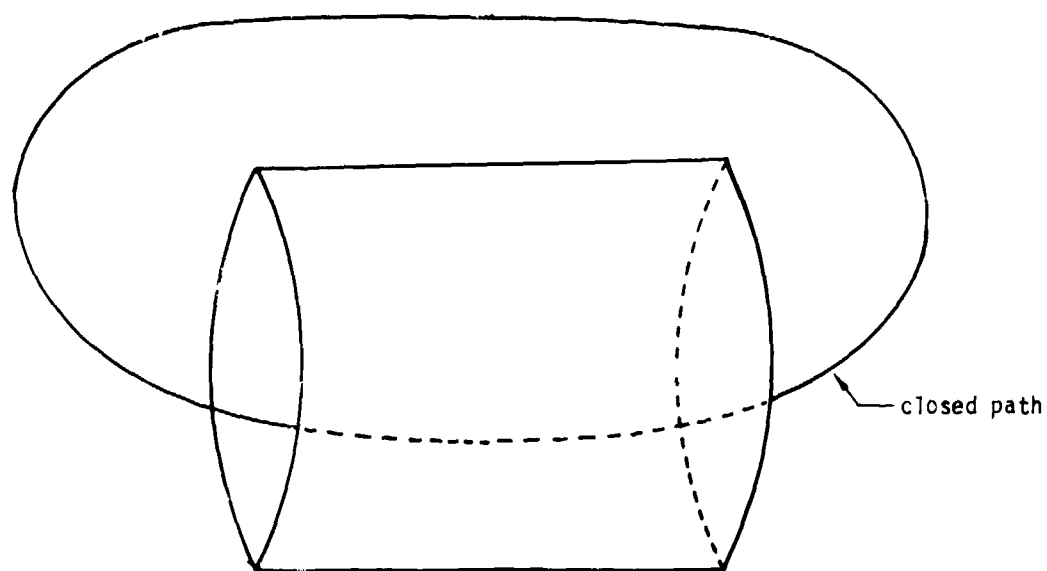


Figure B.8 - A region which fails to be simply connected

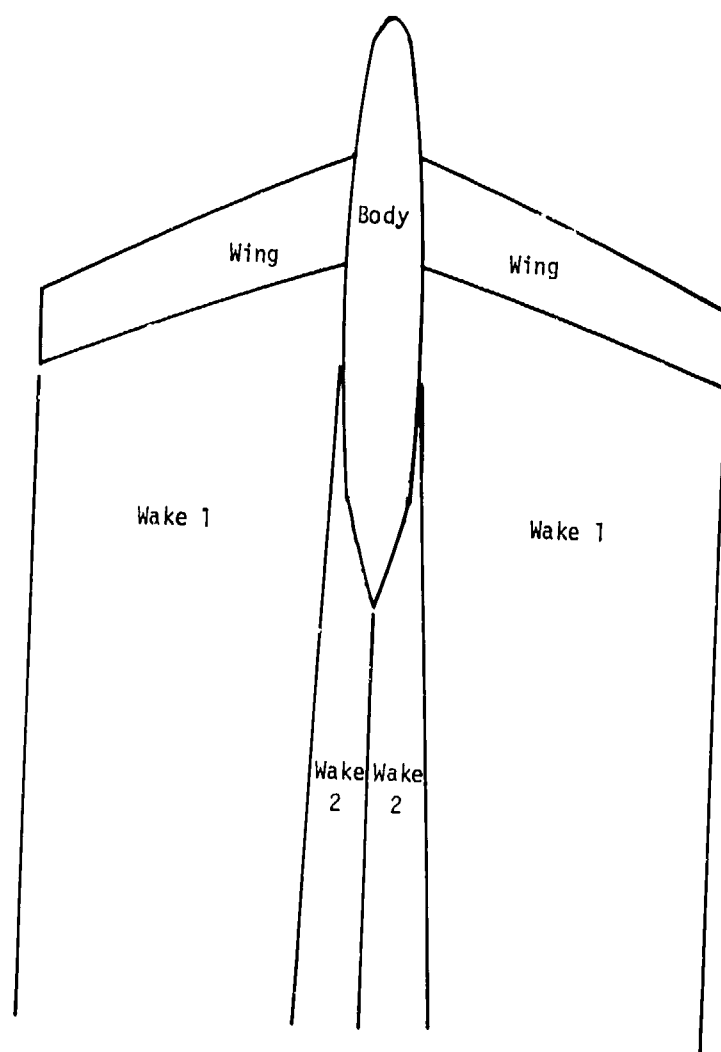


Figure B.9 - Airplane and wake

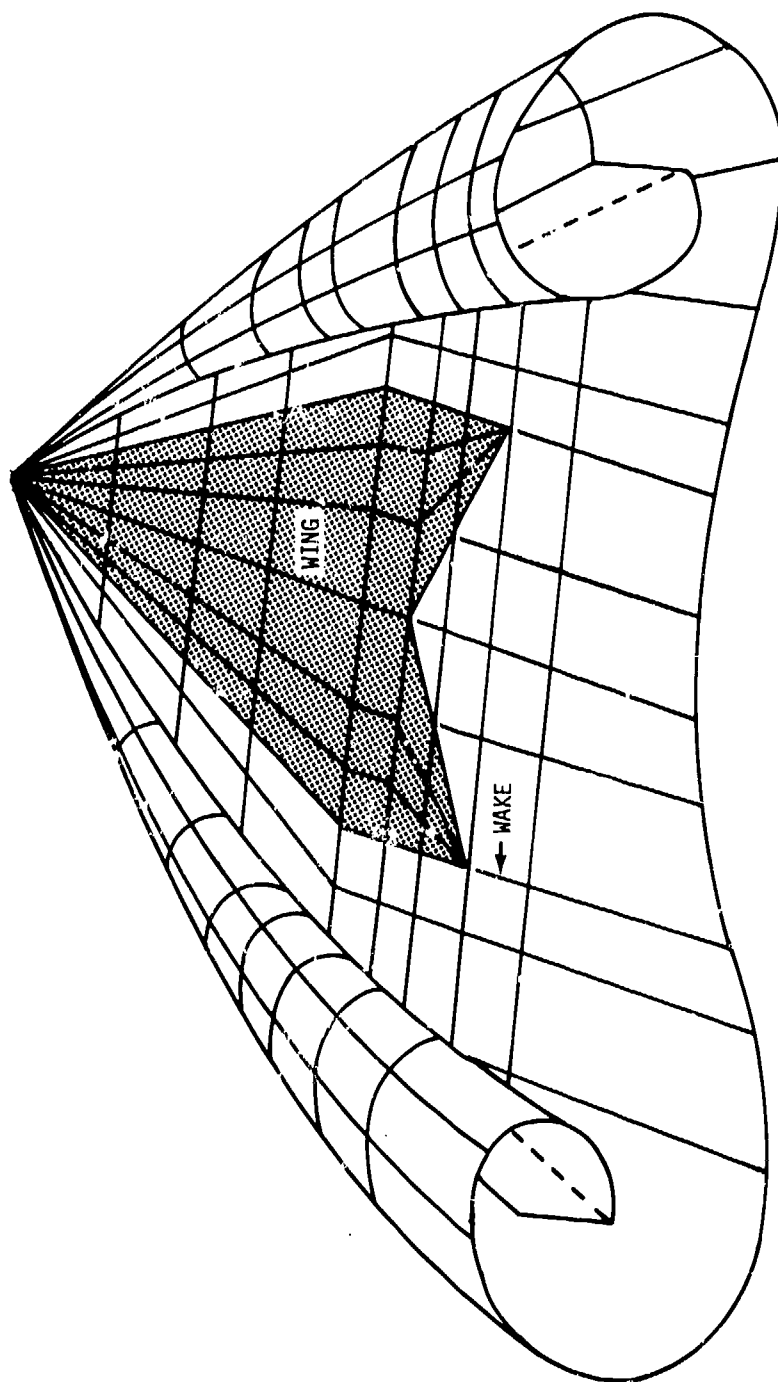


Figure B.10 - Leading edge vortices from a highly swept wing

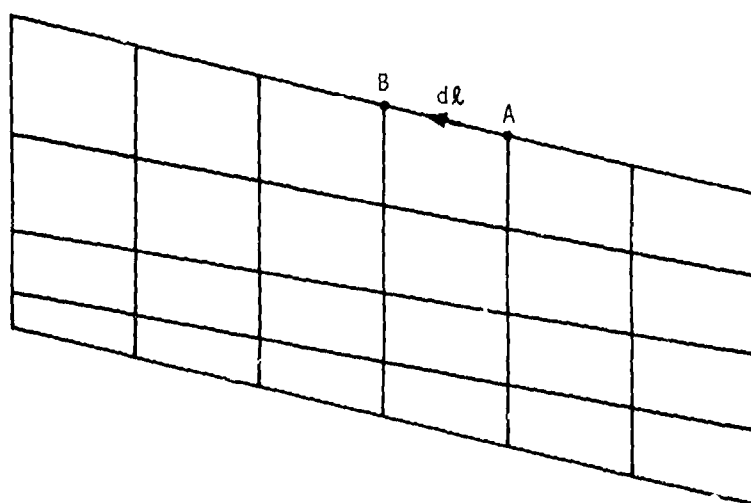


Figure B.11 - Panel edge on a network edge

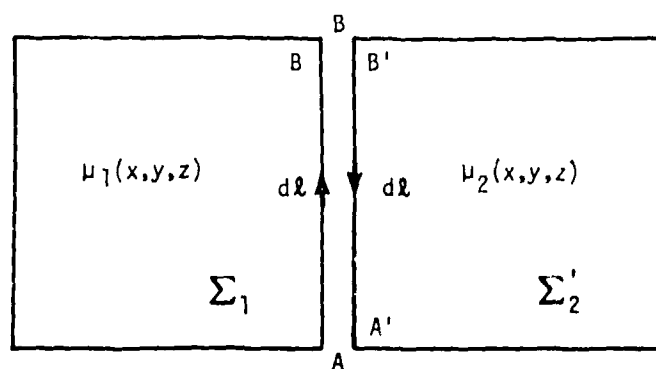


Figure B.12 - Two adjacent panel edges

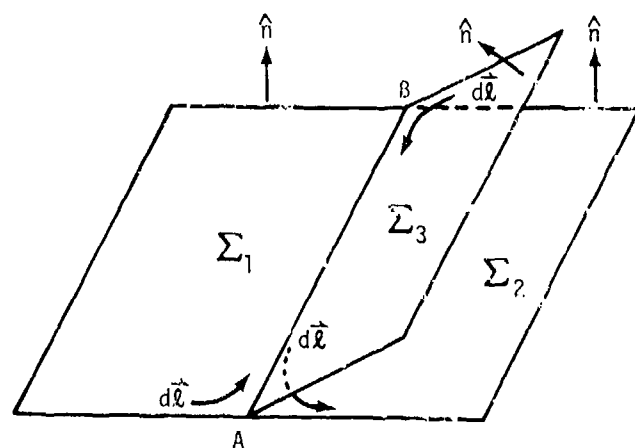


Figure B.13 - Three adjacent panels

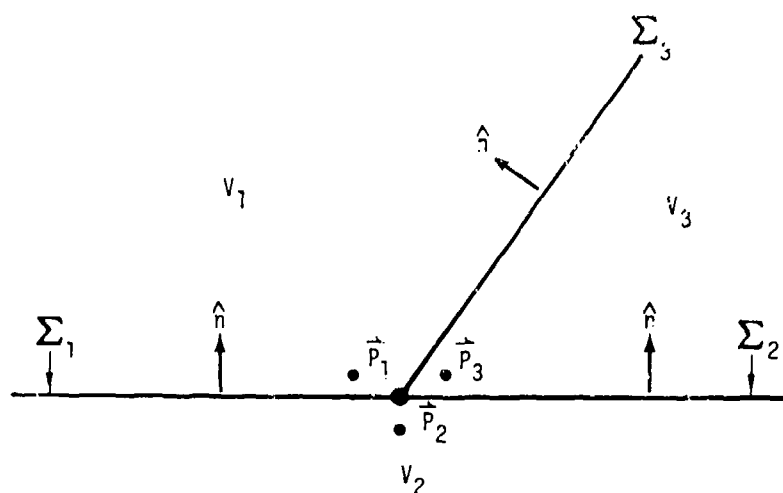


Figure B.14 - Intersection of 3 surfaces (cross-section)

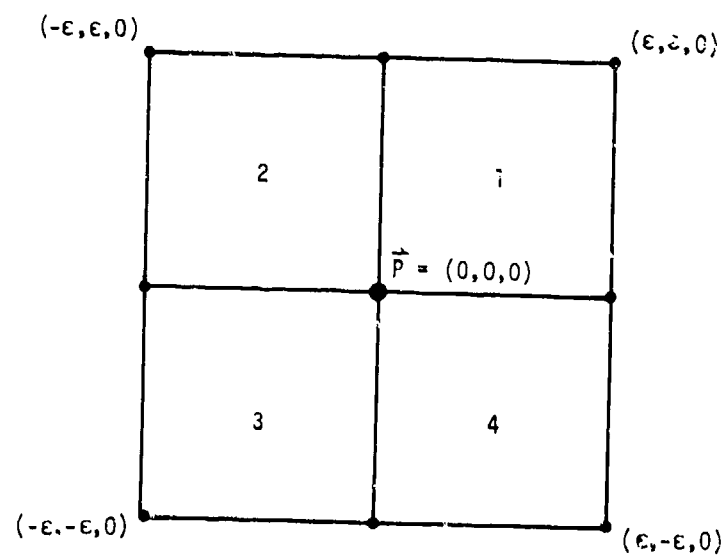


Figure B.15 - Region of integration in neighborhood of  $\vec{P}$

## C.0 The Design Problem

In the design problem the user attempts to obtain a configuration whose shape is unknown, but is subject to certain constraints. For instance, a wing may be required to have a certain planform, but its camber and thickness distributions may be the subject of the design process. The constraints involved in this case would be (1) that the surface be impermeable, and (2) that particular pressure or tangential velocity distributions be required.

Now, specification of both normal and tangential flow on a surface is an overspecification of boundary conditions, and thus in general there is no one step solution to the design problem. The exception is called "linearized design", in which the user is satisfied with a first order approximation to the solution. This method is discussed in section C.1.

In section C.2, we discuss a somewhat more sophisticated procedure, which we call sequential design. This is a non-automatic iterative procedure in which a single loop in the iteration consists of:

- (a) a potential flow analysis (for example, a boundary value problem with impermeability boundary conditions) of the configuration at hand,
- (b) a comparison of the pressures computed in (a) with the desired pressure distribution, leading to the specification of tangential velocity boundary conditions,
- (c) solution of the potential flow problem for the tangential velocity boundary conditions, and computation of the normal flow through the surface, and
- (d) "relofting" of the configuration geometry, using the normal flow data, in order to produce a more nearly impermeable surface.

This procedure can be executed in the first version of PAN AIR, though steps (b) and (d) will have to be performed manually by the program user.

In section C.3, we briefly discuss a still more sophisticated design method, which we simply call "iterative design". This method is distinguished from sequential design in its relofting method.

Finally, in section C.4, we discuss stability problems occurring from the discretization process. These problems generally result when a small perturbation in a boundary condition generates a perturbation in the solution which does not die out with distance. Since the discretization process always results in some numerical error, stability problems can result in a totally incorrect solution.

We do not discuss the imposition of "closure" boundary conditions in this appendix, but rather discuss that subject in section H.2.



### C.1 Linearized Design

The basic assumption of linearized design is that

$$C_p = -2u \quad (C.1.1)$$

where  $C_p$  is the pressure coefficient at a point, and  $u$  is a component of the perturbation velocity

$$\vec{v}(x,y,z) = (u,v,w) \quad (C.1.2)$$

Again, we assume  $|\vec{v}_\infty| = 1$ .

Equation (C.1.1) will be derived in Appendix N. Generally speaking, (C.1.1) is valid only for thin configurations with little camber at small angles of attack, such as the configuration in figure C.1.

Now, the program user wishes to specify a difference in pressure distribution  $\Delta C_{p_s}(x,y,z)$  on the configuration, where

$$\Delta C_p = C_{p, \text{upper}} - C_{p, \text{lower}} \quad (C.1.3)$$

Noting that  $u = \vec{v} \cdot \vec{v}_\infty \quad (C.1.4)$

(since  $|\vec{v}_\infty| = 1$ ) we have

$$\begin{aligned} \Delta C_p &= -2(\vec{v}_U - \vec{v}_L) \cdot \vec{v}_\infty \\ &= -2\vec{\nabla}(\phi_U - \phi_L) \cdot \vec{v}_\infty \\ &= -2\vec{\nabla}\phi \cdot \vec{v}_\infty \end{aligned} \quad (C.1.5)$$

Thus, the boundary condition to impose at  $(x,y,z)$  is

$$(-2\vec{v}_\infty) \cdot \vec{\nabla}\phi = \Delta C_{p_s}(x,y,z) \quad (C.1.6)$$

which is of the form

$$\vec{t}_D \cdot \vec{\nabla}\phi = b \quad (C.1.7)$$

(see (5.4.21) for the general boundary condition equation).

Now, the boundary value problem described by (C.1.7) is solved numerically, in the course of which the total mass flux at the control points is evaluated. The mass flux is used to reloft the surface as follows. The procedure we describe is not incorporated in version 1.0 of PAN AIR.

The relofting takes place one network at a time (for a brief discussion of networks and panels, see section 5.1). Two edges of the network are left fixed or, if the geometry of the adjacent network has been relofted, these edges are adjusted to close the gap. In figure C.2, these edges are edges 1 and 2.

The remainder of the network is relofted one panel corner point at a time. This is done by alternately relofting columns and rows of corner points. For instance, in the example of figure C.2, first point (2,2) is relofted, then (3,2), etc., then (6,2), then (2,3), then (2,4), and then we move one row and column inward, relofting (3,3), ..., (6,3), and then (3,4), and one final time we move one more row and column inward, and then the whole network in figure C.2 has been relofted. Thus a point is relofted only after all the points closer to the network origin (in an indicial sense) have been relofted. We now describe the relofting procedure for a typical point.

The point  $P_4$  (see figure C.3) is relofted to a point  $P_4'$  as follows. Let  $\Delta \vec{P}_4 = \vec{P}_4' - \vec{P}_4$ . Then the user chooses a direction  $\hat{d}$  for  $\Delta \vec{P}_4$ ; that is, requires that

$$\Delta \vec{P}_4 = k \hat{d} \quad (C.1.8)$$

One then determines the value of  $k$  which minimizes  $\vec{W} \cdot \hat{n}'$ , where  $\hat{n}'$  is the normal of the relofted panel. In Appendix D, we show that

$$\hat{n}' = \frac{(\vec{P}_3 - \vec{P}_1) \times (\vec{P}_4' - \vec{P}_2)}{|(\vec{P}_3 - \vec{P}_1) \times (\vec{P}_4' - \vec{P}_2)|} \quad (C.1.9)$$

So, we can equally well minimize

$$|\delta \cdot \vec{W} \cdot \hat{n}'| = |\vec{W} \cdot \{(\vec{P}_3 - \vec{P}_1) \times (\vec{P}_4' - \vec{P}_2)\}| \quad (C.1.10)$$

where  $\delta$  is the denominator of (C.1.9).

$$\text{Writing } \vec{P}_4' = \vec{P}_4 + k \hat{d} \quad (C.1.11)$$

we minimize  $|f(k)|$ , where

$$f(k) = \vec{W} \cdot \{(\vec{P}_3 - \vec{P}_1) \times (\vec{P}_4 - \vec{P}_2)\} + k \vec{W} \cdot (\vec{P}_3 - \vec{P}_1) \times \hat{d} \quad (C.1.12)$$

which, being linear in  $k$ , is zero for

$$k = \frac{-\vec{W} \cdot (\vec{P}_3 - \vec{P}_1) \times (\vec{P}_4 - \vec{P}_2)}{\vec{W} \cdot \{(\vec{P}_3 - \vec{P}_1) \times \hat{d}\}} \quad (C.1.13)$$

This is well defined providing  $\hat{d}$  has been chosen so that it is not parallel to  $(\vec{P}_3 - \vec{P}_1)$  and provided  $\vec{W}$  is not in the plane spanned by  $(\vec{P}_3 - \vec{P}_1)$  and  $\hat{d}$ .

So, (C.1.11) defines  $P_4'$ , and we may continue to the next corner point to be relofted.

In the case of linearized design, we stop here, since we have the best answer we can obtain with the linear pressure formula. The relofted configuration is considered the surface whose distributions of pressure and normal mass flux are the desired ones.

## C.2 Sequential Design

In sequential design, the first step is again to supply a guess at the configuration which will yield the desired pressure distribution, and solve the potential flow problem about that configuration with zero normal flow boundary conditions. This results in a pressure distribution  $C_p(x,y,z)$ . Generally speaking, the second order or isentropic pressure formula would be used to compute this pressure distribution. Now, barring remarkable aerodynamic insight on the part of the user, this pressure distribution will differ from his desired distribution  $C_{p_S}(x,y,z)$ , but hopefully not by too much. We also compute the preliminary perturbation velocity distribution  $\vec{v}(x,y,z)$  resulting from the potential flow solution.

Now, we "linearize" about our previous solution by making the assumption (analogous to (C.1.1)) in that if  $C_{p_S}(x,y,z)$  is close to  $C_p(x,y,z)$ , then

$$C_{p_S}(x,y,z) - C_p(x,y,z) = -2\vec{v}_\infty \cdot (\vec{v}_S(x,y,z) - \vec{v}_p(x,y,z)) \quad (C.2.1)$$

where  $\vec{v}_S$  is the unknown velocity distribution which produces the desired pressure distribution  $C_{p_S}$ . Solving for the freestream component of  $\vec{v}_S$ ,

$$\vec{v}_\infty \cdot \vec{v}_S(x,y,z) = \vec{v}_\infty \cdot \vec{v}_p(x,y,z) - 1/2(C_{p_S} - C_p) \quad (C.2.2)$$

Considering the configuration in figure C.4 (in which  $C_{p,upper} = \Delta C_p$  since  $C_{p,lower} = 0$ ), equation (C.2.2) shows that we apply the boundary condition

$$\vec{t}_n \cdot \vec{\nabla} u = b \quad (C.2.3)$$

$$\text{since} \quad \vec{\nabla} u = \vec{v}_U - \vec{v}_L = \vec{v}_U \quad (C.2.4)$$

where  $\vec{t}_n$  is the projection of  $\vec{v}_\infty$  to the surface

$$\text{and} \quad b = \vec{v}_\infty \cdot \vec{v}_p(x,y,z) - 1/2(C_{p_S} - C_p) \quad (C.2.5)$$

Now, once the potential flow problem with the boundary conditions has been solved, the replotting is performed just as described in section C.1. Then an analysis case (i.e., a potential flow problem with impermeability boundary conditions) is run, and the new pressure and velocity distributions are evaluated, and the next cycle of the procedure continues.

If all goes well, the procedure converges, resulting in a configuration of shape with the desired pressure distribution. Unfortunately, if the initial guess does not yield a pressure distribution  $C_p(x,y,z)$  close to  $C_{p_S}(x,y,z)$ , the procedure may fail to converge.

### C.3 Iterative Design

The procedure we describe briefly in this section is much more accurate and rapidly convergent than sequential design, but also considerably more sophisticated, and not available in PAN AIR. It encompasses two features not found in sequential design. The first one is full automation; the relifting and the formulation of the boundary conditions are performed automatically by the program. The second is a more sophisticated relifting method.

This relifting method involves "differentiated influence coefficients". That is, once the potential flow solution has been performed, and the source and doublet parameters are known, the matrices  $\frac{\partial \vec{v}(P_i)}{\partial CP_j}$  are computed for

all  $i$  and  $j$ , where  $P_i$  is the  $i$ th control point, and  $CP_j$  is the  $j$ th panel corner point. The matrix  $[\partial v / \partial CP_j]$  is a  $3 \times 3$  matrix, one of which exists for each pair of control point  $P_i$  and corner point  $CP_j$ , whose  $k, l$  entry is  $\partial v_k / \partial CP_{jl}$ . Given these matrices, standard optimization techniques can be used in order to generate a revised geometry for which  $\iint_S W \cdot \hat{n}' dS$  is

minimized, subject to user-input constraints such as leaving the planform area the same.

We will not discuss this process further here, since PAN AIR does not make use of differentiated influence coefficients, and thus does not perform iterative design. A more detailed discussion of iterative design, for the special case of leading edge vortices, is given in reference (C.1).

## C.4 Stability

The problem of stability arises from the inherent numerical error in the discretization process, rather than from the theory of the Prandtl-Glauert equation. It is the splining method (see section 5.5 for a discussion of splines) in combination with the boundary conditions which is called stable or unstable. Precisely, a spline is called unstable if the perturbation of a single boundary condition results in a perturbation in the original solution which does not die out with distance from the point at which the boundary condition is located.

In checking for stability, we may make use of the fact that the sum of solutions of the Prandtl-Glauert equation is again a solution. Thus, the solution to any boundary value problem is a linear combination of individual solutions of cases in which one boundary value is set equal to one and the rest are set to zero. We thus check for stability by observing the singularity distribution which occurs when one boundary value is set to one and the rest to zero. The resulting singularity distribution should rapidly diminish in magnitude as the distance from the non-zero boundary condition increases. We consider a spline more stable, the more rapidly the singularity distribution diminishes.

The simplest way to illustrate stability is with two-dimensional examples. Thus, a "network" of "panels" consists of a sequence of intervals. For simplicity, all our splines will be doublet splines, though what we discuss will be applicable to source splines as well.

In figure C.5, we illustrate a doublet spline with singularity parameters and control points located at panel centers, and for which the doublet strength on a panel is constant, and equal to the singularity parameter value. In figure C.6, we illustrate the doublet distribution arising from the boundary conditions  $\mu = 0$  at all but one control point,  $\mu = 1$  at the remaining one. We see that the perturbation induced on the uniformly zero solution by the single non-zero boundary value dies down extremely rapidly; in fact, the perturbation is zero except on the single panel containing the non-zero boundary condition. Thus this spline is very stable. But we know (see Appendix B.4) that locally constant splines are insufficient, so we consider a quadratic spline, as illustrated in figure C.7. Because of the rapid variation a quadratic function may exhibit, control points and singularity parameters are required at the network edges in order to define the singularity strength adequately.

The spline is a piecewise quadratic one, where the quadratic variation is constructed as follows. The value of, for instance,  $\mu(P)$  is determined by finding the quadratic function  $f(x)$  which goes through  $Q_2$  and  $Q_3$  exactly, and then goes through  $Q_1$  and  $Q_4$  in a least squares sense. Then  $\mu(P)$  is given as  $f(P)$ . The details concerning the method by which we obtain the row vector  $S$  of length 4 such that

$$\mu(P) = S \begin{Bmatrix} \mu(Q_1) \\ \mu(Q_2) \\ \mu(Q_3) \\ \mu(Q_4) \end{Bmatrix} \quad (C.4.1)$$

are given in Appendix I.5.

Now, once we know  $u$  at every corner point on the network, the quadratic distribution of  $u$  on an interval is that quadratic function which takes on the computed values at the endpoints, and the singularity parameter value at the panel center. Considering the interval in figure C.8, in the local coordinates illustrated there, we have

$$u(x) = a + bx + cx^2 \quad (C.4.1)$$

$$u(-1) = u(P) = a - b + c \quad (C.4.2)$$

$$u(0) = u(Q) = a \quad (C.4.3)$$

$$u(1) = u(P') = a + b + c \quad (C.4.4)$$

So, subtracting (C.4.2) from (C.4.4),

$$2b = u(P') - u(P) \quad (C.4.5)$$

while, adding these equations,

$$2a + 2c = u(P) + u(P') \quad (C.4.6)$$

$$= 2c + 2u(Q) \quad (C.4.7)$$

Thus (by (C.4.3)) we have values for  $a$ ,  $b$ , and  $c$ , and so

$$u(x) = u(Q) + \frac{u(P') - u(P)}{2} x + \frac{u(P) + u(P') - 2u(Q)}{2} x^2 \quad (C.4.8)$$

In figure C.9, we illustrate the doublet distribution we obtain by setting  $u = 1$  at one control point, and  $u = 0$  at the others, given the spline just described. Note that this spline is nearly as stable as that of figure C.6; the disturbance dies down very quickly.

Further, this spline yields a doublet strength which is continuous across panel edges, something which is very important.

But the same spline, with boundary conditions

$$\frac{\partial u}{\partial x} = 1 \quad (C.4.9)$$

at the last control point, and

$$\frac{\partial u}{\partial x} = 0 \quad (C.4.10)$$

at the others (except  $u = 0$  at the first control point to insure uniqueness) yields the doublet distribution (solving the boundary value problem numerically) illustrated in figure C.10, which compares unfavorably with the identically zero doublet distribution obtained by replacing the right side of (C.4.9) by zero.

But now, consider the doublet parameter and control point locations illustrated in figure C.11. If we impose the boundary conditions (C.4.9) and (C.4.10), we claim that the resulting doublet distribution is illustrated in

figure C.12. While the doublet distribution in figure (C.10) was obtained numerically, that of figure (C.12) can be obtained theoretically in the following manner.

Consider a distribution  $\mu(x) = a+bx+cx^2$  on the interval in figure C.8. Now,

$$\frac{\partial \mu}{\partial x}(Q) = \frac{\partial \mu}{\partial x}(0) = b \quad (C.4.11)$$

and by (C.4.5)

$$b = \frac{\mu(P') - \mu(P)}{2} \quad (C.4.12)$$

Thus,

$$\mu(P') = \mu(P) + 2b = \mu(P) + 2 \frac{\partial \mu}{\partial x}(Q) \quad (C.4.13)$$

So, applying (C.4.12) and (C.4.13) to figure C.12 with  $P=P_0$ ,  $P' = P_1$ ,  $Q=Q_1$ , we obtain

$$\mu(P_1) = 0 \quad (C.4.14)$$

But now that we know  $\mu(P_1)$ , we apply (C.4.14) to the second intervals, and so

$$\mu(P_2) = 0 \quad (C.4.15)$$

We continue this way, obtaining

$$\mu(P_i) = 0, \quad i \leq 6 \quad (C.4.16)$$

$$\mu(P)_7 =$$

$$\mu(P_6) + 2 \frac{\partial \mu}{\partial x}(Q_7) = 2$$

If we now obtain  $\mu(Q_i)$  by least squaring to the 4 surrounding  $P_i$ , we see

$$\mu(Q_i) = 0, \quad i \leq 5 \quad (C.4.17)$$

$$\mu(Q_6) = 0 \quad (C.4.18)$$

$$\mu(Q_7) = 1 \quad (C.4.19)$$

and thus we obtain the doublet distribution of figure C.12.

So, comparing with figure C.10, we see that the imposition of doublet derivative boundary conditions at panel centers requires a different spline than the imposition of boundary conditions defining doublet strength. This situation generalizes to three dimensions, and thus requires different splines for design (that is, doublet gradient) boundary conditions than are used for analysis (that is, normal mass flux) boundary conditions.

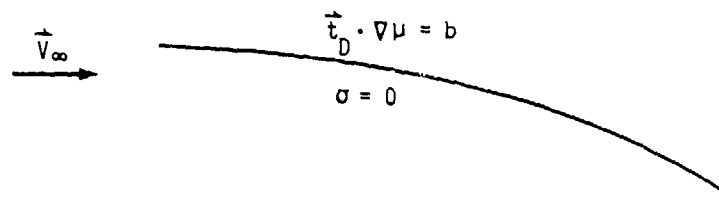


Figure C.1 - Design boundary conditions on a thin configuration

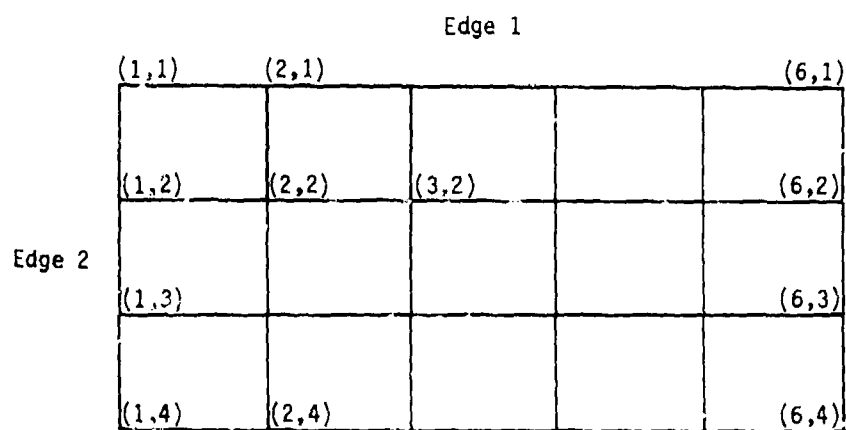


Figure C.2 - Indexing of network points



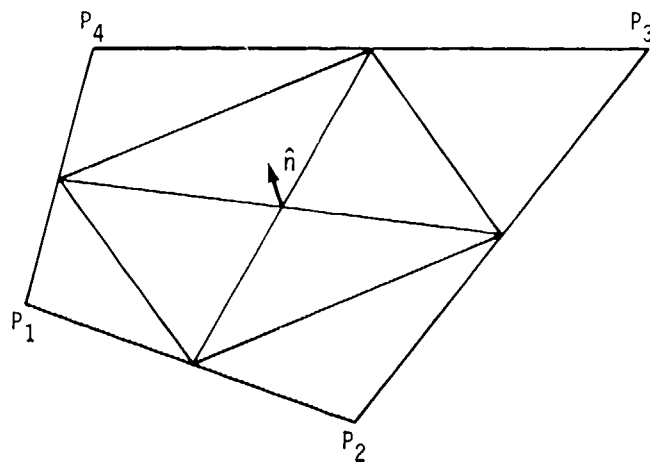
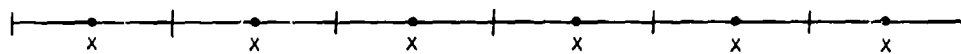


Figure C.3 - A panel



Figure C.4 - Design boundary conditions for a thick wing



• singularity parameter locations  
 x control points

Figure C.5 - A constant doublet strength spline

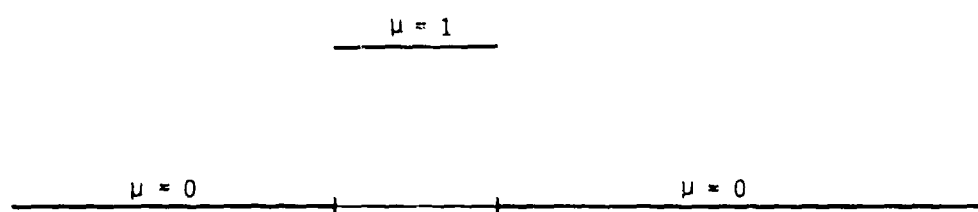


Figure C.6 - Stability for constant doublet spline

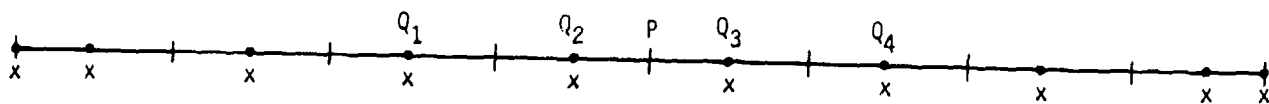


Figure C.7 - Quadratically varying doublet spline

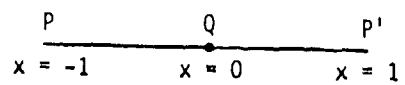


Figure C.8 - A single interval

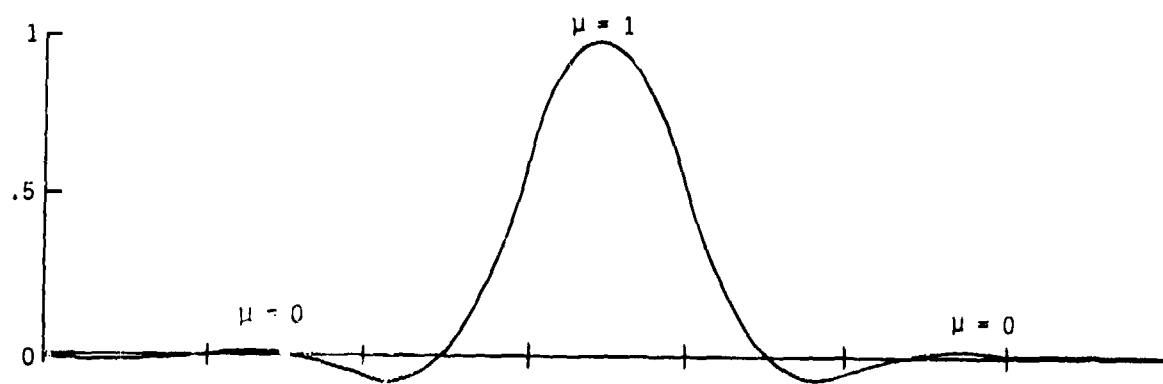


Figure C.9 - Stability for a quadratic doublet spline

C.5-6

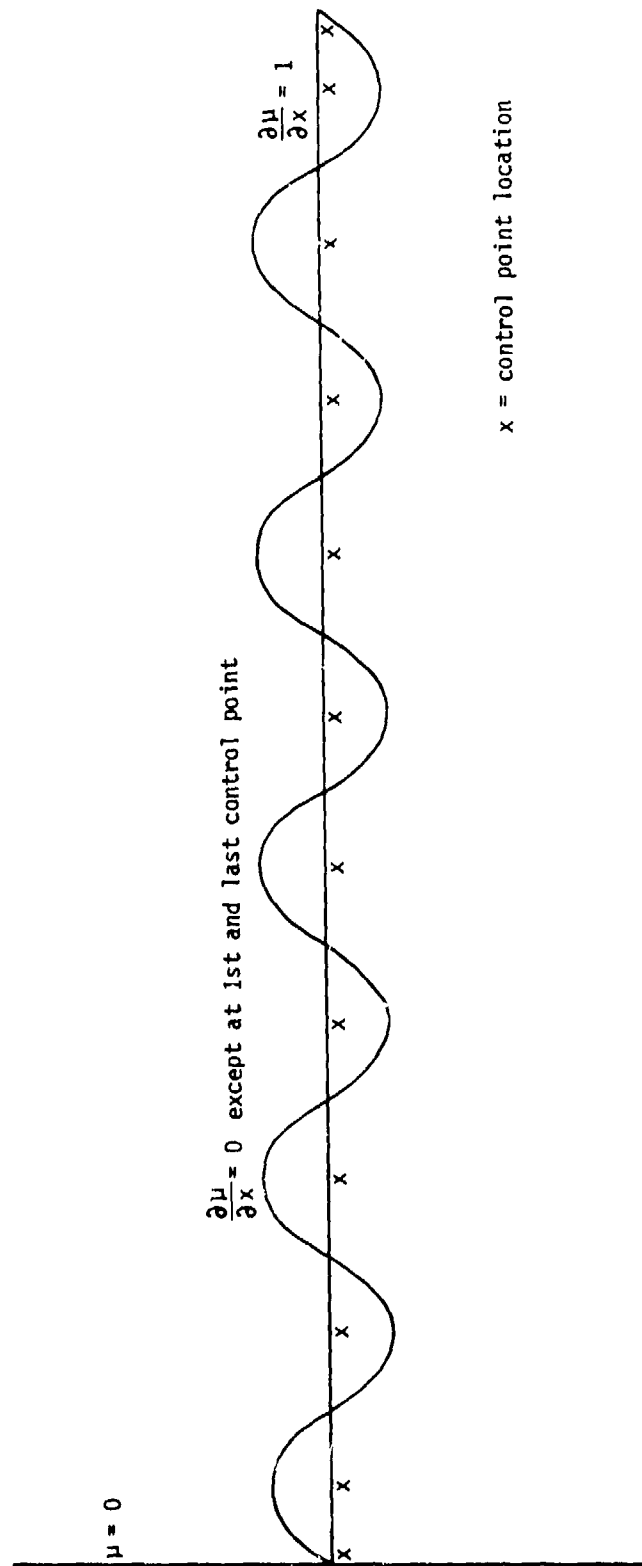


Figure C.10 - Instability of analysis spline with boundary conditions

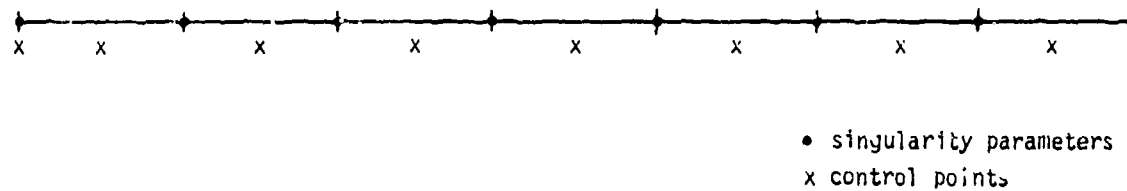


Figure C.11 - A doublet spline for design problems

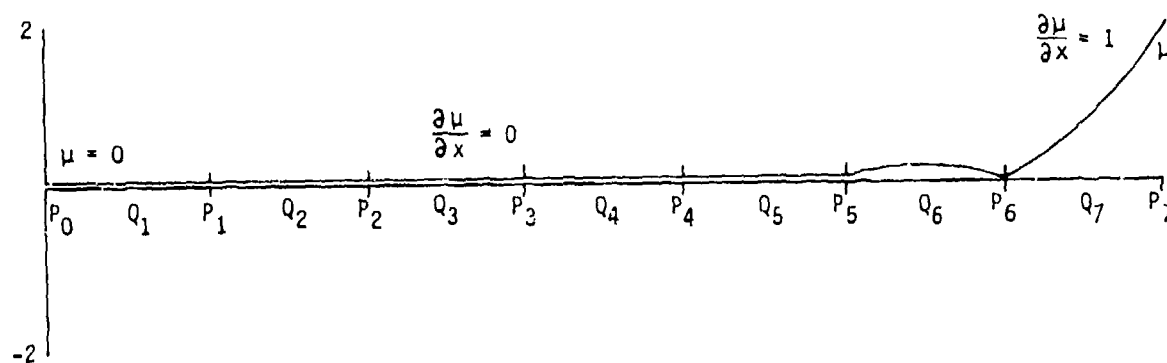


Figure C.12 - Stability for design boundary conditions

#### D.0 Geometry of Networks and Panels

This appendix will discuss the manner in which PAN AIR handles configuration geometry. In section D.1, we will describe the different types of "networks" by which a program user can describe a portion of the configuration. We will also discuss modifications in the geometry generated by the program under certain circumstances. In section D.2, we will discuss basic panel geometry. In section D.3, we will discuss the geometric error detection methods which discover geometric situations which could cause the program to execute improperly or terminate abnormally.

## D.1 Networks

A network is an array (with, say, M rows and N columns) of points in space which define a portion of the configuration geometry. In addition, source and doublet distributions are defined on the network (that is, the network is a "composite" network), with singularity parameter locations and spline methods determined by the network's "source type" and "doublet type".

### D.1.1 Network Types

The possible source types are "analysis", "design" and "null", while the doublet types are "analysis", "design", "wake 1", "wake 2", and "null". Source and doublet analysis networks are used in conjunction with boundary conditions defining impermeability. Design networks are used in conjunction with "design" boundary conditions, that is, those which specify tangential velocity. A network of type "null" is used to denote that the source or doublet strength is zero; one could equally well use an analysis network in conjunction with the uniform boundary condition

$$\sigma = 0 \quad (D.1.1)$$

or 
$$\mu = 0 \quad (D.1.2)$$

To model a wake, as described in section B.2, one would generally use a doublet wake network in conjunction with a source null network. The boundary conditions, which are only imposed at the wake leading edge, specify the matching of doublet strength on that edge to the doublet strength at the trailing edge of the adjacent wing network(s). In figures D.1 through D.3, we illustrate the singularity parameter locations corresponding to each of these network types.

### D.1.2 Wake Networks and the Kutta Condition

Two types of wake networks are available. In wake 1 networks, the doublet strength is variable along the leading edge, and constant in the indicially perpendicular direction. In wake 2 networks, the doublet strength is constant over the entire network. In the example of figure B.9, the wake extending behind the wing would generally be modeled with a wake 1 network, while the portion of the wake extending back from the body would be modeled with a wake 2 network.

The two types of wake networks have distinct purposes. The wake 1 network is PAN AIR's approach to satisfying the Kutta condition (see below), while the purpose of the wake 2 network is to carry over the doublet strength from the wing to the plane of symmetry.

The Kutta condition, which should hold at the trailing edge, is

$$\Delta C_p = 0 \quad (D.1.1)$$

where  $C_p$  is the pressure coefficient. If the freestream direction is the x



direction, and the freestream has unit magnitude, then (cf. (C.1.5)) for a thin wing, the linear expression for  $\Delta C_p$  is

$$\Delta C_p = -2 \frac{\partial \mu}{\partial x} \quad (D.1.2)$$

Now, the boundary conditions on the wake insure doublet continuity from the thin wing to the wake. In addition, it follows from section J.11 that the zero normal mass flux boundary conditions along the trailing edge of the wing insure the continuity of the x-component of the doublet gradient.

Now, the wake spline is such that the doublet strength is constant in the streamwise direction, that is,

$$\left. \frac{\partial \mu}{\partial x} \right|_{\text{wake}} = 0 \quad (D.1.3)$$

Since the normal mass flux boundary conditions insure matching of the doublet x-derivative, we have, in light of (D.1.2),

$$\Delta C_p \Big|_{\text{trailing edge of wing}} = 0 \quad (D.1.4)$$

Thus for a thin wing, the use of a wake 1 network results in the satisfaction of the Kutta condition, using the linear pressure coefficient formula. It is therefore natural to use the wake 1 network to satisfy the Kutta condition for a thick wing. This is done in PAN AIR, even in the absence of a theoretical justification of its validity.

Wake 2 networks have a purpose which is not related to the Kutta condition. In figure B.9, we show a wake 1 network emanating from the wing trailing edge. Now, the body is not a lifting surface, and therefore one would not in general expect a panel method to require a wake emanating from the body. The wake 2 network is required in PAN AIR, however, because in its absence the doublet matching boundary conditions on the wake 1 network would drive the doublet strength to zero along its inboard edge.

Because the doublet strength on the wake is constant, the doublet gradient is zero, and thus the surface vorticity,  $\hat{n} \times \nabla \mu$ , is zero. This corresponds to the physics of the configuration; that is, the body "sheds" no vorticity.

### D.1.3 Indexing

We now discuss the indexing system used internally in PAN AIR. The user specifies an array  $[CP(I,J)]$  of panel corner points, where  $I$ ,  $1 \leq I \leq M$ , is called the row index, and  $J$ ,  $1 \leq J \leq N$ , is called the column index. The upper surface is defined by an upward pointing unit normal  $\hat{n}$  whose direction is the vector cross product (direction of increasing column index)  $\times$  (direction of increasing row index). In figure D.4, we illustrate a network with  $\hat{n}$  pointing up from the paper. The network edges are labeled in counterclockwise fashion as shown, and each panel's corner points are similarly labelled in counterclockwise fashion. The point  $CP(1,1)$  is called the origin of the

network. Finally, a panel  $\Sigma$  is given a row index and column index equal to the row and column index of the point  $P_1$  on  $\Sigma$ .

Singularity parameters are indexed by a distinct integer for each parameter. For each index, the parameter type (source or doublet) and location are stored, and, conversely, for each location on a network, the program stores the indices of any singularity parameter located there.

#### D.1.4 Collapsing of Network Edges

Network edges are collapsed when a network of the type illustrated in figure D.5 is defined by the user. The distance shown there is a user-input "tolerance distance" ( $\epsilon$ ). The short edge of the network in that figure is collapsed as follows: the five panel corner points on that edge are each replaced by the same new point whose coordinates are the averages of the coordinates of the endpoints of the edge. Thus, the revised network has panel corner points as illustrated in figure D.6. The array of points is still a rectangular ( $M \times N$ ) array, except that now the same point occurs five times.

The reason for collapsing a network edge is that the existence of nearly triangular panels (as opposed to exactly triangular panels) such as those in figure D.4 causes nearly singular spline matrices, resulting in significant numerical error. On the other hand, triangular networks (which necessarily have triangular panels) cannot be excluded from consideration because the natural paneling of many surfaces such as delta wings (see figure D.7) requires the use of triangular networks.

A network edge is collapsed whenever the average panel edge length on the network edge is less than the tolerance distance. If, however, the average panel edge length exceeds  $\epsilon$ , yet one or more of the panel edges have length less than  $\epsilon$ , the program terminates. The edge cannot be left uncollapsed because some of the panels are too nearly triangular, it cannot be collapsed because the user-input geometry would be excessively perturbed, and it cannot be partially collapsed because of the indexing problems which would result when singularity parameter locations are assigned.

#### D.1.5 Additional Network Processing

Additional processing is performed on the geometry of each network, but will not be discussed here. This processing includes labeling of all but one singularity parameter on a collapsed network edge as "null", and storing data concerning each network edge separately in preparation for the automatic abutment search described in Appendix F.3. Since this data is associated with computing questions rather than engineering questions, this processing will be discussed in section 3 of the maintenance document.

## D.2 Basic Panel Geometry

In this section we describe some basic quantities concerning panel geometry.

A panel is uniquely defined by its four corner points  $P_i$ ,  $i=1,\dots,4$ , but for convenience we define nine panel defining points as shown in figure D.8, where  $P_5,\dots,P_8$  are panel edge midpoints, and

$$\vec{P}_9 = \frac{1}{4} (\vec{P}_1 + \vec{P}_2 + \vec{P}_3 + \vec{P}_4) \quad (D.2.1)$$

Note that even though  $P_i$ ,  $i=1,\dots,4$ , are arbitrary,  $P_j$ ,  $j=5,\dots,9$  lie in a plane. The proof comes from noting that by definition an edge midpoint is the average of the endpoints of the edge, and so

$$\begin{aligned} \vec{P}_5 &= \frac{1}{2} (\vec{P}_1 + \vec{P}_2) \\ \vec{P}_6 &= \frac{1}{2} (\vec{P}_2 + \vec{P}_3) \\ \vec{P}_7 &= \frac{1}{2} (\vec{P}_3 + \vec{P}_4) \\ \vec{P}_8 &= \frac{1}{2} (\vec{P}_4 + \vec{P}_1) \end{aligned} \quad (D.2.2)$$

and so

$$\begin{aligned} \frac{1}{2} (\vec{P}_5 + \vec{P}_7) &= \frac{1}{4} (\vec{P}_1 + \vec{P}_2 + \vec{P}_3 + \vec{P}_4) = \vec{P}_9 \\ \frac{1}{2} (\vec{P}_6 + \vec{P}_8) &= \frac{1}{4} (\vec{P}_2 + \vec{P}_3 + \vec{P}_4 + \vec{P}_1) = \vec{P}_9 \end{aligned} \quad (D.2.3)$$

Thus  $P_5,\dots,P_8$  lie in the plane defined by the line connecting  $P_5$  and  $P_7$ , and the line connecting  $P_6$  and  $P_8$ .

Thus  $P_9$  is the midpoint of the edge  $P_5P_7$  as well as of the edge  $P_6P_8$ , and so  $P_5,P_9$  and  $P_7$  lie on a line, as do  $P_6,P_9$ , and  $P_8$ . But a basic theorem in geometry states that there exists a plane containing any two intersecting lines, and so  $P_5,\dots,P_9$  lie in that plane, which is called the panel's "average plane".

We define the panel normal  $\hat{n}$  as the unit vector normal to the plane containing  $P_5,\dots,P_9$ , a vector which is unique provided the plane is unique, that is, provided the set  $P_5,\dots,P_9$  contains at least 3 distinct points. The vector  $n$  can be computed in a multitude of ways:

$$\hat{n} = \pm \frac{\vec{V} \times \vec{W}}{|\vec{V} \times \vec{W}|} \quad (D.2.4)$$

for any linearly independent pair of vectors  $V$  and  $W$  lying in the plane. Equation (D.2.4) holds because the cross product of two vectors is perpendicular to each of them; the condition that  $V$  and  $W$  be linearly independent (i.e., non-parallel) insures that

$$\vec{V} \times \vec{W} \neq 0 \quad (D.2.5)$$

$$\text{since} \quad \vec{V} \times \vec{W} = |\vec{V}| |\vec{W}| \sin \theta \quad (D.2.6)$$

where  $\theta$  is the angle between  $V$  and  $W$ . Further,  $|\hat{n}| = 1$  as long as the denominator of (D.2.4) is non-zero.

In practice, PAN AIR derives

$$\begin{aligned} \vec{P}_{10} &= 1/2 (\vec{P}_5 + \vec{P}_6) \\ \vec{P}_{11} &= 1/2 (\vec{P}_6 + \vec{P}_7) \\ \vec{P}_{12} &= 1/2 (\vec{P}_7 + \vec{P}_8) \\ \vec{P}_{13} &= 1/2 (\vec{P}_8 + \vec{P}_5) \end{aligned} \quad (D.2.7)$$

$$\text{and} \quad \hat{n} = \frac{(\vec{P}_{10} - \vec{P}_{12}) \times (\vec{P}_{11} - \vec{P}_{13})}{|(\vec{P}_{10} - \vec{P}_{12}) \times (\vec{P}_{11} - \vec{P}_{13})|} \quad (D.2.8)$$

which insures that  $\hat{n}$  points up out of the paper (see figure D.8). The equation (D.2.8) is used in PAN AIR because that formulation would hold even for "curved panels" (not included in version 1.0 of PAN AIR) for which  $P_5, \dots, P_9$  do not lie in a plane.

We now compute  $n$  by a different method, in order to obtain a result used in section C.1. Applying (D.2.4),

$$\hat{n} = \frac{(\vec{P}_5 - \vec{P}_7) \times (\vec{P}_6 - \vec{P}_8)}{|(\vec{P}_5 - \vec{P}_7) \times (\vec{P}_6 - \vec{P}_8)|} \quad (D.2.9)$$

and thus, substituting (D.2.2) into (D.2.9),

$$\hat{n} = \frac{1/2(\vec{P}_1 + \vec{P}_2 - \vec{P}_3 - \vec{P}_4) \times 1/2(\vec{P}_2 + \vec{P}_3 - \vec{P}_4 - \vec{P}_1)}{|1/2(\vec{P}_1 + \vec{P}_2 - \vec{P}_3 - \vec{P}_4) \times 1/2(\vec{P}_2 + \vec{P}_3 - \vec{P}_4 - \vec{P}_1)|} \quad (D.2.10)$$

The numerator of (D.2.10) is

$$\begin{aligned} & 1/4 \{(\vec{P}_1 - \vec{P}_3) + (\vec{P}_2 - \vec{P}_4)\} \times \{-(\vec{P}_1 - \vec{P}_3) + (\vec{P}_2 - \vec{P}_4)\} \\ &= 1/4 \{(\vec{P}_1 - \vec{P}_3) \times (\vec{P}_2 - \vec{P}_4) - \{(\vec{P}_2 - \vec{P}_4) \times (\vec{P}_1 - \vec{P}_3)\}\} \end{aligned} \quad (D.2.11)$$

$$= 1/2 (\vec{P}_1 - \vec{P}_3) \times (\vec{P}_2 - \vec{P}_4) \quad (D.2.12)$$

Substituting this into (D.2.10),

$$\hat{n} = \frac{(\vec{p}_1 - \vec{p}_3) \times (\vec{p}_2 - \vec{p}_4)}{|(\vec{p}_1 - \vec{p}_3) \times (\vec{p}_2 - \vec{p}_4)|} \quad (D.2.13)$$

a result quoted in section C.1.

Now,  $p_1, \dots, p_4$  need not lie in the plane containing  $p_5, \dots, p_9$ . Thus, a panel contains 5 planar regions; the center region which contains four triangular regions as illustrated in figure D.9, and 4 outer regions containing one triangular region each. The triangular regions are called subpanels, and so a panel contains 8 subpanels, which are labeled in figure D.8.

Much of the geometric data for a panel is computed for each subpanel, though this is occasionally redundant. These include: (1) a subpanel origin and reference to local transformation describing a local subpanel coordinate system (see Appendix E), (2) a subpanel unit normal vector and co-normal, (3) the subpanel area, (4) unit edge tangent vectors for the subpanel edges along with their "compressible" norm, (5) subpanel edge normals in local coordinates, (6) a Jacobian factor relating subpanel area in global coordinates to that in local coordinates, and (7) a flag indicating whether the subpanel is subinclined or superinclined.

To obtain the unit normal to the subpanel illustrated in figure D.9, we compute

$$n = \frac{(\vec{p}_j - \vec{p}_i) \times (\vec{p}_k - \vec{p}_i)}{|(\vec{p}_j - \vec{p}_i) \times (\vec{p}_k - \vec{p}_i)|} \quad (D.2.14)$$

where  $\hat{n}$  is not computed if the denominator is less than  $10^{-10}$ . In that case, the subpanel area is set equal to zero, and no subpanel calculations are performed. The area of the subpanel is (from geometry)

$$A = 1/2 |\vec{p}_j - \vec{p}_i| |\vec{p}_k - \vec{p}_i| \sin \theta \quad (D.2.15)$$

Combining (D.2.6) and (D.2.15),

$$A = 1/2 |(\vec{p}_j - \vec{p}_i) \times (\vec{p}_k - \vec{p}_i)| \quad (D.2.16)$$

The unit edge tangents are

$$\hat{t} = \frac{\vec{p}_j - \vec{p}_i}{|\vec{p}_j - \vec{p}_i|} \quad (D.2.17)$$

etc. The compressible norm of  $\hat{t}$  (see Appendix E for a discussion of this norm) is (by definition)

$$[\hat{t}, \hat{t}] = \hat{t} \cdot \hat{t} - M_{\infty}^2 (C_{\theta} \cdot \hat{t})^2 \quad (D.2.18)$$

The subpanel conormal is defined in compressibility axis coordinates (in which the compressibility direction  $\hat{c}_0 = (1,0,0)$ ) as

$$\tilde{n} = \begin{pmatrix} s\beta^2 n_x \\ n_y \\ n_z \end{pmatrix} \quad (D.2.19)$$

$$= (s\beta^2 - 1) (\hat{c}_0 \cdot \hat{n}) \hat{c}_0 + \hat{n} \quad (D.2.20)$$

since

$$n_x = \hat{c}_0 \cdot \hat{n} \quad (D.2.21)$$

$$\text{Thus,} \quad \tilde{n} = \hat{n} - M_\infty^2 (\hat{c}_0 \cdot \hat{n}) \hat{c}_0 \quad (D.2.22)$$

The Jacobian factor J is given by

$$J = \frac{\text{Area in reference coordinates}}{\text{Area in local coordinates}} \quad (D.2.23)$$

its use will be discussed in Appendices I and J.

Finally, the sub-panel is "subinclined" if

$$\hat{n} \cdot \tilde{n} > 0 \quad (D.2.24)$$

and "superinclined" if

$$\hat{n} \cdot \tilde{n} < 0 \quad (D.2.25)$$

$$\text{If} \quad \hat{n} \cdot \tilde{n} \approx 0 \quad (D.2.26)$$

the subpanel is "Mach-inclined", and the program terminates for reasons which will be discussed in Appendix E.

Some items of data computed for each panel are not concerned with just a single subpanel. For instance, all the data computed for the subpanels is also computed for the "projected panel", the projection of the panel to the average plane. In addition, it is computed for the four "half panels", that is, the triangles  $P_1P_2P_4$ ,  $P_2P_3P_1$ ,  $P_3P_4P_2$ ,  $P_4P_1P_3$ .

These data are needed to compute "intermediate field" influence coefficients, in the computation of which the panel is approximated either by two half panels or by the projected panel. These are used when measuring the influence of the panel on a control point which is sufficiently far not to require the 8-subpanel representation of the panel, but not far enough to permit the far field influence coefficient computation method (see Appendix J.2). All the items are computed for the projected panel or half panels in the same manner as for subpanels. Redundant data is not necessarily computed (e.g., the projected panel is super- or sub-inclined whenever subpanels 5 through 8 are).

Finally, the program calculates, for each panel, its radius, its diameter, and certain skewness parameters. The radius is the distance from the center to the farthest corner point and the diameter is the maximum distance between any two corner points. The skewness parameters result from a non-orthogonal transformation of coordinates after which

$$P_9 = \begin{Bmatrix} 0 \\ 0 \\ 0 \end{Bmatrix}, \quad P_8 = \begin{Bmatrix} 1 \\ 0 \\ 0 \end{Bmatrix}, \quad P_5 = \begin{Bmatrix} 0 \\ 1 \\ 0 \end{Bmatrix}, \quad \hat{n} = \begin{Bmatrix} 0 \\ 0 \\ k \end{Bmatrix}, k > 0 \quad (D.2.27)$$

We may see from figure D.8 that this is not the standard choice of x and y axes, but it results from having derived the relevant formulas with the panel in figure D.8 rotated by 180°.

We use this coordinate system, which we write  $(x^*, y^*, z^*)$  because the interior region bounded by  $P_5, \dots, P_9$  becomes a square, as illustrated in figure D.10. Note that in general (since most panels are not square), this is not an orthogonal coordinate system. The numbers  $C_{ij}$ ,  $j=1, \dots, 4$ ,  $i=1, 2$ , are called skewness parameters since they are all zero for a panel which is a parallelogram in the original coordinate system as

$$(\vec{P}_1 - \vec{P}_9) = (\vec{P}_5 - \vec{P}_9) + (\vec{P}_8 - \vec{P}_9) \quad (D.2.28)$$

for a parallelogram.

The doublet subpanel spline matrices are calculated in the  $(x^*, y^*, z^*)$  coordinate system, but rather than transform the panel coordinates, we compute the matrices using the skewness parameters (see section I.2 for details).

Computing the skewness parameters is fairly straightforward. Combining

$$\vec{P}_1 = \begin{Bmatrix} 1 + C_{11} \\ 1 + C_{21} \end{Bmatrix} \quad (D.2.29)$$

with (D.2.27), (D.2.28) we obtain

$$\begin{aligned} (\vec{P}_1 - \vec{P}_9) &= (1 + C_{11}) (\vec{P}_8 - \vec{P}_9) \\ &+ (1 + C_{21}) (\vec{P}_5 - \vec{P}_9) + \hat{n} \frac{z}{k} \end{aligned} \quad (D.2.30)$$

Taking the cross product on the left with  $(P_8 - P_9)$ , and putting into  $n$ , we obtain

$$\begin{aligned} \{(\vec{P}_8 - \vec{P}_9) \times (\vec{P}_1 - \vec{P}_9)\} \cdot n &= (1 + C_{11}) 0 \cdot \hat{n} \\ &+ (1 + C_{21}) \{(\vec{P}_8 - \vec{P}_9) \times (\vec{P}_5 - \vec{P}_9)\} \cdot n \\ &+ \frac{Z}{K} [(\vec{P}_8 - \vec{P}_9) \times \hat{n}] \cdot \hat{n} \end{aligned} \quad (D.2.31)$$

The final term is zero, and so

$$\begin{aligned} C_{21} &= \frac{\{(\vec{P}_8 - \vec{P}_9) \times (\vec{P}_1 - \vec{P}_9)\} \cdot \hat{n}}{(\vec{P}_8 - \vec{P}_9) \times (\vec{P}_5 - \vec{P}_9) \cdot \hat{n}} - 1 = \\ &\frac{\{(\vec{P}_8 - \vec{P}_9) \times (\vec{P}_1 - \vec{P}_9)\} \cdot \hat{n}}{(\vec{P}_8 - \vec{P}_9) \times (\vec{P}_5 - \vec{P}_9) \cdot \hat{n}} \end{aligned} \quad (D.2. )$$

Similarly

$$\{(\vec{P}_1 - \vec{P}_9) \times (\vec{P}_5 - \vec{P}_9)\} \cdot \hat{n} = ((1 + C_{11})(\vec{P}_8 - \vec{P}_9) \times (\vec{P}_5 - \vec{P}_9)) \cdot \hat{n} \quad (D.2.33)$$

and thus  $C_{11} = \frac{\{(\vec{P}_1 - \vec{P}_9) \times (\vec{P}_5 - \vec{P}_9)\} \cdot \hat{n}}{(\vec{P}_8 - \vec{P}_9) \times (\vec{P}_5 - \vec{P}_9) \cdot \hat{n}} - 1$

$$= \frac{\{(\vec{P}_1 - \vec{P}_8) \times (\vec{P}_5 - \vec{P}_9)\} \cdot \hat{n}}{\{(\vec{P}_8 - \vec{P}_9) \times (\vec{P}_5 - \vec{P}_9)\} \cdot \hat{n}} \quad (D.2.34)$$

Examination of figure D.10 gives us

$$\begin{aligned} C_{12} &= C_{11} \\ C_{22} &= -C_{21} \\ C_{13} &= -C_{11} \\ C_{23} &= -C_{21} \\ C_{14} &= -C_{11} \\ C_{24} &= C_{21} \end{aligned} \quad (D.2.35)$$

This concludes the discussion of basic panel geometric quantities.

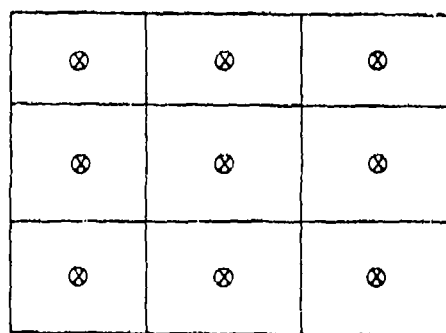


### D.3 Error Checks

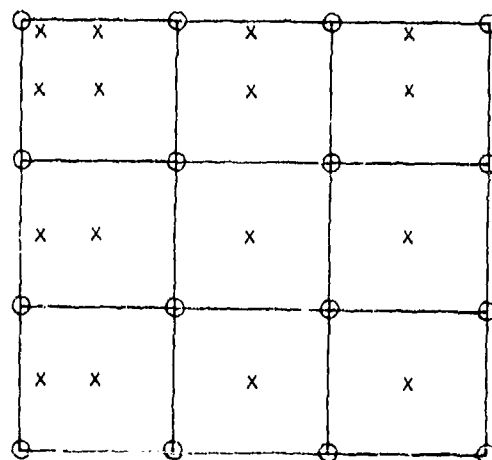
In this section, we summarize the basic checks performed by the program to insure that the geometry of the configuration is admissible. These checks are the following:

- a. Check if the average panel edge length on a network edge exceeds the tolerance  $\epsilon$ , while some panel edge length is less than  $\epsilon$  (violation is a fatal error).
- b. Check if two adjacent edges of network collapse. This is inadmissible because the calculation of spline matrices would be impossible for panels near both collapsed edges. See figure D.11 for a network in which adjacent edges are collapsed.
- c. Check if a panel edge in the network interior has length less than  $\epsilon$ . This is inadmissible because of logic problems which would occur in calculating the spline matrices if the edge were collapsed, and numerical inaccuracies occurring from nearly triangular panels.
- d. Check the panel aspect ratio. This is the ratio of the furthest distance from the panel center to its boundary over the smallest distance. Large aspect ratios cause numerical error in spline and influence coefficient calculation (this has only been verified experimentally). Aspect ratios over  $10^6$  are forbidden and those over 100 result in a warning message.
- e. A panel or subpanel is essentially Mach inclined. If  $\tilde{n} \cdot \tilde{n} < 10^{-4}$  this is a fatal error, and if  $< 1/10$  a warning message is printed.
- f. The panel is seriously skewed. Warning messages are printed if the panel is non-convex ( $1+c_{i1}+c_{i2} < 0$  for some  $i = 1, \dots, 4$ ), nearly non-convex ( $1+c_{i1}+c_{i2} \approx 0$ ), or triangular while having four distinct vertices ( $1+c_{i1}+c_{i2} \approx 0$ ).
- g. A subpanel has zero area when projected to the average plane. If so, a flag is set, no normal or conormal vector is calculated, the subpanel splines are set to zero, etc.

a. Source analysis network



b. Source design network

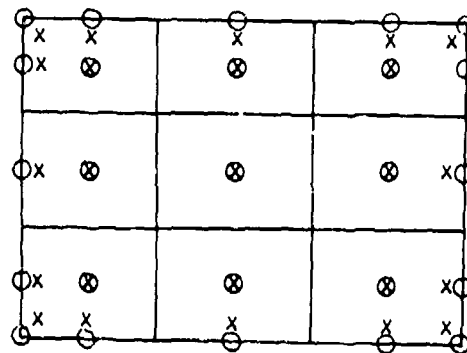


⊗ source parameter locations

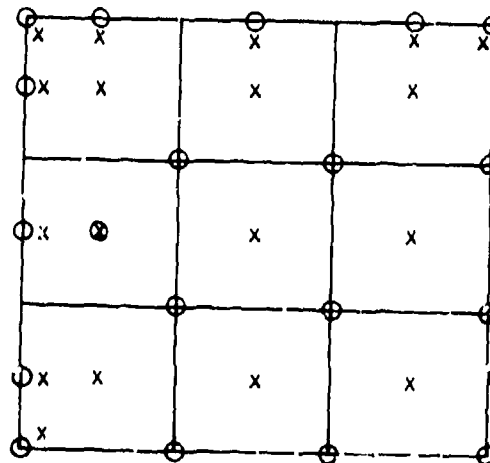
x locations of corresponding non-trivial boundary conditions

Figure D.1 - Locations of source singularity parameters

a. Doublet analysis



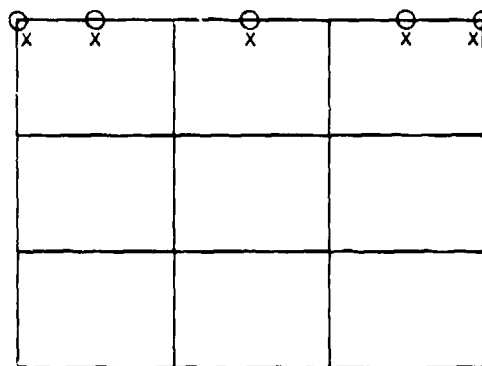
b. Doublet design



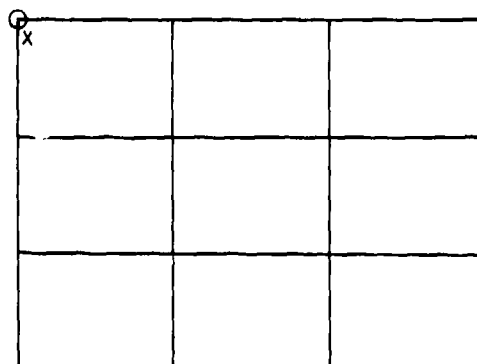
○ doublet parameter locations  
x boundary condition locations

Figure D.2 - Doublet analysis and design singularity parameter locations

a. Doublet wake 1



b. Doublet wake 2



- doublet parameter locations
- x boundary condition locations

Figure D.3 - Doublet wake singularity parameter locations

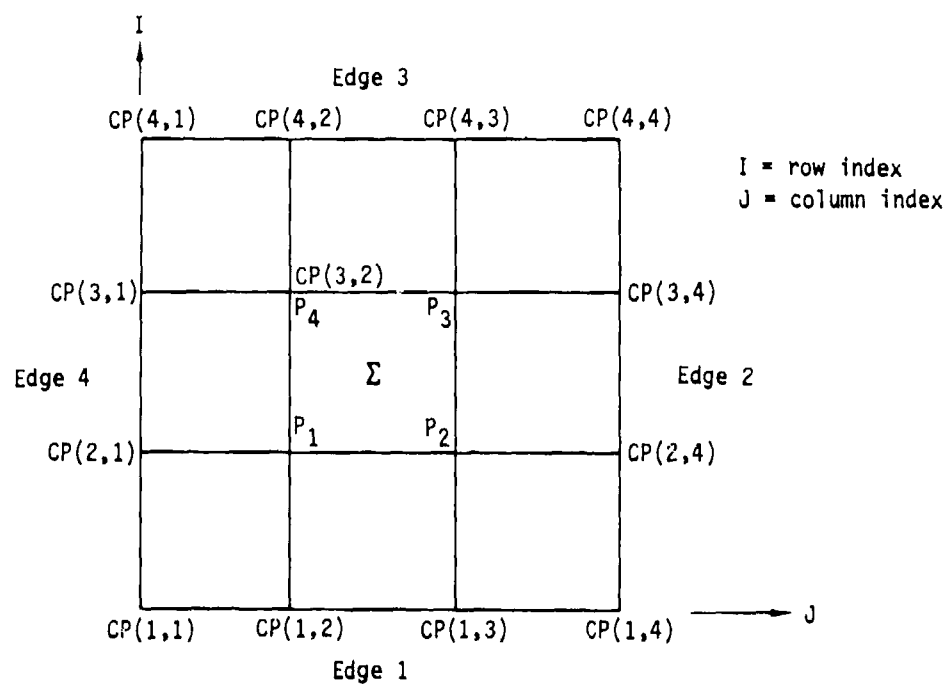


Figure D.4 - Network and panel indexing

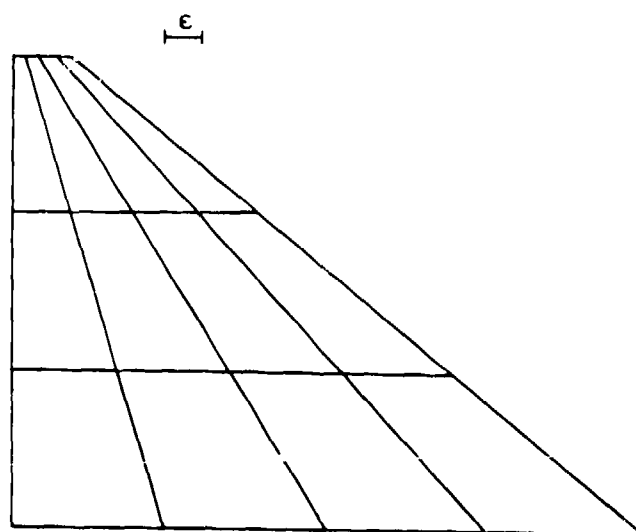


Figure D.5 - Network with an edge to be collapsed by the program

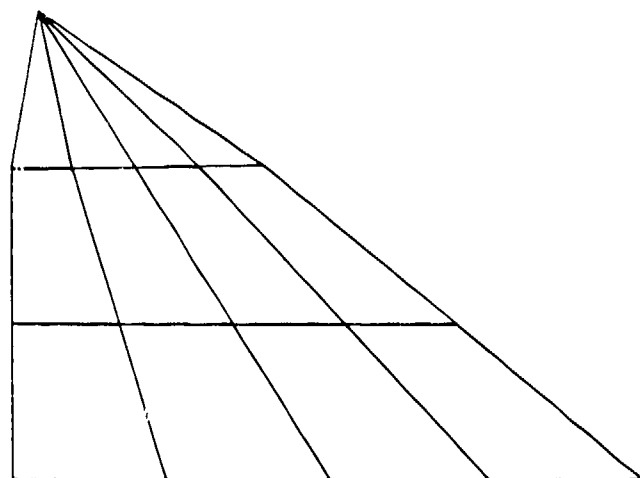


Figure D.6 - Network with revised geometry

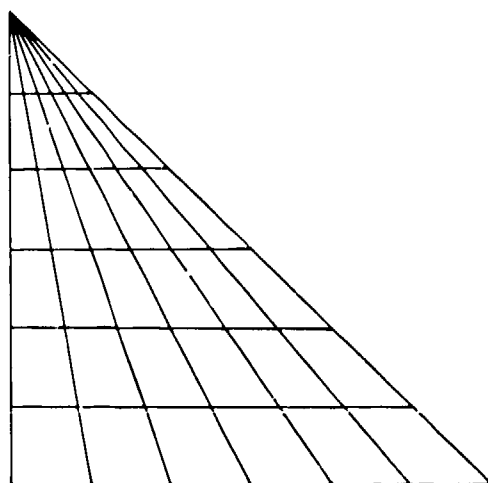


Figure D.7 - Panelling of delta wing

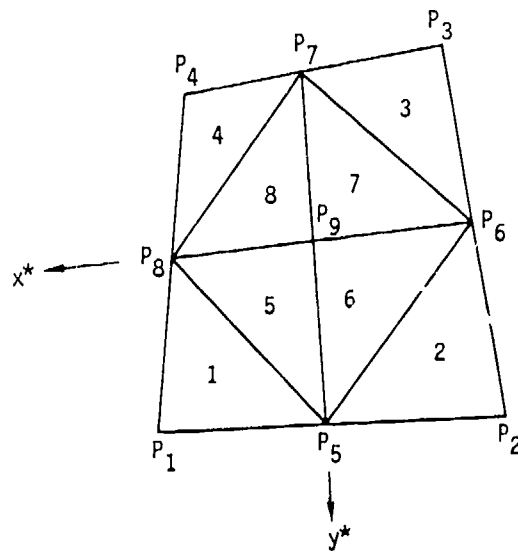


Figure D.8 - A panel

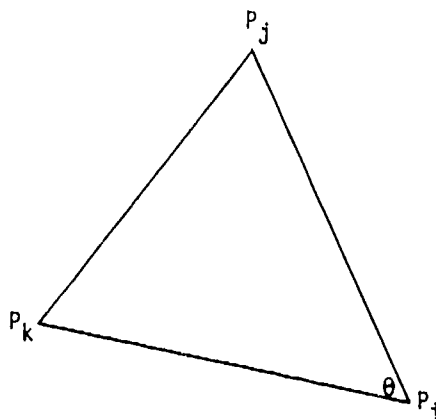


Figure D.9 - A subpanel

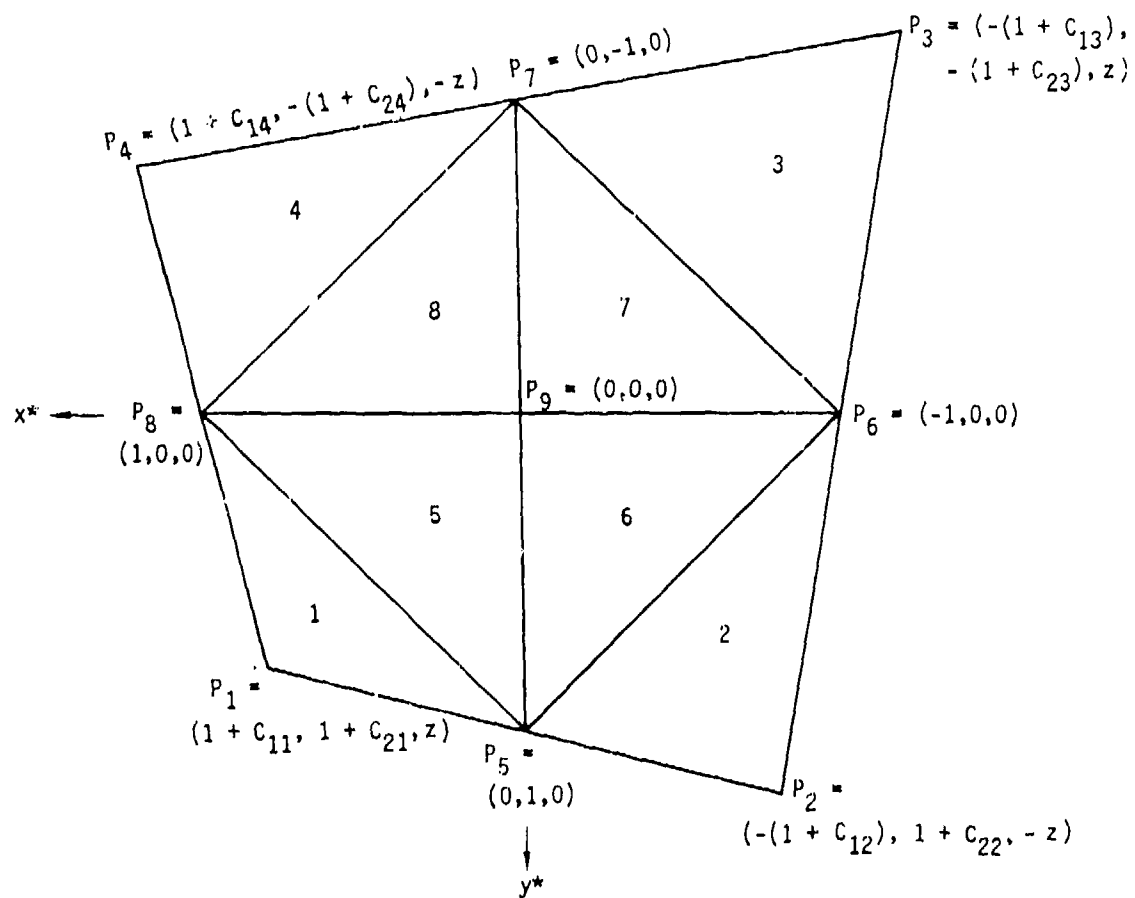


Figure D.10 - Definition of skewness parameters



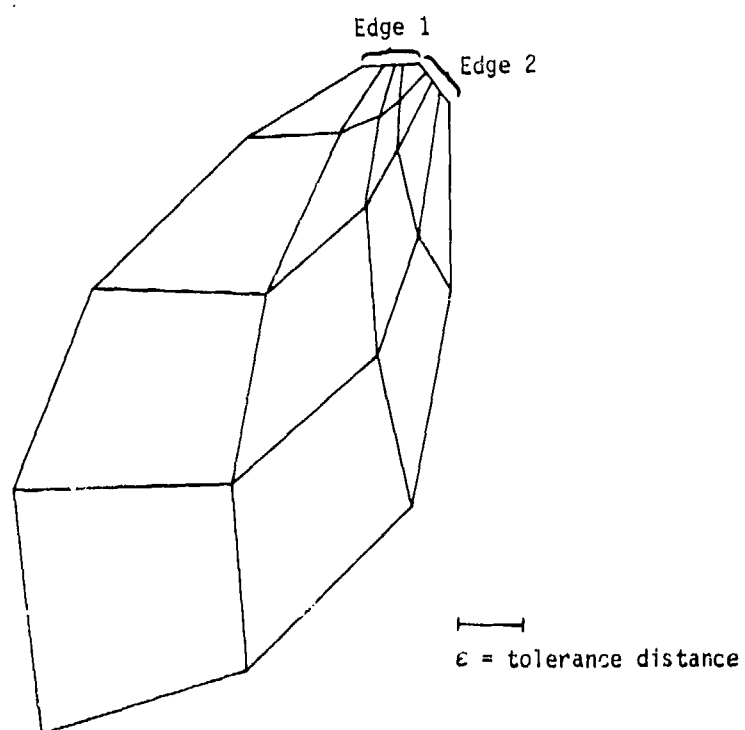


Figure D.11 - Impermissible network (two adjacent collapsed edges)

## E.0 Matrices and Coordinates

The material in this appendix is hardly reflected in the PAN AIR code, but rather provides background material on coordinate systems and transformations. This material is referred to in the course of the influence coefficient derivations of Appendix J. In addition, we derive (in section E.3) the expression for the reference to local transformation (see (5.2.27))

$$A = \begin{bmatrix} \frac{1}{|(\hat{n}_0, \hat{n}_0)|^{1/2}} & [C_0] \hat{u}_0 & \frac{rs}{\beta} [C_0] \hat{v}_0 & \frac{\beta \hat{n}_0}{|(\hat{n}_0, \hat{n}_0)|^{1/2}} \end{bmatrix}^T \quad (E.0.1)$$

and for the transformation between orthogonal coordinate systems (see (5.2.11))

$$\Gamma = \begin{bmatrix} \cos \alpha \cos \beta & -\sin \beta & \sin \alpha \cos \beta \\ \cos \alpha \sin \beta & \cos \beta & \sin \alpha \sin \beta \\ -\sin \alpha & 0 & \cos \alpha \end{bmatrix} \quad (E.0.2)$$

Because  $\Gamma$  is a transformation between two orthogonal coordinate systems, it is in fact an orthogonal matrix. That is, its inverse is its transpose, and for all vectors  $X, Y$ , the Euclidean inner product is invariant under transformation by :

$$(\Gamma X, \Gamma Y) = (X, Y) \quad (E.0.3)$$

This arises from the fact that  $\Gamma$  is a rotation (see section E.3)

In our application,  $\Gamma$  will be the matrix relating reference coordinates and the compressibility coordinate system, in which the x-axis is the compressibility direction.

The matrix  $A$  is less well-behaved, however. This transformation is the product

$$A = GS\Gamma \quad (E.0.4)$$

where we have

$$X_0 \xrightarrow{\Gamma} X \xrightarrow{S} X \xrightarrow{G} X' \quad (E.0.5)$$

Here,  $X_0$  is the reference coordinate system defined by the program user,  $X$  is the compressibility coordinate system in which the freestream is in the x-direction,  $X$  is a coordinate system in which the y- and z-axes have been scaled according to (3.1.3), and  $X'$  is the local coordinate system in which (5.2.19) holds.

While the matrices  $\Gamma$  and  $G$  are orthogonal, the scaling matrix  $S$  is not, and so the product matrix  $A$  is not orthogonal either. The bulk of the complexity of this appendix arises from this fact. In figure E.1, we illustrate a surface  $S$  in the compressibility coordinate system  $X$  and its image  $S'$  in the scaled coordinate system  $X'$ . We illustrate vectors  $\hat{t}$  and  $\hat{n}$ , tangent and normal to

the surface  $S$  respectively, and their images  $\bar{\mathbf{t}}'$  and  $\bar{\mathbf{n}}$  in the scaled coordinate system  $X'$ .

In section E.1, we consider the properties of vectors and their images under an arbitrary transformation. The reader may find some benefit in verifying

the results of E.1 for a "typical" matrix  $A$ , such as a diagonal matrix which is not the identity. In section E.2, we derive the properties of some special inner products. In section E.3, we verify that the matrix (E.0.1) has all the properties we require of a reference-to-local transformation. We do so, in fact, without ever constructing the transformation  $G$  of (E.0.5).

## E.1 Vectors and Dual Vectors

We consider here the effect of the coordinate transformation  $A = [a_{ij}]$

$$A: X_0 \rightarrow X' \quad (E.1.1)$$

by which a position vector  $\vec{x}_0 = \begin{Bmatrix} x_1 \\ x_2 \\ x_3 \end{Bmatrix}$ , expressed in the coordinate

system  $X_0$ , is transformed into an image vector  $\vec{x}' = \begin{Bmatrix} x_1' \\ x_2' \\ x_3' \end{Bmatrix}$ , expressed in the

coordinate system  $X'$ . This image vector represents the same physical quantity (such as location) as the original vector, but in a different coordinate system. It is a different vector only in the sense that its entries are distinct from those of  $\vec{x}$ .

The entries  $x_i'$  of the image vector  $\vec{x}'$  are given by the formulas

$$x_i' = \sum_{j=1}^3 a_{ij} x_j = \{A \vec{x}_0\}_i \quad i = 1, 2, 3 \quad (E.1.2)$$

where  $a_{ij}$  are the entries of the transformation matrix  $A$ . We shall occasionally find it convenient to write this equation using the summation convention for repeated indices, that is,  $x_i' = a_{ij} x_j$ . Examples of other vectors which transform according to the formula (E.1.2) include the vector element of arc length,  $dl$ , and surface tangent vectors  $t$ :

$$dl_i' = a_{ij} dl_j = \{A d\vec{l}\}_i \quad (E.1.3)$$

$$t_i' = a_{ij} t_j = \{A \vec{t}\}_i \quad (E.1.4)$$

Equation (E.1.4) may be interpreted to assert that when  $\vec{t}_0$  is a surface tangent to some surface  $S$  at some point  $y_0$  in  $S$ , then  $\vec{t}' = A \vec{t}_0$  will be a surface tangent vector to the image surface  $S'$

$$S' = \{ \vec{x}' : \vec{x}' = [A] \vec{x}_0 \text{ for some } \vec{x}_0 \text{ in } S \} \quad (E.1.5)$$

at the image point  $\vec{y}' = [A] \vec{y}$ . Unless  $[A]$  is an orthogonal matrix, however, we need not expect that  $\vec{t}'$  will be a unit vector even when  $\vec{t}$  is. However, if  $\hat{\vec{t}} = \vec{t}/|\vec{t}|$  is any unit vector, then we define the corresponding image unit vector by

$$\hat{\vec{t}}' = A \hat{\vec{t}} / |A \hat{\vec{t}}| \quad (E.1.6)$$

Thus the transformation rule for unit vectors is somewhat more complicated than the corresponding rule for vectors. In particular, the image of a unit vector as scaled in (E.1.6) is a distinct vector from the original one. Here,

and from now on, we use a  $\hat{\cdot}$  to denote a vector of unit length.

We now turn to a discussion of dual vectors. A dual vector is, by definition, a real-valued linear function on the vector space. Whereas the typical vector was the position vector  $x_0$ , the typical dual vector is the unit normal vector  $n_0$  or gradient operator

$$\vec{\nabla} = \begin{Bmatrix} \partial/\partial x \\ \partial/\partial y \\ \partial/\partial z \end{Bmatrix} = \begin{Bmatrix} \partial/\partial x_1 \\ \partial/\partial x_2 \\ \partial/\partial x_3 \end{Bmatrix} \quad (\text{E.1.7a})$$

It should be noted that tensor analysis works generally refer to vectors as "contravariant vectors," and dual vectors as "covariant vectors." Both the normal vector and the gradient operator are linear functions on the vector space in a natural manner through the dot product

$$\vec{\nabla} \cdot \vec{Y} = \sum_i \frac{\partial}{\partial x_i} (Y_i) \quad (\text{E.1.7b})$$

$$\hat{n}_0 \cdot \vec{Y} = \sum_i n_i Y_i \quad (\text{E.1.7c})$$

The transformation rules for dual vectors  $\vec{\nabla}_0$  (such as  $\vec{\nabla}$  and  $\hat{n}_0$ ) is that the image  $\vec{\nabla}'$  in the coordinate system  $X'$  satisfies

$$\vec{\nabla}' \cdot \vec{Y}' = \vec{\nabla}_0 \cdot \vec{Y} \quad (\text{E.1.8a})$$

for every vector  $Y$ .

Now,

$$\vec{\nabla}' \cdot \vec{Y}' = \vec{\nabla}'^T \vec{Y}' = \vec{\nabla}'^T [A] \vec{Y} \quad (\text{E.1.8b})$$

while

$$\vec{\nabla}_0 \cdot \vec{Y} = \vec{\nabla}_0^T \vec{Y} = \vec{\nabla}_0^T [A^{-1} A] \vec{Y} \quad (\text{E.1.8c})$$

Thus, for (E.1.8a) to hold, we require

$$\vec{\nabla}'^T = \vec{\nabla}_0^T [A^{-1}] = \left\{ [A^{-T}] \vec{\nabla}_0 \right\}^T \quad (\text{E.1.8d})$$

or

$$\vec{\nabla}' = [A^{-T}] \vec{\nabla} \quad (\text{E.1.8e})$$

where the superscript  $-T$  denotes the inverse of the transpose matrix, which is the same as the transpose of the inverse.

Thus dual vectors transform by  $A^{-T}$ , while ordinary vectors transform (cf. (E.1.2)) by  $A$ . It should be noted that if  $A$  happens to be an orthogonal matrix,  $A = A^{-T}$  and is length-preserving, and thus regular vectors, unit

vectors, and dual vectors transform identically.

The gradient operator may also be applied to functions  $f$  of position  $x$ . We see that if we define  $\nabla'$  by

$$\nabla' f(\vec{x}') = \frac{\partial}{\partial x'_i} f(\vec{x}') \equiv \frac{\partial}{\partial x_i} f(\vec{x}_0) \bigg|_{\vec{x}_0 = A^{-1} \vec{x}'} \quad (\text{E.1.9})$$

we obtain

$$\begin{aligned} (\nabla' f(x))_i &= \frac{\partial f}{\partial x_k} \frac{\partial}{\partial x_i} [A^{-1}]_{kj} x'_j = \frac{\partial f}{\partial x_k} [A^{-1}]_{kj} \delta_{ij} = \\ &= \frac{\partial f}{\partial x_k} [A^{-1}]_{ki} = [A^{-1}]_{ki} \frac{\partial}{\partial x_k} f \end{aligned} \quad (\text{E.1.10a})$$

where  $\delta_{ij}$  is the Kronecker delta:

$$\delta_{ij} = \begin{cases} 1 & \text{if } i = j \\ 0 & \text{if } i \neq j \end{cases} \quad (\text{E.1.10b})$$

We thus obtain

$$\nabla' = A^{-T} \nabla \quad (\text{E.1.11})$$

which is consistent with our transformation rule (E.1.8e) for dual vectors.

Next we see that, whenever  $w_1$  and  $w_2$  are vectors in  $X_0$  then  $w_1 \times w_2$  is "almost" a dual vector in the sense that

$$w'_1 \times w'_2 = (Aw_1) \times (Aw_2) = (\det A) A^{-T} (w_1 \times w_2) \quad (\text{E.1.12})$$

This equation is proved below. Thus, apart from the factor of  $\det A$ , the cross product of two vectors transforms in the same way as a dual vector. In a similar vein, we note as well that the cross product of two dual vectors,  $\vec{v}_1 \times \vec{v}_2$ , transforms very much like a vector

$$\vec{v}'_1 \times \vec{v}'_2 = (A^{-T} \vec{v}_1) \times (A^{-T} \vec{v}_2) = (\det A)^{-1} A (\vec{v}_1 \times \vec{v}_2) \quad (\text{E.1.13})$$

It is appropriate at this time that we give brief proofs of the above assertions. In addition, we will show that  $\hat{n} dS$ , the surface unit normal times the element of surface area, transforms like an "almost" dual vector, (cf. (E.1.12)).

A vector  $\vec{t}$  that is tangent to some surface  $S$  at some point  $x$  may be regarded as the tangent to some curve  $\vec{c}(\tau)$ , parametrized by  $\tau$  and lying completely on  $S$ , as that curve passes through the point  $x$ . In other words, when  $\vec{t}$  is a tangent to  $S$  at  $x_0$ , there exists a curve  $\vec{c}(\tau)$  such that  $\vec{c}(\tau)$  lies in  $S$ ,  $x_0 = \vec{c}(\tau_0)$  and

$$\left. \frac{d}{d\tau} \vec{c}(\tau) \right|_{\tau = \tau_0} = \vec{t} \quad (E.1.14)$$

Given this specification of  $\vec{t}$ , it is easy to see how tangent vectors transform. The image tangent vector  $\vec{t}'$  will simply be the tangent to the image curve  $\vec{c}'(\tau) = A \vec{c}(\tau)$  evaluated at the point

$$\vec{x}_0' = \vec{c}'(\tau) = A \vec{c}(\tau) = A \vec{x}_0. \text{ Thus}$$

$$\left. \frac{d}{d\tau} \vec{c}'(\tau) \right|_{\tau = \tau_0} = \left. \frac{d}{d\tau} A \vec{c}(\tau) \right|_{\tau = \tau_0} = A \left. \frac{d}{d\tau} \vec{c}(\tau) \right|_{\tau = \tau_0} = A \vec{t} = \vec{t}' \quad (E.1.15)$$

as asserted.

Next we prove equation (E.1.12) for vectors  $v$  and  $w$ . Recall from section B.3 that

$$(\vec{v} \times \vec{w})_r = \epsilon_{pqr} v_p w_q \quad (E.1.16)$$

where  $\epsilon_{pqr}$  is defined there. So,

$$(A\vec{v} \times A\vec{w})_r = \epsilon_{pqr} (A\vec{v})_p (A\vec{w})_q = \epsilon_{pqr} A_{pi} v_i A_{qj} w_j \quad (E.1.17)$$

Multiplying by  $A^T$  on the left,

$$(A^T (A\vec{v} \times A\vec{w}))_s = [A^T]_{sr} (A\vec{v} \times A\vec{w})_r = \epsilon_{pqr} A_{pi} v_i A_{qj} w_j \quad (E.1.18)$$

But, generalizing the definition of determinant

$$\det A = \epsilon_{pqr} A_{p1} A_{q2} A_{r3} \quad (E.1.19)$$

we see

$$\epsilon_{ijs} \det A = \epsilon_{pqr} A_{pi} A_{qj} A_{rs} \quad (E.1.20)$$

and thus substituting in (E.1.18),

$$(A^T (A\vec{v} \times A\vec{w}))_s = \epsilon_{ijs} (\det A) v_i w_j = (\det A) (\vec{v} \times \vec{w})_s \quad (E.1.21)$$

and so

$$A^T (A\vec{v} \times A\vec{w}) = (\det A) (\vec{v} \times \vec{w}) \quad (E.1.22)$$

or

$$A\vec{v} \times A\vec{w} = (\det A)[A^T] (\vec{v} \times \vec{w}) \quad (\text{E.1.23})$$

which is equivalent to (E.1.12)

Next we examine the transformation law for unnormalized normal vectors  $\vec{n}$ . Such vectors are specified only up to an arbitrary multiplicative constant; their principle characteristic is that they are perpendicular to all tangent vectors. Thus, if  $\vec{t}_1$  and  $\vec{t}_2$  are two linearly independent tangent vectors,  $\vec{n}$  is given by

$$\vec{n} = \alpha (\vec{t}_1 \times \vec{t}_2) \quad (\text{E.1.24})$$

where  $\alpha$  may be chosen arbitrarily non-zero.

Next, we note that the image  $\vec{n}'$  of  $\vec{n}$  must be perpendicular to the images  $\vec{t}'_1, \vec{t}'_2$ , of  $\vec{t}_1$  and  $\vec{t}_2$ ; thus

$$\vec{n}' = \alpha' (\vec{t}'_1 \times \vec{t}'_2) \quad (\text{E.1.25})$$

Using equation (E.1.4) we find

$$\begin{aligned} \vec{n}' &= \alpha' \{ A\vec{t}_1 \times A\vec{t}_2 \} = \alpha' (\det A) A^{-T} \{ \vec{t}_1 \times \vec{t}_2 \} \\ &= \frac{\alpha'}{\alpha} (\det A)[A^{-T}] \vec{n} \end{aligned} \quad (\text{E.1.26})$$

Choosing  $\alpha' = \frac{\alpha}{\det A}$ , we obtain the desired results.

Finally we note that  $\hat{n}dS$  transforms as in equation (E.1.12). This observation follows immediately from the definitions (see figure (E.2))

$$\begin{aligned} \hat{n}_0 dS &= d\vec{l}_1 \times d\vec{l}_2 \\ \hat{n}' dS &= d\vec{l}'_1 \times d\vec{l}'_2 \\ d\vec{l}'_i &= (Ad\vec{l})_i \end{aligned} \quad (\text{E.1.27})$$

Upon applying equation (E.1.12) we find that

$$\vec{n}' dS' = (\det A) A^{-T} \vec{n} dS \quad (\text{E.1.28})$$



We conclude our discussion of vectors and dual vectors with the observation that the Euclidean inner product of a vector  $\vec{w}$  with a dual vector  $\vec{v}$  is invariant under transformation, that is

$$\begin{aligned} (\vec{v}, \vec{w}) &= \vec{v}^T \vec{w} = \vec{v}^T [A^{-1} A] \vec{w} = (A^{-T} \vec{v})^T A \vec{w} = \vec{v}'^T \vec{w}' \\ &= (\vec{v}', \vec{w}') \end{aligned} \tag{E.1.29}$$

## E.2 Metric Matrices, Dual Metrics and Inner Products

The introduction of metric and dual metric matrices is best motivated by a careful consideration of the Prandtl-Glauert equation (3.9.1) (for the dual metric) and the definition of the function  $R$  (5.2.14) (for the metric matrix). First we define the metric matrix  $C$ .

Recall from section B.0 that  $R^2$  is given in terms of a control point  $P$  and a surface point  $Q$  in the compressibility coordinate system  $(x, y, z)$  by

$$R^2 = (P_1 - Q_1)^2 - s\beta^2 (P_2 - Q_2)^2 - s\beta^2 (P_3 - Q_3)^2 \quad (\text{E.2.1})$$

This relation may be written in matrix-vector form as

$$R^2 = (\vec{P} - \vec{Q})^T \begin{bmatrix} 1 & 0 & 0 \\ 0 & s\beta^2 & 0 \\ 0 & 0 & s\beta^2 \end{bmatrix} (\vec{P} - \vec{Q}) \quad (\text{E.2.2})$$

This equation motivates us to define the metric matrix  $C$  by

$$[C] = \begin{bmatrix} 1 & & \\ & s\beta^2 & \\ & & s\beta^2 \end{bmatrix} \quad (\text{E.2.3})$$

Corresponding to  $C$ , we define the compressible inner product  $[w_1, w_2]$  of two vectors  $\vec{w}_1, \vec{w}_2$  by

$$[\vec{w}_1, \vec{w}_2] = \vec{w}_1^T [C] \vec{w}_2 = (\vec{w}_1, [C] \vec{w}_2) \quad (\text{E.2.4})$$

Turning now to the definition of the dual metric matrix  $B$ , we note that the Prandtl-Glauert equation can be written (since  $s\beta^2 = 1 - M_\infty^2$ )

$$\left( \frac{\partial}{\partial x} \frac{\partial}{\partial y} \frac{\partial}{\partial z} \right) \begin{bmatrix} s\beta^2 & & \\ & 1 & \\ & & 1 \end{bmatrix} \begin{Bmatrix} \frac{\partial \phi}{\partial x} \\ \frac{\partial \phi}{\partial y} \\ \frac{\partial \phi}{\partial z} \end{Bmatrix} = 0 \quad (\text{E.2.5})$$

In matrix vector form this reads

$$\left\{ \vec{\nabla}^T [B] \vec{\nabla} \right\} \phi = 0 \quad (\text{E.2.6})$$

where  $[B]$  is defined by (cf. (5.2.5), where reference and compressibility coordinates are assumed to be identical)

$$[B] = \begin{bmatrix} s\beta^2 & & \\ & 1 & \\ & & 1 \end{bmatrix} \quad (\text{E.2.7})$$

Since the operator  $\vec{\nabla}$  transforms like a dual vector (cf. (E.1.8e), equation (E.2.6) motivates us to define the dual compressible inner product  $\{\vec{v}_1, \vec{v}_2\}$  of two dual vectors by

$$\{\vec{v}_1, \vec{v}_2\} = \vec{v}_1^T [B] \vec{v}_2 = (\vec{v}_1, [B]\vec{v}_2) \quad (\text{E.2.8})$$

An important relationship between B and C is the identity

$$[B] [C] = s\beta^2 [I] \quad (\text{E.2.9})$$

When we investigate the transformation rules for [B] and [C] we will find that this relationship is preserved under linear transformations.

Careful examination of equations (E.2.5) and (E.2.8) shows that we may define modified vectors  $\vec{w}$  and modified dual vector  $\vec{v}$  by

$$\vec{w} = C\vec{w} \quad (\text{modified vector}) \quad (\text{E.2.10})$$

$$\vec{v} = B\vec{v} \quad (\text{modified dual vector}) \quad (\text{E.2.11})$$

With modified vectors defined in this fashion, it is easy to see that the inner product relations (E.2.4) and (E.2.8) can be written

$$[\vec{w}_1, \vec{w}_2] = (\vec{w}_1, \vec{w}_2) = (\vec{w}_1, \vec{w}_2) \quad (\text{E.2.12})$$

$$\{\vec{v}_1, \vec{v}_2\} = (\vec{v}_1, \vec{v}_2) = (\vec{v}_1, \vec{v}_2) \quad (\text{E.2.13})$$

Two examples of modified dual vectors include the conormal,

$$\vec{n} = [B] \hat{n} \quad (\text{E.2.14})$$

and the modified gradient operator,  $\vec{\nabla}$ , defined by (5.2.4).

We now examine the transformation rules for metrics and dual metrics. When a coordinate transformation of the form (E.1.1) is performed, the metric matrix C and dual metric matrix B in the new coordinate system  $X'$  are defined by the invariance requirements that

$$[\vec{w}'_1, \vec{w}'_2] = \vec{w}'_1^T [C'] \vec{w}'_2 = [\vec{w}_1, \vec{w}_2] \quad (\text{E.2.15})$$

$$\{\vec{v}'_1, \vec{v}'_2\} = \vec{v}'_1^T [B'] \vec{v}'_2 = \{\vec{v}_1, \vec{v}_2\} \quad (\text{E.2.16})$$

whenever  $\vec{w}'_i = A\vec{w}_i$ ,  $\vec{v}'_i = [A^{-T}]^T \vec{v}_i$ . For the metric matrix  $C'$ , (E.2.15) implied that, for arbitrary vectors  $\vec{w}_1, \vec{w}_2$

$$\vec{w}_1^T [C] \vec{w}_2 = [\vec{w}_1, \vec{w}_2] = \vec{w}_1'^T [C'] \vec{w}_1' = \vec{w}_1'^T [A^T C' A] \vec{w}_2 \quad (\text{E.2.17})$$

Consequently we find that

$$C = A^T C' A, \quad C' = A^{-T} C A^{-1} \quad (\text{E.2.18})$$

Similarly, equation (E.2.16) provides us with the transformation rule

$$B = A^{-1} B' A^{-T}, \quad B' = A B A^T \quad (\text{E.2.19})$$

It is now an easy matter to verify that the relationship (E.2.9) is preserved under transformation; calculation gives

$$B' C' = (A B A^T) (A^T C A^{-1}) = A (B C) A^{-1} = A (s_B^2 I) A^{-1} = s_B^2 I \quad (\text{E.2.20})$$

There is no a priori condition that determines how  $\vec{w}$  transforms, so we make the reasonable requirement that

$$(\vec{w})' = (\vec{w}')^{\sim} \quad (\text{E.2.21})$$

Then

$$\vec{w}' = (\vec{w}')^{\sim} = C' \vec{w}' = C' A \vec{w} = [C' A C^{-1}] \vec{w} \quad (\text{E.2.22})$$

From equation (E.2.18) we see that

$$C' A C^{-1} = A^{-T} \quad (\text{E.2.23})$$

so that

$$\vec{w}' = A^{-T} \vec{w} \quad (\text{E.2.24})$$

This shows that modified vectors are in fact dual vectors.

Similarly, one may show that modified dual vectors are vectors. That is, assuming, for a dual vector  $\vec{v}$ , that

$$(\vec{v})' = (\vec{v}')^{\sim} \quad (\text{E.2.25})$$

then

$$\vec{v}' = A \vec{v} \quad (\text{E.2.26})$$

These observations provided us with an interesting interpretation of equations (E.2.12) and (E.2.13):  $[\vec{w}_1, \vec{w}_2]$ , which is the compressible product of the vectors  $w_1$  and  $w_2$ , is the same as the Euclidean inner product of the vector  $w_1$  and the dual vector  $w_2$ ; similarly  $(\vec{v}_1, \vec{v}_2)$ , the dual compressible inner product of the dual vectors  $v_1$  and  $v_2$  is the Euclidean inner product of  $\vec{v}_1$  (a vector) and  $\vec{v}_2$  (a dual vector). This observation shows that the invariance properties (E.2.15) and (E.2.16) are closely related to the invariance relation (E.1.29).

### E.3 Coordinate Transformations

We recall from section E.0 the reference coordinate system  $X_0$ , the compressibility system  $X$ , the scaled system  $X_s$ , and the local system  $X'$ . In this section, we will determine the properties required by the transformation  $A: X_0 \rightarrow X'$ , and then show that the matrix (E.0.1) is the unique matrix with these properties.

In general the x-axis of coordinate system  $X_0$  need not line up with the free stream. Thus it is necessary to define a new coordinate system  $X$  in which the x-axis is lined up with the free stream axis (that is the x-axis of the Prandtl-Glauert equation (3.0.1)). This is possible if the user provides the compressibility direction by means of a compressibility vector  $\hat{c}_0$ .

The PAN AIR program user will specify the compressibility axis by giving an angle of attack  $\alpha_c$  and a sideslip angle  $\beta_c$  as shown in fig. E.3. The orientation of the compressibility axis is given by the unit vector (cf. (5.2.12))

$$\hat{c}_0 = \begin{Bmatrix} \cos \alpha_c \cos \beta_c \\ -\sin \beta_c \\ \sin \alpha_c \cos \beta_c \end{Bmatrix} \quad (E.3.1)$$

A free stream oriented coordinate system  $X$  must be defined such that the compressibility vector  $c_0$  lies along the x-axis of this new coordinate system. The transformation from  $X_0$  to  $X$  may be characterized as an angle of attack rotation of  $(-\alpha_c)$  about the  $y_0$ -axis followed by an angle of sideslip rotation of  $(-\beta_c)$  about the resulting z axis. Note that coordinates transform in the opposite manner from basis vectors. Thus if we denote the transformation from  $X_0$  to  $X$  by  $\Gamma_c$  so that

$$\Gamma_c: X_0 \longrightarrow X \quad (E.3.2)$$

we have

$$\begin{aligned} \Gamma_c &= R_z(-\beta_c) R_y(-\alpha_c) = \begin{bmatrix} \cos \beta_c & -\sin \beta_c & 0 \\ \sin \beta_c & \cos \beta_c & 0 \\ 0 & 0 & 1 \end{bmatrix} \begin{bmatrix} \cos \alpha_c & 0 & \sin \alpha_c \\ 0 & 1 & 0 \\ -\sin \alpha_c & 0 & \cos \alpha_c \end{bmatrix} \\ &= \begin{bmatrix} \cos \alpha_c \cos \beta_c & -\sin \beta_c & \sin \alpha_c \cos \beta_c \\ \cos \alpha_c \sin \beta_c & \cos \beta_c & \sin \alpha_c \sin \beta_c \\ -\sin \alpha_c & 0 & \cos \alpha_c \end{bmatrix} \quad (E.3.3) \end{aligned}$$

Here  $R_y$  and  $R_z$  denote rotations about the respective axes.

Thus the compressibility axis in coordinate system X is given by

$$\hat{c} = \Gamma_c \hat{c}_0 = \begin{Bmatrix} 1 \\ 0 \\ 0 \end{Bmatrix} \quad (\text{E.3.4})$$

which is the desired result.

In fact, if  $\Gamma_c$  is partitioned by rows, we see immediately that the first row of  $\Gamma_c$  is simply  $\hat{c}_0^T$  while the remaining two rows are orthogonal to  $\hat{c}_0$  and to one another:

$$\Gamma_c = \begin{Bmatrix} \hat{c}_0^T \\ \hat{s}_0^T \\ \hat{t}_0^T \end{Bmatrix} \quad (\text{E.3.5})$$

In fact,  $\Gamma_c$  is an orthogonal matrix;  $\Gamma_c^T \Gamma_c = I$

A matrix of the form  $\Gamma_c$ , transforming reference coordinates orthogonally to another user-defined system, is used after the potential flow solution has been obtained.

This axis system  $X^*$  is defined by an angle of attack  $\alpha^*$  and an angle of sideslip  $\beta^*$ , with the transformation  $\Gamma^*: X_0 \rightarrow X^*$  defined by

$$\Gamma^* = \begin{bmatrix} \cos \alpha^* \cos \beta^* & -\sin \beta^* & \sin \alpha^* \cos \beta^* \\ \cos \alpha^* \sin \beta^* & \cos \beta^* & \sin \alpha^* \sin \beta^* \\ -\sin \alpha^* & 0 & \cos \alpha^* \end{bmatrix} \quad (\text{E.3.6})$$

The angles  $\alpha^*$  and  $\beta^*$  are user-supplied, and describe the coordinate system in which the user wishes PAN AIR to calculate forces or moments.

Before we consider the transformation from reference ( $X_0$ ) to local ( $X'$ ) coordinates, let us consider the transformations (see (E.2.18) and (E.2.19), substituting  $c$  for A)

$$\begin{aligned} [C_0] &= \Gamma_c^T C \Gamma_c \\ [B_0] &= \Gamma_c^T B \Gamma_c \end{aligned} \quad (\text{E.3.7})$$

The matrices  $B_0$  and  $C_0$  have the same properties in reference coordinates that  $B$  and  $C$  have in compressibility coordinates. That is, equations (E.2.2), (E.2.4), and (E.2.8) hold for  $B_0$  and  $C_0$  if the vectors in these equations are written in reference coordinates.

Now, from (E.2.3) and (E.2.7)

$$\begin{aligned} [C] &= s\beta^2 I + (1-s\beta^2) \hat{e}_1 \hat{e}_1^T \\ [B] &= I + (s\beta^2 - 1) \hat{e}_1 \hat{e}_1^T \end{aligned} \quad (E.3.8)$$

where  $\hat{e}_i$  is the  $i$ th column of the identity matrix  $I$ .

Now, since  $\Gamma_C^{-1} = \Gamma_C^T$  because  $\Gamma_C$  is orthogonal, and

$$\Gamma_C^T \hat{e}_1 = \hat{c}_0$$

by (E.3.5),

$$\begin{aligned} [C_0] &= s\beta^2 I + (1-s\beta^2) \hat{c}_0 \hat{c}_0^T \\ [L_0] &= I + (s\beta^2 - 1) \hat{c}_0 \hat{c}_0^T \end{aligned} \quad (E.3.9)$$

Let us now consider the properties we require of the transformation

$$A: X_0 \rightarrow X' \quad (E.3.10)$$

where  $X'$  is the local coordinate system for each subpanel.

The reasons for these requirements are given following (E.3.15).

First, recalling (5.2.19) through (5.2.22), we require, for points  $p$  and  $q$ , that

$$\begin{aligned} R^2 &= (p'_1 - q'_1)^2 + (p'_2 - q'_2)^2 \\ &\quad + (p'_3 - q'_3)^2 \quad \text{for subsonic flow} \\ &= (p'_1 - q'_1)^2 - (p'_2 - q'_2)^2 \\ &\quad - (p'_3 - q'_3)^2 \quad \text{for subinclined panels in supersonic flow} \\ &= -(p'_1 - q'_1)^2 - (p'_2 - q'_2)^2 \\ &\quad + (p'_3 - q'_3)^2 \quad \text{for superinclined panels.} \end{aligned} \quad (E.3.11)$$

Second, we require that on the subpanel on which the  $X'$  coordinate system is



defined,

$$z' = 0 \quad (E.3.12)$$

Third, we require that the "upstream" direction be the  $x' < 0$  direction for subsonic flow or subinclined panels, (cf. (E.3.13)) and that the upstream direction be preserved for superinclined panels. (cf. (E.3.14)). That is, if the surface normal in reference coordinates is pointing into the flow, then so should the surface normal in local coordinates, and similarly if the normal is pointed with the flow. Precisely, we require

$$(\hat{c}_0, A^{-1} \hat{e}_1) > 0 \quad (E.3.13)$$

in the former case, and

$$\text{sign} (\hat{c}_0, A^{-1} \hat{e}_3) = \text{sign} (\hat{c}_0, \hat{n}_0) \quad (E.3.14)$$

in the latter case. The fourth requirement is

$$\det A > 0 \quad (E.3.15)$$

Before proving that these requirements are satisfied, let us discuss them further. Equation (E.3.11) is necessary in order to obtain reasonable formulas for the influence coefficients, that is, formulas which do not have scaling coefficients all over. The requirement that the subpanel lie in a coordinate plane makes the integrals needed for influence coefficient calculation computable, the  $z' = 0$  plane is chosen throughout in order to permit uniform formulas for all three cases. The constraint on the upstream direction makes the notation for the derivation of the influence coefficient formulas simpler. Finally, the requirement that  $A$  have positive determinant insures that the local coordinate system will be a right-handed one.

In the remainder of this appendix, we will rigorously prove that the matrix  $A$  in (E.0.1) satisfies the requirements. We will not, however, explain where  $A$  came from, since we did not arrive at  $A$  through a rigorous procedure.

Recall that we claim that

$$A^T = \begin{bmatrix} \frac{1}{|\hat{n}_0, \hat{n}_0|^{1/2}} & [C_0] \hat{u}_0 & \frac{rs}{B} [C_0] \hat{v}_0 & \frac{B \hat{n}_0}{|\hat{n}_0, \hat{n}_0|^{1/2}} \end{bmatrix} \quad (E.3.16a)$$

satisfies the requirements (E.3.11-15), where

$\hat{n}_0$  = unit normal vector

$\hat{v}_0 = (\hat{n}_0 \times \hat{c}_0) / |\hat{n}_0 \times \hat{c}_0|$

$r = \text{sign} (\hat{n}_0, \hat{n}_0)$

$\hat{u}_0 = \hat{v}_0 \times \hat{n}_0 \quad (E.3.16b)$

The subscript 0 indicates these vectors are in reference coordinates.

If  $\hat{n}_0$  is parallel to  $\hat{c}_0$ ,  $\hat{v}_0$  may be chosen arbitrarily as any unit vector perpendicular to them. Since  $\hat{n}_0$  and  $\hat{v}_0$  are linearly independent vectors orthogonal to  $\hat{n}_0$ , the second requirement on A, (E.3.12) is equivalent to

$$(A \hat{u}_0, \hat{e}_3) = 0$$

$$(A \hat{v}_0, \hat{e}_3) = 0 \quad (E.3.17)$$

$$\text{or } (\hat{u}_0, A^T \hat{e}_3) = (\hat{v}_0, A^T \hat{e}_3) = 0 \quad (E.3.18)$$

$$\text{or } A^T \hat{e}_3 = k \hat{n}_0, \quad k \neq 0 \quad (E.3.19)$$

But this just says that the third column of  $A^T$  should be proportional to  $\hat{n}_0$ , which is satisfied by the matrix in (E.0.1).

Next, by definition,

$$R^2 = (p_1 - q_1)^2 + s_B^2 (p_2 - q_2)^2 + s_B^2 (p_3 - q_3)^2$$

$$= (\vec{p} - \vec{q})^T \begin{bmatrix} 1 & & \\ & s_B^2 & \\ & & s_B^2 \end{bmatrix} (\vec{p} - \vec{q}) \quad (E.3.20)$$

$$= \{ \Gamma_C (\vec{p}_0 - \vec{q}_0) \}^T [C] \quad \Gamma_C (\vec{p}_0 - \vec{q}_0)$$

$$= (\vec{p}_0 - \vec{q}_0)^T [\Gamma_C^T \quad C \quad \Gamma_C] (\vec{p}_0 - \vec{q}_0) \quad (E.3.21)$$

$$= (\text{by (E.2.18)})$$

$$(\vec{p}_0 - \vec{q}_0)^T [C_0] (\vec{p}_0 - \vec{q}_0) \quad (E.3.22)$$

On the other hand, we can unify (E.3.11) by noting that  $r = -1$  if and only if the panel is superinclined, and so (E.3.11) becomes

$$R^2 = \{ A (\vec{p}_0 - \vec{q}_0) \}^T \begin{bmatrix} r & & \\ & s & \\ & & rs \end{bmatrix} A (\vec{p}_0 - \vec{q}_0) \quad (E.3.23)$$

Combining with (E.3.22), we obtain the requirement on  $[A]$ :

$$[A^T] \begin{bmatrix} r & & \\ & s & \\ & & rs \end{bmatrix} [A] = [C_0] \quad (E.3.24)$$

Inverting (E.3.24)

$$A^{-1} \begin{bmatrix} r & & \\ & s & \\ & & rs \end{bmatrix} A^{-T} = [C_0]^{-1} \quad (E.3.25)$$

or

$$\begin{bmatrix} r & & \\ & s & \\ & & rs \end{bmatrix} = [A][C_0]^{-1} [A^T] \quad (E.3.26)$$

$$\text{But, by (E.3.7), } [C_0]^{-1} = \Gamma_c^T [C^{-1}] \Gamma_c \quad (E.3.27)$$

$$= \Gamma_c^T \begin{bmatrix} 1 & & \\ & 1/s\beta^2 & \\ & & 1/s\beta^2 \end{bmatrix} \Gamma_c \quad (E.3.28)$$

$$= \frac{1}{s\beta^2} \begin{bmatrix} \Gamma_c^T & B & \Gamma_c \end{bmatrix} = \frac{1}{s\beta^2} B_0 \quad (E.3.29)$$

$$= (\text{by E.3.9}) \frac{1}{s\beta^2} [I] + \left(1 - \frac{1}{s\beta^2}\right) [\hat{c}_0, \hat{c}_0^T] \quad (E.3.30)$$

Thus, we must show that

$$\begin{aligned} [D] &\equiv A C_0^{-1} A^T = \frac{1}{s\beta^2} [A A^T] + \left(1 - \frac{1}{s\beta^2}\right) [A \hat{c}_0 \hat{c}_0^T A^T] \\ &= \begin{bmatrix} r & & \\ & s & \\ & & rs \end{bmatrix} \end{aligned} \quad (E.3.31)$$

Now,

$$\begin{aligned}
 [D]_{11} &= \frac{1}{|\hat{n}_0, \hat{n}_0|} \left( \frac{1}{s\beta^2} \hat{u}_0^T [C_0]^T [C_0] \hat{u}_0 \right. \\
 &\quad \left. + \left( 1 - \frac{1}{s\beta^2} \right) \hat{u}_0^T [C_0]^T \hat{c}_0 \hat{c}_0^T [C_0] \hat{u}_0 \right)
 \end{aligned}
 \tag{E.3.32}$$

But from (E.3.9)

$$\begin{aligned}
 [C_0]^T C_0 &= \beta^4 [I] + 2 s\beta^2 (1 - s\beta^2) [\hat{c}_0 \hat{c}_0^T] \\
 &\quad + (1 - s\beta^2)^2 [\hat{c}_0 \hat{c}_0^T \hat{c}_0 \hat{c}_0^T]
 \end{aligned}
 \tag{E.3.33}$$

$$= \beta^4 [I] + (2s\beta^2 - 2\beta^4 + 1 - 2s\beta^2 + \beta^4) [\hat{c}_0 \hat{c}_0^T]
 \tag{E.3.34}$$

$$= \beta^4 [I] + (1 - \beta^4) [\hat{c}_0 \hat{c}_0^T]
 \tag{E.3.35}$$

Next,

$$\begin{aligned}
 [C_0]^T \hat{c}_0 \hat{c}_0^T C_0 &= [s\beta^2 I \hat{c}_0 \hat{c}_0^T s\beta^2 I] \\
 &+ [s\beta^2 I \hat{c}_0 \hat{c}_0^T (1 - s\beta^2) \hat{c}_0 \hat{c}_0^T] \\
 &+ [(1 - s\beta^2) \hat{c}_0 \hat{c}_0^T \hat{c}_0 \hat{c}_0^T s\beta^2 I] \\
 &+ [(1 - s\beta^2) \hat{c}_0 \hat{c}_0^T \hat{c}_0 \hat{c}_0^T (1 - s\beta^2) \hat{c}_0 \hat{c}_0^T]
 \end{aligned}
 \tag{E.3.36}$$

$$\begin{aligned}
 &= \beta^4 [\hat{c}_0 \hat{c}_0^T] + (s\beta^2 - \beta^4) [\hat{c}_0 \hat{c}_0^T] \\
 &+ (s\beta^2 - \beta^4) [\hat{c}_0 \hat{c}_0^T] + (1 - s\beta^2)^2 [\hat{c}_0 \hat{c}_0^T]
 \end{aligned}
 \tag{E.3.37}$$

$$= [\hat{c}_0 \hat{c}_0^T]
 \tag{E.3.38}$$

$$\begin{aligned}
 \text{So, } \hat{u}_0^T [C_0]^T C_0 \hat{u}_0 &= \beta^4 \hat{u}_0^T \hat{u}_0 \\
 &+ (1 - \beta^4) \hat{u}_0^T \hat{c}_0 \hat{c}_0^T \hat{u}_0
 \end{aligned}
 \tag{E.3.39}$$

$$= \beta^4 + (1 - \beta^4) (\hat{u}_0, \hat{c}_0)^2
 \tag{E.3.40}$$

and

$$\hat{u}_0^T [C_0]^T [\hat{c}_0 \hat{c}_0^T] [C_0] \hat{u}_0 = (\hat{u}_0, \hat{c}_0)^2
 \tag{E.3.41}$$

So,

$$[D]_{11} = \frac{1}{|(\hat{n}_0, \hat{n}_0)|} \left[ \frac{\beta^4}{s\beta^2} + \frac{1-\beta^4}{s\beta^2} (\hat{u}_0, \hat{c}_0)^2 \right. \\ \left. + \left(1 - \frac{1}{s\beta^2}\right) (\hat{u}_0, \hat{c}_0)^2 \right] \quad (E.3.42)$$

$$= \frac{1}{|(\hat{n}_0, \hat{n}_0)|} (s\beta^2 + (1 - s\beta^2) (\hat{u}_0, \hat{c}_0)^2) \quad (E.3.43)$$

Now, for vectors A, B, C,

$$(\vec{A} \times \vec{B}) \cdot \vec{C} = \epsilon_{ijk} A_i B_j C_k = \epsilon_{jki} B_j C_k A_i = (\vec{B} \times \vec{C}) \cdot \vec{A} \quad (E.3.44)$$

Thus, applying (E.3.16b),

$$\hat{u}_0 \cdot \hat{c}_0 = (\hat{v}_0 \times \hat{n}_0) \cdot \hat{c}_0 = (\hat{n}_0 \times \hat{c}_0) \cdot \hat{v}_0 \\ = (\hat{n}_0 \times \hat{c}_0)(\hat{v}_0 \cdot \hat{v}_0) = \hat{n}_0 \times \hat{c}_0 \quad (E.3.45)$$

Thus

$$\hat{u}_0 \cdot \hat{c}_0 = |\hat{n}_0 \times \hat{c}_0| = \sin \theta \quad (E.3.46)$$

where  $\theta$  is the angle between  $\hat{n}_0$  and  $\hat{c}_0$ .

On the other hand by (E.3.9)

$$\hat{n}_0, \hat{n}_0 = \hat{n}_0^T B_0 \hat{n}_0 = \hat{n}_0^T \hat{n}_0 \\ + (s\beta^2 - 1) (\hat{n}_0 \cdot \hat{c}_0)^2 \quad (E.3.47)$$

$$= 1 + (s\beta^2 - 1) (\hat{n}_0 \cdot \hat{c}_0)^2 = 1 + (s\beta^2 - 1) \cos^2 \theta \quad (E.3.48)$$

since  $(\hat{n}_0, \hat{c}_0) = \cos \theta$ .

$$\text{So, } D_{11} = \frac{s\beta^2 + (1 - s\beta^2) \sin^2 \theta}{r (1 + (s\beta^2 - 1) \cos^2 \theta)} \quad (E.3.49a)$$

(since  $r(\hat{n}_0, \hat{n}_0) = |(\hat{n}_0, \hat{n}_0)|$ ) (E.3.49b)

$$= \frac{s\beta^2 + (1 - s\beta^2) (1 - \cos^2 \theta)}{(1 + (s\beta^2 - 1) \cos^2 \theta) r} \quad (E.3.50)$$

$$= \frac{1 + (1 - s\beta^2) (-\cos^2 \theta)}{(1 + (s\beta^2 - 1) \cos^2 \theta) r} = r \quad (\text{E.3.51})$$

Next, let us consider  $D_{22}$ . By (E.3.31) and (E.0.1),

$$\begin{aligned} D_{22} &= \frac{1}{s\beta^2} \frac{r^2 s^2}{\beta^2} (C_0 \hat{v}_0)^T C_0 \hat{v}_0 \\ &+ \left(1 - \frac{1}{s\beta^2}\right) \frac{r^2 s^2}{\beta^2} (C_0 \hat{v}_0)^T [\hat{c}_0 \hat{c}_0^T] C_0 \hat{v}_0 \end{aligned} \quad (\text{E.3.52})$$

$$= \frac{1}{s\beta^4} \hat{v}_0^T C_0^T C_0 \hat{v}_0 + \left(1 - \frac{1}{s\beta^2}\right) \frac{1}{\beta^2} \hat{v}_0^T [C_0^T \hat{c}_0 \hat{c}_0^T C_0] \hat{v}_0 \quad (\text{E.3.53})$$

$$\text{Now, } \hat{c}_0^T \hat{v}_0 = 0 \quad (\text{E.3.54})$$

and applying (E.3.35) we therefore get

$$\frac{1}{s\beta^4} \hat{v}_0^T [C_0^T C_0] \hat{v}_0 = \frac{1}{s} \hat{v}_0^T \hat{v}_0 = s \quad (\text{E.3.55})$$

Applying (E.3.38) we find that the second term of (E.3.53) vanishes, and thus

$$D_{22} = s \quad (\text{E.3.56})$$

Next (by (E.0.1) and (E.3.31)),

$$D_{33} = \frac{\beta^2}{s\beta^2} \frac{\hat{n}_0^T \hat{n}_0}{|\{\hat{n}_0, \hat{n}_0\}|} + \left(1 - \frac{1}{s\beta^2}\right) \frac{\beta^2}{|\{\hat{n}_0, \hat{n}_0\}|} \hat{n}_0^T \hat{c}_0 \hat{c}_0^T \hat{n}_0 \quad (\text{E.3.57})$$

Using (E.3.48)

$$D_{33} = \frac{s}{|\{\hat{n}_0, \hat{n}_0\}|} + \frac{\beta^2 (1 - 1/s\beta^2) \cos^2 \theta}{|\{\hat{n}_0, \hat{n}_0\}|} \quad (\text{E.3.58})$$

$$= \frac{s + (\beta^2 - s) \cos^2 \theta}{|\{\hat{n}_0, \hat{n}_0\}|} = \quad (\text{E.3.59})$$

(by (E.3.48) and (E.3.49a))

$$\frac{s (1 + (s\beta^2 - 1) \cos^2 \theta)}{r (1 + (s\beta^2 - 1) \cos^2 \theta)} = rs \quad (\text{E.3.60})$$

Next, we consider  $D_{12}$ . By (E.0.1) and (E.3.31),

$$\begin{aligned} D_{12} = & \frac{rs}{s\beta^3 |(n_0, n_0)|^{1/2}} (C_0 \hat{u}_0)^T C_0 \hat{v}_0 \\ & + \frac{1}{1 - s\beta^2} \frac{rs}{\beta |(n_0, n_0)|^{1/2}} C_0 \hat{u}_0 [\hat{c}_0 \hat{c}_0^T] C_0 \hat{v}_0 \end{aligned} \quad (\text{E.3.61})$$

Applying (E.3.35) and (E.3.38), we see that each term contains either  $\hat{c}_0^T \hat{v}_0$  or  $\hat{u}_0^T \hat{v}_0$ , both of which are zero by (E.3.16b), and thus

$$D_{12} = 0 \quad (\text{E.3.62})$$

Next,  $D_{13} =$

$$\frac{\beta}{|(\hat{n}_0, \hat{n}_0)|} \frac{1}{s\beta^2} \hat{u}_0^T [C_0^T] \hat{n}_0 + \left(1 - \frac{1}{s\beta^2}\right) \hat{u}_0^T [C_0^T \hat{c}_0 \hat{c}_0^T] \hat{n}_0 \quad (\text{E.3.63})$$

= (by (E.3.9))

$$\begin{aligned} & \frac{\beta}{|(n_0, n_0)|} \frac{1}{s\beta^2} \hat{u}_0^T s\beta^2 \hat{n}_0 + \frac{1-s\beta^2}{s\beta^2} \hat{u}_0^T \hat{c}_0 \hat{c}_0^T \hat{n}_0 \\ & + \left(1 - \frac{1}{s\beta^2}\right) \hat{u}_0^T s\beta^2 \hat{c}_0 \hat{c}_0^T \hat{n}_0 \\ & + \left(1 - \frac{1}{s\beta^2}\right) (1 - s\beta^2) \hat{u}_0^T \hat{c}_0 \hat{c}_0^T \hat{c}_0 \hat{c}_0^T \hat{n}_0 \end{aligned} \quad (\text{E.3.64})$$

= (by (E.3.16))

$$\begin{aligned} & \frac{\beta}{|(n_0, n_0)|} \left(0 + \frac{1}{s\beta^2} - 1\right) (\hat{u}_0^T \hat{c}_0 \hat{c}_0^T \hat{n}_0) \\ & + (s\beta^2 - 1) (\hat{u}_0^T \hat{c}_0 \hat{c}_0^T \hat{n}_0) + \left(2 - \frac{1}{s\beta^2} - s\beta^2\right) (\hat{u}_0^T \hat{c}_0 \hat{c}_0^T \hat{n}_0) \end{aligned} \quad (E.3.65)$$

$$= \frac{\beta}{|(n_0, n_0)|} \cdot 0 = 0 \quad (E.3.66)$$

Finally,  $D_{23}$  can be expressed by (E.3.63), changing the factor in front to

$$\frac{rs}{|(n_0, n_0)|^{1/2}}, \text{ and replacing } \hat{u}_0 \text{ by } \hat{v}_0. \text{ But since we also have}$$

(by (E.3.16))

$$\hat{v}_0^T \hat{n}_0 = 0 \quad (E.3.67)$$

we can follow the steps (E.3.63-66) again to obtain

$$D_{23} = 0 \quad (E.3.68)$$

Now, combining the fact that  $D$  is symmetric (see (E.3.31)) with (E.3.51), (E.3.56), (E.3.60), (E.3.62), (E.3.66), and (E.3.68), we have

$$[D] = \begin{bmatrix} r & & \\ & s & \\ & & rs \end{bmatrix} \quad (E.3.69)$$

which we have shown is equivalent to (E.3.31) (see the argument from (E.3.20) to (E.3.31)).

So, we have proved that  $R^2$  has the appropriate form in the  $X'$  system (E.3.11), and earlier we showed that the subplane lies in the  $z' = 0$  plane.

To show that the upstream direction transforms correctly, we exhibit  $A^{-1}$  first. We claim

$$A^{-1} = r \begin{bmatrix} \hat{u}_0 & \hat{v}_0 & B_0 \hat{n}_0 \\ \frac{1}{|(n_0, n_0)|^{1/2}} & \frac{1}{\beta} & \frac{1}{\beta |(n_0, n_0)|^{1/2}} \end{bmatrix} \quad (E.3.70)$$

Verifying that  $[AA^{-1}] = [I]$  is tedious, and uses the same sort of arguments as evaluating  $D$ .

First,



$$[AA^{-1}]_{11} = \frac{r}{|(n_0, n_0)|} \hat{u}_0^T C_0^T \hat{u}_0 \quad (E.3.71)$$

= (by E.3.9)

$$\frac{r}{|(n_0, n_0)|} (s\beta^2 \hat{u}_0^T \hat{u}_0 + (1 - s\beta^2) \hat{u}_0^T \hat{c}_0 \hat{c}_0^T \hat{u}_0) \quad (E.3.72)$$

= (by (E.3.46), (E.3.48), and (E.3.48a))

$$\frac{r}{r(1 + (s\beta^2 - 1) \cos^2 \theta)} (s\beta^2 + (1 - s\beta^2) \sin^2 \theta) = 1 \quad (E.3.73)$$

Next,

$$[AA^{-1}]_{22} = \frac{r^2 s}{\beta^2} \hat{v}_0^T C_0^T \hat{v}_0 = \quad (E.3.74)$$

= (by (E.3.9))

$$\frac{s}{\beta^2} (s\beta^2 \hat{v}_0^T \hat{v}_0 + (1 - s\beta^2) \hat{v}_0^T \hat{c}_0 \hat{c}_0^T \hat{v}_0) \quad (E.3.75)$$

$$= (\text{by (E.3.16)}) \quad \hat{v}_0^T \hat{v}_0 = 1 \quad (E.3.76)$$

Next,

$$[AA^{-1}]_{33} = \frac{r}{|(n_0, n_0)|} \hat{n}_0^T B_0 \hat{n}_0 \quad (E.3.77)$$

= (by definition)

$$\frac{r (\hat{n}_0, \hat{n}_0)}{|(n_0, n_0)|} = 1 \quad (E.3.78)$$

by (E.3.49a).

Next,

$$r\beta|\hat{n}_0, \hat{n}_0|^{1/2} [AA^{-1}]_{12} = \hat{u}_0^T C_0^T \hat{v}_0 = \quad (E.3.79)$$

(by (E.3.9), since  $C_0$  is its own transpose by (E.3.24))

$$(1 - s\beta^2) \hat{u}_0^T \hat{C}_0 \hat{C}_0^T \hat{v}_0 + s\beta^2 \hat{u}_0^T \hat{v}_0 = 0 \quad (E.3.80)$$

by (E.3.16).

$$\text{Next, } r\beta|\hat{n}_0, \hat{n}_0| [AA^{-1}]_{13} = \hat{u}_0^T [C_0 B_0] \hat{n}_0$$

But from (E.2.20) we see

$$C_0 B_0 = s\beta^2 I \quad (E.3.81)$$

and thus by (E.3.16),

$$[AA^{-1}]_{13} = 0 \quad (E.3.82)$$

Next,

$$\beta^2 r^2 s |\hat{n}_0, \hat{n}_0|^{1/2} [AA^{-1}]_{23} = \hat{v}_0^T [C_0^T B_0] \hat{n}_0 \quad (E.3.83)$$

Once again applying (E.3.81) and (E.3.16), we obtain

$$[AA^{-1}]_{23} = 0 \quad (E.3.84)$$

Next,

$$\frac{\beta |\hat{n}_0, \hat{n}_0|^{1/2}}{r^2 s} [AA^{-1}]_{21} = v_0^T C_0 u_0 = 0 \quad (E.3.85)$$

by (E.3.80).

Next,

$$\frac{r |\hat{n}_0, \hat{n}_0|}{\beta} [AA^{-1}]_{31} = \hat{n}_0^T \hat{u}_0 = 0 \quad (E.3.86)$$

by (E.3.16).

Finally

$$r |\hat{n}_0, \hat{n}_0|^{1/2} [AA^{-1}]_{32} = \hat{n}_0^T \hat{v}_0 = 0 \quad (E.3.87)$$

by (E.3.16).

Thus we have shown that

$$[AA^{-1}] = I \quad (E.3.88)$$

Applying (E.3.70) when  $r = +1$ ,

$$[A^{-1}] \begin{Bmatrix} 1 \\ 0 \\ 0 \end{Bmatrix} = \frac{\hat{u}_0}{|\{\hat{n}_0, \hat{n}_0\}|^{1/2}} \quad (\text{E.3.89})$$

and so

$$\hat{c}_0^T A^{-1} \begin{Bmatrix} 1 \\ 0 \\ 0 \end{Bmatrix} = \frac{(\hat{c}_0, \hat{u}_0)}{|\{\hat{n}_0, \hat{n}_0\}|^{1/2}} = \frac{\hat{n}_0 \times \hat{c}_0}{|\{\hat{n}_0, \hat{n}_0\}|^{1/2}} > 0 \quad (\text{E.3.90})$$

This proves (E.3.13). Applying (E.3.70) when  $r = -1$ ,

$$[A^{-1}] \begin{Bmatrix} 0 \\ 0 \\ 1 \end{Bmatrix} = \frac{-[B_0]\hat{n}_0}{\beta|\{\hat{n}_0, \hat{n}_0\}|^{1/2}} \quad (\text{E.3.91})$$

and so

$$\hat{c}_0^T [A^{-1}] \begin{Bmatrix} 0 \\ 0 \\ 1 \end{Bmatrix} = -\frac{\hat{c}_0^T [B_0] \hat{n}_0}{\beta|\{\hat{n}_0, \hat{n}_0\}|^{1/2}} \quad (\text{E.3.92})$$

(by (E.3.9) and (E.3.48))

$$= \frac{1}{\beta|\{\hat{n}_0, \hat{n}_0\}|^{1/2}} (\hat{c}_0^T \hat{n}_0 + (s\beta^2 - 1) \hat{c}_0^T \hat{c}_0 \hat{c}_0^T \hat{n}_0) \quad (\text{E.3.93})$$

$$= \frac{-s\beta (\hat{c}_0, \hat{n}_0)}{\beta|\{\hat{n}_0, \hat{n}_0\}|^{1/2}} \quad (\text{E.3.94})$$

which has the same sign as  $(\hat{c}_0, \hat{n}_0)$  since  $s = -1$ , thus proving (E.3.14).

Finally, we show that  $\det A > 0$ .

Applying (E.1.12) to  $\hat{u}_0$  and  $\hat{v}_0$ ,

$$A\hat{u}_0 \times A\hat{v}_0 = (\det A) [A^{-T}] (\hat{u}_0 \times \hat{v}_0) = (\det A) [A^{-T}] \hat{n}_0 \quad (\text{E.3.95})$$

(by E.3.16).

Applying (E.3.70),

$$A^{-T} n_0 = \begin{Bmatrix} \frac{r}{|\{\hat{n}_0, \hat{n}_0\}|^{1/2}} \hat{u}_0 \cdot \hat{u}_0 \\ \frac{r}{B} \hat{v}_0 \cdot \hat{n}_0 \\ \frac{r}{B |\{\hat{n}_0, \hat{n}_0\}|^{1/2}} \hat{n}_0^T B_0 \hat{n}_0 \end{Bmatrix} \quad (\text{E.3.96})$$

$$= \begin{Bmatrix} 0 \\ 0 \\ \frac{1}{B} |\{n_0, n_0\}|^{1/2} \end{Bmatrix} \quad (\text{E.3.97})$$

Now, recalling from (E.3.79) that  $\hat{u}_0^T [C_0] \hat{v}_0 = 0$ , and applying (E.3.16),

$$[A] \hat{u}_0 = \begin{Bmatrix} \frac{\hat{u}_0^T [C_0] \hat{u}_0}{|\{\hat{n}_0, \hat{n}_0\}|^{1/2}} \\ 0 \\ 0 \end{Bmatrix} = \begin{Bmatrix} r |\{\hat{n}_0, \hat{n}_0\}|^{1/2} \\ 0 \\ 0 \end{Bmatrix} \quad (\text{E.3.98})$$

by (E.3.71-73).

Next, applying (E.3.16) and (E.3.79),

$$[A] \hat{v}_0 = \begin{Bmatrix} 0 \\ -\frac{rs}{B} \hat{v}_0^T [C_0^T] \hat{v}_0 \\ 0 \end{Bmatrix} = \begin{Bmatrix} 0 \\ rs \\ 0 \end{Bmatrix} \quad (\text{E.3.99})$$

by (E.3.74-76).

So,

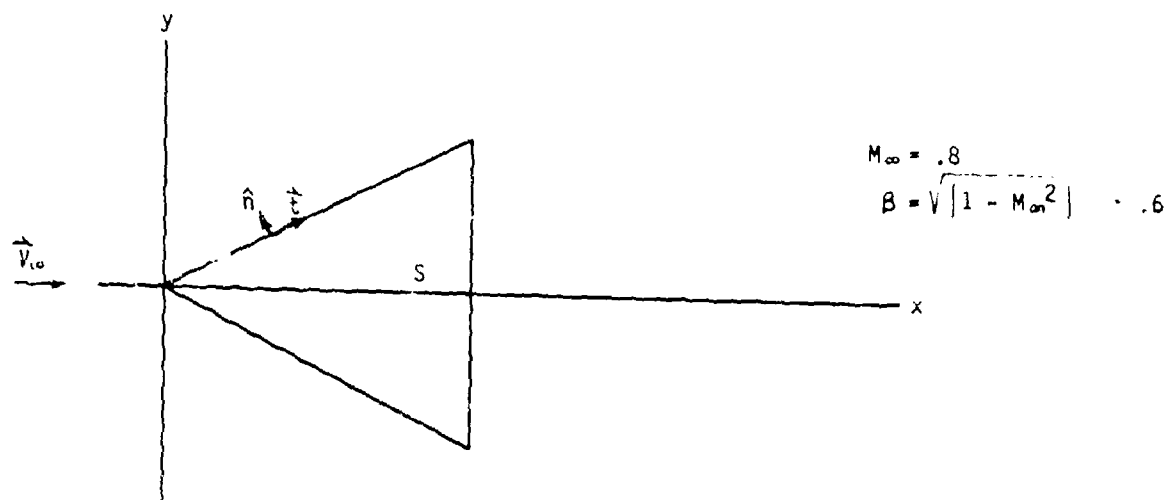
$$A \hat{u}_0 \times A \hat{v}_0 = \begin{Bmatrix} 0 \\ 0 \\ \beta | \{n_0, n_0\} |^{1/2} \end{Bmatrix} =$$

$$\text{(by (E.3.80))} \quad \beta^2 [A^{-T}] n_0 \quad \text{(E.3.100)}$$

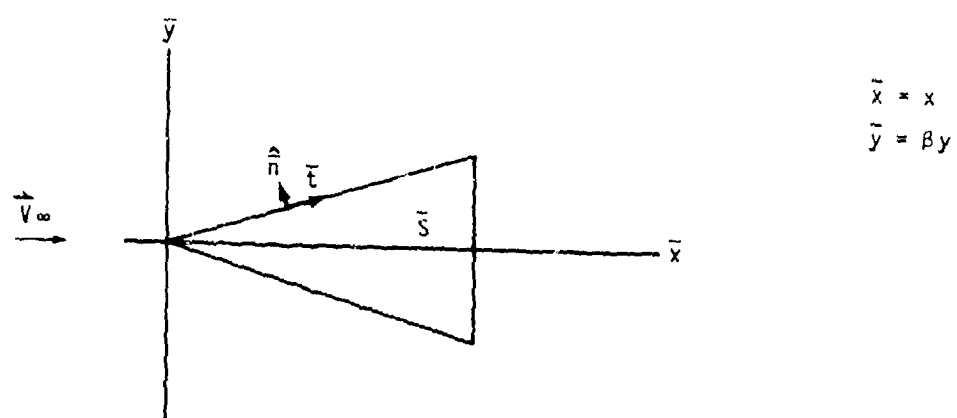
Substituting in (E.3.95), we see that

$$\det A = \beta^2 > 0 \quad \text{(E.3.101)}$$

This concludes our proof that  $[A]$  satisfies (E.3.11-15).



a. Compressibility coordinates



b. Scaled coordinates

Figure E.1 - Surface S in compressibility and scaled coordinates

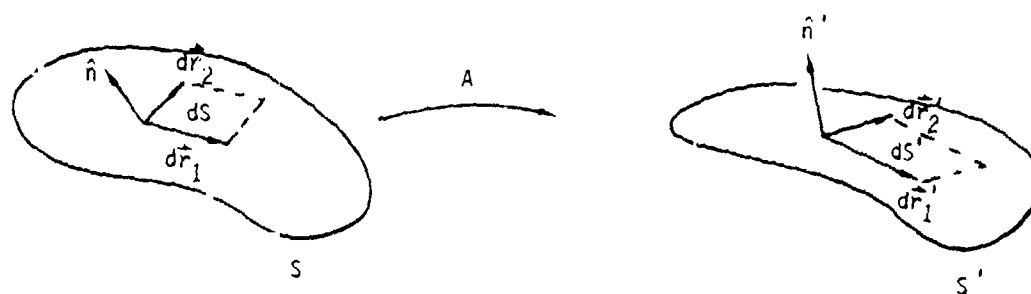


Figure E.2 - Illustration of the transformation law for  $\hat{n} dS$

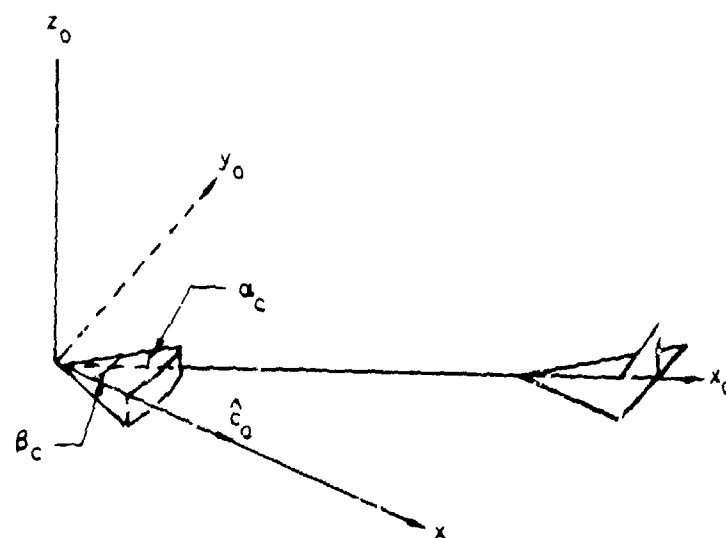


Figure E.3 - Definition of the compressibility vector  $\hat{c}_0$  in terms of  $\alpha_c$  and  $\beta_c$

## F.0 Edge Matching

In this appendix, we will discuss the process by which the program performs "edge matching", that is, insures "continuity" of doublet strength. In section F.1 we will supply the theoretical background, summarizing section 8.3 and discussing a few points not mentioned there. In section F.2, we will discuss the concept of abutments between networks, introducing some of the terminology used within the program. In section F.3, we discuss the process by which the program determines the list of abutments defined by the user-input configuration. In section F.4, we describe the assignment of one edge in the abutment to be the matching edge, and show how this assignment insures doublet matching along the abutment. In section F.5, we discuss the special techniques used by the program to process "abutment intersections", points in space at which abutments meet. In section F.6, we discuss "gap-filling panels," which are added by the program along abutments where gaps between network edges exceed the user-input tolerance distance.



## F.1 Continuity Requirements

Recall equation (B.3.12), that along any panel edge we should have

$$\sum_{i=1}^n s_i u_i = 0 \quad (F.1.1)$$

where  $n$  is the number of panel edges meeting, and  $s_i = \pm 1$  is determined by the direction of the panel normal. We supplied three distinct types of justification for (F.1.1). First, it is physically reasonable. Second, it has been experimentally shown to be necessary for the analysis of supersonic flow. Third, (F.1.1) can be used to increase the efficiency of the program by allowing the removal of the "line vortex terms."

The imposition of (F.1.1) is effected in one of three ways. Within the interior of the network, it is effected by splines, discussed in Appendix I, which impose the equation

$$u_1 - u_2 = 0 \quad (F.1.2)$$

along all panel edges. Note that therefore two networks must not meet except along network edges; else, the value of  $n$  along the line of intersection would be at least 3, while the spline methods assume  $n = 2$ . In figure F.1, we illustrate such an impermissible intersection of networks. Along network edges, boundary conditions (called edge matching boundary conditions) are used to impose (F.1.2). The curve along which network edges meet is called an abutment. If an abutment consists of only two network edges, the user may specify it as a "smooth abutment", in which case a splining method (discussed in Appendix I), is used in place of boundary conditions to impose (F.1.2). This results in fewer boundary conditions, and thus reduces the size of the system of equations to be solved.

The use of smooth abutments is restricted to networks which, together, define a continuously smooth surface. If the surface defined by the networks is not smooth, the doublet gradient at the intersection should in fact be discontinuous, while the smooth abutment specification will make the gradient approximately continuous, resulting in an erroneous solution. For the same reason, a single network should never be used to describe a surface containing a discontinuity of slope.

There is one case in which (F.1.1) does not hold. This case is that of a leading edge vortex (see figure B.10). The true physics of the situation is that the vortex rolls up tighter and tighter (see figure F.2) until it dissipates due to viscous effects. A potential flow program could only simulate the roll-up of the wake by supplying a wake with infinitely many turns in it. This not being practical, wake roll-up can be simulated by replacing the "core" (the region where viscous effects predominate) by a "line vortex" (see figure F.3). Along this network edge, the doublet strength is in fact discontinuous; that is, it is non-zero on the wake, while it is zero in the region of space surrounding the free edge of the wake. The discontinuity of doublet strength means that when the influence of the wake on a control

point is computed, the "line vortex terms" must be added in, that is

$$\int_{as} u \quad \tilde{\nabla} \left( \frac{1}{R} \right) \times \vec{dl} \quad (F.1.3)$$

must be computed. We describe the computation of this quantity in appendix J.

The mechanism by which the program user causes the line vortex term (F.1.3) to be added into the influence coefficient matrix is the following. He specifies "no doublet matching" for a particular network edge. The program then insures that the boundary conditions imposed at the control points along the edge are not those of doublet matching (that is, of the form (F.1.1)), and furthermore adds in the line vortex contribution for each panel edge lying along the network edge when measuring the influence of the panel on a control point.

## F.2 Network Abutments

PAN AIR deals with a number of distinct data sets called abutments. There are "pairwise abutments", "user-defined abutments", "empty space abutments", and "program-generated abutments". The latter three types of abutments are end products of the procedure which generates a list of all existing network abutments. User-defined abutments are those described by the user, either in order to indicate that they are smooth, or else because the user is not sure that the "automatic abutment search" described in section F.3 will define that abutment. Empty space abutments are those which describe a network edge or portion thereof which does not lie in proximity to any other network edge. Program-generated abutments (those which are neither user-defined nor empty space abutments) are computed in a two step procedure. The first step is the computation of pairwise abutments, each of which lists two network edges or portions thereof which lie in proximity to one another. In the second step, the program distills the list of pairwise abutments into a non-redundant list of program-generated abutments. The latter procedure is described in some detail in the Maintenance Document (see section 4-G), and will not be discussed further here.

### F.3 Automatic Abutment Searches

In this section, we will briefly describe the procedure used by the program to construct "pairwise abutments"; that is, pairs of network edge portions belonging to the same abutment.

The program searches for pairwise abutments one network edge at a time. For each point  $P$  on an edge  $E_0$ , it searches for network edges  $E_i$  which lie within the user-specified tolerance distance  $\epsilon$  of  $P$ . Here we say that  $E_i$  lies within  $\epsilon$  of  $P$  if there is some point  $P_i$  on  $E_i$  such that  $|\vec{P} - \vec{P}_i| < \epsilon$ . If  $E_i$  lies within  $\epsilon$  of two adjacent panel corner points  $P$  and  $P'$ , then the panel edge connecting  $P$  and  $P'$  belongs to an abutment containing  $E_0$  and  $E_i$ .

The program then proceeds along the network edge until it arrives at the endpoint of the edge, or at a panel corner point for which  $E_i$  fails to lie within  $\epsilon$ . The program then defines a pairwise abutment between  $E_0$  and  $E_i$  extending from the first panel corner point on the edge to the last corner point on the edge such that  $E_i$  lies within  $\epsilon$  for the endpoints and the intermediate corner points. If the situation illustrated in figure F.4 occurs, several pairwise abutments may be defined which involve edges  $E_0$  and  $E_i$ . There are, however, limitations on the permissibility of configurations of the form of figure F.4. These limitations are noted in the User's Manual.

#### F.4 Doublet Matching along Abutments

The purpose of doublet matching boundary conditions is to insure that equation (F.1.1) holds at every point along an abutment, even though a boundary condition of this form is imposed at only a finite number of points. The ability of a finite number of boundary conditions to cause doublet matching along the full abutment depends directly on the splining techniques used to define the doublet strength along network edges. We discuss this subject in section I.1.2.5, but we will summarize here the results we derive there.

Given any pair of network edges belonging to an abutment, we call the first edge a refinement of the other if, at every point where a panel corner is located on the second edge, a panel corner is also located on the first edge. According to this definition, each network edge in figure F.5 is a refinement of the other, while in figure F.6, edge 1 is a refinement of edge 2.

We show in section I.1.2.5 that if an abutment contains edges  $E_1, \dots, E_n$ , and some edge  $E_k$  is a refinement of each of the other  $(n-1)$  edges of the abutment, then doublet matching can be forced to take place along the entire abutment provided it occurs at the endpoints of the abutments, and at the panel edge midpoints on edge  $E_k$ . In practice, precise doublet matching will not occur because Pan Air uses a "least squares" rather than a differentiable edge spline (see section I.1.2.5). The extent to which doublet matching fails to occur is very small, and has been found experimentally to be negligible.

The program takes into consideration the above results when assigning one edge of an abutment to be the "matching edge", that is, the edge at whose panel edge midpoints doublet matching boundary conditions are imposed. Thus, when no special considerations intervene, the edge with the densest paneling is assigned to be the matching edge. Assuming that the program user has in fact provided one edge in the abutment which is a refinement of all the other edges, then that edge is clearly the most densely paneled edge, and so doublet matching will occur.

Under certain circumstances, the program does not assign the most densely paneled edge in the abutment as the matching edge. The first such case arises from a matching edge of a doublet design or doublet wake network taking part in the abutment.

Unlike doublet analysis networks, design and wake networks are asymmetric; boundary conditions are only imposed along certain edges of these networks, called matching edges, as illustrated in figures D.2 and D.3. When a matching edge of a design or wake network belongs to an abutment, the program assigns it to be the matching edge for the abutment, even if it is not the most densely paneled edge. This is done mostly for convenience; the user is not likely to know what boundary condition to impose at the control points along the matching edge and so the program evades this dilemma by assigning doublet matching boundary conditions there.

The other circumstances under which the most densely paneled edge is not chosen as the matching edge is illustrated in figure F.7. To be specific, whenever the curve defined by an abutment is "supersonic" (that is, no point on the edge is in the domain of dependence of any other point), then that network edge which is a leading edge (that is, upstream of the remainder of the network) is assigned as a matching edge.

The basis for this assignment is largely empirical. Experience with the PAN AIR "pilot code" with the configuration shown in figure F.8a, illustrates the need for imposing doublet matching on the leading supersonic edges of networks in supersonic flow. When doublet matching was imposed along the trailing edges of networks 1, 2, and 3, the solution was completely erratic, while shifting the matching boundary conditions to the leading edges of networks 4, 5, and 6 resulted in a solution which was physically reasonable.

The reasons for the numerical problems resulting from the assignment of matching edges as shown in figure F.8a are not precisely known. It is known, however, that specification of normal mass flux in a two-dimensional, linearized, planar, supersonic flow problem is equivalent to specification of the doublet gradient. We may see this by combining equation (C.1.5), which states that  $\Delta C_p$  is proportional to  $\partial u / \partial x$ , with equations (11-1) and (11-3) of reference F.1, which states that  $\Delta C_p$  is proportional to normal mass flux.

Thus for a two-dimensional configuration, the specification of zero normal mass flux at panel center points, in combination with doublet matching at the trailing edge, is equivalent to the situation in figure C.10, with the trailing edge boundary condition becoming specification of  $u$ . But this set of boundary conditions, in conjunction with the doublet analysis spline, does not have a unique solution. We see this by noting that the doublet distribution  $u_0(x)$  shown in figure F.8b satisfies  $u = 0$  at the leading and trailing edges, and  $\partial u / \partial x = 0$  at panel centers. Thus, if some solution  $u(x)$  exists which satisfies the boundary conditions above, so does  $u(x) + \alpha u_0(x)$  for all real numbers  $\alpha$ . Thus it is not permissible to specify  $u$  at the trailing edge of a two-dimensional network on which normal mass flux is specified at panel centers.

Of course, the configuration in figure F.8a is not a two-dimensional one. Nevertheless, it seems to have enough resemblance to a two-dimensional configuration that the imposition of doublet strength specification on the trailing edge of networks 1, 2, and 3 is an unstable boundary condition specification for the doublet analysis network spline in use on those networks.

Summarizing, the program assigns a matching edge of a doublet design or wake network as the matching edge in an abutment whenever one is available. If there is none, and the abutment is "supersonic", the leading edge of the most "downstream-pointing" network is assigned as the matching edge. In all other cases, the most densely paneled edge is assigned as the matching edge.

Thus, to insure precise doublet matching, a program user must be sure, for every abutment containing a matching edge of a doublet design or wake network, that this edge is a refinement of all the other network edges. Similarly, if it is a supersonic abutment, the leading edge of the most downstream pointing network must be a refinement of the others. Finally, in all other cases, some edge must be a refinement of all the others (recall that, if two edges have identical paneling, each is a refinement of the other).

If these rules are followed, the edge chosen by the program as the matching edge will in fact always be the most densely paneled one, so precise doublet matching will occur. This does not necessarily mean that minor violations of the rules will be serious. For instance, in figure F.9 (ignoring the gap - filling panels for the moment), the edge of the network A is not quite a refinement of the edge of network B. There is no reason to believe, however, that the doublet discontinuities which result from the small discrepancies in figure F.9 are significant.

## F.5 Abutment Intersections

Within the interior of an abutment, the equation

$$\sum s_j u_j = 0 \quad (F.5.1)$$

can easily be imposed by assigning a particular edge as the matching edge, and imposing (F.5.1) at the panel edge midpoints on this edge.

At abutment intersections, points where two or more abutments meet, (see figure F.10), the choice of points at which to impose (F.5.1) becomes more difficult. Only one matching boundary condition may be imposed at a network corner point (since only one control point is located there), yet the corner point lies at the end of two distinct abutments. We will say that a corner point C is "assigned" to an abutment A if the boundary condition imposed at C is doublet matching across A.

A second complication is the danger of overspecification. Consider the abutment intersection, formed by four networks, illustrated in figure F.10. Let us define  $u_i$  to be the doublet strength at the corner of network  $N_i$  at this intersection. In order to obtain doublet matching, we require

$$u_1 = u_2 = u_3 = u_4 \quad (F.5.2)$$

But these are only three equations. Thus, if we assign corner point  $C_1$  to abutment  $A_1$ ,  $C_2$  to  $A_2$ , and  $C_3$  to  $A_3$ , that is, impose the boundary conditions

$$u_1 = u_2 \text{ at } C_1$$

$$u_2 = u_3 \text{ at } C_2 \quad (F.5.3)$$

$$\text{and } u_3 = u_4 \text{ at } C_3$$

we have satisfied (F.5.2). If we were to assign corner point  $C_4$  to abutment  $A_4$  in addition, the resulting boundary condition

$$u_4 = u_1 \text{ at } C_4 \quad (F.5.4)$$

would be redundant, since it follows from (F.5.3). If a row of the AIC matrix corresponding to (F.5.4) were generated, the resulting matrix would therefore be singular, since this row would be a linear combination of three rows corresponding to (F.5.3).

Thus overspecification must be avoided if the program is to provide a numerical solution to the potential flow problem. This is straightforward for any reasonable example, but clearly the program must follow a well-defined method which assigns corner points to abutments in such a manner that doublet matching occurs at all abutments while no overspecification occurs. As an example, the abutment intersection in figure F.11 may arise from a realistic airplane configuration, yet an automatic procedure assigning corner points to abutments is not obvious.

Before we outline such a procedure, we must obtain a few facts about abutment intersections. We will not prove these facts in general, but will



justify them by showing that they hold for the abutment intersections in figures F.10 and F.11. The interested reader is urged to make up examples of his own, and establish these facts for those examples.

The first such fact is that some linear combination of the  $n$  doublet matching equations arising at the abutment intersection (where  $n$  is the number of abutments in the intersection) is a trivial equation reducible to  $0 = 0$ . Further, the linear combination can be defined with all the coefficients being  $\pm 1$ .

In the case of figure F.10, the four matching equations are

$$\begin{aligned} u_1 - u_2 &= 0 \\ u_2 - u_3 &= 0 \\ u_3 - u_4 &= 0 \\ u_4 - u_1 &= 0 \end{aligned} \tag{F.5.5}$$

and their sum is  $0 = 0$ .

In figure F.11, let us assume the normals on networks 1, 3, and 4 point up, out of the paper, the normals on 2 and 5 point down, and the normals on 6 and 7 point to the left. Then the doublet matching equations, by abutment, are

$$\begin{aligned} A_1: u_1 - u_2 - u_3 &= 0 \\ A_2: u_3 - u_4 - u_6 &= 0 \\ A_3: u_4 + u_5 &= 0 \\ A_4: u_6 - u_7 &= 0 \\ A_5: u_2 - u_5 &= 0 \\ A_6: u_7 - u_1 &= 0 \end{aligned} \tag{F.5.6}$$

Note that the plus sign for abutment 3 follows from the opposite orientations of networks 4 and 5. For a precise description of the computation of the signs  $s_i$  in the doublet matching boundary condition (F.5.1), see section B.3. Once again, the sum of all the equations in (F.5.6) is  $0 = 0$ .

Next, we claim that  $(n-1)$  of the  $n$  equations that occur at an intersection of  $n$  abutments are linearly independent. Considering (F.5.5), we see that each equation (except the last one) introduces a variable which had not previously been introduced. Thus each equation is independent of the previous ones, and so the first three equations are linearly independent.

Similarly, consider equations 2, 3, 4, 5, and 6 of (F.5.6). Equation 3 introduces  $u_5$ , 4 introduces  $u_7$ , 5 introduces  $u_2$ , and 6 introduces  $u_1$ , and thus these five equations are linearly independent.

Next, let us consider one more example of an abutment intersection (see figure F.12). The doublet matching equations are (assuming  $\hat{n}$  points leftward

from  $N_1$ , upward from  $N_4$ , and out of the paper from  $N_2$  and  $N_3$ ):

$$A_1: u_1 - u_2 + u_3 = 0$$

$$A_2: u_2 = 0$$

$$A_3: u_4 - u_3 = 0$$

$$A_4: u_1 + u_4 = 0 \quad (F.5.7)$$

Again, we see that the second, third, and fourth equations of (F.5.7) are linearly independent, since each introduces a new variable, while the sum of the first three equations minus the fourth is  $0 = 0$ .

Thus, for our three examples, the right number of doublet matching boundary conditions to impose at an abutment intersection is one less than the number of abutments, for then matching occurs everywhere, with no overspecification.

We now make the rash generalization that we should always impose one fewer doublet matching boundary condition than we have abutments. While not proven in general, this principle has been shown to be valid for a large number of examples.

We are still left with two questions. First, if there are more network corner points at an abutment intersection than the number of abutments minus one, then at which corner points should doublet matching boundary conditions not be imposed. For example, in figure F.10 there are 4 corner points and 4 abutments. Second, to which of two possible abutments should a corner point be assigned for matching, once the program decides to assign it to some abutment. In figure F.10, for instance, the boundary condition available at  $C_2$  may be used to impose doublet matching on either  $A_1$  or  $A_2$ .

We are able to provide a systematic approach to the assignment problem by constructing a pictorial model for an arbitrary abutment intersection. Let us first observe that each network corner point lies at the end of two distinct network edge segments, and therefore there are exactly two abutments associated with any corner point. For example, associated with corner point  $C_4$  in network  $N_4$  of figure F.10 are the two abutments  $A_3$  and  $A_4$ . On the other hand, one, two, or many corner points are associated with each abutment belonging to an abutment intersection. For example, corner points  $C_1$  and  $C_4$  are associated with abutment  $A_4$  in figure F.10. The same two observations hold about points in space, and line segments connecting these points, under the correspondence

corner points  $\longleftrightarrow$  line segments

(F.5.8)

abutments  $\longleftrightarrow$  points in space

That is, each line segment has exactly two endpoints, while a given point may be the endpoint of any number of line segments. This correspondence is not a natural one, since we are letting points correspond to lines and vice versa. Nevertheless, it is an extremely valuable tool in analyzing abutment intersections.

We illustrate in figures F.13a, b, and c the collections of line segments and points which correspond to the abutment intersections in figures F.10, F.11, and F.12. Segments are labeled  $C_i$  to emphasize that they represent corners of network  $N_i$ , and points are labeled  $A_i$  to represent abutments.

We may use the graphs of the type in figure F.13 as a tool to describe a systematic assignment of corner points to abutments in such a manner that each assignment introduces a new variable  $u_i$ , and thus assures the linear independence of the boundary conditions which are imposed.

To describe this systematic assignment, we must first make an observation. Suppose we pick an arbitrary abutment, and assign any corner point which belongs to the abutment. Next, we move to the other abutment associated with that corner point, and assign any corner point, other than the one previously assigned, to it. Once again, we pick the other associated abutment, always making sure no corner point is assigned twice.

We now note that in general, as long as we are not forced into a "dead end", or into an abutment to which we have already assigned a corner point, and as long as we stop when we reach the last abutment but one, or earlier, each abutment involves a new network corner point, which has not been associated with a previous abutment. That is, each time we jump from point to point, we come across a new line segment.

But this means that if we assign corner points to abutments subject to the restrictions above, we are always introducing a new variable in each equation we produce, and thus the linear equations must be independent.

So, for an arbitrary graph of the form in figure F.13, we must find a "path" or a sequence of paths through the graph, such that each time we come to a new abutment, a new line segment occurs (associated with that abutment), which did not occur before. If we ever come to a new abutment for which no new line segment occurs, we have reached a dead end, since the corner points corresponding to those line segments have already been used for matching.

For example, in figure F.13a, we may assign  $C_2$  to  $A_1$ , then  $C_3$  to  $A_2$ , and then  $C_4$  to  $A_3$ . In figure F.13b, we may assign  $C_1$  to  $A_1$ ,  $C_7$  to  $A_6$ ,  $C_6$  to  $A_4$ ,  $C_4$  to  $A_2$ , and  $C_5$  to  $A_3$ . In figure F.13c, we may assign  $C_2$  to  $A_2$ ,  $C_1$  to  $A_1$ , and  $C_4$  to  $A_4$ . In each case, we have assigned one fewer corner point than there are abutments.

In choosing these paths through the three graphs, we obeyed the following principles.

- a. We started at an abutment with empty space (that is, an abutment with only one associated corner point) wherever one existed, in order to avoid ending a path in one (e.g.,  $A_2$  in figure F.12).
- b. We were sure not to circle around an entire "closed loop." An example of a closed loop would be assigning (in figure F.13c)  $C_1$  to  $A_1$ , and  $C_4$  to  $A_4$ . Had we done so, all variables  $u_i$  would already have occurred somewhere, and we could not be sure that the

equation generated by assigning some corner point to some third abutment would be linearly independent of the previous equations.

- c. As required earlier, we never assigned the same corner point twice, we never assigned two corner points to the same abutment, and we made one fewer assignment than there were abutments.

The above principles are followed by the program in the assignment of corner points to abutments. Certain items introduce greater complexity, such as the presence of matching corner points of wake or design networks, and planes of symmetry. These subjects will be discussed in the Maintenance Document (section 4-H).

## F.6 Gap-Filling Panels

Whenever a gap whose size is greater than the user-specified tolerance distance occurs between portions of two or more network edges which form an abutment, gap-filling panels are defined. The placement of gap-filling panels is illustrated for an abutment containing two network edges in figure F.9.

We now briefly outline the process by which gap-filling panels are constructed, first considering the case of two network edges. First, each edge in the abutment is "parametrized." That is, each panel corner point on the edge is assigned a real number  $t$  between 0 and 1 inclusive, where  $t$  is the ratio of two distances. The first distance is the sum of the lengths of the panel edges between the starting point of the abutment and the panel corner point in question, while the second distance is the sum of the lengths of all the panel edges on a network edge. Thus  $t$  represents the proportion of the entire edge length which one has traveled in proceeding from the start of the abutment to the panel corner point in question. In figure F.9, each panel corner point is given a value  $t$ .

Now, suppose the distinct values of  $t$  which occur for the two network edges are  $\{t_0, t_1, \dots, t_n\}$ , where

$$0 = t_0 < t_1 < \dots < t_n = 1 \quad (\text{F.6.1})$$

In the example of figure F.9,  $n = 9$ , since there are 11 panel corner points other than the initial points, and the values  $t = .80$  and  $t = 1.0$  occur twice.

Now, up to  $n$  gap-filling panels may be constructed to fill the gap in the abutment. For each integer  $i$ ,  $1 < i < n$ , the quadrilateral region with corner points lying on the two network edges, with respective parameter values  $t = t_{i-1}$  and  $t = t_i$  is examined. If  $t_i$  is not the parameter value of a corner point (for instance, .30 is not the parameter value of any cornerpoint on network A in figure F.9), linear interpolation between corner points is used to find the point on the panel edge with that parameter value. If three or more of the four edges of this quadrilateral region have length greater than the user-specified tolerance distance  $\epsilon$ , a gap-filling panel is defined.

Thus, for the abutment in figure F.6, no gap-filling panels would be defined, since the gap size is uniformly smaller than  $\epsilon$ , and so all potential gap-filling panels have two edges of length less than  $\epsilon$ . On the other hand, if, in figure F.9,  $\epsilon$  were approximately .05 times the abutment length, seven gap-filling panels would be defined, while two potential ones would be discarded because two edges of the panels would be too short. The reason that very small gap-filling panels are never defined is that numerical difficulties could occur in measuring the influence of these panels on control points. It is not known at this time under which circumstances the resulting doublet discontinuity might be significant.

Next, we address the question of how to define the doublet strength on the gap-filling panels so that doublet continuity is attained. The edge splines constructed in appendix I assure that, if one edge is a refinement of the other, then the doublet strength matches at points on the two network edges with the same parameter value  $t$ . Thus we want the doublet strength to be constant on the panel along the direction perpendicular to the direction of the abutment.

We illustrate this in figure F.14. The four corner points of the panel are  $P_i$  and  $P_{i+1}$  on edge A and  $P_i'$  and  $P_{i+1}'$  on edge B. We then define  $M_i$  as the midpoint of the segment  $P_i P_{i+1}$ , and  $M_i'$  similarly. Then, since  $P_i$ ,  $P_{i+1}$ , and  $M_i$  each has the same parameter value as its primed counterpart, it also has the same doublet strength, namely  $\mu$ ,  $\mu_{i+1}$ , or  $\mu_i^+$  respectively. Thus, we have defined  $\mu$  at six of the nine panel defining points, and we define  $\mu$  at the remaining three panel defining points in the natural way.

This defines  $\mu$  uniquely on the whole panel (see section 5.5). Further, it insures continuity of  $\mu$  on the whole edge  $P_i P_{i+1}$  and the whole edge  $P_i' P_{i+1}'$ , since these two gap-filling panel edges are subsets of ordinary panel edges. Thus the doublet strength on the network edges is defined by a single quadratic function in one variable, and therefore agrees with the doublet strength on the gap-filling panel edge everywhere, since it agrees at three points.

Finally we must consider the case of three or more network edges meeting in an abutment, as illustrated in cross-section in figure F.15. There, network  $E_0$  is the most densely paneled network edge, and so, if the user has followed the paneling rules, it is a refinement of edges  $E_1$  and  $E_2$ . We construct gap-filling panels as illustrated in order to fill the gap in the abutment.

It still remains to be decided how to define the doublet strength on the gap filling panels. We want the doublet strength to be continuous across edges  $E_1$  and  $E_2$ , while at  $E_0$  we want

$$\mu_0 - \mu(1) - \mu(2) = 0 \quad (F.6.2)$$

where  $\mu(i)$  is the doublet strength on the gap-filling panel spanning the gap from  $E_0$  to  $E_i$ . On the other hand, the doublet edge splines and matching boundary conditions insure

$$\mu_0 - \mu_1 - \mu_2 = 0 \quad (F.6.3)$$

where  $\mu_i$  is the doublet strength on edge  $E_i$ . Thus the specification

$$\begin{aligned} \mu(1) &= \mu_1 \\ \mu(2) &= \mu_2 \end{aligned} \quad (F.6.4)$$

insures doublet continuity (in the form (F.1.1)) everywhere.

Thus the general procedure used by Pan Air for gap-filling panels in

abutments with three or more network edges is:

- a. choose the most densely paneled edge (which should be a refinement of all the other network edges),
- b. define gap-filling panels in the gap between the finest edge  $E_0$  and each other edge  $E_j$ , just as if this were an abutment with only two edges, and
- c. define the doublet strength on the gap-filling panels to be equal to the doublet strength on the edge  $E_j$ .

Note that this procedure works even if there are only two edges in the abutment. Further, it insures that the equation

$$\sum s_j u_j = 0 \quad (F.6.5)$$

is imposed along all network edges.

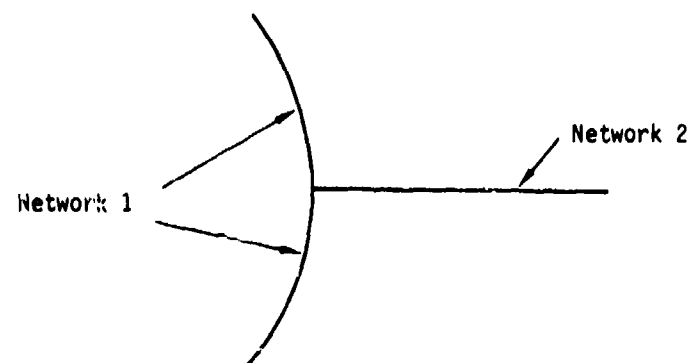
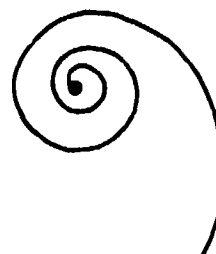


Figure F.1 - Impermissible network intersection  
(in cross-section)



• - region where viscous  
effects dominate

Figure F.2 - Leading edge vortex (in cross-section)





Figure F.3 - Simulation of a vortex core  
by a line vortex

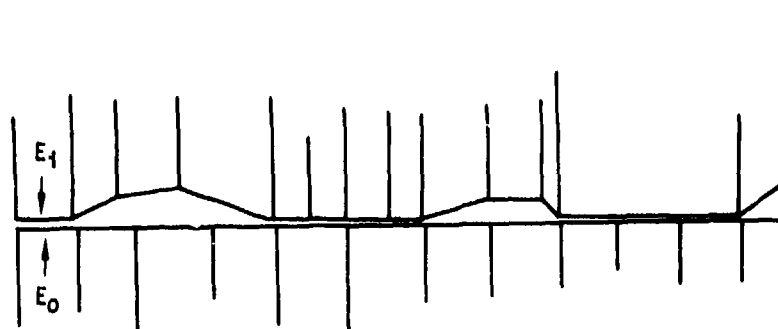


Figure F.4 - Multiple pairwise abutments involving  
the same edges

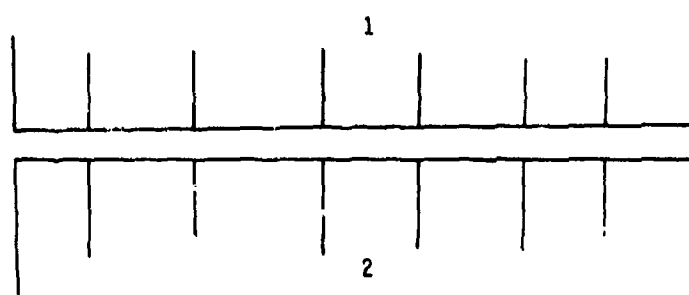


Figure F.5 - Each network edge is a refinement of the other

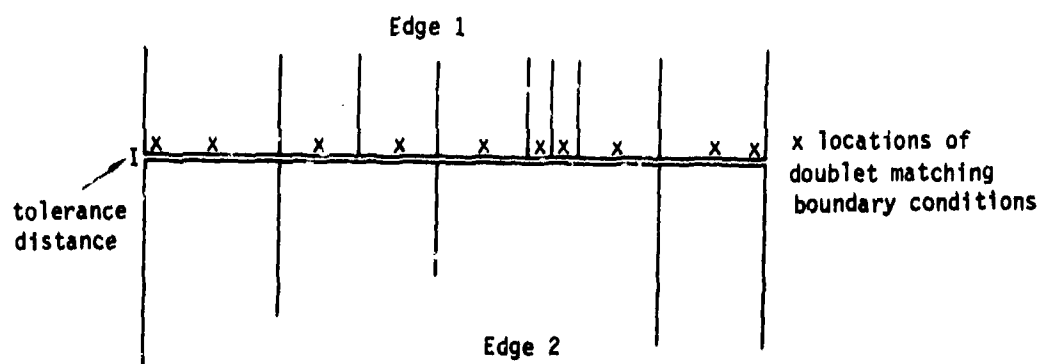
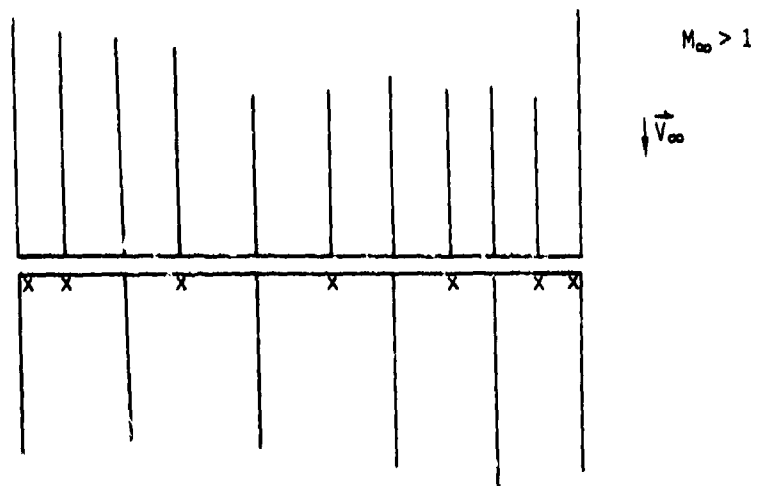


Figure F.6 - Edge 1 is a refinement of edge 2



x control points used for doublet matching

Figure F.7 - Control points on a supersonic leading edge are used for doublet matching

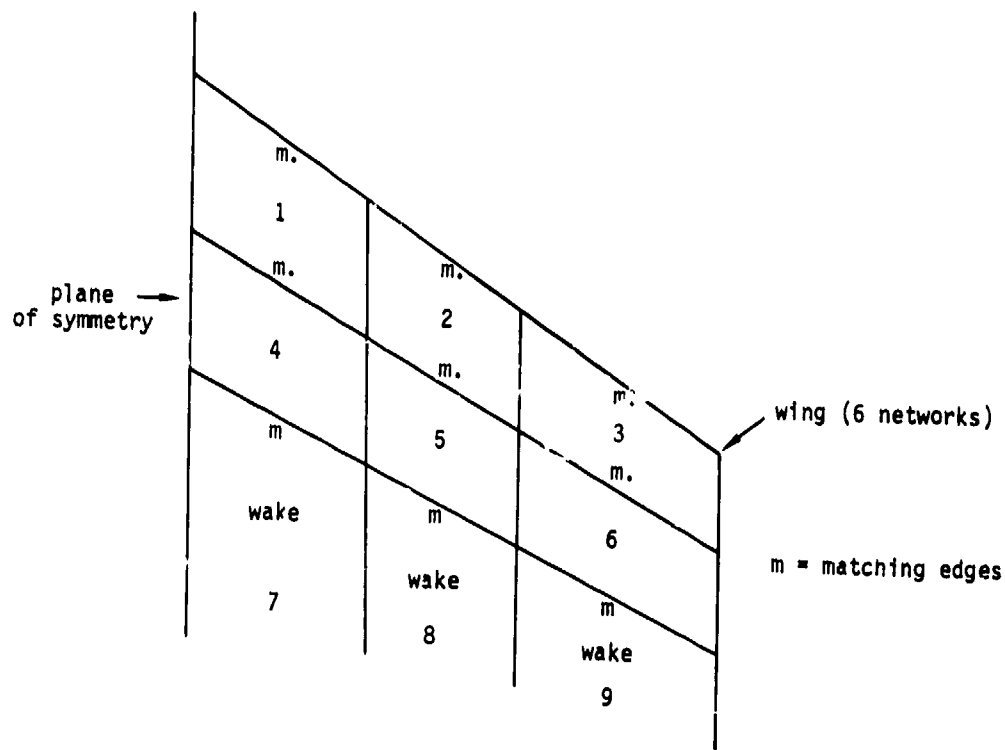


Figure F.8a - Six network wing with wakes

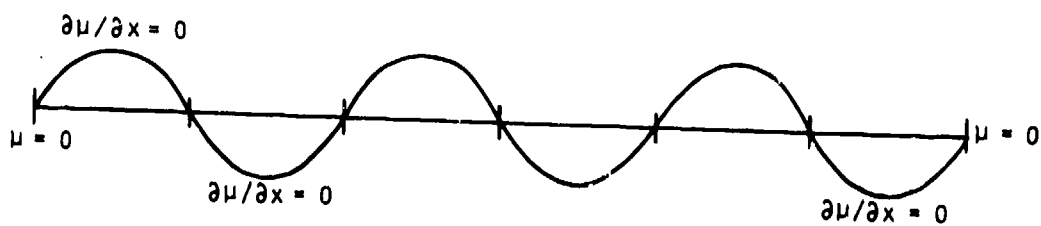


Figure F.8t Doublet distribution arising from specification of  $\mu$  at trailing edge

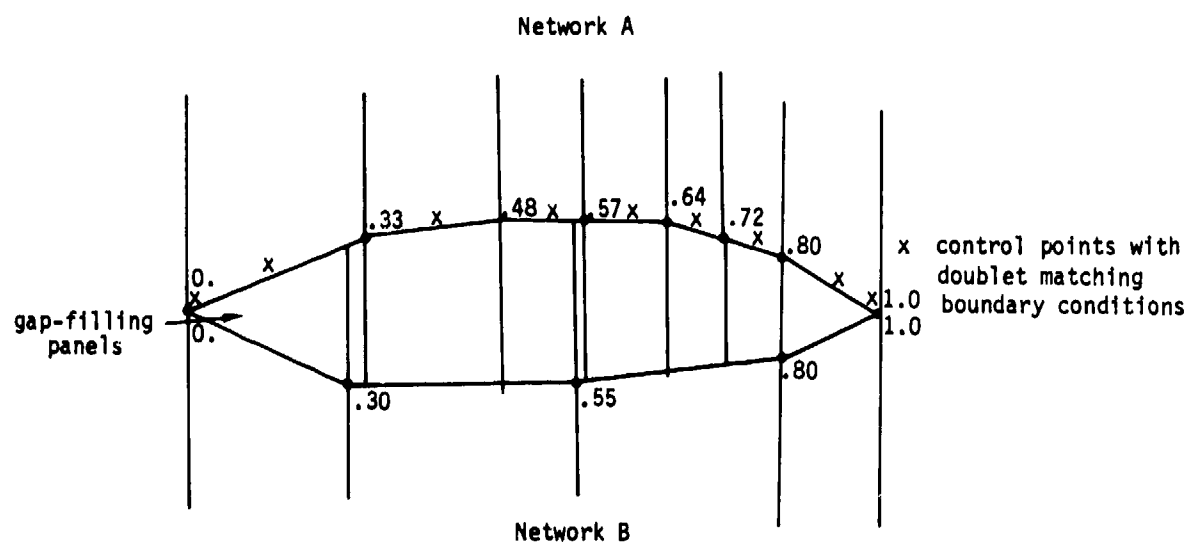


Figure F.9 - One edge is not precisely a refinement of the other

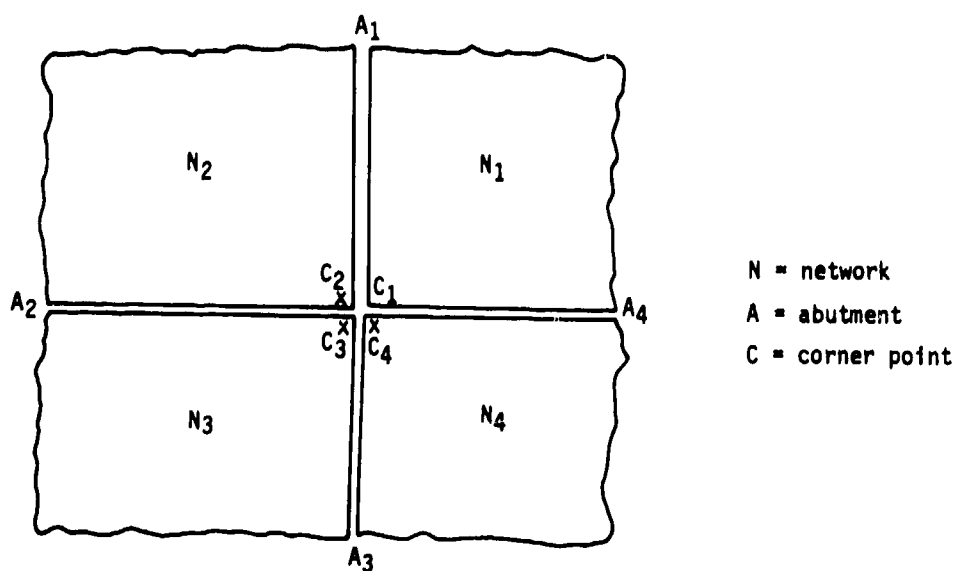


Figure F.10 - An abutment intersection with 4 abutments

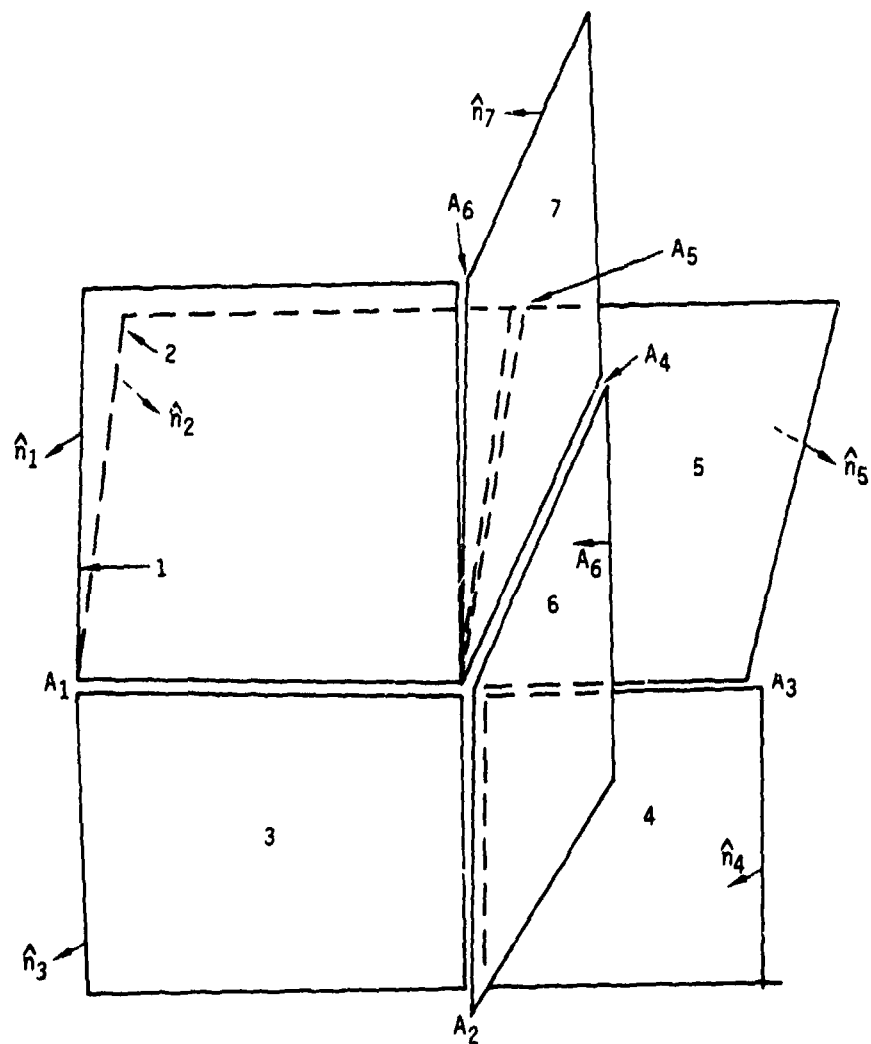


Figure F.11 - An abutment intersection with 6 abutments

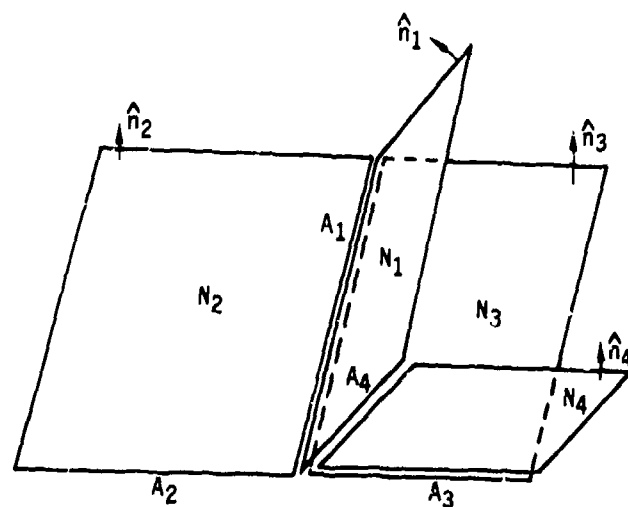
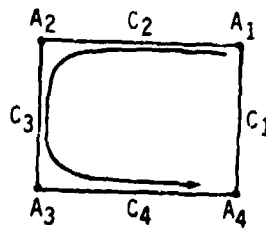
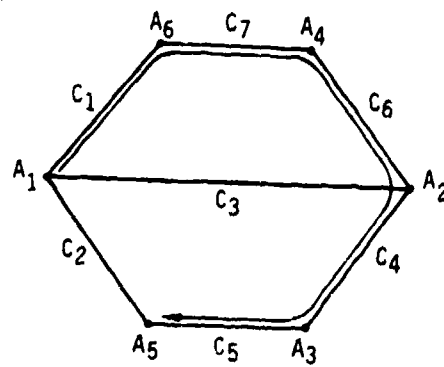


Figure F.12 - Another abutment intersection with 4 abutments

a.



b.



paths discussed  
in text

c.

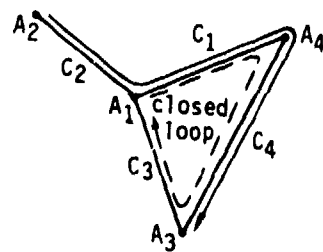


Figure F.13 - Line segment and point diagrams corresponding to three abutment intersections



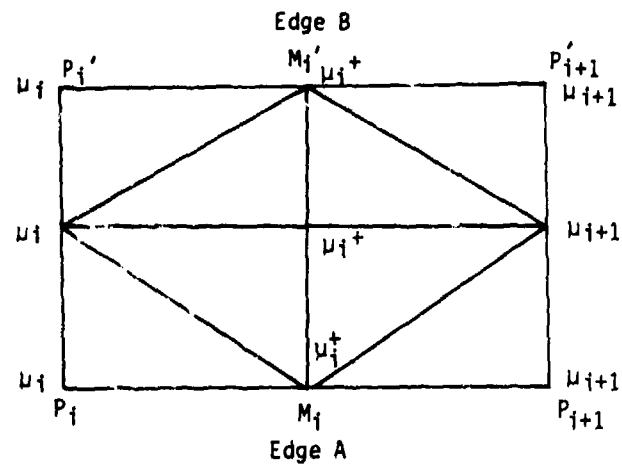


Figure F.14 - Gap-filling panel

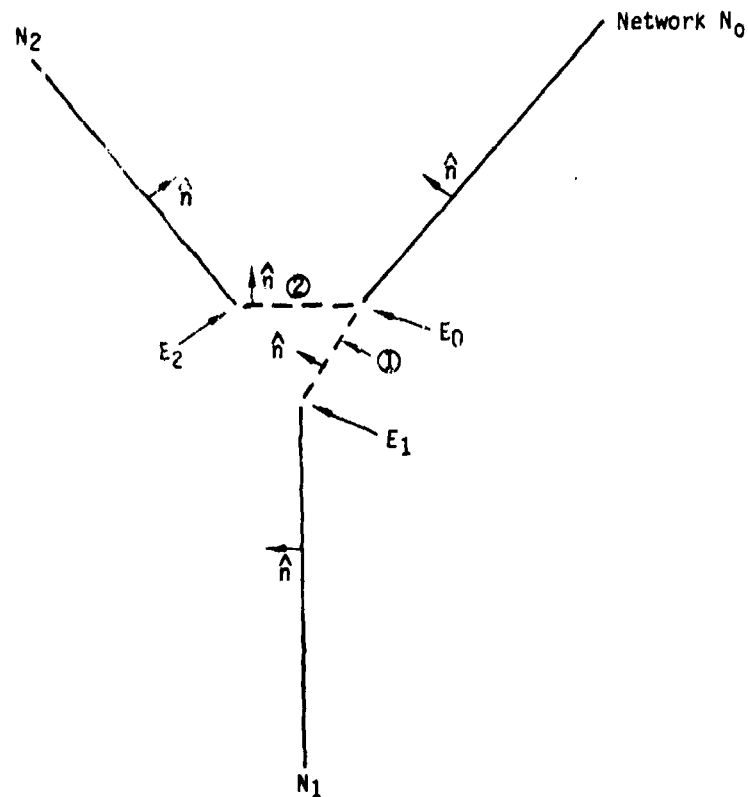


Figure F.15 - Gap-filling panels on an abutment with 3 network edges

## G.0 Control Point Locations

In figure G.1 we illustrate the possible location of points on a network, called control points, at which boundary conditions are defined. These locations are independent of the source type or doublet type of the network; however, we will see in Appendix H that meaningful boundary conditions are not necessarily imposed at all control points (for instance, on wake networks, boundary conditions are only imposed along one edge).

Note that controls points are illustrated as being located near, but not directly on, midpoints of panel edges lying on network edges. This is due to the disastrous results which would occur from attempting to measure the velocity or potential at a control point that lies directly on a panel edge (see section J.11). Later in this section we describe the procedure used to recede control points from the panel edge.

When a network edge is divided into distinct portions belonging to separate abutments, as illustrated in figure G.2, an extra control point, in addition to those in figure G.1, is defined. The same data is computed for these control points as for ordinary control points.

In order to determine its location, a control point is placed in one of three categories: panel center control points, edge midpoint control points, and panel corner control points. The latter two categories are only defined along the network perimeter. The control point is defined by prescribing a "hypothetical location" (the center point, edge midpoint, or corner point at which the control point would ideally be located), and a "recession vector" which describes the extent to which the control point is receded into a subpanel from its hypothetical location.

The size of the "recession vector" has been determined experimentally. Basically, it has been chosen as small as possible without causing severe numerical error. We refer to figure G.3 in defining the recession vectors. There, we show an edge control point as  $P_5$  and a corner point at  $P_1$ ; for control points at other points or edge midpoints the procedure is identical.

Panel center control points are only receded very slightly from the center point  $P_9$  since the doublet distribution is differentiable and the source distribution is continuous at  $P_9$ ; as a result (see section J.11) the potential and velocity induced by the singularity distributions are very well behaved at  $P_9$ . It is still necessary to recede the control point slightly, however, because influence coefficients can not be computed for a point lying directly on a sub-panel edge, because the calculations yield singular results there. So, we choose the recession vector to be

$$\vec{R} = \frac{(\vec{P}_8 - \vec{P}_9) + (\vec{P}_7 - \vec{P}_9)}{1000} \quad (G.0.1)$$

Edge control points are receded considerably further because of the discontinuities in doublet derivative, surface slope, and source strength which occur at network edges. Thus, for the control point located at  $P_5$ , we

define its recession vector to be

$$\vec{R} = \frac{(\vec{P}_9 - \vec{P}_5) + (\vec{P}_8 - \vec{P}_E)}{20} \quad (G.0.2)$$

and similarly for other edge control points.

For corner control points, the situation is complicated by the fact that not all panels look like the one in figure G.3, for which the control point at  $P_1$  would be receded in some obvious manner into the first subpanel. In figure G.4(a), the first subpanel is tiny, while in G.4(b) it does not exist at all.

We thus determine a recession vector for this case as follows. Let  $A_i$  be the area of the  $i$ th subpanel projected to the average plane. Then if

$$A_1 > A_5/10 \quad (G.0.3)$$

we set

$$\vec{R} = \frac{(\vec{P}_8 - \vec{P}_1) + (\vec{P}_5 - \vec{P}_1)}{20} \quad (G.0.4)$$

otherwise, we pick  $P_{10}$  "between"  $P_1$  and  $P_9$  as described below, and set

$$\vec{R} = (\vec{P}_{10} - \vec{P}_1) + \frac{1}{60} (\vec{P}_9 - \vec{P}_{10}) + \frac{1}{60} (\vec{P}_8 - \vec{P}_{10}) + \frac{1}{60} (\vec{P}_5 - \vec{P}_{10}) \quad (G.0.5)$$

To evaluate  $A_1$  and  $P_{10}$  let us consider the panel coordinate system discussed in section D.2 and illustrated in figure D.11. In this coordinate system, the area of subpanel 5 is  $1/2$ . Subpanel 1, projected to the average ( $z = 0$ ) plane, is illustrated in figure G.5. Its area (see D.2.16) is

$$A_1 = 1/2 |(\vec{P}_5 - \vec{P}_1) \times (\vec{P}_8 - \vec{P}_1)| = 1/2 \left| \begin{pmatrix} -1-C_{11} \\ -C_{21} \\ 0 \end{pmatrix} \times \begin{pmatrix} -C_{11} \\ -1-C_{21} \\ 0 \end{pmatrix} \right| \quad (G.0.6)$$

$$= 1/2 (1 + C_{11}) (1 + C_{21}) - C_{21} C_{11} = \frac{1 + C_{11} + C_{21}}{2} \quad (G.0.7)$$

So, (G.0.3) holds if

$$1 + C_{11} + C_{21} > 1/10 \quad (G.0.8)$$

Otherwise, we define  $P_{10}$  as the point lying both on  $P_5 P_8$  and on the line connecting  $P_9$  with the projection of  $P_1$ . Thus, in our panel coordinates

$$\vec{P}_{10} = a \begin{pmatrix} 1 + C_{11} \\ 1 + C_{21} \\ 0 \end{pmatrix} \quad (G.0.9)$$

where  $a$  is determined by the condition that  $P_5 P_8$  lies on the line

$$x + y = 1 \quad (G.0.10)$$

$$\text{Thus} \quad a (1 + C_{11} + C_{21}) = 1 \quad (G.0.11)$$

or

$$\vec{P}_{10} = \begin{pmatrix} (1 + C_{11})/(2 + C_{11} + C_{21}) \\ (1 + C_{21})/(2 + C_{11} + C_{21}) \\ 0 \end{pmatrix} \quad (G.0.12)$$

In reference coordinates, therefore,

$$\vec{P}_{10} = \left( \frac{1 + C_{11}}{2 + C_{11} + C_{21}} \right) \vec{P}_8 + \left( \frac{1 + C_{21}}{2 + C_{11} + C_{21}} \right) \vec{P}_5 \quad (G.0.13)$$

Equation (G.0.5) can now be used to define the recession vector, which thus locates the control point on subpanel 5 (see figure 5.4a).

Some geometric quantities in addition to location and hypothetical location are computed by the program for each control point. One of these is the subpanel on which the control point actually lies. This is needed later (see section J.8) to insure that an over-in potential and velocity are computed correctly in measuring the influence that the sub-panel on which the control point lies exerts on the control point.

Also, for each edge or corner control point at which a matching boundary condition is imposed, a set of "extra hypothetical locations" and their

associated sign is computed. These arise from the matching boundary condition (see section F.1)

$$\sum s_i \mu_i = 0 \quad (G.O.14)$$

where the  $\mu_i$  are the values of doublet strength on different networks.

In figure G.6, we illustrate an abutment containing three network edges. Although the control point is receded from the edge, the matching boundary condition involves singularity strengths at the edge; in this example (G.O.14) becomes

$$\sum_{i=0}^2 s_i \mu(H_i) = 0 \quad (G.O.15)$$

where  $H_0$  is the (default) hypothetical location of the control point, while  $H_1$  and  $H_2$  are extra hypothetical locations.

In Appendix F we indicate how the signs  $s_i$  are computed; here we describe the computation of the extra hypothetical locations. Hypothetical locations are computed one abutment at a time by parametrizing the abutment (see section F.4), a process that assigns to each panel corner point or edge midpoint  $P$  on that portion of a network edge belonging to an abutment a real number  $t(P)$  between 0 and 1.

In figure G.7, we illustrate an abutment with two network edges. Given the control point and default hypothetical location  $H_0$ , we compute the extra hypothetical location  $H_1$  as follows. Parametrization of the abutment gives us  $t(H_0)$ , and also assigns a value  $t$  to every panel corner point and edge midpoint on the edge of network 1.

By interpolation between these points, we find  $H_1$  as the point satisfying

$$t(H_1) = t(H_0) \quad (G.O.16)$$

In addition to the coordinates of the extra hypothetical locations, the program determines the panel and subpanel on which each extra hypothetical location lies, so that the doublet strength can be computed there later.

Our discussion of matching boundary conditions has assumed we are dealing with doublet matching. In the case of a source matching boundary condition (which may occur on the edge of a source design network)

$$\sum s_i \sigma_i = 0 \quad (G.O.17)$$

extra hypothetical locations and signs are computed as before.

There are two final pieces of geometric data, associated with control points, which we have not yet discussed. These are the normal and conormal of the subpanel on which the control point lies. The normal is needed in post-processing to compute velocity from the potential and the normal mass

flux (see Appendix N), while the conormal  $\hat{n}$  is needed to compute the normal mass flux from the velocity influence coefficient matrix by the formula

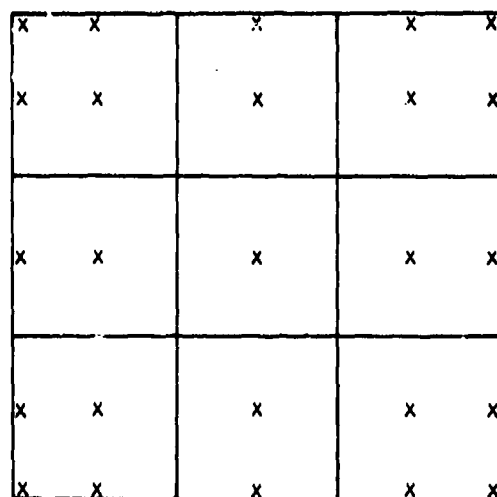
$$\vec{v} \cdot \tilde{n} = \vec{w} \cdot \hat{n} \quad (G.0.18)$$

The computation of the normal is described in section D.2, while

$$\tilde{n} = [B_0] \hat{n} \quad (G.0.19)$$

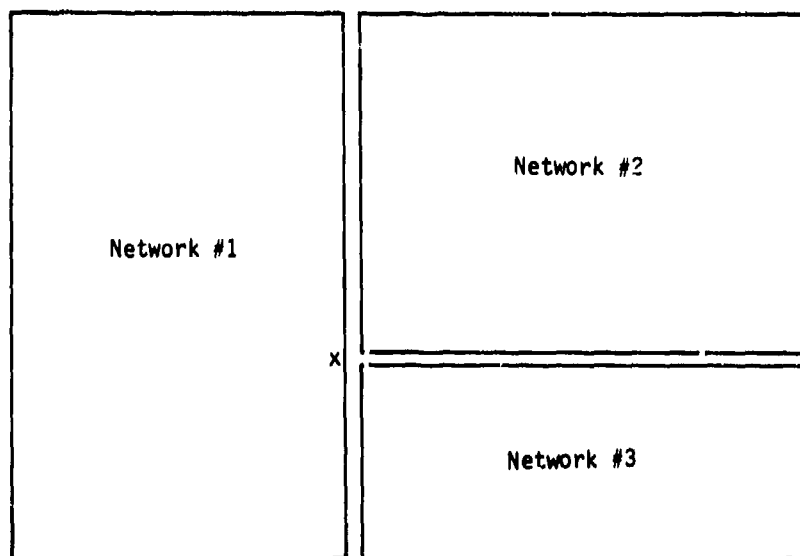
$$\text{where } [B_0] = I + (s\beta^2 - 1) \hat{c}_0 \hat{c}_0^T \quad (G.0.20)$$

by equation (E.3.9).



x = control point location

Figure G.1 - Control point locations



x = extra control point

Figure G.2 - Division of network edge into two abutments

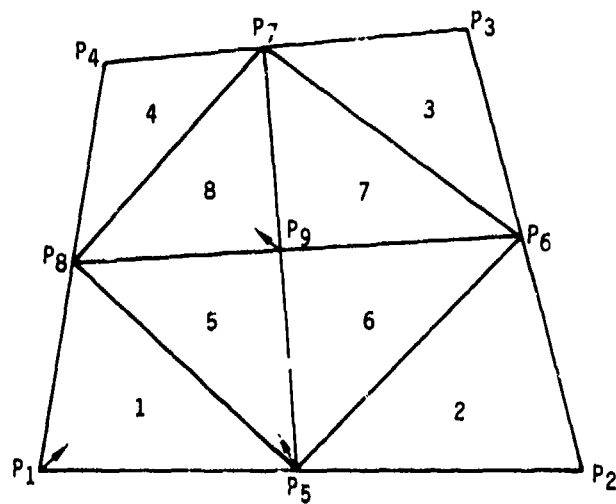


Figure G.3 - Control point recession vectors

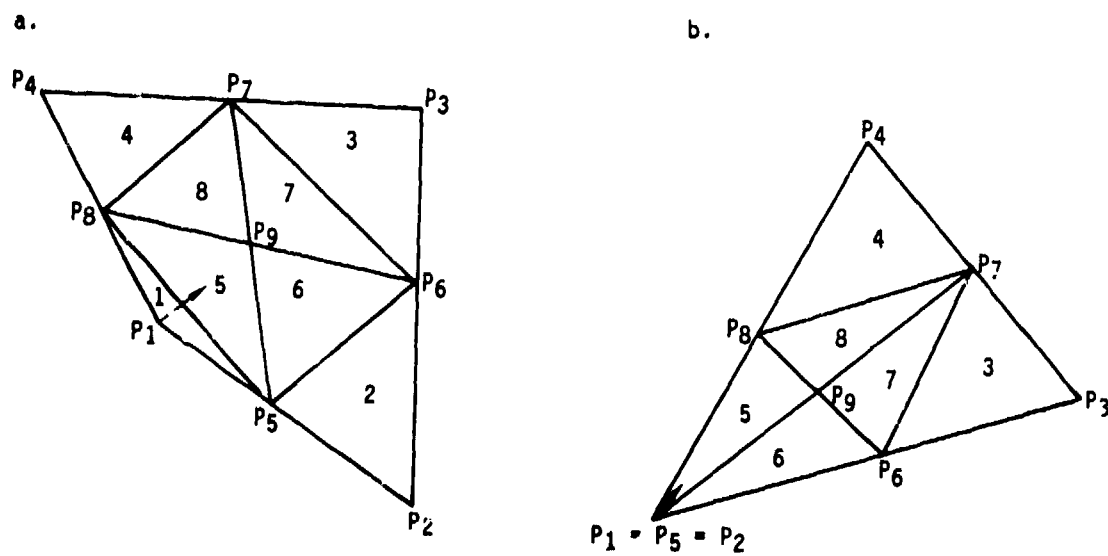


Figure G.4 - Recession of corner control points when subpanel is triangular or nearly triangular



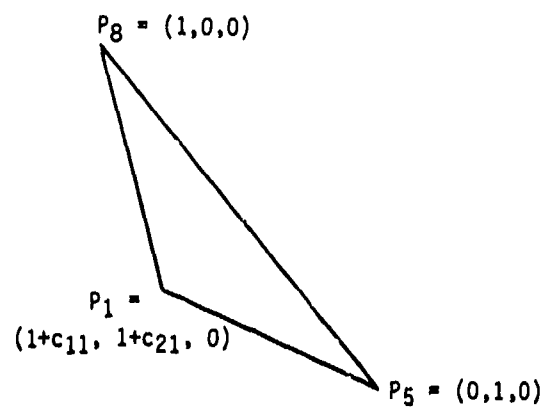


Figure G.5 - Subpanel 1, projected

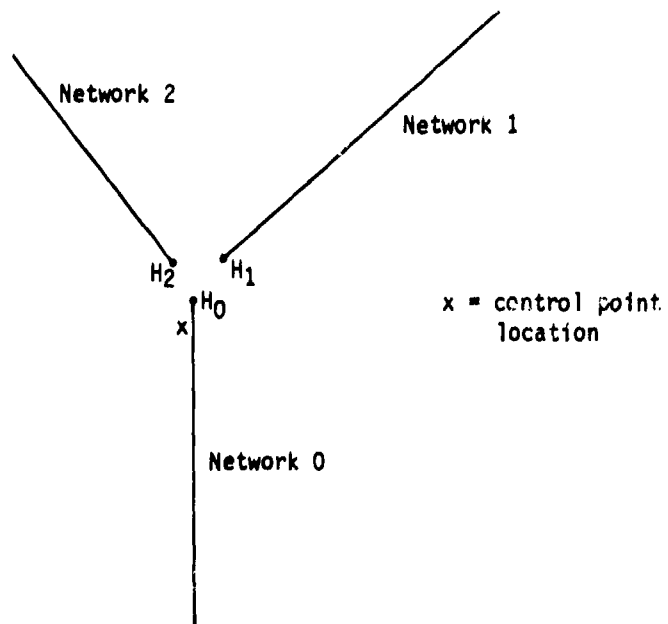


Figure G.6 - Abutment with 3 network edges (cross-section)

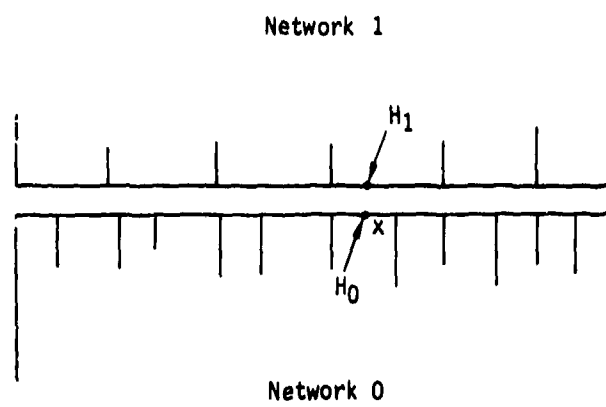


Figure G.7 - Hypothetical locations of a control point

## H.0 Boundary Conditions and Onset Flows

In this appendix, we describe the processing of the user-input boundary condition data by the program. The program is not (with one exception) concerned with the nature of the boundary value problem defined by the user (that is, whether or not it is well posed). Under certain circumstances, however, user-specified boundary conditions are over-ridden by the program.

In section H.1, we discuss the standard boundary condition equation,

$$\begin{aligned} a_A \vec{w}_A \cdot \hat{n} + c_A \phi_A + \vec{t}_A \cdot \vec{v}_A \\ + a_D \sigma + c_D u + \vec{t}_D \cdot \vec{\nabla} u = b \end{aligned} \quad (H.0.1)$$

and describe how the program computes the coefficients of the left hand side of the equation. In section H.2, we discuss program overrides of the user-specified boundary conditions. In section H.3, we discuss the computation of the right hand side of (H.0.1) via onset flows.

## H.1 Reduction of User-Specified Boundary Conditions to Standard

### Formulation

The program user usually defines two boundary conditions at each control point. Generally this is done on a network-wide basis (especially in defining the left hand side of (H.0.1)), but it may be done on a point-by-point basis. The User's Manual (section 3) explains how to define the boundary condition coefficients; for standard cases it is done automatically by the program. In any case, the user-input boundary condition can be much more general than (H.0.1); it can be of the form (though almost all coefficients would generally be zero);

$$\begin{aligned}
 & a_U^I \vec{w}_U \cdot \hat{n} + c_U^I \phi_U + \vec{t}_U^I \cdot \vec{v}_U + e_U^I \vec{v}_U \cdot \hat{n} \\
 & + a_L^I \vec{w}_L \cdot \hat{n} + c_L^I \phi_L + \vec{t}_L^I \cdot \vec{v}_L + e_L^I \vec{v}_L \cdot \hat{n} \\
 & + a_A^I \vec{w}_A \cdot \hat{n} + c_A^I \phi_A + \vec{t}_A^I \cdot \vec{v}_A + e_A^I \vec{v}_A \cdot \hat{n} \\
 & + a_D^I \sigma + c_D^I \mu + \vec{t}_D^I \cdot \vec{\nabla} \mu + e_D^I \vec{v}_D \cdot \hat{n} = b
 \end{aligned}
 \tag{H.1.1}$$

Here, the subscripts U, L, A, D refer to upper, lower, average, and difference, while the superscript I specifies that these are user-input quantities.

Letting X stand for any of the quantities w,  $\phi$ , or v, we have, by definition,

$$\begin{aligned}
 X_A &= 1/2 (X_U + X_L) \\
 X_D &= X_U - X_L
 \end{aligned}
 \tag{H.1.2}$$

Inverting (H.1.2) we have

$$\begin{aligned}
 X_U &= X_A + 1/2 X_D \\
 X_L &= X_A - 1/2 X_D
 \end{aligned}
 \tag{H.1.3}$$

$$\text{Thus, } a_U X_U + a_L X_L = (a_U + a_L) X_A + 1/2 (a_U - a_L) X_D
 \tag{H.1.4}$$

where  $a_U$  and  $a_L$  are any real numbers.

Substituting (H.1.4) into (H.1.1), we have

$$\begin{aligned}
& (a_U^I + a_L^I + a_A^I) \vec{w}_A \cdot \hat{n} + (c_U^I + c_L^I + c_A^I) \phi_A \\
& + (\vec{t}_U^I + \vec{t}_L^I + \vec{t}_A^I) \cdot \vec{v}_A + (e_U^I + e_L^I + e_A^I) \vec{v}_A \cdot \hat{n} \\
& + (1/2 a_U^I - 1/2 a_L^I + a_D^I) \sigma \\
& + (1/2 c_U^I - 1/2 c_L^I + c_D^I) \mu \\
& + (1/2 \vec{t}_U^I - 1/2 \vec{t}_L^I + \vec{t}_D^I) \cdot \vec{\nabla} \mu \\
& + (1/2 e_U^I - 1/2 e_L^I + e_D^I) \vec{v}_D \cdot \hat{n} = b
\end{aligned} \tag{H.1.5}$$

Here, we have used the facts that  $\sigma = \vec{w}_D \cdot \hat{n}$  and  $\mu = \phi_D$ . So we have replaced upper and lower flow quantities in (H.1.1) with average and difference quantities. But in order to put the equation in the non-redundant form (H.0.1), we still have to eliminate the normal velocity terms which may be selected by a program user in place of normal mass flux.

Now, we have already shown (see 5.4.16a) that

$$\vec{w} \cdot \hat{n} = \vec{v} \cdot \tilde{n} \tag{H.1.6}$$

where  $\tilde{n}$  is the co-normal. Now, assuming

$$\hat{n} \cdot \tilde{n} \neq 0 \tag{H.1.7}$$

( $\hat{n} \cdot \tilde{n} = 0$  is the case of a forbidden "Mach-inclined" panel), we have the identity

$$\hat{n} = \frac{1}{\hat{n} \cdot \tilde{n}} \hat{n} + \tilde{\tau} \tag{H.1.8}$$

where

$$\tilde{\tau} = \hat{n} - \frac{1}{\hat{n} \cdot \tilde{n}} \tilde{n} \tag{H.1.9}$$

Now

$$\hat{n} \cdot \tilde{\tau} = 1 - \frac{\hat{n} \cdot \tilde{n}}{\hat{n} \cdot \tilde{n}} = 0 \quad (H.1.10)$$

and so  $\tilde{\tau}$  is in fact a tangent vector or zero.

Thus, by (H.1.8),

$$\vec{v} \cdot \hat{n} = \frac{1}{\hat{n} \cdot \tilde{n}} \vec{v} \cdot \tilde{n} + \tilde{\tau} \cdot \vec{v} = \frac{1}{\hat{n} \cdot \tilde{n}} \vec{v} \cdot \hat{n} + \tilde{\tau} \cdot \vec{v} \quad (H.1.11)$$

Substituting (H.1.11) into (H.1.5), we obtain

$$\begin{aligned} & a_U^I + a_L^I + a_A^I + \frac{1}{\hat{n} \cdot \tilde{n}} (e_U^I + e_L^I + e_A^I) \vec{w}_A \cdot \hat{n} \\ & + (c_U^I + c_L^I + c_A^I) \phi_A \\ & + (\vec{t}_U^I + \vec{t}_L^I + \vec{t}_A^I + (e_U^I + e_L^I + e_A^I) \tilde{\tau}) \cdot \vec{v}_A \\ & + (1/2 a_U^I - 1/2 a_L^I + a_D^I + \frac{1}{\hat{n} \cdot \tilde{n}} (1/2 e_U^I - 1/2 e_L^I + e_D^I)) \sigma \\ & + (1/2 c_U^I - 1/2 c_L^I + c_D^I) \mu \\ & + (1/2 \vec{t}_U^I - 1/2 \vec{t}_L^I + \vec{t}_D^I + (1/2 e_U^I - 1/2 e_L^I + e_D^I) \tilde{\tau}) \cdot \vec{\nabla} \mu = b \end{aligned} \quad (H.1.12)$$

Thus, (H.1.5) is of the form (H.0.1), with

$$a_A = a_U^I + a_L^I + a_A^I + \frac{1}{\hat{n} \cdot \tilde{n}} (e_U^I + e_L^I + e_A^I)$$

$$c_A = c_U^I + c_L^I + c_A^I$$

$$\vec{t}_A = \vec{t}_U^I + \vec{t}_L^I + \vec{t}_A^I + (e_U^I + e_L^I + e_A^I) \left( \hat{n} - \frac{1}{\hat{n} \cdot \tilde{n}} \tilde{n} \right)$$

$$a_D = 1/2 a_U^I - 1/2 a_L^I + a_D^I + \frac{1}{\hat{n} \cdot \tilde{n}} (1/2 e_U^I - 1/2 e_L^I + e_D^I)$$

$$\vec{t}_D = 1/2 \vec{t}_U^I - 1/2 \vec{t}_L^I + \vec{t}_D^I + (1/2 e_U^I - 1/2 e_L^I + e_D^I) \left( \hat{n} - \frac{1}{\hat{n} \cdot \tilde{n}} \tilde{n} \right)$$

(H.1.13)

## H.2 Program Overrides of User Boundary Condition Specifications

The program overrides that can occur are:

- (1) reformulation of boundary conditions on a superinclined panel to specify conditions on the downstream side,
- (2) nullification of the boundary condition if no corresponding singularity parameter exists,
- (3) imposing matching of doublet or source strength, and
- (4) imposition of a closure boundary condition.

### H.2.1 Superinclined Panel Override

In describing the program override which occurs on superinclined panels, that is, those for which

$$\hat{n} \cdot \hat{n} < 0 \quad (H.2.1)$$

we will assume for convenience that the "upper" surface of the panel is the "upstream" surface, that is, that

$$\hat{n} \cdot \hat{c}_0 < 0 \quad (H.2.2)$$

where  $\hat{c}_0$  is the compressibility vector.

This assumption is not made within the program, of course. Under this assumption, any upper surface specification is ill-posed, or very nearly so. Nevertheless, such a boundary condition could accidentally occur if a panel significantly inclined to the freestream becomes superinclined as the Mach number is increased.

We say that an upper surface condition has been specified if all the coefficients of  $X_L$ 's are zero, where  $X_L$  is defined in (H.1.3), and  $X$  stands for  $\vec{w} \cdot \hat{n}$ ,  $\phi$ , or  $\vec{v}$ . Using (H.1.3), we see that

$$X_A - 1/2 X_D = X_L \quad (H.2.3)$$

Now, an upper surface boundary condition specification has occurred if

$$\begin{aligned} a_L &= 0 \\ c_L &= 0 \\ \text{and } t_L &= 0 \end{aligned} \quad (H.2.4a)$$

that is, if

$$\begin{aligned} a_A &= 2 a_D \\ c_A &= 2 c_D \\ \text{and } t_A &= 2 t_D \end{aligned} \quad (H.2.4b)$$



Whenever (H.2.4) occurs, the boundary condition (H.0.1) is replaced by the revised boundary condition

$$\vec{w}_L \cdot \hat{n} = \vec{w}_A \cdot \hat{n} - 1/2 \sigma = 0 \quad (\text{H.2.5})$$

or, if that boundary condition has already been specified as the other boundary condition at the control point, (H.0.1) is replaced by

$$\phi_L = 0 \quad (\text{H.2.6})$$

Finally, if the boundary condition (H.0.1) is

$$\sigma = b \quad (\text{H.2.7})$$

the program assumes this to be an indirect upper surface boundary condition associated with interior perturbation stagnation, and thus replaces this with the boundary condition (H.2.5).

#### H.2.2 Nullification of User-Input Boundary Conditions

The program override of a user-specified boundary condition just discussed differs from the other overrides in that one boundary condition of the standard form (H.0.1) is replaced by another boundary condition of the same form. The other program assigned boundary conditions have non-standard form.

Let us consider the method by which the program decides the number of non-trivial boundary conditions to impose at a control point. Here, the underlying principle is that the number of boundary conditions must equal the number of singularity parameters.

This principle is achieved by the following algorithm. Initially, the number is zero. Next, we compare the control point location (see figure G.1) with the boundary condition locations, for the network source type, illustrated in figure H.1. If a boundary condition location appears at the control point location we increment the boundary condition count, unless the source type is null, in which case we do not increment the count. Next, we compare the control point location to the boundary condition locations for doublet networks illustrated in figure H.2, again incrementing the count only if a boundary condition location appears in the control point location. This gives us the number of boundary conditions to be imposed at the control point.

For "extra" control points, at most one boundary condition is imposed, depending on the doublet type. One boundary condition is imposed if the extra control point lies on a doublet analysis network, or on the matching edge of a doublet wake 1 or doublet design network.

For the typical case (that of a source analysis/doublet analysis network) this algorithm results in the imposition of two boundary conditions (such as  $\phi_L = 0$ ,  $\sigma = -\vec{w}_A \cdot \hat{n}$ ) at panel centers, and one boundary condition (such as  $\phi_L = 0$ ) at edge control points.

Now, the program may decide that zero, one, or two boundary conditions are required at a control point. It then determines a list of user-input boundary conditions, possibly modified by the program in the case of a superinclined panel. Again, there may be zero, one, or two of these. Next, it determines a list of program-generated boundary conditions of the form of doublet or source matching, or closure. If the total number of non-trivial boundary conditions to be assigned exceeds the number of program-assigned boundary conditions, additional boundary conditions are assigned from the list of user-input boundary conditions. If an insufficient number of user-input boundary conditions is available, the program prints an error message and terminates. If fewer than two non-trivial boundary conditions are needed at a control point, the remaining boundary conditions are labeled "null", so that, formally, two boundary conditions are defined at each control point. The null boundary conditions are ignored when the aerodynamic influence coefficient matrix is computed. If more user-input boundary conditions are entered than are required, the program chooses which one to impose according to a procedure described in section H.2.5.

#### H.2.3 Source and Doublet Matching Boundary Conditions

The program-assigned boundary conditions of source or doublet matching or closure only occur at network edges. Source matching and closure boundary conditions only occur for design networks, while doublet matching boundary conditions may occur on an edge of any network whose doublet type is not "null".

Recall from section F.3 that for each network abutment, at most one network edge segment is labelled to the effect that its control points will be used for doublet matching. All the edge midpoint control points on that network edge segment now receive a program-assigned boundary condition of doublet matching. Similarly, it may occur that at most one network edge segment is labelled source matching. The edge control points on that segment are then assigned a boundary condition of source matching.

Similarly, at each "abutment intersection", some of the corner control points belonging to the intersection may be labelled as doublet matching control points. These control points are assigned a doublet matching boundary condition.

#### H.2.4 Closure Boundary Conditions

Closure boundary conditions occur when one particular edge of a source or a doublet design network is designated as a "closure edge" by the program user. Then, for each edge midpoint control point on the network edge, the boundary condition

$$\oint_C (a_A \vec{w}_A \cdot \hat{n} + a_D \sigma) dS = b \quad (H.2.8)$$

C

is imposed, where C is the row or column of panels headed by that control point, as illustrated in figure H.3. The coefficients  $a_A$ ,  $a_D$ , and  $b$  are user-supplied, and once again can be redundantly defined in terms of upper, lower, average, and difference terms. We will explain (H.2.8) by means of a simple example.

In figure H.4, we illustrate a thick wing on the upper surface of which we desire a specified pressure distribution (see Appendix C for a discussion of the design process). Now, after solving the potential flow problem and refoiting the surface, we obtain a refoited surface, whose trailing edge may or may not coincide with the unchanged trailing edge of the lower surface. The closure boundary condition can be used to insure that the trailing edge coincide after refoiting, that is, that the airfoil "closes".

But now, suppose the boundary condition

$$\int_A^B \vec{w}_U \cdot \hat{n} \, d\Gamma = 0 \quad (H.2.9)$$

is satisfied, where A and B are shown in figure H.4. Then clearly a streamline originating on the wing upper surface at A will end up at B. It can not end up "above" B, since then a streamline starting slightly below A would end up slightly above B, and thus the integral of the mass flux through the surface would be non-zero (see figure H.5).

Now, a wing is a 3-dimensional object, and thus, in order to insure that any streamline originating at the leading edge of the design network will arrive at the trailing edge of the design network, equation (H.2.9) must be imposed on a dense set of integration contours originating at the leading edge, and following the wing surface in a streamwise direction to the trailing edge. Then the refoited surface, which is required to be impermeable, must necessarily be the surface defined by the streamlines originating at the leading edge and ending at the trailing edge. So, the imposition of (H.2.9) on a dense set of integration lines would insure that the trailing edge of the refoited surface agrees with the trailing edge of the design network.

Now, a panel method being a discretization method, we do not impose (H.2.9) at a dense set of lines, but instead on a set of narrow two-dimensional surfaces aligned streamwise, namely, rows or columns of panels. Thus we impose the boundary condition

$$\iint_C \vec{w}_U \cdot \hat{n} \, dS = 0 \quad (H.2.10)$$

Now,  $\vec{w}_U = \vec{V}_\infty + \vec{w}_L$  (H.2.11)

$$\vec{w}_U \cdot \hat{n} = \vec{w}_A \cdot \hat{n} + 1/2 \, \sigma \quad (H.2.12)$$

and  $\vec{w}_L = 0$  (H.2.13)

because of the perturbation stagnation boundary conditions ( $\phi_L = 0$ ). Thus (H.2.10) can be written

$$\iint_C (\sigma + \vec{V}_\infty \cdot \hat{n}) dS = 0 \quad (\text{H.2.14})$$

or

$$\iint_C \sigma dS = b = - \iint_C V_\infty n dS \quad (\text{H.2.15})$$

which is of the form (H.2.8), with  $a_D = 1$ ,  $a_A = 0$ . The more general form of (H.2.8) is available for program users solving non-standard problems.

This completes our discussion of closure boundary conditions at this time. In section K.5, we describe the manner in which equation (H.2.8) is converted into a linear equation in the set of singularity parameters.

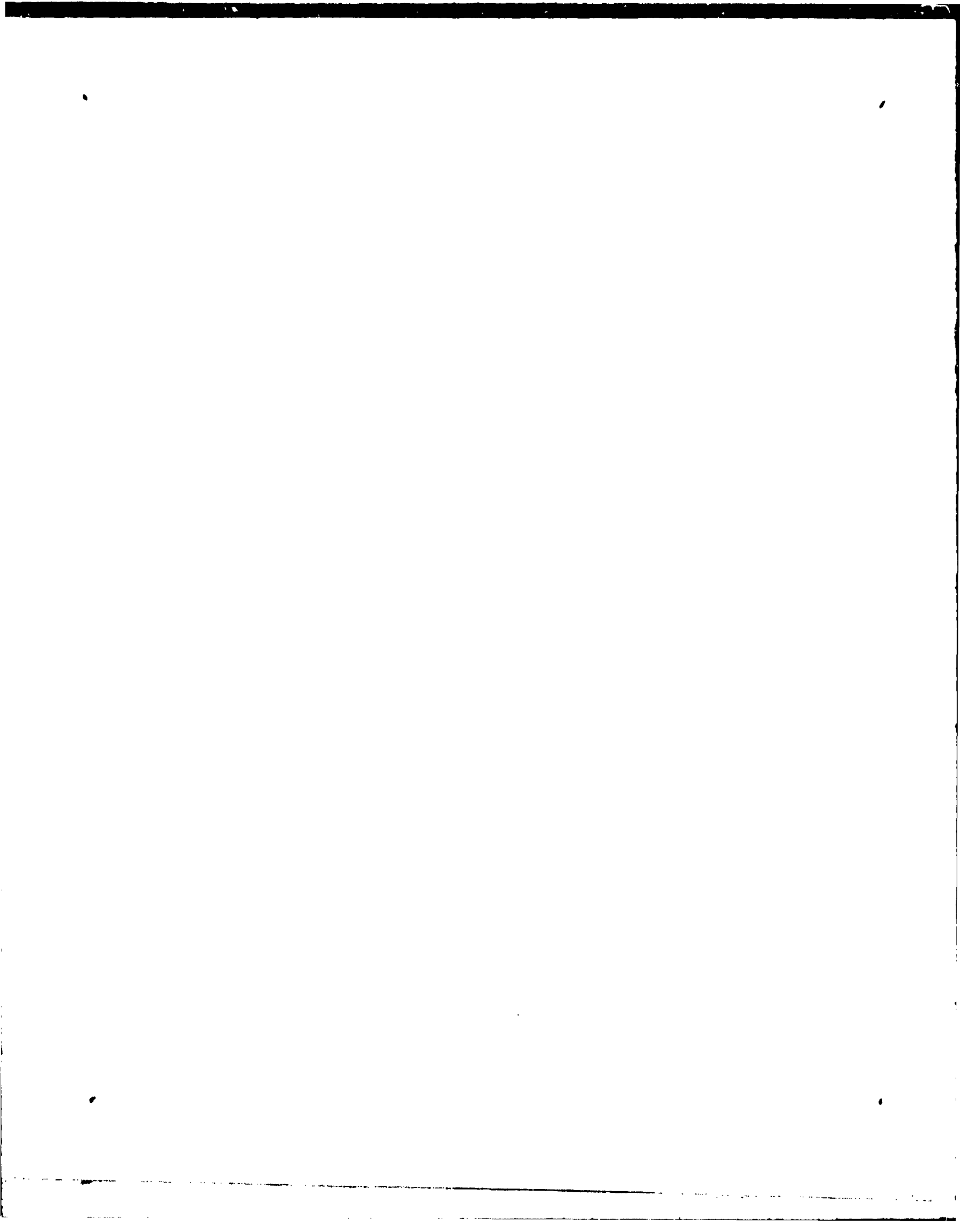
#### H.2.5 The Boundary Condition Hierarchy

Now we consider the case where there are more user-supplied boundary conditions than are needed. Obviously, if zero boundary conditions are needed, the solution is to choose none of them. So, let us assume one boundary condition is needed and two are supplied by the user. Whenever two boundary conditions are supplied by the user, they are given an ordering, and if only one is needed, the first one is chosen.

The ideas behind the ordering method are:

- (a) potential and doublet strength are quadratically varying, while source strength and velocity are linearly varying; therefore the former should be specified rather than the latter, since quadratic functions are not amenable to extrapolation, but need to be "pinned down" at network edges.
- (b) tangential velocity boundary conditions are less stable than normal velocity ones, therefore the latter should be specified, given a choice, and
- (c) there are fewer source parameters than doublet parameters on a network, in general, so specifying source strength (especially on network edges) risks overspecification and a singular AIC matrix.

Based on these considerations, we give six mutually exclusive categories of boundary conditions in figure H.6. We order the two boundary conditions so that the one belonging to the category with the lowest index comes first, choosing arbitrarily if both belong to the same category. If the doublet or source type of the network is null, however, no boundary condition in category 1 or 5, respectively, may be imposed, or else a singular AIC matrix would result. In concluding this discussion, we reiterate that the definitions of the categories in figure H.4, and their order, are not rigorously justifiable, but only based on example and the principles above.



### H.3 Onset Flows

Equation (H.0.1) is the most general possible equation in  $\phi$  and its derivatives, but it is often inconvenient for the user to evaluate the scalar  $b$  on the right hand side of (H.0.1). The most common example arises from the boundary condition

$$\vec{W}_U \cdot \hat{n} = 0 \quad (H.3.1)$$

where  $\vec{W}$  is total mass flux. Since

$$\vec{W} = \vec{w} + \vec{V}_\infty \quad (H.3.2)$$

equation (H.3.1) becomes

$$\vec{w}_U \cdot \hat{n} = -\vec{V}_\infty \cdot \hat{n} = b \quad (H.3.3)$$

The scalar  $b$  could, of course, be computed by the user at every control point, but much labor is saved by having the program do so.

Similarly, consider the tangential velocity boundary condition

$$\vec{t}_U \cdot \vec{V}_U = \beta \quad (\text{where } \beta \text{ is user-specified}), \quad (H.3.4)$$

which becomes

$$\vec{t}_U \cdot \vec{V}_U = \beta - V_\infty \cdot \vec{t}_U \quad (H.3.5)$$

Finally, suppose a program user wishes to define total internal stagnation, as opposed to perturbation stagnation. The boundary conditions to be imposed should therefore indirectly (that is by specifying potential) specify

$$\vec{W}_L = 0 \quad (H.3.6)$$

Thus, we specify

$$\bar{\Phi}_L = 0 \quad (H.3.7)$$

where  $\bar{\Phi}$  is defined by

$$\vec{W} = \vec{\nabla} \bar{\Phi} \quad (H.3.8)$$

on the surface, as illustrated in figure H.7.

Note that  $\bar{\Phi} \neq \Phi$ , where  $\vec{V} = \nabla \Phi$

Now, we prove that up to a constant, (H.3.8) requires that

$$\bar{\Phi}(x) = \frac{1}{s_B^2} [\vec{V}_\infty \cdot \vec{x}] + \phi(\vec{x}) \quad (H.3.9)$$

We now prove (H.3.9). We use reference coordinates. By (5.2.4)

$$\tilde{\nabla}_i [\vec{V}_\infty, \vec{x}] = \sum_j [B_0]_{ij} \frac{\partial}{\partial x_j} [\vec{V}_\infty, \vec{x}] \quad (\text{H.3.10a})$$

= (by (E.2.4))

$$\sum_{j,k,m} [B_0]_{ij} \frac{\partial}{\partial x_j} (\{\vec{V}_\infty\}_k [C_0]_{km} \vec{x}_m) \quad (\text{H.3.10b})$$

Noting that  $\vec{V}_\infty$  and  $[C_0]$  are independent of  $x_j$ , while

$$\frac{\partial}{\partial x_j} (x_m) = \delta_{jm} \quad (\text{H.3.11a})$$

(the Kronecker delta), we have

$$\begin{aligned} \tilde{\nabla}_i [\vec{V}_\infty, \vec{x}] &= \\ \sum_{j,k,m} [B_0]_{ij} \{\vec{V}_\infty\}_k [C_0]_{km} \delta_{jm} &= \\ [B_0]_{ij} [C_0]_{kj} \{\vec{V}_\infty\}_k & \end{aligned} \quad (\text{H.3.11b})$$

Now, applying (E.2.9) to  $B_0$  and  $C_0$ , and noting by (F.3.9) that  $C_0$  is its own transpose,

$$\tilde{\nabla} [\vec{V}_\infty, \vec{x}] = s_B^2 \vec{V}_\infty \quad (\text{H.3.12a})$$

Thus,

$$\tilde{\nabla} \left( \frac{1}{s_B^2} [\vec{V}_\infty, \vec{x}] + \phi(\vec{x}) \right) = \vec{V}_\infty + \tilde{\nabla} \phi = \vec{W} \quad (\text{H.3.12b})$$

which implies (H.3.9).

So, the boundary condition (H.3.7) is equivalent to

$$\phi_L(\lambda) = \frac{-1}{s_B^2} [\vec{V}_\infty, \vec{x}] \quad (\text{H.3.13})$$

The right hand side quantities of equations (H.3.3), (H.3.5), and (H.3.13) are automatically computed in PAN AIR for user convenience. But, in fact, PAN AIR offers more general right hand side options which have a rather empirical

justification for existence. These options arise from the introduction of an "onset flow"  $\vec{U}_0$  with the assumption

$$\vec{W} = \vec{U}_0 + \vec{w} \quad (\text{H.3.15})$$

Now, there is nothing empirical about (H.3.15) unless we make the assumption

$$\vec{U}_0 \neq \vec{V}_\infty \quad (\text{H.3.16})$$

where  $\vec{V}_\infty$  is the uniform freestream, aligned with the compressibility direction  $\hat{e}_0$ .

Even so, at Mach zero, the boundary condition

$$\vec{W} \cdot \hat{n} = 0 \quad (\text{H.3.17})$$

combined with (H.3.15), where  $\vec{U}_0$  is a uniform vector field  $\vec{U}_0$  which is not parallel to  $\vec{V}_\infty$  (see figure H.8) is still theoretically valid, since the Prandtl-Glauert equation reduces to Laplace's equation, and therefore has no preferred direction.

Now, at non-zero Mach number, it is still possible for the small perturbation assumptions to be satisfied if  $\vec{U}_0$  is very close to  $\vec{V}_\infty$  everywhere. The most common application of this is to simulate flow conditions at multiple angles of attack which only differ slightly by varying the uniform onset flow without varying the compressibility direction  $\hat{e}_0$ . The advantage is that as long as  $\vec{V}_\infty = \hat{e}_0$  is not varied, the same AIC matrix may be used each time, thus saving on computation time.

If the perturbation to the freestream defined by the onset flow is small, it need not be uniform. Consider the case of a propeller slipstream (see figure H.9). The action of the propellers causes an increased flow which does not arise from the solution of Prandtl-Glauert equation. Thus the appropriate boundary condition to impose is (H.3.17) where

$$\vec{W} = \vec{V}_\infty + \Delta\vec{U}_1 + \vec{w} \quad (\text{H.3.18})$$

and  $\Delta\vec{U}_1$  is the "local incremental onset flow", in this case the incremental flow due to the action of the propellers. Once again, we can put  $\vec{W}$  in the form (H.3.15) by setting

$$\vec{U}_0 = \vec{V}_\infty + \Delta\vec{U}_1 \quad (\text{H.3.19})$$

As a third example, we consider a case in which the onset flow is not a small perturbation of the freestream, but is so in the neighborhood of the configuration. Consider the case of an airplane undergoing a small rolling motion of magnitude  $|\vec{\omega}|$  in a "right handed" rotation about an axis with direction  $\vec{\omega}$  through a point  $P_0$  (see figure H.10).

Computation of the magnitude  $|\vec{\omega}|$  from a particular roll rate (in radians per unit time) is discussed in section 7 of the User's Manual. This is an unsteady phenomenon, but we simulate it (calling the flow "quasi-steady") by defining an onset flow

$$\vec{U}_0(\vec{r}) = \vec{U}_\infty + \vec{\omega} \times (\vec{r} - \vec{P}_0) \quad (\text{H.3.20})$$



where P is the control point, and imposing the boundary condition.

$$\vec{w} \cdot \hat{n} = -\vec{U}_0 \cdot \hat{n} \quad (\text{H.3.21})$$

Note that  $U_0$  is unbounded as  $|\vec{P} - \vec{P}_0|$  becomes large, and thus a rotational onset flow is never a "small perturbation" in all of space, no matter how small the rotation rate. Thus no theoretical justification for the use of rotational onset flows exists, and so rotational onset flows must be used with extreme caution. The use of a rotational onset flow is generally valid, however, if the perturbation it induces is small in the neighborhood of the configuration, and may be used to estimate aerodynamic derivatives due to steady roll, pitch, and yaw rates.

PAN AIR provides for all these right hand side boundary condition options by permitting an arbitrary linear combination of the options described. Thus, in general, the user may define an arbitrary onset flow at a control point P by

$$\vec{U}_0(P) = U_\infty + \Delta \vec{U}_1(P) + \vec{w} \times (\vec{P} - \vec{P}_0) \quad (\text{H.3.22})$$

where the user defines  $\vec{U}_\infty$ ,  $\Delta \vec{U}_1$ ,  $\vec{w}$ , and  $P_0$ . The vector  $\vec{U}_\infty$  is defined by a magnitude  $|\vec{U}_\infty|$ , an angle of attack  $\alpha$  and angle of sideslip  $\beta$ , such that (compare with (E.3.1))

$$\vec{U}_\infty = |\vec{U}_\infty| \begin{Bmatrix} \cos \alpha \cos \beta \\ -\sin \beta \\ \sin \alpha \cos \beta \end{Bmatrix} \quad (\text{H.2.23})$$

The vector  $\Delta \vec{U}(P)$  is specified by the user on a control point by control point basis either as a vector in reference coordinates, or by specifying a magnitude  $U_1$ , and angles  $\alpha_1$ , and  $\beta_1$  (1 stands for local) such that

$$U_1 = \vec{U}_\infty + \vec{U}_1 = U_1 \begin{Bmatrix} \cos \alpha_1 \cos \beta_1 \\ -\sin \beta_1 \\ \sin \alpha_1 \cos \beta_1 \end{Bmatrix} \quad (\text{H.3.24})$$

Now, the general right hand side expression which may be defined by a user for a boundary condition is

$$b(P) = b_0 - b_n \vec{U}_0 \cdot \hat{n} - \vec{t}_T \cdot \vec{U}_0 - \frac{b_\theta}{s\beta^2} [\vec{U}_\infty, \vec{P}] \quad (\text{H.3.25})$$

where  $b_0$ ,  $b_n$ ,  $\vec{t}_T$  and  $b_\theta$  are user-defined quantities. We mention in passing that various default options are available to define the standard

combinations which occur. These options are described in the PAN AIR User's Manual.

This concludes our discussion of boundary conditions. One exception is that we have not discussed the effect of symmetry planes on the boundary condition processing. This is covered in section K.1.

a. Source analysis

x	x	x
x	x	x
x	x	x

b. Source design

x	x	x	x
x	x	x	x
x	x	x	x
x	x	x	x

matching or closure edge

Figure H.1 - Boundary condition locations for source networks

a. Doublet analysis

x	x		x	x	x
x	x		x		x
x	x		x		x
x	x		x		x
x	x		x		x

b. Doublet wake 1

x	x	

matching edge

c. Doublet wake 2

x		

matching corner

Figure H.2 - Boundary condition locations for doublet networks

d. Doublet analysis network with smooth abutment

x	x		x		x	x
x		x		x		x
x		x		x		x
x		x		x		x
x						x

smooth abutment

e. Doublet design

x	x		x		x
x		x		x	
x		x		x	
x		x		x	
x	x		x		x

matching or closure edge

Figure H.2 - Concluded

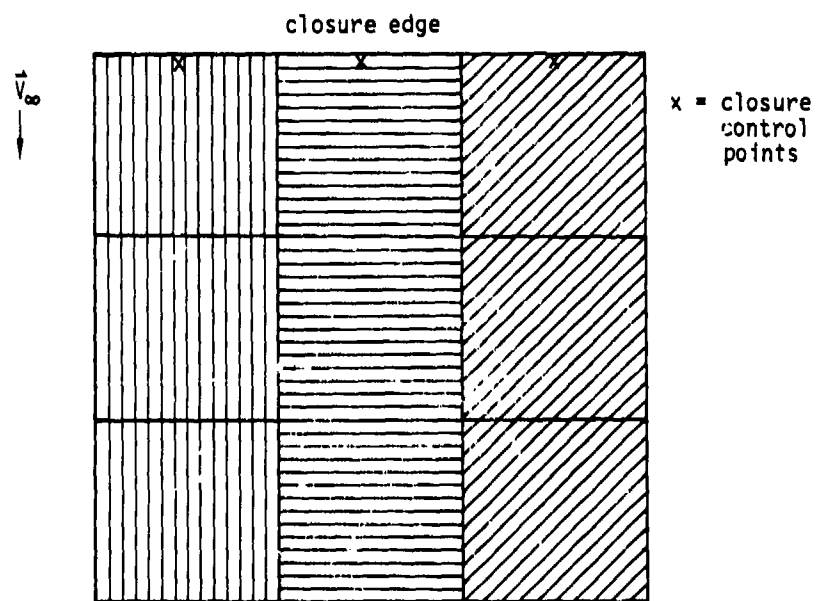


Figure H.3 - Columns of panels illustrated by cross-hatching

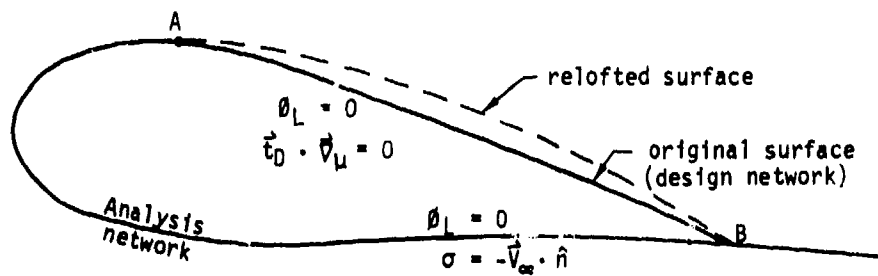


Figure H.4 - Design of upper surface of thick wing

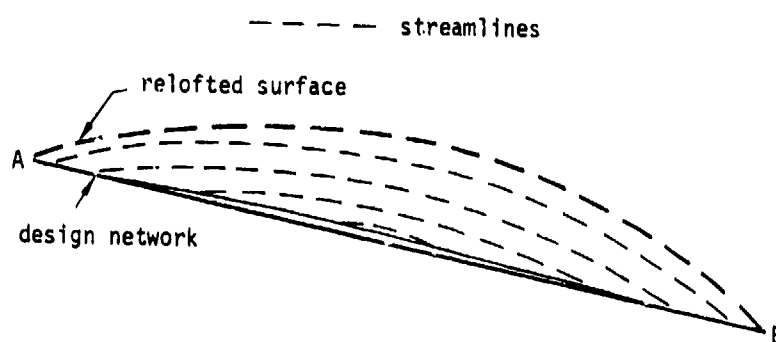


Figure H.5 - Pattern of streamlines on imposition of a closure boundary condition

Order in Hierarchy	Coefficient restrictions	example
1.	$C_D \neq 0$ , all others = 0	$\mu = b$
2.	$C_A \neq 0$ , $a_A = T_A = 0$	$\theta = b$
3.	$a_A \neq 0$ , $T_A = 0$	$W_A \cdot N = b$
4.	$T_A \neq 0$	$V_A \cdot T_A = b$
5.	$T_D \neq 0$ , $a_A = C_A = T_A = a_D = 0$	$T_D \cdot \nabla \mu = b$
6.	$a_D \neq 0$ , $a_A = C_A = T_A = 0$	$\sigma = b$

Figure H.6 - Boundary condition categories

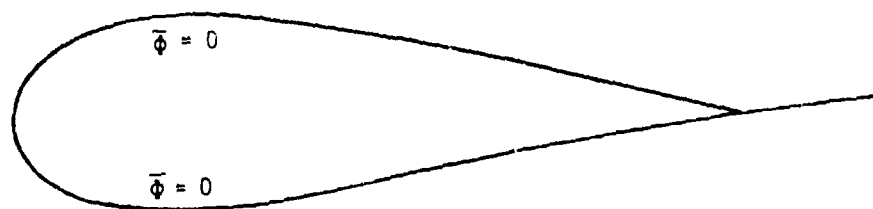


Figure H.7 - Total internal stagnation

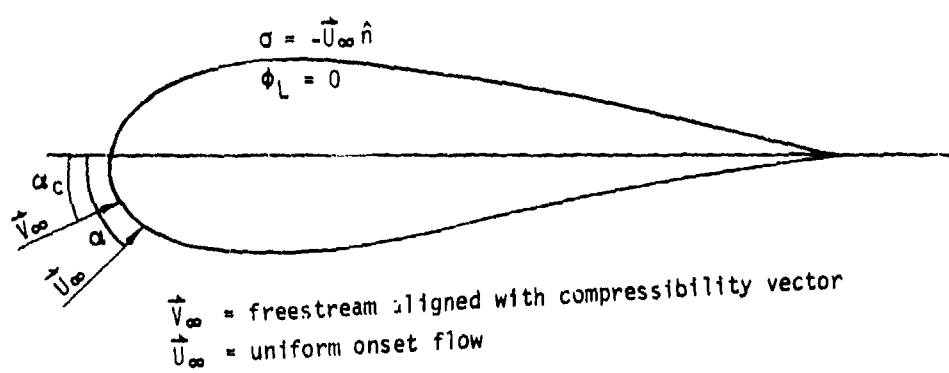


Figure H.8 - Onset flow, not parallel to compressibility direction



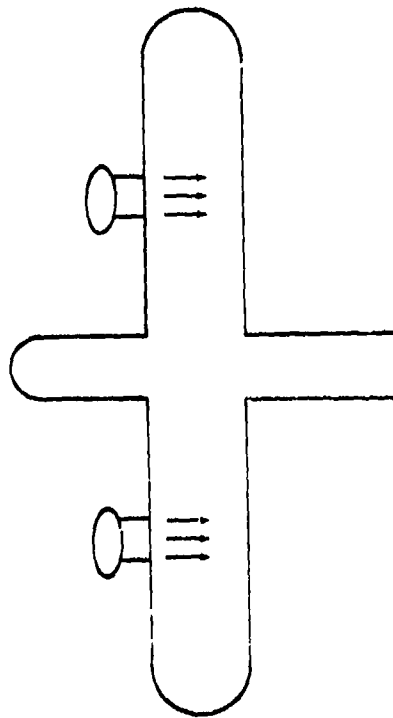


Figure H.9 - Propeller slipstream

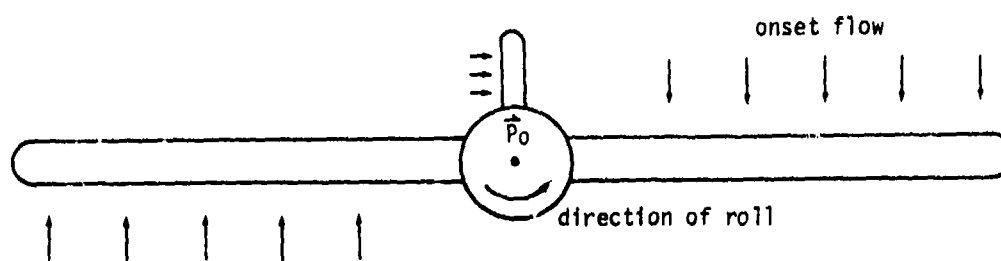


Figure H.10 - Airplane undergoing small rolling motion

## I.0 Singularity Splines

Singularity splines define the source and doublet distributions on the entire configuration in terms of the source and doublet singularity parameters. These distributions are defined by a collection of matrices. First, the source and doublet distributions on a subpanel (recall from section 5.5 that a panel is partitioned into eight subpanels) are each defined by a "subpanel spline matrix" (denoted, respectively,  $SPSPL^S$  and  $SPSPL^D$ ) in terms of five "panel source parameters" and nine "panel doublet parameters." Thus there are eight of each of these matrices associated with each panel.

Next, the panel source and doublet parameters are defined by "outer spline matrices" (denoted, respectively, by  $BS^S$  and  $BD^D$ ) in terms of singularity parameters located in the neighborhood of the panel. There is one of each of these matrices associated with each panel. There is one of each of these matrices associated with each panel.

The subpanel spline matrices are defined by equation (5.5.7). That is,  $[SPSPL^S]^{3 \times 5}$  relates the three coefficients  $\sigma_0, \sigma_1, \sigma_n$  (which define a linear source distribution on the subpanel) to the five panel source parameters (that is, the source strengths at the five points on the panel illustrated in figure I.1a). Similarly,  $[SPSPL^D]^{6 \times 9}$  relates the six coefficients  $\mu_0, \dots, \mu_{nn}$  (which define a quadratic doublet distribution on the subpanel) to the nine panel doublet parameters (whose locations are illustrated in figure I.1b).

The outer spline matrices are defined by equation (5.5.8). That is,  $[BS^S]$  defines the five panel source parameters in terms of the neighboring source singularity parameters (generally nine in number), while  $[BD^D]$  defines the panel doublet parameters in terms of the neighboring doublet parameters (generally 21 in number).

The subpanel and outer spline matrices are used in the influence coefficient calculations. The subpanel spline matrices are first used in order to compute "panel influence coefficient" (PIC) matrices (see sections 4.4.2 and J.1), and the PIC matrices are multiplied by the outer spline matrices to obtain potential and velocity influence coefficient matrices ( $[PIC]$  and  $[VIC]$ ) which give the perturbation potential and velocity at a point, in terms of all singularity parameters, due to all the panels in the configuration (see sections 4.2.3 and 5.9.1).

In section I.1 we discuss the construction of outer spline matrices. While their construction is simple in principle, based on a least square procedure, in practice it is quite involved because there are many special cases. In particular, a special "edge spline" is used near network edges,

which, in conjunction with the doublet matching boundary conditions discussed in Appendix F, results in precise matching of doublet strength along network edges. In section 1.2 we describe the construction of subpanel spline matrices.

In section 1.3 we discuss full panel and half panel spline matrices. These matrices define source and doublet distributions specified by single polynomials over the whole panel or half the panel, respectively, also in terms of the panel singularity parameters. The distributions are rough approximations to the 8 subpanel distributions defined by the subpanel splines. They are used in "intermediate field" influence coefficient calculation.

Next, in section 1.4, we discuss "far field moments", matrices describing integrals of the singularity strength over a panel in terms of the panel singularity parameters. The matrices are used in far field influence coefficient calculation. Finally, in section 1.5, we discuss the theory of the least squares procedure.

We now briefly discuss the reasoning behind the subpanel and outer spline construction techniques. First (cf. section C.3), we require the spline to be stable: the disturbance in the singularity distribution caused by a perturbation of a boundary condition should die off quickly.

Second, the source spline should be linearly accurate and the doublet spline quadratically accurate. That is, if the source parameters are defined by a linear function, the source distribution defined by the spline matrices should be exactly that linear function. An analogous property should hold for the doublet splines. The justification for a linear source and quadratic doublet distribution are given in section B.5.

Third, the spline must be local in nature. That is, the singularity distribution on a panel must depend on a reasonably small number of singularity parameters. This is due to the storage problems which would occur otherwise. That is, too much core and disk storage would otherwise be required for each panel.

Fourth, the doublet strength should be continuous (see section B.4). It is preferable to have a differentiable doublet strength, continuous source strength, and smooth geometry as well; unfortunately only the continuous source strength is easily feasible and thus is produced in PAN AIR, even though its value in the absence of a differentiable doublet strength and smooth geometry is questionable (see section J.12).

Finally, the entries of the PIC matrices, which are defined as sums of integrals, should be computable in closed form. That is, numerical integration should not be required for the evaluation of the integrals. The reason for this requirement is one of simplicity. The integrands in (5.6.9-10) are far too singular to be integrated numerically as they stand. It might be possible to partition the integral into a regular part, integrable numerically, and singular part, integrable in closed form, but such a method has not yet been developed.

It is the avoidance of numerical integration, in combination with the maintenance of geometric continuity, that causes much of the complexity of the spline construction. Geometric continuity between panels can be maintained either by breaking up a panel into flat subpanels, or by defining a single curved panel. The integrals over the curved panel are not computable in closed form in supersonic flow, however.

Once one has decided to use flat subpanels, a minimum of five planar regions (those of figure 5.2) is mandated to achieve geometric continuity. The use of eight subpanels has been chosen because it offers a convenient method of defining a continuous doublet distribution, while not requiring polynomials of degree greater than two. An explicit polynomial distribution has been chosen rather than a parametric distribution because the integration in parametric coordinates can not be performed in closed form.

## I.1 Outer Splines

The construction of outer splines is a two step process. In the first step, row vectors  $SP^S$  and  $SP^D$  (called "spline vectors") are formulated for grid points as illustrated in Figure I.1c for some typical cases. These row vectors define the source or doublet strength at each enriched grid point in the network as a linear combination of surrounding singularity parameter values. In the second step, matrices  $[B^S]$  and  $[B^D]$  are constructed for each panel, giving the source or doublet strength at the appropriate grid points on the panel (panel singularity values) as linear combinations of values of singularity parameters in the neighborhood of the panel.

Thus the matrices  $[B^S]$  have five rows while the  $[B^D]$  have nine rows, since the source strength is defined at five points on a panel (the panel source parameter locations) by row vectors  $SP^S$ , while the doublet strength is defined at nine points by row vectors  $SP^D$  (see Figure I.1). The number of columns in a matrix  $B$  is variable: it equals the total number of distinct singularity parameters on which the panel source or doublet parameters depend. The matrices  $B$  are assembled from the required row vectors  $SP$  in a fairly straightforward manner described in the maintenance manual (see the preface of SUBROUTINE VECUNM of the DQG module). Briefly, first row vectors  $SP$  are computed for every grid point in the configuration (except that row vectors  $SP^S$  are not needed for panel source parameter locations) and stored on disk. Then, when the spline quantities for a single panel are being computed, the five (or nine) row vectors for each of the panel source (or doublet) singularity parameter are fetched from the disk. These row vectors are then amalgamated into a single matrix  $B^S$  (or  $B^D$ ) by VECUNM.

In this section we will concentrate our attention on the computation of individual row vectors  $SP^S$  or  $SP^D$ . The basic principle is simple. For source splines, the source strength at a grid point is fit in a linearly accurate manner to as few surrounding source parameters as possible while for doublet splines we do the same in a quadratically accurate manner. But while the basic principle is simple, implementation is complex because of a myriad of special cases which do not fit the general rules.

We will cover these cases on order of reducing generality. First, we will discuss source splines for analysis networks. Then we will discuss doublet splines for analysis and wake networks. Finally we will discuss source and doublet splines for design networks.

### I.1.1 Source Spline Vectors for Analysis Networks

Computing the row vector describing the source strength at the center of a panel in analysis network is particularly simple, since a source singularity parameter is located there. Thus the source strength is just the singularity parameter value; that is,

$$\sigma_g = \lambda_k^S = [1] \lambda_k^S \quad (I.1.1a)$$

$$\text{or } [SP^S] = [1] \quad (I.1.1b)$$

the row vector of length 1 with unit value.

### I.1.1.1 Neighboring Singularity Parameters

Next, to find the source strength at a panel corner, we perform a "bilinear fit" (a process to be described below) to the four surrounding source parameter values. In Figure I.2, we show the variety of cases which may occur in the course of determining the four neighboring source parameter locations. In the "standard" case (A), the four source parameters are the obvious adjacent ones. In cases (B) and (C), the network edge precludes the existence of some of the obvious choices, and neighboring parameters must be obtained by reaching toward the interior of the network. The logic used for points B or C, however, when extended to D, results in a large number of neighboring source parameters. To keep storage to a minimum, we choose (in a fairly arbitrary manner) from this set of points, those points which are as far as possible in index from the uncollapsed edges of the network.

### I.1.1.2 Computation of a Local Coordinate System

Next we compute the source strength at a panel corner in terms of the four surrounding singularity parameter values, once we have in fact located these four parameters. The first step is to form a local coordinate system whose  $(\xi, \eta)$  plane is the one in which the source strength is to vary linearly.

The four singularity parameter locations determine (generally non-orthogonal) basis vectors  $\vec{v}_\xi$  and  $\vec{v}_\eta$ , connecting pairs of panel edge midpoints, for this coordinate system as follows. Let  $P_0$  be the grid point at which we wish to find the source strength. Then for any point  $P$  on the network, we want to be able to determine coordinates  $\xi(P)$ ,  $\eta(P)$ ,  $\zeta(P)$ , such that

$$(\vec{P} - \vec{P}_0) = \xi(P) \vec{v}_\xi + \eta(P) \vec{v}_\eta + \zeta(P) \vec{v}_\zeta \quad (I.1.2)$$

The  $(\xi, \eta, \zeta)$  coordinates used here (in section I.1) are not related to the  $X'$  coordinate system (also denoted  $(\xi, \eta, \zeta)$  at times) used in Appendix E and section I.2. Here,  $\vec{v}_\zeta$  is a vector perpendicular to the plane spanned by  $\vec{v}_\xi$  and  $\vec{v}_\eta$ . Such a vector is, of course, a multiple of  $\vec{v}_\xi \times \vec{v}_\eta$ , but a simple dimensional argument shows that if  $\vec{v}_\zeta$  is to be independent of the scale of coordinates (that is, if  $\vec{v}_\zeta$  is to be doubled when every point coordinate in the network is doubled), we must have

$$\vec{v}_\zeta = \frac{\vec{v}_\xi \times \vec{v}_\eta}{|\vec{v}_\xi \times \vec{v}_\eta|^{1/2}} \quad (I.1.3)$$

Now, to find the functions which define  $\xi$ ,  $\eta$ , and  $\zeta$ , let us first take the cross product of (I.1.2) with  $\vec{v}_\xi$  on the left, and then the dot product with  $\vec{v}_\xi$ . Next, we take the cross product with  $\vec{v}_\eta$  on the right, and then take the dot product with  $\vec{v}_\eta$ . Since

$$\begin{aligned} \vec{v}_\xi \times \vec{v}_\xi &= 0 = \vec{v}_\eta \times \vec{v}_\eta \\ \vec{v}_\xi \cdot \vec{v}_\xi &= 1 = \vec{v}_\eta \cdot \vec{v}_\eta \\ (\vec{v}_\xi \times \vec{v}_\xi) \cdot \vec{v}_\zeta &= 0 = (\vec{v}_\eta \times \vec{v}_\eta) \cdot \vec{v}_\zeta \end{aligned} \quad (I.1.4)$$

we obtain

$$\begin{aligned}\vec{v}_\xi \times (\vec{P} - \vec{P}_0) &= n(P) (\vec{v}_\xi \times \vec{v}_n) \\ (\vec{P} - \vec{P}_0) \times \vec{v}_n &= \xi(P) (\vec{v}_\xi \times \vec{v}_n) \\ (\vec{P} - \vec{P}_0) \cdot \vec{v}_\xi &= \zeta(P) (\vec{v}_\xi \cdot \vec{v}_\xi)\end{aligned}\quad (1.1.5)$$

Dotting the first two equations with  $\vec{v}_\xi$ , we have

$$\vec{v}_\xi \times (\vec{P} - \vec{P}_0) \cdot \vec{v}_\xi = n(P) (\vec{v}_\xi \times \vec{v}_n) \cdot \vec{v}_\xi = n(P) |\vec{v}_\xi \times \vec{v}_n|^{3/2} \quad (1.1.6)$$

$$\text{Thus, } \xi(P) = \frac{(\vec{P} - \vec{P}_0) \times \vec{v}_n \cdot \vec{v}_\xi}{|\vec{v}_\xi \times \vec{v}_n|^{3/2}} \quad \zeta(P) = \frac{(\vec{P} - \vec{P}_0) \cdot \vec{v}_\xi}{|\vec{v}_\xi \times \vec{v}_n|} \quad (1.1.7)$$

### 1.1.1.3 The Bilinear Fit at Panel Corner Points

Now, let  $P_1, \dots, P_4$  be the four source parameter locations for any of the cases illustrated in figure 1.2, and let  $\lambda_i^S = \sigma(P_i)$  denote these source singularity parameters. Then these four values of source strength define a "bilinear" function in  $\xi$  and  $n$ , that is, a function

$$\sigma(\xi, n) = \sigma_0 + \sigma_1 \xi + \sigma_2 n + \sigma_3 \xi n \quad (1.1.8)$$

(where the symbol  $\sigma_0$  as used in section 1.1 has a different meaning than in section 5 or the remainder of Appendix I), which takes on exactly these four values. The function  $\sigma(\xi, n)$  is defined by

$$\begin{Bmatrix} \lambda_1^S \\ \lambda_2^S \\ \lambda_3^S \\ \lambda_4^S \end{Bmatrix} = \begin{bmatrix} 1 & \xi(P_1) & n(P_1) & \xi(P_1)n(P_1) \\ - & - & - & - \\ 1 & \xi(P_4) & n(P_4) & \xi(P_4)n(P_4) \end{bmatrix} \begin{Bmatrix} \sigma_0 \\ \sigma_1 \\ \sigma_2 \\ \sigma_3 \end{Bmatrix}$$

$$= [BL] \begin{Bmatrix} \sigma_0 \\ \sigma_1 \\ \sigma_2 \\ \sigma_3 \end{Bmatrix} \quad (I.1.9)$$

and thus

$$\begin{Bmatrix} \sigma_0 \\ \sigma_1 \\ \sigma_2 \\ \sigma_3 \end{Bmatrix} = [BL]^{-1} \begin{Bmatrix} \lambda_1^S \\ \lambda_2^S \\ \lambda_2^S \\ \lambda_4^S \end{Bmatrix} \quad (I.1.10)$$

The points  $P_1, \dots, P_4$  are not coplanar in general, and thus computing  $\sigma(\xi, n)$  by (I.1.10) in terms of surrounding source parameters, ignores the  $\xi$ -component of the parameter locations; in other words, we project the parameter locations to the plane defined by  $\vec{v}_\xi$  and  $\vec{v}_n$ . This is justifiable in view of the fact that a reasonable number of panels should be used in defining a geometric surface, and thus the distortions due to curvature can be neglected locally.

Now, by (I.1.7),  $\xi(P_0) = n(P_0) = 0$ , and thus by (I.1.8),

$$\sigma(P_0) = \sigma_0 \quad (I.1.11)$$

Thus by (I.1.10),

$$\sigma(P_0) = \sigma_0 = \begin{bmatrix} 1 & 0 & 0 & 0 \end{bmatrix} [BL]^{-1} \begin{Bmatrix} \lambda_1^S \\ \lambda_2^S \\ \lambda_2^S \\ \lambda_4^S \end{Bmatrix} \quad (I.1.12)$$

Setting

$$\begin{bmatrix} \lambda_1^S & \lambda_2^S & \lambda_2^S & \lambda_4^S \end{bmatrix} = \begin{bmatrix} 1 & 0 & 0 & 0 \end{bmatrix} [BL]^{-1} \quad (I.1.13)$$



we see that

$$\sigma(P_0) = \underline{LSPS} \begin{Bmatrix} S \\ \lambda_1 \\ \vdots \\ S \\ \lambda_4 \end{Bmatrix} \quad (I.1.14)$$

Note that  $\underline{LSPS}$  is just the first row of  $[BL]^{-1}$ . Now, by (I.1.14),  $\underline{SPS}$  is just the row vector we seek; namely, it gives the value of source strength at the point  $P_0$  as a linear combination of four neighboring singularity parameters. A spline vector may similarly be constructed for every panel corner point in the network, whereupon matrices  $B^S$  may be computed for each panel as discussed at the beginning of section I.1.

This concludes the discussion of spline vector construction for source analysis networks. Two special cases, networks with only one row or column, and networks with only one panel; are discussed in the maintenance document (see section 4-I.4 and SUBROUTINE ONDFIT of the DQG module).

#### I.1.2 Doublet Spline Vectors for Analysis Networks

Doublet spline vectors  $SPD$  are more complex to compute for a variety of reasons. First, the requirement of quadratic accuracy forces the doublet strength at a grid point to depend on a greater number of singularity parameters than the source strength. Second, to insure doublet continuity across network edges on non-smooth abutments (along which boundary conditions specifying the matching of doublet strength are imposed), we require that the doublet strength at any point on a network edge depend only on the singularity parameters located on the network edge. The example of a thin wing with a curved planform illustrates the need for this requirement (cf., Figure I.3). The doublet strength is zero at the singularity parameter locations on the free network edge. If the doublet strength at a panel corner point on the edge depended on singularity parameters in the interior, it could not be zero, independent of conditions in the network interior, as we wish it to be. But by insisting that it only depend on edge parameters, we insure that it is zero.

A third cause of increased complexity in determining doublet spline row vectors is the introduction of "smooth abutments." These are abutments consisting of portions of two distinct network edges, along which splines rather than boundary conditions are used to enforce continuity of doublet strength.

For grid points which do not lie on a network edge, obtaining the row vector  $SPD$  which describes the doublet strength at each grid point in terms of surrounding singularity parameters is a two step process. First, the set of surrounding singularity parameters is determined. Second, the doublet strength at the grid point is determined in a quadratically accurate manner in terms of the neighboring singularity parameters.

### 1.1.2.1 The Quadratic Least Squares Fit for Panel Corners or Panel Edge Midpoints

This quadratically accurate procedure is somewhat more complex than the bilinear fit employed for source splines. While there is generally a bilinear function which exactly fits values at four points (unless three of the four lie on a line, which is unlikely if they are panel centers), a quadratic function is less well behaved. There is a unique quadratic through six points, unless these points all lie on two lines. With very regular paneling, however, it is quite likely that six center points chosen as neighbors of a grid point will, in fact, lie on two lines. Thus, the procedure we chose for the quadratic fit is a "least squares" procedure.

That is, we choose an excessive number of neighboring singularity parameters, and find the quadratic function which takes on the values of the closest singularity parameters exactly, while taking on the values of the remaining singularity parameters in a "least squares" sense. The row vector  $SP^D$  for the grid point that is, panel corner or edge midpoint determined by the value the function takes on at the grid point as a linear combination of the singularity parameter values.

We now describe this least squares procedure more precisely. Let  $(\lambda_i^D, i = 1, \dots, k)$  be the singularity parameters (in the neighborhood of the selected grid point) to which we fit the quadratic function exactly. Let  $(\lambda_i^D, i = k+1, \dots, k+m)$  be the remaining neighboring singularity parameters. Let  $\lambda_i^D$  be located at  $(\xi_i, \eta_i, \zeta_i)$ , where the computation of these coordinates will be discussed shortly. Once again, however, this is not the local  $(\xi, \eta, \zeta)$  coordinate system denoted  $X'$  in Appendix E.

Let A be the matrix

$$A = \begin{bmatrix} 1 & \xi_1 & \eta_1 & 1/2 \xi_1^2 & \xi_1 \eta_1 & 1/2 \eta_1^2 \\ \vdots & \vdots & \vdots & \vdots & \vdots & \vdots \\ 1 & \xi_k & \eta_k & 1/2 \xi_k^2 & \xi_k \eta_k & 1/2 \eta_k^2 \end{bmatrix} \quad (1.1.15)$$

This is the matrix for which any function

$$f(\xi, \eta) = f_1 + f_2 \xi + f_3 \eta + 1/2 f_4 \xi^2 + f_5 \xi \eta + 1/2 f_6 \eta^2 \quad (1.1.16)$$

taking on the values

$$f(\xi_i, \eta_i) = \lambda_i^D \quad i = 1, \dots, k \quad (I.1.17)$$

satisfies

$$[A]^{k \times 6} \begin{Bmatrix} f_1 \\ f_2 \\ \vdots \\ f_6 \end{Bmatrix} = \begin{Bmatrix} \lambda_1^D \\ \lambda_2^D \\ \vdots \\ \lambda_k^D \end{Bmatrix} \quad (I.1.18)$$

Now, whenever  $k < 6$ , as it will be in the current applications, equation (I.1.18) does not fully specify the coefficients of  $f$ . The coefficients are completely specified by requiring the minimization of

$$I = \sum_{i=k+1}^{k+m} w_i^2 [f(\xi_i, \eta_i) - \lambda_i^D]^2 \quad (I.1.19)$$

where  $w_i$  is a "weight", to be discussed shortly, which depends on the relative locations of the singularity parameter and the grid point.

If we write

$$[A_1]^{m \times 6} = \begin{bmatrix} 1 & \xi_{k+1} & \eta_{k+1} & 1/2 \xi_{k+1}^2 & \xi_{k+1} \eta_{k+1} & 1/2 \eta_{k+1}^2 \\ 1 & \xi_{k+m} & \eta_{k+m} & 1/2 \xi_{k+m}^2 & \xi_{k+m} \eta_{k+m} & 1/2 \eta_{k+m}^2 \end{bmatrix} \quad (I.1.20)$$

equation (I.1.19) becomes

$$I = \sum_{i=k+1}^{k+m} w_i^2 \left( \sum_{s=1}^6 (A'_{i-k,s}) f_s - \lambda_i^D \right)^2 \quad (I.1.21)$$

The method by which we minimize (I.1.21), subject to the exact conditions (I.1.18), is called a "constrained least squares" procedure, and is discussed

in section I.5. The result of performing this procedure is a  $(6 \times (k+m))$  matrix LSQ such that

$$\begin{Bmatrix} f_1 \\ \vdots \\ f_6 \end{Bmatrix} = [LSQ] \begin{Bmatrix} \lambda_1^D \\ \vdots \\ \lambda_{k+m}^D \end{Bmatrix} \quad (I.1.22)$$

Now, we will construct our  $(\xi, \eta, \zeta)$  coordinate system such that at the grid point  $P_0$  we have

$$\begin{aligned} \xi(P_0) &= 0 \\ \eta(P_0) &= 0 \end{aligned} \quad (I.1.23)$$

Thus,

$$f(P_0) = f_1 = [LSQ]_{1,\cdot} \begin{Bmatrix} \lambda_1^D \\ \vdots \\ \lambda_{k+m}^D \end{Bmatrix} \quad (I.1.24)$$

But we required the row vector  $SP^D$  to define the value at  $P_0$  of the quadratic function  $f$  which satisfied (I.1.18) while minimizing (I.1.21), and thus

$$[SP^D] = [LSQ]_{1,\cdot} \quad (I.1.25)$$

that is,  $SP^D$  is the first row vector of the matrix LSQ defined by the constrained least squares procedure.

In describing the construction of  $SP^D$  for a grid point in a network interior, we have deferred the discussion of three items. These are the determination of the set of neighboring singularity parameters, their  $(\xi, \eta, \zeta)$  coordinates, and the corresponding weights  $w_i$ . We will discuss them in order as follows.

#### I.1.2.2 Neighboring Points for Least Squares Fit

Figure I.4a illustrates the location of neighboring singularity parameters for grid points which do not lie near a network edge. Note that, since a singularity parameter is located at each panel center, the spline vector  $SP^D$  for a panel center point is (like the spline vector  $SP^S$ ) a vector of length 1 with a unit entry.

Now, if the grid point (panel corner or edge midpoint) lies near (but not on) a network edge, the set of neighbors must include singularity parameters on the network edge. Actually, we fit a quadratic function to neighboring grid points, where these grid points need only be singularity parameter locations when they are in the interior of the network. The value of doublet strength at those grid points which lie on the network edge depends in turn on a small number of singularity parameters located on the network edge. This is a procedure which is defined in detail in the maintenance document (see section 4-1).

Figure 1.4.b illustrates the neighboring points we use for the quadratic fit to obtain a spline vector for a grid point which lies near (but not on) a network edge which does not belong to a smooth abutment. Recall that only one singularity parameter is located on a collapsed edge of a network.

Figure 1.4.c illustrates the set of neighboring points when the grid point in question lies near a smooth abutment. In this case, we see that the set of "neighboring points" may lie in two distinct networks. This is because the singularity parameters on the network edges on the smooth abutment (though not at the corner points at the ends of the abutment) have been removed for reasons of economy. The neighboring points in the same network as the point  $P_0$  are chosen in the usual manner (see Figure 1.4a) while those in the adjacent network are chosen as illustrated. The precise method by which the latter points are picked is described in the maintenance document (section 4-1.2.1.2).

### 1.1.2.3 Construction of a Local Coordinate System

Next we discuss the construction of a  $(\xi, \eta, \zeta)$  coordinate system. This system is similar but not identical to that of section 1.1.1.2, and totally distinct from the  $X'$  coordinate system  $X'$  of Appendix E or section 1.2.2.5. First, we construct basis vectors  $\vec{v}_\xi$  and  $\vec{v}_\eta$  as illustrated in Figure 1.5. That is,  $\vec{v}_\xi$  and  $\vec{v}_\eta$  span pairs of enriched grid points adjacent to the base point  $P_0$ . Next, we define  $\vec{v}_\zeta$  by (1.1.3). Then, analogously to (1.1.17), we define

$$\begin{aligned} \bar{\xi}(P) &= \frac{(\vec{P} - \vec{P}_0) \times \vec{v}_\eta \cdot \vec{v}_\zeta}{|\vec{v}_\xi \times \vec{v}_\eta|^{3/2}} & \bar{\eta}(P) &= \frac{\vec{v}_\zeta \times (\vec{P} - \vec{P}_0) \cdot \vec{v}_\xi}{|\vec{v}_\xi \times \vec{v}_\eta|^{3/2}} & \bar{\zeta}(P) &= \frac{(\vec{P} - \vec{P}_0) \cdot \vec{v}_\zeta}{|\vec{v}_\xi \times \vec{v}_\eta|} \end{aligned} \quad (1.1.26)$$

The bars indicate that these are preliminary coordinate values which will be adjusted to account for surface curvature. Consider a cylindrical surface, as illustrated in Figure 1.6. If we use the coordinates  $\bar{\xi}$  and  $\bar{\eta}$  above, we are essentially projecting the surface down to the tangent plane at the point  $P_0$ . When the surface is highly curved, this makes the points A and D appear to be closer to  $P_0$  than they really are, since we are dealing with their projected images A' and D'. The points B' and C' are also closer to the grid point than B and C, but not in the same proportion.

We rectify this by scaling the  $\xi$  and  $\eta$  coordinates of a point according to its height above the tangent plane. We define a scaling factor

$$A(P) = \frac{\xi(P)^2 + \eta(P)^2 + \zeta(P)^2}{\xi(P)^2 + \eta(P)^2}^{1/2} \quad (I.1.27)$$

Then we define

$$\begin{aligned} \bar{\xi}(P) &= A(P) \xi(P) \\ \bar{\eta}(P) &= A(P) \eta(P) \end{aligned} \quad (I.1.28)$$

This coordinate scaling assures that the contribution of distant points is more accurately measured. Note that the denominator of  $A(P)$  is non-zero provided  $P \neq P_0$ .

#### I.1.2.4 Weights for the Least Squares Fit

Next we consider the weights  $w_i$  for the least squares procedure. In order to provide stability, we would like to fit more closely to nearby singularity parameters than further ones. This is done in part by fitting the quadratic function exactly to the nearest parameters, as illustrated by Figure I.4.

A second consideration in determining weights is the desire to give heavier weights in supersonic flow to points which are upstream of the grid point than to those which are downstream. This weighting has been found experimentally to reduce instabilities problems which arise at high Mach numbers. In recognition of these requirements, we set  $w_i =$

$$w(P) = \frac{1 + k M_\infty (1 - \epsilon_0 \cdot (\vec{P} - \vec{P}_0) / |\vec{P} - \vec{P}_0|)}{(1 + 2 k M_\infty)} \quad (I.1.29)$$

The constant  $k$  is set to zero in subsonic flow in view of the lack of a preferred upstream direction. That is, the compressibility direction  $c_0$  may be replaced by  $-c_0$  without changing the solution to the equation. In supersonic flow,  $k$  has been chosen by experiment, and has order of magnitude 1.

Since the dot product of unit vectors lies between -1 and 1, the numerator of (I.1.29) lies between 1 and  $(1 + 2k M_\infty)$ . Thus the ratio of weight (neglecting the effect of distance) at a directly upstream point to that at a directly downstream point is  $1 + 2k M_\infty$ . For  $M_\infty = 3$ , and  $k = 1$  (the provisional choice for  $k$ ), this ratio is 7. This concludes our discussion of the construction of doublet spline vectors for grid points lying in the interior of an analysis network.

#### 1.1.2.5 Edge Splines for Non-Smooth Abutments

Finally we consider grid points (panel corner points or edge midpoints) lying on a network edge. A network edge is divided into distinct portions belonging to different abutments. A doublet parameter is located at the grid points which form the endpoints of the portion of the edge belonging to the abutment (if such an endpoint is not a network corner point, the doublet parameter is an "extra" singularity parameter (see figure 5.13)). Doublet parameters are also located at the panel edge midpoints unless the abutment is a smooth one, in which case the parameters are removed (doublet parameters located at abutment endpoints are retained for simplicity).

We discuss first the case of a non-smooth abutment. In that case, the value of doublet strength at a grid point depends only on singularity parameters located on the network edge.

Consider the abutment illustrated in Figure 1.7a, with one network edge panelled more finely than the other and with a panel corner on the more finely paneled network located wherever the more coarsely paneled network edge has a panel corner. The goal is to find a splining method such that the imposition of doublet matching boundary conditions of some or all of the control points on the edge results in the exact matching of doublet strength on the whole edge.

Experimentation with least-squares-type splines shows that they cannot satisfy the above considerations. Let us consider, on the other hand, a differentiable spline. Let the edge be divided into  $n$  intervals, as illustrated in Figure 1.7b. It is reasonable to ask how many differentiable functions exist, defined by a single quadratic on each of the  $n$  intervals. Now, there are  $3n$  linearly independent quadratic functions altogether (since a quadratic function on an interval has 3 coefficients), and requiring continuity at  $P_2, \dots, P_{n-1}$  yields  $(n-1)$  constraints on the set of functions, while requiring continuity of derivative at these points provides  $(n-1)$  additional constraints. Thus, there are  $(n+2)$  linearly independent piecewise quadratic functions with continuous derivatives.

But this is equal to the number of control points on the edge, and so there is a unique differentiable function which takes on a prescribed set of  $(n+2)$  values at the midpoints of the intervals and the endpoints of the edge.

We can apply this result to the situation illustrated by Figure 1.7a. The doublet distribution on the edge 1 will consist of some differentiable function defined by a single quadratic on each interval of edge 1. If we now impose doublet matching boundary conditions at the control points of edge 2, we obtain on edge 2 the unique differentiable doublet distribution defined as a single quadratic on each interval of edge 2, which agrees with the doublet distribution on edge 1 at the specified points. But, since every interval of edge 2 is a subset of a corresponding interval on edge 1, the doublet distribution on edge 1 satisfies the above criterion too. So, since the distribution is unique, the doublet distributions on edge 1 and edge 2 are identical.

Summarizing, we have shown that if edges 1 and 2 form an abutment, and the paneling on edge 2 is a "refinement" of the paneling on edge 1 (that is, every corner point of edge 1 is also a corner point on edge 2, though edge 2 may have additional corner points), then the imposition of doublet matching at the control points of edge 2 results in exact matching of doublet strength along the entire abutment. Generalizing, if several network edges meet in an abutment, and one edge is a refinement of each of the other edges, then the imposition of doublet matching boundary conditions on that edge forces the alternating sum of the doublet strengths to zero:

$$\sum s_j u_j = 0 \quad (I.1.30)$$

where  $s_j = \pm 1$ .

Unfortunately, the differentiable edge spline, while leading to doublet continuity under a greater variety of circumstances, does not permit forward weighting in supersonic flow. As a result, the differentiable edge spline is insufficiently stable and cannot be used in Pan Air. This fact was determined fairly late in the development of Pan Air, and thus a discussion of the differentiable edge spline has been included in this document.

The spline which is actually implemented in Pan Air is a one dimension quadratic least squares fit. Consider, for instance, a network edge as illustrated in figure I.7b. The points  $P_1, \dots, P_{n+1}$ , and  $M_i$ ,  $i=1, \dots, n$ , are singularity parameter locations, and the doublet strength there is defined to be equal to the value of the singularity located there. Thus the doublet spline vector  $SP^D$  for each of these points is a unit vector of length one, as it is for panel center points in a doublet analysis network.

Next, the doublet strength at the points  $P_i$ ,  $i=2, \dots, n-1$ , is obtained by a constrained least squares analogous to that described in section I.1.2.1, but in one dimension. That is, the quadratic function  $f(t)$  ( $t$  a variable defining distance along the network edge) is found such that

$$f(M_k) = u(M_k) = \lambda_k^D \quad k = i, i+1 \quad (I.1.31a)$$

$$\text{and } f(M_r) = u(M_r) = \lambda_r^D \quad r = i-1, i+2 \quad (I.1.31b)$$

in a least squares sense.

Then the row vector  $SP^D$  which defines  $u(P_i)$  in terms of the singularity parameters ( $\lambda_k^D$ ,  $k = i-1, \dots, i+2$ ), is such that

$$u(P_i) = f(P_i) \quad (I.1.31c)$$

We now discuss the differentiable edge spline which is not implemented in Pan Air. First we must compute the spline matrices which correspond to this differential piecewise quadratic distribution. It can be shown numerically that such a function, if it has a non-zero value at one panel center, and is zero at all other panel centers and the endpoints of the edge, is never identically zero.



Rather, it behaves as illustrated in Figure 1.8; oscillating with an amplitude which diminishes rapidly but never reaches zero. Thus, the spline is stable under doublet specification boundary conditions; however, it is not local, since the doublet strength on an interval depends weakly on the doublet strength at a panel center far away.

In order to avoid storing lengthy spline vectors, we must redefine our doublet parameters to make the spline local. That is, a doublet parameter on a network edge will not have as its value the doublet strength at its location. For this purpose, consider the interval  $[-1, 1]$  on which we define the quadratic function

$$\mu(x) = a + bx + cx^2 \quad (I.1.32a)$$

$$\begin{aligned} \text{Now, } \mu(-1) &= a - b + c \\ \mu(1) &= a + b + c \end{aligned} \quad (I.1.32b)$$

$$\begin{aligned} \frac{d\mu}{dx}(-1) &= b - 2c \\ \frac{d\mu}{dx}(1) &= b + 2c \end{aligned} \quad (I.1.33)$$

Thus,

$$\mu(-1) + \frac{d\mu}{dx}(-1) = a - c = \mu(1) - \frac{d\mu}{dx}(1) \quad (I.1.34)$$

Generalizing (I.1.34) to the interval  $[P_i, P_{i+1}]$  in Figure 1.7b, we have

$$\begin{aligned} &\mu(P_i) + 1/2 \mu'(P_i) (P_{i+1} - P_i) \\ = &\mu(P_{i+1}) + 1/2 \mu'(P_{i+1}) (P_i - P_{i+1}) \end{aligned} \quad (I.1.35)$$

We thus define

$$\lambda_i^D = \mu(P_i) + 1/2 \mu'(P_i) \cdot (\vec{P}_{i+1} - \vec{P}_i) \quad i = 1, \dots, n \quad (I.1.36)$$

$$\lambda_i^D = \mu(P_i), \quad i = 0, n+1 \quad (I.1.37)$$

Now, by (I.1.35)

$$\lambda_{i-1}^D = \mu(P_i) + 1/2 \nabla \mu(P_i) \cdot (\vec{P}_{i-1} - \vec{P}_i) \quad i = 2, \dots, n+1 \quad (I.1.38)$$

Combining (I.1.40) and (I.1.42), and noting that  $\nabla \mu$  is continuous, we have

$$\begin{aligned} (P_i - P_{i-1}) \lambda_i^D + (P_{i+1} - P_i) \lambda_{i-1}^D = \\ (P_i - P_{i-1}) \mu(P_i) + 1/2 \frac{d\mu}{dx}(P_i) (P_{i+1} - P_i) (P_i - P_{i-1}) \\ + (P_{i+1} - P_i) \mu(P_i) + 1/2 \frac{d\mu}{dx}(P_i) (P_i - P_{i-1}) (P_{i+1} - P_i) \end{aligned} \quad (I.1.39)$$

Thus,

$$\begin{aligned} \mu(P_i) = & \frac{|\vec{P}_i - \vec{P}_{i-1}|}{|\vec{P}_i - \vec{P}_{i-1}| + |\vec{P}_{i+1} - \vec{P}_i|} \lambda_i^D \\ & + \frac{|\vec{P}_{i+1} - \vec{P}_i|}{|\vec{P}_i - \vec{P}_{i-1}| + |\vec{P}_{i+1} - \vec{P}_i|} \lambda_{i-1}^D \end{aligned} \quad (I.1.40)$$

This defines the spline vector for  $P_i$  as computed with the differentiable edge spline, which is not implemented in Pan Air.

Now, we wish to evaluate  $\mu(M_i)$ ,  $i=1, \dots, n$ . Again consider a function  $\mu(x)$  on  $[-1, 1]$  defined by (I.1.31).

Then

$$\begin{aligned} \mu(-1) &= a - b + c \\ \mu(1) &= a + b + c \\ \mu(-1) + \frac{d\mu}{dx}(-1) &= a - c \end{aligned} \quad (I.1.41)$$

So,

$$\begin{aligned} \mu(0) &= a = \\ 1/4 \mu(-1) + 1/4 \mu(1) + 1/2 [\mu(-1) + \frac{d\mu}{dx}(-1)] \end{aligned} \quad (I.1.42)$$

Applying this to Figure I.7b, we see

$$\begin{aligned} \mu(M_i) &= 1/4 \mu(P_i) + 1/4 \mu(u_{i+1}) + 1/2 \lambda_i^0 \\ i &= 1, \dots, n \end{aligned} \quad (I.1.43)$$

This defines the spline vector for  $M_i$ .

Equations (I.1.37), (I.1.41), and (I.1.43) together describe  $\mu$  at grid points which lie on a network edge belonging to a non-smooth abutment as linear combinations of neighboring singularity parameters on the edge. We again point out that this procedure is not implemented in Pan Air.

#### I.1.2.6 Edge Splines for Smooth Abutments

We now describe the computation of spline vectors for grid points lying on smooth abutments. Once again, to obtain matching of doublet strength we require that one network be paneled as a refinement of the other, as in the example of Figure I.7a. Then, spline vectors for grid points on the more coarsely paneled edge are computed first, followed by spline vectors for grid points on the more finely paneled edge.

Spline vectors for grid points on the coarser edge are also computed by a constrained least squares procedure, even though again the "neighboring points" lie in two networks. Figure I.9a shows some representative examples which illustrate the procedure for choosing the set of neighboring points. The method is described precisely in the Maintenance Document (see Appendix I of section 4).

Now, continuity of doublet strength along a smooth abutment is insured by requiring the doublet strength at a grid point on the more finely paneled network to be identical (as a linear combination of surrounding singularity parameters) to that at the "corresponding" point on the coarsely paneled network. We determine the corresponding point by "parametrizing" the abutment, that is, assigning to each grid point a real number  $t$ ,  $0 < t < 1$ , which specifies the proportion of the total abutment length that the grid point is distant from the starting point of the abutment. This procedure is discussed in more detail in the maintenance document (see SUBROUTINE PRMEDG of the DQG module).

Figure I.9b illustrates the parametrization of an abutment. Now, some grid point  $P'_i$  on the fine network will have parameter value  $t'_i$ , where

$$t_j < t'_i < t_{j+1} \quad (I.1.44)$$

for some integer  $j$ , that is, the corresponding point on the coarse network is not a grid point. But,  $\mu$  must vary quadratically on the panel edge, so we can obtain  $\mu(P'_i)$  as a linear combination of  $\mu(P_j)$ ,  $\mu(P_{j+1})$ , and  $\mu(P_{j+2})$ .

Now, it follows from (I.1.31-32) that on an interval  $[-1, 1]$ ,

$$\begin{aligned} u(x) &= a + bx + cx^2 = \\ u(0) &+ (1/2 u(1) + 1/2 u(-1))x \\ &+ [1/2 u(1) + 1/2 u(-1) - u(0)]x^2 \end{aligned} \quad (I.1.45)$$

We can apply this to the interval in Figure I.9c by making the transformation

$$x' = \frac{t - t_j}{t_{j+2} - t_j} \quad (I.1.46)$$

$$\begin{aligned} x &= 2x' - 1 \\ &= \frac{2t - t_{j+2} - t_j}{t_{j+2} - t_j} \end{aligned} \quad (I.1.47)$$

Equation (I.1.46) maps the interval in Figure I.9c to  $[0, 1]$ , which in turn is mapped to  $[-1, 1]$  by (I.1.47).

Substituting (I.1.47) in (I.1.45), we obtain

$$\begin{aligned} u(t) &= u(P_{j+1}) + [1/2 u(P_{j+2}) - 1/2 u(P_j)] \frac{2t - t_{j+2} - t_j}{t_{j+2} - t_j} \\ &+ [1/2 u(P_{j+2}) + 1/2 u(P_j) - u(P_{j+1})] \frac{2t - t_{j+2} - t_j^2}{t_{j+2} - t_j} \end{aligned} \quad (I.1.48)$$

Setting  $t = t'_i$ , we have  $u(P_i)$  as a linear combination of  $u(P_j)$ ,  $u(P_{j+1})$ , and  $u(P_{j+2})$ :

$$\begin{aligned} u(P'_i) &= (-1/2 + 1/2 \tau^2) u(P_j) \\ &+ (1 - \tau^2) u(P_{j+1}) + (1/2 + 1/2 \tau^2) u(P_{j+2}) \end{aligned} \quad (I.1.49)$$

$$\text{where } \tau = \frac{2 t'_i - t_{j+2} - t_j}{t_{j+2} - t_j} \quad (I.1.50)$$

This concludes our discussion of spline vector construction for doublet analysis networks. We have now discussed the computation of doublet spline vectors for all enriched grid points in a doublet analysis network. In practice, these vectors are all computed and stored on a disk. Then, within a

loop over panels, the spline vectors corresponding to the nine panel defining points are retrieved from the disk, and merged into an outer spline matrix  $B^0$  by VECUNM.

### I.1.3 Doublet Spline Vectors for Wake Networks

Singularity parameter locations for doublet wake networks are illustrated in Figure D.3. In addition, if the edge of the wake I networks on which singularity parameters are located forms part of more than one abutment, an extra singularity parameter is located at the abutment endpoints lying in the interior of the edge.

The purpose of a doublet wake I network is to model a wake surface on which the doublet strength is constant in the streamwise direction. Thus, spline vectors for grid points are constructed as follows. First, spline vectors are constructed for each grid point on the edge containing singularity parameters, just as though the edge were part of a non-smooth abutment of an analysis network (it should be noted in passing that smooth abutments are only permitted between analysis networks). Then, the spline vector constructed for a particular grid point on the edge is also used for every grid point lying in the column or row of points emanating in an indicially perpendicular direction from the edge. This produces a doublet strength which is constant in one indicial direction, as desired. In general this direction is the direction of increasing row index, though this program default may be overridden by the user. See section 7, record N12, of the User's Manual.

Doublet wake 2 networks are used to define a constant strength doublet sheet, whose strength is the value of the one singularity parameter in the network. Thus, the identical spline vector is constructed for every grid point on the network; namely the row vector of length one with unit entry.

### I.1.4 Source Splines for Design Networks

Singularity locations for source design networks are given by Figure D.1. Since a source parameter is located at every panel corner, the spline vectors for these grid points are just unit vectors of length 1. Spline vectors for panel centers are also straightforward to compute:

$$SPS = \begin{bmatrix} 1/4 & 1/4 & 1/4 & 1/4 \end{bmatrix} \quad (I.1.51)$$

That is, the source strength at a panel center is defined as the average of the source strengths at all the panel corners.

### I.1.5 Doublet Splines for Design Networks

Figure D.2 shows the location of singularity parameters on a doublet design network. For grid points in the interior of the network, spline vectors are computed by fitting to neighboring points, as illustrated in Figure I.10a. For grid points on the "matching edges" (which have singularity parameters located at the panel edge midpoints), the doublet analysis edge spline of section I.1.2.5 is used.

The only unusual aspect of doublet design splines is the edge spline for non-matching edges. The doublet parameters are located at panel corners along these edges (rather than panel edge midpoints) for stability, since the boundary conditions in the vicinity of non-matching edges tend to be doublet gradient boundary conditions. For nonmatching edges, as for matching edges, a differentiable edge spline and a least squares edge spline are available, though once again the least squares spline is implemented in Pan Air. The least squares spline is similar to that for matching edges, except that now it is at panel edge midpoints that the doublet strength is defined by least squaring to the four surrounding edge doublet parameters, while at panel corners the doublet strength is defined by a unit spline vector.

We now discuss the construction of the differentiable edge spline. Let  $\lambda_i^D$  be the value of the doublet parameter located at a panel corner  $P_i$  as illustrated in Figure I.10b. We define a row vector  $\gamma_i$ ,  $0 \leq i \leq n$  ( $n$  the number of panel corners on the network edge) of length  $n$  as follows. We define  $\gamma_0$  and  $\gamma_n$  to be row vectors with the entries 1 in the first entry and the  $n$ th entry, respectively, and otherwise zero. For  $1 < i < n-1$ , we obtain  $\gamma_i$  by performing a one-dimensional least squares fit to the 4 (or 3, if  $i=1$  or  $n-1$ ) neighboring singularity parameters on the edge.

Thus, at each edge midpoint, and at the endpoints of the edge, a row vector  $\gamma_i$  is defined. This is analogous to the situation for the differentiable doublet analysis edge spline. We now obtain  $u$  at corner points and edge midpoints by using the doublet analysis edge spline, but in terms of the  $\gamma_i$  rather than the singularity parameters.

For example, we have, analogously to (I.1.40),

$$u(P_5) = \frac{|\vec{P}_6 - \vec{P}_5|}{|\vec{P}_6 - \vec{P}_5| + |\vec{P}_5 - \vec{P}_4|} \gamma_4 \{\lambda_i^D\} + \frac{|\vec{P}_5 - \vec{P}_4|}{|\vec{P}_6 - \vec{P}_5| + |\vec{P}_5 - \vec{P}_4|} \gamma_5 \{\lambda_i^D\} \quad (I.1.52)$$

This concludes our discussion of spline vector construction. Details of the construction are contained in the Maintenance Document (section 4-I.2.3). We note that the "RESERVE" spline discussed there is in fact the least squares edge spline implemented in Pan Air.

## I.2 Subpanel Splines

### I.2.1 Source Subpanel Splines

#### I.2.1.1 Preliminaries

Consider two panels in one network, side by side (cf., Figure 11). The points A and B are common to both panels and are locations of panel source parameters. Because of the manner in which the outer source spline is constructed, the source strength is continuous at these points. To insure linear accuracy, and insure that  $\sigma$  is continuous on the entire segment AB, we require  $\sigma$  to vary linearly between A and B.

Illustrating panel  $\Sigma_2$  in Figure 1.12, we see, since  $P_8$  is the midpoint of  $P_1P_4$ , that is,

$$\sigma_8 = u(P_8) = 1/2 (\sigma_1 + \sigma_4) \quad (1.2.1)$$

Similarly for all the other edge midpoints, the value of source strength there is the average of the values at the vertices of the edge. Since  $P_8$  is a panel source parameter location, we thus have the source strength at all nine "panel defining points" in terms of the five panel source parameters.

To "fill in" the source distribution on each subpanel, we note that a linear function in two variables can be specified at exactly three distinct non-collinear points. Thus, the specification of  $\sigma$  at the three vertices of a subpanel uniquely specifies the linear variation of source strength on the subpanel.

Consider the subpanel in Figure 1.13, with the vertices specified in local coordinates (the third coordinate is omitted since it is zero). The local coordinate system we use here is the system  $X'$  of Appendix E. That is, the matrix A of equation (E.0.1) defines the transformation from reference coordinates to this local system. We will not use primes to denote local coordinates in this appendix, however. The origin of the local coordinate system is always one of the vertices of the subpanel. If the subpanel is an interior one, the origin is the panel center, while the origin for each of the four corner subpanels is the corresponding panel corner. The local coordinate system  $X'$  is distinct from the local systems used in section I.1. The latter systems are used only in section I.1, and appear nowhere else in this document.

We now compute the distribution

$$\sigma(\xi, \eta) = \sigma_0 + \sigma_\xi \xi + \sigma_\eta \eta \quad (1.2.2)$$

(where  $\sigma_0$ ,  $\sigma_\xi$  and  $\sigma_\eta$  are constant coefficients) which assumes the values  $\sigma_i$ ,  $\sigma_j$ , and  $\sigma_k$  at  $P_i$ ,  $P_j$ , and  $P_k$ .

Now, we clearly have

$$\sigma_i = \sigma(P_i) = \sigma(\xi_i, \eta_i) = \sigma_0 + \sigma_\xi \xi_i + \sigma_\eta \eta_i \quad (1.2.3)$$

Similar equations hold for  $\sigma_j$  and  $\sigma_k$ , so in matrix form we have

$$\begin{Bmatrix} \sigma_i \\ \sigma_j \\ \sigma_k \end{Bmatrix} = \begin{bmatrix} 1 & \xi_i & \eta_i \\ 1 & \xi_j & \eta_j \\ 1 & \xi_k & \eta_k \end{bmatrix} \begin{Bmatrix} \sigma_0 \\ \sigma \\ \sigma_n \end{Bmatrix} = [GS] \begin{Bmatrix} \sigma_0 \\ \sigma \\ \sigma_n \end{Bmatrix} \quad (1.2.4)$$

Inverting, we find

$$\begin{Bmatrix} \sigma_0 \\ \sigma \\ \sigma_n \end{Bmatrix} = [GS]^{-1} \begin{Bmatrix} \sigma_i \\ \sigma_j \\ \sigma_k \end{Bmatrix} \quad (1.2.5)$$

#### 1.2.1.2 Inversion of the Matrix of Coordinates

Now, we can find  $\sigma_0$ ,  $\sigma$ , and  $\sigma_n$  in one of three ways. A standard program for numerical solutions is not suitable since we need the solution for an arbitrary "constraint" or "right hand side" vector (this is made clear by equation (1.2.27)). Now, we can invert the matrix numerically, then performing the matrix multiplication in (1.2.5). Or, we can invert the matrix analytically (that is, find the inverse as a function of the  $\xi$ 's and  $\eta$ 's) and perform the multiplication in (1.2.5).

The approach taken in PAN AIR is based on practical considerations. Because a matrix inverse routine using the Gauss-Jordan method (see Ref. 1.1) is already available, the first method is used in solving small systems of equations, even though greater numerical accuracy would be obtained by analytic inversion of the matrices.

Now, analytic inversion of the 3x3 matrix in (1.2.4) is, of course, straightforward; however, we will demonstrate a round-about method for calculating this inverse, using triangular coordinates, since this method can be generalized to 6x6 and 10x10 matrices which need inverting later on. The equations in the remainder of section 1.2.1.2 are not implemented in Pan Air, but are included here for the interested reader.

In Figure I.14, we illustrate a triangle with vertices  $Q_i$ ,  $i=1,2,3$  (in our applications, the  $Q_i$  will be three of the panel defining points) and triangular coordinates  $L_i$ ,  $i=1,2,3$ . These coordinates are defined in the following manner. Let  $(\xi_i, \eta_i)$  be the local coordinates of  $Q_i$ . Then (with all subscripts modulo 3), a counter-clockwise tangent vector (not of unit length) parallel to the edge opposite  $Q_i$  is

$$\vec{t}_i = \vec{Q}_{i+2} - \vec{Q}_{i+1} = (\xi_{i+2} - \xi_{i+1}, \eta_{i+2} - \eta_{i+1}) \quad (1.2.6)$$



Thus, an inward pointing normal vector to the edge opposite  $Q_i$  is

$$\vec{n}_i = (- (n_{i+2} - n_{i+1}), \xi_{i+2} - \xi_{i+1}) \quad (1.2.7)$$

Now, for any point  $Q$ , let

$$L_i(Q) = \frac{(\vec{Q} - \vec{Q}_{i+1}) \cdot \vec{n}_i}{(\vec{Q}_i - \vec{Q}_{i+1}) \cdot \vec{n}_i} \quad (1.2.8)$$

We can see that

$$L_i(Q_i) = 1; \quad L_i(Q_{i+1}) = L_i(Q_{i+2}) = 0 \quad (1.2.9)$$

Now, the coordinates  $L_1, L_2$ , and  $L_3$  are not independent (after all, points in a plane are specified uniquely by two independent coordinates). Inspection of the points  $Q_i, i=1,2,3$ , shows that

$$L_1(Q) + L_2(Q) + L_3(Q) = 1 \quad (1.2.10)$$

for any point  $Q$ . On the other hand, no two of the  $L_i$  are dependent, and thus any linear function is some combination of the  $L_i$ .

Thus, given a linear function  $\sigma$ ,

$$\sigma(Q) = \sigma_1 L_1(Q) + \sigma_2 L_2(Q) + \sigma_3 L_3(Q) \quad (1.2.11)$$

where

$$\sigma_i = \sigma(Q_i) \quad (1.2.12)$$

$$\text{But, applying (1.2.8), and writing } Q=(\xi, n), \quad (1.2.13)$$

$$L_i(Q) = \frac{(\xi - \xi_{i+1}, n - n_{i+1}) \cdot \vec{n}_i}{(\xi_i - \xi_{i+1}, n_i - n_{i+1}) \cdot \vec{n}_i} = a_i + b_i \xi + c_i n \quad (1.2.14)$$

where, applying (1.2.7),

$$\begin{aligned} a_i &= [\xi_{i+2} (n_{i+2} - n_{i+1}) - n_{i+1} (\xi_{i+2} - \xi_{i+1})] / \Delta_i \\ &= [\xi_{i+1} n_{i+2} - n_{i+1} \xi_{i+2}] / \Delta_i \end{aligned} \quad (1.2.15)$$

where

$$\begin{aligned} \Delta_i &= -(\xi_i - \xi_{i+1})(\eta_{i+2} - \eta_{i+1}) + (\eta_i - \eta_{i+1})(\xi_{i+2} - \xi_{i+1}) \\ &= -(\vec{Q}_i - \vec{Q}_{i+1}) \times (\vec{Q}_{i+2} - \vec{Q}_{i+1}) \cdot \begin{Bmatrix} 0 \\ 0 \\ 1 \end{Bmatrix} \end{aligned} \quad (1.2.16)$$

$$= 2A \quad (1.2.17)$$

where A is the triangle area computed in local coordinates. Note that a triangle's area depends on the coordinate system, since the transformation (E.0.1) is not orthogonal, and therefore not distance-preserving. Equation (1.2.17) follows from (1.2.16) because the cross product of two vectors in the  $z = 0$  plane is a multiple of  $(0,0,1)$ , and thus its magnitude is plus or minus its dot product with  $(0,0,1)$ . Here the right hand rule insures the plus sign.

Now, similarly

$$b_i = \frac{\eta_{i+1} - \eta_{i+2}}{2A} \quad (1.2.18)$$

$$c_i = \frac{\xi_{i+2} - \xi_{i+1}}{2A} \quad (1.2.19)$$

Now, for the definition of  $\sigma_0, \sigma_\xi, \sigma_\eta$  in (1.2.2), and from (1.2.12-14), we obtain

$$\begin{Bmatrix} \sigma_0 \\ \sigma_\xi \\ \sigma_\eta \end{Bmatrix} = \begin{bmatrix} a_1 & a_2 & a_3 & \sigma_1 \\ b_1 & b_2 & b_3 & \sigma_2 \\ c_1 & c_2 & c_3 & \sigma_3 \end{bmatrix} \begin{Bmatrix} \sigma_1 \\ \sigma_2 \\ \sigma_3 \end{Bmatrix} \quad (1.2.20)$$

Thus, substituting (1.2.15-19) in (1.2.20), and reverting to the notation of Figure 1.13, the inverse of the matrix  $G^S$  in (1.2.4) is

$$[G^S]^{-1} = \frac{1}{2A} \begin{bmatrix} \xi_j \eta_k - \eta_j \xi_k & \xi_k \eta_i - \eta_k \xi_i & \xi_i \eta_j - \eta_i \xi_j \\ \eta_j - \eta_k & \eta_k - \eta_i & \eta_i - \eta_j \\ \xi_k - \xi_j & \xi_i - \xi_k & \xi_j - \xi_i \end{bmatrix} \quad (1.2.21)$$

Note, therefore, that  $G^S$  is invertible whenever the triangle has non-zero area.

### I.2.1.3 The Extension Matrix

In order to compute the matrix  $SPSPL^S$  such that

$$\begin{Bmatrix} \sigma_0 \\ \sigma_1 \\ \sigma_2 \\ \sigma_3 \\ \sigma_4 \\ \sigma_5 \\ \sigma_6 \\ \sigma_7 \\ \sigma_8 \\ \sigma_9 \end{Bmatrix} = [SPSPL^S] \begin{Bmatrix} \sigma_1 \\ \sigma_2 \\ \sigma_3 \\ \sigma_4 \\ \sigma_5 \\ \sigma_6 \\ \sigma_7 \\ \sigma_8 \\ \sigma_9 \end{Bmatrix} \quad (I.2.22)$$

we first compute a  $3 \times 5$  "extension matrix"  $XT^S$  such that  $\sigma_i, \sigma_j, \sigma_k$ , the source strength at the three vertices of the subpanel are given by

$$\begin{Bmatrix} \sigma_i \\ \sigma_j \\ \sigma_k \end{Bmatrix} = [XT^S] \begin{Bmatrix} \sigma_1 \\ \sigma_2 \\ \sigma_3 \\ \sigma_4 \\ \sigma_5 \end{Bmatrix} \quad (I.2.23)$$

From (I.2.1) and its analogs, we see that  $[XT^S]$  is the matrix whose first, second, and third rows are the  $i$ th,  $j$ th, and  $k$ th rows of the  $9 \times 5$  matrix

$$V = \begin{bmatrix} 1 & 0 & 0 & 0 & 0 \\ 0 & 1 & 0 & 0 & 0 \\ 0 & 0 & 1 & 0 & 0 \\ 0 & 0 & 0 & 1 & 0 \\ 1/2 & 1/2 & 0 & 0 & 0 \\ 0 & 1/2 & 1/2 & 0 & 0 \\ 0 & 0 & 1/2 & 1/2 & 0 \\ 1/2 & 0 & 0 & 1/2 & 0 \\ 0 & 0 & 0 & 0 & 1 \end{bmatrix} \quad (I.2.24)$$

since

$$\begin{Bmatrix} \sigma_1 \\ \vdots \\ \sigma_8 \\ \sigma_9 \end{Bmatrix} = [V] \begin{Bmatrix} \sigma_1 \\ \vdots \\ \sigma_4 \\ \sigma_9 \end{Bmatrix} \quad (1.2.25)$$

Combining (1.2.5) and (1.2.23), and comparing with (1.2.22), we see that

$$[SPSPLS] = [GS]^{-1} [XTS] \quad (1.2.26)$$

As specified by (1.2.22),  $SPSPLS$  is the matrix which defines the three coefficients of a linearly varying source strength on a subpanel in terms of the five panel source parameters. It should be noted, however, that while the source subpanel splines insure that the source strength varies linearly over each subpanel, and linearly along panel edges, the source distribution is only piecewise linear over a panel as a whole.

## 1.2.2 Doublet Subpanel Splines

Now we consider doublet subpanel splines. The outer spline matrix  $B$  defines the nine panel doublet parameters, that is, the values of doublet strength at the nine panel defining points. The quadratic accuracy to be achieved by the doublet distribution gives us more leeway in choosing the distribution over each subpanel than linear accuracy, since it requires the specification of values at six points to define a unique quadratic function.

### 1.2.2.1 Continuity Requirements

Let us consider a quadratically varying function on a triangular region, such as the one in Figure 1.14. On each edge, the function is just a quadratic on one variable, and thus, the behavior of the function on the whole edge is determined by the values at three distinct points on the edge; say, the edge midpoint and the two vertices. So, we can determine the behavior of the function on the entire boundary of the triangle if, and only if, we know its values at the edge midpoints and three vertices of the triangle. On the other hand, specification of the value of the function at these six points defines the function on the whole triangle. So, the specification of quadratic variations on each of the three edges of the triangle defines a unique quadratic function in the interior of the triangle which assumes the specified values on the boundary. Therefore, to specify a quadratic doublet distribution on each subpanel, we need only specify the doublet variation on all the subpanel edges. This insures doublet continuity within the panel in addition, since the doublet strength is uniquely defined on the set of points common to two or more subpanels.

The requirement of continuity of doublet strength across panel edges makes it clear how we must define  $\mu$  on the panel edges. Since the outer spline matrix  $B^D$  forces continuity of  $\mu$  at only three points (the vertices and midpoint) on a panel edge (see section I.1), the value of  $\mu$  on the entire edge must be determined by these three values. Thus we require  $\mu$  to be a single quadratic function on each panel edge.

This leaves eight interior subpanel edges on which  $\mu$  is not yet fully defined. One possibility considered in the course of the development of the doublet subpanel splines was to minimize the discontinuities in doublet gradient in the interior of the panel. Experimentation showed that this method was unacceptable. An indication of the numerical error introduced by this method can be seen in Figure I.15, which illustrates the values of panel doublet parameters and doublet strengths at all the subpanel edge midpoints which result from the minimization of derivative discontinuities. In fact, in this example, the panel is square and there are no discontinuities in doublet gradient. It is thought that the oscillatory behavior on the vertical edge midpoint connector results in instabilities.

No theoretical study has been performed on the above problem; however, an alternate approach has been found to be experimentally successful. In this approach, the doublet strength on the edge midpoint connectors is defined to be the single quadratic function defined by the values at the endpoints and midpoint. Subject to this constraint, the discontinuities in doublet gradient are minimized. The panel doublet parameters illustrated in Figure I.15 now produce the doublet distribution illustrated in Figure I.16. The latter distribution does not exhibit the oscillatory behavior of the former distribution.

#### I.2.2.2 Definition of "Kappa" Quantities

We will now describe the computation of the subpanel splines by the second approach, the one which is incorporated in PAN AIR. For reasons which will soon become clear (that is, in order to derive (I.2.36), (I.2.45), and (I.2.47)), we describe the quadratically varying doublet strength on an interval AB, (which will later be used to represent either a subpanel edge or a panel edge) as illustrated in Figure I.17, by specifying  $\mu(A)$ ,  $\mu(B)$ , and

$$\kappa_{AB} = \mu(A) + 1/2 \vec{\nabla}\mu(A) \cdot (\vec{B} - \vec{A}) \quad (I.2.27)$$

$$= \kappa_{BA} = \mu(B) + 1/2 \vec{\nabla}\mu(B) \cdot (\vec{A} - \vec{B}) \quad (I.2.28)$$

the quantity  $\kappa_{AB}$  being specified rather than  $\mu(M)$ . Equations (I.2.27-28) are proved in section I.1.

Now let M be the midpoint of AB (Figure I.17). Then

$$\vec{\nabla}\mu(M) \cdot (\vec{B} - \vec{A}) = \mu(B) - \mu(A) \quad (I.2.29)$$

for any quadratic function on AB. Thus

$$\vec{\nabla}\mu(M) \cdot (\vec{B} - \vec{M}) = \frac{\mu(B) - \mu(A)}{2} \quad (I.2.30)$$

It follows from (I.2.28) that

$$\kappa_{MB} = u(M) + 1/2 \vec{\nabla} u(M) \cdot (\vec{B} - \vec{M}) = u(M) + 1/4 u(B) - 1/4 u(A) \quad (I.2.31)$$

$$\text{Similarly } \kappa_{MA} = u(M) + 1/4 u(A) - 1/4 u(B) \quad (I.2.32)$$

$$\text{Also } \kappa_{MA} = \kappa_{AM} = u(A) + 1/2 \vec{\nabla} u(A) \cdot (\vec{M} - \vec{A}) \quad (I.2.33)$$

$$\begin{aligned} \text{Thus } \vec{\nabla} u(A) \cdot (\vec{M} - \vec{A}) &= 2 \kappa_{MA} - 2u(A) \\ &= 2u(M) + 1/2u(A) - 1/2u(B) - 2u(A) \end{aligned} \quad (I.2.34)$$

$$= 2u(M) - 3/2 u(A) - 1/2u(B) \quad (I.2.35)$$

We can apply (I.2.31) and (I.2.32) to a panel on which the doublet strength is a single quadratic on the panel edges and on the lines connecting opposing edge midpoints that is,  $P_5 P_7$  and  $P_6 P_8$  of figure 1.12. Writing  $\kappa_{ij}$  for the quantity  $\kappa_{p_i p_j}$ , we see that (cf., Figure 1.12)

$$\begin{aligned} \kappa_{15} &= u_5 + 1/4 u_1 - 1/4 u_2 \\ \kappa_{52} &= u_5 - 1/4 u_1 + 1/4 u_2 \\ \kappa_{26} &= u_6 + 1/4 u_2 - 1/4 u_3 \\ \kappa_{63} &= u_6 - 1/4 u_2 + 1/4 u_3 \\ &\text{etc.} \end{aligned} \quad (I.2.36)$$

#### I.2.2.3 Computation of "Kappa" Quantities On Lines Containing only two Panel Defining Points

It remains, however, to determine  $\kappa_{56}$ ,  $\kappa_{67}$ ,  $\kappa_{78}$  and  $\kappa_{85}$ . Because these lines contain only two panel defining points, no obvious method exists. We therefore construct a procedure by which derivative discontinuities are minimized. We consider the standard panel in Figure D.11, and project it down to the  $z=0$  plane. One way to compute  $\kappa_{58}$  for example, would be to define it based on the doublet gradient at  $P_5$  given by the doublet strength on  $P_5 P_9 P_7$  and on  $P_1 P_5 P_2$ .

Applying (1.2.35) to  $P_5, P_9, P_7$ , and using the skewness parameters and coordinate system of section 0.2, we see that

$$\vec{\nabla}_\mu(P_5) \cdot (\vec{P}_9 - \vec{P}_5) = \vec{\nabla}_\mu(P_5) \cdot \begin{Bmatrix} 0 \\ 1 \end{Bmatrix} = -1/2\mu_7 - 3/2\mu_5 + 2\mu_9 \quad (1.2.37)$$

On the other hand, applying (1.2.30),

$$\begin{aligned} \vec{\nabla}_\mu(P_5) \cdot (\vec{P}_1 - \vec{P}_5) &= \vec{\nabla}_\mu(P_5) \cdot \begin{Bmatrix} 1 + c_{11} \\ c_{21} \end{Bmatrix} \\ &= 1/2\mu_1 - 1/2\mu_2 \end{aligned} \quad (1.2.38)$$

Now,

$$(\vec{P}_8 - \vec{P}_5) = \begin{Bmatrix} 1 \\ -1 \end{Bmatrix} = \frac{1 + c_{11} + c_{21}}{1 + c_{11}} \begin{Bmatrix} 0 \\ -1 \end{Bmatrix} + \frac{1}{1 + c_{11}} \begin{Bmatrix} 1 + c_{11} \\ c_{21} \end{Bmatrix} \quad (1.2.39)$$

$$= \frac{1 + c_{11} + c_{21}}{1 + c_{11}} (\vec{P}_9 - \vec{P}_5) + \frac{1}{1 + c_{11}} (\vec{P}_1 - \vec{P}_5) \quad (1.2.40)$$

Thus, if we require continuity of doublet strength at  $P_5$ , we have

$$\begin{aligned} \vec{\nabla}_\mu(P_5) \cdot (\vec{P}_8 - \vec{P}_5) &= \\ &= \frac{1 + c_{11} + c_{21}}{1 + c_{11}} \vec{\nabla}_\mu(P_5) \cdot (\vec{P}_9 - \vec{P}_5) + \frac{1}{1 + c_{11}} \vec{\nabla}_\mu(P_5) \cdot (\vec{P}_1 - \vec{P}_5) \end{aligned} \quad (1.2.41)$$

$$= \frac{1 + c_{11} + c_{21}}{1 + c_{11}} (-1/2\mu_7 - 3/2\mu_5 + 2\mu_9) + \frac{1}{1 + c_{11}} (1/2\mu_1 - 1/2\mu_2) \quad (1.2.42)$$

So, by (1.2.28), we have

$$\kappa_{85}^{(5)} = u_5 + 1/2 \vec{\nabla} u(P_5) (\vec{P}_8 - \vec{P}_5) =$$

$$\frac{1}{4(1+c_{11})} \begin{pmatrix} u_1 - u_2 - 3(1+c_{11}+c_{21})u_5 + 4(1+c_{11})u_5 \\ - (1+c_{11}+c_{21})u_7 + 4(1+c_{11}+c_{21})u_9 \end{pmatrix} \quad (1.2.43)$$

$$\frac{1}{4(1+c_{11})} [u_1 - u_2 + (1+c_{11}-3c_{21})u_5 - (1+c_{11}+c_{21})u_7$$

$$+ 4(1+c_{11}+c_{21})u_9] \quad (1.2.44)$$

On the other hand, we could just as well calculate  $\kappa_{85}$  by requiring a differentiable doublet strength at  $P_8$ . We follow exactly the same procedure as before. The analog to (1.2.39-40) is

$$(\vec{P}_5 - \vec{P}_8) = \begin{Bmatrix} -1 \\ 1 \end{Bmatrix} = \frac{1+c_{11}+c_{21}}{1+c_{21}} \begin{Bmatrix} -1 \\ 0 \end{Bmatrix} + \frac{1}{1+c_{21}} \begin{Bmatrix} c_{11} \\ 1+c_{21} \end{Bmatrix} \quad (1.2.45)$$

$$= \frac{1+c_{11}+c_{21}}{1+c_{21}} (\vec{P}_9 - \vec{P}_8) + \frac{1}{1+c_{21}} (\vec{P}_1 - \vec{P}_8) \quad (1.2.46)$$

As an analog to (1.2.44), we obtain

$$\kappa_{85}^{(8)} = \frac{1}{4(1+c_{21})} \begin{pmatrix} u_1 - u_4 + (1+c_{21}-3c_{11})u_8 \\ - (1+c_{11}+c_{21})u_6 + 4(1+c_{11}+c_{21})u_9 \end{pmatrix} \quad (1.2.47)$$

Now, clearly, the definition we use for  $\kappa_{58}$  should be some weighted average of the two values we have calculated. Further, if  $(1+c_{11})$  or  $(1+c_{21})$  is zero, one of the values of  $\kappa_{58}$  goes to infinity, indicating the impossibility of providing a continuous doublet gradient on that occasion (this situation occurs whenever the panel is triangular). Thus, our weighted average should be such that zero weight is given to an infinite value of  $\kappa_{58}$ . The simplest such weighted average is given below:

$$\kappa_{58} = \frac{1+c_{11}}{2+c_{11}+c_{21}} \kappa_{58}^{(5)} + \frac{1+c_{21}}{2+c_{11}+c_{21}} \kappa_{58}^{(8)} \quad (1.2.48)$$



Combining equations (I.2.44), (I.2.47), and (I.2.48) we obtain

$$\kappa_{85} = \frac{1}{4 + c_{11} + c_{21}} \left( 2u_1 - u_2 - u_4 + (1 + c_{11} - 3c_{21})u_5 - (1 + c_{11} + c_{21})u_6 \right. \\ \left. - (1 + c_{11} + c_{21})u_7 + (1 + c_{21} - 3c_{11})u_8 + 8(1 + c_{11} + c_{21})u_9 \right) \quad (I.2.49)$$

Equation (I.2.49) can be rewritten to more clearly show geometric symmetry and thus give us the analogous quantities  $\kappa_{56}$ ,  $\kappa_{67}$ , and  $\kappa_{78}$  easily.

Let

$$F_j = 1 + c_{1j} + c_{2j} \quad j = 1, \dots, 4 \quad (I.2.50)$$

Then

$$F_1 = 1 + c_{11} + c_{21} \quad (I.2.51)$$

and by (D.2.35)

$$\begin{aligned} F_2 &= 1 + c_{12} + c_{22} = 1 + c_{11} - c_{21} \\ F_3 &= 1 - c_{11} - c_{21} \\ F_4 &= 1 - c_{11} + c_{21} \end{aligned} \quad (I.2.52)$$

The quantities  $F_j$  are very naturally associated with the interior edge of the  $j$ th subpanel (for which is to be determined) because every point  $P' = (x', y')$  on this edge, if written as  $P' = (1 + c'_{1j}, 1 + c'_{2j})$ , has the property

$$F'_j = 0 \quad (I.2.53)$$

where  $F'_j$  is defined by (I.2.51-52) with  $c'_{ij}$  replacing  $c_{ij}$ .

Now, using (I.2.52) in (I.2.49) we see

$$\kappa_{85} = \frac{1}{4(1 + F_1)} \left( 2u_1 - u_2 - u_4 + (2F_2 - F_1)u_5 \right. \\ \left. - F_1u_6 - F_1u_7 + (2F_4 - F_1)u_8 + 8F_1u_9 \right) \quad (I.2.54)$$

Using this formulation, we can construct the other 3 's by symmetry.

$$\kappa_{56} = \frac{1}{4(1 + F_2)} \left( 2u_2 - u_1 - u_3 + (2F_3 - F_2)u_6 \right. \\ \left. - F_2u_7 - F_2u_8 + (2F_1 - F_2)u_5 + 8F_2u_9 \right) \quad (I.2.55)$$

$$\kappa_{67} = \frac{1}{4(1 + F_3)} \left( 2u_3 - u_2 - u_4 + (2F_4 - F_3)u_7 \right. \\ \left. - F_3u_8 - F_3u_5 + (2F_2 - F_3)u_6 + 8F_3u_9 \right) \quad (I.2.56)$$

$$\kappa_{78} = \frac{1}{4(1 + F_4)} \left( 2u_4 - u_3 - u_1 + (2F_1 - F_4)u_8 \right. \\ \left. - F_4u_5 - F_4u_6 + (2F_3 - F_4)u_7 + 8F_4u_9 \right) \quad (I.2.57)$$

#### I.2.2.4 The Doublet Extension Matrix

Using equations (I.2.36) and (I.2.54-57), we can compute a doublet extension matrix  $XT^D$ , so that, for the panel in Figure I.13

$$\begin{Bmatrix} \mu_i \\ \mu_j \\ \mu_k \\ \kappa_{jk} \\ \kappa_{ki} \\ \kappa_{ij} \end{Bmatrix} = [XT^D] \begin{Bmatrix} \mu_1 \\ \cdot \\ \cdot \\ \cdot \\ \cdot \\ \mu_9 \end{Bmatrix} \quad (I.2.58)$$

The first three rows consist of a 1 in the  $i$ th,  $j$ th, or  $k$ th column, respectively, and the remaining entries zero. As an example, the extension matrix  $XT^D$  for the first subpanel is

$$\begin{Bmatrix} \mu_1 \\ \mu_5 \\ \mu_8 \\ \kappa_{58} \\ \kappa_{18} \\ \kappa_{15} \end{Bmatrix} = [XT_1^D] \begin{Bmatrix} \mu_1 \\ \cdot \\ \cdot \\ \cdot \\ \cdot \\ \mu_9 \end{Bmatrix} \quad (I.2.59)$$

where  $[XT_1^D] =$

$$\begin{bmatrix} 1 & 0 & 0 & 0 & 0 & 0 & 0 & 0 & 0 \\ 0 & 0 & 0 & 0 & 1 & 0 & 0 & 0 & 0 \\ 0 & 0 & 0 & 0 & 0 & 0 & 0 & 1 & 0 \\ \frac{1}{2(1+F_1)} & \frac{-1}{4(1+F_1)} & 0 & \frac{-1}{4(1+F_1)} & \frac{2F_2-1}{4(1+F_1)} & \frac{-F_1}{4(1+F_1)} & \frac{-F_1}{4(1+F_1)} & \frac{2F_4-F_1}{4(1+F_1)} & \frac{2F_1}{1+F_1} \\ 1/4 & 0 & 0 & -1/4 & 0 & 0 & 0 & 1 & 0 \\ 1/4 & -1/4 & 0 & 0 & 1 & 0 & 0 & 0 & 0 \end{bmatrix} \quad (I.2.60)$$

#### I.2.2.5 The Matrix of Coordinates $[G^D]$

Next, we define a matrix  $G^D$ , such that the doublet distribution on a subpanel in local coordinates (that is, the system  $X'$  of the Appendix E),

$$\mu(\xi, \eta) = \mu_0 + \mu_\xi \xi + \mu_\eta \eta + 1/2 \mu_{\xi\xi} \xi^2 + \mu_{\xi\eta} \xi\eta + 1/2 \mu_{\eta\eta} \eta^2 \quad (I.2.61)$$

is given by

$$\begin{Bmatrix} \mu_i \\ \mu_j \\ \mu_k \\ \kappa_{jk} \\ \kappa_{ki} \\ \kappa_{ij} \end{Bmatrix} = [G^D] \begin{Bmatrix} \mu_0 \\ \cdot \\ \cdot \\ \cdot \\ \cdot \\ \mu_9 \end{Bmatrix} \quad (1.2.62)$$

Inverting (1.2.62) and substituting in (1.2.58) we obtain

$$\begin{Bmatrix} \mu_0 \\ \vdots \\ \mu_{nn} \end{Bmatrix} = [G^D]^{-1} [X^T D] \begin{Bmatrix} \mu_1 \\ \vdots \\ \mu_9 \end{Bmatrix} \quad (1.2.63)$$

Comparing with (1.0.4), we see that

$$[SPSP L^D] = [G^D]^{-1} [X^T D] \quad (1.2.64)$$

To compute  $G^D$ , let us consider that triangular region in Figure 1.18. Again, all subscripts will be considered modulo 3. Now, the quadratic doublet distribution gives

$$\mu(Q_i) = \mu_0 + \mu_\xi \xi_i + \mu_\eta \eta_i + \dots + 1/2 \mu_{nn} \eta_i^2 \quad (1.2.65)$$

$$\text{So,} \quad \kappa_{i,i+1} = \mu(Q_i) + 1/2 \bar{\nabla} \mu(Q_i) \cdot (\bar{Q}_{i+1} - \bar{Q}_i) \quad (1.2.66)$$

Differentiating (1.2.65), we see that

$$\bar{\nabla} \mu(Q_i) = \begin{Bmatrix} \mu_\xi + \mu_{\xi\xi} \xi_i + \mu_{\xi\eta} \eta_i \\ \mu_\eta + \mu_{\eta\xi} \xi_i + \mu_{\eta\eta} \eta_i \end{Bmatrix} \quad (1.2.67)$$

while

$$\bar{Q}_{i+1} - \bar{Q}_i = \begin{Bmatrix} \xi_{i+1} - \xi_i \\ \eta_{i+1} - \eta_i \end{Bmatrix} \quad (1.2.68)$$

Thus, (1.2.66) becomes

$$\begin{aligned}
\kappa_{i,i+1} = & \mu_0 + 1/2(\xi_i + \xi_{i+1})\mu + 1/2(\eta_i + \eta_{i+1})\mu_\eta \\
& + 1/2 \xi_i \xi_{i+1} \mu_{\xi\xi} + 1/2(\xi_{i+1} \eta_i + \xi_i \eta_{i+1})\mu_{\xi\eta} \\
& + 1/2 \eta_i \eta_{i+1} \mu_{\eta\eta}
\end{aligned} \tag{I.2.69}$$

Applying (I.2.65) and (I.2.69) to (I.2.62) for the triangle in Figure I.18 (with  $i=1, j=2, k=3$  in equation (I.2.62)), we obtain  $[G^D] =$

$$\begin{bmatrix}
1 & \xi_1 & \eta_1 & 1/2\xi_1^2 & \xi_1 \eta_1 & 1/2\eta_1^2 \\
1 & \xi_2 & \eta_2 & 1/2\xi_2^2 & \xi_2 \eta_2 & 1/2\eta_2^2 \\
1 & \xi_3 & \eta_3 & 1/2\xi_3^2 & \xi_3 \eta_3 & 1/2\eta_3^2 \\
1 & \frac{\xi_2 + \xi_3}{2} & \frac{\eta_2 + \eta_3}{2} & \frac{\xi_2 \xi_3}{2} & 1/2 \left( \frac{\xi_2 \eta_3 + \xi_3 \eta_2}{\xi_3 \eta_2} \right) & \frac{\eta_2 \eta_3}{2} \\
1 & \frac{\xi_1 + \xi_3}{2} & \frac{\eta_1 + \eta_3}{2} & \frac{\xi_1 \xi_3}{3} & 1/2 \left( \frac{\xi_1 \eta_3 + \xi_3 \eta_1}{\xi_3 \eta_1} \right) & \frac{\eta_1 \eta_3}{2} \\
1 & \frac{\xi_1 + \xi_2}{2} & \frac{\eta_1 + \eta_2}{2} & \frac{\xi_1 \xi_2}{2} & 1/2 \left( \frac{\xi_1 \eta_2 + \xi_2 \eta_1}{\xi_2 \eta_1} \right) & \frac{\eta_1 \eta_2}{2}
\end{bmatrix} \tag{I.2.70}$$

#### I.2.2.6 Inversion of $[G^D]$

As with  $G^S$ ,  $G^D$  may be inverted analytically or numerically. In practice, Pan Air performs numerical inversion. We again supply the analytic method for the interest of the user. Again we use triangular coordinates to invert  $G^D$  analytically. We claim that for  $P = Q_1, Q_2, Q_3$ , or the edge midpoint  $M_1, M_2, M_3$  in Figure I.18,

$$\begin{aligned}
\mu(P) = & \mu_1 L_1(P)^2 + \mu_2 L_2(P)^2 + \mu_3 L_3(P)^2 \\
& + 2 \kappa_{23} L_2(P)L_3(P) + 2 \kappa_{13} L_1(P)L_3(P) + 2 \kappa_{12} L_1(P)L_2(P)
\end{aligned} \tag{I.2.71}$$

This is proven below.

Equation (I.2.71) certainly holds for the points  $Q_1, Q_2, Q_3$ , since

$$L_i(Q_j) = \delta_{ij} \tag{I.2.72}$$

Further

$$\begin{aligned}
L_i(M_k)L_j(M_k) = & 1/4 \text{ if } i \neq k \text{ and } j \neq k \\
= & 0 \text{ otherwise}
\end{aligned} \tag{I.2.73}$$

since the  $L_i$  are linear functions. Thus, the right side of (I.2.71), applied to  $M_k$ , is

$$\begin{aligned} & \mu_{k+1} L_{k+1}(M_k)^2 + \mu_{k+2} L_{k+2}(M_k)^2 \\ & + 2 \kappa_{k+1,k+2} L_{k+1}(M_k) L_{k+2}(M_k) \\ & = 1/4 \mu_{k+1} + 1/4 \mu_{k+2} + 1/2 \kappa_{k+1,k+2} \end{aligned} \quad (I.2.74)$$

Now, referring to Figure I.17, and applying (I.2.28) and (I.2.35), we see that

$$\kappa_{AB} = -1/2 \mu(A) - 1/2 \mu(B) + 2\mu(M) \quad (I.2.75)$$

Applying this to Figure I.18, we see

$$\kappa_{k+1,k+2} = -\frac{1}{2}\mu(Q_{k+1}) - \frac{1}{2}\mu(Q_{k+2}) + 2\mu(M_k) \quad (I.2.76)$$

$$\text{or } \mu(M_k) = \frac{1}{2} \kappa_{k+1,k+2} + \frac{1}{4} \mu(Q_{k+1}) + \frac{1}{4} \mu(Q_{k+2}) \quad (I.2.77)$$

Comparing (I.2.74) and (I.2.77), we see that (I.2.71) holds. Now, since (I.2.71) holds at six independent points on the triangular region, it holds everywhere in the region.

Next, we substitute (I.2.14) and (I.0.2) in (I.2.71) for an arbitrary point  $P=(\xi, n)$ , obtaining

$$\begin{aligned} & \mu_0 + \mu_\xi \xi + \mu_n n + \dots + 1/2 \mu_{nn} n^2 = \\ & \mu_1 (a_1 + b_1 \xi + c_1 n)^2 + \mu_2 (a_2 + b_2 \xi + c_2 n)^2 \\ & + \mu_3 (a_3 + b_3 \xi + c_3 n)^2 \\ & + 2\kappa_{23} (a_2 + b_2 \xi + c_2 n) (a_3 + b_3 \xi + c_3 n) \\ & + 2\kappa_{13} (a_1 + b_1 \xi + c_1 n) (a_3 + b_3 \xi + c_3 n) \\ & + 2\kappa_{12} (a_1 + b_1 \xi + c_1 n) (a_2 + b_2 \xi + c_2 n) \end{aligned} \quad (I.2.78)$$

where the  $a_i$ ,  $b_i$ , and  $c_i$  are defined by (I.2.15-19).

Since (I.2.78) holds for an arbitrary point  $(\xi, n)$ , each coefficient of a term  $\xi^m n^n$ ,  $0 \leq m + n \leq 2$ , on the left must equal the coefficient of the

corresponding term on the right. Matching coefficients of  $\mu_0$ , for instance,

$$\mu_0 = \begin{bmatrix} a_1^2 & a_2^2 & a_3^2 & 2a_2a_3 & 2a_3a_1 & 2a_1a_2 \end{bmatrix} \begin{Bmatrix} \mu_1 \\ \mu_2 \\ \mu_3 \\ \kappa_{23} \\ \kappa_{13} \\ \kappa_{12} \end{Bmatrix} \quad (1.2.79)$$

We obtain five more such equations, obtaining, altogether,

$$\begin{Bmatrix} \mu_0 \\ \mu_\xi \\ \mu_\eta \\ \mu_{\xi\xi} \\ \mu_{\xi\eta} \\ \mu_{\eta\eta} \end{Bmatrix} = \begin{bmatrix} a_1^2 & a_2^2 & a_3^2 & 2a_2a_3 & 2a_3a_1 & 2a_1a_2 \\ 2a_1b_1 & 2a_2b_2 & 2a_3b_3 & 2\begin{pmatrix} a_2b_3 \\ a_3b_2 \end{pmatrix}^+ & 2\begin{pmatrix} a_3b_1 \\ a_1b_3 \end{pmatrix}^+ & 2\begin{pmatrix} a_1b_2 \\ a_2b_1 \end{pmatrix}^+ \\ 2a_1c_1 & 2a_2c_2 & 2a_3c_3 & 2\begin{pmatrix} a_2c_3 \\ a_3c_2 \end{pmatrix}^+ & 2\begin{pmatrix} a_3c_1 \\ a_1c_3 \end{pmatrix}^+ & 2\begin{pmatrix} a_1c_2 \\ a_2c_1 \end{pmatrix}^+ \\ 2b_1^2 & 2b_2^2 & 2b_3^2 & 4b_2b_3 & 4b_1b_3 & 4b_1b_2 \\ 2b_1c_1 & 2b_2c_2 & 2b_3c_3 & 2\begin{pmatrix} b_2c_3 \\ b_3c_2 \end{pmatrix}^+ & 2\begin{pmatrix} b_1c_3 \\ b_3c_1 \end{pmatrix}^+ & 2\begin{pmatrix} b_1c_2 \\ b_2c_1 \end{pmatrix}^+ \\ 2c_1^2 & 2c_2^2 & 2c_3^2 & 4c_2c_3 & 4c_1c_3 & 4c_1c_2 \end{bmatrix} \begin{Bmatrix} \mu_1 \\ \mu_2 \\ \mu_3 \\ \kappa_{23} \\ \kappa_{13} \\ \kappa_{12} \end{Bmatrix} \quad (1.2.80)$$

Comparing to equation (1.2.62), we see that (1.2.80) defines  $[G^D]^{-1}$ . Thus, applying (1.2.64), we have computed  $[SPSPL^D]$ . In practice, however, PAN AIR inverts the matrix  $G^D$  (1.2.70) and multiplies by  $XT^D$ , to obtain  $SPSPL^D$ . This completes the discussion of subpanel splines.

### 1.3 Full Panel and Half Panel Splines

Measuring the influence of a panel on which eight separate singularity distributions are defined requires a considerable amount of computation, and, thus, is reserved for control points which are very near to the panel. For points which are somewhat further from the panel, one of two "intermediate field" procedures is used for the computation of a panel influence coefficient matrix. In these procedures, the panel containing five planar regions and the singularity strength defined distinctly on eight triangular regions are replaced by approximations in order to reduce computation costs.

#### 1.3.1 Full Panel Spline Matrices

In the "one region intermediate field" procedure, the panel is replaced by its projection to the average plane (thus, panels now have gaps between them, but, presumably, the control point is far enough away in hyperbolic distance  $R$ , defined by (5.6.6), that the gaps do not matter). The source and doublet distributions on the panel are approximated by a single linear function and a single quadratic function, respectively, whose strengths are not continuous across panel edges. We now describe the computation of these functions.

Precisely, our goal is to calculate matrices  $PSPL^S$  and  $PSPL^D$  ( $PSPL$  stands for "panel spline") such that in a local coordinate system  $(\xi, \eta)$  defined on the average plane (that is, defined by (E.0.1), with  $\hat{n}$  the normal to the average plane) and with its origin at the panel center,

$$\sigma(\xi, \eta) = \sigma_0 + \sigma_\xi \xi + \sigma_\eta \eta \quad (1.3.1)$$

$$u(\xi, \eta) = u_0 + \dots + 1/2 u_{\eta\eta} \eta^2 \quad (1.3.2)$$

and

$$\begin{Bmatrix} \sigma_0 \\ \sigma_\xi \\ \sigma_\eta \end{Bmatrix} = [PSPL^S] \begin{Bmatrix} \sigma_1 \\ \sigma_2 \\ \sigma_3 \\ \sigma_4 \\ \sigma_9 \end{Bmatrix} \quad (1.3.3)$$

$$\begin{Bmatrix} u_0 \\ \cdot \\ \cdot \\ \cdot \\ \cdot \end{Bmatrix} = [PSPL^D] \begin{Bmatrix} u_1 \\ \cdot \\ \cdot \\ \cdot \\ \cdot \\ u_9 \end{Bmatrix} \quad (1.3.4)$$

The panel spline matrices are computed by a constrained least square procedure. They define the linear source or quadratic doublet distribution on the panel which exactly takes on the value at the panel center, and takes on the values at the four remaining panel source parameter locations (or eight remaining panel doublet parameter locations) in a least squares sense. Precisely,  $PSPL^S$  is the matrix such that  $\sigma_0$ ,  $\sigma$ , and  $\sigma_n$  defined by (I.3.3) satisfy

$$\begin{bmatrix} 1 & \xi_9 & \eta_9 \end{bmatrix} \begin{Bmatrix} \sigma_0 \\ \sigma_\xi \\ \sigma_\eta \end{Bmatrix} = \sigma_9 \quad (I.3.5)$$

while minimizing

$$\left| \begin{bmatrix} 1 & \xi_1 & \eta_1 \\ 1 & \xi_2 & \eta_2 \\ 1 & \xi_3 & \eta_3 \\ 1 & \xi_4 & \eta_4 \end{bmatrix} \begin{Bmatrix} \sigma_0 \\ \sigma_\xi \\ \sigma_\eta \end{Bmatrix} - \begin{Bmatrix} \sigma_1 \\ \sigma_2 \\ \sigma_3 \\ \sigma_4 \end{Bmatrix} \right|^2 \quad (I.3.6)$$

Similarly,  $\mu_0, \dots, \mu_{nn}$ , as defined by  $PSPL^D$  in (I.3.4) satisfy

$$\begin{bmatrix} 1 & \xi_9 & \eta_9 & 1/2\xi_9^2 & \eta_9\xi_9 & 1/2\eta_9^2 \end{bmatrix} \begin{Bmatrix} \mu_0 \\ \cdot \\ \cdot \\ \cdot \\ \mu_{nn} \end{Bmatrix} = \mu_9 \quad (I.3.7)$$

while minimizing

$$\left| \begin{bmatrix} 1 & \xi_1 & \eta_1 & 1/2\xi_1^2 & \xi_1\eta_1 & 1/2\eta_1^2 \\ \cdot & \cdot & \cdot & \cdot & \cdot & \cdot \\ 1 & \xi_8 & \eta_8 & 1/2\xi_8^2 & \xi_8\eta_8 & 1/2\eta_8^2 \end{bmatrix} \begin{Bmatrix} \mu_0 \\ \cdot \\ \cdot \\ \cdot \\ \mu_{nn} \end{Bmatrix} - \begin{Bmatrix} \mu_1 \\ \cdot \\ \cdot \\ \cdot \\ \mu_9 \end{Bmatrix} \right|^2 \quad (I.3.8)$$

The constrained least squares procedure is discussed in section I.5. The purpose of the exact constraint, which insures that the singularity strength exactly takes on the value at the panel center, is to guarantee stability. This exact constraint is only used for analysis networks, for which a singularity parameter is located at the panel center. We thus assure that the singularity distribution takes on the value at the singularity parameter location



### 1.3.2 Half Panel Spline Matrices (Background Material)

We now describe a "two region intermediate field" PIC calculation method, used for control points at which the influence need not be measured by the near field method, but for which the one region intermediate field method is insufficient. This procedure is not included in version 1.0 of Pan Air, but is presented for reader interest. Here, the panel is divided into two regions along one of the two diagonals, with the partitioning which is chosen dependent on the control point's location. If the panel is partitioned along diagonal  $P_1 P_3$ , two half panels, labeled half panels 2 and 4, are generated. If the panel is partitioned along diagonal  $P_2 P_4$ , half panels 1 and 3 are generated, as illustrated in figure 1.19. The half panel index is that of the panel vertex, lying in the half panel, which lies opposite the diagonal.

In order to approximate the eight region singularity distributions fairly accurately with only two regions, we increase the degree of the polynomials. Thus we define a quadratic source strength and a cubic doublet strength on each of the four half panels. It must be emphasized that this does not give us quadratic or cubic accuracy for the source or doublet strength respectively. For example, a source distribution varying quadratically on a global scale will not be exactly produced by the piecewise quadratic source strength to be constructed here.

In Figure 1.20, we illustrate an  $i$ th arbitrary half panel with center point (average of the three vertices)  $C_i$ . For the remainder of this section we will deal with the triangular region in Figure 1.21.

#### 1.3.2.1 Requirements for the Source Half Panel Spline Matrix

Consider first the source coefficients  $\sigma_0, \dots, \sigma_{nn}$  of a quadratically varying source strength in local coordinates.

$$\sigma(\xi, \eta) = \sigma_0 + \sigma_\xi \xi + \sigma_{\eta\eta} + 1/2 \sigma_\xi \xi^2 + \sigma_{\eta\eta} \eta + 1/2 \sigma_{\eta\eta} \eta^2 \quad (1.3.9)$$

Note that since the  $i$ th half panel shares parts of two edges with the  $i$ th subpanel and they are therefore coplanar subpanel (see Figure D.8), we may use the local coordinate system of that subpanel.

Now,  $HPSPL^S$  is defined by the equation

$$\begin{Bmatrix} \sigma_0 \\ \cdot \\ \cdot \\ \cdot \\ \sigma_{nn} \end{Bmatrix} = [HPSPL^S] \begin{Bmatrix} \sigma_1 \\ \cdot \\ \cdot \\ \cdot \\ \sigma_4 \\ \sigma_9 \end{Bmatrix} \quad (1.3.10)$$

Now we require the quadratic source distribution on the half panel to satisfy the following conditions. It should be linear on the three edges, in order to match exactly the source distribution on the neighboring panel or half panel. In addition, it should take on the value of the source strength at  $C'$ , the projection of half panel center  $C$  to the panel, for stability. Finally, we require the source distribution to take on the values at the three triangles vertices. This comes to seven conditions, while a quadratic function can only satisfy six.

Now consider the function

$$f(P) = \sigma_1 L_1(P) + \sigma_2 L_2(P) + \sigma_3 L_3(P) \quad (I.3.12)$$

where

$$\sigma_i = \sigma(Q_i) \quad (I.3.13)$$

This is a linear function taking on the correct values at the corners and edge midpoints of the triangle. On the other hand,

$$\begin{aligned} g(P) &= (3 \sigma(C) - \sigma_1 - \sigma_2 - \sigma_3) \cdot \\ &\quad (L_2(P) L_3(P) + L_1(P) L_3(P) + L_1(P) L_2(P)) \end{aligned} \quad (I.3.14)$$

has the property

$$\begin{aligned} f(C) + g(C) &= 1/3(\sigma_1 + \sigma_2 + \sigma_3) + (3 \sigma(C) - \sigma_1 - \sigma_2 - \sigma_3) (3/9) \\ &= \sigma(C) \end{aligned} \quad (I.3.15a)$$

since

$$L_i(C) = 1/3 \quad i = 1, 2, 3 \quad (I.3.15b)$$

Thus,  $f(P)$  satisfies six of our conditions, while  $(f+g)(P)$  satisfies the seventh (stability) but not all six continuity conditions. The extent to which  $f$  fails to satisfy the seventh condition is

$$\sigma(C) - f(C) = \epsilon = 1/3 (3\sigma(C) - \sigma_1 - \sigma_2 - \sigma_3) \quad (I.3.16)$$

while  $(f+g)$  fails to satisfy three continuity conditions by zero:

$$f(Q_i) + g(Q_i) - \sigma_i = f(Q_i) - \sigma_i = 0 \quad (I.3.17)$$

and three continuity conditions by  $3/4 \epsilon$ :

$$\begin{aligned} f(M_i) + g(M_i) - 1/2 (\sigma_{i+1} + \sigma_{i+2}) &= 3/4 \epsilon \\ &= 1/4 (3 \sigma(C) - \sigma_1 - \sigma_2 - \sigma_3) \end{aligned} \quad (I.3.18)$$

So, a likely candidate for approximating  $\sigma(P)$  is

$$\sigma'(P) = f(P) + ag(P) + b \quad (I.3.19)$$

where  $a$  and  $b$  chosen to minimize the error in some weighted sense.

Then, combining (I.3.12), (I.3.14), (I.3.16), and (I.3.17),

$$\sigma'(Q_i) = f(Q_i) + ag(Q_i) + b = \sigma_i + b \quad (I.3.20)$$

$$\sigma'(M_i) = 1/2 (\sigma_{i+1} + \sigma_{i+2}) + 3/4 a\epsilon + b \quad (I.3.21)$$

$$\sigma'(C) = 1/3 (\sigma_1 + \sigma_2 + \sigma_3) + a\epsilon + b = \sigma(C) - (1-a)\epsilon + b \quad (I.3.22)$$

We want to choose  $a$  and  $b$  so that stability and continuity at the corners are emphasized more strongly than continuity at the edge midpoints. Choosing

$$\begin{aligned} a &= .8 \\ b &= -\epsilon/10 \end{aligned} \quad (I.3.23)$$

we find

$$\begin{aligned} \sigma'(Q_i) &= \sigma(Q_i) - \epsilon/10 \\ \sigma'(M_i) &= \sigma(M_i) + \epsilon/2 \\ \sigma'(C) &= \sigma(C) - 3/10 \epsilon \end{aligned} \quad (I.3.24)$$

This is a reasonable compromise, being a source distribution which is not quite (linear (or continuous) on the half panel edges, and not quite taking on the desired value at  $C$ , but nearly meeting all these requirements, and thus we want the quadratic source strength on the triangular region in Figure 1.21 to be defined by (I.3.19) and (I.3.23).

#### 1.3.2.2 Computation of $[D^S]$

We now want to calculate the matrix  $D^S$  such that

$$\begin{Bmatrix} \sigma_0 \\ . \\ . \\ . \\ \sigma_{nn} \end{Bmatrix} = [D^S] \begin{Bmatrix} \sigma_1 \\ \sigma_2 \\ \sigma_3 \\ \sigma(C) \end{Bmatrix} \quad (I.3.25)$$

Now, by (I.3.12), (I.3.14), (I.3.19), (I.3.23) and (I.3.24),

$$\begin{aligned} \sigma(P) &= \sigma'(P) = \sigma_1 L_1(P) + \sigma_2 L_2(P) + \sigma_3 L_3(P) \\ &+ \frac{8}{10} (3\sigma(C) - \sigma_1 - \sigma_2 - \sigma_3) (L_2(P) L_3(P) + L_1(P) L_3(P) + L_1(P) L_2(P)) \\ &- \frac{1}{10} (3\sigma(C) - \sigma_1 - \sigma_2 - \sigma_3) \end{aligned} \quad (I.3.26)$$

$$\begin{aligned} &\sum_{i=1}^3 \sigma_i (a_i + b_i \xi + c_i \eta) \\ &+ \frac{8}{10} (3\sigma(C) - \sigma_1 - \sigma_2 - \sigma_3) \sum_{i=1}^3 (a_{i+1} + b_{i+1} \xi + c_{i+1} \eta)(a_{i+2} + b_{i+2} \xi + c_{i+2} \eta) \\ &- \frac{1}{10} (3\sigma(C) - \sigma_1 - \sigma_2 - \sigma_3) \end{aligned} \quad (I.3.27)$$

Equations (I.3.9) and (I.3.27) together define  $[D^S]$  by the requirement that the coefficients of  $1, \dots, \eta^2$  be equal, since a quadratic distribution is uniquely defined by specifying its six coefficients. For convenience, we write

$$[D^S] = [D_1^S] + [D_2^S] + [D_3^S] \quad (I.3.28)$$

where  $[D_i^S]$  are the matrices specifying the coefficients of source distribution resulting from the first, second, and third expressions in (I.3.27).

Now, analogous to (I.2.20),

$$[D_1^S] = \begin{bmatrix} a_1 & a_2 & a_3 & 0 \\ b_1 & b_2 & b_3 & 0 \\ c_1 & c_2 & c_3 & 0 \\ 0 & 0 & 0 & 0 \\ 0 & 0 & 0 & 0 \\ 0 & 0 & 0 & 0 \end{bmatrix} \quad (I.3.29)$$

The last three rows of  $[D^S]$  are zero since  $L_j$  is a linear function and thus the quadratic coefficients are zero.

Next, we see that

$$[D_2^S] = \frac{\varepsilon}{10} \begin{Bmatrix} \Sigma(a_{i+1})(a_{i+2}) \\ \Sigma(a_{i+1})(b_{i+2}) + (a_{i+2})(b_{i+1}) \\ \Sigma(a_{i+1})(c_{i+2}) + (a_{i+2})(c_{i+1}) \\ 2 \Sigma(b_{i+1})(b_{i+2}) \\ \Sigma(b_{i+1})(c_{i+2}) + (b_{i+2})(c_{i+1}) \\ 2 \Sigma(c_{i+1})(c_{i+2}) \end{Bmatrix} \begin{bmatrix} -1 & -1 & -1 & 3 \end{bmatrix} \quad (I.3.30)$$

Finally,

$$[D_3^S] = \frac{-1}{10} \begin{Bmatrix} 1 \\ 0 \\ 0 \\ 0 \\ 0 \\ 0 \\ 0 \end{Bmatrix} \begin{bmatrix} -1 & -1 & -1 & 3 \end{bmatrix}$$

The last five rows of  $[D_3^S]$  are zero since the third expression in (I.3.27) is a constant function. So, equations (I.3.28-31) define  $[D^S]$ .

### I.3.2.3 The Extension Matrix $[XHS]$

The matrix  $D^S$  is, of course, the analog of the matrix  $[G^S]^{-1}$  which occurs in the computation of subpanel splines. Also, analogously, we have

$$[HPSPL^S] = [D^S] [XHS] \quad (I.3.32)$$

where  $[XHS]$  is an extension matrix defined by

$$\begin{Bmatrix} \sigma_i \\ \sigma_{i+1} \\ \sigma_{i+2} \\ \sigma(C_i) \end{Bmatrix} = [XHS] \begin{Bmatrix} \sigma_1 \\ \vdots \\ \sigma_4 \\ \sigma_9 \end{Bmatrix} \quad (I.3.33)$$

The first three rows of  $[XHS]$  consist of a solitary unit entry, while the fourth row is computed with the aid of the subpanel splines. The quantity  $\sigma(C_i)$  is defined as the source strength at the point  $C_i$  obtained by projecting  $C_i$  to the panel. Now, if  $C_i = (\xi_i, \eta_i)$  in the local

coordinates of the subpanel on which it lies,

$$\sigma(C_j) = \sum_{i=1}^9 \xi_i n_i [SPSPL_j^S] \begin{Bmatrix} \sigma_1 \\ \vdots \\ \sigma_4 \\ \sigma_9 \end{Bmatrix} \quad (I.3.34)$$

and thus, the fourth row is  $XHS$  is

$$\sum_{i=1}^9 \xi_i n_i [SPSPL_j^S]$$

Thus, we have computed  $[XHS]$ , and so by (I.3.28-32), we have defined  $HPSPL_j^S$ .

#### I.3.2.4 Requirements for the Doublet Half Panel Spline Matrix

Finally, we compute  $[HPSPL^D]$ , which is defined by an equation analogous to (I.3.10). Consider the half panel in Figure I.20. We require that the doublet strength be quadratic on the three triangle edges, and take on the values of  $\mu$  at the three corners, the three edge midpoints, and the triangle center. By making the function quadratic on the edges, we insure continuity of the doublet strength. In contrast to the quadratic source distribution, here we have enough degrees of freedom to fulfill these conditions. In fact, the cubic function satisfying these conditions is

$$\begin{aligned} \mu'(P) = & \sum_{i=1}^3 (\mu_i L_i(P)^2 + 2 \kappa_{i+1,i+2} L_{i+1}(P) L_{i+2}(P)) \\ & + a L_1(P) L_2(P) L_3(P) \end{aligned} \quad (I.3.35)$$

where  $a$  is chosen such that  $\mu'(C) = \mu(C)$ . The other cubic terms do not appear because they do not produce quadratic functions on the triangle edges, since

$$\begin{aligned} L_i(C) &= \frac{1}{3} \\ \mu'(C) &= \frac{1}{9} (\mu_1 + \mu_2 + \mu_3) + \frac{2}{9} \sum_{i=1}^3 \kappa_{i+1,i+2} + \frac{9}{27} \end{aligned} \quad (I.3.36)$$

and thus

$$a = 27\mu(C) - 3(\mu_1 + \mu_2 + \mu_3) - 6 \sum_{i=1}^3 \kappa_{i+1,i+2} \quad (I.3.37)$$

Thus,

$$\begin{aligned} u'(P) &= \sum_{i=1}^3 (\mu_i L_i(P)^2 + 2 \kappa_{i+1, i+2} L_{i+1}(P) L_{i+2}(P)) \\ &+ 27(u(C) - \frac{1}{9} \sum_i \mu_i - \frac{2}{9} \sum_i \kappa_{i+1, i+2}) L_1(P) L_2(P) L_3(P) \end{aligned} \quad (1.3.38)$$

#### 1.3.2.5 Computation of $[DD]$

Analogously to the case of source matrices, we can write

$$\begin{aligned} u(\xi, n) &= \mu_0 + \dots + 1/2 \mu_{nn} n^2 \\ &+ 1/6 \mu_{\xi\xi\xi} \xi^3 + 1/2 \mu_{\xi\xi n} \xi^2 n + 1/2 \mu_{\xi n n} \xi n^2 + 1/6 \mu_{nnn} n^3 \end{aligned} \quad (1.3.39)$$

Then,

$$\begin{Bmatrix} \mu_0 \\ \cdot \\ \cdot \\ \cdot \\ \cdot \\ \mu_{nnn} \end{Bmatrix} = [DD] \begin{Bmatrix} \mu_1 \\ \mu_2 \\ \mu_3 \\ 23 \\ 13 \\ 12 \\ \mu(C) \end{Bmatrix} \quad (1.3.40)$$

We can write

$$[DD] = [D_1^D] + [D_2^D] \quad (1.3.41)$$

where  $D_1^D$  supplies the contribution due to the first expression in (1.3.35) and  $D_2^D$  supplies the contribution due to the second expression. Since the first expression is just the quadratic function determined by the values on the boundary of the triangle, we may apply (1.2.62), (1.2.71) and (1.2.78) to verify that





Further, we can write the quantity  $\mu$  from (1.3.37) as

$$\mu = 27 \left[ -\frac{1}{9} - \frac{1}{9} - \frac{1}{9} - \frac{2}{9} - \frac{2}{9} - \frac{2}{9} \right] \begin{pmatrix} \mu_1 \\ \mu_2 \\ \mu_3 \\ \kappa_{23} \\ \kappa_{13} \\ \kappa_{12} \\ \mu(C) \end{pmatrix} \quad (1.3.44)$$

Combining (1.3.35), (1.3.39-41), and (1.3.43) we obtain  $[D_2^0] =$

$$\left\{ \begin{array}{l} a_1 a_2 a_3 \\ a_1 a_2 b_3 + a_1 b_2 a_3 + b_1 a_2 a_3 \\ a_1 a_2 c_3 + a_1 c_2 a_3 + c_1 a_2 a_3 \\ 2(a_1 b_2 b_3 + b_1 a_2 b_3 + b_1 b_2 a_3) \\ \left( \begin{array}{l} a_1 b_2 c_3 + a_1 c_2 b_3 + b_1 a_2 c_3 \\ + b_1 c_2 a_3 + c_1 a_2 b_3 + c_1 b_2 a_3 \end{array} \right) \\ 2(a_1 c_2 c_3 + c_1 a_2 c_3 + c_1 c_2 a_3) \\ 6 b_1 b_2 b_3 \\ 2(b_1 b_2 c_3 + b_1 c_2 b_3 + c_1 b_2 b_3) \\ 2(b_1 c_2 c_3 + c_1 b_2 c_3 + c_1 c_2 b_3) \\ 6 c_1 c_2 c_3 \end{array} \right\} \begin{pmatrix} -3 & -3 & -3 & -6 & -6 & -6 & 27 \end{pmatrix} \quad (1.3.45)$$

Equations (1.3.41), (1.3.42), and (1.3.45) define  $[DD]$ .

### 1.3.2.6 The Extension Matrix $[XH^D]$

In order to complete the computation of the doublet half panel spline matrices, we must compute the extension matrix  $XH^D$  such that

$$\begin{matrix} u_1 \\ u_j \\ u_k \\ \kappa_{jk} \\ \kappa_{ik} \\ \kappa_{ij} \\ u(C) \end{matrix} = [XH^D] \begin{Bmatrix} u_1 \\ \cdot \\ \cdot \\ \cdot \\ \cdot \\ u_8 \\ u_9 \end{Bmatrix} \quad (1.3.46)$$

for an arbitrary half panel as illustrated in Figure 1.20. The first three rows consists of a single unit entry. The computation of the fourth through sixth rows follows from equation (1.2.30-31). Restating equation (1.2.75),

$$\kappa_{AB} = 2u(M) - 1/2u(A) - 1/2u(B) \quad (1.3.47)$$

Applying to Figure 1.20,

$$\kappa_{i, i(\text{mod}4)+1} = 2u_{i+4} - 1/2u_i - 1/2u_{i(\text{mod}4)+1} \quad (1.3.48)$$

with similar equations holding for the remaining two  $\kappa$ 's.

Thus to compute one of the  $\kappa$ 's, we require  $u(M_i)$ . Similarly, to compute the last row of  $[XH^D]$ , we need  $u(C_i)$ . These quantities are computed, as a linear combination to the nine panel doublet parameters, by projecting  $M_i$  and  $C_i$  to points  $M'_i$  and  $C'_i$  lying on the true (8 region) panel, and using  $u(M'_i)$  and  $u(C'_i)$ . Analogously to (1.3.34), the row vector describing  $u$  at a point  $P'$  with local coordinates  $(\xi', n')$  is

$$u(P') = \begin{bmatrix} 1 & \xi' & n' & 1/2\xi'n' & 1/2n'^2 \end{bmatrix} [SPSPL^D] \quad (1.3.49)$$

So, using (1.3.48) and (1.3.49), we may calculate the remaining rows of  $[XH^D]$ . Then, combining (1.3.40) and (1.3.46), we have

$$[HPSPL^D] = [D^D] [XH^D] \quad (1.3.50)$$

where  $\text{HPSP}^D$  is defined by the equation

$$\begin{Bmatrix} u_0 \\ \cdot \\ \cdot \\ \cdot \\ u_{nnn} \end{Bmatrix} = [\text{HPSP}^D] \begin{Bmatrix} u_0 \\ \cdot \\ \cdot \\ \cdot \\ u_g \end{Bmatrix} \quad (1.3.51)$$

## 1.4 Far Field Moments

"Far field moments" are matrices and tensors which describe various integrals of the singularity strength over a panel as a linear combination of the panel singularity parameters. In this section we define these tensors and show how they are computed from subpanel splines, and other quantities which depend only on the panel under consideration. These tensors occur in the computation of far field influence coefficients (see section J.10). They are discussed here because of their close relation with spline matrices. Section 1.4.1 defines the far field moments and section 1.4.2 shows how they are constructed.

### 1.4.1 The Defining Equations

For an arbitrary point  $Q_0$  on the panel, let

$$\begin{aligned}\vec{Q} &= \vec{Q}_0 - \vec{P}_g \\ \tilde{Q} &= [C] \vec{Q}\end{aligned}\quad (1.4.1)$$

where  $C$  is the compressible scaling matrix defined in Appendix E (for convenience, we neglect the subscript 0 in this section).

$$[C] = sa^2[1] + (1 - sa^2)[c_0 \ c_0^T] \quad (1.4.2)$$

#### 1.4.1.1 Source Far Field Moments

Recall the constant  $\kappa$  ( $2\pi$  for supersonic flow,  $4\pi$  for subsonic flow), and let  $dA_g$  be an area element in reference coordinates,  $dA_L$  ( $u d\xi d\eta$ ) an area element in local coordinates. Again, the transformation from reference to local coordinates is defined by the non-orthogonal transformation (E.0.1), and thus  $dA_g$  need not equal  $dA_L$ . Denote a panel by  $\Sigma$ .

Then before symmetrization (a process we define later) is performed, the source far field moments are a row vector  $FFM_1^S$  of length 5, a  $3 \times 5$  matrix  $FFM_2^S$ , and a  $3 \times 3 \times 5$  tensor  $FFM_3^{S,0}$ , defined by

$$\frac{1}{\kappa} \iint_{\Sigma} \sigma dA_g = [FFM_1^S] \vec{\sigma} \quad (1.4.3)$$

$$\frac{1}{\kappa} \iint_{\Sigma} \tilde{Q} \sigma dA_g = [FFM_2^S] \vec{\sigma} \quad (1.4.4)$$

$$\frac{1}{\kappa} \iint_{\Sigma} \tilde{Q}_i \tilde{Q}_j \sigma dA_g = [FFM_3^{S,0}]_{i,j,\dots} \vec{\sigma} \quad (1.4.5)$$

$$\text{where } \vec{\sigma} = \begin{Bmatrix} \sigma_1 \\ \cdot \\ \cdot \\ \cdot \\ \sigma_4 \\ \sigma_9 \end{Bmatrix} \quad (I.4.6)$$

We now briefly explain the subscript notation we use in section I.4. Let  $A$  be a vector,  $[B]$  a matrix, and  $\{C\}$  a three-dimension tensor. Then  $A_i$  is the  $i$ th entry of  $A$ ,  $[B]_{ij}$  is the  $(i,j)$  entry of  $B$ , and  $\{C\}_{ijk}$  is the  $(i,j,k)$  entry of  $C$ . Further,  $\{B_{\cdot,j}\}$  and  $\{B_{i,\cdot}\}$  are, respectively, the row and column vectors whose  $i$ th entry is  $[B]_{ij}$ . Finally,  $[C_{i,\cdot,\cdot}]$  is the matrix whose  $(j,k)$  entry is  $\{C\}_{ijk}$ . Other vectors and matrices, such as  $\{B_{i,\cdot,\cdot}\}$ ,  $\{C_{\cdot,j,k}\}$ , and  $[C_{\cdot,j,\cdot}]$  are defined analogously. Thus a dot as a subscript is used to define a matrix or vector which is a subset of the original tensor or matrix. A single dot corresponds to only one varying index, and thus represents a row or column vector, while a pair of dots represents a matrix.

#### I.4.1.2 Symmetrization

We will also perform partial symmetrization on tensors as follows. First, let  $\{A_{ijn}\}$  be a tensor such that  $i$  and  $j$  run from 1 to 3.

Then the symmetrization of  $A_{ijn}$  over the first two indices is the  $(6 \times N)$  matrix  $[A]$  ( $N$  the maximum of  $n$ )

$$\begin{aligned} A_{kn} &= A_{kkn} & k &= 1, 2, 3 \\ A_{k+3,n} &= A_{i(k),j(k),n} + A_{j(k),i(k),n} & n &= 1, \dots, N \end{aligned} \quad (I.4.9)$$

where

$$\begin{aligned} i(k) &= k(\text{mod } 3) + 1 \\ j(k) &= (k+1)(\text{mod } 3) + 1 \end{aligned} \quad (I.4.10)$$

Later, we will also come across the symmetrization over three indices  $i, j, m$  of a 4-tensor  $B_{ijmn}$ , where  $i, j, m$  run from 1 to 3. The result is a

10xN matrix [B] (N the maximum of n):

$$B_{kn} = B_{kkkn}$$

$$B_{k+3,n} = B_{k,i(k),i(k),n} + B_{i(k),k,i(k),n} + B_{i(k),i(k),k,n}$$

$$B_{k+6,n} = B_{k,j(k),j(k),n} + B_{j(k),k,j(k),n} + B_{j(k),j(k),k,n}$$

$$k = 1, 2, 3, \quad n = 1, \dots, N$$

$$B_{10,n} = B_{123n} + B_{132n} + B_{213n} + B_{231n} + B_{312n} + B_{321n}$$

$$n = 1, \dots, N$$

(1.4.11)

Now, the matrix  $FFM_3^S$  is the symmetrization of  $FFM_3^{S,0}$  over the first two indices.

#### 1.4.1.3 Doublet Far Field Moments

Next, the doublet far field moments are defined as follows.  $FFM_0^D$  is the row vector of length 9 defined by

$$\frac{sb^2}{\kappa} \iint_{\Sigma} \mu \, dA_g = [FFM_0^D] \vec{\mu} \quad (1.4.12)$$

$$\text{where } \vec{\mu} = \begin{Bmatrix} \mu_1 \\ \vdots \\ \mu_9 \end{Bmatrix}$$

(1.4.13)

$FFM_1^D$  is a (3x9) matrix defined by

$$\frac{sb^2}{\kappa} \iint_{\Sigma} \mu \hat{n} dA_g = [FFM_1^D] \mu \quad (1.4.14)$$

where  $\hat{n}$  is the unit normal in reference coordinates.

$FFM_2^D$  is the (6x9) matrix which is the symmetrization over i and j of the (3x3x9) tensor  $(FFM_2^{D,0})_{ijn}$

$$\frac{sb^2}{\kappa} \iint_{\Sigma} \mu \hat{n}_i \tilde{Q}_j dA_g = [FFM_2^{D,0}]_{i,j,\dots} \vec{\mu} \quad (1.4.15)$$

$FFM_3^D$  is the (10x9) matrix which is the symmetrization over i,j,k of the (3x3x3x9) tensor  $FFM_3^{D,0}$  :

$$\frac{sB^2}{K} \iint_{\Sigma} \mu \hat{n}_i \tilde{Q}_j dA_g = [FFM_3^{D,0}]_{ijk,..} \vec{u} \quad (1.4.16)$$

#### 1.4.1.4 Doublet Velocity Far Field Moments

Now, because of the removal of the line vortex terms from the doublet velocity (see section B.3), we need further far field moments defining integrals related to the quantity  $\hat{n} \times \vec{\nabla}_\mu$  (cf., (B.3.9)). The first of these is the (3x9) matrix  $FFM_4^D$ :

$$\frac{sB^2}{K} \iint_{\Sigma} (\vec{\nabla}_\mu \times \hat{n})^T dA_g = [FFM_4^D] \vec{u} \quad (1.4.17)$$

Next is  $FFM_5^D$ , the 3x3x9 tensor defined by

$$\frac{sB^2}{K} \iint_{\Sigma} (\vec{\nabla}_\mu \times \hat{n})_i \tilde{Q}_j dA_g = [FFM_5^D]_{i,j,..} \vec{u} \quad (1.4.18)$$

Finally,  $FFM_6^D$  is the (3x6x9) tensor which is the symmetrization in j and k (but not i) of the (3x3x3x9) tensor  $(FFM_6^{D,0})_{ijkn}$ :

$$\frac{sB^2}{2K} \iint_{\Sigma} (\vec{\nabla}_\mu \times \hat{n})_i \tilde{Q}_j \tilde{Q}_k dA_g = [FFM_6^{D,0}]_{i,j,k,..} \vec{u} \quad (1.4.19)$$

#### 1.4.2 Construction of the Far Field Moments

##### 1.4.2.1 Preliminaries

Now, over each subpanel,  $\mu$  varies quadratically, while  $\sigma$ , ( $\mu \times n$ ), and  $Q$  vary linearly in local coordinates. If we inspect the far field moment defining equations, we see that the integrals may be as much as fourth order in local coordinates and  $n$ . Thus for each subpanel, we will have to compute

$$C_{MN} = \int \xi^{M-1} n^{N-1} d\xi dn, \quad M + N \leq 6 \quad (1.4.20)$$

where  $\Delta_i$  is the  $i$ th subpanel.

The quantities  $C_{MN}^i$  are computed by a recursive process which we discuss in section 1.4.3.

#### 1.4.2.2 [FFM<sub>1</sub><sup>S</sup>]

We will now compute the far field moment tensors. Starting with FFM<sub>1</sub><sup>S</sup>, let us consider equation (1.4.3). Defining the area Jacobian,

$$J_i = \frac{dA_g}{d\xi d\eta} \quad (1.4.21)$$

the fact that the reference to local transformation is linear with constant coefficients implies that  $J_i$  is a constant over a subpanel, and that we may compute  $J_i$  by

$$J_i = \frac{\text{Area of subpanel in reference coordinates}}{\text{Area of subpanel in local coordinates}} \quad (1.4.22)$$

Here, what we mean by the area of a triangle in a particular coordinate system is that we express the vertices in that coordinate system and then apply (D.2.16).

Now,

$$\iint \sigma dA_g = \sum_{i=1}^8 \iint_{\Delta_i} \sigma(\xi, \eta) J_i d\xi d\eta \quad (1.4.23)$$

$$= \sum_{i=1}^8 \iint_{\Delta_i} (\sigma_0 + \sigma_\xi \xi + \sigma_\eta \eta) J_i d\xi d\eta \quad (1.4.24)$$

$$= \sum_{i=1}^8 J_i \begin{bmatrix} C_{11}^i & C_{21}^i & C_{12}^i \end{bmatrix} \begin{bmatrix} \sigma_0 \\ \sigma_\xi \\ \sigma_\eta \end{bmatrix} \quad \text{ith subpanel} \quad (1.4.25)$$

Since

$$\begin{bmatrix} \sigma_0 \\ \sigma \\ \sigma_\eta \end{bmatrix}_i = [\text{SPSPL}_i^S] \sigma \quad (1.4.26)$$

we have

$$\iint \sigma dA_g = \sum_{i=1}^8 J_i \begin{bmatrix} C_{11}^i & C_{21}^i & C_{12}^i \end{bmatrix} [\text{SPSPL}_i^S] \sigma \quad (1.4.27)$$

Comparing to (1.4.3), we have

$$\text{FFM}_1^S = \sum_{i=1}^8 [\text{SPFFM}_{1,j}^S] \quad (1.4.28a)$$



where

$$[\text{SPFFM}_i^S] = \frac{J_i}{K} [C_{11}^i \ C_{21}^i \ C_{12}^i] [\text{SPSPL}_i^S] \quad (1.4.28b)$$

SPFFM stands for subpanel far field moment. In order to generalize (1.4.28) to the remaining far field moments, while avoiding equations even more complicated than those which follow, we introduce additional notation.

We define  $D_i^S$  to be the  $2 \times 2 \times 5$  tensor defined by

$$\begin{bmatrix} \sigma_n & \sigma_n \\ \sigma_\xi & 0 \end{bmatrix}_{jk} = L_i^S j,k,j \vec{\sigma} \quad (1.4.29)$$

Here the subscripts  $j,k$  on a matrix mean the  $(j,k)$ th entry of the matrix. We see by comparison to (1.4.26) that

$$\begin{aligned} (D_i^S)_{11n} &= [\text{SPSPL}_i^S]_{1n} \\ (D_i^S)_{21n} &= [\text{SPSPL}_i^S]_{2n} \\ (D_i^S)_{12n} &= [\text{SPSPL}_i^S]_{3n} \\ (D_i^S)_{22n} &= 0 \end{aligned} \quad (1.4.30a)$$

In a similar vein, we later use the  $(3 \times 3 \times 9)$  tensor  $(D_i^D)$ , defined by

$$\begin{bmatrix} u_0 & u_n & \frac{1}{2} u_{nn} \\ u_\xi & u_n & 0 \\ \frac{1}{2} u & 0 & 0 \end{bmatrix}_{jk} = L_i^D j,k,j \vec{u} \quad (1.4.30b)$$

Entries of  $D_i^D$  correspond to entries of  $\text{SPSPL}_i^D$  under the correspondence below, where a zero denotes the corresponding entry of  $D_i^D$  is zero.

Subscript of  $D_i^0$

1,1,n

2,1,n

1,2,n

3,1,n

2,2,n

1,3,n

3,2,n

2,3,n

3,3,n

$\Leftrightarrow$

Subscript of  $SPSPL_i^0$

1,n

2,n

3,n

4,n

5,n

6,n

0

0

0

(1.4.30c)

In this notation, we can write the nth entry of  $FFM_1^S$  as

$$(FFM_1^S)_n = \frac{1}{K} \sum_{i=1}^8 (J_i) \sum_{j=1}^2 \sum_{k=1}^2 (C_{JK}) \left( D_i^S \right)_{JKn} \quad (1.4.31)$$

1.4.2.3  $[FFM_2^S]$

Next, we consider  $FFM_2^S$ . The quantity  $\vec{Q} = [C] (\vec{Q}_0 - \vec{P}_g)$  can be written in local coordinates as

$$\vec{Q} = [C] (\vec{Q}_0 - \vec{P}_g) = C \vec{Q} = [CA^{-1}] \begin{Bmatrix} \xi - \xi_g \\ \eta - \eta_g \\ \zeta - \zeta_g \end{Bmatrix} \quad (1.4.32)$$

where A is the reference to local transformation and  $P_g$  has the local coordinates

$$\begin{Bmatrix} \xi_g \\ \eta_g \\ \zeta_g \end{Bmatrix}$$

where  $\xi_g$  is zero if  $P_g$  lies on the plane of the subpanel.

Now,

$$\begin{aligned}
 & \frac{1}{K} \sum_{i=1}^8 \iint_{\Delta_i} \sigma(\xi, \eta) \tilde{Q} \, dA_g = \\
 & \frac{1}{K} \sum_{i=1}^8 \iint_{\Delta_i} \sum_{j=1}^2 J_i \begin{bmatrix} 1 & \eta \\ \xi & \xi_\eta \end{bmatrix}_{JK} \begin{bmatrix} \sigma_0 & \sigma_\eta \\ \sigma & 0 \end{bmatrix}_{JK} [CA^{-1}] \begin{Bmatrix} \xi \\ \eta \\ 0 \end{Bmatrix} d\xi d\eta \\
 & = \frac{1}{K} \sum_{i=1}^8 \sum_{j=1}^2 \iint_{\Delta_i} J_i \begin{bmatrix} 1 & \eta \\ \xi & \xi_\eta \end{bmatrix}_{JK} \begin{bmatrix} \sigma_0 & \sigma_\eta \\ \sigma & 0 \end{bmatrix}_{JK} [CA^{-1}] \begin{Bmatrix} \xi_g \\ \eta_g \\ \zeta_g \end{Bmatrix} d\xi d\eta
 \end{aligned}
 \tag{I.4.33}$$

Now,  $\begin{Bmatrix} \xi_g \\ \eta_g \\ \zeta_g \end{Bmatrix}$  are the local coordinates of  $\vec{P}_g - \vec{C}_i$ , where  $\vec{C}_i$  is the

origin of the coordinate system of the  $i$ th sub-panel. Recall from section I.2.1.1 that  $C_i = P_i$  if  $i \leq 4$ , and otherwise  $C_i = P_g$ . So,

$$[CA^{-1}] \begin{Bmatrix} \xi_g \\ \eta_g \\ \zeta_g \end{Bmatrix} = -[C] (\vec{C}_i - \vec{P}_g)
 \tag{I.4.34}$$

where  $C_i$  and  $P_g$  are in reference coordinates.

Applying (I.4.3), (I.4.28), and (I.4.34), we see that the integrand of the second term of (I.4.33) is

$$[C] (\vec{C}_i - \vec{P}_g) \text{SPFFM}_{1,i} \vec{S}
 \tag{I.4.35}$$

Now, the first expression in (I.4.33) is the column vector whose  $j$ th entry is

$$\frac{1}{\kappa} \sum_{q=1}^5 \sum_{i=1}^8 \sum_{n=1}^3 J_i [CA^{-1}]_{jn} \begin{Bmatrix} \xi \\ n \\ 0 \end{Bmatrix} \sum_{J=1}^2 \sum_{K=1}^2 \begin{bmatrix} 1 & n \\ \xi & \xi_n \end{bmatrix}_{JK} (D_i^S)_{JKq} \sigma_q d\xi d_n \quad (1.4.36)$$

$$n = 1, 2, 3$$

$$q = 1, \dots, 4, 5$$

where we denote  $\sigma_q$  as  $\sigma_5$  for simplicity.

Let us define the matrix  $[K^{S,i}]$  whose  $(n,q)$  entry is

$$K_{nq}^{S,i} = \sum_{J=1}^2 \sum_{K=1}^2 \begin{Bmatrix} \xi \\ n \\ 0 \end{Bmatrix}_n \begin{bmatrix} 1 & n \\ \xi & \xi_n \end{bmatrix}_{JK} (D_i^S)_{JKq} d\xi d_n \quad (1.4.37)$$

So, the expression in (1.4.36) becomes

$$\frac{1}{\kappa} \sum_{i=1}^8 \sum_{j=1}^3 \sum_{q=1}^5 J_i [CA^{-1}]_{jn} (K_{nq}^{S,i}) \sigma_q \quad (1.4.38)$$

while (1.4.37) can also be written

$$K_{nq}^{S,i} = \sum_{J=1}^2 \sum_{K=1}^2 (D_i^S)_{JKq} \begin{Bmatrix} C_{J+1,K}^i \\ C_{J,K+1}^i \\ 0 \end{Bmatrix}_n \quad (1.4.39)$$

Replacing the first and second terms on the right hand side of equation (1.4.33) with the expressions given by (1.4.38) and (1.4.35), respectively, we get

$$\frac{1}{\kappa} \sum_{i=1}^8 \sigma(\xi, n) \tilde{Q} dA_g =$$

$$\frac{1}{\kappa} \sum_{i=1}^8 \sum_{n=1}^3 \sum_{q=1}^5 J_i [CA^{-1}]_{jn} K_{nq}^{S,i} \sigma_q + \frac{1}{\kappa} \sum_{i=1}^8 [C](\vec{C}_i - \vec{P}_g) \underline{SPFFM}_{1,1}^S \vec{\sigma} \quad (1.4.40)$$

Comparing with (I.4.4), we have

$$[FFM_2^S] = \sum_{i=1}^9 [SPFFM_{2,i}^S] \quad (I.4.41)$$

where

$$[SPFFM_{2,i}^S] = \frac{J_i}{K} [CA^{-1}] [KS, i] + \frac{1}{K} [C] (\vec{C}_i - \vec{P}_g) [SPFFM_{1,i}^S] \quad (I.4.42)$$

#### I.4.2.4 $[FFM_3^S]$

Construction of  $FFM_3^S$  is even more complex.  
First,

$$\frac{1}{2K} \iint_{\Delta_1} \sigma(\xi, \eta) \tilde{Q}_j \tilde{Q}_k dA_g =$$

$$\frac{J_1}{2K} \iint_{\Delta_1} \left( \sum_{j=1}^2 \sum_{k=1}^2 \begin{bmatrix} 1 & n \\ \xi & \xi_n \end{bmatrix}_{JK} \begin{bmatrix} \sigma_0 & \sigma_n \\ \sigma \xi & 0 \end{bmatrix}_{JK} [CA^{-1}] \begin{Bmatrix} \xi - \xi_g \\ n - n_g \\ \xi - \xi_g \end{Bmatrix}_j \right) \quad (I.4.43)$$

$$\cdot [CA^{-1}] \begin{Bmatrix} \xi - \xi_g \\ n - n_g \\ \xi - \xi_g \end{Bmatrix}_k \Bigg) d\xi d\eta =$$

$$\frac{J_1}{2K} \iint_{\Delta_1} \sum_{j=1}^2 \sum_{k=1}^2 \begin{bmatrix} 1 & n \\ \xi & \xi_n \end{bmatrix}_{JK} \begin{bmatrix} \sigma_0 & \sigma_n \\ \sigma \xi & 0 \end{bmatrix}_{JK} \left( [CA^{-1}] \begin{Bmatrix} \xi \\ n \\ 0 \end{Bmatrix}_j \right) \left( [CA^{-1}] \begin{Bmatrix} \xi \\ n \\ 0 \end{Bmatrix}_k \right) d\xi d\eta$$

$$- \frac{1}{2} \left( [CA^{-1}] \begin{Bmatrix} \xi_g \\ n_g \\ \xi_g \end{Bmatrix}_j \right) \left( [SPFFM_{2,i}^S] \vec{\sigma} \right)_k - \frac{1}{2} \left( [CA^{-1}] \begin{Bmatrix} \xi_g \\ n_g \\ \xi_g \end{Bmatrix}_k \right) [SPFFM_{2,i}^S] \sigma$$

$$+ \frac{1}{2} \left( [CA^{-1}] \begin{Bmatrix} \xi - \xi_g \\ n - n_g \\ \xi - \xi_g \end{Bmatrix}_j \right) \left( [CA^{-1}] \begin{Bmatrix} \xi - \xi_g \\ n - n_g \\ \xi - \xi_g \end{Bmatrix}_k \right) [SPFFM_{1,i}^S] \vec{\sigma} \quad (I.4.44)$$

Equation (I.4.44) follows from (I.4.28) and (I.4.42). Now, let us introduce the (3x3x5) tensor  $R^{S,i}$ :

$$(R^{S,i})_{nsq} = \sum_{J=1}^2 \sum_{K=1}^5 \int_{\Delta_i} \begin{Bmatrix} \xi \\ n \\ 0 \end{Bmatrix}_n \begin{Bmatrix} \xi \\ n \\ 0 \end{Bmatrix}_s \begin{bmatrix} 1 & n \\ \xi & \xi_n \end{bmatrix}_{JK} (D_i^S)_{JKq} d\xi d_n \quad (I.4.45)$$

Then

$$(R^{S,i})_{nsq} = \sum_{J=1}^2 \sum_{K=1}^5 \begin{bmatrix} C_{J+2,K}^i & C_{J+1,K+1}^i & 0 \\ C_{J+1,K-1}^i & C_{J,K+2}^i & 0 \\ 0 & 0 & 0 \end{bmatrix}_{ns} (D_i^S)_{JKq} \quad (I.4.46)$$

Substituting (I.4.45) in (I.4.44) and noting that

$$[A^{-1}] \begin{Bmatrix} \xi_9 \\ n_9 \\ 0 \end{Bmatrix} = (\vec{P}_9 - \vec{C}_i) \quad (I.4.47)$$

we obtain

$$\begin{aligned} \frac{1}{2\kappa} \int_{\Delta_i} \sigma(\cdot, n) Q_j Q_k dA_g &= \frac{J_i}{2\kappa} \sum_{n=1}^3 \sum_{q=1}^5 [CA^{-1}]_{jn} [CA^{-1}]_{ks} (R^{S,i})_{nsq} \sigma_q \\ &- \frac{1}{2} ([C] (\vec{P}_9 - \vec{C}_i))_j ([SPFFM_2^S, i] \vec{\sigma})_k - \frac{1}{2} ([C] (\vec{P}_9 - \vec{C}_i))_k ([SPFFM_2^S, i] \vec{\sigma})_j \\ &+ \frac{1}{2} ([C] (\vec{P}_9 - \vec{C}_i))_j ([C] (\vec{P}_9 - \vec{C}_i))_k [SPFFM_1^S, i] \vec{\sigma} \end{aligned} \quad (I.4.48)$$

Comparing with (I.4.5),

$$\{FFM_3^{S,0}\} = \frac{1}{2} \sum_{i=1}^8 \{SPFFM_3^S, i\} \quad (I.4.49)$$

where  $(SPFFM_{3,i})_{ikq}$

$$\frac{J_i}{K} \sum_{n=1}^3 \sum_{s=1}^3 [CA^{-1}]_{jn} [CA^{-1}]_{ks} (RS, i)_{nsq}$$

$$\begin{aligned} & - ([C] (\vec{p}_g - \vec{c}_i))_j [SPFFM_{2,i}^S]_{kq} - ([C] (\vec{p}_g - \vec{c}_i))_k [SPFFM_{2,i}^S]_{jq} \\ & + ([C] (\vec{p}_g - \vec{c}_i))_j ([C] (\vec{p}_g - \vec{c}_i))_k [SPFFM_{1,i}^S]_{jq} \end{aligned} \quad (I.4.50)$$

I.4.2.5  $FFM_0^D$

Next we consider doublet far field moments. First,

$$\iint_{\Delta i} \mu(\xi, n) dA_g = J_i \iint_{\Delta i} \sum_{J=1}^3 \sum_{K=1}^9 \begin{bmatrix} 1 & n & n^2 \\ \xi & \xi_n & n^2 \\ \xi^2 & \xi_n^2 & \xi^2 n^2 \end{bmatrix} JK \begin{bmatrix} \mu_0 & \mu_n & 1/2 \mu_{nn} \\ \mu & \mu \xi_n & 0 \\ 1/2 \mu \xi \xi_n & 0 & 0 \end{bmatrix} JK \quad (I.4.51)$$

$$= J_i \iint_{\Delta i} \sum_{J=1}^3 \sum_{K=1}^9 \begin{bmatrix} 1 & n & n^2 \\ \xi & \xi_n & \xi_n^2 \\ \xi^2 & \xi_n^2 & \xi^2 n^2 \end{bmatrix} (D_i^D)_{JKq} \mu_q d\xi d_n \quad (I.4.52)$$

and so, by (I.4.12) and (I.4.30b)

$$FFM_0^D = \sum_{i=1}^8 SPFFM_{0,i}^D \quad (I.4.53)$$

where

$$(SPFFM_{0,i}^D)_q = J_i \frac{s_B^2}{K} \sum_{J=1}^3 \sum_{K=1}^9 C_{JK}^i (D_i^D)_{JKq} \quad (I.4.54)$$

#### 1.4.2.6 $FFM_1^D$

Inserting the vector  $\hat{n}$  in (1.4.51) and (1.4.52) does not change the validity of the equations, and thus by (1.4.14)

$$[FFM_1^D] = \sum_{i=1}^8 [SPFFM_{1,i}^D] \quad (1.4.55)$$

where

$$[SPFFM_{1,i}^D]_{jq} = \frac{J_i s b^2}{\kappa} \hat{n}_j \sum_{J=1}^3 \sum_{K=1}^3 C_{JK}^i (D_i^D)_{JKq} \quad (1.4.56)$$

#### 1.4.2.7 $FFM_2^{D,0}$ and $FFM_3^{D,0}$

Now, the formulas for  $FFM_2^{D,0}$  and  $FFM_3^{D,0}$  are computed in the same manner as the corresponding source<sup>3</sup>far field moments, except that the introduction of the normal vector adds an extra dimension to each tensor, the summation over J and K goes to 3, and there are nine panel doublet parameters where there were five panel source parameters.

So, analogously to (1.4.41), we have

$$\begin{Bmatrix} D,0 \\ FFM_2 \end{Bmatrix} = \sum_{i=1}^8 \begin{Bmatrix} D,0 \\ SPFFM_{2,i} \end{Bmatrix} \quad (1.4.57)$$

where

$$(SPFFM_{2,i}^{D,0})_{jkq} = \frac{s b^2}{\kappa} \hat{n}_j \sum_{n=1}^3 [CA^{-1}]_{kn} (K_{nq}^{D,i}) + ([C](\vec{C}_i - \vec{P}_q))_j [SPFFM_{1,i}^D]_{kq} \quad (1.4.58)$$

and

$$[K^{D,i}]_{nq} = \sum_{J=1}^3 \sum_{K=1}^3 (D_i^D)_{JKq} \begin{Bmatrix} C_{J+1,K}^i \\ C_{J,K+1}^i \\ 0 \end{Bmatrix}_n \quad (1.4.59)$$

And, analogously to (1.4.49),

$$\begin{Bmatrix} D,0 \\ FFM_3 \end{Bmatrix} = \frac{1}{2} \sum_{i=1}^8 \begin{Bmatrix} D \\ SPFFM_{3,i}^D \end{Bmatrix} \quad (1.4.60)$$



where

$$\begin{aligned}
 (\text{SPFFM}_3^D)_{mj kq} &= \frac{J_1 s \beta^2}{\kappa} \hat{n}_m \sum_{n=1}^3 \sum_{s=1}^3 [\text{CA}^{-1}]_{jn} [\text{CA}^{-1}]_{ks} (R^D, i)_{nsq} \\
 &- ([C] (\hat{p}_g - \hat{c}_i))_j [\text{SPFFM}_2^D]_{mkq} - ([C] (\hat{p}_g - \hat{c}_i))_k [\text{SPFFM}_2^D]_{jmq} \\
 &+ ([C] (\hat{p}_g - \hat{c}_i))_j ([C] (\hat{p}_g - \hat{c}_i))_k [\text{SPFFM}_1^D]_{mq} \quad (I.4.61)
 \end{aligned}$$

and

$$(R^D, i)_{nsq} = \sum_{J=1}^3 \sum_{K=1}^3 \begin{bmatrix} c_{J+2,K}^i & c_{J+1,K+1}^i & 0 \\ c_{J+1,K+1}^i & c_{J,K+2}^i & 0 \\ 0 & 0 & 0 \end{bmatrix} (D^D)_{JKq} \quad (I.4.62)$$

#### I.4.2.8 [FFM<sub>4</sub><sup>D</sup>]

Next we consider the doublet far field moments which involve  $(\hat{n} \times \hat{\nabla} u)$ .  
First,  $\hat{\nabla} u =$

$$\begin{aligned}
 \begin{bmatrix} \partial u / \partial x \\ \partial u / \partial y \\ \partial u / \partial z \end{bmatrix} &= (\text{by (E.1.11)}) \quad [A]^T \begin{bmatrix} \partial u / \partial \xi \\ \partial u / \partial \eta \\ \partial u / \partial \zeta \end{bmatrix} = \\
 [A]^T &= \begin{bmatrix} \mu_\xi + \mu_{\xi\xi} \xi + \mu_{\eta\eta} \\ \mu_\eta + \mu_{\xi\eta} \xi + \mu_{\eta\eta\eta} \\ 0 \end{bmatrix} \quad (I.4.63)
 \end{aligned}$$

Now,

$$\frac{\partial \mu}{\partial \xi} = \mu_{\xi} + \mu_{\xi} \xi + \mu_{\xi \eta} \eta =$$

$$\frac{1}{\xi} \sum_{J=1}^3 \sum_{K=1}^9 \begin{bmatrix} 0 \cdot \mu_0 & 0 \cdot \mu_{\eta} & 0 \cdot \frac{1}{2} \\ 1 \cdot \mu_{\xi} & 1 \cdot \mu_{\xi \eta} & 1 \cdot 0 \\ 2 \cdot \frac{1}{2} \mu_{\xi \xi} & 2 \cdot 0 & 2 \cdot 0 \end{bmatrix}_{JK} \begin{bmatrix} 1 & \eta & \eta^2 \\ \xi & \xi \eta & \xi \eta^2 \\ \xi^2 & \xi^2 \eta & \xi^2 \eta^2 \end{bmatrix}_{JK}$$

$$= \sum_{J,K} \sum_{q=1}^9 (D_i^D)_{JKq} \mu_q \cdot (J-1) \xi^{J-2} \eta^{K-1} \quad (1.4.64)$$

Similarly,

$$\frac{\partial \mu}{\partial \eta} = \sum_{J=1}^3 \sum_{K=1}^9 (D_i^D)_{JKq} \mu_q (K-1) \xi^{J-1} \eta^{K-2} \quad (1.4.65)$$

So,

$$\iint_{\Delta_1} \begin{Bmatrix} \partial \mu / \partial \xi \\ \partial \mu / \partial \eta \\ 0 \end{Bmatrix} d\xi d\eta = [GRM_i] \mu \quad (1.4.66)$$

where  $[GRM_i]$  is the  $3 \times 9$  matrix

$$[GRM_i]_{jq} = \sum_{J,K} (D_i^D)_{JKq} \begin{Bmatrix} (J-1) C_{J-1,K}^i \\ (K-1) C_{J,K-1}^i \\ 0 \end{Bmatrix}_j \quad (1.4.67)$$

Note that  $C_{r,0}^i$  and  $C_{0,s}^i$  are not defined; however, these are multiplied by zero wherever they occur, and the intended value of the product is zero.

Now,  $[A]$  is a matrix of constant coefficients, and  $\hat{n}$  is constant over a

subpanel, and thus they can be removed from the integral:

$$\begin{aligned}
 \frac{s\beta^2}{\kappa} \iint_{\Delta_1} (\hat{n} \times \vec{\nabla} u) d\xi d\eta &= \frac{s\beta^2}{\kappa} \iint_{\Delta_1} \hat{n} \times \left( [A^T] \begin{Bmatrix} \partial u / \partial \xi \\ \partial u / \partial \eta \\ 0 \end{Bmatrix} \right) d\xi d\eta \\
 &= \frac{s\beta^2}{\kappa} \hat{n} \times ([A^T] [GRM_i] \vec{u}) = \\
 &= \frac{s\beta^2}{\kappa} \sum_{q=1}^9 \sum_{k=1}^3 (\hat{n} \times [A^T]_{.,k}) [GRM_i]_{k,q} u_q
 \end{aligned} \tag{1.4.68}$$

Thus,

$$[FFM_4^D] = \sum_{i=1}^8 [SPFFM_{4,i}^D] \tag{1.4.69}$$

where

$$[SPFFM_{4,i}^D]_{.,q} = - \frac{J_i s\beta^2}{\kappa} \sum_{k=1}^3 (\hat{n} \times \{A_{k,.}\}) [GRM_i]_{kq} \tag{1.4.70}$$

The minus sign occurs because  $FFM_4^D$  is determined as an integral of  $(\vec{\nabla} u \times \hat{n})$ , while for readability we have used  $(\hat{n} \times \vec{\nabla} u)$ .

#### 1.4.2.9 $[FFM_5^D]$

Next we consider  $FFM_5^D$ . We have

$$\begin{aligned}
 \frac{s\beta^2}{\kappa} \iint_{\Delta_1} \left( \hat{n} \times A^T \begin{Bmatrix} \partial u / \partial \xi \\ \partial u / \partial \eta \\ 0 \end{Bmatrix} \right)_j \tilde{Q}_k d\xi d\eta &= \\
 \frac{s\beta^2}{\kappa} \iint_{\Delta_1} \sum_{n=1}^3 (\hat{n} \times (A^T_{.,n}))_j \begin{Bmatrix} \partial u / \partial \xi \\ \partial u / \partial \eta \\ 0 \end{Bmatrix}_n \left( [CA^{-1}] \begin{Bmatrix} \xi - \xi_9 \\ \eta - \eta_9 \\ \zeta - \zeta_9 \end{Bmatrix} \right)_k d\xi d\eta
 \end{aligned} \tag{1.4.71}$$

$$= \frac{s\theta^2}{\kappa} \sum_{n=1}^3 \sum_{q=1}^9 (\hat{n} \times (A_n, \cdot))_j \sum_{\substack{J=1 \\ K=1}}^3 [CA^{-1}] \begin{bmatrix} (J-1)\xi^{J-1}_{nK-1} & (K-1)\xi^{J_{nK}-2} & 0 \\ (J-1)\xi^{J-2}_{nK} & (K-1)\xi^{J-1}_{nK-1} & 0 \\ 0 & 0 & 0 \end{bmatrix}_{kn}$$

$$- \frac{s\theta^2}{\kappa} \iint_{\Delta_1} \sum_{n=1}^3 (\hat{n} \times (A_n, \cdot))_j \left( [CA^{-1}] \begin{Bmatrix} \xi_9 \\ \eta_9 \\ \zeta_9 \end{Bmatrix} \right)_k \begin{Bmatrix} \partial \nu / \partial \\ \partial \nu / \partial \eta \\ 0 \end{Bmatrix}_n d\xi d\eta$$

(1.4.72)

$$= \frac{s\theta^2}{\kappa} \sum_{\substack{n=1 \\ s=1}}^3 \sum_{q=1}^9 (\hat{n} \times ([A]_{n, \cdot}))_j [CA^{-1}]_{ks} (GRMD_i)_{snq} \mu_q$$

(1.4.73)

$$+ \frac{1}{J_i} ([C] (\vec{P}_9 - \vec{C}_i))_k [SPFFM^D_{4,1}]_{jq} \mu_q$$

where

$$(GRMD_i)_{snq} = \sum_{\substack{l=1 \\ K=1}}^3 (D_i^D)_{JKq} \begin{bmatrix} (J-1)C^i_{JK} & (K-1)C^i_{J+1,K-1} & 0 \\ (J-1)C^i_{J-1,K+1} & (K-1)C^i_{JK} & 0 \\ 0 & 0 & 0 \end{bmatrix}_{sn}$$

(1.4.74)

Thus,

$$(FFM^D_5) = \sum_{i=1}^8 (SPFFM^D_{5,i})$$

(1.4.75)

where

$$(SPFFM^D_{s,i})_{jkq} = - \frac{J_i s\theta^2}{\kappa} \sum_{\substack{n=i \\ s=1}}^3 (\hat{n} \times (A_n, \cdot))_j [CA^{-1}]_{ks} (GRMD_i)_{nsq}$$

$$- ([C] (\vec{P}_9 - \vec{C}_i))_k [SPFFM^D_{4,1}]_{jq}$$

(1.4.76)

I.4.2.10 FFM<sub>6</sub><sup>D,0</sup>

Finally we calculate FFM<sub>6</sub><sup>D,0</sup>. Now,

$$\frac{s\beta^2}{\kappa} \iint_{\Delta} \left( \hat{n} \times [A^T] \begin{pmatrix} \partial u / \partial \xi \\ \partial u / \partial \eta \\ 0 \end{pmatrix} \right)_j \tilde{Q}_k \tilde{Q}_m d\xi d\eta =$$

$$\frac{s\beta^2}{\kappa} \sum_{n=1}^3 (\hat{n} \times (A^T_{\cdot,n}))_j \begin{pmatrix} \partial u / \partial \eta \\ \partial u / \partial \eta \\ 0 \end{pmatrix}_n \left\{ [CA^{-1}] \begin{pmatrix} \xi - \xi_9 \\ \eta - \eta_9 \\ \zeta - \zeta_9 \end{pmatrix} \right\}_k \left\{ [CA^{-1}] \begin{pmatrix} \xi - \xi_9 \\ \eta - \eta_9 \\ \zeta - \zeta_9 \end{pmatrix} \right\}_m d\xi d\eta$$

(I.4.77)

$$= \frac{s\beta^2}{\kappa} \sum_{n=1}^3 (\hat{n} \times (A_{n,\cdot}))_j \begin{pmatrix} \partial u / \partial \eta \\ \partial u / \partial \eta \\ 0 \end{pmatrix}_n \left\{ [CA^{-1}] \begin{pmatrix} \xi \\ \eta \\ 0 \end{pmatrix} \right\}_k \left\{ [CA^{-1}] \begin{pmatrix} \xi \\ \eta \\ 0 \end{pmatrix} \right\}_m d\xi d\eta$$

$$+ \sum_{q=1}^9 ([C] (\vec{p}_9 - \vec{c}_1))_k (SPFFM^D_{5,1})_{jmq} \mu_q + \frac{1}{J_1} \sum_{q=1}^9 \mu_q ([C] (p_9 - c_1))_m (SPFFM^D_{5,1})_{jkl}$$

$$- \frac{1}{J_1} \sum_{q=1}^9 ([C] (\vec{p}_9 - \vec{c}_1))_k ([C] (\vec{p}_9 - \vec{c}_1))_m [SPFFM^D_{4,1}]_{jq} \mu_q$$

(I.4.78)

Now,

$$\iint_{\Delta_1} \begin{pmatrix} \partial u / \partial \xi \\ \partial u / \partial \eta \\ 0 \end{pmatrix}_n \begin{pmatrix} \xi \\ \eta \\ 0 \end{pmatrix}_k \begin{pmatrix} \xi \\ \eta \\ 0 \end{pmatrix}_m d\xi d\eta =$$

$$\iint_{\Delta_1} \sum_{J,K} \sum_{q=1}^9 (D_1^D)_{JKq} \begin{pmatrix} (J-1)\xi^{J-2}\eta^{K-1} \\ (K-1)\xi^{J-1}\eta^{K-2} \\ 0 \end{pmatrix}_n \begin{pmatrix} \xi \\ \eta \\ 0 \end{pmatrix}_k \begin{pmatrix} \xi \\ \eta \\ 0 \end{pmatrix}_m \mu_q d\xi d\eta$$

$$= \sum_{q=1}^9 (GRMDD_1)_{nkmq} \mu_q$$

(I.4.79)

where  $(GRMDD_i)_{jkmq} =$

$$\sum_{J=1}^3 \sum_{K=1}^3 (J-1) (D_i^D)_{JKq} \begin{bmatrix} C_{J+1,K-1}^i & C_{J,K+1}^i & 0 \\ C_{J,K+1}^i & C_{J-1,K+2}^i & 0 \\ 0 & 0 & 0 \end{bmatrix}_{km} \quad (1.4.80)$$

$$(GRMDD_i)_{2kmq} = \sum_{J=1}^3 \sum_{K=1}^3 (K-1) (D_i^D)_{JKq} \begin{bmatrix} C_{J+2,K-1}^i & C_{J+1,K}^i & 0 \\ C_{J+1,K}^i & C_{J+1,K}^i & 0 \\ 0 & 0 & 0 \end{bmatrix}_{km} \quad (1.4.81)$$

$$\text{and } (GRMDD_i)_{3kmq} = 0 \quad (1.4.82)$$

Thus the first term in (1.4.78) is

$$\frac{s\delta^2}{K} \sum_{n=1}^3 \sum_{q=1}^9 (\hat{n} \times (A_{n..})_j [CA^{-1}]_{ms} (GRMDD_i)_{nrsq} \nu_q \quad (1.4.83)$$

Combining (1.4.19), (1.4.78), and (1.4.83), we have

$$FFM_6^{D,0} = \sum_{i=1}^8 (SPFFM_{6,i}^{D,0})$$

$$\text{where } (SPFFM_{6,i}^D)_{jknq} = -J_i \frac{s\delta^2}{2K} \sum_{r=1}^3 \sum_{s=1}^9 (n \times (A_{n..}))_j [CA^{-1}]_{kr} [CA^{-1}]_{ms}$$

$$\begin{aligned} (GRMDD_i)_{nrsq} &= \frac{1}{2} ([C](\vec{P}_9 - \vec{C}_1))_k (SPFFM_{5,i}^D)_{jmq} - \frac{1}{2} ([C](\vec{P}_9 - \vec{C}_1))_m (SPFFM_{5,i}^D)_{jknq} \\ &+ \frac{1}{2} ([C](\vec{P}_9 - \vec{C}_1))_k ([C](\vec{P}_9 - \vec{C}_1))_m [SPFFM_{4,i}^D]_{j,q} \end{aligned} \quad (1.4.85)$$

#### 1.4.3 Basic Far Field Moments

This completes our discussion of far field moment computation, except that

we have deferred the computation of

$$C_{MN}^i = \iint_{\Delta_i} \xi^{M-1} \eta^{N-1} d\xi d\eta \quad (I.4.86)$$

#### I.4.3.1 Reduction to Line Integrals

In Figure I.22 we illustrate a subpanel, located arbitrarily in the  $(\xi, \eta)$  plane. Now, defining  $\eta_j$  to be the function, such that if  $(\xi, \eta)$  lies on side  $j$  then

$$\eta = \eta_j(\xi) \quad (I.4.87)$$

we can write  $C_{MN}$  as an integral over regions 1 and 4, plus another integral over regions 2 and 3:

$$C_{MN} = \int_{\xi_1}^{\xi_3} \int_{\eta_3(\xi)}^{\eta_2(\xi)} \xi^{M-1} \eta^{N-1} d\xi d\eta + \int_{\xi_3}^{\xi_2} \int_{\eta_3(\xi)}^{\eta_1(\xi)} \xi^{M-1} \eta^{N-1} d\xi d\eta \quad (I.4.88)$$

Integrating with respect to  $\eta$ ,

$$C_{MN} = \int_{\xi_1}^{\xi_3} \xi^{M-1} \left( \frac{1}{N} \right) \eta^N \Big|_{\eta_3(\xi)}^{\eta_2(\xi)} d\xi + \int_{\xi_3}^{\xi_2} \xi^{M-1} \left( \frac{1}{N} \right) \eta^N \Big|_{\eta_3(\xi)}^{\eta_1(\xi)} d\xi \quad (I.4.89)$$

$$= \frac{1}{N} \int_{\xi_1}^{\xi_3} (\xi^{M-1}) \eta_2(\xi)^N d\xi + \frac{1}{N} \int_{\xi_3}^{\xi_2} \xi^{M-1} \eta_1(\xi)^N d\xi - \frac{1}{N} \int_{\xi_1}^{\xi_2} \xi^{M-1} \eta_3(\xi)^N d\xi \quad (I.4.90)$$

Similarly, we could write

$$\xi = \xi_i(\eta) \quad (I.4.91a)$$

on side  $i$ , and integrate first with respect to  $\xi$ , obtaining

$$\begin{aligned}
 C_{MN} &= \int_{n_2}^{n_1} \int_{\xi_3(n)}^{\xi_1(n)} \xi^{M-1} n^{N-1} d\xi dn + \int_{r,1}^{n_3} \int_{\xi_2(n)}^{\xi_1(n)} \xi^{M-1} n^{N-1} d\xi dn = \\
 &= \frac{1}{M} \int_{n_3}^{n_1} \xi_1(n)^M n^{N-1} dn - \frac{1}{M} \int_{n_1}^{n_3} \xi_2(n)^M n^{N-1} dn \\
 &\quad - \frac{1}{M} \int_{n_2}^{n_1} \xi_3(n)^M n^{N-1} dn
 \end{aligned} \tag{I.4.92}$$

Now, let  $\hat{n}_i$  be the outward pointing unit normal to side  $i$ . Then, if

$$\hat{t}_i = \begin{Bmatrix} \hat{\xi}_i \\ \hat{n}_i \end{Bmatrix} \tag{I.4.93}$$

is a unit edge tangent, we see that

$$\begin{Bmatrix} \hat{n}_i, \xi \\ \hat{n}_i, n \end{Bmatrix} = \hat{n}_i = \begin{Bmatrix} n_i \\ -\xi_i \end{Bmatrix} \tag{I.4.94}$$

Now, on edge  $i$ ,

$$\begin{aligned}
 d\xi &= \hat{\xi}_i dl \\
 dn &= n_i dl
 \end{aligned} \tag{I.4.95}$$

By (I.4.94), we have along side  $i$ ,

$$d\xi = -\hat{n}_i, n dl \tag{I.4.96}$$

$$dn = \hat{n}_i, \xi dl \tag{I.4.97}$$



Substituting (I.4.96) in (I.4.90), we get

$$C_{MN} = \frac{1}{N} \int_{\text{side 2}} \xi^{M-1} \eta^N \hat{n}_{2,\xi} d\xi \\ + \frac{1}{N} \int_1 \xi^{M-1} \eta^N \hat{n}_{1,\eta} d\eta + \frac{1}{N} \int_3 \xi^{M-1} \eta^N \hat{n}_{3,\eta} d\eta \quad (I.4.98)$$

Substituting (I.4.97) in (I.4.92), we get, similarly,

$$C_{MN} = \frac{1}{M} \int_1 \xi^M \eta^{N-1} \hat{n}_{1,\xi} d\xi + \frac{1}{M} \int_2 \xi^M \eta^{N-1} \hat{n}_{2,\xi} d\xi \\ + \frac{1}{M} \int_3 \xi^M \eta^{N-1} \hat{n}_{3,\xi} d\xi \quad (I.4.99)$$

Taking  $\frac{N}{M+N}$  times (I.4.98) plus  $\frac{M}{M+N}$  times (I.4.99) we have

$$C_{MN} = \frac{1}{M+N} \sum_{i=1}^3 \int_{\text{side } i} \xi^{M-1} \eta^{N-1} (\xi \hat{n}_{i,\xi} + \eta \hat{n}_{i,\eta}) d\xi \quad (I.4.100a)$$

$$\text{Now, call } d_j = \left\{ \begin{matrix} \xi \\ \eta \end{matrix} \right\} \hat{n}_j \\ \xi \hat{n}_{j,\xi} + \eta \hat{n}_{j,\eta} = \left\{ \begin{matrix} \xi \\ \eta \end{matrix} \right\} \hat{n}_j \quad (I.4.101)$$

Then  $d_j$  can be considered the distance (with sign) from the origin to the line containing side  $i$ . Defining

$$G_{MN}^j = \int_{\text{side } j} \xi^{M-1} \eta^{N-1} d\xi \quad (I.4.102)$$

we have

$$C_{MN} = \frac{1}{M+N} \sum_{j=1}^3 d_j G_{MN}^j \quad (I.4.103)$$

#### I.4.3.2 Computation of the Line Integrals

We obtain two recursion relations for the  $G_{MN}^j$ . First, substitution

of (I.4.102) and (I.4.103) in (I.4.100), yields

$$d_j G_{MN}^j = \hat{n}_{j, \epsilon} G_{M+1, N}^j + \hat{n}_{j, n} G_{M, N+1}^j \quad (I.4.104)$$

Second, using intergration by parts (with all subscripts modulo 3):

$$\begin{aligned} \int_{\epsilon_{j+1}}^{\epsilon_{j+2}} M (\epsilon^{M-1}) n_j(\epsilon)^N d\epsilon &= (\epsilon_{j+2})^M (n_{j+2})^N - (\epsilon_{j+1})^M (n_{j+1})^N \\ &- \int_{\epsilon_{j+1}}^{\epsilon_{j+2}} (\epsilon^M)^N n_j(\epsilon)^{N-1} \frac{dn_j}{d\epsilon} d\epsilon \end{aligned} \quad (I.4.105)$$

But by (I.4.97)

$$\frac{dn_j}{d\epsilon} = - \frac{\hat{n}_{j, \epsilon}}{\hat{n}_{j, n}} \quad (I.4.106)$$

and so

$$\begin{aligned} M \int_{\epsilon_{j+1}}^{\epsilon_{j+2}} (\epsilon^{M-1}) n_j(\epsilon)^N d\epsilon &= (\epsilon_{j+2})^M (n_{j+2})^N - (\epsilon_{j+1})^M (n_{j+1})^N \\ &- N \int_{\text{side } j} (\epsilon^M)^{N-1} \hat{n}_{j, \epsilon} d\epsilon \end{aligned} \quad (I.4.107)$$

Applying (I.4.96) and (I.4.102), we have

$$-N \hat{n}_{j, n} G_{M, N+1}^j = (\epsilon_{j+2})^M (n_{j+2})^N - (\epsilon_{j+1})^M (n_{j+1})^N - N \hat{n}_{j, \epsilon} G_{M+1, N}^j \quad (I.4.108)$$

Defining

$$D_{MN}^j = \epsilon_{j+2}^{M-1} n_{j+2}^{N-1} - \epsilon_{j+1}^{M-1} n_{j+1}^{N-1} \quad (I.4.109)$$

we get

$$N \hat{n}_{j, \epsilon} G_{M+1, N}^j - M \hat{n}_{j, n} G_{M, N+1}^j = D_{M+1, N+1}^j \quad (I.4.110)$$

We now apply (I.4.104) and (I.4.110) to obtain  $G_{M, N}^j$ . We consider two cases.

Case 1  $\hat{n}_{j,n} < \hat{n}_{j,\xi}$

Setting  $M=0$  in (I.4.110) yields

$$G_{1,N}^j = \frac{1}{N\hat{n}_{j,\xi}} D_{1,N+1}^j \quad (I.4.111)$$

Substituting  $M$  for  $M+1$  in (I.4.104) gives

$$G_{M,N}^j = \frac{d_j}{\hat{n}_{j,\xi}} G_{M-1,N}^j - \frac{\hat{n}_{j,n}}{\hat{n}_{j,\xi}} G_{M-1,N+1}^j \quad (I.4.112)$$

Equations (I.4.111) and (I.4.112) allow us to obtain any  $G_{MN}^j$  we wish, since  $\hat{n}_{j,\xi} > 0$

Case 2  $n_{j,\xi} < n_{j,n}$

Setting  $N=0$  in (I.4.110) gives

$$G_{M,1}^j = \frac{-1}{M\hat{n}_{j,n}} D_{M+1,1}^j \quad (I.4.113)$$

Substituting  $N$  for  $N+1$  in (I.4.104) gives

$$G_{M,N}^j = \frac{d_j}{\hat{n}_{j,n}} G_{M,N-1}^j \quad (I.4.114)$$

This concludes our discussion of basic far field moments, which are defined by (I.4.103), (I.4.109), and the above recursions.

## I.5 Constrained Least Squares

### I.5.1 Definition of the Problem

In this section we discuss the solution to the following rather general problem, called the constrained least squares problem. Let  $A$  be a  $j \times n$  matrix,  $0 < j < n$ , of rank  $j$ . Let  $A'$  be a  $k \times n$  matrix,  $j + k \geq n$ . Let  $\vec{b}$ ,  $\vec{b}'$ , and  $\vec{w}$  be vectors of length  $j$ ,  $k$ , and  $k$ , respectively. Then we wish to find the  $n \times (j+k)$  matrix LSQ such that the vector  $\vec{x}$  satisfying

$$[A]_{j \times n} \vec{x}_{n \times 1} = \vec{b} \quad (I.5.1)$$

while minimizing

$$J = \sum_{i=1}^k w_i^2 \left( \sum_{s=1}^n A'_{is} x_s - b'_i \right)^2 \quad (I.5.2)$$

is given by

$$\vec{x} = [LSQ]_{n \times (j+k)} \begin{pmatrix} \vec{b} \\ \vec{b}' \end{pmatrix} \quad (I.5.3)$$

### I.5.2 Elimination of the Weights

Now, first we simplify (I.5.2) by noting that if we define a  $(k \times k)$  matrix  $[W]$ :

$$[W]_{ij} = \delta_{ij} w_i \quad (I.5.4)$$

then

$$\begin{aligned} J &= \sum_{i=1}^k \left( \sum_{s=1}^n w_i A'_{is} x_s - w_i b'_i \right)^2 \\ &= \sum_{i=1}^k \left[ \sum_{j=1}^k \left( \sum_{s=1}^n w_{ij} A'_{js} x_s - w_{ij} b'_j \right) \right]^2 \\ &= \sum_{i=1}^k \left( \sum_{s=1}^n \bar{A}'_{is} x_s - b_i \right)^2 \end{aligned} \quad (I.5.5)$$

where

$$\begin{aligned} [\bar{A}] &= [W] [A'] \\ \vec{b} &= [W] \vec{b}' \end{aligned} \quad (I.5.6)$$

### I.5.3 The Case of No Exact Constraints

First, we will consider the minimization of  $J$  in (I.5.5) in the special case when  $j=0$ ; that is, when there are no exact constraints on  $x$  of the form (I.5.1). Now, the quantity  $J$  is a quadratic function in the variables  $(x_s)$ , and since it is a non-negative function, we see that it is minimized for that vector  $x$  for which all first derivatives of the expression with respect to the  $x_s$ 's are zero. That is, minimization of (I.5.5) is equivalent to the requirement

$$\frac{\partial}{\partial x_l} \sum_{i=1}^k \left( \sum_{s=1}^n \bar{A}_{is} x_s - b_i \right)^2 = 0 \quad (I.5.7)$$

$l = 1, \dots, n$

Now,

$$\frac{\partial}{\partial x_l} \sum_{i=1}^k \left( \sum_{s=1}^n \bar{A}_{is} x_s - b_i \right)^2 =$$

$$\sum_{i=1}^k 2 \left( \sum_{s=1}^n \bar{A}_{is} x_s - b_i \right) \frac{\partial}{\partial x_l} \sum_{s=1}^n \bar{A}_{is} x_s = \quad (I.5.8)$$

$$2 \sum_{i=1}^k \left( \sum_{s=1}^n \bar{A}_{is} x_s - b_i \right) \bar{A}_{il} = \quad (I.5.9)$$

$$2 \sum_{i=1}^k \bar{A}_{il} (A\bar{x} - \bar{b})_i = 2(\bar{A}^T \bar{A} \bar{x} - \bar{A}^T \bar{b})_l = 0 \quad (I.5.10)$$

Since (I.5.10) holds for each value of  $l, l = 1, \dots, n$ , we have

$$[\bar{A}^T \bar{A}] \bar{x} = [\bar{A}^T] \bar{b} \quad (I.5.11)$$

or

$$\bar{x} = [[\bar{A}^T \bar{A}]^{-1} \bar{A}^T] \bar{b} \quad (I.5.12)$$

Comparing to (I.5.3) and (I.5.6), and recalling  $j=0$ , we get

$$[LSQ] = [A^T W^T W A]^{-1} [A^T W^T] [W] \quad (I.5.13)$$

Within the PAN AIR code, equation (I.5.11) is solved without actually forming  $[A^T A]$  and inverting it. The method actually used there, which involves factorization of  $[A^T A]$  into a product of lower triangular and upper triangular matrices, is more efficient and more precise than the method indicated by (I.5.13).

#### I.5.4 Reduction of the General Case

Next, let us assume  $j > 0$ , so that there are non-trivial exact constraints of the form (I.5.1). Since  $A$  has rank  $j$ , its columns can be rearranged (that is, "pivoting" performed) so that the first  $j$  columns of the revised matrix  $A^*$  are linearly independent, and thus

$$[A^*] = [A_{11} \ j \times j \quad | \quad A_{12} \ j \times (n-j)] \quad (I.5.14)$$

Here, the relationship between  $A^*$  and  $A$  is that

$$[A^*]_{j \times n} = [A]_{j \times n} [P]_{n \times n} \quad (I.5.15a)$$

where  $[P]$  is a product of matrices which are the identity except for one non-zero off-diagonal term (for any real number  $a$ , adding  $a$  times column  $i$  to column  $j$  is performed by multiplying on the right by the matrix with 1's on the diagonal, the value  $a$  in the  $(i,j)$  position, and 0's elsewhere; its inverse has  $-a$  in the  $(i,j)$  position).

That is, a typical matrix  $P$  is

$$P = \begin{bmatrix} 1 & & & 0 \\ 0 & 1 & & \\ 0 & 0 & 1 & \\ 0 & a & 0 & 1 \end{bmatrix} \quad (I.5.15b)$$

$$P^{-1} = \begin{bmatrix} 1 & & & 0 \\ 0 & 1 & & \\ 0 & 0 & 1 & \\ 0 & -a & 0 & 1 \end{bmatrix} \quad (I.5.15c)$$

So, (I.5.1) becomes

$$[A] \vec{x} = [A^*] [P]^{-1} \vec{x} = [A_{11} \ A_{12}]_{j \times n} (P^{-1} \vec{x})_{n \times 1} = \vec{b} \quad (I.5.16)$$

Writing

$$p-1 \vec{x} = \begin{Bmatrix} \vec{x}_1^{j \times 1} \\ \vec{x}_2^{(n-j) \times 1} \end{Bmatrix} \quad (1.5.17)$$

we have

$$[A_{11} \ A_{12}] \begin{Bmatrix} \vec{x}_1 \\ \vec{x}_2 \end{Bmatrix} = \vec{b} \quad (1.5.18)$$

while we also want to minimize

$$\left| [A_{21} \ A_{22}] \begin{Bmatrix} \vec{x}_1 \\ \vec{x}_2 \end{Bmatrix} - \vec{b}' \right|^2 \quad (1.5.19)$$

where

$$[A_{21}^{k \times j} \ A_{22}^{k \times (n-j)}] = [A]^{k \times n} [p-1]^{n \times n} \quad (1.5.20)$$

Now, since the  $j$  columns of  $A_{11}$  are independent,  $A_{11}$  is invertible, and thus, by (1.5.18),

$$[A_{11}] x_1 = -[A_{12}] x_2 + b \quad (1.5.21)$$

or

$$\vec{x}_1^{(j \times 1)} = [A_{11}^{-1}]^{j \times j} - [A_{12}]^{j \times (n-j)} \vec{x}_2^{(n-j) \times 1} + \vec{b}^{(j \times 1)} \quad (1.5.22)$$

Substituting (1.5.22) into (1.5.19), we want to minimize

$$\begin{aligned} & \left| [A_{21}] \vec{x}_1 + [A_{22}] \vec{x}_2 - \vec{b}' \right|^2 = \\ & \left| \begin{aligned} & -[A_{21}]^{k \times j} [A_{11}^{-1}]^{j \times j} [A_{12}]^{j \times (n-j)} \vec{x}_2^{(n-j) \times 1} \\ & + [A_{21}]^{k \times j} [A_{11}^{-1}]^{j \times j} \vec{b}^{(j \times 1)} - \vec{b}'^{(k \times 1)} + [A_{22}] \vec{x}_2 \end{aligned} \right|^2 \end{aligned} \quad (1.5.23)$$

But this is just a least squares problem with no exact constraints, that is, it requires the minimization of

$$\left| [A^0] \vec{x}_2 - \vec{b}_0 \right|^2 \quad (1.5.24)$$

where

$$[A^0]^{k \times (n-j)} = -[A_{21}]^{k \times j} [A_{11}^{-1}]^{j \times j} [A_{12}]^{j \times (n-j)} + [A_{22}] \quad (1.5.25)$$

and

$$\vec{b}_0^{k \times 1} = -[A_{21}]^{(k \times j)} [A_{11}^{-1}]^{j \times j} \vec{b}^{(j \times 1)} + \vec{b}^{(k \times 1)} \quad (1.5.26)$$

This minimization procedure is described by equations (1.5.5-12), and results in a matrix  $LSQ^0$  such that

$$\vec{x}_2^{(n-j) \times 1} = [LSQ^0]^{(n-j) \times k} \vec{b}_0^{(k \times 1)} \quad (1.5.27)$$

Combining (1.5.22), (1.5.26), and (1.5.27), we have obtained  $\vec{x}_1$  and  $\vec{x}_2$ , and as linear combinations of entries of  $\vec{b}$  and  $\vec{b}'$ . Thus, we have shown in principle how the constrained least square problem is solved. Considerations of efficiency cause complexities which will not be discussed here.



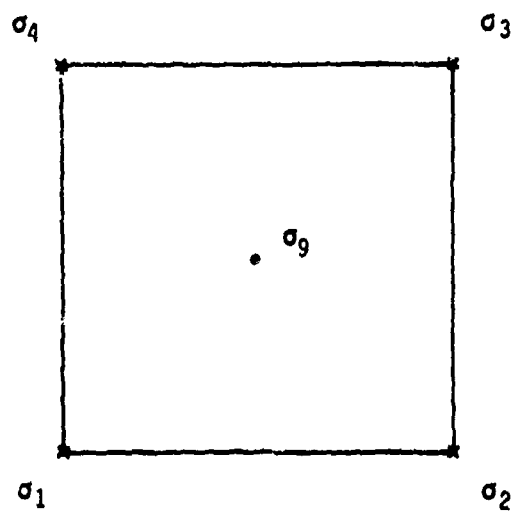


Figure I.1a - Panel source parameter locations

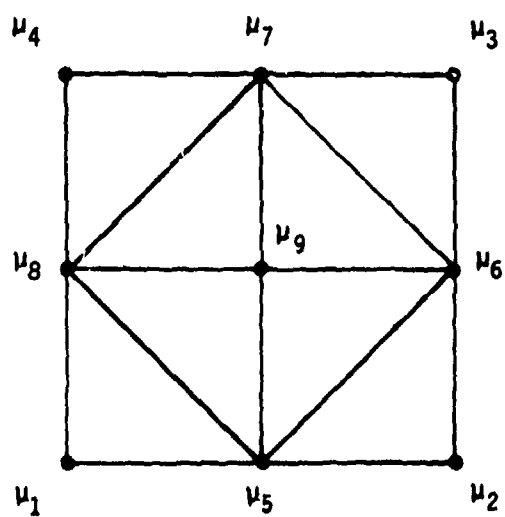


Figure I.1b - Panel doublet parameter locations

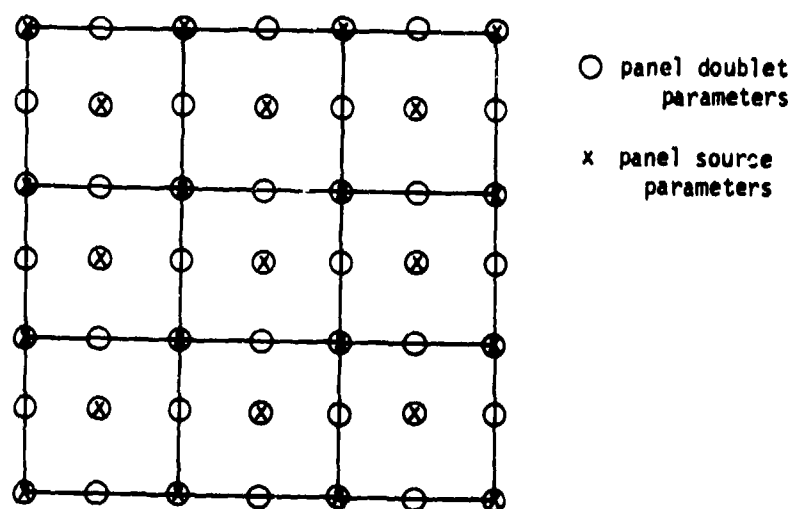


Figure I.1c - Panel singularity parameter locations for a nine-panel network

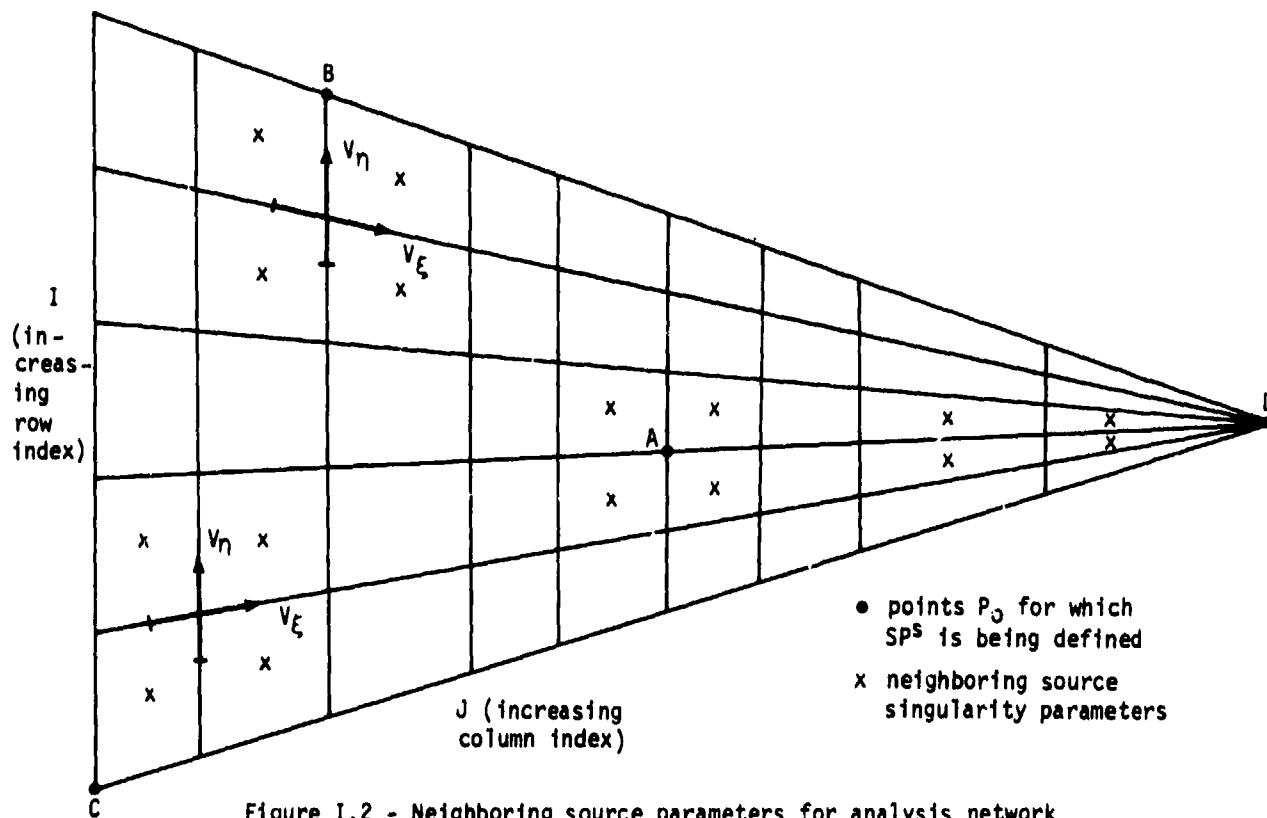


Figure I.2 - Neighboring source parameters for analysis network

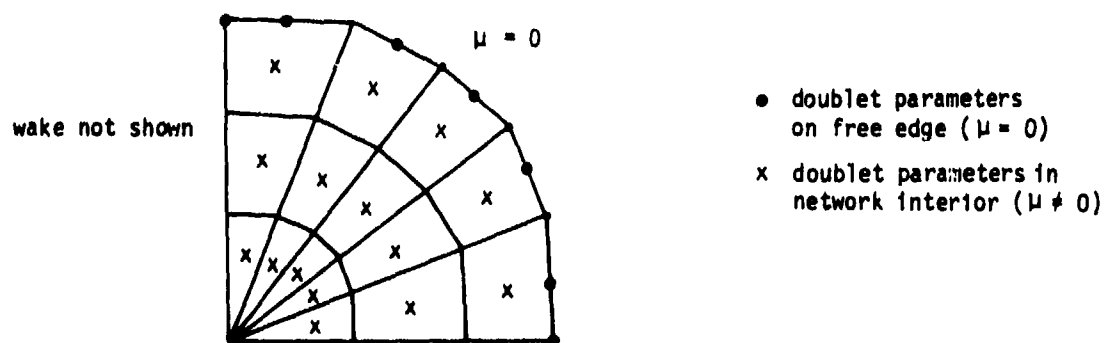


Figure I.3 - Thin wing with curved planform

- x points  $P_0$  for which  $SP^D$  is being defined
- neighboring singularity parameters for exact fit
- neighboring singularity parameters for weighted least squares fit

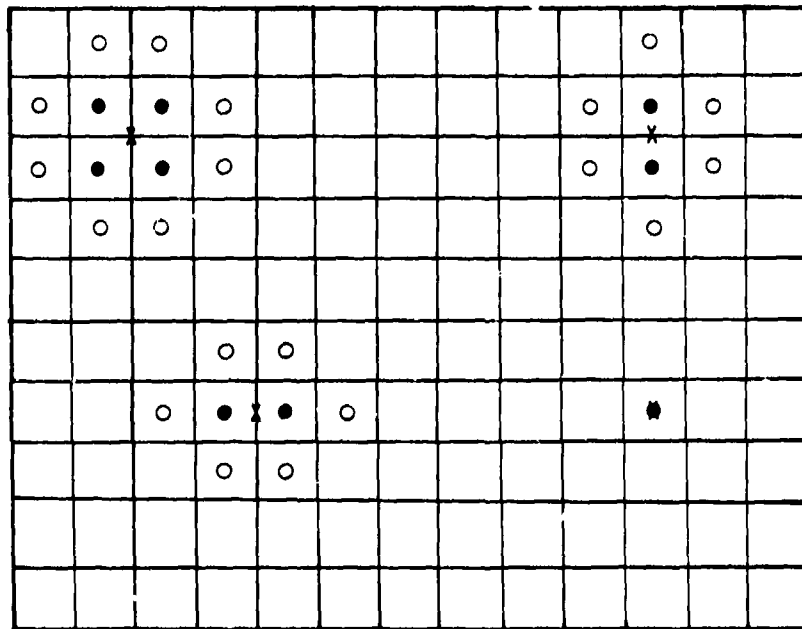


Figure 1.4a - Neighboring singularity parameters ( $P_0$  away from network edge)

- x points  $P_0$
- + neighbors for exact fit
- neighbors for least squares fit

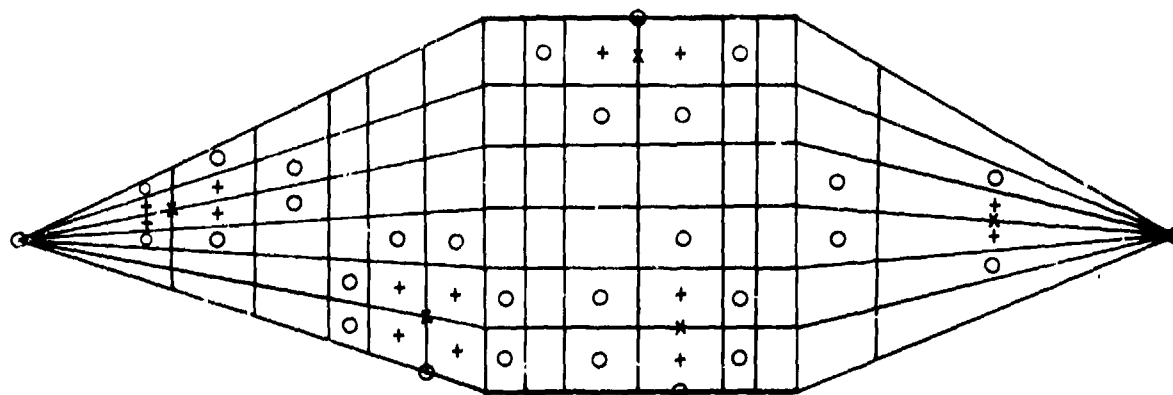


Figure 1.4b - Neighboring points for least squares fit ( $P_0$  near network edge)

- x points  $P_0$
- neighboring singularity parameters for exact fit
- o neighboring singularity parameters for least squares fit

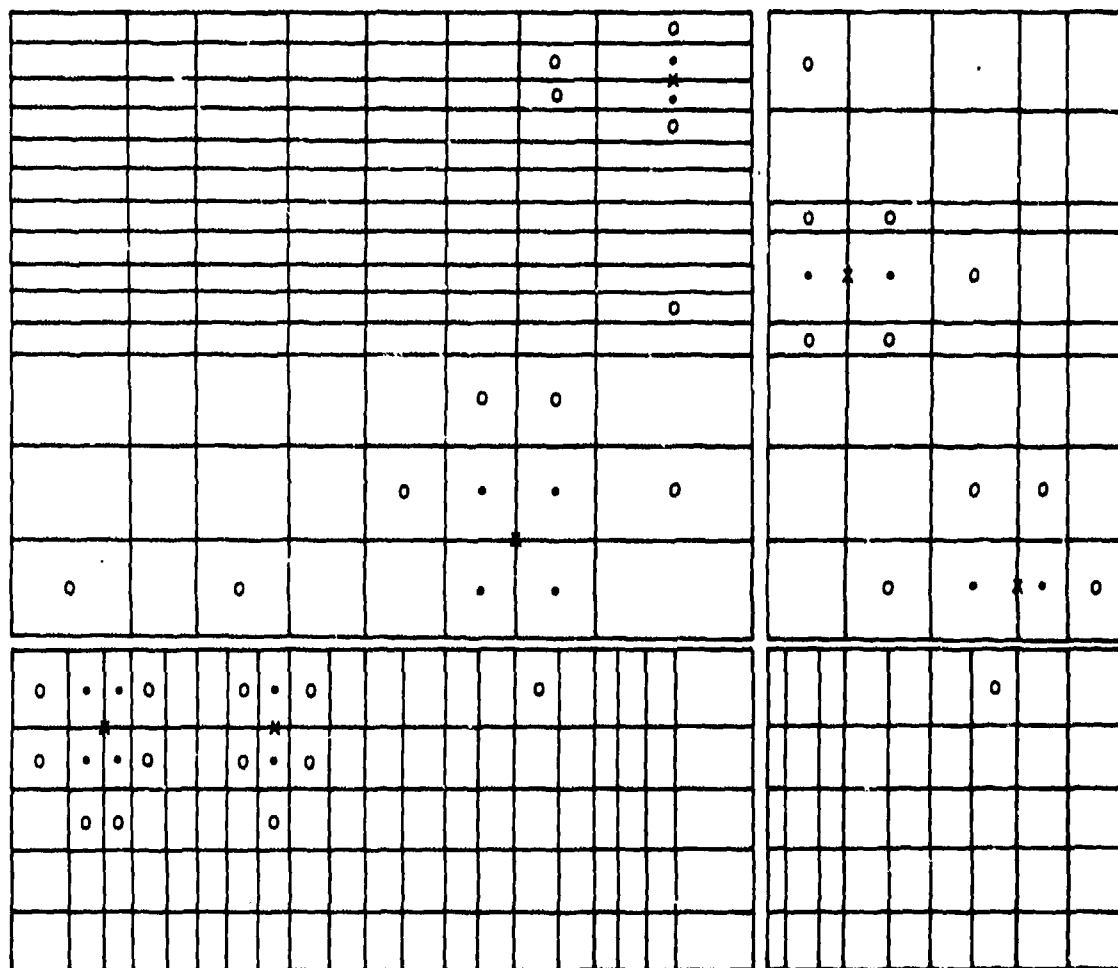


Figure 1.4c - Neighboring points for least squares fit  
( $P_0$  near a smooth abutment)

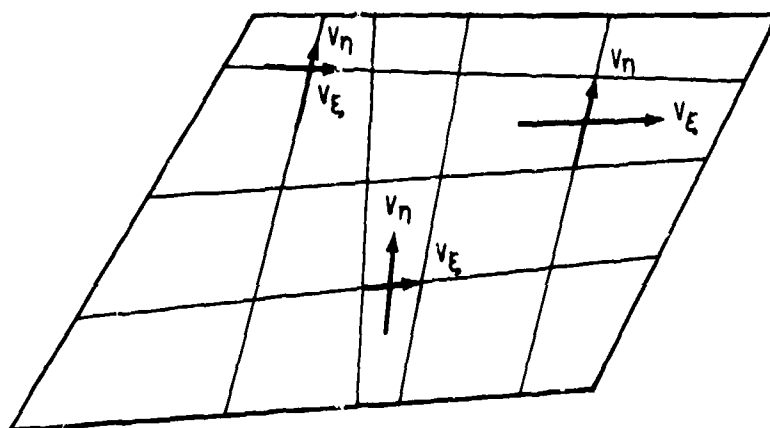


Figure I.5 - Basis Vectors for local Coordinate System for Spline Vector Construction

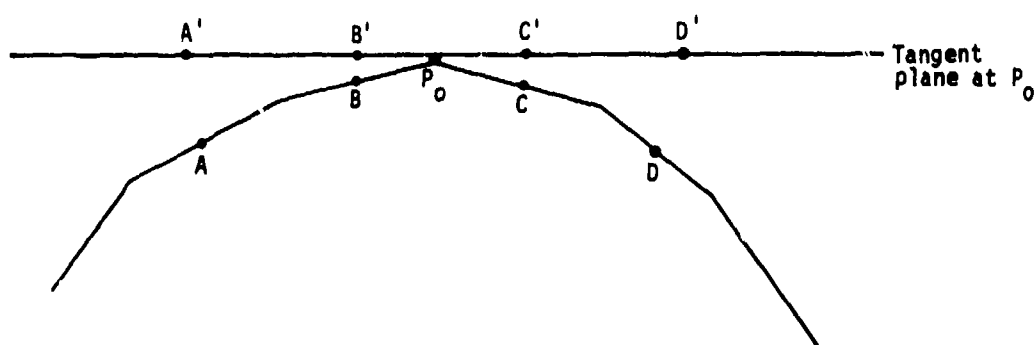


Figure I.6 - Projections to Tangent Plane of Points on Curved Surface

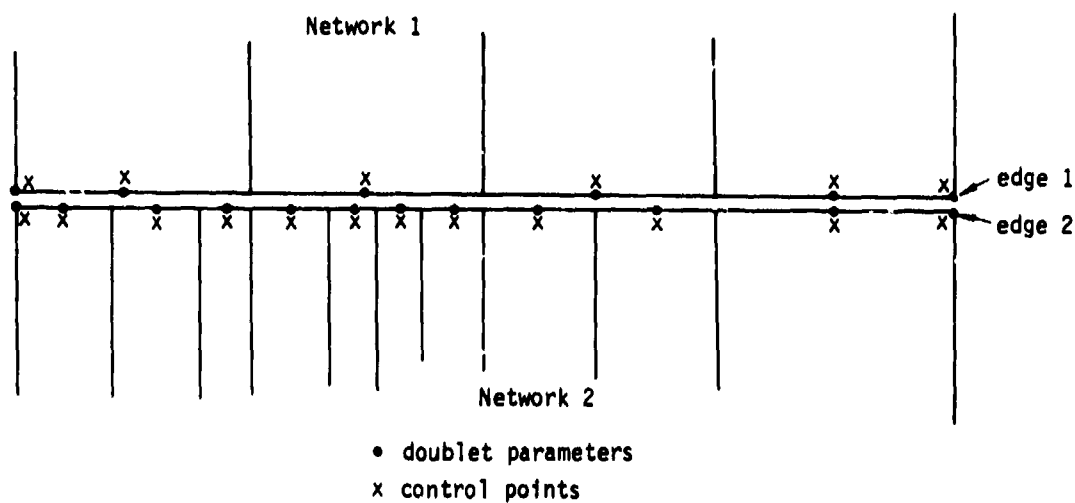


Figure I.7a - Unequal spacing in a non-smooth abutment  
(second edge is a refinement of the first)

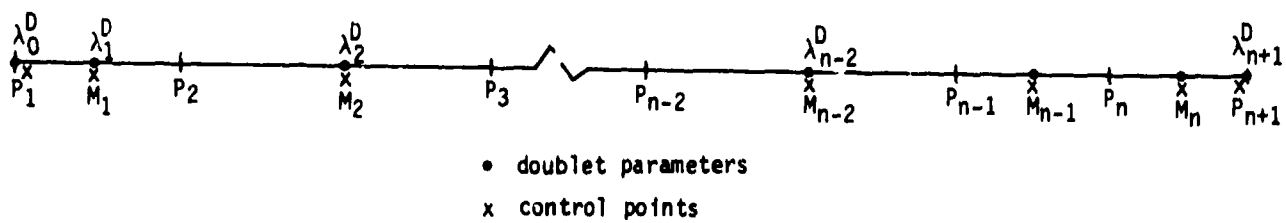


Figure I.7b - Identification of points on a network edge

$\mu(M_5) = 1$   
 All other  $\mu(M_i) = 0$

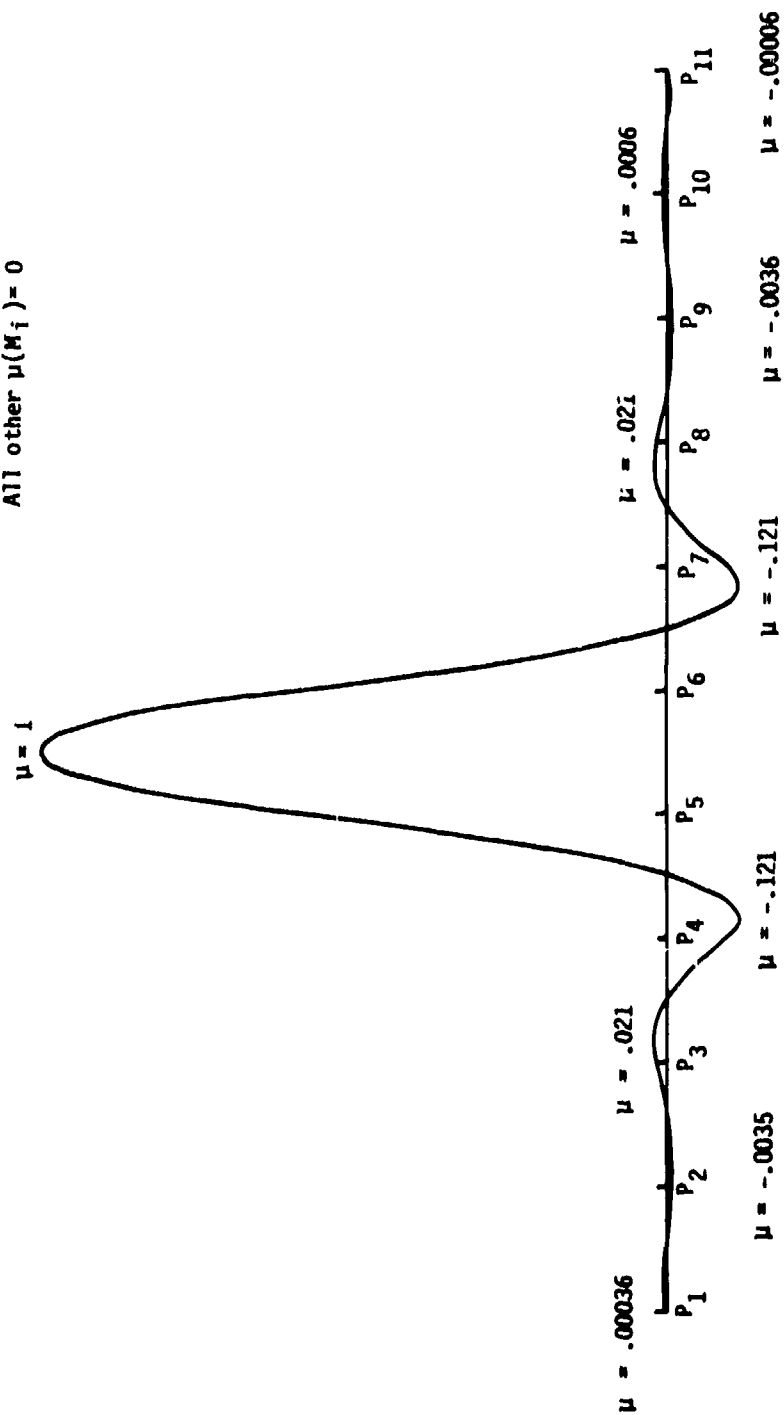
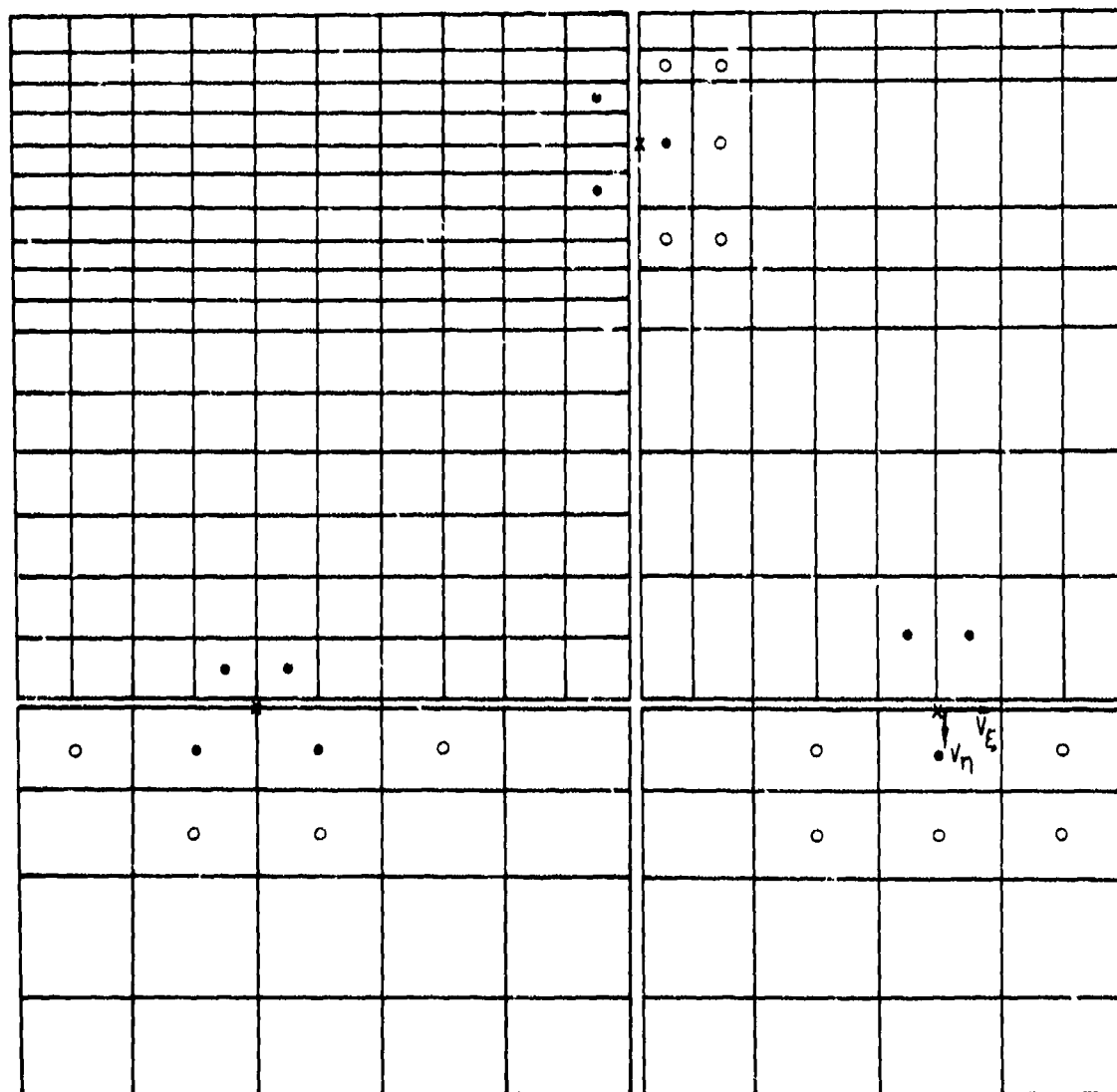


Figure I.8 - Differentiable 2-D quadratic spline



neighbors for grid points on smooth abutments



x point  $P_0$   
 • exact fit  
 o least squares fit

Figure I.9a - Neighboring singularity parameters for points  $P_0$  on a smooth abutment

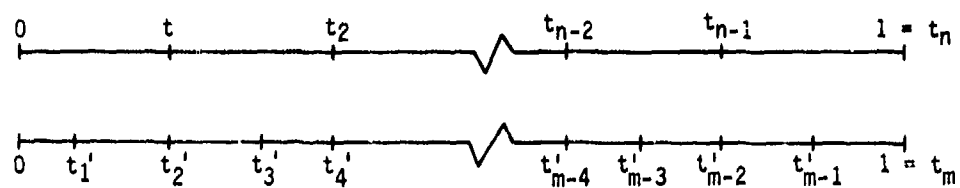


Figure 1.9b - Parameterization of an abutment

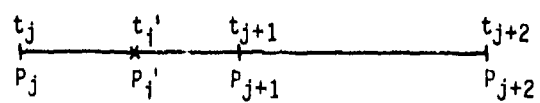


Figure 1.9c - Panel edge on coarse network

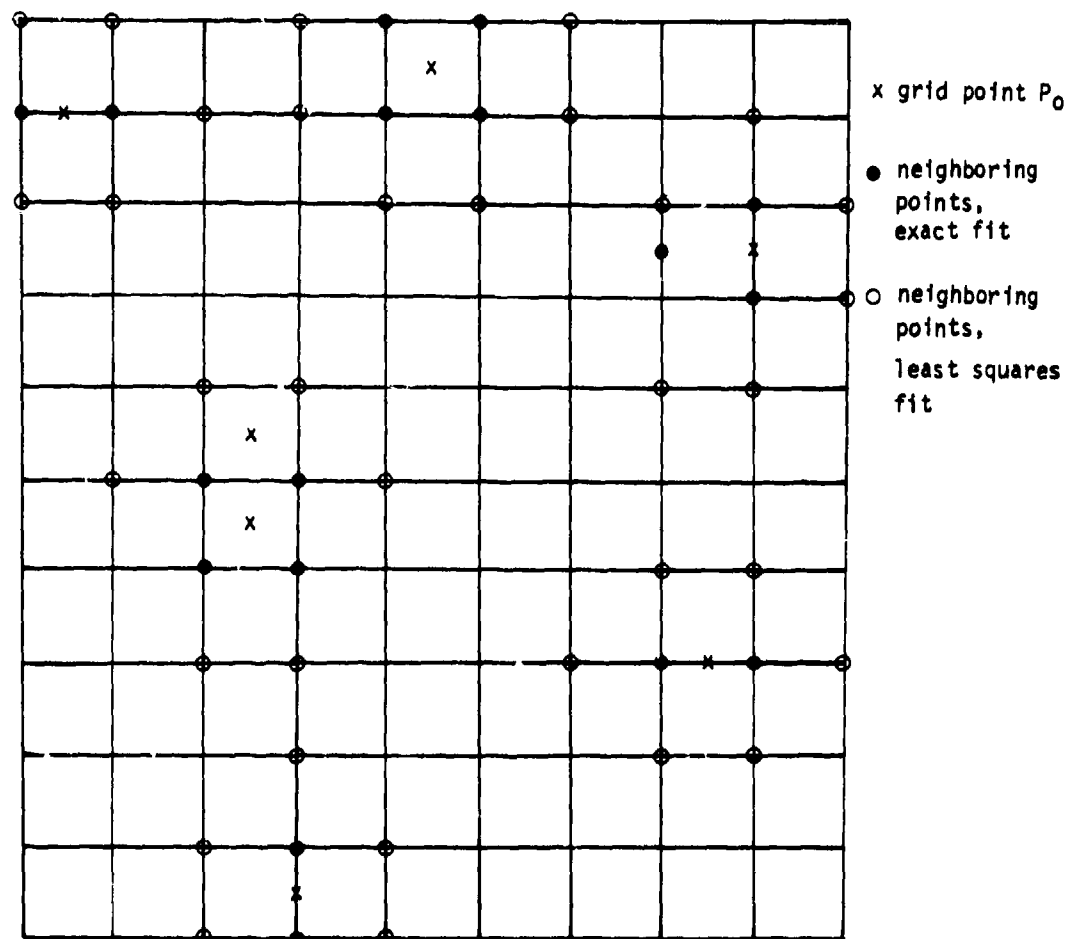


Figure I.10a - Neighboring point for least square fit ( $P_0$  on a doublet design network)

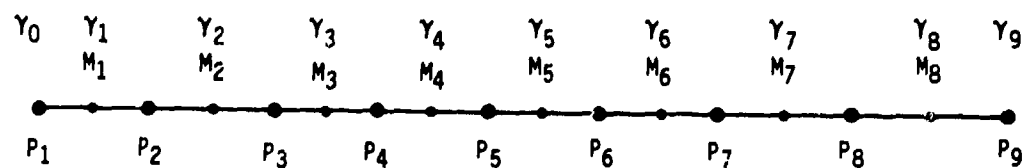


Figure I.10b - Edge of a doublet design network

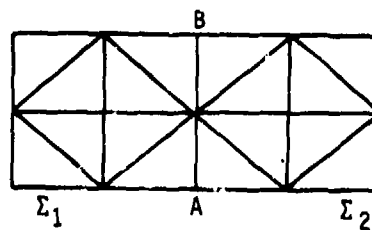
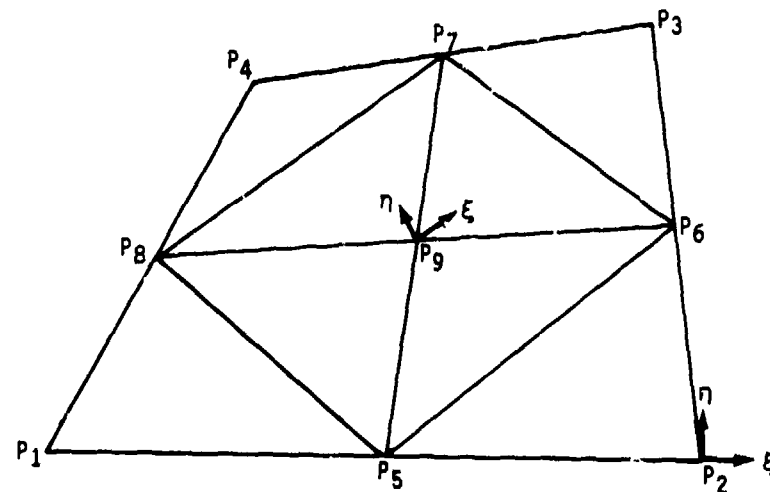


Figure 1.11 - Adjacent panels



- points  $P_1$  and  $P_3$  lie above average plane
- $P_2$  and  $P_4$  lie below plane
- $P_5$  through  $P_9$  lie in a plane

Figure 1.12 - Panel defining points and subpanel local coordinate systems

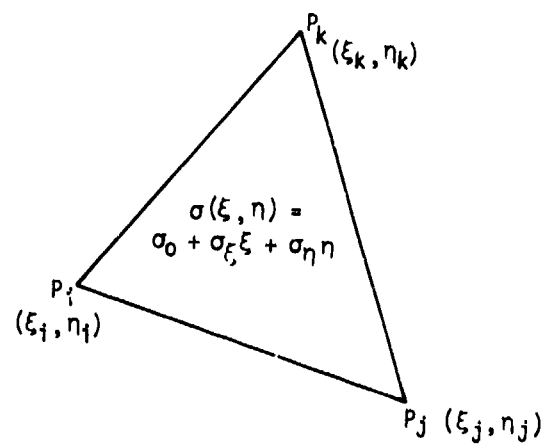


Figure I.13 - Subpanel local coordinates

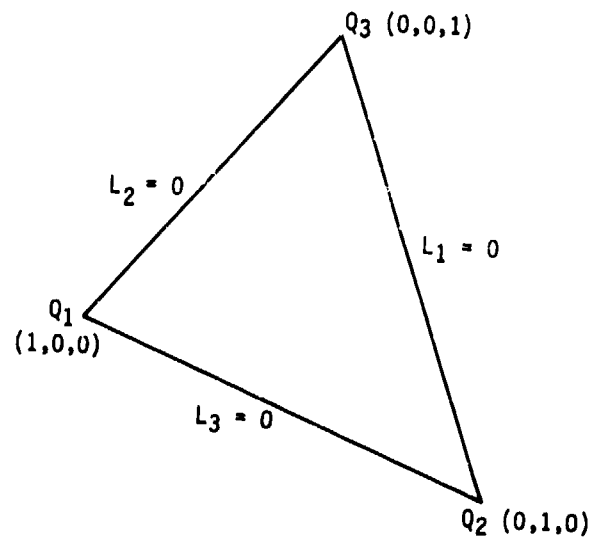


Figure I.14 - Triangular coordinates

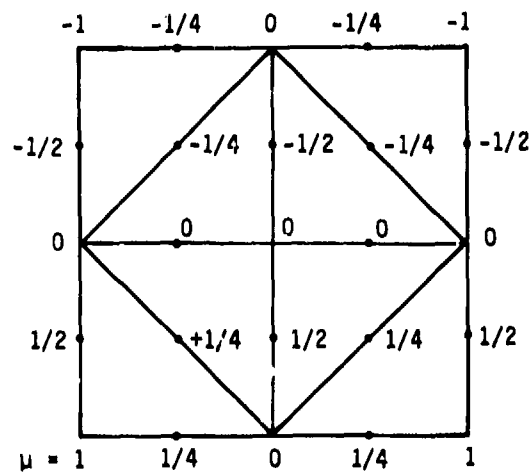


Figure I.15 - Values of differentiable doublet distribution on a square panel

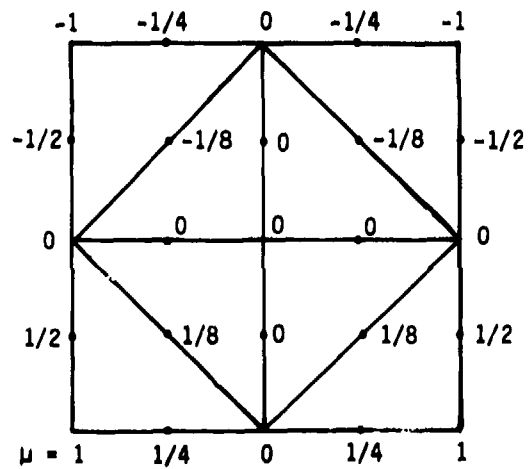


Figure I.16 - Values of doublet distribution on square panel with Pan Air spline

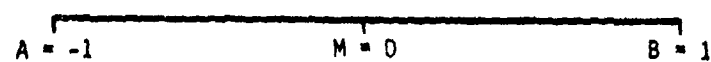


Figure 1.17 - An interval with midpoint

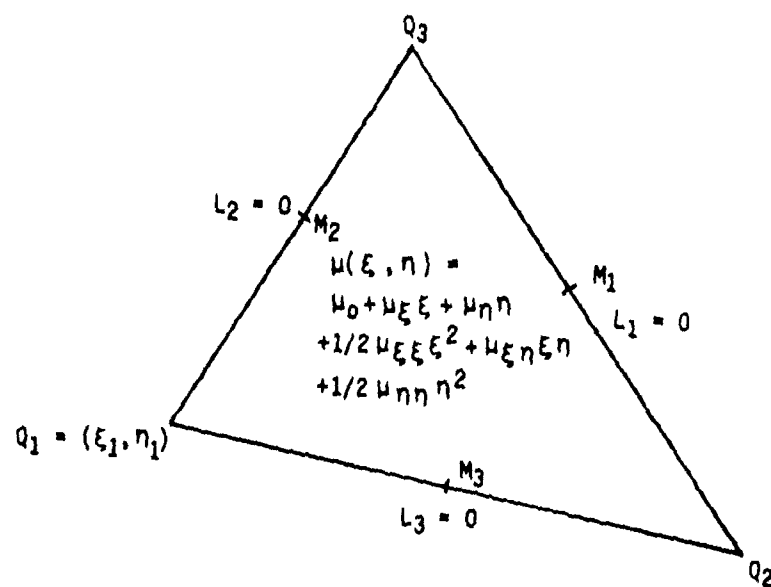


Figure 1.18 Quadratic doublet distribution on a subpanel

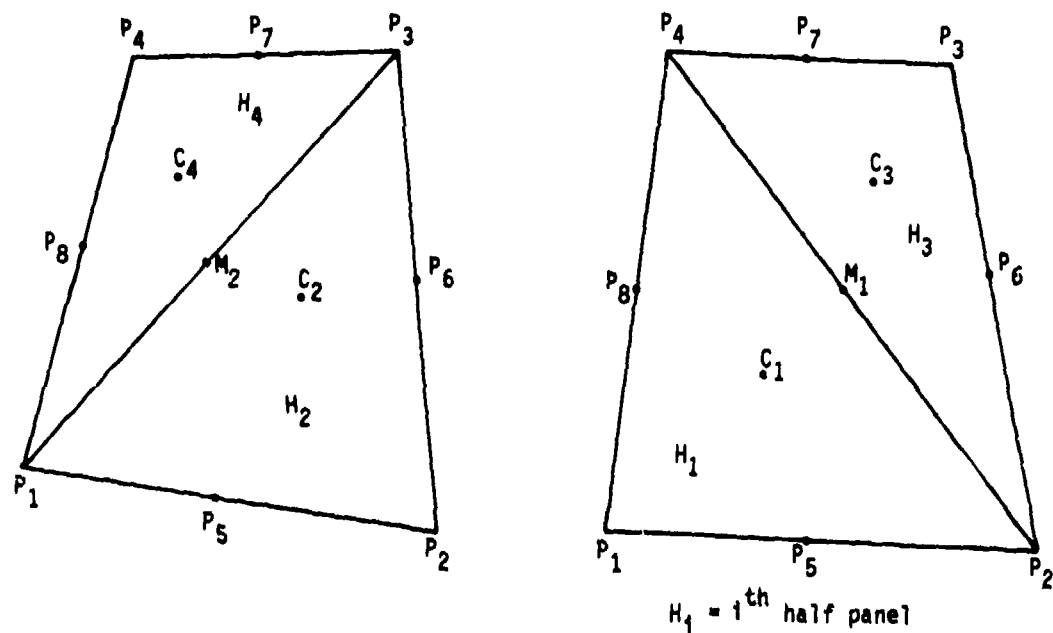


Figure I.19 - Division on panel into half panels

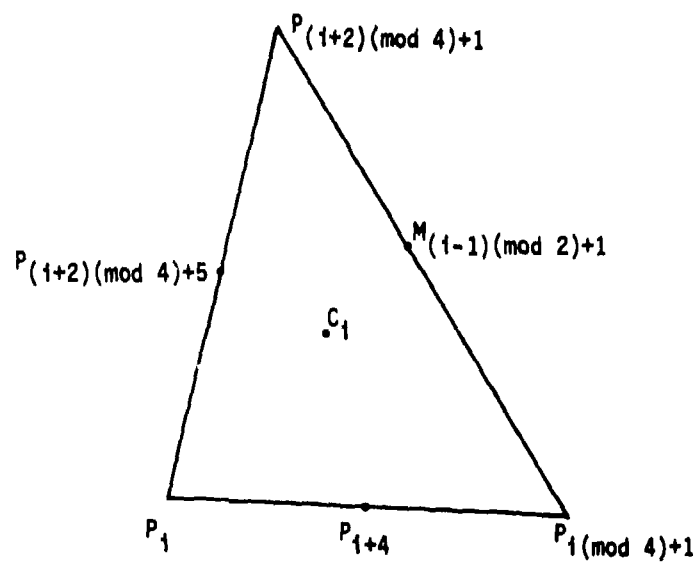


Figure I.20 - Diagram of half panel 1



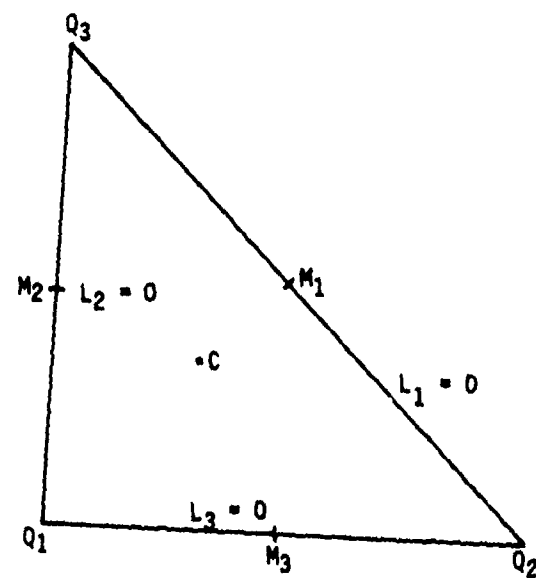


Figure 1.21 - Standard half panel

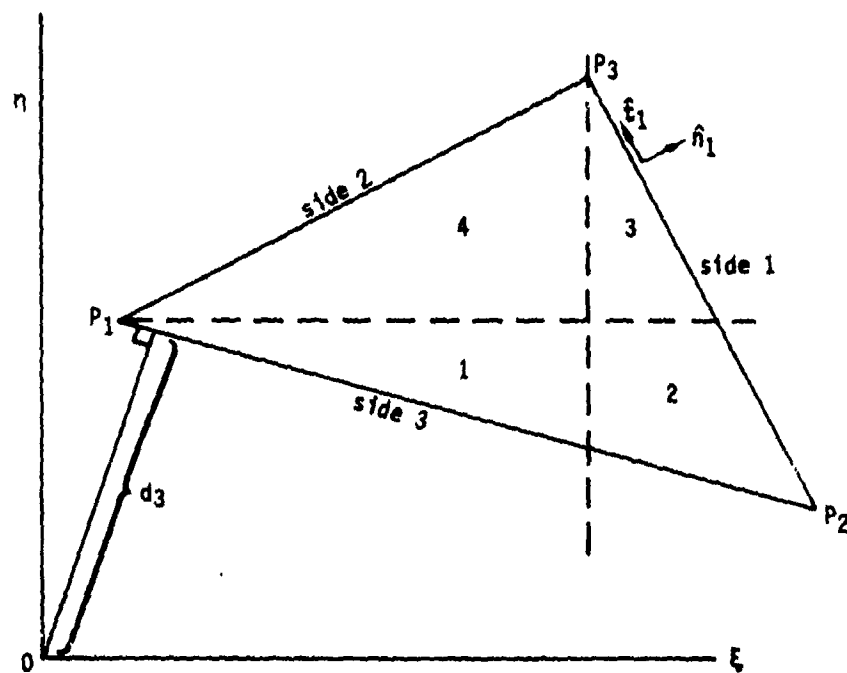


Figure 1.22 - Computation of basic far field moments

## J.0 Panel Influence Coefficient Calculation

### J.1 Introduction and Notation

In this appendix we discuss the construction of a panel influence coefficient matrix (PIC). Two such matrices (one corresponding to the source distribution on the panel, the other to the doublet distribution) are defined for every pair of panel and control point. Thus, for this entire appendix, we will assume we are dealing with a single panel and a single control point. We will see that as the location of the control point with respect to the panel changes, the method used to compute the PIC matrices may vary.

The multiplicity of methods is necessary for efficiency: the "near field" method, which is always accurate, is too expensive always to be used, while the less expensive intermediate and far field methods are not always accurate. In this appendix, we will discuss the various methods and when to use each, and will examine the behavior of the entries of the PIC matrices in certain limiting circumstances.

#### J.1.1 Definitions

Given a panel  $\Sigma$  and a control point  $P$ , we define matrices  $PIC^S$  and  $PIC^D$  as follows. Let  $\sigma_1, \dots, \sigma_4, \sigma_9$  be the five panel source parameters,  $\nu_1, \dots, \nu_9$  the nine panel doublet parameters. Let  $\phi_s$  and  $\vec{v}_s$  be the perturbation potential and velocity which the source distribution on the panel defined by  $\sigma_1, \dots, \sigma_9$  induce at the control point, that is, (see (B.0.1) and (B.3.9))

$$\phi_s = -\frac{1}{\kappa} \iint_{\Sigma \cap D_P} \sigma(Q) \left(\frac{1}{R}\right) dS \quad (J.1.1)$$

$$\vec{v}_s = -\frac{1}{\kappa} \iint_{\Sigma \cap D_P} \sigma(Q) \vec{\nabla}_P \left(\frac{1}{R}\right) dS \quad (J.1.2)$$

Then we define  $PIC^S$  by the equation

$$\begin{bmatrix} \phi_s \\ \vec{v}_s \end{bmatrix} = [PIC^S]^{4 \times 5} \begin{bmatrix} \sigma_1 \\ \sigma_2 \\ \sigma_3 \\ \sigma_4 \\ \sigma_9 \end{bmatrix} \quad (J.1.3)$$

Next, let  $\phi_D$  be the perturbation potential, and  $\vec{v}_D$  the regular part of the perturbation velocity, which the doublet distribution on the panel defined by  $\nu_1, \dots, \nu_9$  induce at the control point. That is (again, see (B.0.1) and (B.3.9)),

$$\phi_D = \frac{1}{\kappa} \iint_{\Sigma \cap D_P} [\mu(q) \hat{n} \cdot \tilde{\nabla}(\frac{1}{R})] dS \quad (J.1.4)$$

$$\vec{v}_D = \frac{1}{\kappa} \iint_{\Sigma \cap D_P} (\hat{n} \times \tilde{\nabla} Q \mu) \times \tilde{\nabla}(\frac{1}{R}) dS \quad (J.1.5)$$

Then we define  $[PIC^D]$  by the equation

$$\begin{Bmatrix} \phi_D \\ - \\ \vec{v}_D \end{Bmatrix} = [PIC^D]^{4 \times 9} \begin{Bmatrix} \mu_1 \\ \vdots \\ \mu_9 \end{Bmatrix} \quad (J.1.6)$$

In the actual operation of the program, fewer than 4 rows of the PIC matrices may be computed for reasons of efficiency. This subject is discussed in the Maintenance Document (see section 5-E and the preface of SUBROUTINE BLOCK of the MAG module); in this appendix, we will always consider the full (4-row) matrix.

Finally, let  $\vec{v}_{D,i}^*$  be the line vortex component of the velocity that the doublet distribution defined by  $\mu_1, \dots, \mu_9$ , restricted to the  $i$ th edge of the panel, induces at the control point. That is,

$$\vec{v}_{D,i}^* = \frac{1}{\kappa} \int_{\substack{\text{ith edge of} \\ D_P}} \mu \tilde{\nabla} Q(\frac{1}{R}) \times d\vec{l} \quad (J.1.7)$$

Then we define matrices  $[LINV_i]$  by

$$\vec{v}_{D,i}^* = [LINV_i]^{3 \times 9} \begin{Bmatrix} \mu_1 \\ \vdots \\ \mu_9 \end{Bmatrix} \quad (J.1.8)$$

The computation of the matrix  $[LINV_i]$  is not available in version 1.0 of Pan Air.

## J.1.2 Summary

### J.1.2.1 Near Field Versus Far Field

The first step in computation of the PIC matrices is to determine which

method should be used to compute them. In the near field method, the integration required to evaluate the PIC matrices is performed analytically over each of the eight subpanels. The resultant PIC matrices satisfy (J.1.3) and (J.1.6) "exactly" that is, with no error other than that due to roundoff in arithmetic calculations.

The near field method involves considerable computation, however, and thus its use is reserved for the cases where the other methods are inaccurate. Generally speaking, the farther (using a compressible distance metric) the control point lies from the panel, the more accurate the intermediate field and far field methods become. The algorithms summarized below, and described in detail in section J.2, are purely empirical, and thus subject to modification in time.

The first step is to determine if the panel center is in the domain of dependence of the control point. A far field PIC is never computed unless this holds, in which case we require in addition that the distance from the panel center to the control point is at least five times the panel radius, where all distances are measured by means of a compressible inner product.

If the far field test fails, an intermediate field test, described in section J.2, is performed. If the test is successful, an intermediate field PIC is computed. In computing such a PIC, the 8-segment panel and the singularity distribution on it are approximated, while the influences defined by these approximations are determined analytically.

#### J.1.2.2 The Domain of Dependence

In supersonic flow, the domain of dependence of a control point P is limited to the forward Mach cone from P, as illustrated in figure J.1. The panel  $\Sigma$  illustrated there is outside  $D_p$ , and thus has zero influence on P.

For subinclined panels, we will see in section J.3 that  $\Sigma$  lies outside  $D_p$  whenever all four edges do. For superinclined panels, this does not hold, as illustrated in figure J.2. The test performed on a superinclined panel to determine if it intersects  $D_p$  is also described in section J.3.

#### J.1.2.3 Near Field and Intermediate Field PIC Calculation

The principal step in computing a near field PIC matrix is the computation, for each subpanel, of "sub-panel integral" matrices  $SPINT_j^S$  and  $SPINT_j^D$  such that

$$\begin{Bmatrix} \phi_S \\ \partial\phi_S/\partial\xi' \\ \partial\phi_S/\partial\eta' \\ \partial\phi_S/\partial\zeta' \end{Bmatrix} = [SPINT_j^S] \begin{Bmatrix} \sigma_0 \\ \sigma_\xi \\ \sigma_\eta \end{Bmatrix} \quad (J.1.9)$$

$$\begin{Bmatrix} \phi_D \\ \partial\phi_D/\partial\xi' \\ \partial\phi_D/\partial\eta' \\ \partial\phi_D/\partial\zeta' \end{Bmatrix} = [\text{SPINT}^D] \begin{Bmatrix} \mu_0 \\ \mu_\xi \\ \cdot \\ \cdot \\ \cdot \\ \mu_{\eta\eta} \end{Bmatrix} \quad (\text{J.1.10})$$

where  $\phi_S$  and  $\phi_D$  are the perturbation potentials induced respectively by the linear source distribution defined by  $\sigma_0$ ,  $\sigma_\xi$ , and  $\sigma_\eta$ , and the quadratic doublet distribution defined by  $\mu_0, \dots, \mu_{\eta\eta}$ .

Equations (J.1.9) and (J.1.10) define a perturbation velocity in local  $(\xi', \eta', \zeta')$  coordinates. It is easy to show (c.f., equation K.3.15) that

$$\begin{Bmatrix} \partial\phi/\partial x_0 \\ \partial\phi/\partial y_0 \\ \partial\phi/\partial z_0 \end{Bmatrix} = [A_0^T] \begin{Bmatrix} \partial\phi/\partial\xi' \\ \partial\phi/\partial\eta' \\ \partial\phi/\partial\zeta' \end{Bmatrix} \quad (\text{J.1.11})$$

where  $A_0$  is the matrix sending reference coordinates to local coordinates:

$$[A_0] \begin{Bmatrix} x_0 \\ y_0 \\ z_0 \end{Bmatrix} = \begin{Bmatrix} \xi' \\ \eta' \\ \zeta' \end{Bmatrix} \quad (\text{J.1.12})$$

Finally, recall the definitions of subpanel splines from section I.2.

$$\begin{Bmatrix} \sigma_0 \\ \sigma_\xi \\ \sigma_\eta \end{Bmatrix} = [\text{SPSPL}^S] \begin{Bmatrix} \sigma_1 \\ \cdot \\ \cdot \\ \cdot \\ \sigma_4 \\ \sigma_9 \end{Bmatrix} \quad (\text{J.1.13})$$

$$\begin{Bmatrix} \mu_0 \\ \cdot \\ \cdot \\ \cdot \\ \mu_{\eta\eta} \end{Bmatrix} = [\text{SPSPL}^D] \begin{Bmatrix} \mu_1 \\ \cdot \\ \cdot \\ \cdot \\ \mu_9 \end{Bmatrix} \quad (\text{J.1.14})$$

Then, we may combine (J.1.3), (J.1.9), (J.1.11), and (J.1.13) to obtain

$$[PICS]^{4 \times 5} = \sum_{i=1}^8 [\tilde{A}_i]^{4 \times 4} [SPINT_i^S]^{4 \times 3} [SPSPL_i^S]^{3 \times 5} \quad (J.1.15)$$

where the subscript  $i$  refers to the  $i$ th subpanel, and

$$[\tilde{A}_i] = \begin{bmatrix} 1 & 0 & 0 & 0 \\ 0 & \vdots & \vdots & \vdots \\ 0 & \vdots & A_i^T & \vdots \\ 0 & \vdots & \vdots & \vdots \end{bmatrix} \quad (J.1.16a)$$

Similarly, for the 2-region intermediate field method, we have a corresponding equation

$$[PICS]^{4 \times 5} = \sum_{i=1}^2 [\tilde{A}_i]^{4 \times 4} [HPINT_i^S]^{4 \times 6} [HPSPL_i^S]^{6 \times 5} \quad (J.1.16b)$$

where  $i$  ranges over two "half panels," the half panel integral matrix  $HPINT^S$  defines the influence of the half panel on the control point, and the half panel spline matrix  $HPSPL^S$ , defined in section I.3, gives a quadratic source distribution in terms of the five panel source parameters.

Finally, the one region intermediate field procedure approximates the panel by its projection to an average plane. In this procedure,

$$[PICS]^{4 \times 5} = [\tilde{A}]^{4 \times 4} [PINT^S]^{4 \times 3} [PSPL^S]^{3 \times 5} \quad (J.1.17)$$

where  $PINT^S$  ("panel integral") defines the influence of the projected panel on the control point, and  $[PSPL^S]$  defines a source distribution on the projected panel in terms of the panel singularity parameters.

Equations corresponding to (J.1.15-17) hold for the doublet distribution as well. Thus the computation of PIC matrices by near field or intermediate field methods has been discussed, except for the computation of the subpanel, half panel, and panel integral matrices.

This is a rather complex subject and is discussed in full detail in section J.6. In that section the influence  $[S_0]$  of a quadratic source distribution over a polygonal region and the influence  $[D_0]$  of a cubic doublet distribution over a polygonal region are computed in terms of certain fundamental integrals we call "edge functions" and "panel functions". These edge and panel functions are computed in section J.7, though the formulas

derived there do not consider numerical instabilities which may occur during the computation. These numerical instabilities are avoided by means of rationalization formulas discussed in section J.8.

#### J.1.2.4 Far Field PIC's

Recall from (B.O.1) that the denominator in the fundamental integral is  $1/R$ , where in compressibility coordinates

$$R^2 = (\xi - x)^2 + s\beta^2(\eta - y)^2 + s\beta^2(\zeta - z)^2 \quad (J.1.18)$$

where the control point  $\vec{P} = (x, y, z)$ , and the point of integration

$$\vec{Q} = (\xi, \eta, \zeta).$$

Recalling from section E.2 the inner product

$$[\vec{x}, \vec{y}] = \vec{x}^T [C_0] \vec{y} \quad (J.1.19)$$

where in compressibility coordinates,

$$[C_0] = \begin{bmatrix} 1 & & \\ & s\beta^2 & \\ & & s\beta^2 \end{bmatrix} \quad (J.1.20)$$

we see that

$$R^2 = [\vec{P} - \vec{Q}, \vec{P} - \vec{Q}] \quad (J.1.21)$$

Letting  $Q_0$  be the panel center,

$$\begin{aligned} \Delta\vec{Q} &= \vec{Q}_0 - \vec{Q} \\ \vec{R}_0 &= \vec{P} - \vec{Q}_0 \end{aligned} \quad (J.1.22a)$$

we have

$$R^2 = [\vec{R}_0 + \Delta\vec{Q}, \vec{R}_0 + \Delta\vec{Q}] \quad (J.1.22b)$$

Now, the expression  $R^{-N}$ ,  $N = 1$  or  $3$ , occurs in the fundamental integrals, and the basis for the far field method is the equation

$$\begin{aligned} R^{-N} &= [\vec{R}_0 + \Delta\vec{Q}, \vec{R}_0 + \Delta\vec{Q}]^{-N/2} \\ &= ([\vec{R}_0, \vec{R}_0] + 2[\vec{R}_0, \Delta\vec{Q}] + [\Delta\vec{Q}, \Delta\vec{Q}])^{-N/2} \end{aligned} \quad (J.1.23)$$

$$= [\vec{R}_0, \vec{R}_0]^{-N/2} \left( 1 + 2 \frac{[\vec{R}_0, \Delta\vec{Q}]}{[\vec{R}_0, \vec{R}_0]} + \frac{[\Delta\vec{Q}, \Delta\vec{Q}]}{[\vec{R}_0, \vec{R}_0]} \right)^{-N/2} \quad (J.1.24)$$

The factor  $[\vec{R}_0, \vec{R}_0]^{-N/2}$  is independent of  $Q$  and may thus be taken out of the integral, while the remaining factor may be expressed by a power series in  $\Delta Q$  for which we ignore any terms of cubic or higher order.

We will show in section J.9 that the integrations (J.1.1) and (J.1.2) can then be performed as a sum of multiplication of matrices, one whose entries are computed from  $R_0$ , and one whose entries are integrals of powers of  $\Delta Q$ , which, since they are independent of  $P$ , may be performed in advance (and thus need not be repeated for each control point).

### J.1.3 Integration Techniques

The computation of the entries of the subpanel integral matrices [SPINT] (cf., J.1.9-10) involves considerable detail (see sections J.4 through J.6). At this time, however, we will give a brief outline of the process described in those sections.

In sections J.4 and J.5 we establish, respectively, special cylindrical and hyperbolic coordinate system, the former for use in subsonic flow or with superinclined panels, the latter for use with subinclined panels in supersonic flow. The coordinate systems have two advantages. First, the kernel  $1/R$  of the integrals (J.1.1-2) has a very simple form (cf., J.6.59). Second, the limits of integration may also be expressed conveniently (cf., (J.4.62) and (J.5.107)). In section J.6, we first express the entries of a subpanel integral matrix in terms of fundamental integrals ( $a$ ,  $\bar{a}$ , etc., cf., (J.6.152) and (J.6.164)). We then use the results of sections J.4 and J.5 to evaluate these integrals.

It is worth noting, however, that there exist other ways of computing the entries of the subpanel integral matrices. While all these methods are equivalent in that, if correct, they yield the same real numbers for the influence of a particular subpanel on a particular control point, they may have quite different structures. We now briefly summarize three alternate methods.

One such method (for zero Mach number) is described in Appendix D.2 of reference J.1. There, the entries of the subpanel integral matrices are given in terms of fundamental integrals, some of which are singular even when the control point is away from the panel. It can be shown that the singular integrals always cancel, however, and thus the entries of the subpanel integral matrix are finite.

A second approach is given in Appendix D.5 of reference J.1. Here, an additional integration by parts is performed, with the result that the entries of the subpanel integral matrices are computed exclusively as combinations of non-singular integrals. Of all published methods for PIC computation, this one most closely resembles that of section J.6. The fundamental integrals are also similar, with  $H(1,1,3)$  in reference J.1 being a multiple of the integral  $a$  (cf., (J.6.165)). In fact, the computation of  $H(1,1,3)$ , which uses cylindrical coordinates as well, closely parallels the computation of  $a$ .

A third approach to PIC computation is contained in Reference 4.9 (Ehlers, et.al.). There, rectilinear coordinates are used in evaluation of the integrals. The resulting formulas appear totally different from those of



section J.6 because the entries of the subpanel integral matrices are expressed in terms of different (and also non-singular) fundamental integrals. The verification that the entries of the subpanel integral matrices as computed in reference 4.9 are in fact identical to the entries as computed in section J.6 is a major one.

#### J.1.4 Notation

The discussion of PIC computation is lengthy, and many terms are defined and then not used again until much later. The most frequently used terms are listed in figure J.3 for convenient reference. All vectors and matrices are in reference coordinates unless otherwise specified, except that those marked with a prime are in local coordinates unless otherwise specified.

## J.2 Distance Algorithm

In this section we discuss the algorithms we use to determine whether to compute a far field, a one region intermediate field, a two region intermediate field, or a near field PIC. First, we consider the requirements for performing a far field PIC.

### J.2.1 The Far Field Criterion

Consider equation (J.1.24). In order to ignore cubic terms in  $\vec{\Delta Q}$ , we must have

$$[\vec{R}_0, \vec{\Delta Q}] \ll [\vec{R}_0, \vec{R}_0] \quad (J.2.1)$$

To determine a condition on  $R_0$  for which (J.2.1) holds, we digress into the realm of linear algebra.

Let  $(\cdot, \cdot)_p$  be a positive definite inner product (not necessarily the standard Euclidean inner product); that is,

$$(\vec{X}, \vec{X})_p > 0 \quad (J.2.2)$$

if  $\vec{X}$  is non-zero. Let

$$|\vec{X}|_p = (\vec{X}, \vec{X})_p \quad (J.2.3)$$

Then we have the triangle inequality (see, for instance, page 11 of reference J.2):

$$|\vec{X}|_p + |\vec{Y}|_p \geq |\vec{X} + \vec{Y}|_p \quad (J.2.4)$$

Squaring (J.2.4),

$$(\vec{X}, \vec{X})_p + 2(\vec{X}, \vec{Y})_p + (\vec{Y}, \vec{Y})_p \leq (\vec{X}, \vec{X})_p + 2|\vec{X}|_p |\vec{Y}|_p + (\vec{Y}, \vec{Y})_p \quad (J.2.5)$$

or

$$(\vec{X}, \vec{Y})_p \leq |\vec{X}|_p |\vec{Y}|_p \quad (J.2.6)$$

a relation called the Cauchy-Schwartz inequality.

We generalize (J.2.6) for the specific positive definite inner product

$$[\vec{X}, \vec{Y}]_p = \vec{X}^T [C_0] \vec{Y} \quad (J.2.7)$$

where  $C_0$  is the positive definite matrix

$$C_0 = \beta^2 I + (1 - \beta^2) \hat{c}_0 \hat{c}_0^T \quad (J.2.8)$$

Then one can show (though we will not do so) that

$$[\vec{X}, \vec{Y}] \leq |\vec{X}|_p |\vec{Y}|_p = \sqrt{(\vec{X}^T C_0 \vec{X}) (\vec{Y}^T C_0 \vec{Y})} \quad (J.2.9)$$

Substituting  $\vec{R}_0$  for  $\vec{X}$  and  $\vec{\Delta Q}$  or  $\vec{R}_0$  for  $\vec{Y}$ , we get

$$[\vec{R}_0, \vec{\Delta Q}] \leq |\vec{R}_0|_P |\vec{\Delta Q}|_P \quad (J.2.10)$$

and

$$[\vec{R}_0, \vec{R}_0] \leq |\vec{R}_0|_P \quad (J.2.11)$$

Then consider the requirement

$$|\vec{R}_0|_P |\vec{\Delta Q}|_P \ll [\vec{R}_0, \vec{R}_0] \quad (J.2.12)$$

If (J.2.12) holds, we obtain

$$[\vec{R}_0, \vec{\Delta Q}] \leq |\vec{R}_0|_P |\vec{\Delta Q}|_P \ll [\vec{R}_0, \vec{R}_0] \quad (J.2.13)$$

Thus, imposing (J.2.12), or the equivalent condition

$$|\vec{\Delta Q}|_P \ll \frac{[\vec{R}_0, \vec{R}_0]}{|\vec{R}_0|_P} \quad (J.2.14)$$

we insure that the condition (J.2.1) holds and we may perform a far field PIC computation.

Now, the condition (J.2.14) must hold for all points Q on the panel, that is, defining the "compressible panel radius"

$$CR(\Sigma) = \max_{Q \text{ in } \Sigma} |\vec{Q} - \vec{Q}_0|_P \quad (J.2.15)$$

we must have

$$k CR(\Sigma) = \frac{[\vec{R}_0, \vec{R}_0]}{|\vec{R}_0|_P} \quad (J.2.16)$$

where k is a "large" number.

Now, as the panel radius gets smaller and smaller compared to the "distance" from the control point to the panel center, we may neglect first the quadratic terms and finally neglect even the linear terms in  $\Delta Q$  in the expansion (J.1.24). The corresponding far field computations are called dipole and monopole computations respectively, with the retention of quadratic terms in  $\Delta Q$  (but not higher ones) called the quadrupole computation.

In practice, we perform a monopole computation if the factor k in (J.2.16) exceeds 24, a dipole computation for  $8 < k \leq 24$ , a quadrupole computation for  $5 < k \leq 8$ , and a one region intermediate field computation if  $2 < k \leq 5$ . These are empirical results not justifiable by a rigorous error analysis.

### J.2.2 The Intermediate Field Criterion

As noted above, we perform a one-region intermediate field PIC computation when the constant  $k$  in (J.2.16) exceeds 2. We now discuss the circumstances under which we perform a two region intermediate field calculation, and if so, which pair of half panels we use. This is background material, since version 1.0 of Pan Air does not in fact perform two region intermediate field calculations.

Consider the panel approximations illustrated in figure J.4. The outer edges of the approximate panel coincide with the outer edges of the true panel; therefore our approximation preserves surface continuity. Furthermore, the doublet strength on the half panels, computed in section I.3, is identical to that of the exact panel on the panel edges; therefore doublet continuity is preserved. Thus we may perform a two region intermediate field PIC computation even though the control point is fairly close to the panel.

We require two criteria to hold before permitting a two region intermediate field computation. The first is that the constant  $k$  in (J.2.16) exceeds 1.2. Essentially, this means the "distance" from the control point to the panel center must exceed 1.2 panel radii; in particular, the control point does not lie on the panel.

To define the second criterion, let us recall some definitions from appendix I. We construct a special panel-wide local coordinate system similar to that constructed in section I.1, but we use different rotation to avoid confusion with the coordinates  $(\xi, \eta, \zeta)$  which occur in this appendix.

Let

$$\begin{aligned}\vec{W}_1 &= \vec{P}_8 - \vec{P}_9 \\ \vec{W}_2 &= \vec{P}_5 - \vec{P}_9\end{aligned}\tag{J.2.17}$$

Now, analogously to (I.1.3), let

$$W_3 = \frac{|\vec{W}_1 \times \vec{W}_2|}{|\vec{W}_1 \times \vec{W}_2|^{1/2}}\tag{J.2.18}$$

Next, for any control point  $P$ , analogously to (I.1.7), let

$$\begin{aligned}
\lambda_1(P) &= \frac{((\vec{P} - \vec{P}_g) \times \vec{W}_2) \cdot \vec{W}_3}{|\vec{W}_1 \times \vec{W}_2|^{3/2}} \\
\lambda_2(P) &= \frac{(\vec{W}_1 \times (\vec{P} - \vec{P}_g)) \cdot \vec{W}_3}{|\vec{W}_1 \times \vec{W}_2|^{3/2}} \\
\lambda_3(P) &= \frac{(\vec{P} - \vec{P}_g) \cdot \vec{W}_3}{|\vec{W}_1 \times \vec{W}_2|}
\end{aligned} \tag{J.2.19}$$

Also, recall from section P.2 the "skewness parameters"

$$\begin{aligned}
C_{11} &= \frac{((\vec{P}_1 - \vec{P}_g) \times \vec{W}_2) \cdot \hat{n}}{(\vec{W}_1 \times \vec{W}_2) \cdot \hat{n}} - 1 \\
C_{21} &= \frac{(\vec{W}_1 \times (\vec{P}_1 - \vec{P}_g)) \cdot \hat{n}}{(\vec{W}_1 \times \vec{W}_2) \cdot \hat{n}} - 1
\end{aligned} \tag{J.2.20}$$

These parameters are zero if the panel is a parallelogram.

Now, we perform a two region intermediate field PIC if

$$\sum_{i=1}^3 \lambda_i(P)^2 \geq (1 + |C_{11}|)^2 + (1 + |C_{12}|)^2 \tag{J.2.21}$$

For a square panel, this permits a two region intermediate field PIC to be performed unless the control point lies in the sphere, about the panel center, whose radius is the panel radius (see figure J.5). For skewed panels, the presence of  $C_{11}$  and  $C_{12}$  in (J.2.21) insures that the control point is further from the panel.

Finally, the choice of diagonal along which the panel is sliced into two half panels is chosen as follows: the value  $i$ ,  $1 \leq i \leq 4$ , for which

$$[\vec{P} - \vec{P}_i, \vec{P} - \vec{P}_i] \quad \text{is minimized, is computed.}$$

Then, the panel is split in two along the diagonal which does not lie on  $P_i$ , that is, the diagonal with endpoints  $P_{(i+1) \pmod 4}$  and  $P_{(i+3) \pmod 4}$ . An example of splitting a panel is shown in figure J.6. Note there that since

$P_1$  lies closest to  $P$  in hyperbolic distance, the panel  $\Sigma$  is split along the diagonal connecting  $P_2$  and  $P_4$ .

In closing this section, we note that whenever we fail to compute a far field or intermediate field PIC, we compute a near field PIC. In the course of this computation, we may determine that the panel has no influence on the control point if the flow is supersonic, a subject we will discuss in the next section.

### J.3 Supersonic Influence Test

In order to compute the influence of a subpanel on a control point P in supersonic flow, one must know

- (a) whether the subpanel intersects  $D_p$ ,
- (b) if so, which of its edges intersect  $D_p$ , and
- (c) which of its corners lie in  $D_p$ .

Rather than compute this data one subpanel at a time, the program takes several short cuts, which, if results are successful, give much or all of this data for a minimum of computation. First, a simple test is performed to check if the panel lies outside  $D_p$  (this test does not find all panels lying outside  $D_p$ , but does eliminate many of them). Second, a test which identifies panels lying wholly within  $D_p$  is performed. Finally, for panels which are identified neither as lying outside  $D_p$  or wholly within  $D_p$ , the influence test must be performed one subpanel at a time.

#### J.3.1 Definition of $D_p$

Given a control point P, we define  $D_p$  as the points Q, lying in the upstream pointing Mach cone from P. The condition that Q lie upstream from P is given by

$$(\vec{P} - \vec{Q}) \cdot \hat{c}_0 \geq 0 \quad (J.3.1)$$

The condition that Q lie in either the upstream or downstream Mach cone from P is given by

$$[\vec{P} - \vec{Q}, \vec{P} - \vec{Q}] \geq 0 \quad (J.3.2)$$

A point Q satisfying both (J.3.1) and (J.3.2) lies in  $D_p$ .

#### J.3.2 A Zero Influence Test

In this section, we determine the minimum distance  $d(Q, \partial D_p)$  from a point Q to the boundary  $\partial D_p$  of the domain of independence of P. We use this as follows. Let  $R(\Sigma)$  be the true radius (as opposed to compressible radius) of the panel:

$$R(\Sigma) = \max_{1 \leq i \leq 4} |P_g - P_i| \quad (J.3.3)$$

Then if  $P_g$  does not lie in  $D_p$ , and

$$d(P_g, \partial D_p) > R(\Sigma) \quad (J.3.4)$$

no point on  $\Sigma$  can lie in  $D_p$ , and thus  $\Sigma$  is wholly outside  $D_p$  and so its influence on P is zero.

The computation of  $d(Q, a D_p)$  is performed in the following manner. This distance is most easily computed in a coordinate system  $\tilde{x}$  centered at the control point P, aligned with the compressibility vector  $\hat{c}_0$  and oriented such that Q-P lies in the  $\tilde{x}$ - $\tilde{y}$  plane with positive  $\tilde{y}$  coordinate, where the  $\tilde{y}$  axis is orthogonal to  $\hat{c}_0$ , as illustrated in figure J.7.

Now, in this coordinate system, the Mach cone is defined by the lines

$$\tilde{y} = \pm \frac{\tilde{x}}{\beta} \quad (J.3.5)$$

since points on that line satisfy

$$\tilde{x}^2 + \beta^2 \tilde{y}^2 = 0 \quad (J.3.6)$$

The line perpendicular to that defined by (J.3.5), passing through the origin, is

$$\tilde{y} = \beta \tilde{x} \quad (J.3.7)$$

and thus the line through Q perpendicular to the Mach line closer to Q is

$$\tilde{y} - \tilde{y}_0 = \beta(\tilde{x} - \tilde{x}_0) \quad (J.3.8)$$

Thus the point on  $a D_p$  lying closest to Q is the point  $(\tilde{x}, \tilde{y})$  lying on the lines

$$\tilde{y} - \tilde{y}_0 = \beta(\tilde{x} - \tilde{x}_0) \quad (J.3.9)$$

$$\tilde{y} = \frac{-\tilde{x}}{\beta}$$

Substituting (J.3.10) in (J.3.9),

$$-\frac{\tilde{x}}{\beta} + \tilde{y}_0 = \beta(\tilde{x} - \tilde{x}_0) \quad (J.3.11)$$

or

$$\tilde{x} = \frac{\beta \tilde{x}_0 - \tilde{y}_0}{\beta + 1/\beta} \quad (J.3.12)$$

and so

$$\tilde{y} = \frac{-\tilde{x}}{\beta} = \frac{-\beta \tilde{x}_0 + \tilde{y}_0}{\beta^2 + 1} \quad (J.3.13)$$

J.3-2



Then,

$$d(Q, a D_p) = \sqrt{(\tilde{x} - \tilde{x}_0)^2 + (\tilde{y} - \tilde{y}_0)^2} \quad (J.3.14)$$

So,  $d(Q, a D_p)^2 =$

$$\left( \frac{\beta \tilde{x}_0 - \tilde{y}_0}{\beta + 1/\beta} - \tilde{x}_0 \right)^2 + \left( \frac{-\beta \tilde{x}_0 + \tilde{y}_0}{\beta^2 + 1} - \tilde{y}_0 \right)^2 \quad (J.3.15)$$

$$= \frac{1}{(\beta^2 + 1)} [\beta^2 \tilde{x}_0 - \beta \tilde{y}_0 - (\beta^2 + 1) \tilde{x}_0]^2 + \frac{1}{(\beta^2 + 1)^2} (-\beta \tilde{x}_0 - \beta^2 \tilde{y}_0)^2 \quad (J.3.16)$$

$$= \frac{1}{(\beta^2 + 1)^2} (-\tilde{x}_0 - \beta \tilde{y}_0)^2 + \frac{1}{(\beta^2 + 1)^2} (-\beta \tilde{x}_0 - \beta^2 \tilde{y}_0)^2 \quad (J.3.17)$$

$$= \frac{1 + \beta^2}{(\beta^2 + 1)^2} \tilde{x}_0^2 + \frac{2(1 + \beta^2)(\tilde{x}_0 + \beta \tilde{y}_0)^2}{(\beta^2 + 1)^2} + \frac{(1 + \beta^2)(\beta^2 \tilde{y}_0)^2}{(\beta^2 + 1)^2} \quad (J.3.18)$$

$$= \frac{(\tilde{x}_0 + \beta \tilde{y}_0)^2}{1 + \beta^2} \quad (J.3.19)$$

So,  $d(Q, a D_p) =$

$$\frac{\tilde{x}_0 + \beta \tilde{y}_0}{1 + \beta^2} \quad (J.3.20)$$

This formula holds as long as the nearest point on  $a D_p$  to  $Q$  is found by dropping a perpendicular to the Mach line, that is whenever (see figure J.7)

$$\tilde{y}_0 > \beta \tilde{x}_0 \quad (J.3.21)$$

Otherwise, the nearest point on  $D_p$  to  $Q$  is  $P$ , that is,

$$d(Q, a D_p) = |\vec{P} - \vec{Q}| \quad (J.3.22)$$

Finally, we compute  $\tilde{x}_0$  and  $\tilde{y}_0$  as follows. First, since the x-axis is aligned with  $\hat{c}_0$ ,

$$\tilde{x}_0 = (\vec{Q} - \vec{P}) \cdot \hat{c}_0 \quad (J.3.23)$$

Next, since there is no coordinate scaling, we want

$$\tilde{x}_0^2 + \tilde{y}_0^2 = |\vec{Q} - \vec{P}|^2 \quad (J.3.24)$$

or

$$\tilde{y}_0 = \sqrt{|\vec{Q} - \vec{P}|^2 - \tilde{x}_0^2} \quad (J.3.25)$$

Then, summarizing,  $d(Q, a D_p)$  is computed as

$$\begin{aligned} d(Q, a D_p)^2 &= (\tilde{x}_0 + b \tilde{y}_0)^2 / (1 + b^2) & \tilde{y}_0 &\geq b \tilde{x}_0 \\ d(Q, a D_p)^2 &= |\vec{Q} - \vec{P}|^2 & \tilde{y}_0 &< b \tilde{x}_0 \end{aligned} \quad (J.3.26)$$

### J.3.3 Panels Wholly within the Mach Cone

Just as a panel whose center lies further from a  $D_p$  than the panel radius has no influence on the control point if its center lies outside  $D_p$ , it analogously lies wholly within  $D_p$  if its center does. That is, if  $P_0$  lies in  $D_p$ , and

$$d(P_0, a D_p) > R(\Sigma) \quad (J.3.27)$$

then  $\Sigma$  lies within  $D_p$ .

### J.3.4 The Influence Test for a Subpanel

Finally, let us assume that the panel passes none of the simple tests described above. For each subpanel (or half panel or projected panel, in the case of intermediate field computations) we must determine which corners lie in  $D_p$ , which edges intersect  $D_p$ , and whether the region as a whole intersects  $D_p$ .

The corners of a subpanel are tested one at a time to see if they satisfy (J.3.1) and (J.3.2). If all corners do, then the entire subpanel lies in  $D_p$ . This follows from the fact that  $D_p$  is a "convex" region. A convex region is one such that the line segment joining any two points in the region also lies in the region. Thus if all vertices of a subpanel lie in  $D_p$ , then any point on an edge lies in  $D_p$ . Thus, since any point in the interior of the subpanel lies on some line segment joining points on edges, every point on the subpanel lies in  $D_p$ . Next, if one vertex of an edge lies in  $D_p$  and another does not, it is clear that both the edge and the subpanel lie partially within  $D_p$ .

#### J.3.4.1 The Point of Closest Approach

Let us assume neither vertex of an edge lies in  $D_p$ . Then we determine whether the edge intersects  $D_p$  as follows.

First, suppose the edge is a "subsonic edge." That is, let  $\hat{t}_0$  be a unit vector parallel to the edge. Then defining

$$\tau = [\hat{t}_0, \hat{t}_0] \quad (J.3.28)$$

we call the edge subsonic if  $\tau > 0$ , supersonic if  $\tau < 0$ , and sonic if  $\tau = 0$  (see figure J.8). A subsonic edge is inclined to the compressibility direction at less than the Mach angle; thus every point on the edge is in the domain of dependence of the most downstream point. So, if the most upstream point lies outside  $D_p$ , the entire edge does. In particular, if both vertices of a subsonic edge lie outside  $D_p$ , the entire edge does.

For a supersonic edge, this property does not hold, as illustrated in figure J.8. Thus, for a supersonic edge whose vertices lie outside  $D_p$ , we must check if the "point of closest approach" on the edge lies in  $D_p$ . If not, then the entire edge lies outside  $D_p$ .

What we mean by the point of closest approach is that point  $R_*$  on the line containing the edge which lies closest to the line through  $P$  parallel to the compressibility direction  $\hat{c}_0$ , as illustrated in figure J.9. We find  $R_*$  as follows. Let

$$\vec{\Delta R} = \vec{R}^+ - \vec{R}^- \quad (J.3.29)$$

where  $\vec{R}^+$  and  $\vec{R}^-$  are the vertices of the edge.

Now, let us write

$$\vec{R} = \alpha \vec{R}^- + (1 - \alpha) \vec{R}^+ = \vec{R}^+ - \alpha \vec{\Delta R} \quad (J.3.30)$$

for an arbitrary point on the line.

Then, the projection of  $R$  to the line parallel to  $\hat{c}_0$  containing  $P$  is

$$\vec{P} + \hat{c}_0 \hat{c}_0^T (\vec{R} - \vec{P}) \quad (J.3.31)$$

and so the square of the distance from  $R$  to that line is

$$d^2 = |\vec{R} - \vec{P} - \hat{c}_0 \hat{c}_0^T (\vec{R} - \vec{P})|^2 \quad (J.3.32)$$

$$= (\vec{R} - \vec{P}) \cdot (\vec{R} - \vec{P}) - (\hat{c}_0 \cdot (\vec{R} - \vec{P}))^2 \quad (J.3.33)$$

= (by (J.3.30))

$$\begin{aligned} & (\vec{R}^+ - \alpha \vec{\Delta R} - \vec{P}) \cdot (\vec{R}^+ - \alpha \vec{\Delta R} - \vec{P}) \\ & - (\hat{c}_0 \cdot (\vec{R}^+ - \alpha \vec{\Delta R} - \vec{P}))^2 \end{aligned} \quad (J.3.34)$$

Now,  $d^2$  is minimized by setting

$$\frac{d}{da} (d^2) = 0 = 2(\vec{R}^+ - a\vec{\Delta R} - \vec{P}) \cdot (-\vec{\Delta R})$$

$$-2(\hat{C}_0 \cdot (\vec{R}^+ - a\vec{\Delta R} - \vec{P})) (-\hat{C}_0 \cdot \vec{\Delta R}) \quad (J.3.35)$$

$$= [2(\vec{\Delta R} \cdot \vec{\Delta R}) - 2(\hat{C}_0 \cdot \vec{\Delta R})^2] a$$

$$-2(\vec{R}^+ - \vec{P}) \cdot \vec{\Delta R} + 2(\hat{C}_0 \cdot (\vec{R}^+ - \vec{P})) (\hat{C}_0 \cdot \vec{\Delta R}) \quad (J.3.36)$$

So,  $d^2$  is minimized for

$$a = a^* = \frac{(\vec{R} - \vec{P}) \cdot \vec{\Delta R} - (\hat{C}_0 \cdot (\vec{R} - \vec{P})) (\hat{C}_0 \cdot \vec{\Delta R})}{(\vec{\Delta R} \cdot \vec{\Delta R}) - (\hat{C}_0 \cdot \vec{\Delta R})^2} \quad (J.3.37)$$

Thus, the point  $P_*$  on the line containing the edge which is the point of closest approach is

$$\vec{R}_* = a_* \vec{R} + (1 - a_*) \vec{R} \quad (J.3.38)$$

Thus if  $R^+$  and  $R^-$  both lie outside  $D_p$ , we compute  $a_*$ . If  $0 < a_* < 1$ , the point of closest approach lies in the interior of the edge, and we thus test if  $R_*$  lies in  $D_p$ . If it does not, the entire edge lies outside  $D_p$ .

For reasons of efficiency, the program actually computes

$$a_* = \frac{(\hat{C}_0 \times \vec{\Delta R}) \cdot (\hat{C}_0 \times (\vec{R}^+ - \vec{P}))}{|\hat{C}_0 \times \vec{\Delta R}|^2} \quad (J.3.39)$$

The equivalence of (J.3.37) and (J.3.39) is easily seen in compressibility coordinates, where

$$\hat{C}_0 = \begin{Bmatrix} 1 \\ 0 \\ 0 \end{Bmatrix} \quad (J.3.40)$$

Then,

$$\hat{C}_0 \cdot \vec{\Delta R} = (\vec{\Delta R})_x \quad (J.3.41)$$

and so the denominator of (J.3.37) is

$$(\vec{\Delta R})_y^2 + (\vec{\Delta R})_z^2 \quad (J.3.42)$$

On the other hand

$$\hat{c}_0 \times \Delta \vec{R} = \begin{pmatrix} 0 \\ -\Delta R_z \\ \Delta R_y \end{pmatrix} \quad (J.3.43)$$

and so the expression (J.3.42) defines the denominator of (J.3.39).

Next,

$$(\hat{c}_0 \times \Delta \vec{R}) \cdot (\hat{c}_0 \times (\vec{R}^+ - \vec{P})) = \begin{pmatrix} 0 \\ -\Delta R_z \\ \Delta R_y \end{pmatrix} \cdot \begin{pmatrix} 0 \\ -(\vec{R}^+ - \vec{P})_z \\ (\vec{R}^+ - \vec{P})_y \end{pmatrix} = \quad (J.3.44)$$

$$\Delta R_y (\vec{R}^+ - \vec{P})_y + \Delta R_z (\vec{R}^+ - \vec{P})_z \quad (J.3.45)$$

$$= \Delta \vec{R} \cdot (\vec{R}^+ - \vec{P}) - (\hat{c}_0 \cdot \Delta \vec{R}) (\hat{c}_0 \cdot (\vec{R}^+ - \vec{P})) \quad (J.3.46)$$

and thus the numerators of (J.3.37) and (J.3.39) are equal.

#### J.3.4.2 The Winding Number Test

Finally, let us assume that none of the edges of the subpanel intersect  $D_p$ . Then if the panel is subinclined, we can see from figure J.10 that the entire panel lies outside  $D_p$ , while for supersonic panels this does not hold.

Thus in this case we compute the point  $P_*$ , on the plane containing the subpanel, which is the intersection of the line through  $P$  parallel to  $c_0$  with the plane of subpanel. It is clear that if  $P_*$  lies in the interior of the subpanel, the subpanel intersects  $D_p$ , while if it lies in the exterior of the subpanel, the subpanel lies wholly outside  $D_p$ .

Now, we can write

$$\vec{P}_* = \vec{P} + s \hat{c}_0 \quad (J.3.47)$$

and since  $P_*$  lies on the subpanel,

$$(\vec{P}_* - \vec{P}_1) \cdot \hat{n}_0 = 0 \quad (J.3.48)$$

where  $\hat{n}_0$  is the subpanel normal and  $\vec{P}_1$  is a vertex. Substituting (J.3.47) in (J.3.48),

$$(\vec{P} - \vec{P}_1) \cdot \hat{n}_0 + s(\hat{c}_0 \cdot \hat{n}_0) = 0 \quad (J.3.49)$$

or

$$A = \frac{(\vec{P}_i - \vec{P}) \cdot \hat{n}_0}{\hat{c}_0 \cdot \hat{n}_0} \quad (J.3.50)$$

Now, if  $P_*$  lies in the subpanel, the angles formed by  $P_i$ ,  $P_*$ , and  $P_{i(\text{mod } 3) + 1}$  are all of the same sign. That is,  $P_*$  is inside the subpanel if and only if

$$((\vec{P}_i - \vec{P}_*) \times (\vec{P}_{i(\text{mod } 3)+1} - \vec{P}_*)) \cdot \hat{n}_0 \quad (J.3.51)$$

has the same sign for  $i = 1, 2, 3$ .

#### J.3.4.3 Half Panels and Projected Panels

Everything we have said about subpanels holds equally well for half panels, since they are also triangular regions. It also holds equally well for projected panels, used in the one region intermediate field computation, provided the projected panel is convex. When the panel is not convex, there is a small risk that the influence will be calculated erroneously. For this reason, the program checks for non-convex panels and warns the user of their existence.

#### J.4 Cylindrical Coordinates

When the integrals (J.1.1), (J.1.2), (J.1.4) and (J.1.5) are transformed to local coordinates, they become integrals of the general form

$$\iint_{\Sigma' \cap D_p} \begin{Bmatrix} \sigma(\xi', n') \\ \mu(\xi', n') \end{Bmatrix} f(R') d\xi' dn' \quad (J.4.1)$$

where (see section E.3)

$$R'^2 = r(\xi' - x')^2 + s(n' - y')^2 + rs(\zeta' - z')^2 \quad (J.4.2)$$

When  $rs = 1$  (this covers both the case of subsonic flow and of superinclined panels), these integrals are very naturally evaluated using cylindrical coordinates. In section J.4, we derive basic results which are necessary to perform these integrations. The case of  $rs = -1$  (subinclined panels in supersonic flow) is best handled by hyperbolic coordinates discussed in section J.5.

##### J.4.1 Fundamental Results

Recall from section E.3 that in the local coordinate system, the flow is in the  $x'$  direction for subsonic flow and in the  $z'$  direction for superinclined panels. Thus  $D_p$  is all space for subsonic flow, and (writing  $P = (x', y', z')$  in local coordinates)

$$D_p = \{(\xi', n', \zeta') \mid (\zeta' - z')^2 - (\xi' - x')^2 - (n' - y')^2 > 0 \text{ and } (\zeta' - z') \text{ sign}(\hat{c}_0 \cdot \hat{n}_0) \leq 0\} \quad (J.4.3)$$

(where  $\hat{n}_0$  is the subpanel normal) for superinclined panels. We can rewrite (J.4.3) as

$$D_p = \{(\xi', n', \zeta') \mid \sqrt{(\xi' - x')^2 + (n' - y')^2} < -\text{sign}(\hat{c}_0 \cdot \hat{n}_0)(\zeta' - z')\} \quad (J.4.4)$$

Because both the function  $R'$  and the domain of dependence  $D_p$  exhibit circular symmetry with respect to the point  $(x', y')$ , we will find it convenient to use cylindrical coordinates centered at  $(x', y')$  to perform the required integrations. In addition, because the boundary of the panel image  $\Sigma'$  is composed of straight lines (the edges), local coordinate systems having axes perpendicular and parallel to the edges also arise naturally.

We should note here that our results will hold for any planar region which is convex. This, of course, includes subpanels and half panels, though not necessarily projected panels (see section J.3.4.3).

#### J.4.2 The Mach Disk

Since  $\zeta'$  is a constant on the surface of integration  $\Sigma'$  (see section E.3), the region of integration  $\Sigma' \cap D_p$  may equally well be taken to be  $\Sigma' \cap C_h$  where  $C_h$  the "Mach disk" is defined by

$$C_h = \{(\zeta', n') \mid (\zeta' - x')^2 + (n' - y')^2 \leq \bar{h}\} \quad (J.4.5)$$

where

$$+ \infty \text{ if } s = 1$$

$$\bar{h} =$$

$$\text{sign}(\hat{n}_0 \cdot \hat{c}_0)h \text{ if } s = -1 \quad (J.4.6)$$

where

$$h = z' - \zeta' \quad (J.4.7)$$

The region of integration  $\Sigma' \cap C_h$  for a typical panel image  $\Sigma'$  is shown in Figure J.12. Note that since both  $\Sigma'$  and  $C_h$  are convex, so is  $\Sigma' \cap C_h$ .

A careful examination of figure J.12 reveals that the boundary of  $\Sigma' \cap C_h$  denoted  $a(\Sigma' \cap C_h)$  is composed of both curved and straight line segments. Furthermore  $a(\Sigma' \cap C_h)$  has sharp corners in two possible instances,

- (i) Whenever a corner of  $\Sigma'$  lies inside  $C_h$ .
- (ii) Whenever an edge  $\Sigma'$  intersects the boundary of  $C_h$ .

We will develop a scheme for numbering the edges,  $E_k$ , corner points  $p_k^*$ , and phases of corner points  $\phi_k^*$  of the region  $\Sigma' \cap C_h$ . At the outset of this discussion, we distinguish three separate cases

- (a)  $\Sigma' \cap C_h$  is empty
- (b)  $\Sigma' \cap C_h = C_h$  (that is,  $C_h \subset \Sigma'$ )
- (c)  $\Sigma' \cap C_h$  is a proper subset of  $C_h$

Case (a) is of absolutely no consequence since  $\Sigma' \cap C_h$  is null and all integrals over it are zero.

#### J.4.3 The Case of the Mach Disk Lying within the Panel

Case (b) is handled in the following fashion (see fig. J.13). In the first place, no edges are defined when  $\Sigma' \cap C_h = C_h$ . Next, some point  $(\xi', n')$  lying on the boundary of  $C_h$  is chosen at random and  $p = (s_1, t_1)$  is defined by



$$\vec{p} = (\xi' - x', \eta' - y') \quad (J.4.8)$$

Next,  $\vec{p}_1^+$ ,  $\vec{p}_2^-$ ,  $\phi_1^+$ ,  $\phi_2^-$  are defined by

$$\begin{aligned} \vec{p}_1^- &= \vec{p}_1^+ = \vec{p}_2^- = \vec{p} \\ \phi_1^- &= \phi_1^+ = \text{ph}(s_1, t_1) \\ \phi_2^- &= \phi_1^+ + 2\pi \end{aligned} \quad (J.4.9)$$

Here,  $\text{ph}$  is the "phase function" in two real variables

$$\text{ph}(x,y) = \arg(x + iy) \quad (J.4.10)$$

where  $\arg$  is the complex argument function. Precisely, for any two real numbers  $x$  and  $y$ , one of them non-zero, the equations

$$\begin{aligned} -\pi &< \text{ph}(x,y) \leq \pi \\ \cos(\text{ph}(x,y)) &= x \\ \sin(\text{ph}(x,y)) &= y \end{aligned} \quad (J.4.11)$$

uniquely define  $\text{ph}(x,y)$ . It should be noted in passing that  $\text{ph}(x,y)$  equals the FORTRAN function  $\text{ATAN2}(y,x)$ .

With these definitions, it is clear that the integral  $J$  defined by

$$J = \frac{d\xi' d\eta'}{\sqrt{h^2 - (\xi' - x')^2 - (\eta' - y')^2}} \quad (J.4.13)$$

may equally well be computed by the expression

$$J = \left[ \int_{\phi_1^-}^{\phi_1^+} d\phi + \int_{\phi_1^+}^{\phi_2^-} d\phi \right] \int_0^{|h|} \frac{\rho d\rho}{h^2 - \rho^2}$$

(where  $C_h \subset \Sigma'$ ) and  $\rho = |\vec{p}|$ , since

$$\rho d\rho d\phi = d\xi' d\eta' \quad (J.4.14)$$

#### J.4.4 Arbitrary Intersection of the Mach Disk with the Panel

We now take up the difficult and interesting case (c), when  $\Sigma' \cap C_h \neq C_h$ . For this discussion, the reader is referred back to Fig. J.12. Starting with any edge of  $\Sigma'$  that has some points lying inside  $C_h$ , we denote this edge  $E_1$  and begin proceeding around the boundary of  $\Sigma' \cap C_h$  in a

counterclockwise (positive) fashion. As we traverse  $\partial(\Sigma' \cap C_h)$ , we will move along straight and possibly curved pieces of boundary. The straight pieces of boundary are named  $E_1, E_2, \dots, E_n$  as they are encountered. Here,  $n$  is the number of edges of  $\Sigma'$  that have some points lying inside  $C_h$  (see Fig. J.14).

#### J.4.4.1 Corner Points

Having described the edge naming convention, the corner points  $\rho_k^\pm$  are defined by

$$\vec{\rho}_k^- = (\xi', n') \mid \begin{array}{c} \text{lower edge} \\ \text{of } E_k \end{array} \quad -(x', y') \quad (\text{J.4.15})$$

The components of  $\vec{\rho}_k^\pm$  are denoted  $(s_k^\pm, t_k^\pm)$  as follows

$$(s_k^\pm, t_k^\pm) = \vec{\rho}_k^\pm \quad (\text{J.4.16})$$

Also, the special corner point  $\vec{\rho}_{n+1}^-$  is defined

$$\vec{\rho}_{n+1}^- = \vec{\rho}_1^- \quad (\text{J.4.17})$$

#### J.4.4.2 The Phase Function

Finally, the phases of the corner points,  $\phi_k^\pm$ , are defined recursively by

$$\begin{aligned} \phi_1^- &= \text{ph}(s_1^-, t_1^-) \\ \phi_k^+ &= \phi_k^- + \int_{\rho_k^-}^{\rho_k^+} d\phi \end{aligned} \quad (\text{J.4.18})$$

Great care must be taken here because of the problem of "phase wrap." That is, the phase function is discontinuous on a closed path in the  $x'-y'$  plane which does not contain the origin. Thus in the former case (that of the second or third illustration in figure J.14)  $\phi_n^+$  is almost  $2\pi$  greater than  $\phi_1$ , while in the latter case the increment of  $2\pi$  does not occur.

Next we compute

$$d\phi = \frac{\partial \phi}{\partial s} ds + \frac{\partial \phi}{\partial t} dt \quad (\text{J.4.19})$$

Now, since, up to an additive constant,

$$\begin{aligned} \phi &= \text{ph}(s, t) = \arg(s+it) \\ &= \text{Im} \log(s+it) \end{aligned} \quad (\text{J.4.20})$$

(where  $\text{Im}$  is the imaginary part), we have

$$\begin{aligned} \frac{\partial \phi}{\partial s} &= \text{Im} \frac{\partial}{\partial s} \log(s+it) = \text{Im} \left( \frac{1}{s+it} \right) \\ &= \text{Im} \left( \frac{s-it}{s^2+t^2} \right) = \frac{-t}{s^2+t^2} \end{aligned} \quad (\text{J.4.21})$$

Similarly,

$$\frac{\partial \phi}{\partial t} = \text{Im} \left( \frac{i}{s+it} \right) = \text{Im} \left( \frac{is-t}{s^2+t^2} \right) = \frac{s}{s^2+t^2} \quad (\text{J.4.22})$$

Combining these results, we have

$$d\phi = \frac{sdt - tds}{s^2+t^2}$$

(by definition of  $\vec{\rho}$ )

$$\frac{(\vec{\rho} \times d\vec{\rho})}{\rho^2} \quad (\text{J.4.23})$$

The integrals in (J.4.18) are straightforward to evaluate. Since (see figure J.15) the angle  $\phi$  between  $\vec{\rho}_k^-$  and  $\vec{\rho}_k^+$  satisfies

$$\begin{aligned} (\vec{\rho}_k^- \times \vec{\rho}_k^+)_z &= \rho_k^- \rho_k^+ \sin \phi \\ \vec{\rho}_k^- \cdot \vec{\rho}_k^+ &= \rho_k^- \rho_k^+ \cos \phi \end{aligned} \quad (\text{J.4.24a})$$

we have (by J.4.11)

$$\phi = \int_{\rho_k^+}^{\rho_{k+1}^-} d\phi = \text{ph}(\rho_k^+ \cdot \rho_{k+1}^+, (\rho_k^+ \times \rho_{k+1}^+)_z) \quad (\text{J.4.24b})$$

Now, geometric reasoning shows that in this case,

$$(\rho_k^+ \times \rho_{k+1}^+)_z > 0 \quad (\text{J.4.25})$$

and thus  $0 \leq \phi \leq \pi$ .

On the other hand, the angle  $\phi'$  between  $\rho_k^+$  and  $\rho_{k+1}^-$  may exceed  $\pi$  (see figure J.15), and must be correctly evaluated in view of phase wrap, and thus

$$\phi' = \int_{\rho_k^+}^{\rho_{k+1}^-} d\phi = \hat{\text{ph}}(\rho_k^+ \cdot \rho_{k+1}^-, (\rho_k^+ \times \rho_{k+1}^-)_z) \quad (\text{J.4.26})$$

where  $\hat{\text{ph}}$  is defined by

$$\hat{\text{ph}}(x, y) = \text{ph}(x, y) + 2\pi n$$

$$0 \leq \hat{\text{ph}}(x, y) < 2\pi$$

$$n = 0 \text{ or } 1 \quad (\text{J.4.27})$$

With phases  $\phi_k^*$  defined in this fashion, the phase of a point  $\rho$  on the bound.  $\Gamma \cap C_h$ , defined by

$$\phi(\vec{\rho}) = \phi_1^- + \int_{\rho_1^-}^{\rho} d\phi = \phi_1^- + \text{ph}(\rho_1^- \cdot \vec{\rho}, (\rho_1^- \times \vec{\rho})_z) \quad (\text{J.4.28})$$

is a continuous function for all points on the boundary satisfying

$$\phi(\rho_k^*) = \phi_k^* \quad k = 1, \dots, n \quad (\text{J.4.29})$$

Because of phase wrap, it may happen that  $\phi_{-n+1} \neq \phi_{-1}$  but rather  $\phi_{-n+1} = \phi_{-1} + 2\pi$ . If this happens, it indicates that the center of our coordinate system  $(x', y')$  lies inside  $\Sigma'$ . Defining the center indicator  $C_\bullet$  by

$$C_\bullet = \begin{cases} 1 & \text{if } (x', y') \in \Sigma' \\ 0 & \text{otherwise} \end{cases} \quad (\text{J.4.30})$$

we observe that

$$\phi_{-n+1} = \phi_{-1} + 2\pi C_\bullet \quad (\text{J.4.31})$$

#### J.4.4.3 Edges and the Mach Disk

The discussion given above provides a very precise definition of the phases  $\phi_k^*$  once the corner points are known; however, the determination of the edges  $E_k$  and the corner points  $\rho_k^*$  will require some more detail which we now provide.

An edge  $E_k$  of the region  $\Sigma' \cap C_h$  must be either part of, or all of an edge  $E$  of  $\Sigma'$ . Thus given an edge  $E$  of  $\Sigma'$ , we seek to answer the question of when an edge  $E$  of  $\Sigma'$  is also an edge  $E_k$  of  $\Sigma' \cap C_h$ . Toward answering this question, we assume that the upper or lower endpoints of the edge  $E$  are given by (see figure J.15)

$$\text{Edge } E \text{'s lower endpoint} = (x', y') + \vec{\rho}^-$$

$$\text{Edge } E \text{'s upper endpoint} = (x', y') + \vec{\rho}^+ \quad (\text{J.4.32})$$

Thus  $\vec{\rho}^-(\vec{\rho}^+)$  describes the vector from  $(x', y')$  to the lower (upper) end point of  $E$ . (The upper and lower endpoints of  $E$  may be assumed known because they are essential to the definition of  $\Sigma'$ ). The components of  $\vec{\rho}^\pm$  are denoted  $(s^\pm, t^\pm)$ , i.e.,

$$(s^\pm, t^\pm) = \vec{\rho}^\pm \quad (\text{J.4.33})$$

It should be noted that the designations "lower" and "upper" are designations associated with the orientation of  $\Sigma'$ ; as one traverses  $\partial\Sigma'$  in a positive (counterclockwise) fashion, one moves along edges from their lower to their upper end.

#### J.4.4.4 Edge Tangents and Normals

Next, we define the edge tangent  $t$  by

$$\vec{t} = n(\vec{\rho}^+ - \vec{\rho}^-) \quad (\text{J.4.34})$$

where  $n$  denotes the normalization operation

$$n(x) = \frac{\vec{x}}{|\vec{x}|} \quad (J.4.35)$$

In component notation,  $t$  may be written

$$\vec{t} = (t_\xi, t_n) \quad (J.4.36)$$

We use this representation to define the edge outer normal  $\vec{n}$  by

$$\vec{n} = (t_n, -t_\xi) = (n_\xi, n_n) \quad (J.4.37)$$

Clearly,  $\vec{n}$  and  $\vec{t}$  so defined satisfy the conditions

$$\text{Normalization Conditions} \quad |\vec{t}| = (t_\xi^2 + t_n^2)^{1/2} = 1$$

$$\vec{n} = (n_\xi^2 + n_n^2)^{1/2} = 1 \quad (J.4.38)$$

Orthogonality

$$\vec{n} \cdot \vec{t} = n_\xi t_\xi + n_n t_n = 0 \quad (J.4.39)$$

Cross Product

$$(\vec{n} \times \vec{t})_\xi = n_\xi t_n - n_n t_\xi = 1 \quad (J.4.40)$$

As a consequence of (J.4.38-40), the vector pair  $(\vec{n}, \vec{t})$  (in that order) comprises a right handed basis for  $(u, v)$  space as shown in Fig. J.16.

The  $(s, t)$  system illustrated there has been previously introduced and is given by

$$\vec{p} = (s, t) = (\xi' - x', n' - y') \quad (J.4.41)$$

The coordinate functions  $u, v$  are defined by

$$\begin{aligned} u &= \vec{n} \cdot \vec{p} \\ v &= \vec{t} \cdot \vec{p} \end{aligned} \quad (J.4.42)$$

or

$$\begin{Bmatrix} u \\ v \end{Bmatrix} = \begin{bmatrix} t_n & -t_\xi \\ t_\xi & t_n \end{bmatrix} \begin{Bmatrix} s \\ t \end{Bmatrix} = [A] \begin{Bmatrix} s \\ t \end{Bmatrix} \quad (J.4.43)$$

Since  $A$  is orthogonal,

$$A^{-1} = A^T$$

and so

$$\vec{p} = \begin{Bmatrix} s \\ t \end{Bmatrix} = A^T \begin{Bmatrix} u \\ v \end{Bmatrix} = \begin{bmatrix} t_n & t_\xi \\ -t_\xi & t_n \end{bmatrix} \begin{Bmatrix} u \\ v \end{Bmatrix} = u \begin{Bmatrix} t_n \\ -t_\xi \end{Bmatrix} + v \begin{Bmatrix} t_\xi \\ t_n \end{Bmatrix} \quad (J.4.44)$$

or

$$\vec{\rho} = \vec{u}\vec{n} + \vec{v}\vec{t} \quad (\text{J.4.45})$$

For points lying on the edge E, we note that

$$\vec{\rho}|_E = \vec{\rho}^- + s\vec{t} \quad (\text{J.4.46})$$

where s denotes arc length along E. Taking the dot product of (J.4.46) with  $\vec{n}$  and taking account of (J.4.39), we find

$$\vec{n} \cdot \vec{\rho}|_E = \vec{n} \cdot \vec{\rho}^- \quad (\text{J.4.47})$$

that is, the expression  $\vec{n} \cdot \vec{\rho}$  is a constant along the edge E; this observation motivates the definition of a, the edge distance

$$a = \vec{n} \cdot \vec{\rho}|_E = \vec{n} \cdot \vec{\rho}^- = \vec{n} \cdot \vec{\rho}^+ \quad (\text{J.4.48})$$

We may now express the vectors  $\rho^\pm$  in the new coordinate system as follows. Using (J.4.45) we have

$$\vec{\rho}^\pm = (\vec{n} \cdot \vec{\rho}^\pm) \vec{n} + (\vec{t} \cdot \vec{\rho}^\pm) \vec{t} \quad (\text{J.4.49})$$

Now, defining  $v^\pm$  by

$$v^\pm = \vec{\rho}^\pm \cdot \vec{t} \quad (\text{J.4.50})$$

we find by (J.4.48) that (as illustrated in figure J.16)

$$\vec{\rho}^\pm = a\vec{n} + v^\pm \vec{t} \quad (\text{J.4.51})$$

Equation (J.4.51) describes the endpoints of the edge E; for points interior to the edge E we have

$$\vec{\rho}|_E = a\vec{n} + v\vec{t} \quad (\text{J.4.52})$$

where

$$v = \vec{\rho} \cdot \vec{t}$$

The representation (J.4.52) now provides us with the information necessary to answer the question posed earlier (when is an edge E of  $\Sigma$  also an edge of  $\Sigma \cap C_h$ ). To see how this is done, we refer to figure J.17. First we note that what we are really trying to determine is if any points interior to E are also interior to  $C_h$ . In particular, if either  $\vec{\rho}^-$  or  $\vec{\rho}^+$  lies inside  $C_h$  the answer is YES. On the other hand, for all points  $\vec{\rho}$  in  $C_h$ ,  $|\vec{\rho}| \leq h$ . Since the smallest that  $|\vec{\rho}|_E$  can become is  $|a|$  (see equation (J.4.52)), we see that if  $|a| > h$  then the answer is NO. Now if  $|\vec{\rho}^+| > h$ ,  $|\vec{\rho}^-| > h$  and  $|a| \leq h$ , we must still determine whether or not E passes through  $C_h$  without either of its endpoints actually lying inside. This will happen provided  $v^- \leq 0 \leq v^+$ . Otherwise, E will not pass through  $C_h$ . Thus we have determined in all circumstances whether E intersects  $C_h$ . These can be summarized by the following algorithm.

Algorithm: (Does an edge E have any points in  $C_h$ )

$|a| > \bar{h} \Rightarrow \text{NO}$

$|a| < \bar{h} :$

$|\vec{\rho}^+| < \bar{h} \text{ or } |\vec{\rho}^-| < \bar{h} \Rightarrow \text{YES}$

$|\vec{\rho}^+| \geq \bar{h} \text{ and } |\vec{\rho}^-| \geq \bar{h}$

$0 \text{ in } [v-, v+] \Rightarrow \text{YES}$

$0 \text{ not in } [v-, v+] \Rightarrow \text{NO}$

Once we have made the determination that an edge E has points inside  $C_h$ , we must assign it a number k (for  $E_k$ ) and define the end points  $\rho_k^\pm$  for  $E_k$ .

If we define the critical value of  $v_c$  by

$$v_c = \sqrt{h^2 - a^2} \quad (\text{J.4.54})$$

then  $\rho_k^\pm$  are determined by the procedure

$$\vec{\rho}_k^- = \vec{\rho}^- \text{ if } |\vec{\rho}^-| < \bar{h}$$

$$= \vec{a}n - v_c \vec{t} \text{ if } |\vec{\rho}^-| \geq \bar{h}$$

$$\vec{\rho}_k^+ = \vec{\rho}^+ \text{ if } |\vec{\rho}^+| < \bar{h}$$

$$= \vec{a}n + v_c \vec{t} \text{ if } |\vec{\rho}^+| \geq \bar{h} \quad (\text{J.4.55})$$

#### J.4.4.5 The Function $P(\phi)$

We have now given complete procedures for the specification of  $E_k$ ,  $\rho_k^\pm$ ,  $\phi_k^\pm$ . Before we can evaluate the integrals (J.4.1), we must define a function  $P(\phi)$  (see Figure J.18) that describes the upper limit of integration from  $(x', y')$  to the boundary of  $\Sigma' \cap C_h$ .  $P(\phi)$  is defined as follows:

$$P(\phi) = \begin{cases} |h| & \text{if } \phi_k^\pm < \phi < \phi_{k+1}^\pm \\ P_k(\phi) & \text{if } \phi_k^- \leq \phi \leq \phi_k^+ \end{cases} \quad (\text{J.4.56})$$

where on each edge  $E_k$ ,  $P_k(\phi)$ , is the distance from  $(x', y')$  to  $E_k$

$$P_k(\phi) = \sqrt{a_k^2 + v_k(\phi)^2} \quad (\text{J.4.57})$$



In equation (J.4.57),  $v_k(\theta)$  denotes the local edge coordinate  $v$ , evaluated on the edge  $E_k$  and expressed as a function of  $\theta$ . Although we will never use it explicitly, we record it here for the sake of completeness

$$v_k(\theta) = a_k \tan(\theta - \theta_k' + \phi(a_k, v_k)) \quad (J.4.58)$$

With all these definitions available, it is now a fairly simple matter to write down the integrals (J.4.1) using polar coordinates. For the sake of concreteness, we evaluate the integral  $J$

$$J = \iint_{\Sigma' \cap C_h} \frac{d\xi' d\eta'}{\sqrt{h^2 - (\xi' - x')^2 - (\eta' - y')^2}} \quad (J.4.59)$$

Converting to polar coordinates centered at  $(x', y')$ , we have

$$d\xi' d\eta' = \rho d\rho d\theta \quad (J.4.60)$$

$$(\xi' - x')^2 + (\eta' - y')^2 = \rho^2 \quad (J.4.61)$$

so that (see Figure J.19 for limits of integration)

$$\begin{aligned} J &= \iint_{\Sigma' \cap C_h} \frac{\rho d\rho d\theta}{\sqrt{h^2 - \rho^2}} \\ &= \sum_{k=1}^n \left( \int_{\theta_k^-}^{\theta_k^+} d\theta \int_0^{P_k(\theta)} \frac{\rho d\rho}{h^2 - \rho^2} + \int_{\theta_k^+}^{\theta_{k+1}^-} d\theta \int_0^{|h|} \frac{\rho d\rho}{h^2 - \rho^2} \right) \end{aligned} \quad (J.4.62)$$

Evaluating the inner integrals in (J.4.62), we note

$$\int_0^P \frac{\rho d\rho}{\sqrt{h^2 - \rho^2}} = -\sqrt{h^2 - \rho^2} \Big|_0^P = -\sqrt{h^2 - P^2} + |h| \quad (J.4.63)$$

so that

$$\begin{aligned}
 J &= \sum_{k=1}^n \left( \int_{\phi_k^-}^{\phi_k^+} d\phi \left( |h| - \sqrt{h^2 - p_k(\phi)^2} \right) + \int_{\phi_k^+}^{\phi_{k+1}^-} |h| d\phi \right) \\
 &= h \sum_{k=1}^n \left( \int_{\phi_k^-}^{\phi_k^+} d\phi + \int_{\phi_k^+}^{\phi_{k+1}^-} d\phi \right) - \sum_{k=1}^n \int_{\phi_k^-}^{\phi_k^+} d\phi \sqrt{h^2 - p_k(\phi)^2} \\
 &= |h| (\phi_{n+1}^- - \phi_1^-) - \sum_{k=1}^n \int_{\phi_k^-}^{\phi_k^+} d\phi \sqrt{h^2 - p_k(\phi)^2} \quad (J.4.64)
 \end{aligned}$$

Now equation (J.4.23) for  $d\phi$  may be combined with the representation (J.4.45) for  $\rho$  to yield

$$\begin{aligned}
 \rho^2 d\phi &= (\vec{\rho} \times \vec{d\rho})_z = \\
 &= (\vec{u}\vec{n} + \vec{v}\vec{t}) \times (\vec{n} du + \vec{t} dv) \\
 &= u dv - v du \quad (J.4.65)
 \end{aligned}$$

Now if we agree to restrict  $\vec{\rho}$  to the edge  $E_k$ , we find  $u = \text{const.}$   
 $= a_k$ ,  $du = 0$ , and for  $d\phi$ ,

$$d\phi = \frac{u dv}{\rho^2} = \frac{a_k dv}{a_k^2 + v^2} \quad (J.4.66)$$

Substituting this into (J.4.64) and noting that when  $\phi = \phi_k^\pm$ ,  $v = v_k^\pm$ ,  
 (at the points  $\phi_k^\pm$ ) we obtain

$$J = |h| 2\pi C_0 - \sum_{k=1}^n \int_{v_k^-}^{v_k^+} \frac{a_k dv}{a_k^2 + v^2} \sqrt{h^2 - a_k^2 - v^2} \quad (J.4.67)$$

where we have used  $p_k(\phi)^2 = a_k^2 + v^2$  on edge  $E_k$ . The integral  
 on the right may be evaluated by elementary means to yield

$$J = 2\pi C_0 |h| - \sum_{k=1}^n [h \phi h(a_k R_k(v), hv) + a_k \phi h(v, R_k(v))]_{v_k^-}^{v_k^+} \quad (J.4.68)$$

where

$$R_k(v) = \sqrt{h^2 - a_k - v^2}$$

This integral is verified in section J.7.1.4, where it is identified as "I(X)."

## J.5 Hyperbolic Coordinates

Having examined the geometry of the circle in such gruesome detail we now do the same for the hyperbola. The motivation for this exercise stems from a desire to develop effective tools to deal with integrals of the following form arising from application of the transformations described in section (E.3) for subinclined panels:

$$\iint_{\Sigma' \cap D_p} \begin{Bmatrix} \sigma(\xi, n) \\ \nu(\xi, n) \end{Bmatrix} f(R) d\xi' dn' \quad (J.5.1)$$

where

$$\begin{aligned} R &= (\xi' - x')^2 - (n' - y')^2 - (\zeta' - z')^2 \\ D_p &= \{P' = (\xi', n', \zeta') \mid (\xi' - x')^2 \leq - (n' - y')^2 + (\xi' - z')^2\} \end{aligned} \quad (J.5.2)$$

and  $\Sigma'$  is some convex region lying in the  $(\xi', n')$  plane with oriented normal  $\vec{n}' = (0, 0, 1)$ . The points in  $\Sigma'$  are described by  $(\xi', n', \zeta')$  in the coordinate system  $X'$ , with  $\zeta'$  constant.

### J.5.1 Fundamental Results

As before,  $D_p$  denotes the domain of dependence described in the plane? local coordinate system  $X'$ .

Because the geometry of the hyperbola is much less intuitive than that of the circle, our discussion will have to rely rather heavily upon algebraic arguments. We will, however, try to parallel the discussion of section (J.4) as closely as possible.

We begin our discussion of (J.5.1) with a trivial change of variables. Variables  $s$  and  $t$  are defined by (see Fig. J.20)

$$\begin{aligned} s &= \xi' - x' \\ t &= n' - y' \end{aligned} \quad (J.5.4)$$

and the constant  $h$  is defined by

$$h = z' - \zeta' \quad (J.5.5)$$

Using these new variables, the integral (J.5.1) can be written

$$\iint_{\Sigma' \cap M_h} \begin{Bmatrix} \sigma(x' + s, y' + t) \\ \nu(x' + s, y' + t) \end{Bmatrix} f(R) ds dt \quad (J.5.6)$$

where the panel  $\Sigma'$  is of course translated, and  $H_h$  denotes the hyperbolic region

$$H_h = \{(s,t) \mid s \leq -\sqrt{t^2 + h^2}\} \quad (J.5.7)$$

Using the new variables, the distance function  $R$  is

$$R = \sqrt{s^2 - t^2 - h^2} \quad (J.5.8)$$

Having made this transformation of variables, we now remark that both the function  $R$  and the region  $H_h$  exhibit hyperbolic symmetry with respect to the origin (of the  $s$ - $t$  coordinate system). By this we mean that if  $s, t$  are defined by

$$\begin{bmatrix} \tilde{s} \\ \tilde{t} \end{bmatrix} = [A] \begin{bmatrix} s \\ t \end{bmatrix} \quad (J.5.9a)$$

where

$$A = \begin{bmatrix} a & b \\ b & a \end{bmatrix} \quad (J.5.9b)$$

$$\text{and} \quad a^2 - b^2 = 1$$

$$a > 0 \quad (J.5.9c)$$

and  $\tilde{H}_h, \tilde{R}$  by

$$\begin{aligned} \tilde{H}_h &= \{(\tilde{s}, \tilde{t}) \mid \tilde{s} \leq -\sqrt{\tilde{t}^2 + h^2}\} \\ \tilde{R} &= \sqrt{\tilde{s}^2 - \tilde{t}^2 - h^2} \end{aligned} \quad (J.5.10)$$

then

$$\tilde{R} = R$$

$$\text{and} \quad A H_h = \tilde{H}_h \quad (J.5.11)$$

that is to say, both the function  $R$  and the region  $H_h$  are invariant in form with respect to transformations of the type (J.5.9). We will use this fact very heavily in the treatment of the integrals (J.5.1).

A careful examination of the region of integration  $\Sigma' \cap H_h$  (see fig. J.20) reveals that its boundary is composed of both straight and curved segments. If the boundary of  $\Sigma' \cap H_h$  is traversed in a positive (counterclockwise) fashion, the straight segments of boundary are named  $E_1, E_2, \dots, E_n$  (see fig. J.21), in the order they are encountered. Here,  $n$  is the number of edges of  $\Sigma'$  having some points lying inside  $H_h$ ; the position of the lower end of edge  $E_k$  is denoted  $\bar{p}_k$  while the upper end is denoted  $a_k^+$ . The  $s$ - $t$  coordinates of  $\bar{p}_k^+$  are denoted  $(s_k^+, t_k^+)$ , that is

$$\vec{\rho}_k^- = (s_k^-, t_k^-) = \text{lower end of edge } E_k$$

$$\vec{\rho}_k^+ = (s_k^+, t_k^+) = \text{upper end of edge } E_k \quad (\text{J.5.12})$$

Next, we introduce the hyperbolic coordinate system for the region  $\{(s, t) \mid s < -|t|\}$  of the  $s$ - $t$  plane. For a point  $\vec{\rho} = (s, t)$  lying in this region, hyperbolic phase  $\phi$  and hyperbolic radius  $\rho$  are defined by the requirement that

$$\vec{\rho} = \begin{pmatrix} s \\ t \end{pmatrix} = \begin{pmatrix} -\rho \cosh \phi \\ -\rho \sinh \phi \end{pmatrix} \quad (\text{J.5.13})$$

Here,

$$\begin{aligned} \cosh x &= 1/2(e^x + e^{-x}) \\ \sinh x &= 1/2(e^x - e^{-x}) \end{aligned} \quad (\text{J.5.14})$$

We define

$$\rho = \sqrt{s^2 - t^2} \quad (\text{J.5.15})$$

and defining

$$\tanh x = \frac{\sinh x}{\cosh x} \quad (\text{J.5.16})$$

and

$$\tanh^{-1} x = y \text{ such that } \tanh y = x \quad (\text{J.5.17a})$$

we obtain

$$\phi = \tanh^{-1} (t/s) \quad (\text{J.5.17b})$$

Solving (J.5.17),

$$\frac{e^\phi - e^{-\phi}}{e^\phi + e^{-\phi}} = \frac{t}{s} \quad (\text{J.5.18})$$

$$\text{or } s(e^\phi - e^{-\phi}) = t(e^\phi + e^{-\phi}) \quad (\text{J.5.19})$$

$$\text{or } (s - t)e^\phi = (s + t)e^{-\phi} \quad (\text{J.5.20})$$

$$\text{or } e^{2\phi} = \frac{s+t}{s-t} \quad (\text{J.5.21})$$

$$\text{or } \phi = 1/2 \log \left( \frac{s+t}{s-t} \right) \quad (\text{J.5.22})$$

In particular, the hyperbolic phase of the points  $\vec{p}_k^*$  is denoted  $\phi_k^*$ :

$$\phi_k^* = 1/2 \log \left( \frac{s_k^* + t_k^*}{s_k^* - t_k^*} \right) \quad (\text{J.5.23})$$

It is well to notice that not nearly as much care is required in the definition of hyperbolic phase as was required in the definition of circular phase in sec. J.4. The reason for this simplicity is that phase wrap simply does not occur when one is dealing with hyperbolic phase.

Having defined the edges  $E_k$ , corner points  $\vec{p}_k^*$ , and corner phases  $\phi_k^*$  of the region  $\Sigma \cap H_h$  we now delve more deeply into the problem of determining which edges  $E$  of  $\Sigma'$  are also edges of  $\Sigma \cap H_h$ . Thus, given an oriented edge  $\vec{E}$  with lower end point  $\vec{p}_-$  and upper end point  $\vec{p}_+$ , we seek to determine if  $E$  has any points lying inside  $H_h$ ; if it does,  $E$ , or part of  $E$  will be an edge  $E_k$  of  $\Sigma \cap H_h$ . In addition, we will also want to determine the point (or points) at which  $E$  enters or exits the region  $H_h$ .

In order to answer these questions precisely, we need to define a number of new concepts. These include:

- (i) A pseudo inner product  $\langle \cdot, \cdot \rangle$
- (ii) The edge tangent  $\vec{t}$
- (iii) The edge normal  $\vec{n}$ , and conformal  $\vec{d}$
- (iv) The edge distance  $a$ , and edge variable  $v$ , and
- (v) Differential arc length,  $ds$ , along an edge.

The pseudo inner product on two vectors, denoted  $\langle \cdot, \cdot \rangle$  is defined by the expression

$$\langle a, b \rangle = -a_\xi b_\xi + a_n b_n \quad (\text{J.5.24})$$

For points  $\vec{p}$  lying inside  $H_h$ , we have

$$\langle \vec{p}, \vec{p} \rangle = -s^2 + t^2 \leq -h^2 \quad (\text{J.5.25})$$

an inequality that follows directly from the specification (J.5.7) of  $H_h$ . This inequality, combined with the condition that  $s$  be negative, provides a very useful characterization of those points lying inside  $H_h$ :

$$\vec{p} \in H_h \text{ if and only if } s < 0 \text{ and } \langle \vec{p}, \vec{p} \rangle \leq -h^2 \quad (\text{J.5.26})$$

The usefulness of this inner product stems from the fact that it is invariant with respect to hyperbolic transformations of the form (J.5.9). Thus, if  $\hat{x}$  and  $\hat{y}$  are vectors of length two, and  $\tilde{x}$  and  $\tilde{y}$  are defined by

$$\begin{aligned}\tilde{x} &= A\hat{x} \\ \tilde{y} &= A\hat{y}\end{aligned}\quad A = \begin{bmatrix} a & b \\ b & a \end{bmatrix}, \quad a^2 - b^2 = 1 \quad (J.5.27)$$

then

$$\langle \tilde{x}, \tilde{y} \rangle = \langle \hat{x}, \hat{y} \rangle \quad (J.5.28)$$

The edge tangent  $\hat{t}$  to an edge  $f$ , with lower end point  $\hat{\phi}$  and upper end point  $\hat{\phi}^*$ , is defined by the expression

$$t = (t_x, t_y) = \frac{\hat{\phi}^* - \hat{\phi}}{\langle \hat{\phi}^* - \hat{\phi}, \hat{\phi}^* - \hat{\phi} \rangle} \quad (J.5.29)$$

We have chosen the normalization for  $t$  given by (J.5.29) because this particular normalization is invariant with respect to hyperbolic transformations of the form (J.5.9). With  $t$  defined by (J.5.29), we can give the corresponding edge tangent  $\tilde{t}$  in the coordinate system  $X'$ ; we have,

$$\tilde{t} = \begin{bmatrix} t_x \\ t_y \\ 0 \end{bmatrix} \quad (J.5.30)$$

Recall from (J.5.28) the definition of subsonic and supersonic edges. The inner product  $\langle \tilde{t}, \tilde{t} \rangle$ , defined by

$$\langle \tilde{t}, \tilde{t} \rangle = \tilde{t}^T C_0 \tilde{t} \quad (J.5.31)$$

in reference coordinates, is given in  $X'$  coordinates by

$$\langle \tilde{t}', \tilde{t}' \rangle = \tilde{t}'^T C' \tilde{t}' \quad (J.5.32)$$

where, from section 4.1,

$$C' = \begin{bmatrix} r & s \\ s & r \end{bmatrix} \quad (J.5.33)$$

Note that in this section, we have  $r = 1$  and  $s = -1$  (subinclined panel in supersonic flow). Thus,  $f$  is a subsonic edge if and only if

$$\langle \tilde{t}', \tilde{t}' \rangle > 0 \quad (J.5.34)$$



if and only if

$$t_\xi^2 - t_n^2 > 0 \quad (\text{J.5.35})$$

if and only if

$$\langle \vec{t}, \vec{t} \rangle < 0 \quad (\text{J.5.36})$$

Similarly, E is a supersonic edge when

$$\langle \vec{t}, \vec{t} \rangle > 0 \quad (\text{J.5.37})$$

Note that (J.5.29) is undefined for sonic edges. We will not treat them explicitly in this section; later we will deal with them by a limiting process.

Since the definition (J.5.29) of  $\vec{t}$  ensures that

$$|\langle \vec{t}, \vec{t} \rangle| = 1$$

we obtain the normalization conditions on  $\vec{t}$

$$(\text{subsonic edges}) \quad \langle \vec{t}, \vec{t} \rangle = -t_\xi^2 + t_n^2 = -1 \quad (\text{J.5.38})$$

$$(\text{supersonic edges}) \quad \langle \vec{t}, \vec{t} \rangle = +1 \quad (\text{J.5.39})$$

Next, the edge normal  $\vec{n}$  and conormal  $\vec{v}$  are defined by

$$\vec{n} = \begin{pmatrix} n_\xi \\ n_n \end{pmatrix} = \begin{pmatrix} t_n \\ -t_\xi \end{pmatrix} \quad (\text{J.5.40})$$

$$\vec{v} = \begin{pmatrix} -n_\xi \\ n_n \end{pmatrix} = \begin{pmatrix} -t_n \\ -t_\xi \end{pmatrix} \quad (\text{J.5.41})$$

It is well to note that  $\vec{n}$  as defined by (J.5.40) is an outward edge normal to edge E. That  $\vec{n}$  is normal (i.e. perpendicular) to edge E follows from the computation

$$\vec{n} \cdot \vec{t} = t_n t_\xi + (-t_\xi t_n) = 0 \quad (\text{J.5.42})$$

and that it points outward follows from the computation (see figure 5.22)

$$(\vec{n} \times \vec{t})_\zeta = n_\xi t_n - n_n t_\xi = t_n^2 + t_\xi^2 > 0 \quad (\text{J.5.43})$$

Note that  $\vec{n} \times \vec{t}$  points out of the page (its  $\zeta$  component is positive). Finally we note that for any vector  $\vec{p}$ , the following relationship holds by virtue of the definition (J.5.41) of  $\vec{v}$ .

$$\vec{p} \cdot \vec{n} = \langle \vec{p}, \vec{v} \rangle \quad (\text{J.5.44})$$

The edge distance  $a$  and the edge variable  $v$  are defined by

$$a = \vec{n} \cdot \vec{p} = \langle \vec{v}, \vec{p} \rangle \quad (\text{J.5.45})$$

$$v = \langle \vec{t}, \vec{p} \rangle \quad (\text{J.5.46})$$

where  $\vec{p}$  is any point on the edge  $E$  (see figure J.16 or J.18). The number  $a$ , of course, is independent of which point along the edge  $E$  is used to compute it.

Note that the vectors  $\vec{v}$  and  $\vec{t}$  are linearly independent (i.e., nonparallel). This fact follows from the computation

$$(\vec{v} \times \vec{t})_z = v_x t_n - v_n t_x = -t_n^2 + t_x^2 = \pm 1 \quad (\text{J.5.47})$$

by (J.5.38-39). Thus, the position vector  $\vec{p}$  can be expressed as a linear combination of  $\vec{v}$  and  $\vec{t}$

$$\vec{p} = r_1 \vec{v} + r_2 \vec{t} \quad (\text{J.5.48})$$

Using the normalization conditions

$$\langle \vec{t}, \vec{t} \rangle = -(t_x^2 - t_n^2) \quad (\text{J.5.49a})$$

$$\langle \vec{v}, \vec{v} \rangle = -v_x^2 + v_n^2 = -t_n^2 + t_x^2 \quad (\text{J.5.49b})$$

and the orthogonality condition

$$\langle \vec{v}, \vec{t} \rangle = \vec{n} \cdot \vec{t} = 0 \quad (\text{J.5.49c})$$

we can solve for  $r_1$  and  $r_2$  in terms of  $a$  and  $v$ . Taking the pseudo inner product of (J.5.48) with  $\vec{v}$  gives

$$a = \langle \vec{p}, \vec{v} \rangle = r_1 \langle \vec{v}, \vec{v} \rangle = r_1 (t_x^2 - t_n^2) \quad (\text{J.5.50a})$$

while doing the same thing with  $\vec{t}$  yields

$$v = \langle \vec{p}, \vec{t} \rangle = r_2 \langle \vec{t}, \vec{t} \rangle = -r_2 (t_x^2 - t_n^2) \quad (\text{J.5.50b})$$

Substituting these expressions back into (J.5.48) and taking account of the fact that  $t_x^2 - t_n^2 = \pm 1$  we obtain

$$\vec{p} = (t_x^2 - t_n^2) (a \vec{v} - v \vec{t}) \quad (\text{J.5.51a})$$

or, using (J.5.38-39)

$$\vec{p} = a \vec{v} - v \vec{t} \quad (\text{subsonic edge}) \quad (\text{J.5.51b})$$

$$\vec{p} = -a \vec{v} + v \vec{t} \quad (\text{supersonic edge}) \quad (\text{J.5.51c})$$

Equations (J.5.50-51) now enable us to relate the differential of the edge variable,  $dv$ , to the differential arc length,  $ds$ . Differential arc length  $ds$  is defined by

$$ds = \frac{\vec{t} \cdot d\vec{\rho}}{|\vec{t}|} \quad (\text{J.5.52})$$

Using (J.5.50-51) we then find

$$\begin{aligned} ds &= -|\vec{t}| dv && (\text{subsonic edge}) \\ &= |\vec{t}| dv && (\text{supersonic edge}) \end{aligned} \quad (\text{J.5.53})$$

Thus,  $v$  decreases along subsonic edges and increases along supersonic edges.

With the machinery developed above, we are now in a position to determine which edges  $E$  intersect the region  $H_h$ . In doing this, we will treat the cases of subsonic and supersonic edges separately. First, we treat the subsonic edge.

#### J.5.2 Subsonic Edges

For  $E$  a subsonic edge with tangent  $\vec{t}$  defined by (J.5.29), we define an edge coordinate transformation of the type (J.5.9)

$$\vec{\rho} = \begin{Bmatrix} \tilde{s} \\ \tilde{t} \end{Bmatrix} = A \begin{Bmatrix} s \\ t \end{Bmatrix} = A\vec{s} \quad (\text{J.5.54})$$

where

$$A = \begin{bmatrix} t_E & -t_n \\ -t_n & t_E \end{bmatrix} s_E \quad (\text{J.5.55})$$

The matrix  $A$  defined by (J.5.55) maps the region  $H_h$  into itself and preserves the pseudo-inner product  $\langle \cdot, \cdot \rangle$ . The coordinate functions  $\tilde{s}$ ,  $\tilde{t}$  may be easily expressed using the pseudo inner product as follows

$$\begin{aligned} \tilde{s} &= s_E (t_E \rho_E - t_n \rho_n) = -s_E \langle \vec{t}, \vec{\rho} \rangle \\ \tilde{t} &= s_E (-t_n \rho_E + t_E \rho_n) = -s_E \langle \vec{n}, \vec{\rho} \rangle = -s_E \langle \vec{v}, \vec{\rho} \rangle \end{aligned} \quad (\text{J.5.56})$$

Thus, for points  $\vec{\rho}$  lying on the edge  $E$ , the  $\tilde{s}$  and  $\tilde{t}$  coordinates are given

$$\begin{aligned} \tilde{s} &= -vs_E \\ \tilde{t} &= -a s_E = \text{cons.} \end{aligned} \quad (\text{J.5.57})$$

so that the image of  $E$  under  $A$ , denoted  $\tilde{E}$ , is a line parallel to the  $s$  axis, as shown in figure J.23.

Note that for the edge E in figure J.23,

$$\begin{aligned} s_{\xi} &= 1 \\ a &= (\vec{\sigma}, \vec{n}) < 0 \end{aligned} \quad (J.5.58)$$

and thus

$$\tilde{t} = a > 0 \quad (J.5.59)$$

A careful examination of Figure J.23 reveals that it is a fairly easy matter to determine if an edge image E has any points lying inside  $H_h = \{(\tilde{z}, \tilde{t}) \mid \tilde{z} < (t^2 + h^2)^{1/2}\}$ . Since E is parallel to the s axis and since such lines can intersect the boundary of  $H_h$  at most once, E will have points lying inside  $H_h$  if and only if one of the image end points,  $\vec{\sigma}^-$  or  $\vec{\sigma}^+$ , lies inside  $H_h$ . Furthermore, the point  $\vec{\sigma}_c$  at which the edge E either enters or exits  $H_h$  is given.

$$\vec{\sigma}_c = \begin{pmatrix} \tilde{z}_c \\ t_c \end{pmatrix} = \begin{pmatrix} -\sqrt{h^2 + a^2} \\ -s_{\xi} a \end{pmatrix} \quad (J.5.60)$$

The point  $\vec{\sigma}_c$  will be a point of exit if  $s_{\xi} = +1$  and a point of entry if  $s_{\xi} = -1$ .

Now since the transformation A is invertible, the above remarks about the image edge E can yield similar statements about the original edge E. In doing this, we must relate the position vector  $\rho$  to its image coordinates. This is done by combining (J.5.57) into (J.5.51a) to obtain

$$\vec{\sigma} = a \vec{v} - v \vec{t} = s_{\xi} (-\tilde{t} \vec{v} + \tilde{z} \vec{t}) \quad (J.5.61)$$

With this connection established we can now state an algorithm for determining if a subsonic edge E intersects the region  $H_h$ .

ALGORITHM: Does a subsonic edge E with lower and upper endpoints  $\vec{\sigma}^-$  and  $\vec{\sigma}^+$  intersect  $H_h$ . If it does, compute  $\vec{\rho}_k$  and  $\vec{\rho}_k$  appropriately.

Assume  $-t_{\xi}^2 + t_h^2 = -1$  (subsonic)

$\rho^- \notin H_h$  and  $\rho^+ \notin H_h \rightarrow$  NO

$\rho^- \in H_h$  or  $\rho^+ \in H_h \rightarrow$  YES (J.5.62)

Case  $s_{\xi} = +1$  (Edge E leaves  $H$ )

$$\vec{\rho}_k^+ = \vec{\rho}_c$$

$$\vec{\rho}_k^- = \vec{\sigma}^-$$

(J.5.63)

Case  $s = -1$  (Edge E enters  $H_h$ )

$$\begin{aligned}\vec{\rho}_k^+ &= \vec{\rho}^+ \\ \vec{\rho}_k^- &= \vec{\rho}_c\end{aligned}\quad (J.5.64)$$

where, using (J.5.60) and (J.5.61),

$$\begin{aligned}\vec{\rho}_c &= s_\xi (-\tilde{t}_c \vec{v} + \tilde{s}_c \vec{t}) \\ &= a \vec{v} - s \vec{t} \sqrt{h^2 + a^2}\end{aligned}\quad (J.5.65)$$

We complete our discussion of subsonic edges by developing the relation between the differential of the edge variable,  $dv$ , and the differential of hyperbolic phase,  $d\phi$ .

We define the angle of hyperbolic rotation  $X$  by

$$X = \tanh^{-1} \left( \frac{t_n}{t_\xi} \right) = \text{phh}(|t_\xi|, s_\xi t_n) \quad (J.5.66)$$

where "hyperbolic phase"  $\text{phh}$  is defined by (see J.5.22-23))

$$\text{phh}(x, y) = \tanh^{-1} \left( \frac{y}{x} \right) = \frac{1}{2} \log \left( \frac{x+y}{x-y} \right) \quad (J.5.67)$$

Then, the matrix  $A$  defined by (J.5.55) is given by

$$A = \begin{bmatrix} \cosh X & -\sinh X \\ -\sinh X & \cosh X \end{bmatrix} \quad (J.5.68)$$

Substituting this expression and the expression (J.5.13) for  $\vec{\rho}$  into (J.5.54) yields for  $\vec{\rho}$ :

$$\begin{bmatrix} \cosh X & -\sinh X \\ -\sinh X & \cosh X \end{bmatrix} \begin{bmatrix} -\rho \cosh \phi \\ -\rho \sinh \phi \end{bmatrix} = \begin{bmatrix} -\rho \cosh (\phi - X) \\ -\rho \sinh (\phi - X) \end{bmatrix} \quad (J.5.69)$$

Now, for points lying on the edge E, equation (J.5.57) gives the values for the  $s$ - $t$  coordinates, combining this result with (J.5.69) yields

$$\vec{\rho} = \begin{bmatrix} \tilde{s} \\ \tilde{t} \end{bmatrix} = \begin{bmatrix} -s_\xi v \\ -s_\xi a \end{bmatrix} = \begin{bmatrix} -\rho \cosh (\phi - X) \\ -\rho \sinh (\phi - X) \end{bmatrix} \quad (J.5.70)$$

Solving equation (J.5.70) for  $\phi$  and  $\rho$  now gives

$$\begin{aligned}\rho &= \sqrt{v^2 - a^2} \\ \phi &= \tanh^{-1}(a/v) + X\end{aligned}\quad (\text{J.5.71})$$

We can differentiate the second of these quantities to obtain  $d\phi$ . First, we develop two differentiation formulas which will be of use.

The first of these is

$$\begin{aligned}\frac{d}{dt} \text{ph}(x(t), y(t)) &= \\ \frac{d}{dt} \tan^{-1} \left( \frac{y(t)}{x(t)} \right) &= \\ (\text{after some algebra})\end{aligned}\quad (\text{J.5.72})$$

$$\frac{x \frac{dy}{dt} - y \frac{dx}{dt}}{x^2 + y^2} \quad (\text{J.5.73})$$

The second of these is

$$\begin{aligned}\frac{d}{dt} \text{phh}(x(t), y(t)) &= \\ \frac{d}{dt} \frac{1}{2} \log \left( \frac{x+y}{x-y} \right) &= \\ = \frac{1}{2} \left( \frac{x-y}{x+y} \right) \frac{d}{dt} \left( \frac{x+y}{x-y} \right) &= \\ = \frac{x \frac{dy}{dt} - y \frac{dx}{dt}}{x^2 - y^2} &= \\ \end{aligned}\quad (\text{J.5.74})$$

$$= \frac{1}{2} \left( \frac{x-y}{x+y} \right) \frac{d}{dt} \left( \frac{x+y}{x-y} \right) \quad (\text{J.5.75})$$

$$= \frac{x \frac{dy}{dt} - y \frac{dx}{dt}}{x^2 - y^2} \quad (\text{J.5.76})$$

Applying (J.5.76) to (J.5.71), and noting that  $a$  is a constant,

$$\frac{d\phi}{dv} = \frac{-a \frac{dv}{dv}}{v^2 - a^2} \quad (\text{J.5.77})$$

and thus

$$d\phi = \frac{a}{a^2 - v^2} dv \quad (J.5.78)$$

A quantity that will be useful in our computation of the integrals (J.5.1) is the value of  $v$  along an edge  $E_k$ . Taking the ratio of the two equations contained in (J.5.70) yields

$$v = v_k(\phi) = \frac{a}{\tanh(\phi - \chi)} \quad (J.5.79)$$

(by definition)

$$a \coth(\phi - \chi)$$

This completes our study of subsonic edges. We now turn to the treatment of supersonic edges.

### J.5.3 Supersonic Edges

For  $E$  a supersonic edge with tangent  $\vec{t}$  defined by (J.5.29), we define an edge coordinate transformation of the type (J.5.9)

$$\vec{\sigma} = \begin{pmatrix} \tilde{s} \\ \tilde{t} \end{pmatrix} = A \begin{pmatrix} s \\ t \end{pmatrix} = A\vec{\sigma} \quad (J.5.80)$$

where

$$A = s_n \begin{bmatrix} t_n & -t_\xi \\ -t_\xi & t_n \end{bmatrix} \quad (J.5.81)$$

$$s_n = \text{sign}(t_n)$$

That the matrix  $A$  so defined is a hyperbolic transformation of the form (J.5.9) follows from the normalization condition for  $\vec{t}$ , (J.5.39),  $t_n^2 - t_\xi^2 = 1$ .

For a given point  $p$ , it is a trivial matter to compute the corresponding  $\tilde{s}$ - $\tilde{t}$  coordinate functions. Doing this, and using the pseudo-inner product, we find

$$\begin{aligned}\tilde{s} &= s_n(t_n \rho_{\xi} - t_{\xi} \rho_n) = s_n \vec{n} \cdot \vec{p} = s_n \langle \vec{n}, \vec{p} \rangle \\ \tilde{t} &= s_n(-t_{\xi} \rho_{\xi} + t_n \rho_n) = s_n \langle \vec{t}, \vec{p} \rangle\end{aligned}\quad (J.5.82)$$

Taking account of the definitions of  $a$  and  $v$  (J.5.45-46) we then find that, for points  $\vec{p}$  on  $E$ ,

$$\begin{aligned}\tilde{s} &= s_n a = \text{const.} \\ \tilde{t} &= s_n v\end{aligned}\quad (J.5.83)$$

Thus  $\tilde{E}$ , the image of  $E$ , is a line parallel to the  $t$ -axis as shown in fig. J.24.

Note that for the edge illustrated there,

$$\begin{aligned}s_n &= -1 \\ a &= \vec{p} \cdot \vec{n} > 0\end{aligned}\quad (J.5.84)$$

and thus

$$\tilde{s} = s_n a < 0 \quad (J.5.85)$$

A careful examination of fig. J.24 reveals that the image edge  $E$  can have points lying inside  $H_h$  even when neither endpoint,  $\vec{p}_+$  nor  $\vec{p}_-$  lies inside  $H_h$ . In particular, this can happen when the  $\tilde{s}$  coordinate of the line  $E$  satisfies  $\tilde{s} \leq -|h|$  and the  $t$  coordinate function has opposite signs when it is evaluated at the two endpoints of  $E$ . In light of equation (J.5.83) this criterion can be written

$$\begin{aligned}\tilde{E} \cap \tilde{H}_h &\text{ is not empty if} \\ \tilde{s} = s_n a < -|h| \text{ and } \tilde{t}_- \tilde{t}_+ &= v_- v_+ < 0\end{aligned}$$

where  $v_{\pm}$  are defined

$$v_{\pm} = \langle \vec{t}, \vec{p}_{\pm} \rangle \quad (J.5.87)$$

Having determined whether or not  $\tilde{E}$  intersects  $\tilde{H}_h$ , we now seek to determine the point of entry or exit of the edge  $E$ . Any such entry or exit point must lie on the boundary of  $\tilde{H}_h$ , that is its  $\tilde{s}$ - $\tilde{t}$  coordinates must satisfy

$$\tilde{s}^2 - \tilde{t}^2 = h^2 \quad (J.5.88)$$

Invoking the conditions (J.5.83) for points on  $\tilde{E}$ , this implies

$$a^2 - v^2 = h^2$$

or

$$|v| = v_c = \sqrt{a^2 - h^2} \quad (J.5.89)$$



where the above equation defines  $v_c$ , the critical value of the edge variable. Since the variable  $v$  increases along supersonic edges, (by virtue of (J.5.5')) we have in general

$$v_- < v_+ \quad (\text{J.5.90})$$

Now if an edge  $\tilde{E}$  that intersects  $\tilde{H}_h$  is such that  $\tilde{\rho}^- \notin \tilde{H}_h$ , then we must have

$$v_- < -v_c \quad (\text{J.5.91})$$

and the  $v$ -coordinate of point of entry equal to  $-v_c$ .

Similarly, if  $\tilde{E} \cap \tilde{H}_h \neq \emptyset$  but  $\tilde{\rho}^+ \notin \tilde{H}_h$ , we have

$$v_+ > v_c \quad (\text{J.5.92})$$

and the  $v$ -coordinate of point of exit equal to  $v_c$ .

As in the case of subsonic edges, we may transform these observations about supersonic edges back into the  $s$ - $t$  coordinate system by using the identity (J.5.51)

$$\tilde{\rho} = -a \tilde{v} + v \tilde{t} = -s_n \tilde{s} \tilde{v} + s_n \tilde{t} \tilde{t} \quad (\text{J.5.93})$$

We summarize our observations with the following algorithm.

ALGORITHM: Does a supersonic edge  $E$  with lower and upper endpoints

$\tilde{\rho}^-$  and  $\tilde{\rho}^+$  intersect  $H_h$ . If it does, compute  $\tilde{\rho}_k^-$  and

$\tilde{\rho}_k^+$  appropriately.

Assume  $-t_\xi^2 + t_n^2 = +1$ .

Determination if  $E \cap H \neq \emptyset$

$\tilde{\rho}^- \in H_h$  or  $\tilde{\rho}^+ \in H_h$   $\longrightarrow$  YES

$\tilde{\rho}^- \in H_h$  and  $\tilde{\rho}^+ \in H_h$

$s_n a < -|h|$  and  $v_- v_+ \leq 0$   $\longrightarrow$  YES

otherwise: NO

Determination of Endpoints: If the result of the above performance is YES, do the following

$$\begin{aligned} \text{if } \vec{p}^- \in H_h & \quad \text{then } \vec{p}_k^- = \vec{p}^- \\ & \quad \text{else } \vec{p}_k^- = -a\vec{v} - v_c \vec{t} \\ \text{if } \vec{p}^+ \in H_h & \quad \text{then } \vec{p}_k^+ = \vec{p}^+ \\ & \quad \text{else } \vec{p}_k^+ = -a\vec{v} + v_c \vec{t} \end{aligned}$$

We complete our discussion of supersonic edges by deriving the relationship between  $d\phi$  and  $dv$ . Proceeding as before, we now define  $X$  by

$$X = \tanh^{-1} \left( \frac{t_n}{t_n} \right) = \text{phh}(|t_n|, s_n t_n) \quad (\text{J.5.94})$$

With this definition of  $X$ , the matrix  $A$  of (J.5.81) can be written

$$A = \begin{bmatrix} \cosh & -\sinh \\ -\sinh & \cosh \end{bmatrix} \quad (\text{J.5.95})$$

Proceeding as before, we obtain the following relation analogous to (J.5.70).

$$\vec{p} = \begin{bmatrix} \vec{s} \\ \vec{t} \end{bmatrix} = \begin{bmatrix} s_n a \\ s_n v \end{bmatrix} = \begin{bmatrix} -\rho \cos(\phi - X) \\ -\rho \sinh(\phi - X) \end{bmatrix} \quad (\text{J.5.96})$$

Solving for  $\rho$  and  $\phi$  then yields

$$\begin{aligned} \rho &= \sqrt{a^2 - v^2} \\ \phi &= \tanh^{-1}(v/a) + X \end{aligned} \quad (\text{J.5.97})$$

Differentiating the second of these equations yields (by (J.5.74-76))

$$d\phi = \frac{adv}{a^2 - v^2} \quad (\text{J.5.98})$$

a relation identical to (J.5.78). Finally, we note that along the edge  $E_k$ ,  $v$  is given as a function of hyperbolic phase by

$$v = v_k(\phi) = a_k \tanh(\phi - X) \quad (\text{J.5.99})$$

This completes our study of supersonic edges.

#### J.5.4 Computation of the Integrals

We conclude our discussion of the geometry of the hyperbola by using our plethora of newly defined quantities to evaluate the integral J

$$J = \iint_{\Sigma' \cap H_h} \frac{ds \, dt}{R} \quad (J.5.100)$$

A suitably intricate region of integration,  $\Sigma' \cap H_h$ , is diagrammed in figures J.25a and J.25b. In these figures, the cross-hatched regions make positive contributions to the integral while shaded regions make negative contributions. In Figures J.25 this corresponds to the fact that  $d\theta > 0$  along edges 1,2,3 and 4 while  $d\theta < 0$  on edge 5.

Transforming the integral (J.5.100) to hyperbolic polar coordinates (cf. (J.5.13)), we see that the Jacobian  $\partial(s,t)/\partial(\rho, \theta)$  of the transformation is given by

$$\frac{\partial(s, t)}{\partial(\rho, \theta)} = \begin{bmatrix} -\cosh \theta & -\rho \sinh \theta \\ -\sinh \theta & -\rho \cosh \theta \end{bmatrix} \quad (J.5.101)$$

The determinant of this jacobian is easily computed

$$\det \left( \frac{\partial(s, t)}{\partial(\rho, \theta)} \right) = \rho \quad (J.5.102)$$

since

$$\cosh^2 \theta - \sinh^2 \theta = 1 \quad (J.5.103)$$

so that the element of area is given by

$$ds \, dt = \rho \, d\rho \, d\theta \quad (J.5.104)$$

The function R, given by (J.5.8), may be represented in polar coordinates by

$$R = \sqrt{\rho^2 - h^2} \quad (J.5.105)$$

Substituting (J.5.104-105) into (J.5.100) yields for J

$$J = \iint_{\Sigma' \cap H_h} \frac{\rho \, d\rho \, d\theta}{\rho^2 - h^2} \quad (J.5.106)$$

Now using the definitions given above it is easy to see that J can be evaluated as follows

$$J = \sum_{k=1}^n \int_{\phi_k^-}^{\phi_k^+} d\phi \int_0^{p_k(\phi)} \frac{\rho d\rho}{\sqrt{\rho^2 - h^2}} \quad (J.5.107)$$

where, using (J.5.71) and (J.5.97),  $p_k(\phi)$  is given by

$$p_k(\phi) = \begin{cases} \sqrt{v_k(\phi)^2 - a_k^2} & \text{subsonic edges} \\ \sqrt{a_k^2 - v_k(\phi)^2} & \text{supersonic edges} \end{cases}$$

and, from (J.5.79) and (J.5.99),  $v_k(\phi)$  is given by

$$v_k(\phi) = \begin{cases} a_k \coth(\phi - \chi) & \text{subsonic edges} \\ a_k \tanh(\phi - \chi) & \text{supersonic edges} \end{cases} \quad (J.5.108)$$

Performing the inner integral in (J.5.107) yields for J

$$J = \sum_{k=1}^n \int_{\phi_k^-}^{\phi_k^+} d\phi \sqrt{p_k(\phi)^2 - h^2} \quad (J.5.110)$$

Transforming each of the integrals in (J.5.110) into an edge integral with respect to the edge variable  $v$ , we have

$$d\phi = \frac{adv}{a^2 - v^2} \quad (J.5.111)$$

and

$$J = \sum_{k=1}^n \int_{v_k^-}^{v_k^+} \frac{a_k dv}{a_k^2 - v^2} R_k(v) \quad (J.5.112)$$

where  $R_k(v)$  is defined

$$\sqrt{v^2 - a^2 - h^2} \quad (\text{subsonic edges})$$

$$R_k(v) = \sqrt{\rho_k^2 - h^2} = \sqrt{a^2 - v^2 - h^2} \quad (\text{supersonic edges})$$

(J.5.113)

and  $v_k^\pm$  are defined by the obvious relations

$$v_k^\pm = \langle \vec{\rho}_k^\pm, \vec{t}_k \rangle \quad (\text{J.5.114})$$

Now the integral  $\int a R dv / (a^2 - v^2)$  can be evaluated by elementary means.

Doing this, one obtains (see the integrals  $J(X)$  in section J.7.1)

$$\int \frac{R_k a_k dv}{a_k^2 - v^2} = -h \operatorname{ph}(a_k R_k, h v) - a_k \tanh^{-1}(R_k/v) \quad (\text{subsonic case})$$

$$= -h \operatorname{ph}(a_k R_k, h v) - a_k \operatorname{ph}(v, R_k) \quad (\text{supersonic case})$$

(J.5.115)

Thus, using hyperbolic coordinates, it is a fairly easy matter to evaluate the integrals of type (J.5.1).

## J.6 The Panel Integral Matrices

In this section, we calculate matrices  $[S_0]$  and  $[D_0]$  which define the perturbation potential and velocity induced at a control point by a quadratically varying source strength or a cubically varying doublet strength on a convex, planar, polygonal region. These are  $(4 \times 6)$  and  $(4 \times 10)$  matrices respectively, defined by the equations

$$\begin{Bmatrix} \phi_s' \\ v_s' \end{Bmatrix} = [S_0] \begin{Bmatrix} \sigma_0 \\ \sigma_\xi \\ \vdots \\ \sigma_{\eta\eta} \end{Bmatrix} \quad (J.6.1)$$

and

$$\begin{Bmatrix} \phi_D' \\ v_D' \end{Bmatrix} = [D_0] \begin{Bmatrix} \mu_0 \\ \mu_\xi \\ \vdots \\ \mu_{\eta\eta\eta} \end{Bmatrix} \quad (J.6.2)$$

Here, the perturbation velocity  $\vec{v}_s'$  induced by the source strength and the regular part of  $\vec{v}_D'$  of the perturbation velocity induced by the doublet strength are expressed in a local  $(\xi', \eta', \zeta')$  coordinate system (see section E.3) with the property that  $\Sigma$  lies in the plane  $\zeta' = 0$ , and the compressible distance  $R$  from the control point  $P$  to the point of integration  $Q$  is written

$$R^2 = [P-Q, P-Q] = r(\xi'-x')^2 + s(\eta'-y')^2 + rs(\zeta'-z')^2 \quad (J.6.3)$$

There in local coordinates

$$\begin{aligned} \vec{P} &= (x', y', z') \\ \vec{Q} &= (\xi', \eta', \zeta') \end{aligned} \quad (J.6.4)$$

Now, the values of  $\vec{v}_s'$ ,  $\vec{v}_D'$ , and  $R$  are independent of the origin of the local coordinate system. The coefficients  $\sigma_0, \sigma_{\eta\eta}, \dots, \mu_0, \dots, \mu_{\eta\eta\eta}$  of the source and doublet polynomials are not, however (after all,  $\sigma_0$  and  $\mu_0$  are the source and doublet strengths at the origin). We define  $S$  and  $D$  to be the matrices for which (J.6.1) and (J.6.2) hold if the origin of the  $(\xi', \eta', \zeta')$  coordinate system is the point  $(x', y', 0)$ , that is, the projection of  $P$  to the plane containing  $\Sigma$ . This control point - dependent coordinate system origin is useful for computation of the panel integral matrix. In section J.6.6 we compute the matrices  $S_0$  and  $D_0$  which result from shifting the origin back to the standard one which is independent of the control point location.

## J.6.1 Preliminaries

### J.6.1.1 Transformation Rules

Consider the reference to local transformation,

$$A: X_0 \longrightarrow X' \quad (J.6.5)$$

We now review the transformation properties of various quantities (see section E.3). We have

$$\vec{R}' = [A] \vec{R}$$

$$\text{where } \vec{R} = \vec{P} - \vec{Q} \quad (J.6.6)$$

$$\vec{n}' = [A^{-T}] \vec{n}_0 \quad (J.6.7)$$

where

$$\vec{n}' = \begin{Bmatrix} 0 \\ 0 \\ 1 \end{Bmatrix}$$

$$\vec{n}' dS' = (\det A) [A^{-T}] \hat{n} dS$$

$$\text{and } dS' = \frac{1}{J} dS \quad (J.6.8)$$

where

$$dS' = d\xi' d\eta' \quad (J.6.9)$$

and J is the area Jacobian (the ratio of area in reference coordinates to area in local coordinates). Next,

$$[B'] = s_B^2 \begin{bmatrix} r & s & rs \\ & & \end{bmatrix} = A B_0 A^T \quad (J.6.10)$$

$$[C'] = \begin{bmatrix} r & s & rs \\ & & \end{bmatrix} = A^{-T} C_0 A^{-1} \quad (J.6.11)$$

$$\vec{\nabla}' = B' \vec{\nabla} = [B'] \begin{Bmatrix} \partial/\partial x' \\ \partial/\partial y' \\ \partial/\partial z' \end{Bmatrix} = A \vec{\nabla} \quad (\text{J.6.12})$$

We also define  $\vec{\nabla}_Q'$  and  $\vec{\nabla}_Q$  as gradient operators with respect to the location of the integration point Q whose local coordinates are  $(\xi', \eta', \zeta')$ . We define

$$\vec{G}' = \vec{\nabla}_Q' \left( \frac{1}{R} \right) = [A] \vec{G}_0 \quad (\text{J.6.13a})$$

where

$$\vec{G}_0 = \vec{\nabla}_Q \left( \frac{1}{R} \right) \quad (\text{J.6.13b})$$

#### J.6.1.2 Transformation of the Integrals

Now, recall from (B.0.1) that

$$\phi_s = -\frac{1}{\kappa} \iint_{\Sigma' \cap D_p} \frac{\sigma(Q)}{R} ds \quad (\text{J.6.14a})$$

$$= -\frac{J}{\kappa} \iint_{\Sigma' \cap D_p} \frac{\sigma(\xi', \eta')}{R} d\xi' d\eta' \quad (\text{J.6.14b})$$

$$= J \phi_{s'} \quad (\text{J.6.14c})$$

where

$$\phi_{s'} = -\frac{1}{\kappa} \iint_{\Sigma' \cap D_p} \frac{\sigma(\xi', \eta')}{R} d\xi' d\eta' \quad (\text{J.6.14d})$$

Next,

$$\phi_0 = \frac{1}{\kappa} \iint_{\Sigma' \cap D_p} \mu \hat{n} \cdot \vec{\nabla} \left( \frac{1}{R} \right) dS \quad (\text{J.6.15a})$$

$$= \frac{1}{\kappa \det A} \iint_{\Sigma' \cap D_p} \mu(\xi', \eta') \left\{ A^T \vec{n}' \right\} \cdot \vec{\nabla}_Q \left( \frac{1}{R} \right) d\xi' d\eta' \quad (\text{J.6.15b})$$

$$= \frac{1}{\kappa \det A} \iint_{\Sigma' \cap D_p} \mu(\xi', \eta') (\vec{n}' \cdot \vec{G}) d\xi' d\eta' \quad (\text{J.6.15c})$$



Now, by (E.3.90)

$$\det A = \beta^2 \quad (\text{J.6.16a})$$

and so, letting

$$\vec{H}' = \frac{1}{\beta^2} \vec{G}' \quad (\text{J.6.16b})$$

we have

$$\phi_D = \frac{1}{\kappa} \iint_{\Sigma' \cap D_P} \mu(\xi', n') \vec{H}' \cdot \vec{H}' d\xi' dn' \quad (\text{J.6.16c})$$

Note that

$$\frac{1}{\beta^2} [B'] = s [C'] \quad (\text{J.6.17})$$

and so we can also write

$$\vec{H}' = s[C'] \vec{\nabla}'_Q \left(\frac{1}{R}\right) \quad (\text{J.6.18})$$

Next, applying (B.3.9),

$$\vec{V}_S = \vec{\nabla}_P \phi_S = [A^T] \vec{\nabla}_P' \phi_S = J[A^T] \vec{V}_S' \quad (\text{J.6.20})$$

where

$$\begin{aligned} \vec{V}_S' &= \vec{\nabla}_P' \phi_S' = \\ &= \frac{1}{\kappa} \iint_{\Sigma' \cap D_P} \sigma(\xi', n') \vec{\nabla}_P' \left(\frac{1}{R}\right) d\xi' dn' \end{aligned} \quad (\text{J.6.21})$$

$$= \frac{1}{\kappa} \iint_{\Sigma' \cap D_P} \sigma(\xi', n') \vec{\nabla}_Q' \left(\frac{1}{R}\right) d\xi' dn' \quad (\text{J.6.22})$$

Finally,

$$\vec{V}_D^{*'} = \frac{1}{\kappa} \iint_{\Sigma' \cap D_P} (\vec{R} \times \vec{\nabla}_Q' \mu) \times \vec{\nabla}_Q' \left(\frac{1}{R}\right) dS \quad (\text{J.6.23})$$

Applying the transformation rule for cross products (E.1.12) to

$$\vec{v}_D^{*'} = \frac{1}{K} \iint_{\Sigma' \cap D_p} \left[ \left( \frac{1}{B^2} [A^T] \vec{n}' \, ds' \right) \times (A^T \vec{\nabla}'_Q u) \right] \times (A^{-1} \vec{G}') \quad (J.6.24)$$

we obtain

$$\vec{v}_D^{*'} = \frac{1}{K} \det(A^T) \iint_{\Sigma' \cap D_p} (A^{-1} \left( \frac{1}{B^2} \vec{n}' \, ds' \times \vec{\nabla}'_Q u \right)) \times (A^{-1} \vec{G}') \quad (J.6.25)$$

$$= - \frac{1}{K} [A^T] \iint_{\Sigma' \cap D_p} (\vec{\nabla}'_Q u \times \vec{n}') \times \frac{\vec{G}'}{B^2} \, ds' \quad (J.6.26)$$

$$= [A^T] \vec{v}_D^{*'} \quad (J.6.27)$$

where

$$\vec{v}_D^{*'} = - \frac{1}{K} \iint_{\Sigma' \cap D_p} (\vec{\nabla}'_Q u \times \hat{n}') \times \vec{n}' \, ds' \quad (J.6.28)$$

### J.6.1.3 Singularity Strength Coefficients

In Section J.6, we compute the quantities  $\phi'_s$ ,  $\phi'_D$ ,  $\vec{v}'_s$  and  $\vec{v}'_D$ , in terms of the coefficients describing the source and doublet strength on the panel. We now introduce some notation to describe the variation in singularity strength.

Let

$$\vec{\sigma} = \begin{bmatrix} \sigma_\xi \\ \sigma_n \end{bmatrix} \quad (J.6.29)$$

$$\vec{\mu} = \begin{bmatrix} \mu_\xi \\ \mu_n \end{bmatrix} \quad (J.6.30)$$

$$[\Sigma] = \begin{bmatrix} \sigma_\xi & \sigma_{\xi n} \\ \sigma_{\xi n} & \sigma_{nn} \end{bmatrix} \quad (J.6.31)$$

$$[M] = \begin{bmatrix} \mu_\xi & \mu_{\xi n} \\ \mu_{\xi n} & \mu_{nn} \end{bmatrix} \quad (J.6.32)$$

and let  $\gamma_l$  be the  $2 \times 2 \times 2$  tensor

$$\gamma_{\dots,1} = \begin{bmatrix} \mu_{\xi\xi\xi} & \mu_{\xi\xi\eta} \\ \mu_{\xi\xi\eta} & \mu_{\xi\eta\eta} \end{bmatrix} \quad (J.6.33)$$

$$\gamma_{\dots,2} = \begin{bmatrix} \mu_{\xi\xi\eta} & \mu_{\xi\eta\eta} \\ \mu_{\xi\eta\eta} & \mu_{\eta\eta\eta} \end{bmatrix} \quad (J.6.34)$$

Then,

$$\sigma(\xi', \eta') = \sigma_0 + \vec{\sigma}^T \vec{\rho} + 1/2 [\Sigma] : [\vec{\rho} \vec{\rho}^T] \quad (J.6.35)$$

where

$$\vec{\rho} = \begin{Bmatrix} \xi' \\ \eta' \end{Bmatrix} \quad (J.6.36)$$

and where for matrices A and B

$$[A] : [B] = \sum_{ij} A_{ij} B_{ij} \quad (J.6.37)$$

Similarly

$$\begin{aligned} \mu(\xi', \eta') = & \mu_0 + \vec{\mu}^T \vec{\rho} + 1/2 [M] : [\vec{\rho} \vec{\rho}^T] \\ & + 1/6 \sum_{i,j,k} \gamma_{ijk} \rho_i \rho_j \rho_k \end{aligned} \quad (J.6.38)$$

#### J.6.1.4 Uniform Formulas for Local Variables

Recall from sections J.4 and J.5 that we introduced certain expressions depending on an edge  $E_h$ . These are the radius vector

$$\vec{\rho} = \begin{Bmatrix} \xi' - x' \\ \eta' - y' \end{Bmatrix} \quad (J.6.39)$$

(this is consistent with Section J.6.1.3 if the local coordinate system is centered at the control point) with "magnitude"  $\rho$  satisfying

$$\rho^2 = (\xi' - x')^2 + (\eta' - y')^2 \quad (J.6.40)$$

the height  $h$  above the panel

$$h = z' - \zeta' \quad (\text{J.6.41})$$

the edge tangent

$$\vec{T}_k = \vec{p}_k^+ - \vec{p}_k^- \quad (\text{J.6.42})$$

where  $\vec{p}_k^\pm$  are the endpoints of  $E_k \cap D_p$ , the normalized edge tangent

$$\vec{t}_k = \begin{Bmatrix} t_\xi \\ t_\eta \end{Bmatrix} = \vec{T}_k / |\langle \vec{T}_k, \vec{T}_k \rangle|^{1/2} = \hat{t}_k / \tau \quad (\text{J.6.43})$$

where  $\hat{t}_k$  is a unit edge tangent, and for vectors  $a, b$  we define  $\langle \vec{a}, \vec{b} \rangle$  by

$$\langle \vec{a}, \vec{b} \rangle = rs a_\xi b_\xi + a_\eta b_\eta \quad (\text{J.6.44})$$

the edge normal

$$\vec{n}_k = \begin{Bmatrix} t_\eta \\ -t_\xi \end{Bmatrix} \quad (\text{J.6.45})$$

the edge distance

$$a_k = \vec{n}_k \cdot \vec{p}_k^\pm \quad (\text{J.6.46})$$

and the distance along the edge

$$v_k = \langle \vec{t}_k, \vec{p} \rangle \quad (\text{J.6.47})$$

In addition, we define the edge type indicator

$$q_k = \text{sign} [t_k, t_k] = rt_\xi^2 + st_\eta^2 = s \langle \vec{t}_k, \vec{t}_k \rangle \quad (\text{J.6.48})$$

which is 1 for subsonic edges, -1 for supersonic edges, the edge conormal

$$\vec{v}_k = [G] \vec{n}_k \quad (\text{J.6.49})$$

where

$$[G] = \begin{bmatrix} rs & \\ & 1 \end{bmatrix} \quad (\text{J.6.50})$$

and the edge cotangent

$$\vec{t}_k = [G] \vec{t}_{k1} \quad (J.6.51)$$

In terms of these definitions we have, combining (J.4.51), (J.5.50), (J.5.51), and (J.6.49),

$$\vec{p}_k = q_k r a_k v_k + a_k s v_k \vec{t}_k \quad (J.6.52)$$

From (J.6.44) and (J.6.49) we have

$$\langle \vec{v}_k, \vec{v}_k \rangle = rs t_n^2 + t_\xi^2 = rs \langle \vec{t}_k, \vec{t}_k \rangle \quad (J.6.53)$$

From (J.4.46) and (J.5.53) we obtain the differential of arc length

$$ds = sq |\vec{t}_k| dv \quad (J.6.54)$$

Next,

$$\begin{aligned} \langle \vec{v}_k, \vec{v}_k \rangle &= \langle \vec{n}_k, \vec{n}_k \rangle = t_\xi^2 + rst_n^2 \\ &= rs \langle \vec{t}_k, \vec{t}_k \rangle = rssq = rq \end{aligned} \quad (J.6.55)$$

Further,

$$\langle \vec{v}_k, \vec{t}_k \rangle = \left\langle \begin{pmatrix} rs & t_n \\ -t_\xi & \end{pmatrix}, \begin{pmatrix} t_\xi \\ t_n \end{pmatrix} \right\rangle = 0 \quad (J.6.56)$$

Thus, by (J.6.52)

$$\begin{aligned} \langle \vec{p}_k, \vec{p}_k \rangle &= a_k^2 \langle \vec{v}_k, \vec{v}_k \rangle + v_k^2 \langle \vec{t}_k, \vec{t}_k \rangle \\ &= rq_k a_k^2 + sq_k v_k^2 \end{aligned} \quad (J.6.57)$$

So,

$$\rho_k^2 = rs \langle \vec{p}_k, \vec{p}_k \rangle = sq_k a_k^2 + rq_k v_k^2 \quad (J.6.58)$$

Finally,

$$\begin{aligned} r^2 &= r(\xi', x')^2 + s(n' - y')^2 + rs(\zeta' - z')^2 \\ &= r\rho^2 + rsh^2 = \\ &= rsq_k a_k^2 + q_k v_k^2 + rsh^2 \end{aligned} \quad (J.6.59)$$

The above results will be used extensively in the following sections.

#### J.6.1.5 Differentiation Formulas

Now we introduce

$$\psi = \frac{1}{R} \quad (\text{J.6.60})$$

Many of our formulas will be terms of  $\psi$ ; an interested reader may compute the equations which would result if  $1/R$  were replaced by a different expression such as the Helmholtz kernel  $e^{i\omega R}/R$ .

We now derive some integration and differentiation formulas concerning  $\psi$  which will be useful. First,

$$\frac{\partial \psi}{\partial \xi'} = \frac{\partial}{\partial R} \frac{\partial R}{\partial \xi'} = \quad (\text{J.6.61})$$

(by (J.6.41) and (J.6.59))

$$\frac{\partial}{\partial R} \left( \frac{-rsh}{R} \right) \quad (\text{J.6.62})$$

Similarly,

$$\frac{\partial \psi}{\partial \rho} = \frac{\partial \psi}{\partial R} \frac{\partial R}{\partial \rho} \quad (\text{J.6.63})$$

By (J.6.59),

$$2RdR = 2\rho d\rho \quad (\text{J.6.64})$$

and so

$$\frac{\partial \psi}{\partial \rho} = \frac{r\rho}{R} \frac{\partial \psi}{\partial R} \quad (\text{J.6.65})$$

Thus,

$$\frac{\partial \psi}{\partial \xi'} = \frac{-sh}{\rho} \frac{\partial \psi}{\partial \rho} \quad (\text{J.6.66})$$

Next, defining

$$\vec{\nabla}_{2,Q}^i = [G] \begin{Bmatrix} \partial/\partial \xi' \\ \partial/\partial n' \end{Bmatrix} \quad (\text{J.6.67})$$

(J.6.39-40) yield

$$\vec{\nabla}_{2,Q}^1(\rho^2) = 2rs\vec{p} \quad (\text{J.6.68})$$

or

$$\vec{\nabla}_{2,Q}^1(\rho) = \frac{rs\vec{p}}{\rho} \quad (\text{J.6.69})$$

Thus,

$$\vec{\nabla}_{2,Q}^1(\psi) = \frac{rs\vec{p}}{\rho} \frac{\partial \psi}{\partial \rho} \quad (\text{J.6.70a})$$

and

$$\rho \frac{\partial \psi}{\partial \zeta'} = -\frac{sh\vec{p}}{\rho} \frac{\partial \psi}{\partial \rho} = -rh \vec{\nabla}_{2,Q}^1 \psi \quad (\text{J.6.70b})$$

Finally, let us introduce

$$X(R) = \int_0^R \vec{R} \psi(\vec{R}) d\vec{R} \quad (\text{J.6.71})$$

Then

$$\frac{\partial X}{\partial \rho} = \frac{\partial X}{\partial R} \frac{\partial R}{\partial \rho} = R \left( \frac{r\rho}{R} \right) = \rho \psi \quad (\text{J.6.72})$$

This concludes our derivation of preliminary integral formulas.

## J.6.2 Source Potential and Velocity

In this section we compute the matrix  $S$  defining  $\phi'_S$  and  $v'_S$  in terms of certain fundamental expressions.

### J.6.2.1 Source Potential

From (J.6.18),

$$\phi'_S = -\frac{1}{K} \iint_{\Sigma' \cap D_p} \sigma(\xi', n') d\xi' dn' \quad (\text{J.6.73})$$

= (by (J.6.35))

$$-\frac{1}{K} \left( \iint \sigma_0 dS' + \iint \vec{\sigma}^T \vec{p} dS' + \frac{1}{2} \iint [\Sigma] : [\vec{p} \vec{p}^T] dS' \right) \quad (\text{J.6.74})$$

Here we have used the fact that the coordinate system is centered on the projection of the control point to the panel, and thus

$$\begin{Bmatrix} \xi' - x' \\ \eta' - y' \end{Bmatrix} = \vec{p} \quad (\text{J.6.75})$$

So,

$$\phi_s' = \sigma_0 \left( -\frac{1}{\kappa} \iint \psi dS' \right) + \vec{p}^T \left\{ -\frac{1}{\kappa} \iint \vec{p} \psi dS' \right\} + 1/2 [\Sigma]: \left[ -\frac{1}{\kappa} \iint \vec{p}^T \psi dS' \right] \quad (\text{J.6.76})$$

Using (J.6.69) and (J.6.72),

$$\begin{aligned} \iint_{\Sigma'} \vec{p} \psi dS' &= \iint_{\Sigma'} \frac{\vec{p}}{\rho} (\rho \psi) dS' \\ &= \iint_{\Sigma'} (rs \vec{\nabla}_{2,Q'} \rho) \left( \frac{r \partial X}{\partial \rho} \right) dS' \end{aligned} \quad (\text{J.6.77})$$

$$s \iint_{\Sigma'} \vec{\nabla}_{2,Q'} dS' = s \int_{\partial \Sigma'} \frac{\vec{v}}{|\vec{v}|} X ds \quad (\text{J.6.78})$$

Equation (J.6.78) is obtained by using the two-dimensional version of Gauss' theorem; if  $f$  is any function on a planar region ,

$$\iint_{\Sigma} \vec{\nabla} f dS = \int_{\partial \Sigma} \frac{\vec{n}}{|\vec{n}|} f ds \quad (\text{J.6.79})$$

Applying [G] to (J.6.79), and noting that

$$|\vec{v}| = |\vec{n}| \quad (\text{J.6.80})$$

we obtain

$$\int_{\Sigma} \vec{\nabla}_{2'} f dS = \int_{\partial \Sigma'} \frac{\vec{v}}{|\vec{v}|} f ds \quad (\text{J.6.81})$$

Finally, using (J.6.69) and (J.6.72),

$$\vec{\nabla}_{2'} X = \frac{\partial X}{\partial \rho} \vec{\nabla}_{2'} \rho = s \psi \rho \quad (\text{J.6.82})$$

and thus

$$\iint_{\Sigma'} \vec{p} \vec{p}^T \psi dS' = s \iint_{\Sigma'} \vec{p} \vec{\nabla}_{2'}^T X ds \quad (\text{J.6.83})$$



Combining (J.6.76-78) and (J.6.83), we obtain

$$\begin{aligned} \phi_s' &= \sigma_0 \left( -\frac{1}{\kappa} \iint \psi dS' \right) \\ &+ \partial^T \left( -\frac{s}{\kappa} \int_{\partial \Sigma'} \partial X \frac{ds}{|\vec{n}|} \right) \\ &+ [\Sigma]: \left[ -\frac{s}{2\kappa} \iint_{\Sigma'} \partial^i \partial'^T \chi \quad dS' \right] \end{aligned} \quad (J.6.84)$$

#### J.6.2.2 Tangential Source Velocity

Now, from (J.6.22) and (J.6.35)

$$\vec{v}_{s'} = \frac{1}{\kappa} \iint_{\Sigma'} \sigma(\xi', n') \vec{\nabla}' Q' \psi \quad dS' \quad (J.6.85)$$

where

$$\vec{\nabla}' Q = \begin{Bmatrix} \partial/\partial \xi' \\ \partial/\partial \eta' \\ \partial/\partial \zeta' \end{Bmatrix} = \begin{Bmatrix} \partial'_{2,Q} \\ \partial'_{3,Q} \end{Bmatrix} \quad (J.6.86)$$

So,

$$v'_{s,\xi,n} = \iint_{\Sigma'} \sigma \vec{\nabla}'_{2,Q} \psi \quad dS' \quad (J.6.87)$$

Applying (J.6.35)

$$\begin{aligned} v'_{s,\xi,n} &= \frac{\sigma_0}{\kappa} \iint_{\Sigma'} \vec{\nabla}'_{2,Q} \psi \quad dS' + \\ &\frac{1}{\kappa} \left[ \iint_{\Sigma'} (\vec{\nabla}'_{2,Q} \psi) \partial^T dS' \partial + \right. \\ &\left. \sum_{i,j} \frac{1}{2\kappa} \left( \iint_{\Sigma'} \rho_i \rho_j (\vec{\nabla}'_{2,Q})_k \psi \quad dS' \right) [\Sigma]_{ij} \right] \end{aligned} \quad (J.6.88)$$

Now, applying (J.6.79)

$$\iint_{\Sigma'} \vec{\nabla}'_{2,Q} \psi \quad dS = \int_{\partial \Sigma'} \vec{n} \psi \frac{ds}{|\vec{n}|} \quad (J.6.89)$$

To compute the second term of (J.6.86), we extend (J.6.79) to a product  $fg$  of functions to obtain

$$\begin{aligned}\iint_{\Sigma'} \vec{\nabla}(fg) \, dS &= \iint_{\Sigma'} (f \vec{\nabla}g + g \vec{\nabla}f) \, dS \\ &= \int_{\partial \Sigma'} fg \frac{\vec{n}}{|\vec{n}|} \, ds\end{aligned}\quad (\text{J.6.91})$$

We thus obtain the general two dimensional integration by parts formula

$$\iint_{\Sigma'} f \vec{\nabla}g \, dS = \int_{\partial \Sigma'} fg \frac{\vec{n}}{|\vec{n}|} \, ds - \iint_{\Sigma'} g \vec{\nabla}f \, dS \quad (\text{J.6.92})$$

For later use, note that applying the definitions of  $\vec{\nabla}_2, \vec{\nabla}_2, \vec{\rho}$ , and  $[G]$  (equations (J.6.67), (J.6.36), and (J.6.50))

$$\iint_{\Sigma'} f \vec{\nabla}_2 g \, dS = \int_{\partial \Sigma'} fg \frac{\vec{v}}{|\vec{v}|} \, ds - \iint_{\Sigma'} g \vec{\nabla}f \, dS \quad (\text{J.6.93})$$

Now, applying (J.6.92)

$$\begin{aligned}\vec{\nabla}_2, Q \phi \vec{\rho}^T \, dS' &= \\ \int_{\partial \Sigma'} \psi \frac{\vec{n}}{|\vec{n}|} \vec{\rho}^T \, ds &- \iint_{\Sigma'} \psi [I] \, dS'\end{aligned}\quad (\text{J.6.94})$$

since

$$\vec{\nabla}_2, Q \vec{\rho}^T = \begin{bmatrix} 1 & 0 \\ 0 & 1 \end{bmatrix} = I \quad (\text{J.6.95})$$

Substituting (J.6.89) and (J.6.94) in (J.6.88),

$$\begin{aligned}\vec{v}'_{s, \zeta'} &= \frac{1}{\kappa} \left( \int_{\partial \Sigma'} \vec{n} \psi \frac{ds}{|\vec{n}|} \right) \sigma_0 \\ &+ \frac{1}{\kappa} \left[ \int_{\partial \Sigma'} \vec{n} \vec{\rho}^T \frac{\psi}{|\vec{n}|} \, ds \right] \vec{\sigma} - \frac{1}{\kappa} \left( \iint_{\Sigma'} \psi \, dS' \right) \vec{\sigma} \\ &+ \sum_{i,j} \frac{1}{2\kappa} \left( \iint_{\Sigma'} \rho_i \rho_j \vec{\nabla}'_2 Q \psi \, dS' \right) [\Sigma]_{ij}\end{aligned}\quad (\text{J.6.96})$$

### J.6.2.3 Normal Source Velocity

Finally

$$\vec{v}'_{s, \zeta'} = \frac{1}{\kappa} \iint_{\Sigma'} \sigma \frac{\partial \psi}{\partial \zeta'} \, dS' \quad (\text{J.6.97})$$

(using J.6.66)

$$\frac{-sh}{\kappa} \iint_{\Sigma'} \sigma \frac{1}{\rho} \frac{\partial \psi}{\partial \rho} dS' = \quad (J.6.98)$$

(by J.6.35)

$$\begin{aligned} & \left( \frac{-sh}{\kappa} \iint_{\Sigma'} \frac{1}{\rho} \frac{\partial \psi}{\partial \rho} dS' \right) \sigma_0 - \frac{sh}{\kappa} \iint_{\Sigma'} \frac{\vec{p}^T}{\rho} \frac{\partial \psi}{\partial \rho} dS' \vec{p} \\ & - \frac{1}{2} \left[ \frac{sh}{\kappa} \iint_{\Sigma'} \frac{\vec{p} \vec{p}^T}{\rho} \frac{\partial \psi}{\partial \rho} dS' \right] : [\Sigma] \end{aligned} \quad (J.6.99)$$

Now, by (J.6.70), (J.6.79) and multiplication by [G],

$$\begin{aligned} \iint_{\Sigma'} \frac{\vec{p}}{\rho} \frac{\partial \psi}{\partial \rho} dS' &= \int_{\partial \Sigma'} rs \vec{\nabla}_{2,Q'} \psi ds \\ &= rs \int_{\partial \Sigma'} \psi \frac{\vec{p}}{|\vec{p}|} ds \end{aligned} \quad (J.6.100)$$

Next, by (J.6.70)

$$\iint_{\Sigma'} [\rho \vec{p}^T] \frac{1}{\rho} \frac{\partial \psi}{\partial \rho} dS' = rs \iint_{\Sigma'} (\vec{\nabla}'_{2,Q}) \vec{p}^T dS' \quad (J.6.101)$$

= (using the integration by parts formula (J.6.93))

$$rs \int_{\partial \Sigma'} \frac{\vec{p}}{|\vec{p}|} \vec{p}^T ds - rs \iint_{\Sigma'} \vec{\nabla}'_{2,Q} \vec{p}^T dS' \quad (J.6.102)$$

$$= rs \int_{\partial \Sigma'} \frac{\vec{p}}{|\vec{p}|} \vec{p}^T ds - rs \iint_{\Sigma'} \psi [G] dS' \quad (J.6.103)$$

since

$$\vec{\nabla}_{2,Q'} \vec{p}^T = \begin{Bmatrix} rs & \partial/\partial \xi' \\ 0 & \partial/\partial \eta' \end{Bmatrix} \begin{bmatrix} \xi' & \eta' \end{bmatrix} \quad (J.6.104)$$

$$= \begin{bmatrix} rs & 0 \\ 0 & 1 \end{bmatrix} = [G] \quad (J.6.105)$$

Combining (J.6.99-104), we have

$$\begin{aligned}
 \vec{v}'_{S,\zeta} = & \left( \frac{-sh}{\kappa} \iint_{\Sigma'} \frac{1}{\rho} \frac{\partial \psi}{\partial \rho} dS' \right) \vec{e}_0 \\
 & - \frac{rh}{\kappa} \int_{\partial \Sigma'} \psi \vec{e}^T \frac{ds}{|\vec{e}|} \vec{e} \\
 & + \left[ \frac{-1}{2} \frac{rh}{\kappa} \int_{\partial \Sigma'} \psi \vec{e}^T \frac{ds}{|\vec{e}|} \right] : [\Sigma] \\
 & + \left( \frac{1}{2} \frac{rh}{\kappa} \iint_{\Sigma'} \psi dS' \right) [G] : [\Sigma]
 \end{aligned} \tag{J.6.106}$$

### J.6.3 Doublet Potential and Velocity

#### J.6.3.1 Doublet Potential

From (J.6.10) and (J.6.18)

$$\phi_D' = \frac{s}{\kappa} \iint_{\Sigma'} \mu \vec{n}'^T [C'] \vec{\nabla}'_Q \psi dS' \tag{J.6.107}$$

= (applying (J.6.7) and (J.6.11))

$$\frac{r}{\kappa} \iint_{\Sigma'} \mu \frac{\partial \psi}{\partial \zeta'} dS' \tag{J.6.108}$$

= (applying (J.6.66))

$$\frac{-rsh}{\kappa} \iint_{\Sigma'} \mu \frac{1}{\rho} \frac{\partial \psi}{\partial \rho} dS' = \tag{J.6.109}$$

$$\frac{-rsh}{\kappa} \left( \iint_{\Sigma'} \frac{1}{\rho} \frac{\partial \psi}{\partial \rho} dS' \right) \mu_0$$

$$\frac{-rsh}{\kappa} \int_{\Sigma'} \frac{\vec{p}}{\rho}^T \frac{\partial \psi}{\partial \rho} dS' \vec{p}$$

$$\frac{-rsh}{2\kappa} \left[ \iint_{\Sigma'} \frac{\vec{p} \vec{p}^T}{\rho} \frac{\partial \psi}{\partial \rho} dS' \right] : [M]$$

$$\frac{-rsh}{6\kappa} \sum_{ijk} \left\{ \iint_{\Sigma'} \rho_i \rho_j \rho_k \frac{1}{\rho} \frac{\partial \psi}{\partial \rho} dS' \right\} m_{ijk} \tag{J.6.110}$$

The first three integrals are identical to those arising in the evaluation of  $\vec{v}'_{S,\zeta}$ , and thus we need only consider the fourth integral.

Now, using (J.6.70)

$$\iint_{\Sigma'} \rho_i \rho_j \rho_k \frac{1}{\rho} \frac{\partial \psi}{\partial \rho} dS' =$$

$$rs \iint_{\Sigma'} \rho_i \rho_j (\tilde{\nabla}_2, Q)_k \psi dS' \quad (J.6.111)$$

Now, substituting equations (J.6.100), (J.6.103), and (J.6.111) in (J.6.11), we obtain

$$\phi_j = \frac{-rsh}{\kappa} \left( \iint_{\Sigma'} \frac{1}{\rho} \frac{\partial \psi}{\partial \rho} dS' \right) u_0$$

$$- \frac{h}{\kappa} \int_{\Sigma'} \frac{\vec{v}^T}{|\vec{v}|} ds_j \vec{u}$$

$$- \frac{h}{2\kappa} \left[ \int_{\Sigma'} \psi \frac{\vec{v}^T}{|\vec{v}|} \rho^T ds \right] : [M]$$

$$+ \frac{h}{2\kappa} \left( \iint_{\Sigma'} \psi dS' \right) [G] : [M]$$

$$- \frac{h}{6\kappa} \sum_{i,j,k} \left( \iint_{\Sigma'} \rho_i \rho_j (\tilde{\nabla}_2, Q)_k \psi dS' \right) m_{ijk} \quad (J.6.114)$$

### J.6.3.2 Tangential Doublet Velocity

Combining (J.6.7), (J.6.18), and (J.6.28), we have

$$\vec{v}_0^* = -\frac{1}{\kappa} \iint_{\Sigma'} \left\{ \begin{pmatrix} \partial u / \partial \xi' \\ \partial u / \partial \eta' \\ \partial u / \partial \zeta' \end{pmatrix} \times \begin{pmatrix} 0 \\ 0 \\ 1 \end{pmatrix} \right\} \times \begin{pmatrix} rs \partial \psi / \partial \xi' \\ \partial \psi / \partial \eta' \\ \partial \psi / \partial \zeta' \end{pmatrix} dS'$$

$$= -\frac{1}{\kappa} \iint_{\Sigma'} \begin{bmatrix} \partial u / \partial \eta' \\ -\partial u / \partial \xi' \\ 0 \end{bmatrix} \times \begin{bmatrix} rs \partial \psi / \partial \xi' \\ \partial \psi / \partial \eta' \\ rs \partial \psi / \partial \zeta' \end{bmatrix} dS' \quad (J.6.115)$$

$$= -\frac{1}{\kappa} \iint_{\Sigma'} \begin{pmatrix} -r(\partial u / \partial \xi')(\partial \psi / \partial \zeta') \\ -r(\partial u / \partial \eta')(\partial \psi / \partial \zeta') \\ (\partial u / \partial \eta')(\partial \psi / \partial \xi') \\ + rs (\partial u / \partial \xi')(\partial \psi / \partial \xi') \end{pmatrix} dS'$$

$$= - \left\{ \begin{aligned} & \frac{-r}{\kappa} \iint_{\Sigma'} \vec{\nabla}'_{2\mu} \frac{\partial \psi}{\partial \xi^{\mu}} dS' \\ & \frac{1}{\kappa} \iint_{\Sigma'} \vec{\nabla}'_{2,Q\mu} \cdot \vec{\nabla}'_{2,Q} \psi dS' \end{aligned} \right\} \quad (J.6.116)$$

In particular

$$\vec{v}_0^* = \frac{r}{\kappa} \iint_{\Sigma'} (\vec{\nabla}'_{2,Q\mu}) \frac{\partial \psi}{\partial \xi^{\mu}} dS' \quad (J.6.117)$$

Applying (J.6.38) and (J.6.66)

$$\begin{aligned} \vec{v}_{0,\xi,n}^* &= \frac{-rsh}{\kappa} \iint_{\Sigma'} \frac{1}{\rho} \frac{\partial \psi}{\partial \rho} \cdot \\ & \left\{ \vec{\nabla}'_{2,Q} \mu_0 + [\vec{\nabla}'_{2,Q\mu^T}] \vec{\mu} + \frac{1}{2} \vec{\nabla}'_{2,Q} ([\vec{\mu}\vec{\mu}^T]:[M]) \right. \\ & \left. + \frac{1}{6} \vec{\nabla}'_{2,Q} \left( \sum_{i,j,k} \rho_i \rho_j \rho_k m_{ijk} \right) \right\} dS' \end{aligned} \quad (J.6.118)$$

= (applying (J.6.90))

$$\begin{aligned} & - \frac{rsh}{\kappa} \left( \iint_{\Sigma'} \frac{1}{\rho} \frac{\partial \psi}{\partial \rho} dS' \right) \vec{\mu} - \frac{rsh}{\kappa} \iint_{\Sigma'} \frac{1}{\rho} \frac{\partial \psi}{\partial \rho} [M] \vec{\mu} dS' \\ & - \frac{rsh}{6\kappa} \sum_{i,j} \left( \iint_{\Sigma'} \frac{1}{\rho} \frac{\partial \psi}{\partial \rho} \rho_i \rho_j dS' \right) (m_{.,i,j} + m_{i,.,j} + m_{i,j,.}) \end{aligned} \quad (J.6.119)$$

Inspection of (J.6.33) and (J.6.34) shows that

$$m_{1,i,j} = m_{i,1,j} = m_{i,j,1} \quad (J.6.120)$$

and similarly for  $m_{2,i,j}$ , and thus

$$m_{.,i,j} + m_{i,.,j} + m_{i,j,.} = 3m_{i,j} \quad (J.6.121)$$

Now, substituting (J.6.100), (J.6.103), and (J.6.121) in (J.6.119), we obtain

$$\begin{aligned} \vec{v}_{D,\xi',n'}^* &= -\frac{rsh}{\kappa} \iint_{\Sigma'} \frac{1}{\rho} \frac{\partial \psi}{\partial \rho} dS' \vec{n} \\ &\quad - \frac{h}{\kappa} [M] \iint_{\Sigma'} \frac{\vec{v}}{|\vec{v}|} ds - \frac{h}{2\kappa} \sum_{i,j} \iint_{\Sigma'} \left[ \frac{\vec{v}}{|\vec{v}|} \cdot \vec{x}^T \right]_{i,j} ds \{m_{.,i,j}\} \\ &\quad + \frac{h}{2\kappa} \left( \iint_{\Sigma'} \psi dS' \right) \sum_{i,j} [G]_{ij} \{m_{.,i,j}\} \end{aligned} \quad (J.6.122)$$

### J.6.3.3 Normal Doublet Velocity

By (J.6.116),

$$\vec{v}_{D,\zeta'}^* = -\frac{1}{\kappa} \iint_{\Sigma'} (\vec{\nabla}_{2,Q}^* \mu) \cdot (\vec{\nabla}_{2,Q}^* \psi) dS' \quad (J.6.123)$$

Applying (J.6.38) and (J.6.70)

$$\begin{aligned} \vec{v}_{D,\zeta'}^* &= -\frac{1}{\kappa} \sum_{i,j} \iint_{\Sigma'} \vec{\nabla}_{2,Q,j}^* (\rho_i \mu_i) \frac{rs_{oj}}{\rho} \frac{\partial \psi}{\partial \rho} dS' \\ &\quad - \frac{1}{2\kappa} \sum_{i,j,k} \iint_{\Sigma'} \vec{\nabla}_{2,Q,k}^* (\rho_i \rho_j) [M]_{ij} \frac{rs_{ok}}{\rho} \frac{\partial \psi}{\partial \rho} dS' \\ &\quad - \frac{1}{6} \sum_{ijk1} \iint_{\Sigma'} \vec{\nabla}_{2,Q,1}^* (\rho_i \rho_j \rho_k) (m_{ijk}) \frac{rs_{o1}}{\rho} \frac{\partial \psi}{\partial \rho} dS' \end{aligned} \quad (J.6.124)$$

Applying (J.2.90)

$$\begin{aligned} \vec{v}_{D,\zeta'}^* &= -\frac{rs}{\kappa} \sum_i \left( \iint_{\Sigma'} \frac{\rho_i}{\rho} \frac{\partial \psi}{\partial \rho} dS' \right) \mu_i \\ &\quad - \frac{rs}{2\kappa} \sum_{ijk} \iint_{\Sigma'} (\delta_{ik} \rho_j \rho_k + \delta_{ij} \rho_i \rho_k) \frac{1}{\rho} \frac{\partial \psi}{\partial \rho} dS' [M]_{ij} \\ &\quad - \frac{rs}{6} \sum_{ijk1} \iint_{\Sigma'} dS' (\delta_{i1} \rho_j \rho_k + \delta_{j1} \rho_i \rho_k + \delta_{k1} \rho_i \rho_j) m_{ijk} \frac{\rho_1}{\rho} \frac{\partial \psi}{\partial \rho} \end{aligned} \quad (J.6.125)$$

Using the definition of the delta function,

$$\begin{aligned} \nabla D_{,z}^* &= -\frac{rs}{\kappa} \sum_i \left( \iint_{\Sigma'} \frac{\rho_i}{\rho} \frac{\partial \psi}{\partial \rho} dS' \right) u_i \\ &\quad - \frac{rs}{\kappa} \sum_{ij} \iint_{\Sigma'} \rho_i \rho_j \frac{1}{\rho} \frac{\partial \psi}{\partial \rho} dS' [M]_{ij} \\ &\quad - \frac{rs}{2\kappa} \sum_{ijk} \iint_{\Sigma'} \rho_i \rho_j \rho_k \frac{1}{\rho} \frac{\partial \psi}{\partial \rho} dS' \eta_{ijk} \end{aligned} \quad (J.6.126)$$

Substituting (J.6.70) into (J.6.126),

$$\begin{aligned} \nabla D_{,z}^* &= -\frac{1}{\kappa} \sum_i \iint_{\Sigma'} \left\{ \nabla_{2,Q}^i \right\}_i \psi dS' \bar{u}_i \\ &\quad - \frac{1}{\kappa} \sum_{ij} \iint_{\Sigma'} \rho_i (\nabla_{2,Q}^i)_j \psi dS' [M]_{ij} \\ &\quad - \frac{1}{2\kappa} \sum_{ijk} \iint_{\Sigma'} \rho_i \rho_j (\nabla_{2,Q}^i)_k \psi dS' (\eta)_{ijk} \end{aligned} \quad (J.6.127)$$

Applying (J.6.81), (J.6.93), and (J.6.104-105),

$$\begin{aligned} \nabla D_{,z}^* &= -\frac{1}{\kappa} \int_{\partial \Sigma'} \frac{\nabla^T}{|\nabla|} \psi dS' \bar{u} \\ &\quad - \frac{1}{\kappa} \left[ \int_{\partial \Sigma'} \bar{u} \nabla^T \frac{ds}{|\nabla|} \right] : [M] \\ &\quad + \frac{1}{\kappa} \iint_{\Sigma'} \psi dS' [G] : [M] \\ &\quad - \frac{1}{2\kappa} \sum_{i,j,k} \iint_{\Sigma'} \rho_i \rho_j (\nabla_{2,Q}^i)_k \psi dS' (\eta)_{ijk} \end{aligned} \quad (J.6.128)$$

#### J.6.4 Reduction to Fundamental Integrals

In this section, we will see that the entries of the matrices S and D, describing source and doublet potential and velocity, are all combinations of a small number of fundamental integrals.



#### J.6.4.1 Definition of the Integrals

We define the integrals as follows.

$$a = -\frac{sh}{\kappa} \iint_{\Sigma'} \frac{1}{\rho} \frac{\partial \psi}{\partial \rho} dS' \quad (J.6.129)$$

$$b = -\frac{1}{\kappa} \iint_{\Sigma'} \psi dS' \quad (J.6.130)$$

$$\vec{a} = \frac{1}{\kappa} \int_{\partial \Sigma'} \frac{\vec{n}}{|\vec{n}|} \psi ds \quad (J.6.131)$$

$$\vec{b} = -\frac{s}{\kappa} \int_{\partial \Sigma'} \vec{v} \times \frac{ds}{|\vec{v}|} \quad (J.6.132)$$

$$[B] = \frac{1}{\kappa} \int_{\partial \Sigma'} \frac{\vec{n} \vec{\sigma}^T}{|\vec{n}|} \psi ds - \frac{1}{\kappa} \left( \iint_{\Sigma'} \psi dS' \right) [I] \quad (J.6.133)$$

where I is the identity matrix.

$$[F] = \frac{s}{\kappa} \iint_{\Sigma'} \vec{\sigma} \vec{\nabla}_2^T \cdot \vec{Q} \psi dS' \quad (J.6.134)$$

Finally, let H be the 2x2x2 tensor

$$H_{ijk} = \frac{1}{\kappa} \iint_{\Sigma'} \rho_i \rho_j (\vec{\nabla}_2^T \cdot \vec{Q})_k \psi dS' \quad (J.6.135)$$

#### J.6.4.2 Source Potential and Velocity

Applying the above to (J.6.84), we see

$$\phi_{S'} = b\sigma_0 + \vec{b}^T \vec{\sigma} - 1/2 [F] : [\Sigma] \quad (J.6.136)$$

From (J.6.96) we get

$$\vec{v}'_{S, \xi', \eta'} = \sigma_0 \vec{a} + [B] \vec{\sigma} + \frac{1}{2} \sum_{ij} [\sum_l G_{.,l} H_{ijl}] \Sigma_{ij} \quad (J.6.137)$$

since

$$[G] \vec{\nabla}_2^T \cdot \vec{Q} = \vec{\nabla}_2^T \cdot \vec{Q} \quad (J.6.138)$$

Finally, (J.6.106) yields

$$\begin{aligned} \vec{v}'_{S,\zeta} &= a \sigma_0 - rh (Ga)^T \vec{\sigma} \\ &\quad - \frac{rh}{2} [GB] : [\Sigma] \end{aligned} \quad (J.6.139)$$

With a few simple definitions, we can write down the matrix [S] such that

$$\begin{Bmatrix} \phi'_S \\ v'_{S,\xi',n'} \\ v'_{S,\zeta'} \end{Bmatrix} = [S] \begin{Bmatrix} \sigma_0 \\ \sigma_\xi \\ \sigma_\eta \\ \sigma_{\xi\xi} \\ \sigma_{\xi\eta} \\ \sigma_{\eta\eta} \end{Bmatrix} \quad (J.6.140)$$

First, for a (2x2) matrix [A], let  $\mathcal{A}_3$  be the row vector of length 3:

$$\mathcal{A}_3 = \mathcal{A}_{11} \quad (\mathcal{A}_{12} + \mathcal{A}_{21}) \quad \mathcal{A}_{22} \quad (J.6.141)$$

For a (2x2x2) tensor {T}, let  $\mathcal{T}_4$  be the row vector of length 4:

$$\mathcal{T}_4 = \mathcal{T}_{111} \quad (\mathcal{T}_{112} + \mathcal{T}_{121} + \mathcal{T}_{211}) \quad (\mathcal{T}_{122} + \mathcal{T}_{212} + \mathcal{T}_{221}) \quad \mathcal{T}_{222} \quad (J.6.142)$$

and let  $[T_k]$  (k = 1 or 2) be the 2x2 matrix

$$[T_k]_{ij} = (T)_{ijk} \quad (J.6.143)$$

We easily see that if [A] is a 2x2 matrix,

$$[A] : [\Sigma] = \mathcal{A}_3 \begin{Bmatrix} \sigma_{\xi\xi} \\ \sigma_{\xi\eta} \\ \sigma_{\eta\eta} \end{Bmatrix} \quad (J.6.144)$$

Thus, from (J.6.136)

$$\phi'_S = b\sigma_0 + \vec{b}^T \vec{\sigma} - \frac{1}{2} \mathcal{F}_3 \begin{Bmatrix} \sigma_{\xi\xi} \\ \sigma_{\xi\eta} \\ \sigma_{\eta\eta} \end{Bmatrix} \quad (J.6.145)$$

and by (J.6.139)

$$\begin{aligned} \vec{v}'_{S,\zeta'} &= a\sigma_0 - rh[G] \vec{\sigma}^T \vec{\sigma} \\ &\quad - \frac{rh}{2} \mathcal{G}_3 \begin{Bmatrix} \sigma_{\xi\xi} \\ \sigma_{\xi\eta} \\ \sigma_{\eta\eta} \end{Bmatrix} \end{aligned} \quad (J.6.146)$$

Finally, we note that

$$\sum_j G_{1j} H_{ij} = rs[H_1] \quad (J.6.147)$$

while

$$\sum_j G_{2j} H_{ij} = [H_2] \quad (J.6.148)$$

Thus,

$$\sum_{ij} G_{1j} H_{ij} \Sigma_{ij} = rs[H_1]_3 \begin{Bmatrix} \sigma_{\xi\xi} \\ \sigma_{\xi\eta} \\ \sigma_{\eta\eta} \end{Bmatrix} \quad (J.6.149)$$

while

$$\sum_{ij} G_{2j} H_{ij} \Sigma_{ij} = [H_2]_3 \begin{Bmatrix} \sigma_{\xi\xi} \\ \sigma_{\xi\eta} \\ \sigma_{\eta\eta} \end{Bmatrix} \quad (J.6.150)$$

Applying (J.6.149-150)

$$\begin{aligned} \nabla'_{s,\xi'} &= \sigma_0 a + [B] \vec{\sigma} \\ \nabla'_{s,\eta'} &+ \frac{1}{2} \begin{bmatrix} rs[H_1]_3 \\ [H_2]_3 \end{bmatrix}^{2 \times 3} \begin{Bmatrix} \sigma_{\xi\xi} \\ \sigma_{\xi\eta} \\ \sigma_{\eta\eta} \end{Bmatrix} \end{aligned} \quad (J.6.151)$$

Substituting (J.6.145-146) and (J.6.151) into (J.6.140),

$$[S] = \begin{matrix} & \begin{matrix} 1 & 2 & 3 \end{matrix} \\ \begin{matrix} 1 \\ 2 \\ 1 \end{matrix} & \begin{bmatrix} b & \vec{b}^T & -1/2 [F]_3 \\ \vec{a} & B & \frac{rs}{2} [H_1]_3 \\ a & -hr(G\vec{a})^T & \frac{1}{2} [H_2]_3 \end{bmatrix} \end{matrix} \quad (J.6.152)$$

#### J.6.4.3 Doublet Potential and Velocity

Applying (J.6.129-135) to (J.6.114), we see that

$$\phi_D = r a u_0 - h (G\vec{a})^T \vec{a} - \frac{h}{2} [GB] : [M]$$

$$- \frac{h}{6} \sum_{ijk} H_{ijk} m_{ijk} \quad (J.6.153)$$

Next, from (J.6.122), we obtain

$$\vec{v}_{D,\xi',n'}^* = r a \vec{a} - h[M] (G\vec{a}) - \frac{h}{2} \sum_{ij} [GB]_{ij} m_{.,i,j} \quad (J.6.154)$$

Finally, from (J.6.128),

$$\begin{aligned} \vec{v}_{D,\zeta'}^* &= - (Ga)^T \vec{a} - [GB] : [M] \\ &\quad - \frac{1}{2} \sum_{i,j,k} H_{ijk} m_{ijk} \end{aligned} \quad (J.6.155)$$

Now, recalling the definition (J.6.33-34) of  $m$ , we see that if  $T$  is a  $2 \times 2 \times 2$  tensor,

$$\sum_{ijk} T_{ijk} m_{ijk} = T_{,4} \cdot \begin{Bmatrix} \mu_{EEE} \\ \mu_{EEn} \\ \mu_{Enn} \\ \mu_{nnn} \end{Bmatrix} \quad (J.6.156)$$

where  $T_{,4}$  is defined by (J.6.142).

Now, applying (J.6.156) and the doublet equivalent of (J.6.144) to (J.6.153), we have

$$\begin{aligned} \phi_D &= r a u_0 - h (G\vec{a})^T \vec{a} \\ &\quad - \frac{h}{2} [GB]_3 \begin{Bmatrix} \mu_{EE} \\ \mu_{En} \\ \mu_{nn} \end{Bmatrix} - \frac{h}{6} T_{,4} \begin{Bmatrix} \mu_{EEE} \\ \mu_{EEn} \\ \mu_{Enn} \\ \mu_{nnn} \end{Bmatrix} \end{aligned} \quad (J.6.157)$$

Next, expanding (J.6.154) into two equations,

$$\begin{aligned} \vec{v}'_{D,\xi} &= ra \, \mu_\xi - h \sum_j M_{ij} (Ga)_j \\ &\quad - \frac{h}{2} \sum_{ij} [GB]_{ij} \eta_{1,i,j} \end{aligned} \quad (J.6.158)$$

= (using the definitions (J.6.32-34) of M and  $\eta$ )

$$ra \, \mu_\xi - h(Ga)^T \begin{Bmatrix} \mu_{\xi\xi} \\ \mu_{\xi n} \end{Bmatrix} - \frac{h}{2} GB_{,3} \begin{Bmatrix} \mu_{\xi\xi\xi} \\ \mu_{\xi\xi n} \\ \mu_{\xi nn} \end{Bmatrix} \quad (J.6.159)$$

Similarly,

$$\vec{v}'_{D,\eta} = ra \, \mu_n - h \sum_j M_{2j} (Ga)_j - \frac{h}{2} \sum_{ij} [GB]_{ij} \eta_{2ij} \quad (J.6.160)$$

$$= ra \, \mu_n - h(Ga)^T \begin{Bmatrix} \mu_{\xi n} \\ \mu_{nn} \end{Bmatrix} - \frac{h}{2} GB_{,3} \begin{Bmatrix} \mu_{\xi\xi n} \\ \mu_{\xi nn} \\ \mu_{nnn} \end{Bmatrix} \quad (J.6.161)$$

Finally, applying (J.6.156) and the doublet equivalent of (J.6.144) to (J.6.155),

$$\begin{aligned} \vec{v}'_{D,\zeta} &= - (Ga)^T \vec{d} - GB_{,3} \begin{Bmatrix} \mu_{\xi\xi} \\ \mu_{\xi n} \\ \mu_{nn} \end{Bmatrix} \\ &\quad - \frac{1}{2} H_{,4} \begin{Bmatrix} \mu_{\xi\xi\xi} \\ \mu_{\xi\xi n} \\ \mu_{\xi nn} \\ \mu_{nnn} \end{Bmatrix} \end{aligned} \quad (J.6.162)$$

So, we can now write down the matrix [D] such that

$$\begin{Bmatrix} \phi_{D'} \\ \vec{v}'_{\xi',n} \\ v_{D,\zeta'} \end{Bmatrix} = [D] \begin{Bmatrix} \mu_D \\ \mu_\xi \\ \mu_n \\ \cdot \\ \cdot \\ \mu_{nnn} \end{Bmatrix} \quad (J.6.163)$$

From (J.6.157), (J.6.159), (J.6.161), and (J.6.162), we have  $[D]^{4 \times 10} =$

$$\begin{array}{c}
 \begin{array}{cccc}
 1 & 2 & 3 & 4
 \end{array} \\
 \begin{array}{c}
 1 \\
 2 \\
 1
 \end{array}
 \begin{bmatrix}
 \begin{array}{c|c|c|c}
 ra & -h(G\vec{a})^T & -\frac{h}{2}GB_{,3} & -\frac{h}{6}H_{,4} \\
 \hline
 0 & ra[I] & -h(G\vec{a})^T & 0 \\
 \hline
 0 & -(G\vec{a})^T & -GB_{,3} & -\frac{1}{2}H_{,4}
 \end{array}
 \end{bmatrix}
 \end{array}
 \quad (J.6.164)$$

#### J.6.5 The Fundamental Integrals in Terms of Panel and Edge Functions

The seven fundamental integrals which define the entries of the matrices  $[S]$  and  $[D]$  can themselves be reduced to simpler expressions. The only integrals involved in these expressions are a single "panel function" and one "edge function" for each edge of the region.

##### J.6.5.1 Computation of $a$ .

By (J.6.129),

$$a = -\frac{sh}{\kappa} \iint_{\Sigma'} \frac{1}{\rho} \frac{\partial \psi}{\partial \rho} dS' \quad (J.6.165)$$

Thus, for subsonic flow and superinclined panels

$$a = -\frac{sh}{\kappa} \sum_{\text{edges}} \int_{\phi_k}^{\phi_k^+} d\phi \int_0^{P_k(\phi)} \frac{u d\rho}{\rho} \frac{\partial \psi}{\partial \rho} \quad (J.6.166)$$

by (J.4.56-57) and (J.4.60).

Note that this integral is always finite unless the control point lies on the panel edge.

Now,

$$\begin{aligned} \int_0^{P_k(\phi)} \frac{\partial \psi}{\partial \rho} d\rho &= \psi(P_k(\phi)) - \psi(0) \\ &= \psi(P_k(\phi)) - \frac{1}{ihl} \end{aligned} \quad (J.6.167)$$

Thus,

$$\begin{aligned} a &= -\frac{sh}{\kappa} \sum_{\text{edges}} \int_{\phi_k^-}^{\phi_k^+} \psi d\phi \\ &= -\frac{sh}{\kappa} \left( -\frac{2\pi}{ihl} C_0 \right) \end{aligned} \quad (J.6.168)$$

where  $C_0$  is defined by (J.5.30).

For subinclined panels,

$$\begin{aligned} a &= -\frac{sh}{\kappa} \iint_{\Sigma'} \frac{1}{\rho} \frac{\partial \psi}{\partial \rho} dS' = (\text{cf. (J.5.104)}) \\ &= -\frac{sh}{\kappa} \sum_k \int_{\phi_k^-}^{\phi_k^+} d\phi \int_{|h|}^{P_k(\phi)} \frac{\partial \psi}{\partial \rho} d\rho \end{aligned} \quad (J.6.169)$$

Unlike the integral J.6.166, we will see shortly that this integral is in fact infinite. We have

$$a = -\frac{sh}{\kappa} \left[ \sum_k \lim_{\epsilon \rightarrow 0^+} \int_{\phi_k^-}^{\phi_k^+} d\phi \left[ \left( \rho - \frac{1}{\epsilon} \right) \frac{P_k(\phi)}{\sqrt{h^2 + \epsilon^2}} \right] \right] \quad (J.6.170a)$$

$$= -\frac{sh}{\kappa} \sum_{k=1}^K \int_{\phi_k^-}^{\phi_k^+} d\phi - \lim_{\epsilon \rightarrow 0} \int_{\phi_k^-}^{\phi_k^+} \frac{1}{\epsilon} d\phi \quad (J.6.170b)$$

We now evaluate the first term of this integral, which is the "finite part". We discard the second term, or "infinite part", for reasons discussed in section J.6.7. Thus, setting  $C_0 = 0$  for subinclined panels, we always have

$$a = -\frac{sh}{\kappa} \left[ \sum_k \int_{\phi_k^-}^{\phi_k^+} d\phi - \frac{2\pi}{ihl} C_0 \right] \quad (J.6.171)$$

Setting

$$J_k(\psi) = \int_{\phi_k^-}^{\phi_k^+} d\phi \quad (J.6.172)$$

$$\text{and } J = \sum_k h J_k(\psi) - 2\pi \operatorname{sign}(h) C_\infty \quad (J.6.173)$$

we have

$$a = -\frac{S}{K} J \quad (J.6.174)$$

The function  $J$  is called the panel function.

J.6.5.2 Computation of  $b$ .

By (J.6.130),

$$b = -\frac{1}{K} \iint_{\Sigma'} dS' \quad (J.6.175)$$

Thus

$$b = -\frac{1}{K} \sum_k \int_{\phi_k^-}^{\phi_k^+} d\phi \frac{P_k(\phi)}{|h|} \psi_\phi d\phi \quad (J.6.176)$$

Now, by (J.6.72)

$$\int_\phi \psi d\phi = rX = rR \quad (J.6.177)$$

and thus for subsonic flow or superinclined panels

$$b = -\frac{r}{K} \sum_k \int_{\phi_k^-}^{\phi_k^+} d\phi (R - |h|) \quad (J.6.178)$$

$$= -\frac{r}{K} \left[ \sum_k \int_{\phi_k^-}^{\phi_k^+} R d\phi - 2\pi |h| C_\infty \right] \quad (J.6.179)$$



since  $R = |h|$  when  $\rho = 0$  and thus

$$\int_{|h|}^{P_k(\phi)} \rho d\rho = r(R-|h|) \quad (J.6.180)$$

For subinclined panels,  $R = 0$  when  $\rho = |h|$ , and thus

$$b = -\frac{r}{K} \sum_k \int_{\phi_k^-}^{\phi_k^+} R d\phi \quad (J.6.181)$$

Thus  $b$  is defined in all cases by (J.6.179) by setting  $C_0 = 0$  for subinclined panels.

#### J.6.5.3 Computation of $\vec{a}$ .

By (J.6.131),

$$\vec{a} = -\frac{1}{K} \int_{\partial \Sigma'} \frac{\vec{n}}{|n|} ds \quad (J.6.182)$$

Applying (J.6.54), and noting from (J.6.45) that  $|\vec{e}| = |\vec{n}|$ , we have

$$\vec{a} = \frac{1}{K} \sum_k \int_{\text{edge}} \vec{n} s q \psi dv = \frac{s}{K} \sum_k \vec{n}_k q_k \int_{v_k^-}^{v_k^+} \psi dv \quad (J.6.183)$$

Defining

$$I_k = \int_{v_k^-}^{v_k^+} \psi dv \quad (J.6.184)$$

we have

$$\vec{a} = \frac{s}{K} \sum_k \vec{n}_k q_k I_k \quad (J.6.185)$$

#### J.6.5.4 Computation of $\vec{b}$ .

By (J.6.132),

$$\vec{b} = \frac{-s}{K} \int_{\partial \Sigma'} \vec{\nabla} X \frac{ds}{|\vec{v}|} = \frac{-1}{K} \sum_k \vec{v}_k q_k \int_{v_k^-}^{v_k^+} R dv \quad (J.6.186)$$

= (by (J.6.54))

$$\frac{-s}{K} \int_{\partial \Sigma} \vec{v} \cdot \vec{q} x dv = \frac{-1}{K} \sum_k \vec{v}_k \cdot \vec{q}_k \int_{v_k^-}^{v_k^+} R dv \quad (\text{J.6.189})$$

Integrating by parts,

$$\int R dv = Rv - \int v \frac{\partial R}{\partial v} dv \quad (\text{J.6.190})$$

where (by J.6.59)

$$2R \frac{\partial R}{\partial v} = 2qv \quad (\text{J.6.191})$$

Thus

$$\int_{v_k^-}^{v_k^+} R dv = [Rv] \Big|_{v_k^-}^{v_k^+} - \int_{v_k^-}^{v_k^+} \frac{q}{R} v^2 dv \quad (\text{J.6.192})$$

= (once again applying (J.6.59))

$$[Rv] \Big|_{v_k^-}^{v_k^+} - \int_{v_k^-}^{v_k^+} \frac{R^2 - rsq_k a_k^2 - rsh^2}{R} dv \quad (\text{J.6.193})$$

Collecting terms,

$$2 \int_{v_k^-}^{v_k^+} R dv = [Rv] \Big|_{v_k^-}^{v_k^+} + \int_{v_k^-}^{v_k^+} \frac{rsq_k a_k^2 + rsh^2}{R} dv \quad (\text{J.6.194})$$

Substituting (J.6.184) and (J.6.194) in (J.6.189)

$$b = \frac{-1}{2K} \sum_k \vec{v}_k \cdot \vec{q}_k \Delta(Rv) - \frac{rs}{2K} \sum_k \vec{v}_k \cdot (a_k^2 + q_k h^2) I_k \quad (\text{J.6.195})$$

where, for any quantity f, we define

$$\Delta f = f(v_k^+) - f(v_k^-) \quad (\text{J.6.196})$$

#### J.6.5.5 Computation of B

By (J.6.130) and (J.6.133),

$$[B] = b [I] + \frac{1}{K} \int_{\partial \Sigma} \frac{\vec{n} \cdot \vec{p}^T}{|n|} \psi ds \quad (\text{J.6.197})$$

Applying (J.6.52) and (J.6.54)

$$[B] = b[I] + \frac{1}{\kappa} \sum_k \int_{v_k^-}^{v_k^+} \tilde{n}_k (q_k r a_k \tilde{v}_k^T + q_k s v_k \tilde{t}_k^T) q_k s dv \quad (J.6.198)$$

By (J.6.191),

$$\frac{\partial R}{\partial v} = q v \psi \quad (J.6.199)$$

and thus

$$[B] = b[I] + \frac{rs}{\kappa} \sum_k n_k a_k \tilde{v}_k^T \int_{v_k^-}^{v_k^+} \psi dv + \frac{1}{\kappa} \sum_k q_k \tilde{n}_k \tilde{t}_k^T \Delta R \quad (J.6.200)$$

= (using (J.6.184))

$$b[I] + \frac{rs}{\kappa} \sum_k \tilde{n}_k a_k \tilde{v}_k^T I_k + \frac{1}{\kappa} \sum_k q_k \tilde{n}_k \tilde{t}_k^T \Delta R \quad (J.6.201)$$

J.6.5.6 Computation of F

By (J.6.134),

$$[F] = \frac{s}{\kappa} \iint_{\Sigma'} \tilde{\rho} \tilde{\nabla}_{2,Q}^T X ds' \quad (J.6.202)$$

= (using J.6.93)

$$\frac{s}{\kappa} \int_{\partial \Sigma'} \tilde{\rho} \frac{\tilde{\nabla}^T}{|\tilde{\nabla}|} X ds - \frac{s}{\kappa} \iint_{\Sigma'} X \tilde{\nabla}_{2,Q}^T \tilde{\rho}^T ds' \quad (J.6.203)$$

= (applying (J.6.52) and (J.6.54))

$$\frac{s}{\kappa} \sum_k \int_{v_k^-}^{v_k^+} (q_k r a_k \tilde{v}_k + q_k s v_k \tilde{t}_k) \tilde{v}_k^T X s q_k dv - \frac{s}{\kappa} \left( \iint_{\Sigma'} X ds' \right) [G] \quad (J.6.204)$$

We first compute  $\iint_{\Sigma'} X ds'$ .

We compute the integral using either circular cylindrical or hyperbolic cylindrical coordinates. In the derivation that follows, we assume that  $|h| > 0$  so that we need not concern ourselves with the problem that hyperbolic phase becomes unbound on the lines  $(\xi' - x') = \pm (n' - y')$ . The upper

limit of integration with respect to  $\rho$  is  $P_k(\phi)$ ; the lower limit is 0,  $|h|$  or 0 in accordance with whether  $s = +1$ ,  $rs = -1$ , or  $r = -1$ . We write then,

$$\iint X dS' = \sum_k \int_{\phi_k^-}^{\phi_k^+} d\phi \left. \frac{rR^3}{3} \right|_{\rho=0 \text{ or } |h|} P(\phi) \quad (\text{J.6.205})$$

$$= \sum_k \int_{\phi_k^-}^{\phi_k^+} d\phi \left. \frac{rR^3}{3} \right|_{\rho=0 \text{ or } |h|} P(\phi) \quad (\text{J.6.206})$$

$$= \frac{r}{3} \sum_k \int_{\phi_k^-}^{\phi_k^+} d\phi \left\{ \begin{matrix} R^3 \\ \text{or} \\ R^3 \end{matrix} \right\} \quad (\text{J.6.207})$$

Now the sum over  $k$  in equation (J.6.207) is over all segments of the boundary of  $\Sigma$ ,  $\partial\Sigma$ , both straight and curved segments. On curved segments  $R = 0$  so that we may write

$$\iint X dS' = \frac{r}{3} \sum_{\text{edges } k} \int_{\phi_k^-}^{\phi_k^+} R^3 d\phi - |h|^3 \cdot 2\pi C_0 \quad (\text{J.6.208})$$

We now examine integrals of the form  $\int R^3 d\phi$ . Transforming this integral into an integral with respect to  $v$ , the intrinsic edge variable, we find (using (J.4.66), (J.5.78), and (J.5.98)) that

$$\int_{\phi^-}^{\phi^+} R^3 d\phi = \int_{v^-}^{v^+} \frac{adv}{a^2 + rsv^2} R^3 = \int_{v^-}^{v^+} \frac{adv}{a^2 + rsv^2} R [qrs(a^2 + rsv^2) + rsh^2] \quad (\text{J.6.209})$$

$$\begin{aligned} &= aqrs \int_{v^-}^{v^+} R dv + rsh^2 \int_{v^-}^{v^+} \frac{adv}{a^2 + rsv^2} R \\ &= aqrs \int_{v^-}^{v^+} R dv + rsh^2 \left[ aqrs \int_{v^-}^{v^+} \frac{dv}{R} + rsh^2 \int_{v^-}^{v^+} \frac{adv}{(a^2 + rsv^2)R} \right] \end{aligned} \quad (\text{J.6.210})$$

Defining

$$g^2 = ra^2 + rqh^2, \text{ and } \int R dv = I(X) = \frac{1}{2} [Rv + sqg^2 I(\psi)] \quad (\text{J.6.211})$$

where  $\int \frac{dv}{R} = I(\psi)$  (see J.6.194) (J.6.212)

and  $\int \frac{adv}{(a^2 + rsv^2)R} = \frac{d\psi}{R} = J(\psi)$  (J.6.213)

we find that

$$\int_{\psi^-}^{\psi^+} R^3 d\psi = [aqrs I(X) + (aqrs) rsh^2 I(\psi) + h^4 J(\psi)] \quad (J.6.214)$$

Substituting this expression into (J.6.208) and recalling the definition (J.6.173) of the panel function J we find

$$\iint X ds = \frac{r}{3} (h^3 J + \sum_k aqrs) \quad (J.6.215)$$

Recalling the computed values (J.6.179) and (J.6.181) of b, the integral  $\iint X ds$  can be written

$$\iint X ds = \frac{r}{3} \left( h^2 \left( \frac{-kb}{s} \right) + rs \sum aq I(X) \right) \Bigg|_{v^-}^{v^+} \quad (J.6.216)$$

$$\text{or } \iint X ds = \frac{-rs}{3} h^2 kb + \frac{s}{3} aq I(X) \Bigg|_{v^-}^{v^+} \quad (J.6.217)$$

Applying (J.6.212) and (J.6.194)

$$I(X) \Bigg|_{v^-}^{v^+} = \int_{v^-}^{v^+} R dv = \frac{1}{2} \Delta(Rv) + \frac{1}{2} \int_{v^-}^{v^+} \frac{rsqa^2 + rsh^2}{R} dv \quad (J.6.218a)$$

$$= \frac{1}{2} \Delta(Rv) + \frac{1}{2} (rsqa^2 + rsh^2) I(\psi) \Bigg|_{v^-}^{v^+} \quad (J.6.218b)$$

by (J.6.212).

Recalling the definition (J.6.184) of  $I_k$  we have

$$dS' = \frac{-rs}{3} h^3 b + \frac{s}{6} \sum_k a_k q_k \Delta(Rv) + \frac{s}{6} \sum_k a_k q_k (rs q_k a_k^2 + rsh^2) I_k \quad (J.6.219)$$

We now consider the other terms in (J.6.204).

We have

$$\int_{v_k^-}^{v_k^+} v \times dv = \int_{v_k^-}^{v_k^+} R v dv = \quad (J.6.220)$$

(by (J.6.191))

$$\int R(qR \frac{\partial R}{\partial v}) dv = q \int R^2 \frac{\partial R}{\partial v} dv = \frac{q}{3} \Delta(R^3) \quad (J.6.221)$$

Substituting (J.6.194), (J.6.219), and (J.6.221) in (J.6.204)

$$\begin{aligned} [F] &= \frac{s}{2\kappa} \sum_k q_k r a_k \vec{v}_k \vec{v}_k^T s q_k \left\{ \Delta(Rv) + (rsq_k a_k^2 + rsh^2) I_k \right\} \\ &+ \frac{s}{\kappa} \sum_k q_k \vec{v}_k \vec{v}_k^T q_k \left( \frac{q}{3} \Delta(R^3) \right) - \frac{s}{\kappa} [G] \left( \frac{-rs}{3} h^2 \kappa b + \frac{1}{6} \sum_k s a_k q_k \Delta(Rv) \right) \\ &+ \frac{1}{6} \sum_k a_k q_k (r q_k a_k^2 + rh^2) I_k \end{aligned} \quad (J.6.222)$$

#### J.6.5.7 Computation of H.

Recalling the definition (J.6.135)

$$H_{ijk} = \frac{1}{\kappa} \iint_{\Sigma'} \rho_i \rho_j (\vec{\nabla}'_{2,Q})_k \psi ds' \quad (J.6.223)$$

we apply (J.6.93) to obtain

$$H_{ijl} = \frac{1}{\kappa} \iint_{\Sigma'} \rho_i \rho_j \frac{\vec{v}_l}{|\vec{v}|} \psi ds - \frac{1}{\kappa} \iint_{\Sigma'} \psi (\vec{\nabla}'_{2,Q})_l (\rho_i \rho_j) ds' \quad (J.6.224)$$

Now,

$$(\vec{\nabla}'_{2,Q})_l (\rho_i \rho_j) = \rho_i [G]_{lj} + [G]_{li} \rho_j \quad (J.6.225)$$

Combining (J.6.77-78) with (J.6.132), we see

$$\vec{b} = \frac{-1}{\kappa} \iint_{\Sigma'} \rho \psi ds' \quad (J.6.226)$$

and thus

$$\begin{aligned}
 & -\frac{1}{K} \iint_{\Sigma'} \psi (\vec{\nabla}_{2,Q}^{\cdot})_k (\rho_i \rho_j) dS' = \\
 & -\frac{1}{K} \iint_{\Sigma'} \psi (\rho_i [G]_{kj} + [G]_{ki} \rho_j) dS' \\
 & = [G]_{kj} \vec{b}_i + [G]_{ki} \vec{b}_j
 \end{aligned} \tag{J.6.227}$$

We now consider the first term of (J.6.224).

By (J.6.52) and (J.6.54)

$$\begin{aligned}
 & \int_{\partial \Sigma'} \rho_i \rho_j \frac{\vec{v}_1}{|\vec{v}_1|} \psi ds = \\
 & \int_{\partial \Sigma'} (q r a v_i + q s v t_i) (q r a v_j + q s v t_j) v_1 s q \psi dv
 \end{aligned} \tag{J.6.228}$$

$$\begin{aligned}
 & = \sum_k a_k^2 (\vec{v}_k)_i (\vec{v}_k)_j (\vec{v}_k)_1 s q_k \int_{v_k^-}^{v_k^+} \psi dv \\
 & + \sum_k r s a_k (\vec{v}_k)_i (\vec{t}_k)_j (\vec{v}_k)_1 s q \int_{v_k^-}^{v_k^+} \psi dv \\
 & + (\vec{t}_k)_i (\vec{t}_k)_j (\vec{v}_k)_1 s q \int_{v_k^-}^{v_k^+} \psi v^2 dv
 \end{aligned} \tag{J.6.229}$$

Now by (J.6.191)

$$\frac{\partial R}{\partial v} = \frac{q v}{R} = q v \psi \tag{J.6.230}$$

Thus

$$\int_{v_k^-}^{v_k^+} \psi v dv = a_k \Delta R \tag{J.6.231}$$

and

$$\int_{v_k^-}^{v_k^+} \psi v^2 dv = \int_{v_k^-}^{v_k^+} q_k \frac{\partial R}{\partial v} v dv \quad (J.6.232)$$

= (applying (J.6.194))

$$q_k \Delta(vR) - \frac{1}{2} q_k \Delta(vR) - \frac{q_k}{2} \int_{v_k^-}^{v_k^+} \frac{rsq_k a_k^2 + rsh^2}{R} dv \quad (J.6.233)$$

$$= \frac{1}{2} q_k \Delta(vR) - \frac{q_k}{2} (rsq_k a_k^2 + rsh^2) I_k \quad (J.6.234)$$

where we have used the definition (J.6.184) of  $I_k$ . Applying the latter definition, along with (J.6.231) and (J.6.234) to (J.6.229), we define

$$\begin{aligned} \bar{H}_{ijl} &= \frac{1}{K} \int_{\Sigma} \rho_i \rho_j \frac{v_l}{|v|} \psi ds = \\ &= \frac{S}{K} \sum_k a_k^2 (\vec{v}_k)_i (\vec{v}_k)_j (\vec{v}_k)_l q_k I_k \\ &+ \frac{r}{K} \sum_k a_k (\vec{v}_k)_i (\vec{e}_k)_j (\vec{v}_k)_l \Delta R \\ &+ -\frac{S}{2K} \sum_k (\vec{e}_k)_i (\vec{e}_k)_j (\vec{v}_k)_l \left( \frac{\Delta(vR) - (rsq_k a_k^2 + rsh^2) I_k}{R} \right) \end{aligned} \quad (J.6.235)$$

Substituting (J.6.227) and (J.6.235) in (J.6.224)

$$H_{ijk} = \bar{H}_{ijk} + [G]_{kj} \vec{b}_i + [G]_{ki} \vec{b}_j \quad (J.6.236)$$

This concludes the reduction of fundamental integrals to the edge and panel functions.

#### J.6.6 The Origin Shift

The computation of the entries of the matrices  $[S]$  and  $[D]$  has been based on the assumption that the local  $(\xi', \eta')$  coordinate system is centered on the projection  $(x', y')$  of the control point to the plane of the panel. In practice, however, we require the matrices  $[S_0]$  and  $[D_0]$  corresponding to a  $(\xi_0', \eta_0')$  coordinate system centered on a fixed point  $(0, 0)$  on the panel.



That is, S and D were defined in terms of coefficients  $\sigma_0, \sigma_\xi, \dots, \sigma_{nn}, \mu_0, \mu_\xi, \dots, \mu_{nn}$  defining a source distribution and doublet distribution

$$\sigma(\xi_0', n_0') = \sigma_0 + \dots + \frac{1}{2} \sigma_{nn} (n_0' - y')^2$$

$$\mu(\xi_0', n_0') = \mu_0 + \mu_\xi (\xi_0' - x') + \dots + \frac{1}{6} \mu_{nnn} (n_0' - y')^3 \quad (J.6.237)$$

The matrices  $S_0$  and  $D_0$  are defined in terms of coefficients  $\sigma_0^0, \dots, \sigma_{nn}^0, \mu_0^0, \dots, \mu_{nnn}^0$  defining the same source and doublet distributions by

$$\sigma(\xi_0', n_0') = \sigma_0^0 + \sigma_\xi^0 \xi_0' + \dots + \frac{1}{2} \sigma_{nn}^0 n_0'^2$$

$$\mu(\xi_0', n_0') = \mu_0^0 + \mu_\xi^0 \xi_0' + \dots + \frac{1}{6} \mu_{nnn}^0 n_0'^3 \quad (J.6.238)$$

Then, while [S] and [D] are defined by (J.6.1-2),  $[S_0]$  and  $[D_0]$  are defined by

$$\begin{Bmatrix} \phi_{S'} \\ \vec{v}_{S'} \end{Bmatrix} = [S_0] \begin{Bmatrix} \sigma_0^0 \\ \vdots \\ \sigma_{nn}^0 \end{Bmatrix} \quad (J.6.239)$$

$$\begin{Bmatrix} \phi_{D'} \\ \vec{v}_{D'} \end{Bmatrix} = [D_0] \begin{Bmatrix} \mu_0^0 \\ \vdots \\ \mu_{nnn}^0 \end{Bmatrix} \quad (J.6.240)$$

To obtain  $[S_0]$  and  $[D_0]$  from [S] and [D], we must compute the matrices  $[T_S]^{6 \times 6}$  and  $[T_D]^{10 \times 10}$  such that

$$\begin{Bmatrix} \sigma_0 \\ \vdots \\ \sigma_{nn} \end{Bmatrix} = [T_S] \begin{Bmatrix} \sigma_0^0 \\ \vdots \\ \sigma_{nn}^0 \end{Bmatrix} \quad (J.6.241)$$

$$\begin{Bmatrix} \mu_0 \\ \vdots \\ \mu_{nnn} \end{Bmatrix} = [T_D] \begin{Bmatrix} \mu_0^0 \\ \vdots \\ \mu_{nnn}^0 \end{Bmatrix} \quad (J.6.242)$$

for then, combining (J.6.1-2) with (J.6.239-242), we have

$$[S_0] = [S] [T_S] \quad (J.6.243)$$

$$[D_0] = [D] [T_0] \quad (J.6.244)$$

Thus we need to compute  $[T_S]$  and  $[T_0]$ , or, in particular  $T_0$ , since  $[T_S]$  is just the upper left (6x6) corner of  $[T_0]$ . So, we rewrite the second equation in (J.6.238) as

$$\begin{aligned} \mu(\xi_0', \eta_0') &= \mu_0^0 + \mu_\xi^0 (\xi_0' - x' + x') + \mu_\eta^0 (\eta_0' - y' + y') \\ &\quad + \frac{1}{2} \mu_{\xi\xi}^0 (\xi_0' - x' + x')^2 + \dots \\ &\quad + \frac{1}{6} \mu_{\eta\eta\eta}^0 (\eta_0' - y' + y')^3 \end{aligned} \quad (J.6.245)$$

Now, we equate the coefficients of  $(\xi_0' - x')^i (\eta_0' - y')^j$ ,  $i + j \leq 3$ , in (J.6.237) and (J.6.245) to obtain

$$\begin{aligned} i &= 0 \\ j &= 0 \quad \mu_0 = \mu_0^0 + \mu_\xi^0 x' + \mu_\eta^0 y' + \frac{1}{2} \mu_{\xi\xi}^0 x'^2 + \dots + \frac{1}{6} \mu_{\eta\eta\eta}^0 y'^3 \end{aligned} \quad (J.6.246a)$$

$$\begin{aligned} i &= 1 \\ j &= 0 \quad \mu_\xi = \mu_\xi^0 + \mu_{\xi\xi}^0 x' + \mu_{\xi\eta}^0 y' + \frac{1}{2} \mu_{\xi\xi\xi}^0 x'^2 \\ &\quad + \mu_{\xi\xi\eta}^0 x' y' + \frac{1}{2} \mu_{\xi\eta\eta}^0 y'^2 \end{aligned} \quad (J.6.246b)$$

$$\begin{aligned} i &= 0 \\ j &= 1 \quad \mu_\eta = \mu_\eta^0 + \mu_{\xi\eta}^0 x' + \mu_{\eta\eta}^0 y' + \frac{1}{2} \mu_{\xi\xi\eta}^0 x'^2 \\ &\quad + \mu_{\xi\eta\eta}^0 x' y' + \frac{1}{2} \mu_{\eta\eta\eta}^0 y'^2 \end{aligned} \quad (J.6.246c)$$

$$\begin{aligned} i &= 2 \\ j &= 0 \quad \mu_{\xi\xi} = \mu_{\xi\xi}^0 + \mu_{\xi\xi\xi}^0 x' + \mu_{\xi\xi\eta}^0 y' \end{aligned} \quad (J.6.246d)$$

$$\begin{aligned} i &= 1 \\ j &= 1 \quad \mu_{\xi\eta} = \mu_{\xi\eta}^0 + \mu_{\xi\xi\eta}^0 x' + \mu_{\xi\eta\eta}^0 y' \end{aligned} \quad (J.6.246e)$$

$$\begin{aligned} i &= 0 \\ j &= 2 \quad \mu_{\eta\eta} = \mu_{\eta\eta}^0 + \mu_{\xi\eta\eta}^0 x' + \mu_{\eta\eta\eta}^0 y' \end{aligned} \quad (J.6.246f)$$

$$\begin{aligned}
 i + j = 3 \quad & \mu_{\xi\xi\xi} = \mu_{\xi\xi\xi}^0 \\
 & \mu_{\xi\xi\eta} = \mu_{\xi\xi\eta}^0 \\
 & \mu_{\xi\eta\eta} = \mu_{\xi\eta\eta}^0 \\
 & \mu_{\eta\eta\eta} = \mu_{\eta\eta\eta}^0
 \end{aligned}
 \tag{J.6.246g}$$

Comparing (J.6.242) with (J.6.246), we see that the latter equation defines the entries of  $T_D$  :

$$[T_D] =$$

$$\begin{bmatrix}
 1 & x' & y' & \frac{1}{2}x'^2 & x'y' & \frac{1}{2}y'^2 & \frac{1}{6}x'^3 & \frac{1}{2}x'^2y' & \frac{1}{2}x'y'^2 & \frac{1}{6}y'^3 \\
 0 & 1 & 0 & x' & y' & 0 & \frac{1}{2}x'^2 & x'y' & \frac{1}{2}y'^2 & 0 \\
 0 & 0 & 1 & 0 & x' & y' & 0 & \frac{1}{2}x'^2 & x'y' & \frac{1}{2}y'^2 \\
 0 & 0 & 0 & 1 & 0 & 0 & x' & y' & 0 & 0 \\
 0 & 0 & 0 & 0 & 1 & 0 & 0 & x' & y' & 0 \\
 0 & 0 & 0 & 0 & 0 & 1 & 0 & 0 & 0 & 0 \\
 0 & 0 & 0 & 0 & 0 & 0 & 1 & 0 & 0 & 0 \\
 0 & 0 & 0 & 0 & 0 & 0 & 0 & 1 & 0 & 0 \\
 0 & 0 & 0 & 0 & 0 & 0 & 0 & 0 & 1 & 0 \\
 0 & 0 & 0 & 0 & 0 & 0 & 0 & 0 & 0 & 1
 \end{bmatrix}$$

(J.6.247)

Introducing

$$\vec{d} = \begin{Bmatrix} x' \\ y' \end{Bmatrix} \tag{J.6.248}$$

and recalling the notation (J.6.141-142) which defines row vectors from tensors, and defining  $D$  as the  $2 \times 2 \times 2$  tensor

$$D_{ijk} = d_i d_j d_k \tag{J.6.249}$$

we have

$$T_D =$$

$$T_D = \begin{bmatrix} 1 & 2 & 3 & 4 \\ \begin{array}{c} 1 \\ 0 \\ 0 \\ 0 \end{array} & \begin{array}{c} dT \\ I \\ 0 \\ 0 \end{array} & \begin{array}{c} \frac{1}{2} d^2 T_3 \\ dT \\ 0 \\ 0 \end{array} & \begin{array}{c} \frac{1}{6} d^3 T_4 \\ \frac{1}{2} d^2 T_3 \\ \frac{1}{2} d^2 T_3 \\ dT \\ 0 \end{array} \end{bmatrix} \quad (J.6.250)$$

Similarly,  $T_S$  is just the quadratic portion of  $T$  :

$$T_S = \begin{bmatrix} 1 & d & \frac{1}{2} d^2 T_3 \\ 0 & I & dT \\ 0 & 0 & dT \\ 0 & 0 & I \end{bmatrix} \quad (J.6.251)$$

Combining (J.6.152), (J.6.243) and (J.6.251) we get  $[S_0] =$

$$\begin{bmatrix}
 b & \vec{b}^T + b\vec{d}^T & \frac{1}{2} b \underline{\vec{d}\vec{d}}_3 + \underline{\vec{b}\vec{d}}_3 - \frac{1}{2} \underline{F}_3 \\
 \vec{a} & \underline{\vec{a}\vec{d}}^T + B & \frac{1}{2} \vec{a}_1 \underline{\vec{d}\vec{d}}_3 + \underline{B}_{1..} \vec{d}_3 + r_s \underline{H}_{1,3} \\
 & & \frac{1}{2} \vec{a}_2 \underline{\vec{d}\vec{d}}_3 + \underline{B}_{2..} \vec{d}_3 + \underline{H}_{2,3} \\
 a & \underline{\vec{a}\vec{d}}^T - hr (G\vec{a})^T & \frac{1}{2} a \underline{\vec{d}\vec{d}}_3 - hr \underline{[G]} [\underline{\vec{a}\vec{d}}^T]_3 \\
 & & - \frac{rh}{2} \underline{GB}_3
 \end{bmatrix} \quad (J.6.252)$$

Combining (J.6.164), (J.6.244) and (J.6.247),  $[D_0] =$

$$\begin{bmatrix}
 ra & \underline{\vec{r}\vec{a}\vec{d}}^T - h (G\vec{a})^T & \begin{bmatrix} ra \underline{\vec{d}\vec{d}}_3 - \\ h \underline{[G]} [\underline{\vec{a}\vec{d}}^T]_3 \\ - \frac{h}{2} \underline{GB}_3 \end{bmatrix} & \begin{bmatrix} ra \underline{D}_{,4} - \frac{h}{2} (G\vec{a})_i d_j d_{k,4} \\ - \frac{h}{2} \underline{[GB]}_{ij} d_{k,4} - \frac{h}{6} \underline{H}_{,4} \end{bmatrix} \\
 0 & ra I & \begin{bmatrix} \underline{\vec{r}\vec{a}\vec{d}}^T - h (G\vec{a})^T & 0 \\ 0 & \underline{\vec{r}\vec{a}\vec{d}}^T - h (G\vec{a})^T \end{bmatrix} & \begin{bmatrix} \begin{bmatrix} ra \underline{\vec{d}\vec{d}}_3 \\ h \underline{[G\vec{a}}] \vec{d}_3 - \frac{h}{2} \underline{GB}_3 \end{bmatrix} & 0 \\ \begin{bmatrix} ra \underline{\vec{d}\vec{d}}_3 \\ -h \underline{[G\vec{a}}] \vec{d}_3 - \frac{h}{2} \underline{GB}_3 \end{bmatrix} & \end{bmatrix} \\
 u & -(G\vec{a})^T & \begin{bmatrix} - \underline{[G]} [\underline{\vec{a}\vec{d}}^T]_3 \\ - \underline{GB}_3 \end{bmatrix} & \begin{bmatrix} - \frac{1}{2} (G\vec{a})_i d_j d_{k,4} \\ - \underline{[GB]}_{ij} d_{k,4} - \frac{1}{2} \underline{H}_{,4} \end{bmatrix}
 \end{bmatrix} \quad (J.6.253)$$

### J.6.7 Finite Parts of Integrals

In section J.6.5.1 we evaluated the integral

$$a = \frac{-sh}{\kappa} \iint_{\Sigma' \cap D_p} \frac{1}{\rho} \frac{\partial \psi}{\partial \rho} dS, \quad (J.6.254)$$

for  $\Sigma'$  a subinclined panel. In doing so, we discarded a term, leaving the justification for discarding that term to this section.

We will show in section J.6.7.4 that the term we discard is in fact zero if we only consider the "finite part" of the integral (J.6.254). The finite part of an integral is a concept we define in section J.6.7.1, and for which we cite certain well-known properties in section J.6.7.2. Next, in section J.6.7.3, we review the manipulations of integrals we have performed prior to Appendix J and conclude that they are still valid if we consider only the finite parts of various integrals. We then note in section J.6.7.4 that we really want to compute only the finite part of (J.6.254), and thus we properly discarded the extra term which appeared in section J.6.5.1.

#### J.6.7.1 Definition of a Finite Part

Let  $f$  be a function on a surface  $S$  (though our definition will have an obvious extension to functions on a line or in a volume of space) of finite area. Let  $S_\epsilon$  be the set of points in  $S$  which are distance greater than  $\epsilon$  from any point on  $S$  at which  $f$  is infinite, where  $\epsilon > 0$ . Then we define

$$\iint_S^* f dS = \lim_{\epsilon \rightarrow 0} \iint_{S_\epsilon} f dS \quad (J.6.255)$$

and we call the integral on the left side of (J.6.255) the finite part of the integral of  $f$  over  $S$ . We call

$$\iint_S f dS - \iint_S^* f dS \quad (J.6.256)$$

the infinite part of the integral whenever it is non-zero.

#### J.6.7.2 Properties of a Finite Part

Several important properties of ordinary integrals of bounded functions also hold for finite parts of integrals. First, the standard integration by parts theorems in several variables (the divergence theorem, Stokes' Theorem, Green's Theorem) hold for finite parts of integrals.

Second, differentiation with respect to a parameter on which  $f$  depends may be moved under the integral. That is, if  $f$  is a function of  $t$ ,

$$\frac{\partial}{\partial t} \iint_S^* f dS = \iint_S \frac{\partial f}{\partial t} dS \quad (J.6.257)$$

These results are discussed in the paper of Robinson (reference J.3).

### J.6.7.3 Finite Parts and the Integral Equation

In section B.0, we quoted the fundamental integral equation (B.0.1),

$$\phi = \frac{1}{K} \iint_{SNDP}^* \frac{\sigma}{R} + n \cdot \tilde{\nabla} \left( \frac{1}{R} \right) dS \quad (J.6.258)$$

But thereafter, we treated this integral as though it were an ordinary integral rather than a finite part integral. In particular, we applied Stokes' Theorem and took the gradient operator under the integral equation to obtain (B.3.31)

$$\begin{aligned} \vec{\nabla}(P) = & \frac{1}{K} \iint_{SNDP}^* \left[ -\sigma \vec{\nabla}_P \left( \frac{1}{R} \right) + (\hat{n} \times \vec{\nabla}_Q \mu) \times \tilde{\nabla} \left( \frac{1}{R} \right) \right] dS \\ & + \frac{1}{K} \iint_{SNDP}^* \mu \tilde{\nabla}_Q \left( \frac{1}{R} \right) \times d\vec{l} \end{aligned} \quad (J.6.259)$$

The derivation of (J.6.259) from (J.6.258) is only justifiable, however, in light of the results we quote in section J.6.7.2.

### J.6.7.4 Finite Parts and PIC Computation

Now, in appendix J, we have consistently ignored the fact that we really were interested only in the finite parts of the integrals which defined. Until section J.6.5.1, where we attempted actually to evaluate such an integral, this caused no problem. In that section, however, we obtained an infinite term because we failed to evaluate only the finite part of the integral (J.6.254). That is, we should compute

$$\begin{aligned} a = & \iint_{\Sigma'NDP}^* \frac{1}{\rho} \frac{\partial \psi}{\partial \rho} dS' \\ = & -\frac{sh}{K} \lim_{\epsilon \rightarrow 0} \iint_{\Sigma'_\epsilon} \frac{1}{\rho} \frac{\partial \psi}{\partial \rho} dS' \end{aligned} \quad (J.6.260)$$

where  $\Sigma'_\epsilon$  is a polygonal region, entirely within  $D_p$ , which approaches  $\Sigma' \cap D_p$  as  $\epsilon$  goes to zero (cf., figure J.26)

Then, if  $\Sigma'_\epsilon$  has  $K_\epsilon$  edges, by (J.6.169-170), we have

$$a = \lim_{\epsilon \rightarrow 0} \frac{-sh}{K} \sum_{k=1}^{K_\epsilon} \int_{\phi_k^-}^{\phi_k^+} \psi d\phi - \int_{\phi_k^-}^{\phi_k^+} \frac{1}{\epsilon} d\phi \quad (J.6.261)$$

$$= \lim_{\epsilon \rightarrow 0} \frac{1}{K} \sum_{k=1}^{K_\epsilon} \int_{\phi_k^-}^{\phi_k^+} \psi d\phi$$

$$- \lim_{\epsilon \rightarrow 0} \frac{1}{\epsilon} \sum_{k=1}^{K_\epsilon} \int_{\phi_k^-}^{\phi_k^+} d\phi \quad (J.6.262)$$

But it follows from section J.5 (cf. (J.5.22), along with figure J.20, which shows that  $(s+t)/(s-t) > 0$ ) that  $\phi$  is a smooth function on  $D_p$ , and bounded on  $\Sigma'_\epsilon$ . In particular,  $\phi$  is single-valued. Thus by the fundamental theorem of calculus

$$\sum_{k=1}^{K_\epsilon} \int_{\phi_k^-}^{\phi_k^+} d\phi = \int_{\partial \Sigma'_\epsilon} d\phi = 0 \quad (J.6.263)$$

and thus the second term of (J.6.262) is zero, and thus should be neglected, as we do in section J.6.5.1.

#### J.6.7.5 Summary of Finite Part Integrals

We now briefly summarize the role of finite parts of integrals in influence coefficient computation. First, we state the fundamental integral equation (B.0.1), which involves the finite part of a surface integral, and whose validity we do not prove, but is discussed in Ward (reference 1.5) and in more detail in Ehlers, et. al. (reference 4.9). Second, we derive (B.3.31) from (B.0.1), a derivation which is only valid because of the properties (whose validity we also do not prove) of finite parts of integrals cited in section J.6.7.2. Third, for reasons of clarity, we leave the finite parts symbol off many integrals in appendix J. Fourth, we see that a term which appears in section J.6.5.1 must be discarded, since we only require the finite part of the integral which is being evaluated. In section J.7 we will see that the remaining term in this expression can be evaluated in closed form.



## J.7 Edge and Panel Functions

In section J.7.1, we compute the edge function

$$I_k(\psi) = \int_{v_k^-}^{v_k^+} \psi dv \quad (J.7.1)$$

and the function

$$J_k(\psi) = \int_{\phi_k^-}^{\phi_k^+} \psi d\phi \quad (J.7.2)$$

where the panel function  $J$  is given by (cf. (J.6.173))

$$J = \sum_k h J_k(\psi) - 2\pi \operatorname{sign}(h) C_\bullet \quad (J.7.3)$$

We also compute integrals  $I(X)$  and  $J(X)$  used in sections J.4 - J.6 (cf. (J.4.68), (J.5.115), (J.6.212))

$$I_k(X) = \int_{v_k^-}^{v_k^+} R_k dv \quad (J.7.4)$$

$$J_k(X) = \int_{v_k^-}^{v_k^+} \frac{R_k}{\rho_k^2} dv = \int_{\phi_k^-}^{\phi_k^+} R d\phi \quad (J.7.5)$$

### J.7.1 Edge and Panel Functions

#### J.7.1.1 Subsonic Flow

Since the flow is subsonic,  $r = s = q_k = 1$ , and (J.6.58-59) become

$$\rho_k^2 = a_k^2 + v_k^2 \quad (J.7.6)$$

$$R^2 = a_k^2 + v_k^2 + h^2 \quad (J.7.7)$$

By (J.4.66) we have

$$J_k(\psi) = \int_{v_k^-}^{v_k^+} \frac{a_k}{a_k^2 + v_k^2} dv$$

$$= \int_{v_k^-}^{v_k^+} R_k (a_k^2 + v_k^2) dv \quad (J.7.8)$$

We now exhibit without derivation the functions which are the indefinite integrals  $I(\psi)$ ,  $J(\psi)$ ,  $I(X)$ ,  $J(X)$ . The integrations can be verified by differentiating the functions with respect to  $v$ , while noting (J.7.6-7). The differentiations are tedious but straightforward.

We find

$$I(\psi) = \int \frac{dv}{R} = \frac{1}{2} \log \left( \frac{R+v}{R-v} \right) \quad (J.7.9)$$

$$J(\psi) = \int \frac{a}{R(a^2 + v^2)} dv = \frac{1}{h} \text{ph} (hv, aR) \quad (J.7.10)$$

$$I(X) = \int R dv = \frac{1}{2} (vR + (a^2 + h^2)I(\psi)) \quad (J.7.11)$$

$$J(X) = \int \frac{a R dv}{a^2 + v^2} = h^2 J(\psi) + aI(\psi) \quad (J.7.12)$$

Clearly

$$I_k(\psi) = I(\psi)(R_k^+, v_k^+) - I(\psi)(R_k^-, v_k^-) \quad (J.7.13)$$

Similarly, evaluation at both endpoints of the intersection of the panel edge and the domain of dependence gives us the remaining definite integrals.

#### J.7.1.2 Subsonic Edges of Subinclined Panels in Supersonic Flow

Now (J.6.58-59) become

$$\rho^2 = v^2 - a^2 \quad (J.7.14)$$

$$R^2 = v^2 - a^2 - h^2 \quad (J.7.15)$$

since  $s = -1$ ,  $r = +1$ ,  $q = +1$ . Also, we have

$$J_k(\psi) = \int_{v_k^-}^{v_k^+} \frac{a_k R}{a_k^2 + v^2} dv \quad (J.7.16)$$

The indefinite integrals now become

$$I(\psi) = \int \frac{dv}{R} = \frac{1}{2} \log \left( \frac{v+r}{v-r} \right) \quad (J.7.17)$$

$$J(\psi) = \int \frac{adv}{(a^2 - v^2)R} = -\frac{1}{h} \text{ph} (hv, aR) \quad (J.7.18)$$

$$I(X) = \int R dv = \frac{1}{2} (vR - (a^2 + h^2) I(\psi)) \quad (J.7.19)$$

$$J(X) = \int \frac{aR dv}{a^2 - v^2} = -h^2 J(\psi) - aI(\psi) \quad (J.7.20)$$

#### J.7.1.3 Supersonic Edges of Subinclined Panels

Now  $r = +1$ ,  $s = -1 = q$ , so

$$\rho^2 = a^2 - v^2 \quad (J.7.21)$$

$$R^2 = a^2 - h^2 - v^2 \quad (J.7.22)$$

and

$$J_k(\psi) = \int_{v_k^-}^{v_k^+} \frac{a_k R dv}{a_k^2 - v^2} \quad (J.7.23)$$

The indefinite integrals become

$$I(\psi) = \int \frac{dv}{R} = -\text{ph} (v, R) \quad (J.7.24)$$

$$J(\psi) = \int \frac{adv}{(a^2 - v^2)R} = -\frac{1}{h} \text{ph} (hv, aR) \quad (J.7.25)$$

$$I(X) = \int R dv = \frac{1}{2} (vR + (a^2 - h^2) I(\psi)) \quad (J.7.26)$$

$$J(X) = \int \frac{aR dv}{a^2 - v^2} = -h^2 J(\psi) + aI(\psi) \quad (J.7.27)$$

#### J.7.1.4 Superinclined Panels

Now  $r = s = q = -1$ , and

$$\rho^2 = a^2 + v^2 \quad (J.7.28)$$

$$R^2 = h^2 - a^2 - v^2 \quad (J.7.29)$$

and

$$J_k(\psi) = \int_{v_k^-}^{v_k^+} \frac{a_k dv}{(a_k^2 + v^2)R} \quad (J.7.30)$$

The indefinite integrals become

$$I(\psi) = \int \frac{dv}{R} = -ph(hv, R) \quad (J.7.31)$$

$$J(\psi) = \int \frac{adv}{R(a^2 + v^2)} = \frac{1}{h} ph(hv, aR) \quad (J.7.32)$$

$$I(\chi) = \int R dv = \frac{1}{2} (vR - (a^2 - h^2) I(\psi)) \quad (J.7.33)$$

$$J(\chi) = \int \frac{aR dv}{a^2 + v^2} = h^2 J(\psi) - aI(\psi) \quad (J.7.34)$$

#### J.7.1.5 Uniform Formulas

We unify the results of section J.7.1 for  $I_k(\psi)$  and  $J_k(\psi)$ . We obtain

$$I_k(\psi) = \left. \frac{1}{2} \log \left( \frac{R+v}{R-v} \right) \right|_-^+ \quad s = 1$$

$$\left. \frac{1}{2} \log \left( \frac{v+R}{v-R} \right) \right|_-^+ \quad s = -1, q = 1$$

$$-ph(hv, R) \quad q = -1 \quad (J.7.35)$$

$$J_k(\psi) = \left. -\frac{1}{h} ph(hv, aR) \right|_-^+ \quad (J.7.36)$$

where evaluation occurs at the two endpoints of the intersection of the edge and the domain of dependence.

#### J.7.2 Computation of Edge and Panel Function Arguments in Reference Coordinates

In this section, we compute  $h$ ,  $v$ ,  $a$ , and

$$g = \sqrt{rsq a^2 + rsh^2} \quad (J.7.37)$$

in reference coordinates. These quantities are computed in reference coordinates in PAN AIR to minimize numerical error.

### J.7.2.1 Computation of h

By (J.6.41)

$$h = z' - \zeta' = \begin{pmatrix} 0 \\ 0 \\ 1 \end{pmatrix} \cdot A (P - Q_0) \quad (J.7.38)$$

where  $Q_0$  is any point on the panel, such as the panel center, and  $A$  is the reference to local transformation.

Thus

$$h = \begin{bmatrix} 0 & 0 & 1 \end{bmatrix} [A] (\vec{P} - \vec{Q}_0) \quad (J.7.39)$$

$$= \sum_{j=1}^3 A_{3j} (\vec{P} - \vec{Q}_0)_j \quad (J.7.40)$$

Applying (E.0.1)

$$h = \frac{8}{(\hat{n}_0, \hat{n}_0)} \hat{n}_0 \cdot (\vec{P} - \vec{Q}_0) \quad (J.7.41)$$

### J.7.2.2 Computation of v

By (J.6.47)

$$v = \langle \vec{t}_k, \vec{\rho} \rangle = \vec{t}_k^T [G] \vec{\rho} \quad (J.7.42)$$

where  $G$ ,  $\vec{t}_k$ , and  $\vec{\rho}$  are defined in section J.6.1.4. Now, define a 3-vector

$$\vec{t}' = \begin{pmatrix} \vec{t}_k \\ - \\ 0 \end{pmatrix} \quad (J.7.43)$$

Next, we note from (E.3.24) that

$$\begin{bmatrix} r \\ s \\ r_s \end{bmatrix} = [A^{-T}] C_0 [A^{-1}] \quad (J.7.44)$$

So,

$$v = \vec{t}_k^T \begin{bmatrix} rs & 0 \\ 0 & 1 \end{bmatrix} \vec{\rho}$$

$$= \vec{t}'^T \begin{bmatrix} rs & 1 \\ & s \end{bmatrix} \begin{bmatrix} \vec{\rho} \\ 0 \end{bmatrix} \quad (J.7.45)$$

$$= \vec{st}'^T \begin{bmatrix} r & s \\ & rs \end{bmatrix} A (\vec{Q} - \vec{P}) \quad (J.7.46)$$

$$= \vec{st}'^T [A^{-T}] C_0 (\vec{Q} - \vec{P}) \quad (J.7.47)$$

$$= s [A^{-1} \vec{t}', \vec{Q} - \vec{P}] \quad (J.7.48)$$

$$= s |A^{-1} \vec{t}'| [\vec{t}_0, \vec{Q} - \vec{P}] \quad (J.7.49)$$

where  $\vec{t}_0$  is the unit edge tangent,  $\vec{P}$  is the field point, and  $\vec{Q}$  lies on the edge.

Noting (J.6.42-43), we see that

$$\vec{t}' = \frac{A\vec{t}}{|\langle A\vec{t}, A\vec{t} \rangle|^{\frac{1}{2}}} \quad (J.7.50)$$

where  $\vec{t}$  is any tangent vector in reference coordinates. Thus we define

$$\tau = \frac{1}{|A^{-1} \vec{t}'|} = |\langle A\vec{t}_0, A\vec{t}_0 \rangle|^{\frac{1}{2}}$$

$$= |\vec{t}_0^T A^T \begin{bmatrix} G & 0 \\ 0 & 0 \end{bmatrix} A\vec{t}_0|^{\frac{1}{2}} = |\vec{t}_0^T C \vec{t}_0|^{\frac{1}{2}}$$

$$= |[\hat{t}_0, \hat{t}_0]|^{\frac{1}{2}} \quad (J.7.51)$$

where we have chosen a unit tangent vector  $\hat{t}_0$ .

Then

$$v = \frac{s}{\tau} [\hat{t}_0, \vec{Q} - \vec{P}] \quad (J.7.52)$$

### J.7.2.3 Computation of a

The edge distance  $a_k$  is (cf (J.6.46))

$$a_k = \vec{n}_k \cdot \vec{p}_k \quad (\text{J.7.53})$$

where

$$\vec{n} = \begin{Bmatrix} t_\eta \\ -t_\xi \end{Bmatrix} \quad (\text{J.7.54})$$

Note that

$$\vec{t}' \times \vec{n}' = \begin{Bmatrix} t_\xi \\ t_\eta \\ 0 \end{Bmatrix} \times \begin{Bmatrix} 0 \\ 0 \\ 1 \end{Bmatrix} = \begin{Bmatrix} t_\eta \\ -t_\xi \\ 0 \end{Bmatrix} \quad (\text{J.7.55})$$

Thus

$$a = \left( \vec{t}' \times \begin{Bmatrix} 0 \\ 0 \\ 1 \end{Bmatrix} \right) \cdot (\vec{Q}' - \vec{P}') \quad (\text{J.7.56})$$

$$= \begin{Bmatrix} 0 \\ 0 \\ 1 \end{Bmatrix} \cdot \left( (\vec{Q}' - \vec{P}') \times \vec{t}' \right)$$

$$= \begin{Bmatrix} 0 \\ 0 \\ 1 \end{Bmatrix} \cdot \left\{ A(Q - P) \times \frac{A \hat{t}_0}{\tau} \right\} \quad (\text{J.7.57})$$

$$= (\text{cf. (E.1.12)}) \quad \begin{Bmatrix} 0 \\ 0 \\ 1 \end{Bmatrix} \cdot \frac{\det A}{\tau} A^{-T} \left\{ ((\vec{Q} - \vec{P}) \times \hat{t}_0) \right\} \quad (\text{J.7.58})$$

$$= \frac{\det A}{\tau} (A_{\cdot,3}^{-1}) \cdot ((\vec{Q} - \vec{P}) \times \hat{t}_0) \quad (\text{J.7.59})$$

= (cf (E.3.59))

$$\frac{\det A}{\tau} \frac{r}{B | \{n_0, n_0\} |^2} B_0 \hat{n}_0 \cdot ((\vec{Q} - \vec{P}) \times \hat{t}_0) \quad (\text{J.7.60})$$

Finally, applying (E.3.90) to obtain  $\det A$ ,

$$a = \frac{r \cdot b}{\tau | \{n_0, n_0\} |^2} (\hat{n}_0, (\vec{Q} - \vec{P}) \times \hat{t}_0) \quad (J.7.61)$$

#### J.7.4.2 Computation of $g$

Applying (J.6.59)

$$g^2 = sq (R^2 - qv^2) \quad (J.7.62)$$

$$= sq ( [\vec{Q} - \vec{P}, \vec{Q} - \vec{P}] - \frac{q}{\tau^2} [\hat{t}_0, \vec{Q} - \vec{P}]^2 ) \quad (J.7.63)$$

Now we use the following identity, which we prove shortly. For arbitrary vectors  $a$  and  $b$ , and a matrix  $C$ ,

$$(\vec{a} \times \vec{b})^T [C^{-1}] (\vec{a} \times \vec{b}) = \det (C^{-1}) ((\vec{a}^T \vec{c}_a) (\vec{b}^T \vec{c}_b) - (\vec{a}^T \vec{c}_b)^2) \quad (J.7.64)$$

We apply (J.7.64) to (J.7.63) with

$$\vec{a} = \vec{Q} - \vec{P}$$

$$\vec{b} = \frac{\hat{t}_0}{\tau} = \vec{t}$$

$$[C] = [C_0] \quad (J.7.65)$$

Since (cf. E.2.9))

$$C_0^{-1} = \frac{1}{s\beta^2} B_0 \quad (J.7.66)$$

we get (by J.7.64)

$$\frac{1}{s\beta^2} \left\{ (\vec{Q} - \vec{P}) \times \vec{t}, (\vec{Q} - \vec{P}) \times \vec{t} \right\} =$$

$$\frac{1}{\beta^4} ( [\vec{Q} - \vec{P}, \vec{Q} - \vec{P}] [\vec{t}, \vec{t}] - [\vec{Q} - \vec{P}, \vec{t}]^2 ) \quad (J.7.67)$$

= (cf. (J.7.51))

$$\frac{s}{\beta^4} g^2 \quad (J.7.68)$$

Here we use the fact (cf. (J.7.51))

$$[\hat{t}_0, \hat{t}_0] = q \tau^2 \quad (J.7.69)$$



Thus

$$g^2 = \beta^2 \left\{ (\vec{n} - \vec{p}) \times \frac{\hat{t}_0}{T}, (\vec{q} - \vec{p}) \times \frac{\hat{t}_0}{T} \right\} \quad (J.7.70)$$

We now need only to prove (J.7.64)

We prove in general, for vectors,  $\vec{a}, \vec{b}, \vec{c}, \vec{d}$ , and a matrix  $C$ :

$$\begin{aligned} (\vec{a} \times \vec{b})^T C (\vec{c} \times \vec{d}) &= \\ (\det C) [(\vec{a}^T C^{-1} \vec{c}) (\vec{b}^T C^{-1} \vec{d}) - (\vec{a}^T C^{-1} \vec{d}) (\vec{b}^T C^{-1} \vec{c})] \end{aligned} \quad (J.7.71)$$

Now, by (E.1.23)

$$[C] (\vec{c} \times \vec{d}) = (\det C) (C^{-1} \vec{c}) \times (C^{-1} \vec{d}) \quad (J.7.72)$$

Thus

$$\begin{aligned} (\vec{a} \times \vec{b})^T [C] (\vec{c} \times \vec{d}) &= \\ (\det C) (\vec{a} \times \vec{b}) \cdot (C^{-1} \vec{c} \times C^{-1} \vec{d}) \end{aligned} \quad (J.7.73)$$

Now, using the notation of section B.3, for vectors  $\vec{a}, \vec{b}, \vec{e}, \vec{f}$ ,

$$(\vec{a} \times \vec{b}) \cdot (\vec{e} \times \vec{f}) = \sum_{ijmn} (\epsilon_{ijk} a_i b_j) (\epsilon_{mnk} e_m f_n) \quad (J.7.74)$$

Now, recalling (B.3.31):

$$(\vec{a} \times \vec{b}) \times \vec{c} = -(\vec{b} \cdot \vec{c}) \vec{a} + (\vec{a} \cdot \vec{c}) \vec{b} \quad (J.7.75)$$

we convert to  $\epsilon$  notation and obtain

$$\begin{aligned} ((\vec{a} \times \vec{b}) \times \vec{c})_k &= \\ \sum_{ijmn} \epsilon_{ijk} (\epsilon_{mni} a_m b_n) c_j &= \end{aligned} \quad (J.7.76)$$

$$\begin{aligned} &= (\vec{b} \cdot \vec{c}) a_k + (\vec{a} \cdot \vec{c}) b_k = \\ &= \sum_n (b_n c_n) a_k + \sum_m a_m c_m b_k = \end{aligned} \quad (J.7.77)$$

$$= \sum_{jnm} \delta_{jn} \delta_{km} a_m b_n c_j + \sum_{jmn} \delta_{jm} \delta_{kn} a_m b_n c_j \quad (J.7.78)$$

where  $\delta$  is the Kronecker delta (zero unless the two subscripts are equal, in which case it equals one).

Now, noting that  $\epsilon_{ijk} = \epsilon_{jki}$ , (J.7.76-78) yield

$$\sum_i \epsilon_{jki} \epsilon_{mni} = \delta_{jm} \delta_{kn} - \delta_{jn} \delta_{km} \quad (\text{J.7.79})$$

Applying (J.7.79) to (J.7.74)

$$(\vec{a} \times \vec{b}) \cdot (\vec{c} \times \vec{d}) = \sum_{ijmn} \epsilon_{ijk} \epsilon_{mnk} a_i b_j c_m d_n \quad (\text{J.7.80})$$

$$\begin{aligned} &= \sum_{ijmn} (\delta_{im} \delta_{jn} - \delta_{in} \delta_{jm}) a_i b_j c_m d_n \\ &= (\vec{a} \cdot \vec{c}) (\vec{b} \cdot \vec{d}) - (\vec{a} \cdot \vec{d}) (\vec{b} \cdot \vec{c}) \end{aligned} \quad (\text{J.7.81})$$

Substituting (J.7.80-81) into (J.7.73)

$$\begin{aligned} &(\vec{a} \times \vec{b}) \cdot \vec{c} = (\vec{c} \times \vec{d}) \cdot \vec{a} \\ &(\det C) \begin{pmatrix} (\vec{a}^T C^{-1} \vec{c}) (\vec{b}^T C^{-1} \vec{d}) \\ - (\vec{a}^T C^{-1} \vec{d}) (\vec{b}^T C^{-1} \vec{c}) \end{pmatrix} \end{aligned} \quad (\text{J.7.82})$$

which is (J.7.64) with  $C^{-1}$  replacing  $C$ .

## J.8 Rationalization Formulas

The computation of the edge and panel functions has been described in section J.7. These formulas are not always computationally stable. In this section we describe the actual formulas we use to compute the edge and panel functions.

### J.8.1 Edge Functions

In this section we will discuss the computation of the quantities

$$\hat{I} = \frac{q}{\tau} I(\psi) \Big|_{v^-}^{v^+} \quad (J.8.1)$$

$$\Delta \hat{R} = \hat{R}_+ - \hat{R} \Big|_{r_-} \quad (J.8.2)$$

$$\hat{K} = \frac{1}{\tau^2} (q \Delta R - \frac{1}{2}(v_+ + v_-) I(\psi) \Big|_{v^-}^{v^+}) \quad (J.8.3)$$

where

$$\tau = |[\hat{t}_0, \hat{t}_0]|^{\frac{1}{2}} \quad (J.8.4)$$

$$q = \text{sign} [\hat{t}_0, \hat{t}_0] \quad (J.8.5)$$

$$I(\psi) = \begin{cases} \frac{1}{2} \log \left( \frac{v+R}{v-R} \right) & q = +1 \\ -\text{ph}(V, R) & q = -1 \end{cases} \quad (J.8.6)$$

$$\vec{r} = \vec{p} - \vec{Q} \quad (J.8.7)$$

$$R = [\vec{r}, \vec{r}]^{\frac{1}{2}} \quad (J.8.8)$$

and  $r_+$ ,  $v_+$  denote the values of  $r$  and  $v$  at the upper and lower end points of  $END_E$ , where  $E$  is the edge in question. We use a  $\Delta$  to denote the difference of a value at the endpoints, and a bar to denote the average.

The procedure used to evaluate these edge functions is as follows.

In section J.8.1.1, we will discuss edges for which

$$\tau^2 > 10^{-4} \quad (J.8.9)$$

We will call these non-sonic edges, and will distinguish four cases. We will first consider the case where at most one endpoint of the edge lies in the interior of  $D_p$ , dividing this into the regular case of a supersonic edge or  $R \leq .95v$ , and a special case of a subsonic edge and  $R > .95v$ . We will also consider the case of both endpoints lying within the interior of  $D_p$ . This is divided into a regular case and a special case in which  $v$  changes sign ( $v_- < 0 < v_+$ ) and  $g^2 \ll 1$ .

In section J.8.1.2 we will discuss nearly sonic edges, for which

$$10^{-10} \leq \tau^2 \leq 10^{-4} \quad (J.8.10)$$

Here the regular case is

$$q = 1$$

$$\text{or} \quad \text{sign}(R + R_- + v + v_-) = 1 \quad (J.8.11)$$

In section J.8.13, we will consider essentially sonic edges, for which

$$\tau^2 < 10^{-10} \quad (J.8.12)$$

#### J.8.1.1 Non-Sonic Edges

We will calculate

$$\hat{I} = \frac{q}{\tau} (I(\psi)|_{v_+} - I(\psi)|_{v_-}) \quad (J.8.13)$$

and

$$\Delta R = \vec{R}|_{r_+} - \vec{R}|_{r_-} \quad (J.8.14)$$

When an edge intersects the Mach cone, it is possible to compute these functions without actually evaluating the point of intersection. We have

$$R|_{\text{Mach cone}} = 0 \quad (J.8.15)$$

(subsonic)

$$\begin{aligned} I(\psi)|_{v_+, \text{Mach cone}} &= 0 \\ I(\psi)|_{v_-, \text{M.C.}} &= 0 \end{aligned} \quad q = +1 \quad (J.8.16)$$

(supersonic)

$$\begin{aligned} I(\psi)|_{v_+, \text{M.C.}} &= 0 \\ I(\psi)|_{v_-, \text{M.C.}} &= 0 \end{aligned} \quad q = -1 \quad (J.8.17)$$

Thus, when only one endpoint of the edge E lies inside the Mach cone, (we are now treating the case of supersonic flow), we need compute only one elementary transcendental function. For a subsonic edge, we would then compute

$$I(\psi) = \frac{1}{2} \log \frac{v+R}{v-R} \quad (q = +1) \quad (J.8.18)$$

while for a supersonic edge we would have

$$I(\psi) \Big|_v = -ph(v, R) \quad (q = -1) \quad (J.8.19)$$

If we recall equation (J.7.62) we obtain

$$\begin{aligned} R^2 = qv^2 + sqg^2 = \begin{cases} v^2 - g^2 & (q = +1, s = -1) \\ g^2 - v^2 & (q = -1, s = -1) \end{cases} \end{aligned} \quad (J.8.20)$$

we see that some difficulties may arise in the evaluation of  $I(\psi) \Big|_v$  for subsonic edges when  $g^2$  is very small, for then  $R \approx v$  and the log function in equation (J.8.18) blows up. Thus, for the very special case in which (a) one end of  $END_p$  lies on the Mach cone (E subsonic) and (b)  $g^2$  is very small, the following procedure should be used

$$\begin{aligned} I(\psi) \Big|_v &= \frac{1}{2} \log \frac{v+R}{v-R} \\ &= \log(v+R) - \frac{1}{2} \log(g^2) \quad (v > 0) \\ &= \frac{1}{2} \log(g^2) - \log(R + v) \quad (v < 0) \end{aligned} \quad (J.8.21)$$

$$= \text{sign}(v) (\log(|v| + R) - \frac{1}{2} \log g^2) \quad (J.8.22)$$

where  $g$  should be computed by the relation (see Section J.7.2.4)

$$g^2 = \frac{B^2}{r^2} \{ \vec{r}_0 \times \hat{t}_0, \vec{r}_0 \times \hat{t}_0 \} \quad (J.8.23)$$

The initial test for small  $g$  can be made by asking whether  $R > .95|v|$ . If this test is satisfied,  $g^2$  is small and the special procedure outlined by equation (J.8.22) should be used.

This completes the discussion of what must be done when one endpoint of  $E_{Dp}$  lies on the Mach cone. We now turn our attention to the case in which both endpoints lie inside the Mach cone. We begin this discussion by deriving

some expressions for  $I(\psi) \Big|_{v_-}^{v_+}$  that are generally valid; that is, they do not depend upon the assumption that both endpoints of  $E_{Dp}$  lie inside the Mach cone.

Using equation (J.8.6), we have, for subsonic edges

$$I(\psi) \Big|_{v_-}^{v_+} = \frac{1}{2} \log \frac{v_+ R_-}{v_- R_+} \Big|_{v_-}^{v_+} \quad (J.8.24a)$$

$$= \frac{1}{2} \log \frac{(v_+ v_- - R_+ R_-) + (R_+ v_- - v_- R_+)}{(v_+ v_- - R_+ R_-) - (R_+ v_- - v_- R_+)} \\ = \frac{1}{2} \log \frac{1+z}{1-z} \quad (J.8.24b)$$

where  $z$  is defined by

$$z = \frac{R_+ v_- - R_- v_+}{v_+ v_- - R_- R_+} \quad (J.8.25)$$

The definition (J.8.25) for  $z$  may be arranged somewhat by using equation (J.8.20) to obtain

$$R^2 = v^2 + sg^2 \quad (J.8.26)$$

Then

$$z = \frac{R_+ v_- - R_- v_+}{v_+ v_- - R_- R_+} = \frac{R_+ v_- + R_- v_+}{R_+ v_- + R_- v_+} \quad (J.8.27a)$$

$$= \frac{R_+^2 v_-^2 - R_-^2 v_+^2}{R_+ v_+ (v_-^2 - R_-^2) + R_- v_- (v_+^2 - R_+^2)} \quad (J.8.27b)$$

$$= \frac{v_+^2 - v_-^2}{R_+ v_+ + R_- v_-} \quad (J.8.27c)$$

In a precisely analogous fashion, we have for supersonic edges

$$I(\psi) \Big|_{v_-}^{v_+} = -ph(v, R) \Big|_{v_-}^{v_+} = - \left[ \frac{\pi}{2} - ph(R, v) \right]_{v_-}^{v_+} \quad (J.8.28)$$

$$= ph(R_+, v_+) - ph(R_-, v_-) \\ = ph(R_+ R_- + v_+ v_-, v_+ R_- - v_- R_+) \quad (J.8.29)$$

$$= ph(\sigma, \sigma \tilde{z}) \quad (J.8.30)$$

where in this case we define  $\sigma$  and  $\tilde{z}$  by

$$\sigma = \text{sign}(R_+ R_- + v_+ v_-) \quad (\text{J.8.31})$$

$$\tilde{z} = \frac{v_+ R_- - v_- R_+}{R_+ R_- + v_+ v_-} \quad (\text{J.8.32})$$

As before, the definition of  $\tilde{z}$  may be rearranged somewhat with the help of equation (J.8.20). Doing this, we find

$$\tilde{z} = \tilde{z} \frac{R_+ v_- + R_- v_+}{R_+ v_- + R_- v_+} = \quad (\text{J.8.33})$$

$$= \frac{v_+^2 - v_-^2}{R_+ v_+ + R_- v_-} = z \quad (\text{J.8.34})$$

Thus,  $\tilde{z} = z$  and we can drop the tilde. Summarizing, we have found,

$$I(\psi) \Big|_{v_-}^{v_+} = \begin{cases} \frac{1}{2} \log \frac{1+z}{1-z} & q = +1 \\ \text{ph}(\sigma, \sigma z) & q = -1 \end{cases} \quad (\text{J.8.35})$$

where

$$z = \frac{v_+^2 - v_-^2}{R_+ v_+ + R_- v_-} = \frac{(v_+ - v_-)(v_+ + v_-)}{R_+ v_+ + R_- v_-}$$

$$\sigma = \text{sign}(R_+ R_- + v_+ v_-) \quad (\text{J.8.36})$$

Equation (J.8.35) will permit stable and accurate evaluation of  $I(\psi) \Big|_{v_-}^{v_+}$  in

all instances with the exception that when  $g^2$  is small,  $q = +1$ , and  $v$  changes sign along the edge, some additional care must be taken. We now describe the procedure to be used in this case.

Since  $v$  changes sign along the edge, the flow must be subsonic. Consequently, equation (J.8.20) gives us

$$R^2 = v^2 + g^2 \quad (\text{J.8.37})$$

Next, we note that the function  $I(\psi)$  may be written

$$I(\psi) = \frac{1}{2} \log \frac{v+R}{v-R} = \frac{1}{2} \log \left( -\frac{R+v}{R-v} \right) + \frac{1}{2} \quad (\text{J.8.38})$$

Concentrating on the function  $\frac{1}{2} \log \frac{R+v}{R-v}$ , we find

$$\frac{1}{2} \log \frac{R+v}{R-v} = \log g - \log (R-v) \quad (J.8.39)$$

Evaluating  $I(\psi)$  at the two limits and noting that since  $v_- v_+ < 0$ , we must have  $v_- < 0 < v_+$ , we get

$$\begin{aligned} I(\psi) \Big|_{v_-}^{v_+} &= \left( \frac{1}{2} \log \frac{R+v}{R-v} \right)_{v_+} - \left( \frac{1}{2} \log \frac{R+v}{R-v} \right)_{v_-} \\ &= (\log (R_+ + v_+) - \log g) - (\log g - \log (R_- - v_-)) \\ &= \log ((R_+ + v_+)(R_- - v_-)) - 2 \log g \end{aligned} \quad (J.8.40)$$

or

$$I(\psi) \Big|_{v_-}^{v_+} = \log \frac{(R_+ + v_+)(R_- - v_-)}{g^2} \quad \begin{array}{l} s = 1, q = 1 \\ v_- < 0 < v_+ \end{array} \quad (J.8.41)$$

With  $g^2$  computed from equation (J.8.23), equation (J.8.41) may be used for the evaluation of  $I(\psi) \Big|_{v_-}^{v_+}$  whenever  $g$  is small,  $q = +1$ , and  $v$  changes sign along the edge.

This completes our discussion of non-sonic edges.

#### J.8.1.2 Nearly Sonic Edges

The very fact that we are discussing nearly sonic edges ensures us that the flow itself is supersonic, that is,  $s = -1$ . Thus, equation (J.8.20) gives us

$$R^2 = \begin{cases} v^2 - g^2 & q = +1 \\ g^2 - v^2 & q = -1 \end{cases} \quad (J.8.42)$$

Also, we know that on subsonic edges,  $v$  cannot change sign. Note also that in the evaluation procedure for AIC's for nearly sonic edges, the expression  $\Delta R$  is not needed. However, as we will shortly see, it will be necessary to compute  $\bar{P}_\pm$  for nearly sonic edges (recall that  $\bar{P}_\pm$  are the values of  $\bar{P}-\bar{Q}$  at the first and last points of  $END_p$ ).



The basic idea of the evaluation procedure for nearly sonic edges is to use equation (J.8.35) for  $I(\psi) \Big|_{v_-}^{v_+}$  and at the same time notice two facts: (a)  $z$  will almost always be quite small and (b) on supersonic edges, we will almost always have  $\sigma = +1$ . The first of these two observations follows from the calculation

$$z = \frac{(v_+ - v_-)(v_+ + v_-)}{R_{+v_+} + R_{-v_-}} = \frac{(\Delta v)\bar{v}}{(Rv)} = \frac{qs\Delta s_0\bar{v}}{(Rv)} \quad (J.8.43)$$

where the definition of  $\bar{v}$ ,  $\bar{v} = \tau v$ , and (cf. (J.6.54))

$$\Delta v = \tau qs(\Delta s_0) \quad (J.8.44)$$

have been used. Because of the presence of the coefficient  $\tau$  in equation (J.8.43), we may expect that  $z$  is of order  $\tau$ , and consequently that it is small. The second of these two observations follows from the fact that if  $\sigma$  is to be equal to  $-1$ ,  $v$  must change sign along the edge. Consequently, the edge and control point must be arranged as shown in figure J.27, where the angle  $\epsilon \approx \tau^2/2$  is very small. (Recall that an edge is said to be nearly sonic only if  $\tau < .01$ . This implies  $\epsilon < .00005$ ) Invoking our two assumptions, and expanding equation (J.8.35) in a maclaurin series, we obtain

$$I(\psi) \Big|_{v_-}^{v_+} = \begin{cases} \sum_{j=0}^{\infty} \frac{z^{2j+1}}{2j+1} & q = +1 \\ \sum_{j=0}^{\infty} (-1)^j \frac{z^{2j+1}}{2j+1} & q = -1, \sigma = +1, \\ & |z| < 1 \end{cases}$$

$$I(\psi) \Big|_{v_-}^{v_+} = z \sum_{j=0}^{\infty} \frac{(qz^2)^j}{2j+1} \quad \begin{matrix} q = -1 \\ \sigma = +1 \\ |z| < 1 \end{matrix} \quad (J.8.45)$$

We may now use this expression to obtain stable and accurate expressions for  $I, K$ . We begin by defining the function  $\phi_q(z)$  such that

$$I(\psi) \Big|_{v_-}^{v_+} = z (1 + z^2 \phi_q(z)) \quad (J.8.46)$$

Evidently, for  $|z| < 1$  and  $\sigma = +1$ ,  $\phi_q$  has the expansion

$$\phi_q(z) = q \sum_{j=1}^{\infty} \frac{(qz^2)^{j-1}}{2j+1} \quad (J.8.47)$$

Substituting the expression (J.8.46) into (J.8.1) and (J.8.3) yields the results for  $\hat{I}$ ,  $\hat{K}$

$$\hat{I} = \frac{qz}{\tau} (1 + z^2 \phi_q(z)) \quad (J.8.48)$$

$$\hat{K} = \left(\frac{1}{\tau^2}\right) (q \Delta R - \bar{v} z) - \left(\frac{\bar{v}}{\tau^2}\right) z^3 \phi_q(z) \quad (J.8.49)$$

We now show how to evaluate the three expressions

$$\frac{qz}{\tau}, \frac{1}{\tau^2} (q \Delta R - \bar{v} z), \frac{\bar{v} z^3}{\tau^2} \quad (J.8.50)$$

First,

$$\frac{qz}{\tau} = \frac{(\Delta R)^2}{\tau(2\bar{R}\bar{V})} = \frac{R \Delta R}{\tau(\bar{R}\bar{V})} = \frac{\bar{R} \Delta R}{\bar{R} \bar{V}} \quad (J.8.51)$$

Now

$$\begin{aligned} \bar{R}\bar{V} - \bar{R} \bar{v} &= \frac{1}{2} (R_+ v_+ + R_- v_-) - \frac{1}{4} (R_+ + R_-) (v_+ + v_-) \\ &= \frac{1}{4} \Delta R \Delta v \end{aligned} \quad (J.8.52)$$

Thus

$$\begin{aligned} \frac{qz}{\tau} &= \frac{\bar{R} \Delta R}{\tau(\bar{R}\bar{V} + \frac{1}{4} \Delta R \Delta v)} = \\ &= \frac{\Delta R}{\bar{V} + \frac{1}{4} (sq \tau^2 \Delta s_0) \Delta R / \bar{R}} \end{aligned} \quad (J.8.53)$$

since

$$sq \tau^2 \Delta s_0 = \Delta \hat{v} \quad (J.8.54)$$

Next,

$$(1/\tau) (q \Delta R - \bar{v} z) = (1/\tau^2) (q \Delta R - \bar{v} \frac{\Delta(v^2)}{2\bar{R}\bar{V}}) = \quad (J.8.55)$$

$$\frac{q}{\tau^2(2\bar{R}\bar{V})} [2\bar{R}\bar{V} \Delta R - \bar{v} \Delta(R^2)] = \frac{q}{\tau^2(2\bar{R}\bar{V})} [2\bar{R}\bar{V} \Delta R - 2\bar{v}\bar{R} \Delta R] \quad (J.8.56)$$

$$= \frac{q}{\tau^2 \cdot 2RV} [2\Delta R \cdot \frac{1}{4} \Delta R \Delta V]$$

$$= \frac{1}{4} \left( \frac{q\Delta V}{\tau} \right) \frac{(\Delta R)^2}{\tau RV} \quad (J.8.57)$$

$$= \frac{1}{4} s \Delta s_0 \frac{(\Delta R)^2}{RV} = \frac{1}{4} \frac{R(\Delta R)^3}{R\bar{V}\bar{V}}$$

$$= \frac{1}{4} \left( \frac{qz}{\tau} \right) \frac{(\Delta R)^2}{\bar{V}} \quad (J.8.58)$$

Finally,

$$\frac{vz^3}{\tau^2} = q\tau\bar{V} \left( \frac{qz}{\tau} \right)^3 \quad (J.8.59)$$

where  $(qz/\tau)$  is given by (J.8.53). In deriving these equations, we have used (J.8.54) and the definition of  $\bar{V}$ .

To summarize our procedure then,  $\hat{I}$  and  $\hat{K}$  are to be evaluated using equations (J.8.48-49) for all subsonic edges and for supersonic edges when  $\sigma = +1$ . When  $|z| < .3$ , say, the series (J.8.47) should be used to evaluate  $\phi_q$ ; however for larger  $|z|$ , one should use

$$\phi_q(z) = \frac{\frac{1}{2} \log \frac{1+z}{1-z} - z}{z^3} \quad \begin{matrix} q = +1 \\ |z| > .3 \end{matrix} \quad (J.8.60a)$$

$$\phi_q(z) = \frac{ph(1,z) - z}{z^3} \quad \begin{matrix} q = -1 \\ |z| > .3 \end{matrix} \quad (J.8.60b)$$

where now, Fortran library routines should be used for the evaluations. The expression  $z$  should be computed by

$$z = \tau \frac{qs\Delta s_0 \bar{V}}{RV} \quad (J.8.61)$$

We know in particular that this approach works for supersonic edges even when  $|z| > 1$  provide only that  $\sigma = +1$ . This is because, as long as  $\sigma = +1$ ,

$$I(\psi) \Big|_{v_-}^{v_+} = ph(1,z) = z(1+z^2 \phi_q(z)) \quad (J.8.62)$$

Consequently, we are done except for the case of supersonic, nearly sonic edges for which

$$\sigma = \text{sign}(R_+ R_- + v_+ v_-) = -1 \quad (\text{J.8.63})$$

In this case, both  $\hat{I}$  and  $\hat{K}$  are quite close to an actual singularity of strength  $(1/\tau)$ . Consequently, we will only show how the quantities  $\tau \hat{I}$ ,  $\tau \hat{K}$  can be stably evaluated. The first of these is trivial. Using (J.8.1) and (J.8.35),

$$\tau \hat{I} = q \left. I(\psi) \right|_{v_-}^{v_+} = -\text{ph}(-1, -z) \quad (\text{J.8.64})$$

where  $z$  may again be computed from (J.8.61). For  $\tau \hat{K}$ , we have, using (J.8.2) and (J.8.35),

$$\tau \hat{K} = q \left( \frac{\Delta R}{\tau} \right) - \frac{\bar{v}}{\tau} \text{ph}(-1, -z) \quad (\text{J.8.65})$$

We now conclude our discussion with a prescription of what is to be done in and case of edges that can only be regarded as truly sonic,  $\tau^2 \leq 10^{-10}$ .

### J.8.1.3 Essentially Sonic Edges

In this case, the only reasonable thing to do is to evaluate the limits, as  $\tau \rightarrow 0$  of the functions  $I$ ,  $\Delta R$ ,  $K$ .  $\Delta R$  is trivial to compute, but both  $I$  and  $K$  require great care. We begin with equations (J.8.48-49) and evaluate the following expressions in the limit as  $\tau \rightarrow 0$ :

$$\frac{qz}{\tau}, \frac{1}{\tau^2} (q\Delta R - vz), \frac{vz^3}{2}, z, \phi_q(z) \quad (\text{J.8.66})$$

First, equation (J.8.53) gives us

$$\lim_{\tau \rightarrow 0} \frac{qz}{\tau} = \frac{\Delta R}{\bar{v}} \quad (\text{J.8.67})$$

Next, from (J.8.58)

and

$$\lim_{\tau \rightarrow 0} \bar{R} \bar{v} = \bar{R} \bar{v} \quad (\text{J.8.68})$$

we obtain

$$\lim_{\tau \rightarrow 0} \frac{1}{\tau^2} (q\Delta R - \bar{v}z) = \frac{s\Delta s_0}{4} \frac{(\Delta R)^2}{R \bar{v}} = \frac{1}{4} \frac{(\Delta R)^3}{(\bar{v})^2} \quad (\text{J.8.69})$$

Again, equation (J.8.59) combined with (J.8.67) yields

$$\lim_{\tau \rightarrow 0} \frac{\bar{v}z^3}{\tau^2} = q \bar{v} (\Delta R / \bar{v})^3 \quad (\text{J.8.70})$$

Finally, equation (J.8.67) implies that  $\lim_{\tau \rightarrow 0} z = 0$  so that

$$\lim_{\tau \rightarrow 0} \phi_q(z) = \phi_q(u) = q/3 \quad (\text{J.8.71})$$

Combining all these results, we find

$$\hat{I}|_{\tau=0} = \lim_{\tau \rightarrow 0} \frac{qz}{\tau} = \Delta R / \bar{v} \quad (\text{J.8.72})$$

and

$$\begin{aligned} \hat{K}|_{\tau=0} &= \lim_{\tau \rightarrow 0} \left( \frac{1}{\tau^2} (q\Delta R - \bar{v}z) - \frac{\bar{v}}{\tau^2} \phi_q(z) \right) \\ &= \frac{s\Delta s_0}{4} \frac{(\Delta R)^2}{R \bar{v}} - q \bar{v} \left( \frac{\Delta R}{\bar{v}} \right)^3 \frac{q}{3} \end{aligned} \quad (\text{J.8.73})$$

Now

$$\begin{aligned} (s\Delta s_0)(\bar{v}) &= \frac{q\Delta v}{\tau} \tau \bar{v} = \\ \frac{q}{2} \Delta(v^2) &= \frac{1}{2} \Delta R^2 = \bar{R} \Delta R \end{aligned} \quad (\text{J.8.74})$$

so that

$$\begin{aligned} \hat{K}|_{\tau=0} &= \frac{1}{4} \frac{\bar{R} \Delta R}{\bar{v}} \frac{(\Delta R)^2}{\bar{v}} - \frac{\bar{v}}{3} \left( \frac{\Delta R}{\bar{v}} \right)^3 \\ &= -\frac{1}{12} \frac{(\Delta R)^3}{(\bar{v})^2} \end{aligned} \quad (\text{J.8.75})$$

### J.8.2 Panel Function Computation

The panel function  $J$  is defined by

$$J = -\text{sign}(h) J'$$

$$J' = 2\pi C_\bullet + \sum_{\text{edges}} \text{ph}(|h| v, a_k R) \Big|_{v_k^-}^{v_k^+} \quad (\text{J.8.76})$$

where  $C_\bullet =$

$$\begin{aligned} &1 \text{ if } (x', y') \in \Sigma' \cap D_p' \text{ and } r_s = +1 \\ &0 \text{ otherwise} \end{aligned} \quad (\text{J.8.77})$$

In section J.8.2.1 we compute a "standard rationalization" which is valid even for a panel with sonic edges. In section J.8.2.2 we consider the special case

$$g^2 \ll 1 \quad (\text{J.8.78})$$

In section J.8.2.3 we consider a point on the panel.

#### J.8.2.1 The Standard Rationalization

$$\text{Defining } h' = |h| \quad (\text{J.8.79})$$

we have

$$\begin{aligned} J' &= \sum \text{ph}(h' v_k^+, a_k R_k^+) - (\pi \text{sign } a_k - \text{ph}(-h' v_k^-, a_k R_k^-)) \\ &+ 2\pi C_\bullet = \\ &\sum (\text{ph}(h' v_k^+, a_k R_k^+) + \text{ph}(-h' v_k^-, a_k R_k^-)) - \pi \sum \text{sign } a_k - 2\pi C_\bullet \\ &= \sum_{k \text{ corners}} (\text{ph}(h' v_k^+, a_k R_k^+) + \text{ph}(-h' v_{k+1}^-, a_{k+1} R_{k+1}^-)) - \pi \sum \text{sign } a_k \\ &+ 2\pi C_\bullet \end{aligned} \quad (\text{J.8.80})$$

We now define

$$Q_k = \text{ph}(h' v_k^+, a_k R_k^+) + \text{ph}(-h' v_{k+1}^-, a_{k+1} R_{k+1}^-) \quad (\text{J.8.81})$$

Then, using the sum of angles formulas,

$$\begin{aligned}\cos Q_k &= \frac{1}{R_k R_{k+1}} (-h^2 v_k^+ v_{k+1}^- - a_k a_{k+1} R^2) \\ \sin Q_k &= \frac{1}{R_k R_{k+1}} (h^2 R (a_{k+1} v_k^+ - a_k v_{k+1}^-))\end{aligned}\quad (J.8.82)$$

We then define

$$Q_k = \phi h (-h^2 v_k^+ v_{k+1}^- - a_k a_{k+1} R^2, h^2 R (a_{k+1} v_k^+ - a_k v_{k+1}^-)) \quad (J.8.83)$$

We now investigate the sign of  $a_{k+1} v_k^+ - a_k v_{k+1}^-$ . First, by definition, (cf. Section J.6.1.4)

$$\begin{aligned}a &= \xi t_n - n t_\xi \\ v &= r s \xi t_\xi + n t_n \\ \vec{t}_k &= (t_\xi, t_n), \quad \vec{t}_{k+1} = (\bar{t}_\xi, \bar{t}_n)\end{aligned}\quad (J.8.84)$$

Thus

$$a_{k+1} v_k^+ - a_k v_{k+1}^- = (\xi t_n - n t_\xi)(r s \xi t_\xi + n t_n) \quad (J.8.85)$$

$$\begin{aligned}&= \xi^2 (r s \bar{t}_n t_\xi - r s t_n \bar{t}_\xi) + n (-r s \bar{t}_\xi t_\xi + \bar{t}_n t_n + r s t_\xi \bar{t}_\xi - t_n \bar{t}_n) \\ &\quad + n^2 (-\bar{t}_\xi t_n + t_\xi \bar{t}_n)\end{aligned}\quad (J.8.86)$$

$$\begin{aligned}&= (r s \xi^2 + n^2) (t_\xi \bar{t}_n - \bar{t}_\xi t_n) \\ &= r s \rho^2 (\vec{t}_k \times \vec{t}_{k+1})_\xi\end{aligned}\quad (J.8.87)$$

Now since the region is convex,

$$(t_k \times t_{k+1})_\xi > 0 \quad (J.8.88)$$

Thus

$$\text{sign}(a_{k+1} v_k^+ - a_k v_{k+1}^-) = r s \quad (J.8.89)$$

We first consider the case of  $r s = 1$ .

Careful consideration of the range of  $Q_k$ ,  $Q_k$  and  $a_k$  shows

$$\begin{aligned}J' &= \sum \bar{Q}_k - 2\pi - \pi \text{sign } a_k + 2\pi C_0 \\ &= \sum \bar{Q}_k - \sum_k \pi + 2\pi + K\end{aligned}\quad (J.3.90)$$

where  $m_k = 1$  if  $a_k < 0$  and  $a_{k+1} < 0$ , zero otherwise, and

$$K = \sum_k \pi - 2\pi - \sum_k 2\pi m_k - \sum_k \pi \operatorname{sign} a_k + 2\pi C_0 \quad (J.8.91)$$

Let  $\tau_k = 1$  if  $a_k > 0$

$$\tau_k = 0 \text{ if } a_k < 0 \quad (J.8.92)$$

Then

$$\operatorname{sign} a_k = 2\tau_k - 1$$

$$m_k = (1 - \tau_k)(1 - \tau_{k+1})$$

$$C_0 = \pi \tau_k \quad (J.8.93)$$

and

$$\begin{aligned} K &= \sum_k [\pi - 2\pi(1 - \tau_k)(1 - \tau_{k+1}) - \pi(2\tau_k - 1)] + 2\pi(C_0 - 1) \\ &= \sum_k 2\pi(1 - \tau_k) \tau_{k+1} + 2\pi(C_0 - 1) \end{aligned} \quad (J.8.94)$$

or

$$\frac{K}{2\pi} = \sum_k (1 - \tau_k) \tau_{k+1} + \pi \tau_k - 1 \quad (J.8.95)$$

It follows by a careful analysis from the convexity of the polygonal region that  $K = 0$ .

Next, we assume  $r_s = -1$ .

By definition,  $C_0 = 0$ .

Defining  $l_k = 1$  if  $a_k > 0$  and  $a_{k+1} > 0$ , it follows that

$$Q_k = \bar{Q}_k + 2\pi l_k \quad (J.8.96)$$

Thus

$$\begin{aligned} J' &= \sum \bar{Q}_k + 2\pi l_k - \pi \operatorname{sign} a_k \\ &= (\bar{Q}_k + \pi) - 2\pi + K \end{aligned} \quad (J.8.97)$$

So,

$$K = 2\pi - \sum \pi + \sum 2\pi l_k - \pi \sum \operatorname{sign} a_k \quad (J.8.98)$$



or

$$\begin{aligned}\frac{K}{2\pi} &= 1 - \sum \frac{1}{2} + \sum \tau_k \tau_{k+1} - \frac{1}{2} \sum (2\tau_k - 1) \\ &= 1 + \sum \tau_k (\tau_{k+1} - 1) = 0\end{aligned}\quad (J.8.99)$$

Thus in general

$$J' = \sum_{\text{corners}} \bar{Q}_k + rs(2\pi - \sum_{\text{edges}} \pi) \quad (J.8.100)$$

Now,  $\bar{Q}_k =$

$$\text{ph}(-h^2 v_k^+ v_{k+1}^- - a_k a_{k+1} R^2, h' R r s \rho^2 (\vec{t}_k \times \vec{t}_{k+1})_\xi) \quad (J.8.101)$$

So,

$$J = -\text{sign}(h) J' =$$

$$- \text{sign}(h) rs (2\pi - \sum_E \pi + \sum_C \text{ph}(-h^2 v_k^+ v_{k+1}^- - a_k a_{k+1} R^2, |h| R \rho^2 (\vec{t}_k \times \vec{t}_{k+1})_\xi)) \quad (J.8.102)$$

We now define

$$\begin{aligned}x_k &= -h^2 v_k^+ v_{k+1}^- - a_k a_{k+1} R^2 \\ y_k &= |h| R \rho^2 (\vec{t}_k \times \vec{t}_{k+1})_\xi\end{aligned}\quad (J.8.103)$$

Then

$$x_k = -h^2 v_k^+ v_{k+1}^- - a_k a_{k+1} (rsh^2 + r\rho^2) \quad (J.8.104)$$

Now,

$$\begin{aligned}v_k^+ v_{k+1}^- + rs a_k a_{k+1} &= (rs \xi t_\xi + n t_n)(rs \bar{\xi} \bar{t}_\xi + n \bar{t}_n) \\ &\quad + rs (\xi t_n - n t_\xi)(\bar{\xi} \bar{t}_n - n \bar{t}_\xi)\end{aligned}\quad (J.8.105)$$

$$\begin{aligned}&= \xi^2 (t_\xi \bar{t}_\xi + r s t_n \bar{t}_n) + \xi^2 (t_n \bar{t}_n + r s t_\xi \bar{t}_\xi) \\ &\quad + rs \xi n (t_n \bar{t}_\xi + \bar{t}_n t_\xi - t_\xi \bar{t}_n - \bar{t}_\xi t_n)\end{aligned}\quad (J.8.106)$$

$$= \rho^2 (t_{\xi} \bar{t}_{\xi} + r s t_{\eta} \bar{t}_{\eta}) = \rho^2 r s \langle \bar{t}_k, \bar{t}_{k+1} \rangle \quad (\text{J.8.107})$$

So,

$$X_k = -h^2 \rho^2 r s \langle \bar{t}_k, \bar{t}_{k+1} \rangle - a_k a_{k+1} r \rho^2 \quad (\text{J.8.108})$$

Thus

$$J = -\text{sign}(h) r s (2\pi - \sum_E \pi + \sum_C \text{ph}(X_{k,k+1}, Y_{k,k+1})) \quad (\text{J.8.109})$$

where

$$\begin{aligned} X_{k,k+1} &= -h^2 r s \langle \bar{t}_k, \bar{t}_{k+1} \rangle - r a_k a_{k+1} \\ Y_{k,k+1} &= R h (\bar{t}_k \times \bar{t}_{k+1})_{\xi} \end{aligned} \quad (\text{J.8.110})$$

Using the results of Sections J.7.2.1 and J.7.2.2 we find for  $X_{k+1}$

$$\begin{aligned} X_{k,k+1} &= - \left( \frac{\beta(\hat{n}_0 \cdot (\vec{x}_0 - \vec{\xi}_0))}{|\{\hat{n}_0, \hat{n}_0\}|^{1/2}} \right)^2 r [t_k, t_{k+1}] \\ &- r \left( \frac{\beta}{|\{\hat{n}_0, \hat{n}_0\}|^{1/2}} \right)^2 \{n_0, (\vec{\xi}_0 - \vec{x}_0) \times \vec{t}_{0,k}\} \{ \hat{n}_0, (\vec{\xi}_0 - \vec{x}_0) \times \vec{t}_{0,k+1} \} \end{aligned} \quad (\text{J.8.111})$$

$$\begin{aligned} &= \frac{-\beta^2}{n_0, n_0} [(\hat{n}_0, \vec{x}_0 - \vec{\xi}_0)^2 [t_{0,k}, t_{0,k+1}] \\ &+ \{ \hat{n}_0, (\vec{\xi}_0 - \vec{x}_0) \times \vec{t}_{0,k} \} \{ \hat{n}_0, (\vec{\xi}_0 - \vec{x}_0) \times \vec{t}_{0,k+1} \}] \\ &= \frac{-\beta^2}{\{\hat{n}_0, \hat{n}_0\}} G_0 \end{aligned} \quad (\text{J.8.112})$$

We will now simplify the expression  $G_0$  (J.8.112). Employing the identity (J.7.64) with

$$\begin{aligned} \vec{a} &= \vec{c} = \hat{n}_0, \quad \vec{b} = (\vec{\xi}_0 - \vec{x}_0) \times \vec{t}_k \\ \vec{d} &= (\vec{\xi}_0 - \vec{x}_0) \times \vec{t}_{k+1} \\ C^{-1} &= B_0 \end{aligned} \quad (\text{J.8.113})$$

we find

$$\begin{aligned}
 G_0 = & (\hat{n}_0, \hat{x}_0 - \hat{\xi}_0)^2 [\hat{t}_{0,k}, \hat{t}_{0,k+1}] \\
 & + (\hat{n}_0^T B_0 \hat{n}_0) ((\hat{\xi}_0 - \hat{x}_0) \times \hat{t}_{0,k})^T B_0 ((\hat{\xi}_0 - \hat{x}_0) \times \hat{t}_{0,k+1}) \\
 & - (\hat{n}_0 \times ((\hat{\xi}_0 - \hat{x}_0) \times \hat{t}_{0,k}))^T \frac{B_0^{-1}}{\det B_0 - I} (\hat{n}_0 \times ((\hat{\xi}_0 - \hat{x}_0) \times \hat{t}_{0,k+1}))
 \end{aligned} \tag{J.8.114}$$

Now (cf. (B.3.31))

$$\begin{aligned}
 \hat{n}_0 \times ((\hat{\xi}_0 - \hat{x}_0) \times \hat{t}_{0,k}) &= (\hat{\xi}_0 - \hat{x}_0) (\hat{n}_0, \hat{t}_{0,k}) - \hat{t}_{0,k} (\hat{n}_0, \hat{\xi}_0 - \hat{x}_0) \\
 &= (\hat{x}_0 - \hat{\xi}_0, \hat{n}_0) \hat{t}_{0,k}
 \end{aligned} \tag{J.8.115}$$

Similarly

$$\hat{n}_0 \times ((\hat{\xi}_0 - \hat{x}_0) \times \hat{t}_{0,k+1}) = (\hat{x}_0 - \hat{\xi}_0, \hat{n}_0) \hat{t}_{0,k} \tag{J.8.116}$$

Using the results (cf. Appendix E)

$$\begin{aligned}
 C_0 B_0 &= s\beta^2 I \\
 \det B_0 &= \beta^2
 \end{aligned} \tag{J.8.117}$$

we find

$$\frac{B_0^{-1}}{\det B_0 - I} = C_0 \tag{J.8.118}$$

Consequently, we find for  $G_0$

$$\begin{aligned}
 G_0 = & (\hat{n}_0, \hat{x}_0 - \hat{\xi}_0)^2 [\hat{t}_{0,k}, \hat{t}_{0,k+1}] \\
 & + \{\hat{n}_0, \hat{n}_0\} ((\hat{\xi}_0 - \hat{x}_0) \times \hat{t}_{0,k})^T B_0 ((\hat{\xi}_0 - \hat{x}_0) \times \hat{t}_{0,k+1}) \\
 & - (\hat{n}_0, \hat{x}_0 - \hat{\xi}_0) (\hat{t}_{0,k}^T C \hat{t}_{0,k+1}) (\hat{n}_0, \hat{x}_0 - \hat{\xi}_0)
 \end{aligned} \tag{J.8.119}$$

The first and last terms cancel and we are left with

$$G_0 = \{\hat{n}_0, \hat{n}_0\} ((\hat{\xi}_0 - \hat{x}_0) \times \hat{t}_{0,k})^T B_0 ((\hat{\xi}_0 - \hat{x}_0) \times \hat{t}_{0,k+1}) \tag{J.8.120}$$

Substituting this result into equation (J.8.108) we find

$$x_{k,k+1} = -r\beta^2 ((\hat{\xi}_0 - \hat{x}_0) \times \hat{t}_{0,k})^T B_0 ((\hat{\xi}_0 - \hat{x}_0) \times \hat{t}_{0,k+1}) \tag{J.8.121}$$

Turning now to  $Y_{k,k+1}$ , we find

$$Y_{k,k+1} = R |h(\vec{t}_k \times \vec{t}_{k+1})| \quad (J.8.122)$$

The expression inside the absolute value sign can be written

$$\begin{aligned} h(\vec{t}_k \times \vec{t}_{k+1}) &= (z' - \zeta')(\vec{t}_k \times \vec{t}_{k+1}) \\ &= (\vec{x}' - \vec{\xi}') \cdot (\vec{t}_k \times \vec{t}_{k+1}) \end{aligned} \quad (J.8.123)$$

Transforming this expression into the reference coordinate system we find

$$\begin{aligned} h(\vec{t}_k \times \vec{t}_{k+1}) &= (A(\vec{x}_0 - \vec{\xi}_0)) \cdot (A\vec{t}_{0,k} \times A\vec{t}_{0,k+1}) \\ &= (\vec{x}_0 - \vec{\xi}_0)^T A^T (\det A) A^{-T} (\vec{t}_{0,k} \times \vec{t}_{0,k+1}) = \\ &= \beta^2 (\vec{x}_0 - \vec{\xi}_0) \cdot (\vec{t}_{0,k} \times \vec{t}_{0,k+1}) \end{aligned} \quad (J.8.124)$$

Thus for  $Y_{k,k+1}$  we have

$$Y_{k,k+1} = \beta^2 R |(\vec{x}_0 - \vec{\xi}_0) \cdot (\vec{t}_{0,k} \times \vec{t}_{0,k+1})| \quad (J.8.125)$$

Upon comparing equations (J.8.121) and (J.8.125) we see that the factor  $\beta^2/\tau_k \tau_{k+1}$  can be extracted from each of them and that we can write

$$\text{ph}(X_{k,k+1}, Y_{k,k+1}) = \text{ph}(\bar{X}_{k,k+1}, \bar{Y}_{k,k+1}) \quad (J.8.126)$$

where

$$\begin{aligned} \bar{X}_{k,k+1} &= -\{(\vec{\xi}_0 - \vec{x}_0) \times \hat{t}_{0,k}, (\vec{\xi}_0 - \vec{x}_0) \times \hat{t}_{0,k+1}\} \\ \bar{Y}_{k,k+1} &= R |(\vec{\xi}_0 - \vec{x}_0) \cdot \hat{t}_{0,k} \times \hat{t}_{0,k+1}| \end{aligned} \quad (J.8.127)$$

Thus we obtain the standard rationalization

$$J = -\text{sign}(h) \left( \sum_{\text{edges}} \pi + \sum_{\text{corners}} \text{ph}(\bar{X}_{k,k+1}, \bar{Y}_{k,k+1}) \right) \quad (J.8.128)$$

#### J.8.2.2 A Special Rationalization

In equation (J.8.128) the summation extends over the straight edges of  $\Sigma'$  and over the corners of  $\Sigma'$  internal to  $Dp'$ . When  $h \rightarrow 0$ , the form (J.8.128) may not be sufficiently stable for accurate evaluation if on any edge  $a_k \approx 0$ . The precise situation in which resolvable difficulties can arise is when  $g_k^2 = r(q_k h^2 + a_k^2) \approx 0$  and the panel is subinclined

( $r = +1$ ). Although it can happen that  $g_k^2 \approx 0$  for some edge on a superinclined panel (see figure J.28) the difficulties associated with evaluating the panel function for this configuration are quite unavoidable and the standard rationalization must be regarded as optimal. To illustrate this difficulty, we point out that for the configuration shown, the value of  $|h|$  decreases down to the inner circle.

Having identified the situation  $g^2 \approx 0$  as a source of difficulty, we now show how this problem may be resolved (when it is resolvable). Thus we define the procedure to be used for evaluating  $J'$ .

First, if  $r = -1$

$$\begin{aligned} \text{or } r = 1, s = -1 \text{ and } g_k^2 \geq 10^{-4} \max(a_k^2 + h^2, D_\Sigma^2) \\ \text{on all subsonic or nearly sonic edges} \\ \text{or } r = 1, s = +1, \text{ and } g_k^2 \geq 10^{-4} D_\Sigma^2 \end{aligned} \quad (\text{J.8.129})$$

(where  $D_\Sigma$  is the panel diameter) we use the standard rationalization.

Otherwise, we calculate  $J'$  by

$$J' = 2\pi C_\theta + \sum_{\text{edges}} Q_k \quad (\text{J.8.130})$$

where (cf. (J.8.81))

$$Q_k = \text{ph}(|h|, v, aR) \Big|_{v_k^-}^{v_k^+}$$

We now describe stable methods for computing  $C_\theta$  and  $Q_k$ .

Since either the flow is subsonic or  $C_\theta = 0$ , the most direct way of getting  $C_\theta$  is by the formula

$$C_\theta = \begin{cases} 1 & \text{if } \{\hat{n}, (\vec{Q}_k - \vec{P}_k) \times \vec{t}_k\} > 0 \text{ for all } k \\ 0 & \text{otherwise} \end{cases} \quad (\text{J.8.133})$$

The topological justification of the procedure defined above stems from the following observation. As one traverses the boundary of a convex polygonal region, proceeding in a positive fashion, any point inside the region always lies to the left of the extension of the edge. Thus the edge distance  $a_k$  is always positive.

We now provide a detailed prescription for the computation of  $Q_k$ . This description will consist of two parts.

- (i) Evaluation of  $\text{ph}(|h|v, aR)$  when  $R = 0$  together with the evaluation of  $Q_k$  on edges that intersect the Mach cone, and
- (ii) Evaluation of  $Q_k$  when both end points of edge  $k$  lie inside the domain of dependence  $D_p$ .

It is a fairly straightforward matter to show that the value of  $v$  at the point at which an edge enters the domain of dependence satisfies the inequality

$$v_k^- \Big|_{R=0} < 0 \quad (\text{J.8.134})$$

Similarly, when an edge leaves  $D_p$ ,  $v_k^+$  satisfies the inequality

$$v_k^+ \Big|_{R=0} > 0 \quad (\text{J.8.135})$$

These inequalities can in fact be verified by a careful study of the special cases in figure J.29.

As a consequence of these observations, we see that

$$\text{ph}(|h| v_k^-, a_k R) \Big|_{R=0} = \text{sign}(a_k \pi) \quad (\text{J.8.136})$$

and

$$\text{ph}(|h| v_k^+, a_k R) \Big|_{R=0} = 0 \quad (\text{J.8.137})$$

If just the lower endpoint of the edge intersects  $D_p$ ,  $Q_k$  is given by

$$Q_k = \text{ph}(|h| v_k^+, a_k R_k^+) - \pi \text{sign } a_k \quad (\text{J.8.138})$$

If just the upper endpoint intersects  $D_p$  we have

$$Q_k = -\text{ph}(|h| v_k^-, a_k R_k^-) \quad (\text{J.8.139})$$

Finally if both endpoints intersect  $D_p$

$$Q_k = -\pi \text{sign } a_k \quad (\text{J.8.140})$$

We now develop a rationalization for  $Q_k$  when  $R_k^+ \neq 0$ ,  $R_k^- \neq 0$ .  
Evaluating (J.8.128) we have

$$Q_k = \text{ph}(|h| v, a_k R) \Big|_{v_k^-}^{v_k^+} =$$

$$\text{ph}(|h| v_k^+, a_k R_k^+) - \text{ph}(|h| v_k^-, a_k R_k^-)$$

$$= \bar{Q}_k + 2\pi n \quad n \text{ an integer} \quad (\text{J.8.141})$$

where  $\bar{Q}_k$  is defined by

$$\bar{Q}_k = \text{ph}(h^2 v_k^+ v_k^- + a_k^2 R_k^+ R_k^-, |h| a_k (R_k^+ v_k^- - R_k^- v_k^+)) \quad (\text{J.8.142})$$

In order that we might determine  $n$ , we investigate the sign of  $R_k^+ v_k^- - R_k^- v_k^+$ .

$$R_k^+ v_k^- - R_k^- v_k^+ = R_k^+ R_k^- \left( \frac{v_k^-}{R_k^-} - \frac{v_k^+}{R_k^+} \right) = -R_k^+ R_k^- \int_{v_k^-}^{v_k^+} d\left(\frac{v}{R}\right) \quad (\text{J.8.143})$$

Now  $R^2 = sqg^2 + qv^2$ , hence,

$$d\left(\frac{v}{R}\right) = \frac{1}{R} - \frac{qv^2}{R^3} = \frac{sqg^2}{R^3} \quad (\text{J.8.144})$$

Consequently

$$\text{sign}(R_k^+ v_k^- - R_k^- v_k^+) = -sqk \quad (\text{J.8.145})$$

Thus

$$-sqk \text{ sign}(a_k) Q_k \in (0, \pi) \quad (\text{J.8.146})$$

Now an inspection of equation (J.8.138) shows that  $Q_k \in (0, \pi)$ .  
Consequently we see that no phase wrap is possible, and that  $n = 0$  and

$$Q_k = \bar{Q}_k \quad (\text{J.8.147})$$

Multiplying both arguments of  $Q_k$  by  $(R_k^+ v_k^- + R_k^- v_k^+)$ , we find that

$$Q_k = \bar{Q}_k = \text{ph}(X, Y) \quad (\text{J.8.148})$$

$$\sigma X = R_k^+ v_k^+ (h^2 v_k^{-2} + a_k^2 R_k^{-2}) + R_k^- v_k^- (h^2 v_k^{+2} + a_k^2 R_k^{+2})$$

$$Y = |h| a_k \text{sign}(R_k^+ v_k^- + R_k^- v_k^+) (sqg^2) (v_k^{-2} v_k^{+2}) \quad (J.8.149)$$

Now,

$$\begin{aligned} \text{sign}(R^+ v^- + R^- v^+) &= -sq \text{sign}((R^+ v^-)^2 - (R^- v^+)^2) \\ &= -sq(sq) \text{sign}(v^{-2} - v^{+2}) \\ &= \text{sign}(v^{+2} - v^{-2}) \\ &= \text{sign}(v^+ + v^-) \end{aligned} \quad (J.8.150)$$

Consequently, Y is given by

$$Y = -a_k |h| g^2 |\Delta(R^2)| \quad (J.8.151)$$

Next, we examine X. First, note that

$$\begin{aligned} h^2 v^2 + a^2 R^2 &= (h^2 + qa^2)(v^2 + rsa^2) = rqg^2(v^2 + rsh^2) \\ &= rg^2(qv^2 + rsq) = rg^2(R^2 - rsh^2) \end{aligned} \quad (J.8.152)$$

Consequently  $\sigma X =$

$$(R_k^+ v_k^+ (R_k^{-2} - rsh^2) + R_k^- v_k^- (R_k^{+2} - rsh^2)) rg^2 \quad (J.8.153)$$

Comparing (J.8.152) and (J.8.153) we see that they contain a common factor of  $g^2$ . We remove this common factor to obtain the rationalized expression for  $Q_k$

$$Q_k = -ph(\sigma[R_k^+ v_k^+ (R_k^{-2} - rsh^2) + R_k^- v_k^- (R_k^{+2} - rsh^2)], \tau a_k |h| |\Delta(R^2)|) \quad (J.8.154)$$

This is the basic formula we use to compute  $Q_k$  for subsequent substitution into equation (J.8.130) for  $J'$ . The arguments for the expression (J.8.154) may be computed in the obvious fashion using the relations found in Section (J.7.2).

We can now evaluate  $J'$  if  $|h| = 0$ . In doing this, we use the following formula for  $J'$  (cf. J.8.109-110)

$$J' = rs(2\pi - \sum_E \pi + \sum_C ph(-h^2 rs \langle \vec{t}_k, \vec{t}_{k+1} \rangle - r a_k a_{k+1}, |h| R_k^+ \vec{t}_k \cdot \vec{t}_{k+1})) \quad (J.8.155)$$



Setting  $|h| = 0$  we find

$$J' \Big|_{h=0} = rs(2\pi - \sum_E \pi + \sum_C \pi h(-ra_k a_{k+1}, 0^+)) \quad (J.8.156)$$

Since  $a_k > 0$  for all  $k$ , we then obtain

$$J' \Big|_{h=0} = rs(2\pi - \sum_E \pi + \frac{(1+r)}{2} \sum_C \pi) \quad (J.8.157)$$

We can now examine the three special cases described by Figure J.30. First, consider  $s = 1$ . Then  $r = +1$  and the number of corners in the domain of dependence equals the number of edges ( $=n$ , say). Thus

$$\sum_E \pi = n\pi, \quad \sum_C \pi = n\pi$$

and

$$J' \Big|_{h=0} = 2\pi \quad (J.8.158)$$

Next, suppose  $rs = -1$ . Then  $r = +1$ ,  $s = -1$  and the number of straight edges of  $D'$  exceeds the number of interior corners by 1. Hence

$$\sum_E \pi = (m+1)\pi$$

$$\sum_C \pi = m\pi \quad (J.8.159)$$

and

$$J' \Big|_{h=0} = -\pi \quad (J.8.160)$$

Finally, suppose  $r = -1$ . Here,  $r = -1$ ,  $s = -1$  and  $D'$  has no straight edges or corners. Hence

$$J' \Big|_{h=0} = 2\pi \quad (J.8.161)$$

Summarizing, for a field point lying on the panel

$$J' \Big|_{h=0} = \begin{cases} 2\pi rs & \text{if } rs = 1 \\ \pi rs & \text{if } rs = -1 \end{cases} \quad (J.8.162)$$

In general we write

$$J' \Big|_{h=0} = \frac{\pi}{2}(rs + 3) \quad (J.8.163)$$

Of additional interest is the jump in  $J$  and the average value of  $J$ . In order that we might define the jump in  $J$  we must define it by

$$[J] = \lim_{\epsilon \rightarrow 0^+} [J(\vec{P} + \epsilon \hat{n}) - J(\vec{P} - \epsilon \hat{n})] \quad (\text{J.8.164})$$

The average value,  $(J)_{Av}$ , is the average of these two quantities. First let  $s = 1$ . Here

$$\begin{aligned} [J] &= -2\pi - (2\pi) = -4\pi \\ (J)_{Av} &= \frac{1}{2}(-2\pi + 2\pi) = 0 \end{aligned} \quad (\text{J.8.165})$$

Next, consider  $rs = -1$ . Here

$$\begin{aligned} [J] &= 2\pi \\ (J)_{Av} &= 0 \end{aligned} \quad (\text{J.8.166})$$

Finally let  $r = -1$ . Here we must proceed very carefully. First we must recall that a panel may influence a point only when

$$\text{sign}(h) \text{sign}(\hat{n}, \hat{c}_0) = 1 \quad (\text{J.8.167})$$

Next, we must compute the sign of  $h$  for field points lying just above the panel  $(\vec{P} + \epsilon \hat{n})$  and for points just below the panel. Now

$$\text{sign}(h(\vec{P} \pm \epsilon \hat{n})) = \pm 1 \quad (\text{J.8.168})$$

Thus,

$$\begin{aligned} [J] &= \pi \text{sign}(\hat{n}, \hat{c}_0) \\ (J)_{Av} &= \frac{\pi}{2} \end{aligned} \quad (\text{J.8.169})$$

## J.9 Far Field PIC's

In this section we discuss the computation of PIC matrices under the assumption that the control point  $P$  is sufficiently far from the panel center  $Q_0$  that

$$R = [\vec{P} - \vec{Q}, \vec{P} - \vec{Q}]^{\frac{1}{2}} \quad (J.9.1)$$

may be expressed as a power series in entries of

$$\Delta \vec{Q} = \vec{Q} - \vec{Q}_0 \quad (J.9.2)$$

where  $Q$  is a point of integration.

### J.9.1 The Basic Principle

Without any loss of generality, we may assume the panel center  $Q_0$  lies at the origin of the coordinate system, and then define

$$P = [\vec{P} - \vec{Q}_0, \vec{P} - \vec{Q}_0]^{\frac{1}{2}} = [\vec{P}, \vec{P}]^{\frac{1}{2}} \quad (J.9.3)$$

and

$$\tilde{Q} = [C] (\vec{Q} - \vec{Q}_0) = C \vec{Q} \quad (J.9.4)$$

Then

$$\frac{1}{R} = [\vec{P} - \vec{Q}, \vec{P} - \vec{Q}]^{-\frac{1}{2}} = \quad (J.9.5)$$

$$([\vec{P}, \vec{P}] - 2[\vec{P}, \vec{Q}] + [\vec{Q}, \vec{Q}])^{-\frac{1}{2}} \quad (J.9.6)$$

$$= [\vec{P}, \vec{P}]^{-\frac{1}{2}} \left( 1 - \frac{2[\vec{P}, \vec{Q}]}{p^2} + \frac{[\vec{Q}, \vec{Q}]}{p^2} \right)^{-\frac{1}{2}} \quad (J.9.7)$$

$$= \frac{1}{P} \left( 1 - \frac{2\vec{P} \cdot \vec{Q}}{p^2} + \frac{\vec{Q} \cdot \vec{Q}}{p^2} \right)^{-\frac{1}{2}} \quad (J.9.8)$$

Applying the binomial theorem and retaining only the quadratic and lower order terms in  $|\vec{Q}|/P$ ,

$$\frac{1}{R} = \frac{1}{P} \left[ 1 + \frac{\vec{P} \cdot \vec{Q}}{p^2} - \frac{1}{2} \frac{\vec{Q} \cdot \vec{Q}}{p^2} + \frac{3}{8} \left( \frac{2\vec{P} \cdot \vec{Q}}{p^2} \right)^2 \right] \quad (J.9.9)$$

$$= \frac{1}{p} + \frac{\vec{p} \cdot \vec{Q}}{p^3} - \frac{1}{2} \frac{\vec{Q} \cdot \vec{Q}}{p^3} + \frac{3}{2} \frac{(\vec{p} \cdot \vec{Q})^2}{p^5} \quad (\text{J.9.10})$$

We note that

$$\vec{Q} = [C^{-1}] \vec{Q} \quad (\text{J.9.11})$$

and thus

$$\vec{Q} \cdot \vec{Q} = \sum_{ij} Q_i [C^{-1}]_{ij} \tilde{Q}_j \quad (\text{J.9.12})$$

Thus (J.9.10) becomes

$$\frac{1}{R} = G(0) + \sum_i G_i(1) \tilde{Q}_i + \sum_{ij} G_{ij}(2) \tilde{Q}_i \tilde{Q}_j \quad (\text{J.9.13})$$

where

$$G(0) = \frac{1}{p} \quad (\text{J.9.14})$$

is a constant,

$$G(1) = \frac{\vec{p}}{p^3} \quad (\text{J.9.15})$$

is a vector of length 3, and  $G(2)$  is the 3x3 matrix

$$[G(2)]_{ij} = \frac{3 p_i p_j}{p^5} - \frac{[C^{-1}]_{ij}}{p^3} \quad (\text{J.9.16})$$

But substituting (J.9.13) into

$$\phi_S = -\frac{1}{\kappa} \iint \frac{\sigma}{R} dS \quad (\text{J.9.17})$$

we see that

$$\begin{aligned} \kappa \phi_S &= -G(0) \iint \sigma dS - \sum_i G_i(1) \iint \sigma \tilde{Q}_i dS \\ &\quad - \sum_{ij} G_{ij}(2) \iint \sigma \tilde{Q}_i \tilde{Q}_j dS \end{aligned} \quad (\text{J.9.18})$$

But the integrals depend only on the panel and not on the control point. In fact, the integrals are defined by the far field moment matrices (cf(I.4.3-5))

$$\frac{1}{\kappa} \iint \sigma \, dS = LFFM_1 S_j \begin{Bmatrix} \sigma_1 \\ \vdots \\ \sigma_4 \\ \sigma_9 \end{Bmatrix} \quad (J.9.19)$$

$$\frac{1}{\kappa} \iint \sigma \tilde{Q} \, dS = [FFM_2 S_j] \begin{Bmatrix} \sigma_1 \\ \vdots \\ \sigma_4 \\ \sigma_9 \end{Bmatrix} \quad (J.9.20)$$

and

$$\frac{1}{2\kappa} \iint \sigma \tilde{Q}_i \tilde{Q}_j \, dS = \sum_l (FFM_3^{S,0})_{ijl} \begin{Bmatrix} \sigma_1 \\ \vdots \\ \sigma_4 \\ \sigma_9 \end{Bmatrix}_l \quad (J.9.21)$$

Now, by definition,

$$\phi_S = [PIC S_{1,..}] \begin{Bmatrix} \sigma_1 \\ \vdots \\ \sigma_4 \\ \sigma_9 \end{Bmatrix} \quad (J.9.22)$$

and so

$$\begin{aligned} [PIC S]_{1,1} &= -G^{(0)} LFFM_1 S_j \\ &- \sum_i G_i^{(1)} [FFM_2 S]_{ij} - \sum_{ij} G_{ij}^{(2)} (FFM_3^{S,0})_{ijl} \end{aligned} \quad (J.9.23)$$

Thus, based on the assumption that  $1/R$  may be approximated by a power series in  $Q$ , we have computed the source potential  $PIC$  as a sum of matrix multiplications.

## J.9.2 Computation of the Gradient

In this section we compute a power series expression for  $\vec{\nabla}_p(1/R)$ . We write  $x_i$  for the  $i$ th component of location. Then

$$\frac{\partial}{\partial x_k} \left( \frac{1}{R} \right) = \frac{\partial}{\partial x_k} [\vec{P} - \vec{Q}, \vec{P} - \vec{Q}]^{-\frac{1}{2}} \quad (\text{J.9.24})$$

$$= -\frac{1}{2} [\vec{P} - \vec{Q}, \vec{P} - \vec{Q}]^{-\frac{3}{2}} \frac{\partial}{\partial x_k} [\vec{P} - \vec{Q}, \vec{P} - \vec{Q}] \quad (\text{J.9.25})$$

$$= -\frac{1}{2} [\vec{P} - \vec{Q}, \vec{P} - \vec{Q}]^{-\frac{3}{2}} \frac{\partial}{\partial x_k} ([\vec{P}, \vec{P}] - 2[\vec{P}, \vec{Q}]) \quad (\text{J.9.26})$$

$$= -(\vec{P}_k - \vec{Q}_k) [\vec{P}, \vec{P}]^{-\frac{3}{2}} \left( 1 - \frac{2[\vec{P}, \vec{Q}]}{[\vec{P}, \vec{P}]} + \frac{[\vec{Q}, \vec{Q}]}{[\vec{P}, \vec{P}]} \right)^{-\frac{3}{2}} \quad (\text{J.9.27})$$

where  $\vec{P} = [C] \vec{p}$

Applying the binomial theorem and retaining quadratic and lower order terms,

$$\frac{\partial}{\partial x_k} \left( \frac{1}{R} \right) = \frac{-(\vec{P}_k - \vec{Q}_k)}{p^3} \left( 1 + \frac{3[\vec{P}, \vec{Q}]}{p^2} - \frac{3}{2} \frac{[\vec{Q}, \vec{Q}]}{p^2} + \frac{15}{8} \frac{2[\vec{P}, \vec{Q}]}{p^2} \right)^2 \quad (\text{J.9.28})$$

$$= (\vec{P}_k - \vec{Q}_k) \left( \frac{1}{p^3} + \frac{3[\vec{P}, \vec{Q}]}{2p^5} - \frac{3[\vec{Q}, \vec{Q}]}{2p^5} + \frac{15[\vec{P}, \vec{Q}]^2}{2p^7} \right) \quad (\text{J.9.29})$$

We now note that

$$\vec{Q}_k = \sum_i C_{ik} Q_i$$

and

$$[\vec{Q}, \vec{Q}] = \sum_i \vec{Q}_i \vec{Q}_i = \sum_{ij} C_{ij} Q_i Q_j \quad (\text{J.9.30})$$

Thus

$$\begin{aligned} \frac{\partial}{\partial x_k} \left( \frac{1}{R} \right) &= \frac{-\vec{P}_k}{p^3} + \sum_i Q_i \left( \frac{C_{ik}}{p^3} - \frac{3\vec{P}_i \vec{P}_k}{p^3} \right) \\ &\quad + \frac{1}{2} \sum_{i,j} \frac{Q_i Q_j}{p^5} (3\vec{P}_i C_{jk} + 3\vec{P}_k C_{ij} + 3\vec{P}_j C_{ik} + 15 \frac{\vec{P}_i \vec{P}_j \vec{P}_k}{p^2}) \end{aligned} \quad (\text{J.9.31})$$

We now apply  $-C^{-1}$  and note that

$$\sum_i P_i \tilde{Q}_i = \sum_i \tilde{P}_i Q_i \quad (J.9.32)$$

to obtain

$$\begin{aligned} \left\{ -C^{-1} \vec{\nabla} p \left( \frac{1}{R} \right) \right\}_k = & \\ \frac{P_k}{p^3} + \sum_i \tilde{Q}_i (-[C^{-1}]_{ik}) + \frac{3 P_i P_k}{p^5} & \\ + \frac{1}{2} \sum_{ij} \frac{\tilde{Q}_i \tilde{Q}_j}{p^5} (3P_i [C^{-1}]_{jk} + 3P_k [C^{-1}]_{ij} + 3P_j [C^{-1}]_{ik} + \frac{15}{p^2} P_i P_j P_k) & \end{aligned} \quad (J.9.33)$$

If we define a  $3 \times 3 \times 3$  tensor  $\left\{ G^{(4)} \right\}_{ijk} =$

$$= \frac{3}{p^5} (P_i [C^{-1}]_{jk} + P_j [C^{-1}]_{ik} + P_k [C^{-1}]_{ij}) + \frac{15}{p^7} P_i P_j P_k \quad (J.9.34)$$

we obtain

$$\left\{ -C^{-1} \vec{\nabla} p \left( \frac{1}{R} \right) \right\}_k = G_k^{(1)} + \sum_i Q_i \tilde{G}_{ik}^{(2)} + \sum_{ij} \tilde{Q}_i \tilde{Q}_j G_{ijk}^{(4)} \quad (J.9.35)$$

### J.9.3 Source Velocity

We are now in position to compute a far field expression for source velocity.

Since

$$\dot{\vec{x}} = -\frac{1}{R} \iint \sigma \vec{\nabla} p \left( \frac{1}{R} \right) dS \quad (J.9.36)$$

$$C^{-1} \dot{\vec{x}} = \frac{1}{R} \iint \sigma [-C^{-1} \vec{\nabla} p \left( \frac{1}{R} \right)] dS \quad (J.9.37)$$

So,  $\left\{ C^{-1} \dot{\vec{x}} \right\}_k =$

$$\begin{aligned} G_k^{(1)} + \frac{1}{R} \iint \sigma dS + \sum_i G_{ik}^{(2)} \cdot \frac{1}{R} \iint \sigma \tilde{Q}_i dS & \\ + \frac{1}{2} \sum_{ij} G_{ijk}^{(4)} \cdot \frac{1}{R} \iint \sigma \tilde{Q}_i \tilde{Q}_j dS & \end{aligned} \quad (J.9.38)$$

Applying the definitions (J.9.19-21) of the source far field moments,

$$\begin{aligned} \sum_i [C^{-1}]_{ki} [PICS_{i+1,1}] &= G_k^{(1)} [FFM_1^S]_1 \\ &+ \sum_i G_{ik}^{(2)} [FFM_2^S]_{i1} + \sum_j G_{ijk}^{(4)} \left\{ FFM_3^{S,0} \right\}_{ij1} \end{aligned} \quad (J.9.39)$$

Note that the  $(i+1)$ th row of  $[PICS]$  defines the  $i$ th component of the source velocity.

#### J.9.4 Doublet Potential

We have

$$\phi_D = \frac{1}{\kappa} \iint \mu \hat{n} \cdot \tilde{\nabla}_Q \left( \frac{1}{R} \right) dS \quad (J.9.40)$$

But

$$\begin{aligned} \hat{n} \cdot \tilde{\nabla}_Q &= \hat{n} \cdot \tilde{\nabla}_P = \hat{n} \cdot (-\tilde{\nabla}_P) = \\ &= -\hat{n}^T [B] \tilde{\nabla}_P = \end{aligned} \quad (J.9.41)$$

(applying (E.2.9))

$$-\hat{n}^T [sB^2C^{-1}] \tilde{\nabla}_P = sB^2 \hat{n} \cdot (-C^{-1} \tilde{\nabla}_P) \quad (J.9.42)$$

Thus

$$\phi_D = \frac{sB^2}{\kappa} \iint \mu \hat{n} \cdot (-C^{-1} \tilde{\nabla}_P \left( \frac{1}{R} \right)) dS = \quad (J.9.43)$$

$$\begin{aligned} \sum_k G_k^{(1)} \cdot \left\{ \frac{sB^2}{2\kappa} \iint \mu \hat{n}_k dS \right\} &+ \sum_{i,k} G_{ik}^{(2)} \frac{sB^2}{\kappa} \iint \mu \tilde{Q}_i \hat{n}_k dS \\ &+ \sum_{ijk} G_{ijk}^{(4)} \left\{ \frac{sB^2}{2\kappa} \iint \mu \tilde{Q}_i \tilde{Q}_j \hat{n}_k dS \right\} \end{aligned} \quad (J.9.44)$$

Recalling the definitions (I.4.14-16) of the unsymmetrized doublet potential far field moments we see that

$$\begin{aligned} Q_D &= \sum_{k1} G_k^{(1)} [FFM_1^D]_{k1} u_1 + \\ &+ \sum_{ik1} G_{ik}^{(2)} (FFM_2^{D,0})_{ik1} u_1 + \\ &+ \sum_{ijk1} G_{ijk}^{(4)} (FFM_3^{D,0})_{ijk1} u_1 \end{aligned} \quad (J.9.45)$$



Thus

$$\begin{aligned}
 [PICD]_{1,1} &= \sum_k G_k^{(1)} [FFM_1^D]_{k1} \\
 &+ \sum_{ik} G_{ik}^{(2)} (FFM_2^{D,0})_{ik1} + \sum_{ijk} G_{ijk}^{(4)} (FFM_3^{D,0})_{ijk1} \quad (J.9.46)
 \end{aligned}$$

#### J.9.5 Doublet Velocity

We have

$$\vec{v}_D = \frac{1}{K} \iint (\hat{n} \times \vec{\nabla}_{Qu}) \times \vec{\nabla}_Q \left( \frac{1}{R} \right) dS \quad (J.9.47)$$

Now,

$$\begin{aligned}
 \vec{\nabla}_Q &= B \vec{\nabla}_P = -B \vec{\nabla}_P = \\
 [BC] (-C^{-1} \vec{\nabla}_P) &= sB^2 (-C^{-1} \vec{\nabla}_P) \quad (J.9.48)
 \end{aligned}$$

Thus

$$\begin{aligned}
 \vec{v}_D &= \frac{sB^2}{K} \iint (\hat{n} \times \vec{\nabla}_{Qu}) \times (-C^{-1} \vec{\nabla}_P \left( \frac{1}{R} \right)) dS \\
 &= \frac{sB^2}{K} \iint (-C^{-1} \vec{\nabla}_P \left( \frac{1}{R} \right)) \times (\vec{\nabla}_{Qu} \times \hat{n}) dS \quad (J.9.49)
 \end{aligned}$$

Applying (J.9.35)

$$\begin{aligned}
 v_D &= G^{(1)} \times \frac{sB^2}{K} \iint (\vec{\nabla}_{Qu} \times \hat{n}) dS \\
 &+ \sum_i G_{i..}^{(2)} \times \frac{sB^2}{K} \iint \tilde{Q}_i (\vec{\nabla}_{Qu} \times \hat{n}) dS \\
 &+ \sum_{ij} G_{i,j..}^{(4)} \times \frac{sB^2}{K} \iint \tilde{Q}_i \tilde{Q}_j (\vec{\nabla}_{Qu} \times \hat{n}) dS \quad (J.9.50)
 \end{aligned}$$

Here  $G_{i..}^{(2)}$  and  $G_{i,j..}^{(4)}$  are the vectors whose  $k$ th entries are  $G_{ik}^{(2)}$  and  $G_{ijk}^{(4)}$  respectively. Now, applying the definitions (I.4.17-19) of the doublet

velocity far field moments, we have

$$\begin{aligned}\vec{v}_D = & \sum_i (G^{(1)}) \times [FFM_4^D]_{.,i} \mu_i \\ & + \sum_{i,j} (G^{(2)}) \times (FFM_5^D)_{.,i,j} \mu_i \\ & + \sum_{i,j,l} (G^{(4)}) \times (FFM_6^{D,0})_{.,i,j,l} \mu_i\end{aligned}\quad (J.9.51)$$

Thus  $\sum_i [C^{-1}]_{ki} [PIC^D]_{i+1,1}$  is the  $k$ th entry of

$$\begin{aligned}& G^{(1)} \times [FFM_4^D]_{.,1} \\ & + \sum_i (G^{(2)}) \times (FFM_5^D)_{.,i,1} \\ & + \sum_{i,j,l} (G^{(4)}) \times (FFM_6^{D,0})_{.,i,j,l}\end{aligned}\quad (J.9.52)$$

#### J.9.6 Symmetrization

(i) It is easy to see (cf. (J.9.14-16) and (J.9.34)) that the tensors  $G^{(i)}$ ,  $i = 1, 2, 4$ , are symmetric. This leads to a potential computational saving in computing far field PIC's. For we may symmetrize the far field moments and multiply them by the symmetric portion of the tensors  $G^{(i)}$ .

For instance,

$$\begin{aligned}& \sum_{i=1}^3 \sum_{k=1}^3 G^{(2)}_{ik} (FFM_2^{D,0})_{ik1} = \\ & \sum_{i=1}^3 \sum_{k=1}^{i-1} G^{(2)}_{ik} ((FFM_2^{D,0})_{ik1} + (FFM_2^{D,0})_{k1i}) + G^{(2)}_{11} (FFM_2^{D,0})_{111}\end{aligned}\quad (J.9.53)$$

Thus our summation requires only 6 entries of  $G^{(2)}$ .

We now discuss the symmetrization in a systematic manner.

#### J.9.6.1 Source Potential

Let  $\bar{G}^{(2)}$  be the vector of length 6:

$$\bar{G}_k^{(2)} = G_k k^2$$

$$\bar{G}_{k+3}^{(2)} = G_{i(k)}^{(2)}, j(k)$$

$$k = 1, 2, 3$$

(J.9.54)

where

$$i(k) = k \pmod{3} + 1$$

$$j(k) = (k + 1) \pmod{3} + 1$$

(J.9.55)

Then, from the definition (I.4.9) of the symmetrization of a matrix, (J.9.23) yields

$$[PIC^5]_{1,1} = G^0 [FFM_1 S]_1 + \sum_{i=1}^3 G_i^{(1)} [FFM_2 S]_{i1}$$

$$+ \sum_{k=1}^6 G_k^{(2)} [FFM_3 S]_{k1}$$

(J.9.56)

#### J.9.6.2 Source Velocity

Let us define  $[G]^{(4)}$  as the 6x3 matrix:

$$\bar{G}_{km}^{(4)} = G_{kkm}^{(4)}$$

$$\bar{G}_{k+3,n}^{(4)} = G_{i(k),j(k),n}^{(4)}$$

$$k = 1, 2, 3$$

(J.9.57)

Then (J.9.39) becomes

$$\sum_i [C^{-1}]_{ki} [PIC^5]_{i+1,1} =$$

$$G_k^{(1)} [FFM_1 S]_1 + \sum_i G_i^{(2)} [FFM_2 S]_{i1}$$

$$+ \sum_{k=1}^6 G_k^{(4)} [FFM_3 S]_{k1}$$

(J.9.58)

### J.9.6.3 Doublet Potential

Let us define  $\tilde{G}^{(4)}$  as the vector of length 10:

$$\begin{aligned}\tilde{G}_k^{(4)} &= G_{kkk}^{(4)} \\ \tilde{G}_{k+3}^{(4)} &= G_{i(k),j(k),k}^{(4)} \quad k = 1, 2, 3 \\ \tilde{G}_{10}^{(4)} &= G_{123}^{(4)}\end{aligned}\tag{J.9.59}$$

Then (J.9.46) becomes

$$\begin{aligned}[PIC^D]_{1,1} &= \\ &\sum_{k=1}^3 G_k^{(1)} [FFM_1^D]_k + \sum_{k=1}^6 G_k^{(2)} [FFM_2^D]_{k1} \\ &+ \sum_{k=1}^{10} \tilde{G}_k^{(4)} [FFM_3^D]_{k1}\end{aligned}\tag{J.9.60}$$

### J.9.6.4 Doublet Velocity

Finally (J.9.52) becomes

$$\begin{aligned}\sum_{i=1}^3 [C^{-1}]_{ki} [PIC^D]_{i+1,1} &= \text{the } k\text{th entry of} \\ (G^{(1)}) \times [FFM_4^D]_{.,1} &+ \sum_{i=1}^3 \left\{ G_i^{(2)} \right\} \times (FFM_5^D)_{.,i,1} \\ + \sum_{i=1}^k (G_i^{(4)}) \times (FFM_6^D)_{i,.,1}\end{aligned}\tag{J.9.61}$$

# J.10 Line Vortex PIC's

The line vortex term of the velocity is given by (cf.(B.3.55))

$$\vec{v}_D^* = \frac{1}{\kappa} \int_{\partial S \cap D_p} \mu \vec{\nabla} \left( \frac{1}{R} \right) \times \vec{d}l \quad (J.10.1)$$

Differentiating in compressibility coordinates yields

$$\vec{\nabla} \left( \frac{1}{R} \right) = -s\beta^2 (\vec{Q} - \vec{P}) / R^3 \quad (J.10.2)$$

and thus

$$\vec{v}_D^* = \frac{-s\beta^2}{\kappa} \int_{\partial S \cap D_p} \frac{\mu}{R^3} (\vec{Q}_0 - \vec{P}_0) \times \vec{d}l \quad (J.10.3)$$

In general, the doublet strength is assumed to be continuous everywhere, and thus the line vortex contribution to the velocity cancels and may be ignored. In addition, evaluation of this integral is not possible in supersonic flow without additional assumptions.

In subsonic flow, however, the inclusion of a "line vortex" corresponding to a discontinuity in doublet strength may be meaningful (see Appendix B). The option is not available in version 1.0 of Pan Air, but the theory is included here as background material. In this section, we compute the 3x3 matrix which gives  $\vec{v}_D^*$  in terms of  $\mu$ ,  $\mu_0$ , and  $\mu_+$ , the values of doublet strength at the initial point, center point, and endpoint of a line segment, such as a panel edge.

## J.10.1 Computation of $\vec{v}_D^*$

Now along a straight segment of  $\partial \Sigma_0$ , we have

$$\vec{dx}_0 = \hat{t}_0 ds_0 \quad (J.10.4)$$

where  $\hat{t}_0$  denotes the unit edge tangent in reference coordinates and  $ds_0$  denotes the element of arc length. Also, as one moves along such an edge, the point of integration  $Q_0$  varies according to the rule

$$\vec{Q}_0 = \vec{Q}_0(0) + \hat{t}_0 ds \quad (J.10.5)$$

Thus

$$\vec{\nabla} \left( \frac{1}{R} \right) \times \vec{dx}_0 = -s\beta^2 \iint (\vec{Q}_0(0) - \vec{P}_0) \times \hat{t}_0 \frac{ds_0}{R^3} \quad (J.10.6)$$

Substituting this into equation (J.10.3) we obtain the line vortex velocity due to a straight segment of edge E

$$\vec{v}_D^* = \frac{-s\beta^2}{K} (Q_0(0) - P_0) \times \hat{t}_0 \int_E \frac{\mu ds_0}{R^3} \quad (J.10.7)$$

This equation motivates us to define the integral

$$\omega = \int_E \frac{\mu ds_0}{R^3} \quad (J.10.8)$$

so that  $\vec{v}_D^*$  is given by

$$\vec{v}_D^* = \frac{-s\beta^2}{K} ((\vec{Q}_0(0) - \vec{P}_0) \times \hat{t}_0) \omega \quad (J.10.9)$$

Thus  $\vec{v}_D^*$  is a constant vector times the integral  $\omega$ . We evaluate  $\omega$  by applying a coordinate transformation from the reference system  $X_0$  to a local coordinate system  $X'$  such that in  $X'$ , the element of arc length along the edge image is  $ds' = \int_{\text{edge}} \sqrt{dx'^2} = \int_{\text{edge}} \sqrt{dx'^2}$ . Our new coordinate system is defined by the transformations

$$X_0 \xrightarrow{\Gamma} X \xrightarrow{E} \bar{X} \xrightarrow{A} X' \quad (J.10.10)$$

The transformation  $\Gamma$  is discussed in Appendix E. The coordinates  $X$  are compressibility coordinates, while  $E$  is a scaling transformation,

$$E = \begin{bmatrix} 1 & & \\ & \beta & \\ & & \beta \end{bmatrix} \quad (J.10.11)$$

We define

$$A = \frac{1}{|(\bar{t}, \bar{t})|^{1/2}} \begin{bmatrix} s\bar{t}_x & a & 0 \\ -sa & s\bar{t}_x & 0 \\ 0 & 0 & q \end{bmatrix} \begin{bmatrix} 1 & 0 & 0 \\ 0 & \bar{t}_y/a & \bar{t}_z/a \\ 0 & -\bar{t}_z/a & \bar{t}_y/a \end{bmatrix} \quad (J.10.12)$$

where

$$\begin{aligned} \bar{t} &= E \Gamma \hat{t}_0 \\ a^2 &= \bar{t}_x^2 + \bar{t}_y^2 \\ q &= \text{sign} [\bar{t}, \bar{t}] \end{aligned} \quad (J.10.13)$$

Before proceeding further, we note in passing that when  $t_0$  is chosen to have the normalization

$$[\hat{t}_0, \hat{t}_0] = q = \pm 1 \quad (J.10.14)$$

then  $\hat{e}$ ,  $\bar{e}$ , and  $\hat{e}'$ , defined by

$$\begin{aligned}\hat{e} &= r \hat{e}_0 \\ \bar{e} &= E \hat{e} \\ \hat{e}' &= \bar{A} \bar{e}\end{aligned}\tag{J.10.15}$$

retain this normalization

$$[\hat{e}, \bar{e}]_x = [\bar{e}, \bar{e}]_{\bar{x}} = [\hat{e}', \bar{e}']_{x'} = 1\tag{J.10.16}$$

Because of this nice property, we will assume that  $\hat{e}_0$  has the normalization (J.10.14). We can now prove the two identities

$$ds_0 = |\hat{e}_0| ds'\tag{J.10.17}$$

$$ds' = \text{sq } dx'\tag{J.10.18}$$

The first identity is proved by the calculation

$$\begin{aligned}(ds')^2 &= (\hat{e}' ds') \cdot (\hat{e}' ds') = (\vec{dx}') \cdot (\vec{dx}') \\ &= (\bar{A}\bar{e} \cdot \vec{dx}_0) \cdot (\bar{A}\bar{e} \cdot \vec{dx}_0) =\end{aligned}\tag{J.10.19}$$

$$\begin{aligned}&(\bar{A}\bar{e} \cdot \hat{e}_0 ds_0) \cdot (\bar{A}\bar{e} \cdot \hat{e}_0 ds_0) = \\ &(ds_0)^2 |\bar{A}\bar{e} \cdot \hat{e}_0|^2\end{aligned}\tag{J.10.20}$$

Now since  $\hat{e}_0 = \bar{e}_0/|\bar{e}_0|$ , we find

$$\begin{aligned}(ds')^2 &= (ds_0)^2 |\bar{A}\bar{e} \cdot \bar{e}_0|^2 / |\bar{e}_0|^2 \\ &= (ds_0)^2 |\hat{e}'|^2 / |\hat{e}_0|^2\end{aligned}\tag{J.10.21}$$

where we have used equation (J.10.15) to notice that

$$\hat{e}' = \bar{A}\bar{e} \cdot \bar{e}_0 = \bar{A} \bar{e}\tag{J.10.22}$$

The quantity  $\bar{A} \bar{e}$  is readily computed:

$$\bar{A} \bar{e} = \frac{1}{|[\bar{e}, \bar{e}]|^{1/2}} \begin{Bmatrix} s\bar{e}_x^2 + \bar{e}_y^2 + \bar{e}_z^2 \\ 0 \\ 0 \end{Bmatrix} = \text{sq } \sqrt{|[\bar{e}, \bar{e}]|} \begin{Bmatrix} 1 \\ 0 \\ 0 \end{Bmatrix}\tag{J.10.23}$$

Invoking the normalization condition (J.10.16) we then find that

$$\hat{t}' = \bar{A} \bar{t} = sq \begin{pmatrix} 1 \\ 0 \\ 0 \end{pmatrix}, \quad |\bar{A} \bar{t}| = 1 \quad (\text{J.10.24})$$

Using this in equations (J.10.21-22) then yields the required identity

$$|\hat{t}_0| ds' = ds_0 \quad (\text{J.10.25})$$

The second identity (J.10.18) can be proved by noticing that

$$\hat{t}' = \frac{\hat{t}'}{|\hat{t}'|} = \hat{t}' = sq \begin{pmatrix} 1 \\ 0 \\ 0 \end{pmatrix} \quad (\text{J.10.26})$$

The identity  $d\vec{x}' = \hat{t}' ds'$  then provides the desired result as follows

$$\begin{pmatrix} dx' \\ dy' \\ dz' \end{pmatrix} = d\vec{x}' = \hat{t}' ds' = \begin{pmatrix} sq \\ 0 \\ 0 \end{pmatrix} ds' \quad (\text{J.10.27})$$

It should be noted that the ratio of arc elements,  $|\hat{t}_0|$  (cf. (J.10.17)), is closely related to the quantity  $\tau$  defined by

$$\tau^2 = |[\hat{t}_0, \hat{t}_0]| \quad (\text{J.10.28})$$

To see this relationship note that

$$\hat{t}_0 = \frac{\hat{t}_0}{|[\hat{t}_0, \hat{t}_0]|^{1/2}} = \frac{\hat{t}_0}{\tau} \quad (\text{J.10.29})$$

Taking norms and remembering that  $|\hat{t}_0| = 1$ , we find

$$|\hat{t}_0| = \frac{1}{\tau} \quad (\text{J.10.30})$$

The next piece of information we will need is the form of the function  $R$  in the coordinate system  $X'$ . Using the fact that in  $\bar{X}$ ,  $R^2$  is given by

$$R^2 = (\xi - x)^2 + s(n - y)^2 + s(\zeta - z)^2 \quad (\text{J.10.31})$$

one may then use the definition (J.10.12) of  $A$  to compute  $R^2$  in  $X'$ . One quickly finds that

$$R^2 = q(\xi' - x')^2 + sq(n' - y')^2 + s(\zeta' - z')^2 \quad (\text{J.10.32})$$



If we now define the edge variable  $v$  and the edge parameter  $g$  by

$$v = \xi' - x' \quad (J.10.33)$$

$$sqg^2 = sq(\eta' - y')^2 + s(\xi' - z')^2 \quad (J.10.34)$$

one quickly obtains the necessary expression for  $R^2$

$$R^2 = qv^2 + sqg^2 \quad (J.10.35)$$

We may now write the integral  $\omega$  in the concise form

$$\omega = \int_E \mu \frac{|t_0| ds'}{R^3} = \frac{sq}{T} \int_E \frac{\mu dv}{\sqrt{qv^2 + sqg^2}^3} \quad (J.10.36)$$

Now on a given edge  $E$ ,  $\mu$  is assumed to be a quadratic function, completely determined by its values at the lower and upper endpoints  $v_-$  and  $v_+$  and at the midpoint  $v_0 = 1/2 (v_- + v_+)$ . The corresponding values of  $\mu$  are denoted  $\mu_-$ ,  $\mu_+$ ,  $\mu_0$ . As a function of  $v$ ,  $\mu$  may be written

$$\begin{aligned} \mu &= \mu(v) = \mu_- f_-(v) + \mu_0 f_0(v) + \mu_+ f_+(v) \\ &= [\mu_- \mu_0 \mu_+] \begin{Bmatrix} f_- \\ f_0 \\ f_+ \end{Bmatrix} \end{aligned} \quad (J.10.37)$$

where the functions  $f$  are defined

$$\begin{aligned} f_-(v) &= \frac{(v - v_0)(v - v_+)}{(v_- - v_0)(v_- - v_+)} \\ f_0(v) &= \frac{(v - v_-)(v - v_+)}{(v_0 - v_-)(v_0 - v_+)} \\ f_+(v) &= \frac{(v - v_-)(v - v_0)}{(v_+ - v_-)(v_+ - v_0)} \end{aligned} \quad (J.10.38)$$

If we introduce the basis functions  $\phi_0(v)$ ,  $\phi_1(v)$ ,  $\phi_2(v)$  by the definitions

$$\begin{aligned} \Delta v &= v_+ - v_- \\ \phi_0(v) &= 1 \end{aligned} \quad (J.10.39)$$

$$\phi_1(v) = \frac{v - v_0}{\frac{1}{2} \Delta v}$$

$$\phi_2(v) = \frac{(v - v_0)^2}{\frac{1}{4} (\Delta v)^2} - 1 \quad (\text{J.10.40})$$

we see that the  $f$  functions can be written

$$\begin{Bmatrix} f_- \\ f_0 \\ f_+ \end{Bmatrix} = \begin{bmatrix} \frac{1}{2} & \frac{1}{2} & \frac{1}{2} \\ 0 & 0 & -1 \\ 0 & \frac{1}{2} & \frac{1}{2} \end{bmatrix} \begin{Bmatrix} \phi_0 \\ \phi_1 \\ \phi_2 \end{Bmatrix} \quad (\text{J.10.41})$$

Substituting (J.10.40) into (J.10.36) and thence into (J.10.35) we obtain for  $w$

$$\begin{aligned} w &= \begin{bmatrix} \frac{1}{2} & \frac{1}{2} & \frac{1}{2} \\ 0 & 0 & -1 \\ \frac{1}{2} & \frac{1}{2} & \frac{1}{2} \end{bmatrix} \frac{sq}{\tau} \int_E \begin{Bmatrix} \phi_0 \\ \phi_1 \\ \phi_2 \end{Bmatrix} \frac{dv}{R^3} \\ &= \begin{bmatrix} \frac{1}{2} & \frac{1}{2} & \frac{1}{2} \\ 0 & 0 & -1 \\ \frac{1}{2} & \frac{1}{2} & \frac{1}{2} \end{bmatrix} \begin{Bmatrix} w_0 \\ w_1 \\ w_2 \end{Bmatrix} \quad (\text{J.10.42}) \end{aligned}$$

where  $w_i$  are defined by

$$w_i = \frac{sq}{\tau} \int_E \frac{\phi_i dv}{R^3} \quad (\text{J.10.43})$$

The functions  $w_i$  can be computed by repeated integration by parts. In doing this, we treat the general case of a quadratic basis function  $\phi$ . We consider then

$$w(\phi) = \frac{sq}{\tau} \int \frac{\phi dv}{\sqrt{qv^2 + sqg^2}}^3 \quad (\text{J.10.44})$$

$$U = \phi \quad dV = \frac{dv}{\sqrt{qv^2 + sqg^2}}^3$$

$$dU = \phi'(v) dv \quad V = \frac{v}{sqg^2 R} \quad (\text{J.10.45})$$

Thus

$$\omega(\phi) = \frac{sq}{T} \left[ \frac{\phi v}{sqg^2 R} - \frac{1}{sqg^2} \int \frac{\phi' v}{R} dv \right]_{v_-}^{v_+} \quad (J.10.46)$$

Again integrating by parts, let

$$\begin{aligned} U &= \phi'(v) & dv &= \frac{v}{R} dv \\ dU &= \phi''(v) dv & v &= qR \end{aligned} \quad (J.10.47)$$

Thus,

$$\omega(\phi) = \frac{sq}{sqg^2} \left[ \frac{\phi v}{R} - \phi' qR + q\phi'' \int R dv \right]_{v_-}^{v_+} \quad (J.10.48)$$

Now, note that

$$\begin{aligned} \frac{d}{dv}(vR) &= R + \frac{qv^2}{R} - R + \frac{R^2 - sqg^2}{R} \\ &= 2R - \frac{sqg^2}{R} \end{aligned} \quad (J.10.49)$$

Consequently

$$\int R dv = \frac{1}{2} [vR + sqg^2 \int dv/R] \quad (J.10.50)$$

and we obtain for  $\omega(\phi)$ ,

$$\omega(\phi) = \frac{sq}{sqg^2} \left[ \frac{\phi v}{R} - \phi' qR + \frac{q\phi''}{2} (vR + sqg^2 I(\psi)) \right]_{v_-}^{v_+} \quad (J.10.51)$$

where, of course,  $I(\psi)$  is given by

$$I(\psi) = \int \frac{dv}{R} = \begin{cases} \frac{1}{2} \log \frac{v+R}{v-R} & q = +1 \\ -\text{ph}(v, R) & q = -1 \end{cases} \quad (J.10.52)$$

We now apply the formula (J.10.50) to the evaluation of  $w_i$ ,  $i = 0, 1, 2$ .

$$\begin{aligned} \text{First } w_0 &= \frac{sq}{sqg^2} \left. \frac{v}{R} \right|_{v_-}^{v_+} = \frac{sq/\tau}{sqg^2} \left( \frac{v_+}{R_+} - \frac{v_-}{R_-} \right) \\ &= \frac{sq/\tau}{sqg^2} \frac{R_-v_+ - R_+v_-}{R_+R_-} = \frac{R_-v_+ + R_+v_-}{R_-v_+ + R_+v_-} \end{aligned} \quad (\text{J.10.53})$$

$$= \frac{sq/\tau}{sqg^2} \frac{sqg^2(v_+^2 - v_-^2)}{R_+R_-(R_-v_+ + R_+v_-)} \quad (\text{J.10.54})$$

$$= \frac{sq}{\tau} \frac{2\Delta v v_0}{R_+R_-(R_-v_+ + R_+v_-)} \quad (\text{J.10.55})$$

where

$$v_0 = \frac{1}{2}(v_- + v_+) \quad (\text{J.10.56})$$

In performing this evaluation, we have taken special care that the possibility that  $g^2 \approx 0$  not cause any difficulty.

Next, we consider  $w_1$ , which corresponds to

$$\begin{aligned} \phi_1(v_-) &= -1 \\ \phi_1(v_+) &= +1 \\ \phi_1' &= -2/\Delta v \end{aligned} \quad (\text{J.10.57})$$

Using equation (J.10.50) we find

$$w_1 = \frac{sq}{sqg^2} \left[ \frac{v_+}{R_+} + \frac{v_-}{R_-} - \frac{2q}{\Delta v} (R_+ - R_-) \right] \quad (\text{J.10.58})$$

After considerable manipulation, one then finds

$$w_1 = -\frac{1}{2} \left[ \Delta \left( \frac{1}{R} \right) \right]^2 \frac{s}{\tau(v/R)} \quad (\text{J.10.59})$$

where the overscore denotes the average value of the quantity at the lower and upper endpoints. Finally we compute  $w_2$ , which corresponds to

$$\begin{aligned} \phi_2(v_+) &= \phi_2(v_-) = 0 \\ \phi_2'(v_+) &= -\phi_2'(v_-) = \frac{4}{\Delta v} \\ \phi_2'' &= \frac{8}{(\Delta v)^2} \end{aligned} \quad (\text{J.10.60})$$

Applying equation (J.10.50), we find

$$\begin{aligned}\omega_2 &= \frac{sq}{(sqg^2)} \left[ -\frac{4q}{\Delta v} (R_+ + R_-) + \frac{4q}{(\Delta v)^2} (\Delta(vR) + sqg^2 \Delta I) \right] \\ &= \frac{4s}{sqg^2 (\Delta v)^2} [-\Delta v (R_+ + R_-) + \Delta(vR) + sqg^2 \Delta I]\end{aligned}\quad (J.10.61)$$

Now

$$\begin{aligned}-\Delta v (R_+ + R_-) + \Delta(vR) &= \bar{v} \Delta R + \bar{R} \Delta v - 2\Delta v \bar{R} \\ &= \bar{v} \Delta R - \Delta v \bar{R} = v_- R_+ - v_+ R_-\end{aligned}\quad (J.10.62)$$

$$= \frac{sqg^2 (v_-^2 - v_+^2)}{v_- R_+ + v_+ R_-}\quad (J.10.63)$$

Consequently

$$\omega_2 = \frac{4s}{(\Delta v)^2} \left[ \Delta I - \frac{\Delta(v^2)}{v_- R_+ + v_+ R_-} \right]\quad (J.10.64)$$

This may be written

$$\omega_2 = \frac{4s}{\Delta v} \left[ \frac{\Delta I}{\Delta v} - \frac{\bar{v}}{R_+ R_- - (\bar{v}/R)} \right]\quad (J.10.65)$$

As in the case of  $\omega_0$  and  $\omega_1$ , we have found a form that is perfectly well behaved in the limit  $g^2 \approx 0$ . Of course, the expression  $\Delta I$  must be calculated in a stable manner. This problem has already been considered in Section J.8.1.

## J.11 Singular Behavior of Integrals

In this section we will examine the behavior of the perturbation potential and velocity induced by a discontinuous source strength, a discontinuous doublet strength, or a discontinuous doublet gradient. It can be seen that no generality is lost by examining the potential and velocity induced by various non-zero source and doublet distributions on the triangular region in figure J.31.

We will consider the cases of discontinuous singularity strength or gradient across edges in subsonic flow, and subsonic, supersonic, or nearly sonic edges in supersonic flow. The case of  $\epsilon = 0$ ,  $M_\infty = 0$  will be of sufficient generality in subsonic flow. For supersonic flow, the cases of subsonic and supersonic edges may be treated by considering edge 3, and  $\epsilon$  a small positive or negative real number. Finally, the compressibility direction may always be taken to be the x-direction, except when considering the case of a superinclined panel. Thus with the exception of this last case, the reference to local transformation (cf. (E.0.1)) is the identity.

In the sections which follow, we will first compute the potential and velocity induced by the three discontinuities in singularity strength or gradient in terms of edge and panel functions. We will then evaluate the computed expressions for each of the flow regimes. We will borrow heavily from the notation of Section J.6, especially J.6.1.4 and J.6.5.

### J.11.1 Discontinuous Source Strength

The source strength may be discontinuous across a panel edge in such a fashion that the discontinuity retains the same magnitude along the entire edge, in which case the tangential derivative of source strength is continuous. On the other hand, the magnitude may vary, in which case the tangential derivative is discontinuous. The two representative cases are the constant source strength

$$\sigma_1(x,y) = 1 \quad (J.11.1)$$

and the linearly varying strength

$$\sigma_2(x,y) = 1 \quad (J.11.2)$$

We will now consider the potential and velocity induced by  $\sigma_1$  and  $\sigma_2$ .

We recall the definition of  $[S_0]$

$$\begin{pmatrix} \phi_s \\ \vec{v}_s \end{pmatrix} = [S_0]^{4 \times 6} \begin{pmatrix} \sigma_0 \\ \sigma_x \\ \sigma_y \\ \cdot \\ \cdot \\ \sigma_{yy} \end{pmatrix} \quad (\text{J.11.3})$$

and note that therefore

$$\begin{pmatrix} \phi_s \\ \vec{v}_s \end{pmatrix}_{\text{due to } \sigma_1} = [S_0]^{4 \times 6} \begin{pmatrix} 1 \\ 0 \\ 0 \\ 0 \\ 0 \\ 0 \end{pmatrix} \quad (\text{J.11.4})$$

$$\begin{pmatrix} \phi_s \\ \vec{v}_s \end{pmatrix}_{\text{due to } \sigma_2} = [S_0] \begin{pmatrix} 0 \\ 1 \\ -1 \\ 0 \\ 0 \\ 0 \end{pmatrix} \quad (\text{J.11.5})$$

Applying (J.6.25), we have

$$\begin{pmatrix} \phi_s \\ \vec{v}_s \end{pmatrix}_1 = \begin{pmatrix} b \\ \vec{d} \\ a \end{pmatrix} \quad (\text{J.11.6})$$

and

$$\begin{aligned} \begin{pmatrix} \phi_s \\ \vec{v}_s \end{pmatrix}_2 &= \begin{pmatrix} \vec{b}_1 + b\vec{d}_1 - \vec{b}_2 - b\vec{d}_2 \\ \vec{a}_1\vec{d}_1 + B_{11} - \vec{a}_1\vec{d}_2 - B_{12} \\ \vec{a}_2\vec{d}_1 + B_{21} - \vec{a}_2\vec{d}_2 - B_{22} \\ \vec{a}\vec{d}_1 - hr (G\vec{a})_1 - \vec{a}\vec{d}_2 + hr (G\vec{a})_2 \end{pmatrix} \end{aligned} \quad (\text{J.11.7})$$

where  $a$ ,  $b$ ,  $\vec{a}$ ,  $\vec{b}$ , and  $B$  are the fundamental integrals of Section J.6.5, and

$$\vec{d} = \vec{p}_0' = \begin{pmatrix} x_0' \\ y_0' \end{pmatrix} \quad (\text{J.11.8})$$

the local coordinate value of the field point.

We first consider the potential and velocity induced by the source distribution  $\sigma_1$ .

We have (cf. J.6.179)

$$b = \frac{-r}{\kappa} \left( \sum_k \int_{\phi_k^-}^{\phi_k^+} R d\phi - 2\pi |h| C_0 \right) \quad (J.11.9)$$

= (cf(J.7.5))

$$\frac{-r}{\kappa} \sum_k J_k(X) \quad (J.11.10)$$

= (cf(J.7.3), (J.7.12), (J.7.27), (J.7.34))

$$\frac{-sh}{\kappa} J - \frac{s}{\kappa} \sum a_k q_k I_k \quad (J.11.11)$$

where: (cf(J.7.3))

$$J = \sum_k h J_k(\psi) - 2\pi \text{sign}(h) C_0 \quad (J.11.12)$$

is the panel function and  $I_k$  is the edge function.  $I_k$  and  $J_k$  are defined by (J.7.1) and (J.7.2) respectively.

Next, we have (cf(J.6.174))

$$a = \frac{-s}{\kappa} J \quad (J.11.13)$$

and (cf(J.6.185))

$$\vec{a} = \frac{s}{\kappa} \sum \vec{n}_k q_k I_k \quad (J.11.14)$$

Thus we have

$$\phi_{s,1} = b = \frac{-sh}{\kappa} J - \frac{s}{\kappa} \sum a_k q_k I_k \quad (J.11.15)$$

$$(\vec{v}_{s,1})_{x,y} = \vec{a} = \frac{s}{\kappa} \sum \vec{n}_k q_k I_k \quad (J.11.16)$$

$$(v_{s,1})_z = a = \frac{-s}{\kappa} J \quad (J.11.17)$$



Next we consider the potential and velocity induced by the second source distribution. We have (cf(J.6.195))

$$\bar{b} = \frac{-1}{2\kappa} \sum_k \bar{v}_k q_k \Delta(RV) - \frac{rs}{\kappa} \sum_k \bar{v}_k (a_k^2 + q_k h^2) I_k \quad (J.11.18)$$

Thus

$$\begin{aligned} \bar{b}_{s,2} &= \bar{b}_1 - \bar{b}_2 + b(\bar{d}_1 - \bar{d}_2) = \\ &= \frac{1}{2\kappa} \sum_k (\bar{v}_{k,1} - \bar{v}_{k,2}) q_k \Delta(RV) - \frac{rs}{2\kappa} \sum_k (\bar{v}_{k,1} - \bar{v}_{k,2}) (a_k^2 + q_k h^2) I_k \\ &+ \phi_{s,1} (x_0' - y_0') \end{aligned} \quad (J.11.19)$$

Next, by (J.6.201)

$$[B] = b I + \frac{rs}{\kappa} \sum_k \bar{n}_k a_k \bar{v}_k^T I_k + \frac{1}{\kappa} \sum_k q_k \bar{n}_k \bar{e}_k^T \Delta R \quad (J.11.20)$$

Thus

$$\begin{aligned} \bar{v}_{s,2,x} &= \bar{a}_1(\bar{d}_1 - \bar{d}_2) + B_{11} - B_{12} = \\ &= \bar{v}_{s,1,x} (x_0' - y_0') + \phi_{s,1} + \\ &+ \frac{rs}{\kappa} \sum_k \bar{n}_{k,1} a_k (\bar{v}_{k,2} - \bar{v}_{k,1}) I_k + \\ &+ \frac{1}{\kappa} \sum_k q_k \bar{n}_{k,1} (\bar{e}_{k,1} - \bar{e}_{k,2}) \Delta R \end{aligned} \quad (J.11.22)$$

Similarly,

$$\begin{aligned} \bar{v}_{s,2,y} &= \bar{a}_2(\bar{d}_1 - \bar{d}_2) + B_{21} - B_{22} \\ &= \bar{v}_{s,1,y} (x_0' - y_0') - \phi_{s,1} \end{aligned} \quad (J.11.23)$$

$$\begin{aligned} &+ \frac{rs}{\kappa} \sum_k \bar{n}_{k,2} a_k (\bar{v}_{k,1} - \bar{v}_{k,2}) I_k \\ &+ \frac{1}{\kappa} \sum_k q_k \bar{n}_{k,2} (\bar{e}_{k,1} - \bar{e}_{k,2}) \Delta R \end{aligned} \quad (J.11.24)$$

Finally,

$$\bar{v}_{s,2,z} = a(\bar{d}_1 - \bar{d}_2) - hr((G\bar{a})_1 - (G\bar{a})_2) \quad (J.11.25)$$

Now,

$$G\vec{n} = \vec{v} \quad (J.11.26)$$

and so

$$\begin{aligned} \vec{v}_{s,2,z} &= \vec{v}_{s,1,z}(x_0' - y_0') \\ &= \frac{hrs}{\kappa} \sum_k (\vec{n}_{k,1} - \vec{n}_{k,2}) q_k \vec{i}_k \end{aligned} \quad (J.11.27)$$

#### J.11.2 Discontinuous Doublet Strength

A complete discussion of the potential and velocity induced by a discontinuous doublet strength would require consideration of a varying doublet distribution as well as a constant one, in parallel with the discussion on discontinuous source strength. This process would be lengthy, however, and not contribute any additional insight, and so will be neglected. We thus consider a panel with constant doublet strength  $\mu = 1$  only.

##### J.11.2.1 Doublet Potential

We have

$$\phi_D = [D_0]_{1..}^{1 \times 10} \begin{Bmatrix} \mu_0 \\ \cdot \\ \cdot \\ \cdot \\ \cdot \\ \mu_{nn} \end{Bmatrix} \quad (J.11.28)$$

where  $D_0$  is given by (J.6.253), and  $\mu_0 = 1$ , while all other coefficients are zero.

Thus

$$\phi_D = r_a = \frac{-rs}{\kappa} J \quad (J.11.29)$$

$$= \frac{-rs}{\kappa} \left( \sum_k h J(\psi) - 2\pi \text{sign}(h) C_0 \right) \quad (J.11.30)$$

##### J.11.2.2 Doublet Velocity

To compute the velocity induced by a discontinuous doublet strength, we must use the results of Section J.10. We consider (J.10.41) in light of the fact that  $\mu = 1$  on the entire panel. Thus

$$\mu_1 = \mu_0 = \mu_+ = 1$$

and

$$\omega = \begin{bmatrix} 1 & 0 & 0 \end{bmatrix} \begin{bmatrix} \omega_0 \\ \omega_1 \\ \omega_2 \end{bmatrix} = \omega_0 \quad (\text{J.11.31})$$

$$(\text{J.11.32})$$

Combining (J.10.9) and (J.11.32)

$$\nabla_{D,\text{edge}}^* = \frac{-s\beta^2}{\kappa} ((\vec{Q}_0 - \vec{P}_0) \times \vec{t}_0) \vec{\omega}_0 \quad (\text{J.11.33})$$

where  $Q_0$  is any point on the edge. From (J.10.52),

$$\omega_0 = \frac{1}{\tau_g^2} (v_+^+ - v_-^-) \quad (\text{J.11.34})$$

and thus

$$\nabla_{D,\text{edge}}^* = \frac{-s\beta^2}{\tau_g^2 \kappa} (v_+^+ - v_-^-) (\vec{Q}_0 - \vec{P}_0) \times \vec{t}_0 \quad (\text{J.11.35})$$

### J.11.3 Discontinuities in Doublet Gradient

Since a discontinuity in the tangential derivative of doublet gradient produces a doublet discontinuity of the type we are neglecting to consider, we need only consider a discontinuity in the normal derivative of the doublet gradient across a panel edge. It is clearly not possible to find a panel with a quadratic doublet distribution which has zero doublet strength on its perimeter without being identically the zero distribution. Thus we look at the effect of a discontinuous doublet gradient across a single edge of the panel. We must later consider the possibility that some of the singular behavior of the induced potential or velocity is artificial, resulting from the isolation of a single edge. That is, the contribution from a neighboring panel may cancel the contribution from this panel edge.

We thus assume that the coordinate system is translated so that it lies on the  $k$ th edge of our triangular region,  $k = 1, 2, 3$ , and that the doublet strength on the panel is given by

$$\mu_k(Q) = \vec{Q} \cdot \hat{n}_k$$

where

$$\hat{n}_k = \tau \vec{n}_k \quad (\text{J.11.36})$$

and  $\vec{n}_k$  is the outward pointing edge normal, normalized by (J.6.43) and (J.6.45). Thus  $\mu = 0$  on the  $k$ th edge, while the normal derivative of  $\mu$  jumps by 1 on the edge.

Thus, applying (J.6.240) and (J.6.253), the potential and velocity induced by  $u_k$  is

$$\begin{Bmatrix} \phi_D \\ v_D \end{Bmatrix}_k = \begin{matrix} & \begin{matrix} 1 & 2 \end{matrix} \\ \begin{matrix} 1 \\ 2 \end{matrix} & \begin{bmatrix} ra & ra \vec{d}^T - h (G\vec{a})^T \\ 0 & ra I \end{bmatrix} \\ \begin{matrix} 1 \end{matrix} & \begin{bmatrix} 0 & -(G\vec{a})^T \end{bmatrix} \end{matrix} \begin{Bmatrix} 0 \\ \vec{n}_k \end{Bmatrix} \quad (J.11.37)$$

We now recall that reference and local coordinates are identical. Thus (cf(J.6.39) and (J.6.46))

$$a_k = -\vec{d} \cdot \vec{n}_k = -\frac{1}{r} \vec{d} \cdot \vec{n}_k \quad (J.11.38)$$

and (cf(J.6.44), (J.6.49-50), and (J.6.55))

$$(G \vec{n}_k) \cdot \vec{n}_k = \vec{v}_k \cdot \vec{n}_k = q_k r_\tau \quad (J.11.39)$$

Thus,

$$\begin{aligned} \phi &= ra \vec{d}^T \vec{n}_k - h (G\vec{a})^T \vec{n}_k \\ &= -ra \tau a_k - h (G\vec{a})^T \vec{n}_k \end{aligned} \quad (J.11.40)$$

Thus, by (J.11.13-14), and (J.11.39) the contribution due to the  $k$ th edge is

$$\phi_k = \frac{rsh\tau}{\kappa} J_k a_k - \frac{rsh\tau}{\kappa} I_k \quad (J.11.41)$$

Next,

$$\vec{v} = \begin{Bmatrix} ra \hat{n}_k \\ -(G\vec{a})^T \vec{n}_k \end{Bmatrix} \quad (J.11.42)$$

Thus

$$\vec{v}_{k,x,y} = \frac{-rs}{\kappa} J_k \hat{n}_k \quad (J.11.43)$$

while

$$\vec{v}_{k,z} = \frac{-rs}{\kappa} I_k \quad (J.11.44)$$

This concludes our reduction to fundamental integrals of the potential and velocity due to discontinuous singularity strength or gradient. We now consider the behavior of the panel function  $J$ .

#### J.11.4 Singularities of the Panel Function

The panel function  $J$  is defined by (J.11.12) where (cf Section J.7)

$$J_k(\psi) = \frac{-1}{h} \text{ph}(hr, aR) \Big|_{-}^{+} \quad (\text{J.11.45})$$

We also have (cf. J.8.105-106)

$$J = -\text{sign}(h)rs \ 2\pi - \sum_{\text{edges}} \pi + \sum_{\text{corners}} \text{ph}(x_{k,k+1}, y_{k,k+1}) \quad (\text{J.11.46})$$

where

$$\begin{aligned} x_{k,k+1} &= -h^2rs \ \langle \hat{t}_k, \hat{t}_{k+1} \rangle - ra_k a_{k+1} \\ y_{k,k+1} &= R|h| \ |\hat{t}_k \times \hat{t}_{k+1}| \end{aligned} \quad (\text{J.11.47})$$

##### J.11.4.1 The Plane $h = 0$

We see that a possible region of discontinuity for  $J$  is the plane  $h = 0$ . On this plane,

$$\begin{aligned} x_{k,k+1} &= -ra_k a_{k+1} \\ y_{k,k+1} &= 0 \end{aligned} \quad (\text{J.11.48})$$

Thus  $J$  is not readily defined on the  $h = 0$  plane whenever  $a = 0$  for some edge, that is, whenever the field point lies on the line containing the edge. In addition, on all Mach lines downstream from the panel corners, the number of edges or number of corners in  $D_p$  may change, and thus  $J$  may experience a jump. In figure J.32, we illustrate potential lines of discontinuity for the expression

$$J_+ = \lim_{h \rightarrow 0^+} J = -rs(2\pi - \sum_E \pi + \sum_C \text{ph}(-ra_k a_{k+1}, 0)) \quad (\text{J.11.49})$$

These lines include some which are upstream of the panel and thus apply only in subsonic flow.

We now claim that  $J_+$  has a constant value on the exterior of the panel and a (perhaps different) constant value on the interior of the panel. This assertion may be proved by careful examination of the behavior of  $J_+$  in the vicinity of a Mach line or a panel edge extension. In any region which does not contain such a line, the number of corners and edges in  $D_p$  is a constant, while in addition  $a_k a_{k+1}$  never changes sign, and thus  $J_+$  is a constant.

Now, careful examination of figure J.32 makes it clear how  $J_+$  changes when an extension of a panel edge (though not part of the panel edge) is crossed. If the panel is superinclined it has no influence on the field point since  $h = 0$ . If the flow is subsonic,  $a_k$  changes sign, for some edge  $E_k$ , while all the  $a_i$ ,  $i \neq k$ , have unchanged sign. Thus  $a_{k-1}a_k$  and  $a_k a_{k+1}$  both change sign, and so two of the phase functions change in value, one from zero to  $\pi$ , the other from  $\pi$  to zero. Thus  $J_+$  remains unchanged.

Next, when the extension of the edge  $E_k$  of a subinclined panel in supersonic flow is crossed, then either both the  $(k-1)$  and  $k$ th corners lie in  $D_p$  or neither does. In the former case, the value of  $J_+$  remains unchanged for the same reasons as in subsonic flow. In the latter case, none of terms of  $J$  changes, since the summation over corners includes only those in  $D_p$ .

Next we consider the behavior of  $J_+$  as Mach lines are crossed. Here we need only consider subinclined panel in supersonic flow, since for superinclined panels the Mach cones from panel corners intersect the  $h = 0$  plane only at the corner itself. Careful consideration of figure J.33 yields the following conclusions.

First, suppose  $\text{sign}(a_k a_{k+1}) = +1$ . Then as the field point  $P$  moves such that the  $k$ th corner moves into  $D_p$ , the number of edges intersecting  $D_p$  increases by one. On the other hand, if  $\text{sign}(a_k a_{k+1}) = -1$ , then as the  $k$ th corner moves into  $D_p$ , the number of edges intersecting  $D_p$  increases by zero (if the panel already intersected  $D_p$ ) or by two (if the panel did not previously intersect  $D_p$ ).

Thus in the first case, as the corner enters  $D_p$ , the sum in (J.11.49) over edges decreases by  $\pi$  while the sum over corners increases by  $\pi$ , and so  $J$  remains constant. In the second case (Figure J.33b) the sum over edges is unchanged, but  $-ra_k a_{k+1} > 0$ , and so the sum over corners is changed by

$$\text{ph}(1, 0^+) = 0 \quad (\text{J.11.50})$$

In the third case,  $J_+$  is zero when the corner is outside  $D_p$  since by convexity, the entire panel is outside  $D_p$  (note that (J.11.49) is not valid when the entire panel is outside  $D_p$ ). Now, when the corner enters  $D_p$ ,  $J_+$  becomes

$$J_+ = -rs(2\pi - \sum_E \pi + \sum_{1 \text{ corner}} \text{ph}(1, 0)) = 0 \quad (\text{J.11.51})$$

Thus in all cases,  $J_+$  remains constant across Mach lines, even if the point  $P_0$  lies on the panel. In addition,  $J_+$  remain constant across panel extensions. Thus in supersonic flow,  $J_+ = 0$  whenever  $P_0$  is outside the panel, since it is zero for a point  $P_0$  for which the panel lies outside

$D_p$ . On the other hand, if  $P_0$  lies inside the panel,  $a_k a_{k+1}$  is always positive, and so in both supersonic or subsonic flow we have

$$J_+ = -2\pi rs \quad (J.11.52)$$

by choosing  $P_0$  such that the same number of edges and corners lie in  $D_p$ .

Finally, considering a point  $P_0$  outside the panel in subsonic flow, we see that as  $P_0$  crosses from being inside the panel to outside, sign ( $a_k a_{k+1}$ ) changes from +1 to -1 for exactly two corners, and so  $-rsJ_+$  decreases by  $2\pi$  from its value inside the panel of  $2\pi$ .

Summarizing,

$$\begin{array}{ll} J_+ = -2\pi rs & P_0 \text{ inside panel} \\ J_+ = 0 & P_0 \text{ outside panel} \end{array} \quad (J.11.53)$$

We may go through the same arguments for  $J_-$ ,

$$\begin{aligned} J_- &= \lim_{h \rightarrow 0^-} J = rs(2\pi - \sum_E \pi + \sum_C \text{ph}(-ra_k a_{k+1}, 0^+)) \\ &= -J_+ \end{aligned} \quad (J.11.54)$$

But now, the panel lies outside  $D_p$  for a superinclined panel, and thus

$$\begin{array}{ll} J_- = 2\pi rs & r = +1, \text{ or} \\ & P_0 \text{ inside panel} \\ J_- = 0 & r = -1, \text{ or} \\ & P_0 \text{ outside panel} \end{array} \quad (J.11.55)$$

We thus see that  $J$  is continuous on the  $h = 0$  plane except on the panel itself, where  $J$  experiences a discontinuity

$$J_+ - J_- = \pi(r + 3)s \quad (J.11.56)$$

#### J.11.4.2 Discontinuities Due to $C_0$

Let us recall our original definition of  $J$  (cf(J.11.12) and (J.11 45))

$$J = \sum_k h J_k(\psi) - 2\pi \text{sign}(h) C_0 \quad (J.11.57a)$$

where

$$J_k(\psi) = \frac{-1}{h} \text{ph}(hv, aR) \Big|_{-}^{+} \quad (\text{J.11.57b})$$

We now wish to investigate whether the discontinuity in  $C_\theta$  reflects a true discontinuity in  $J$ . To do so, we consider the formulation (J.11.46-47) of  $J$ . Note that we need only consider subsonic flow and superinclined panels. We also assume  $h = 0$ , and that we are not directly above a corner of the panel. Thus  $v_- < 0 < v_+$ .

Now consider Figure J.34. If the point  $P_0$  is moved so that it lies above the panel, crossing edge 1, then  $a_1$  changes sign, while  $h$ ,  $v_1^+$ , and  $R_1^+$  remain essentially unchanged. If  $R_1^+ > 0$ , we have

$$\text{ph}(hv_1^+, a_1 R_1) = \text{ph}(\text{sign}(hv_1^+), 0^+) \quad (\text{J.11.58})$$

If we first consider the case of  $h = 0$ ,  $a_1 > 0$  we have

$$\text{ph}(hv_1, a_1 R_1) \Big|_{-}^{+} = \text{ph}(1, 0^+) - \text{ph}(-1, 0^+) = -\pi \quad (\text{J.11.59})$$

If  $h = 0$ ,  $a_1 < 0$ , we have

$$\text{ph}(hv_1, a_1 R_1) \Big|_{-}^{+} = \text{ph}(1, 0^-) - \text{ph}(-1, 0^-) = \pi \quad (\text{J.11.60})$$

Thus as  $P_0$  moves from being not above the panel ( $a > 0$ ) to being above it ( $a < 0$ ),

$$\text{ph}(hv, a_1 R_1) \Big|_{-}^{+}$$

jumps by  $2\pi$ . In general, by considering  $h < 0$ , we find

$$J_1(\psi)_{\text{outer}} - J_1(\psi)_{\text{inner}} = 2\pi \text{sign}(h) \quad (\text{J.11.61})$$

On the other hand, when we consider any other edge, we find that the small change in point location has no effect on  $J_k(\ )$ . That is,

$$J_k(\psi)_{\text{outer}} - J_k(\psi)_{\text{inner}} = 0 \quad \text{if } k \neq 1 \quad (\text{J.11.62})$$

If we combine (J.11.56) with (J.11.61-62), we find

$$J_{\text{outer}} - J_{\text{inner}} = 0 \quad (\text{J.11.63})$$

Thus under the assumptions  $v_+ \neq 0$ ,  $R > 0$ , the function  $J$  has no discontinuity where  $C_\theta$  does.



These are not regions of discontinuity either, however. The lines  $v_{\pm} = 0$  cannot be regions where a jump of  $2\pi$  occurs, since jumps in a function can only occur across a surface. The problem of  $R = 0$  may be handled by redefining  $J_k$ :

$$J_k(\psi) = \lim_{R \rightarrow R^+} \text{ph}(hv^+, a_k R) - \lim_{R \rightarrow R^-} \text{ph}(hv^-, a_k R) \quad (\text{J.11.64})$$

Summarizing, we find that the discontinuity in  $C_0$  is exactly matched by a corresponding discontinuity in  $J_k(\psi)$ .

#### J.11.4.3 Discontinuities in $J_k(\psi)$

We note that the function

$$f(x, y) = \text{ph}(x, y) \quad (\text{J.11.65})$$

may be discontinuous if

$$\begin{aligned} & x < 0 \text{ and } y \approx 0 \\ \text{or} \\ & x \approx 0 \text{ and } y \approx 0 \end{aligned} \quad (\text{J.11.66})$$

We have already noted that if  $h \neq 0$ , a discontinuity in  $J_k(\psi)$  due to  $a_k$  changing sign is matched by a corresponding discontinuity in  $C_0$ , provided that  $P_0$  lies directly above the panel. We now consider the case where  $a_k$  changes sign, while  $P_0$  is not directly above the panel. Then defining

$$\Delta J_k = (J_k |_{a_k > 0}) - (J_k |_{a_k < 0}) \quad (\text{J.11.67})$$

$$\begin{aligned} \Delta J_k &= \text{ph}(hv^+, 0^+) - \text{ph}(hv^-, 0^+) \\ &\quad - (\text{ph}(hv^+, 0^-) - \text{ph}(hv^-, 0^-)) \end{aligned} \quad (\text{J.11.68})$$

$$\begin{aligned} &= \text{ph}(hv^+, 0^+) - \text{ph}(hv^+, 0^-) \\ &\quad - (\text{ph}(hv^-, 0^+) - \text{ph}(hv^-, 0^-)) \end{aligned} \quad (\text{J.11.69})$$

Defining

$$\begin{aligned} s^+ &= 0 \quad \text{if } hv^+ > 0 \\ &= 1 \quad \text{if } hv^+ < 0 \end{aligned} \quad (\text{J.11.70})$$

$$\Delta J_k = 2\pi s^+ - 2\pi s^- \quad (\text{J.11.71})$$

since

$$ph(-1, 0^+) - pn(-1, 0^-) = 2\pi \quad (\text{J.11.72})$$

But, looking at the point  $P_0'$  in figures J.34 and J.35, with subsonic flow in figure J.34, we see that if  $a_k$  changes sign and  $P_0$  does not lie directly above the panel, then  $v^+$  and  $v^-$  have the same sign. Thus  $s^+ = s^-$ , and so

$$\Delta J_k = 0 \quad (\text{J.11.73})$$

So, we conclude that if  $a \approx 0$ ,  $h \approx 0$ , then  $J$  is a continuous function.

Thus we can assume that  $aR$  has constant sign (since  $R \geq 0$ ) as  $P_0$  moves slightly, though perhaps with changing magnitude. Since we need only consider the case

$$\begin{aligned} v^+ &\approx 0 \\ R &\approx 0 \\ |a| &> 0 \\ |h| &> 0 \end{aligned} \quad (\text{J.11.74})$$

Now, by (J.6.59),

$$R^2 = rsqa^2 + qv^2 + rsh^2 \geq 0 \quad (\text{J.11.75})$$

Thus (J.11.74) can only be satisfied if

$$rsqa^2 + rsh^2 \approx 0 \quad (\text{J.11.76})$$

that is, if

$$\text{sign}(rsq) = \text{sign}(rs) \quad (\text{J.11.77})$$

But this is equivalent to

$$q = -1 \quad (\text{J.11.78})$$

Thus we need only look at a supersonic edge, as illustrated in figure J.36. For  $P_0$  as located there,

$$\begin{aligned} J_k &= \text{ph}(hv^+, aR^+) - \text{ph}(hv^-, aR^-) \\ &= \text{ph}(hv^+, aR^+) - \text{ph}(hv^-, 0) \end{aligned} \quad (\text{J.11.79})$$

$$= \text{ph}(hv^+, aR^+) - \pi s^- \quad (\text{J.11.80})$$

But as  $P_0$  is moved slightly,  $aR$  may range over small numbers of constant sign, while  $hv^+$  ranges over small number of constant sign. More precisely, for any real number  $\epsilon > 0$ , and any real number  $x$ ,  $-\pi < x < \pi$ , there exists a point  $P$  such that

$$|\vec{P} - \vec{P}_0| < \epsilon$$

and

$$\text{ph}(hv^+(P), aR^+(P)) = x \quad (\text{J.11.81})$$

This, by definition, means that the phase function is discontinuous at  $P_0$ . Since  $s^-$  is a constant which is not dependent on the precise location of  $P_0$ , the function  $J_k$  is in fact discontinuous at  $P_0$ .

Finally, let us consider the behavior of the phase function in the neighborhood of  $P_0'$ . Then if the edge intersects  $D_p$ ,

$$\begin{aligned} -hJ_k &= \text{ph}(hv, aR) \Big|_-^+ \\ &= \lim_{R \rightarrow 0^+} (\text{ph}(hv^+, aR) - \text{ph}(hv^-, aR)) \end{aligned} \quad (\text{J.11.82})$$

Since

$$v^- < 0 < v^+ \quad (\text{J.11.83})$$

we have (considering the four separate cases for sign  $h$  and sign  $a$ )

$$-hJ_k = -\pi \text{sign}(h) \text{sign}(a) \quad (\text{J.11.84})$$

On the other hand, if the edge does not intersect  $D_p$ ,  $J_k$  is zero.

#### J.11.4.4 Summary of Panel Function Behavior

We now summarize the results we have obtained concerning the panel function. We find that  $J$  experiences a simple jump discontinuity of magnitude

$$J_+ - J_- = \pi(r+3) s \quad (\text{J.11.85})$$

across the panel. In addition,  $J$  experiences a jump

$$J_+ - J_- = -\pi \operatorname{sign}(h) \operatorname{sign}(a_k) \quad (\text{J.11.86})$$

across a portion of the boundary "Mach wedge" emanating downstream from any supersonic edge. We illustrate such a Mach wedge in cross-section in figure J.37a, where the plane of the paper is a plane downstream from the edge and perpendicular to the flow direction. If the panel is subinclined, it is a plane of constant  $a_k$ , while if superinclined, it is a plane of constant  $h$ . In figure J.37b, we illustrate a Mach wedge in three dimensions.

Finally, there are certain lines in space along which  $J$  takes infinitely many values over a range of  $2\pi$  as a point on the line is approached from different directions. These lines are the panel edges and the lines emanating from a supersonic panel edge along which  $v = 0$  and  $R = 0$  (see figure J.37a).

#### J.11.5 Singularities of the Edge Function

By (J.7.35)

$$\begin{aligned} I_k(\psi) &= \frac{1}{2} \log \left| \frac{R+v}{R-v} \right| \Big|_{-}^{+} \quad \text{if } q_k = +1 \\ &= -\operatorname{ph}(v, R) \Big|_{-}^{+} \quad \text{if } q_k = -1 \end{aligned} \quad (\text{J.11.87})$$

##### J.11.5.1 Supersonic Edges

We first consider the behavior of the edge function for a supersonic edge. Defining

$$I_k^* = -\operatorname{ph}(v^*, R^*) \quad (\text{J.11.88})$$

we see that  $I_k^*$  is continuous if  $v^* = 0$ , since if  $v^* < 0$  and  $R^* = 0$ ,

$$I_k^* = -\lim_{R \rightarrow 0^+} \operatorname{ph}(v^*, R) = -\operatorname{ph}(-1, 0) = -\pi \quad (\text{J.11.89})$$

But by (J.6.59), for supersonic edges,

$$R^2 = r(a^2 - h^2) - v^2 \quad (\text{J.11.90})$$

Thus

$$R \approx v \approx 0$$

$$|a| \approx |h| \quad (J.11.91)$$

We therefore see that  $I_k$  is discontinuous along the lines defined by the intersection of the Mach cones with the planes  $v_{\pm}^+ = 0$  (cf. figure J.37), the same lines along which  $J_k$  is discontinuous.

Even when  $P_0$  approaches the panel edge (except at its endpoints),  $I_k$  is continuous provided the limit is taken such that the edge intersects  $D_p$ . For then

$$v^{\pm} = \pm |c| \quad c \approx 0$$

$$R^{\pm} = 0 \quad (J.11.92)$$

Thus  $I_k =$

$$\begin{aligned} -\text{ph}(v, R) \Big|_{-}^{+} &= -\text{ph}(|c|, 0^+) + \text{ph}(-|c|, 0^+) \\ &= \pi \end{aligned} \quad (J.11.93)$$

regardless of the direction from which the point approaches the edge, unless the edge is approached so that it does not lie in  $D_p$ , in which case the limit is zero.

#### J.11.5.2 Subsonic Edges

By (J.11.87) we see that  $I_k$  is continuous unless

$$|R^{\pm}| = |v^{\pm}|$$

$$\text{or} \quad R^{\pm 2} - v^{\pm 2} = 0 \quad (J.11.94)$$

By (J.6.59) we have, since  $r = q = 1$ ,

$$R^2 = v^2 + s(a^2 + h^2) \quad (J.11.95)$$

Thus  $I_k$  may be singular when

$$|R^{\pm 2} - v^{\pm 2}| = |s(a^2 + h^2)| = g^2 = 0 \quad (J.11.96)$$

that is, whenever the field point  $P_0$  lies on the line containing the panel edge. Now, if  $P_0$  lies on an extension of the edge,  $v^+$  and  $v^-$  have the

same sign, and are non-zero. Applying the rationalization (J.8.35-36)

$$I_k = \frac{1}{2} \log \left( \frac{1+z}{1-z} \right) \quad (J.11.97)$$

$$z = \frac{(v_+ - v_-)(v_+ + v_-)}{R_+ v_+ + R_- v_-}$$

$$\approx \frac{v_+^2 - v_-^2}{(v_+^2 + v_-^2) \text{sign}(v_+)} \quad (J.11.98)$$

we see that  $|z| < 1$ . Thus  $I_k$  is a continuous function in this case.

Next, suppose  $P_0$  lies very near the panel edge. If the flow is supersonic, this means  $R_- = 0$ , and thus by (J.8.27)

$$z = \frac{v_+^2 - v_-^2}{R_+ v_+} \quad (J.11.99)$$

As long as the point is away from the edge,  $v_+ < R_+$ ,  $v_-^2 > 0$ , and so  $|z| < 1$ , making  $I_k$  continuous. But as  $P_0$  approaches the edge,  $v_+$  approaches  $R_+$ ,  $v_-$  approaches zero, and so  $|z|$  approaches 1. Thus  $I_k$  becomes infinite as the point approaches the panel edge.

For subsonic flow, if  $P_0$  approaches the panel edge,  $v$  changes sign along the edge and we thus use the rationalization (J.8.40-41))

$$I_k = \log \frac{(R_+ + v_+)(R_- + |v_-|)}{g^2} \quad (J.11.100)$$

The denominator is non-zero, and thus we see that in both subsonic and supersonic flow, the edge function  $I_k$  becomes logarithmically infinite when the field point approaches the edge.

### J.11.5.3 Subsonic Nearly Sonic Edges

The same arguments used for subsonic edges show that the only potential singularity occurs when  $v = R_+$ , that is, when the point  $P_0$  is on the line extending the subsonic edge. This situation is illustrated in figure J.33.

Defining a unit edge tangent

$$\hat{t}_0 = \frac{\vec{Q}_+ - \vec{Q}_-}{|\vec{Q}_+ + \vec{Q}_-|} \quad (J.11.101)$$

we see that

$$\begin{aligned} R_{\pm}^2 &= [\vec{Q}_{\pm} - \vec{P}_0, \vec{Q}_{\pm} - \vec{P}_0] \\ &= |\vec{Q}_{\pm} - \vec{P}_0|^2 [\hat{t}_0, \hat{t}_0] = \tau^2 |\vec{Q}_{\pm} - \vec{P}_0|^2 \end{aligned} \quad (\text{J.11.102})$$

while

$$v_{\pm} = [t_0, Q_{\pm} - P_0] = Q_{\pm} - P_0 = R_{\pm} \quad (\text{J.11.103})$$

Applying (J.11.97-98)

$$I_k = \frac{1}{2} \log \left( \frac{1+z}{1-z} \right) \quad (\text{J.11.104})$$

where

$$z = \frac{|\vec{Q}_+ - \vec{P}_0|^2 - |\vec{Q}_- - \vec{P}_0|^2}{|\vec{Q}_+ - \vec{P}_0|^2 + |\vec{Q}_- - \vec{P}_0|^2} = \frac{(s_0 + \Delta s)^2 - s_0^2}{(s_0 + \Delta s)^2 + s_0^2} \quad (\text{J.11.105})$$

where we have used the notation of figure J.38.

So,

$$|z| = \left| \frac{2s_0\Delta s + \Delta s^2}{2s_0^2 + 2s_0\Delta s + \Delta s^2} \right| < 1 \quad (\text{J.11.106})$$

whenever  $s_0 > 0$ . But as  $s_0$  approaches zero,  $z$  approaches 1. In fact

$$\begin{aligned} \lim_{s_0 \rightarrow 0} I_k &= \frac{1}{2} \lim_{s_0 \rightarrow 0} \log \frac{1+z}{1-z} \\ &= \frac{1}{2} \lim_{s_0 \rightarrow 0} \log \left( \frac{2}{1 - \frac{2s_0\Delta s + \Delta s^2}{2s_0^2 + 2s_0\Delta s + \Delta s^2}} \right) \end{aligned} \quad (\text{J.11.107})$$

$$= \frac{1}{2} \lim_{s_0 \rightarrow 0} \log \frac{2(2s_0^2 + 2s_0\Delta s_0 + \Delta s^2)}{2s_0^2} \quad (\text{J.11.108})$$

$$= \frac{1}{2} \lim_{s_0 \rightarrow 0} \log \frac{\Delta s^2}{s_0^2} \quad (\text{J.11.109})$$

Thus as  $P$  approaches the endpoint of the edge,  $I_k$  becomes logarithmically infinite. Otherwise, however,  $I_k$  is continuous.

#### J.11.5.4 Supersonic Nearly Sonic Edges

We have seen that  $v = R$  only when the point  $P_0$  lies on the line containing the edge. But a supersonic edge has the property that no point on the edge lies in the domain of dependence of any point on the line containing the edge. Thus, if  $v = R$ , the edge does not influence  $P_0$ . Thus  $I_k$  is continuous everywhere except along the edge itself.

#### J.11.5.5 Essentially Sonic Edges

Combining (J.8.13) and (J.8.72), we see that for essentially sonic edges

$$I_k(\psi) = \lim_{\tau \rightarrow 0} q \tau \hat{I} = \lim_{\tau \rightarrow 0} \frac{q \tau \Delta R}{\bar{v}} \quad (J.11.110)$$

Now,

$$\frac{\tau}{\bar{v}} = \frac{1}{\frac{\bar{v}_+ + \bar{v}_-}{2\tau}} = \frac{2}{v_+ + v_-} \quad (J.11.111)$$

But  $v$  can not change sign for an essentially sonic edge, in fact, both  $v_+$  and  $v_-$  will be very large numbers (of order  $1/\tau$ ) of the same sign, unless  $P_0$  lies very near to the edge itself. We thus find that  $I_k$  is not only continuous, but of order  $\tau$ , everywhere except at the edge.

#### J.11.6 Singularities in Subsonic Flow

In this section, we consider the effect of a continuous source strength, doublet strength, or doublet gradient on the potential or velocity in subsonic flow. We illustrate the distances  $h, v, a, g$  and  $R$  for subsonic flow in Figure J.39.

##### J.11.6.1 Discontinuous Source Strength

We see by (J.11.15) that the potential due to a panel with source strength 1 is

$$\phi_{s,1} = \frac{-sh}{K} J - \frac{s}{K} \sum a_k q_k I_k \quad (J.11.112)$$

But by Section J.11.4.4,  $J$  is continuous in subsonic flow except for a jump by  $4\pi$  across the panel. Thus  $hJ$  is continuous everywhere in subsonic flow except near the panel edge, where

$$\begin{aligned} I_k &= \log \left( \frac{\text{constant}}{g^2} \right) \\ &= \text{constant} - 2 \log |g| \end{aligned} \quad (J.11.113)$$



But  $g^2 = a^2 + h^2$

or  $|g| \geq |a|$  (J.11.114)

and thus  $a_k I_k$  is continuous and bounded everywhere. We thus see that in subsonic flow the potential due to a constant strength source panel is continuous everywhere.

Next we consider the velocity due to the constant source distribution. By (J.11.6)

$$\vec{v}_s = \begin{pmatrix} \vec{a} \\ -a \end{pmatrix} \quad (\text{J.11.115})$$

where

$$\begin{aligned} \vec{a} &= \frac{1}{K} \sum \vec{n}_k I_k \\ a &= \frac{-S}{K} J \end{aligned} \quad (\text{J.11.116})$$

We thus see that the component of the source velocity perpendicular to the edge becomes logarithmically infinite as we approach the panel edge.

That is,  $\vec{v}_{s,x,y} = \text{bounded terms} - \vec{n}_k \log(g)$  (J.11.117)

as  $P_0$  approaches the  $k$ th panel edge.

In addition, the  $z$ -component of velocity jumps as the panel is crossed, which is to be expected in light of the definition of source strength as the jump in normal mass flux (or normal velocity at Mach zero).

We will leave consideration of the varying source distribution (cf. (J.11.5)) to the reader. We do note, however, that no new discontinuities or singularities appear.

#### J.11.6.2 Discontinuous Doublet Strength

By (J.11.29) the potential induced by a constant strength doublet panel in subsonic flow is

$$\phi_0 = ra = \frac{1}{K} J \quad (\text{J.11.118})$$

This function is continuous in subsonic flow except for a jump across the panel, which is to be expected since the doublet strength is defined as the jump in potential.

Next, the line vortex term of the doublet velocity is given by (cf. (J.11.55))

$$\vec{v}_{D,edge}^* = \frac{-g^2}{g^2} \left( \frac{v_+}{R_+} - \frac{v_-}{R_-} \right) (\vec{Q}_0 - \vec{n}_0) \times \hat{t}_0 \quad (J.11.119)$$

Thus in subsonic flow this velocity is continuous whenever  $g = 0$ . Applying the rationalization (J.10.54) for the case  $g \approx 0$ ,

$$v_{D,edge}^* = \frac{-g^2}{K\tau} \frac{\Delta v(v_+ + v_-)}{R_+R_- (R_-v_+ + R_+v_-)} (\vec{Q}_0 - \vec{P}_0) \times \hat{t}_0 \quad (J.11.120)$$

we see that if

$$R_-v_+ + R_+v_- \neq 0 \quad (J.11.121)$$

the velocity is again well-behaved, since (J.11.120) cannot occur whenever  $R_+$  or  $R_-$  is zero. But if  $g = 0$

$$\begin{aligned} R_-^2 &= v_-^2 \\ R_+^2 &= v_+^2 \end{aligned} \quad (J.11.122)$$

and so

$$\begin{aligned} R_-v_+ + R_+v_- &= 0 \implies \\ R_+ &= v_+ \\ -R_- &= v_- \end{aligned} \quad (J.11.123)$$

That is,  $v_+$  and  $v_-$  have opposite sign unless one of them is zero. Thus, the point  $P_0$  lies on the panel edge. So, the velocity is well-behaved for all points which do not lie on the panel edge.

We now consider the limiting value of the velocity as  $P_0$  approaches the panel edge. By (J.11.122)

$$\frac{v_+}{R_+} - \frac{v_-}{R_-} = 2 \quad (J.11.124)$$

except perhaps at the endpoints of the edge. Further, it is easy to see that

$$|(\vec{Q}_0 - \vec{P}_0) \times \hat{t}_0| = g \quad (J.11.125)$$

and thus

$$\lim_{P_0 \rightarrow \text{edge}} \vec{v}_0^* = \frac{2\beta^2}{\kappa g} \quad (\text{J.11.126})$$

That is, the velocity has a magnitude proportional to the inverse of the distance from the point to the edge.

#### J.11.6.3 Discontinuous Doublet Gradient

We have seen that the potential due to a discontinuity in the normal component of doublet gradient is (cf(J.11.41))

$$\phi_k = \frac{-rsh\tau a_k}{\kappa} J_k + \frac{rsh\tau}{\kappa} I_k \quad (\text{J.11.127})$$

Examination of section J.11.4 shows that the panel function contribution to the potential is continuous except on the panel surface. On the other hand, (J.11.100) describes the edge function behavior in subsonic flow. We thus see that the potential becomes infinite in the neighborhood of a panel edge, and is proportional to the logarithm of the distance from the edge.

#### J.11.7 Discontinuous Source Strength in Supersonic Flow

##### J.11.7.1 Source Potential

We recall from (J.11.15) that the potential due to a constant source panel is

$$\phi_s = \frac{-sh}{\kappa} J - \frac{s}{\kappa} \sum a_k q_k I_k \quad (\text{J.11.128})$$

An examination of the results of Sections J.11.4 and J.11.5 show that  $hJ$  and  $I_k$  are continuous with several exceptions. One exception for  $J$  is that if the  $k$ th edge is supersonic, and  $a = h$ ,  $R_+ = v_+ = 0$ ,  $J_k$  may take on any value (cf. Section J.11.4.3). Also, if  $R_+ = 0 = R_-$ ,  $h = a$ , then  $J_k$  undergoes a jump across the "Mach wedge" located there. On the other hand (cf. Section J.11.5.1)  $I$  has discontinuities at the same locations. Consideration of (J.11.82) and (J.11.88) shows that if  $h = a$

$$-h J_k = -\text{sign}(h) \text{sign}(a) I_k \quad (\text{J.11.129})$$

Thus

$$\frac{-sh}{\kappa} (hJ_k) + \frac{sa_k}{\kappa} I_k = 0 \quad (\text{J.11.130})$$

when  $|h| = |a|$ . So, while  $J_k$  and  $I_k$  are discontinuous away from the panel, the sum  $\phi_s$  is continuous everywhere except on the panel.

#### J.11.7.2 Source Velocity

By (J.11.16-17)

$$\vec{v}_s = \left\{ \frac{\frac{s}{K} \sum_k \vec{n}_k q_k I_k}{-\frac{s}{K} J} \right\} \quad (J.11.131)$$

Thus the z-component of the velocity is always finite, though it is discontinuous on the panel and on the Mach wedges emanating from supersonic edges. On the other hand, by Section J.11.5, the tangential component of becomes logarithmically infinite as the point  $P_0$  approaches a subsonic or sonic edge and is discontinuous as  $P_0$  approaches a supersonic edge.

Now, for nearly sonic edges,  $I_k$  remains bounded but non-zero. Since  $\vec{n}_k = \hat{n}_k/\tau$  is of order  $1/\tau$ , the velocity in a very small region (that is, along the extension of the edge) is of order  $1/\tau$ . This is not a singularity since for any particular nearly sonic edge the resulting velocity is bounded.

Finally, for essentially sonic edges, the edge function is of order  $\tau$  everywhere except at the edge, and thus the source velocity remains bounded.

#### J.11.8 Discontinuous Doublet Strength in Supersonic Flow

By (J.11.29-30), the potential due to a panel with unit doublet strength is

$$\phi_D = \frac{-rs}{K} J \quad (J.11.132)$$

Thus the singularities of the doublet potential are exactly those of the panel function. That is (cf Section J.11.4.4) the potential has a jump across the panel, and across the Mach wedge emanating from any supersonic edge, and is discontinuous with multiple limiting values at panel edges and the lines  $R_+ = V_+ = 0$ .

Next, we consider the doublet velocity. By (J.11.35)

$$\vec{v}_D^* = \frac{-s\beta^2}{g^2} \left( \frac{v_+}{R_+} - \frac{v_-}{R_-} \right) (\vec{Q}_0 - \vec{P}_0) \times \hat{t}_0 \quad (\text{J.11.133})$$

We state here without proof that a "finite part" of the doublet velocity line vortex term may be computed as

$$\vec{v}_{D, \text{finite}}^* = \frac{-s\beta^2}{g^2} (\vec{Q}_0 - \vec{P}_0) \times \hat{t}_0 \cdot \left( \sum_{\text{edge in } D_p} \frac{v}{R} \text{sign(vertex)} \right) \quad (\text{J.11.134})$$

Using (J.11.134), it is straightforward to show that  $\vec{v}$  is bounded over any region of space which does not include the Mach cone emanating downstream from the vertices of the edge. In the vicinity of these cones,  $\vec{v}$  is of order  $(1/R)$ .

#### J.11.9 Discontinuous Doublet Gradient in Supersonic Flow

By (J.11.41), a discontinuous doublet gradient along an edge yields a potential

$$\phi_k = \frac{hrs}{\kappa} \tau_{ak} J_k - \frac{rsh}{\kappa} \tau_{Ik} \quad (\text{J.11.135})$$

It can easily be seen that this function is continuous along panel edges, since  $h$  and  $a_k$  are zero there. In addition, the discontinuities of  $J_k$  and  $I_k$  on the surface  $|h| = |a|$  cancel (cf(J.11.129)). Thus the potential due to a discontinuity in doublet gradient is continuous away from the panel.

Next (cf(J.11.43)),

$$\vec{v}_{k,x,y} = \frac{-rs}{\kappa} J_k \vec{n}_k \quad (\text{J.11.136})$$

and so is discontinuous on the Mach wedge emanating from a supersonic panel edge. Finally (cf(J.11.44))

$$\vec{v}_{k,z} = \frac{-rs}{\kappa} \tau_{Ik} \quad (\text{J.11.137})$$

and so the normal velocity is logarithmically infinite in the neighborhood of subsonic edges, and discontinuous on the Mach wedge emanating from a supersonic edge.

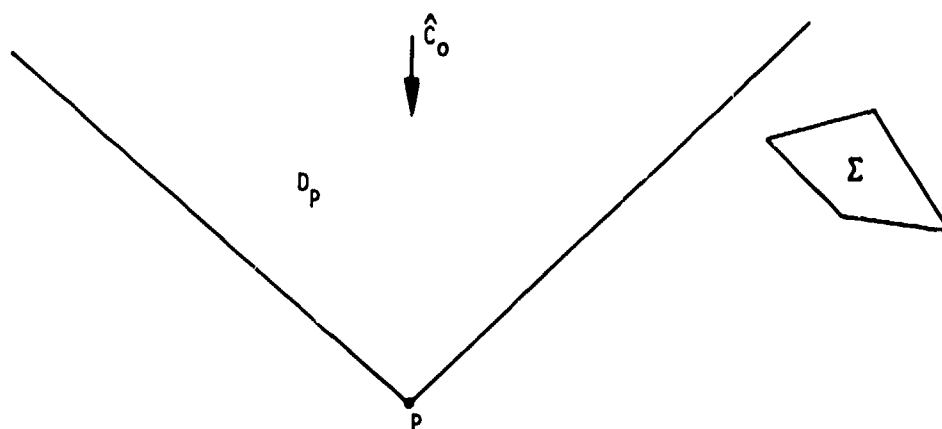


Figure J.1 - Domain of dependence

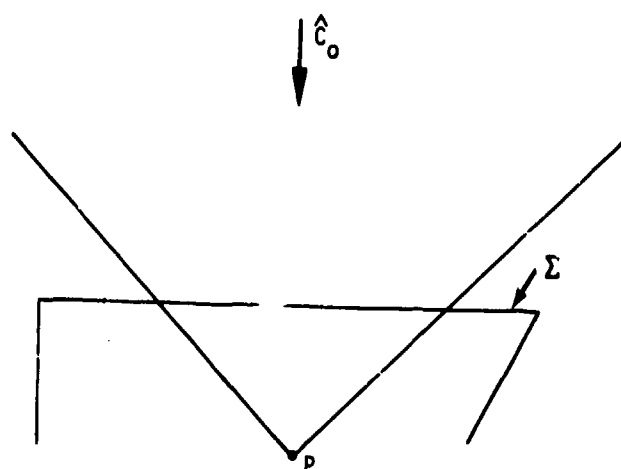
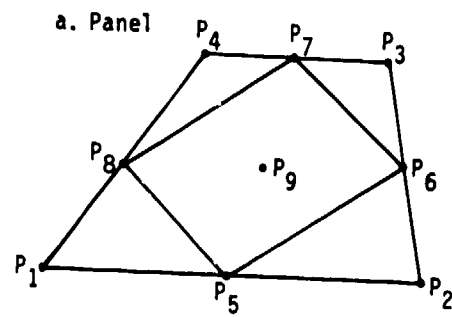


Figure J.2 - Superinclined panel partially within  $D_p$  without corners in  $D_p$

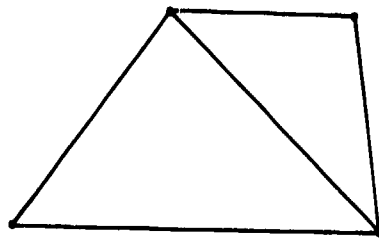
# Notation

$\hat{c}_0$	unit compressibility vector
$[C_0]$	metric matrix $C_0 = sB^2I + (1-sB^2) \hat{c}_0 \hat{c}_0^T$
$[\tilde{C}_0]$	positive definite metric matrix $\tilde{C}_0 = \beta^2I + (1-\beta^2) \hat{c}_0 \hat{c}_0^T$
$D_p$	domain of dependence
$[B_0]$	dual metric matrix $B_0 = I + (s\beta^2-1) \hat{c}_0 \hat{c}_0^T$
$P$	control point or field point
$Q$	point or panel, point of integration
$Q_0$	panel center
$Q_i, i=1,\dots,9$	panel defining points
$[ \cdot ]$	compressible inner product, corresponding to $[C_0]$
$\{ \cdot \}$	dual inner product, corresponding to $[B_0]$
$\vec{R}$	$\vec{Q} - \vec{P}$
$\hat{n}_0$	subpanel unit normal vector
$\hat{t}_0$	unit edge tangent
$A_0$	reference to local transformation
$A_i$	reference to local transformation for $i$ th region

Figure J.3 - Notation used frequently in Appendix J



b. Two half panels



c. Two half panels

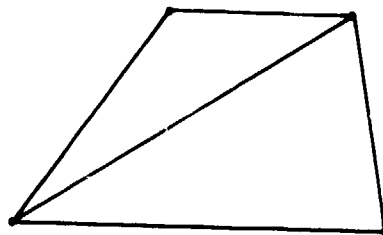


Figure J.4 - Two region approximations to panel



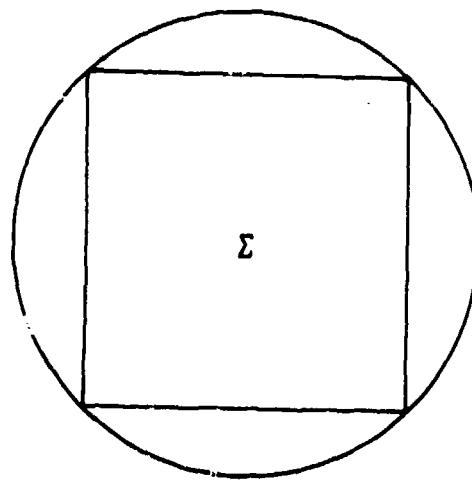


Figure J.5 - Region in which intermediate field PIC is not performed

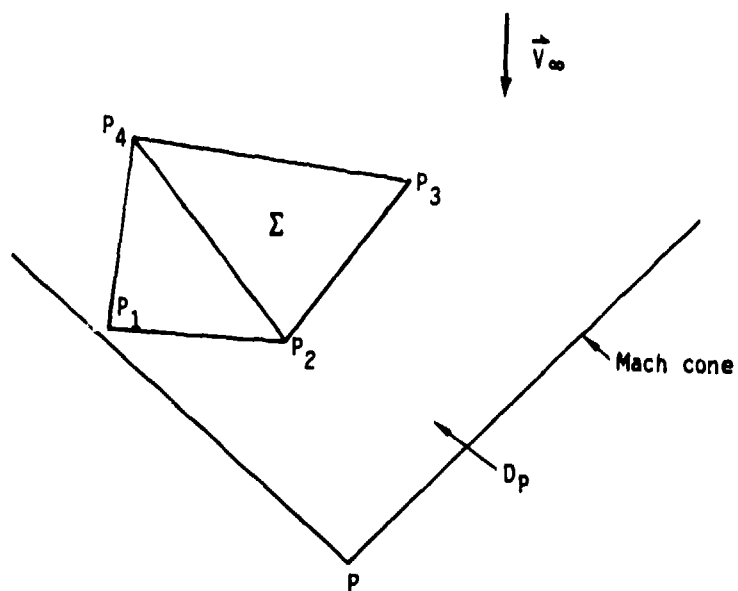


Figure J.6 - Splitting a panel into half panels

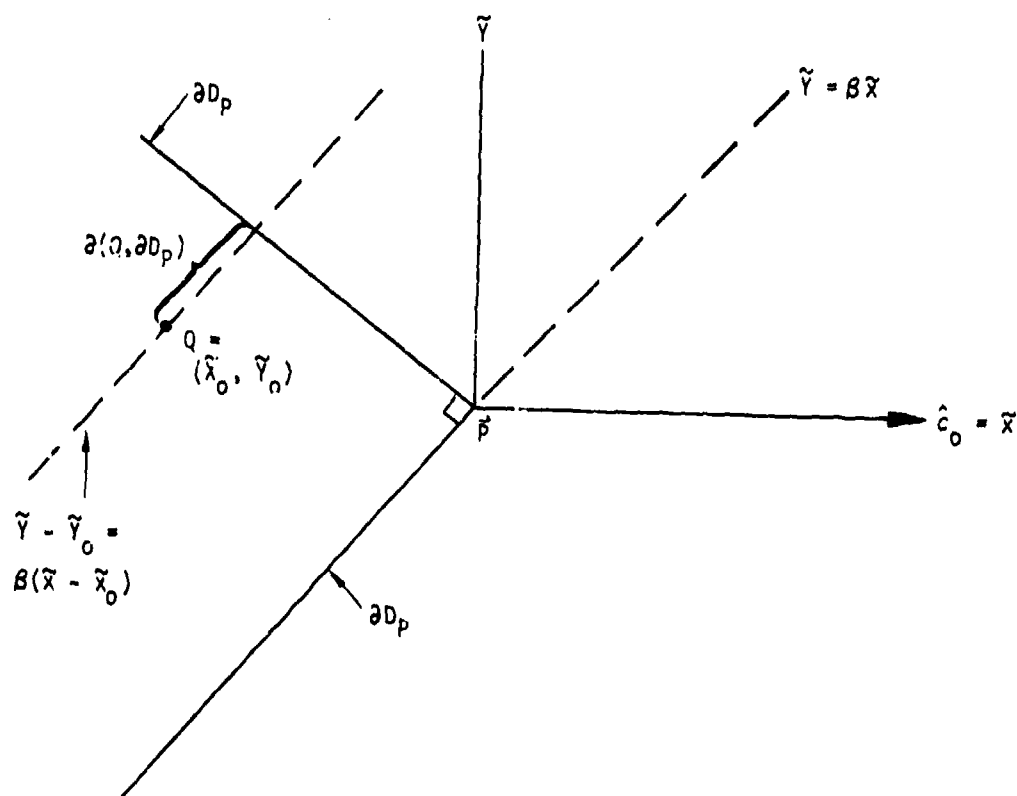


Figure J.7  $(\tilde{X}, \tilde{Y})$  coordinate system

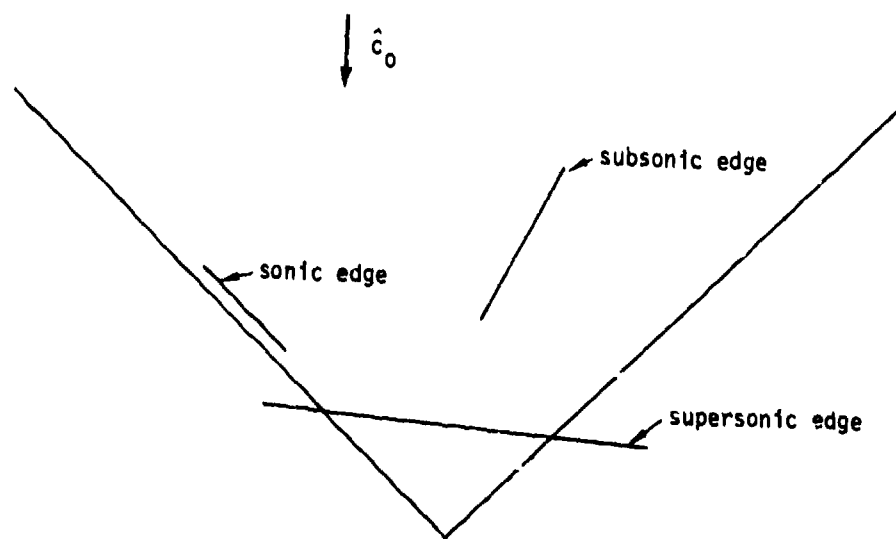


Figure J.8 - Subsonic and supersonic edges

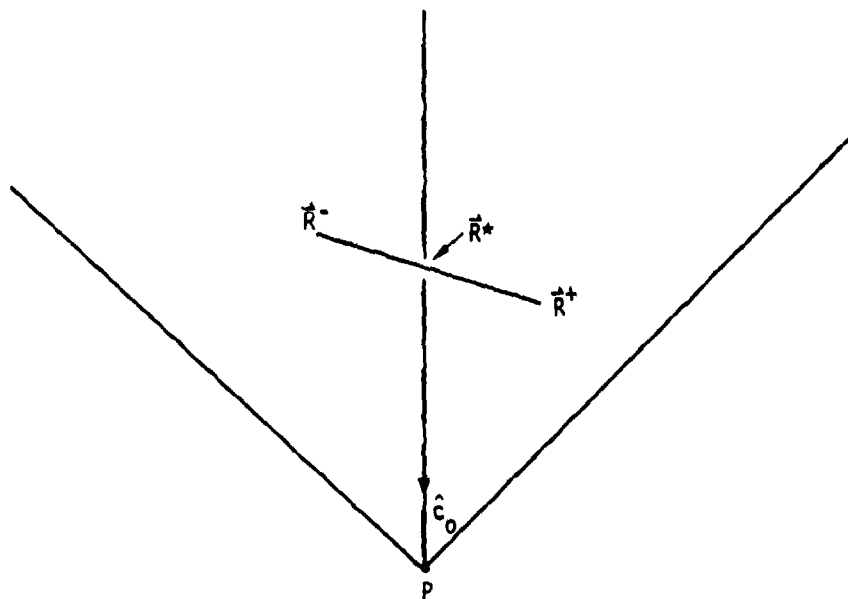


Figure J.9 - Point of closest approach

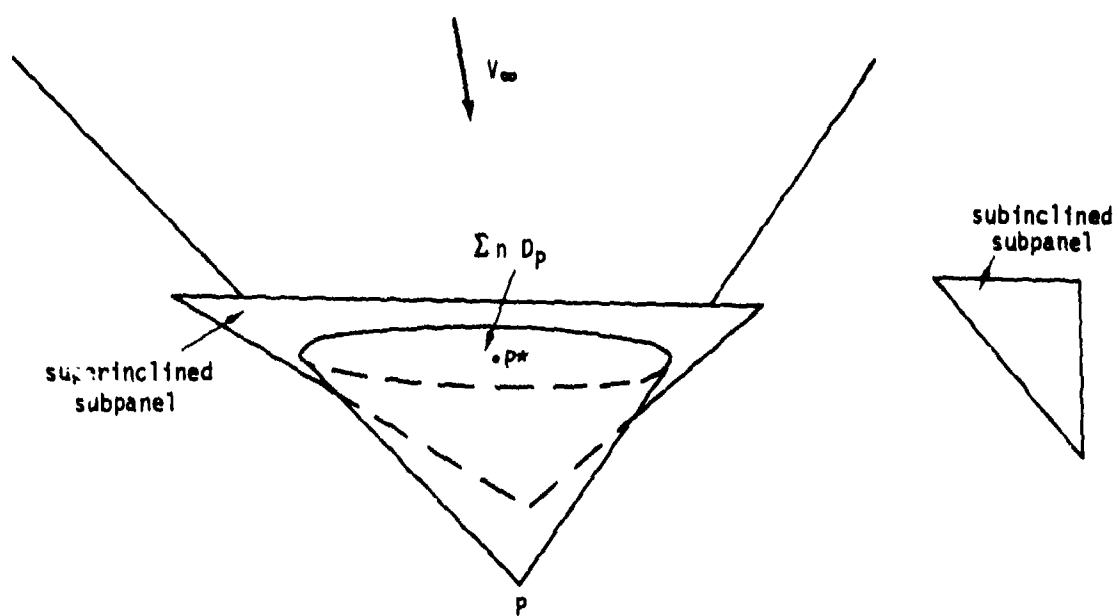


Figure J.10 - Subinclined and superinclined panel

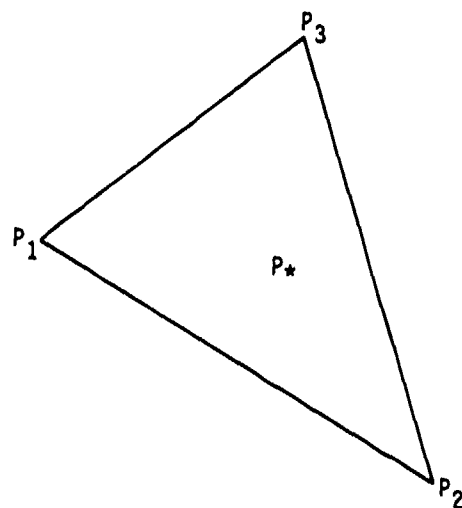


Figure J.11 -  $P_*$  lies in the interior of the subpanel

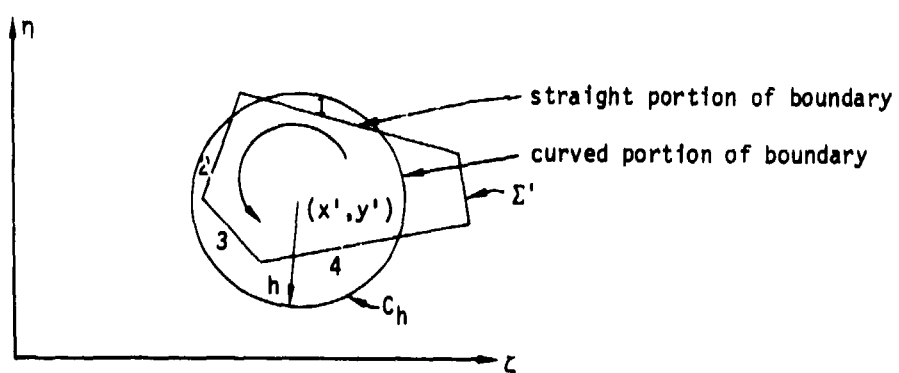


Figure J.12 - Region of integration,  $\Sigma' \cap C_h$  for a typical subpanel

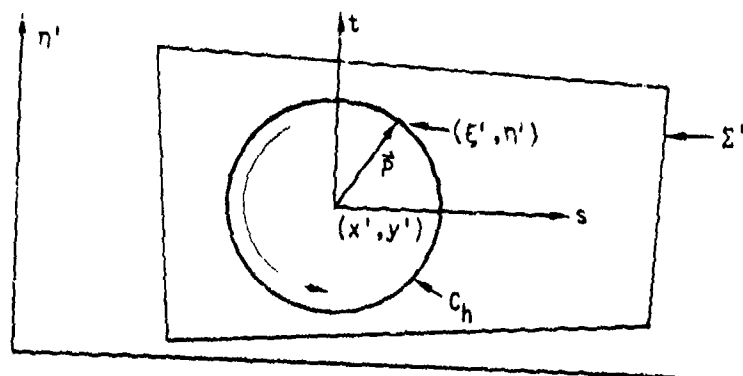


Figure J.13 -  $p_k^{\pm}$ ,  $q_k^{\pm}$  when  $C_h \subset \Sigma'$

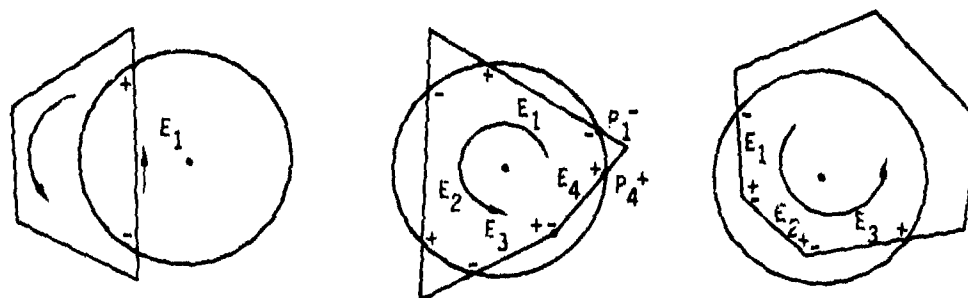


Figure J.14 - Edge numbering for various panel configurations

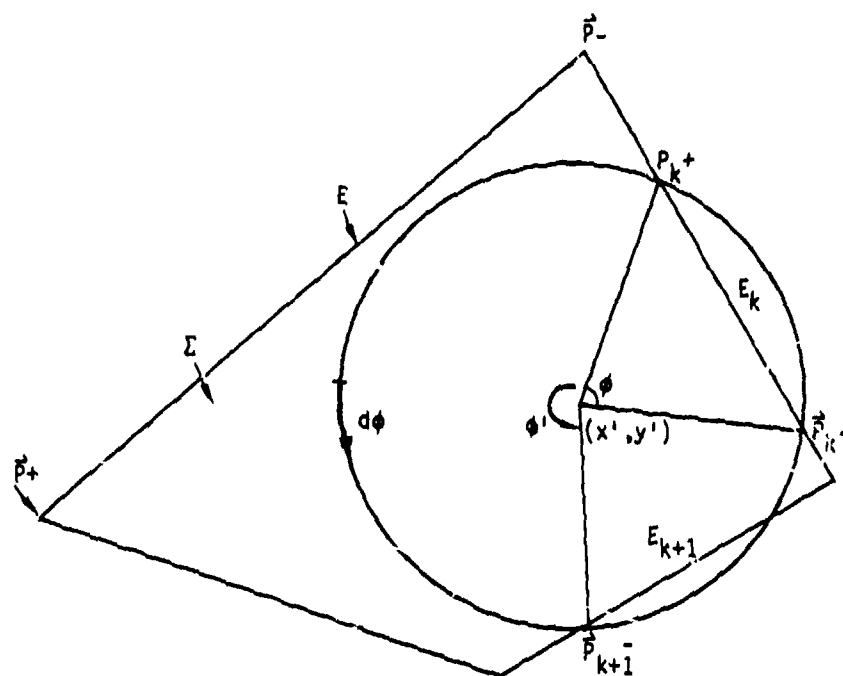


Figure J.15 - Phase angle  $\phi'$  exceeds  $\pi$

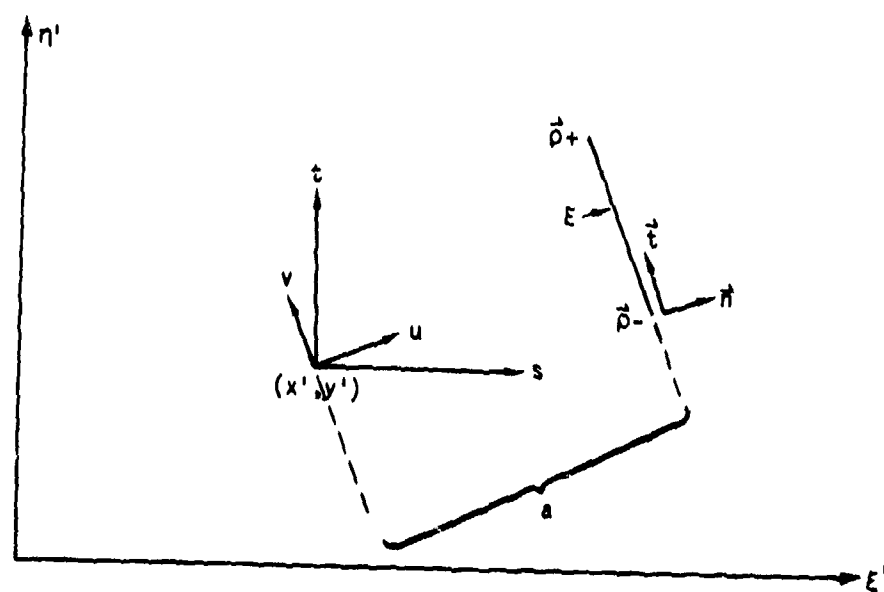


Figure J.16 - Coordinate systems in the  $(\xi', \eta')$  plane

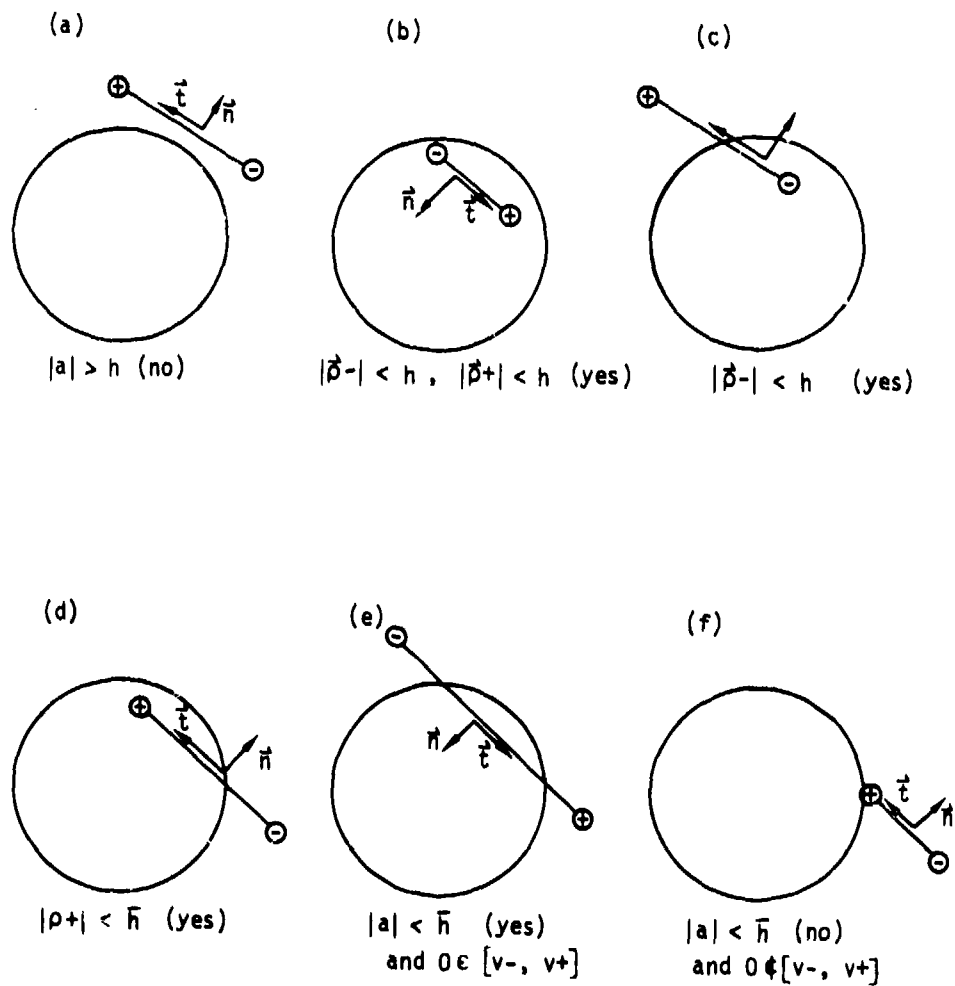


Figure J.17 - Determining if an edge of  $\Sigma'$  is an edge of  $\Sigma' \cap C_h$

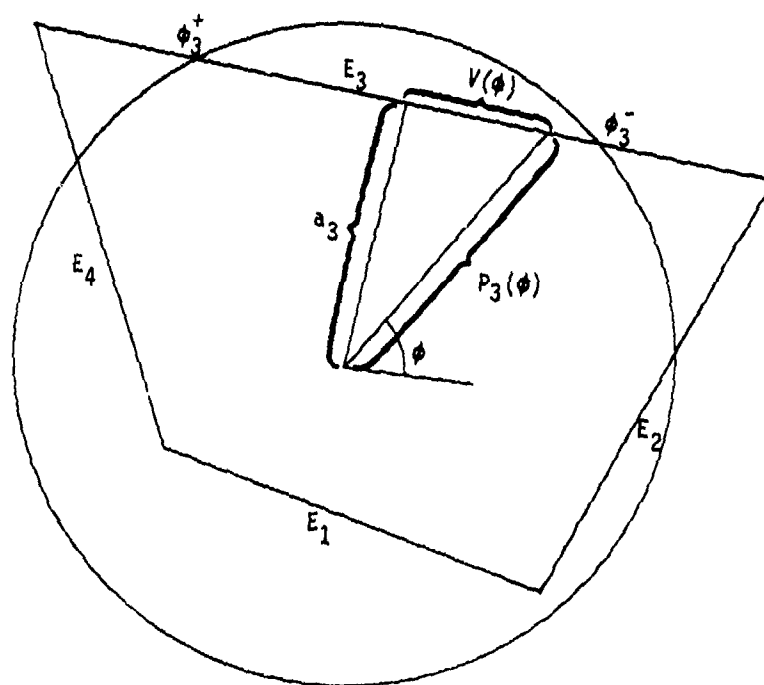


Figure J.18 - Definition of  $P(\phi)$ , the upper limit of integration for  $P$



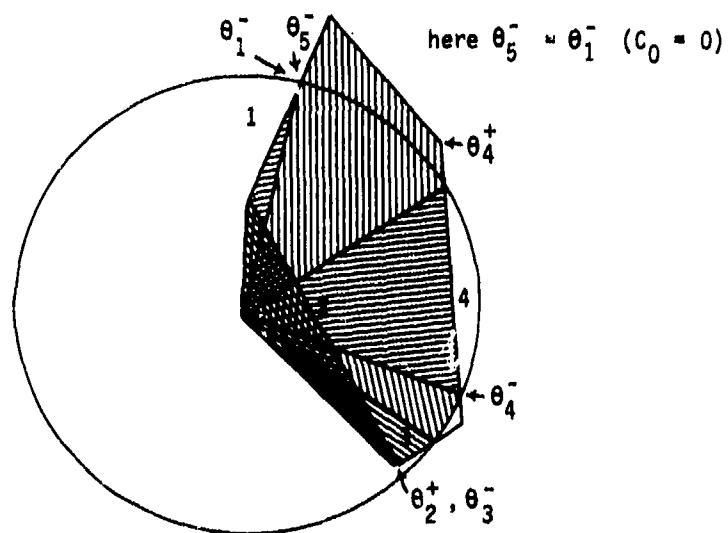
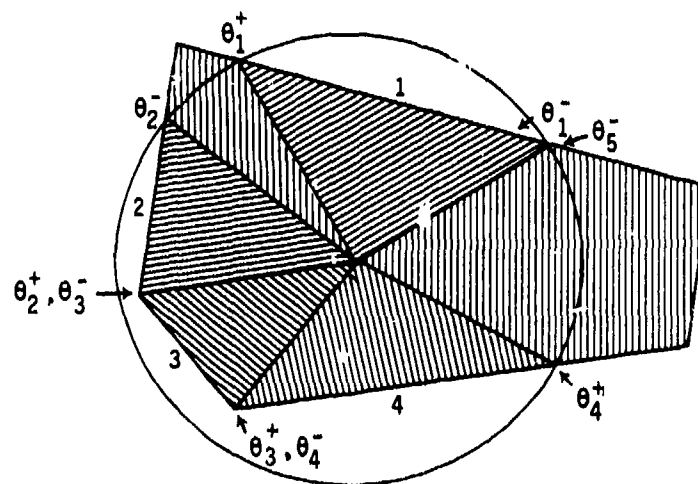


Figure J.19 - Region of integration for superinclined panel

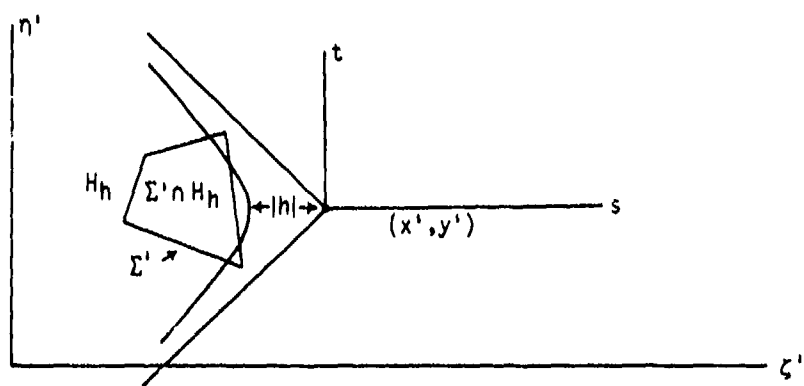


Figure J.20 - Transformation to  $(s, t)$  variables and region of integration

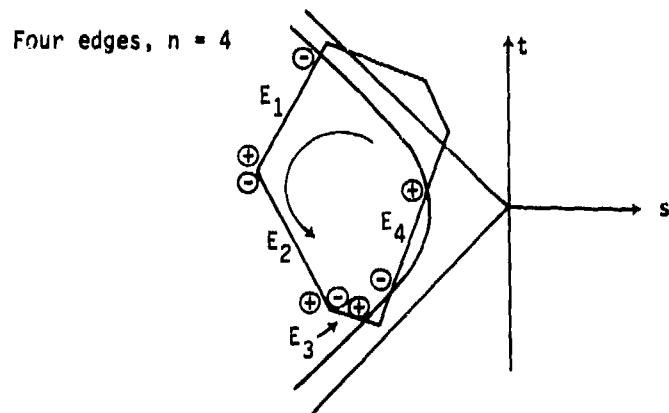


Figure J.21 - Numbering of edges of  $\Sigma' \cap H_h$

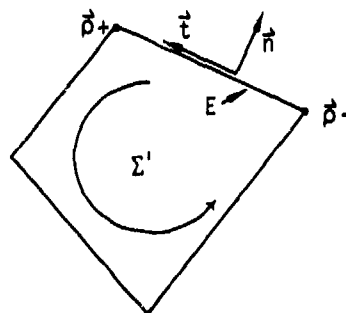


Figure J.22 - A region  $\Sigma'$  with edge  $E$ , oriented tangent  $\vec{t}$  and outward edge normal  $\vec{n}$ .

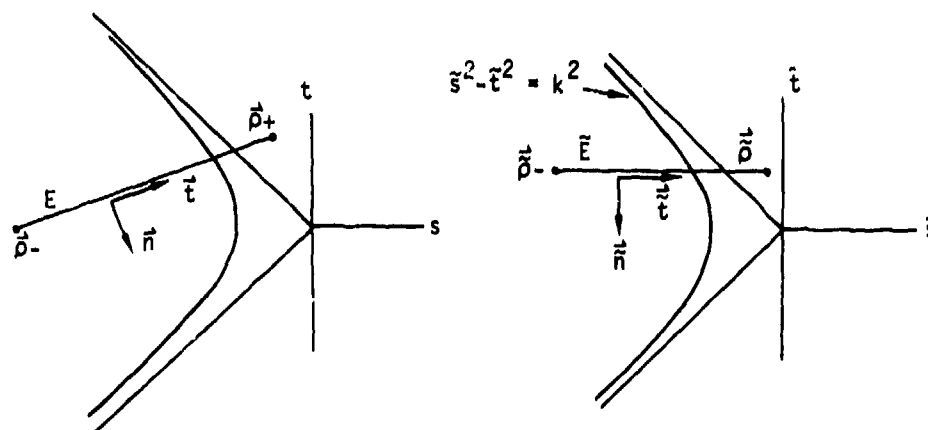


Figure J.23 - An edge  $E$  and its image  $\tilde{E}$  in the  $\tilde{s}$  -  $\tilde{t}$  coordinate system (subsonic edge)

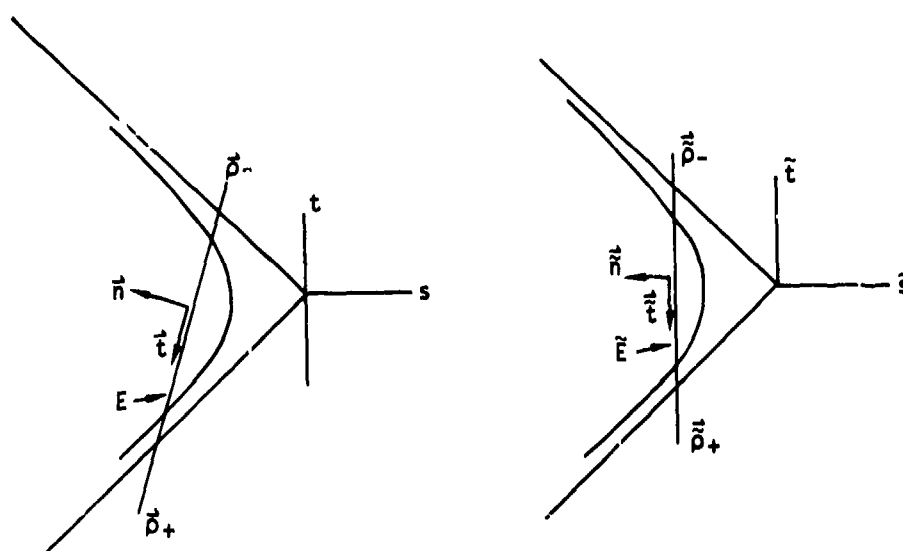
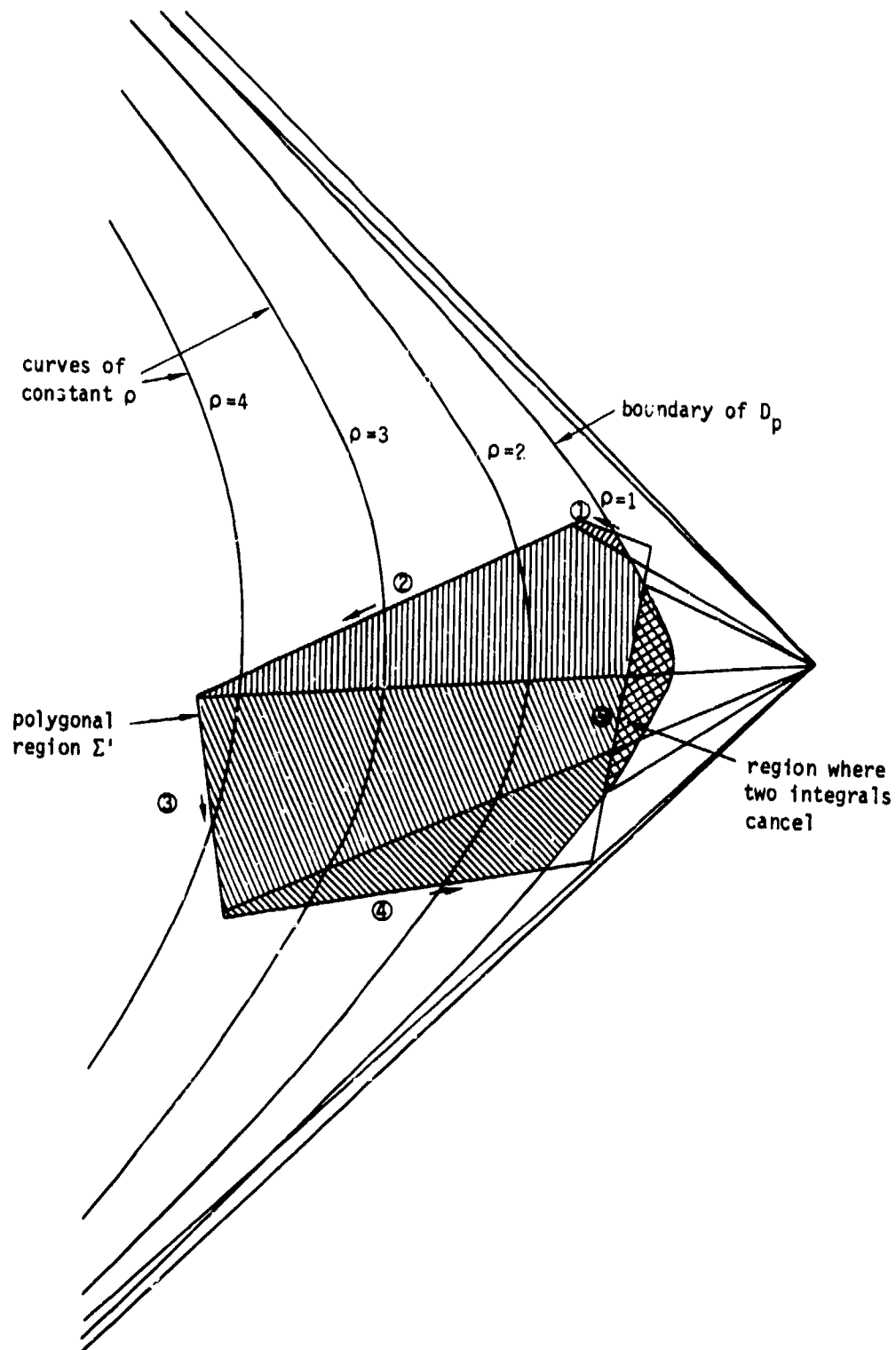


Figure J.24 - An edge  $E$  and its image  $\tilde{E}$  in the  $\tilde{s}$ - $\tilde{t}$  coordinate system (supersonic edge)



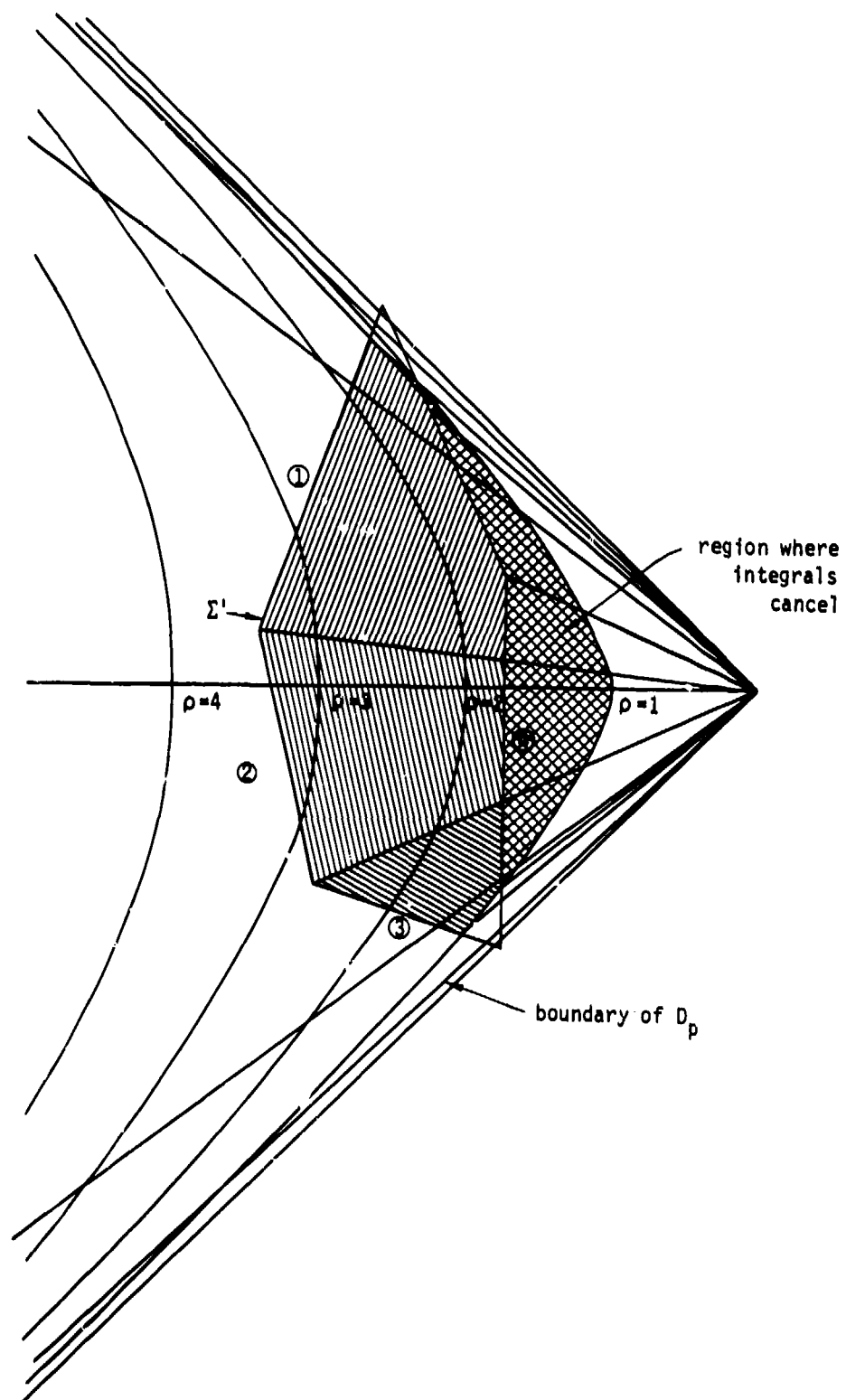


Figure J.25b - Region of integration for subincised panel

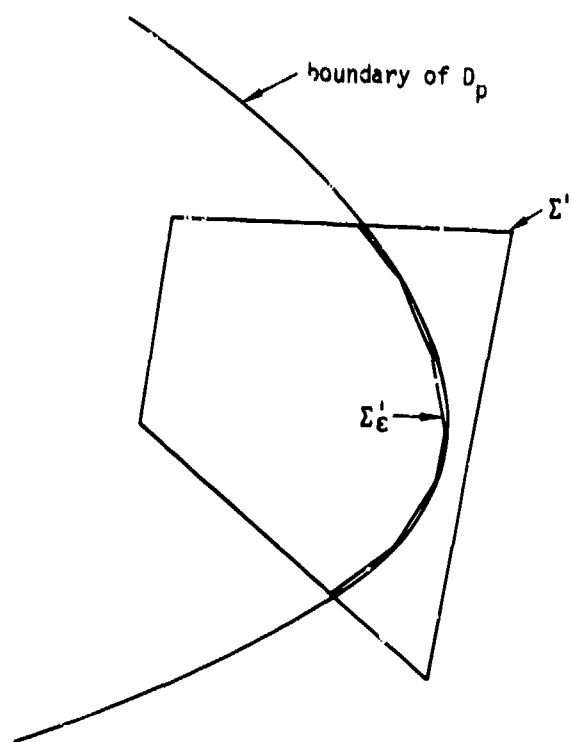


Figure J.26 - Polygon  $\Sigma'_\epsilon$  approximating  $\Sigma'\eta D_p$

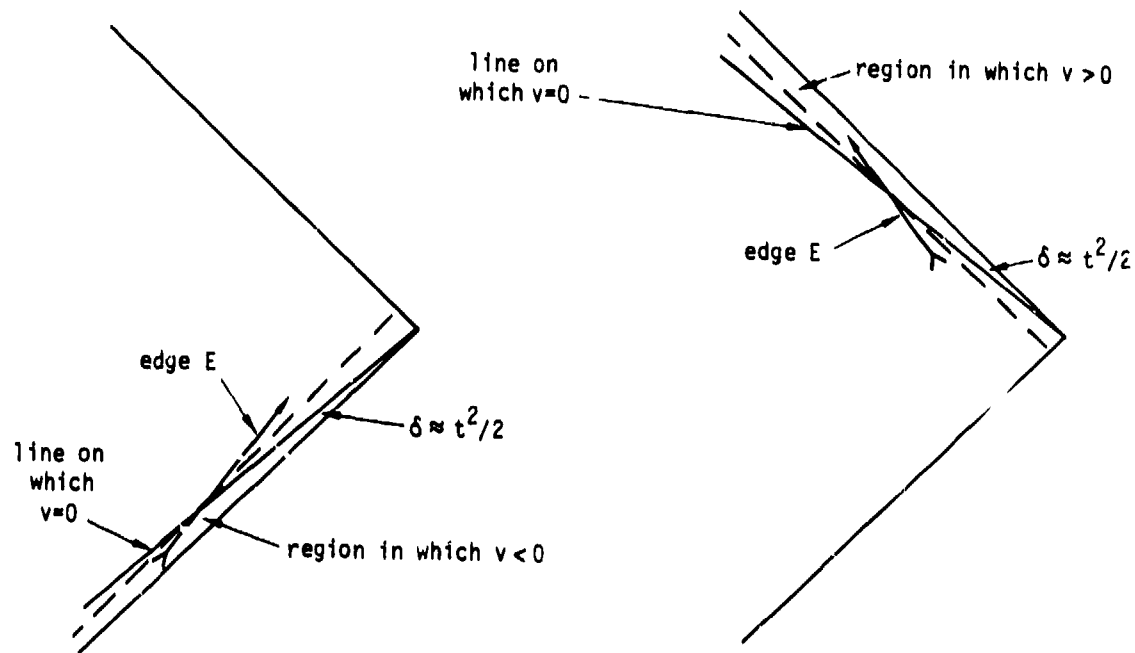


Figure J.27 - Illustration of supersonic, nearly sonic edges on which  $v$  changes sign

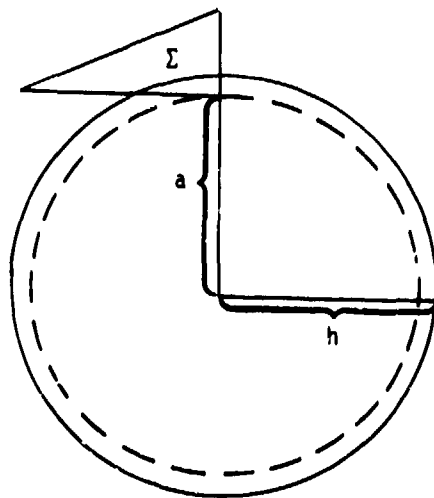


Figure J.28 - An example of a superinclined panel with  $g^2 = h^2 - a^2 \approx 0$



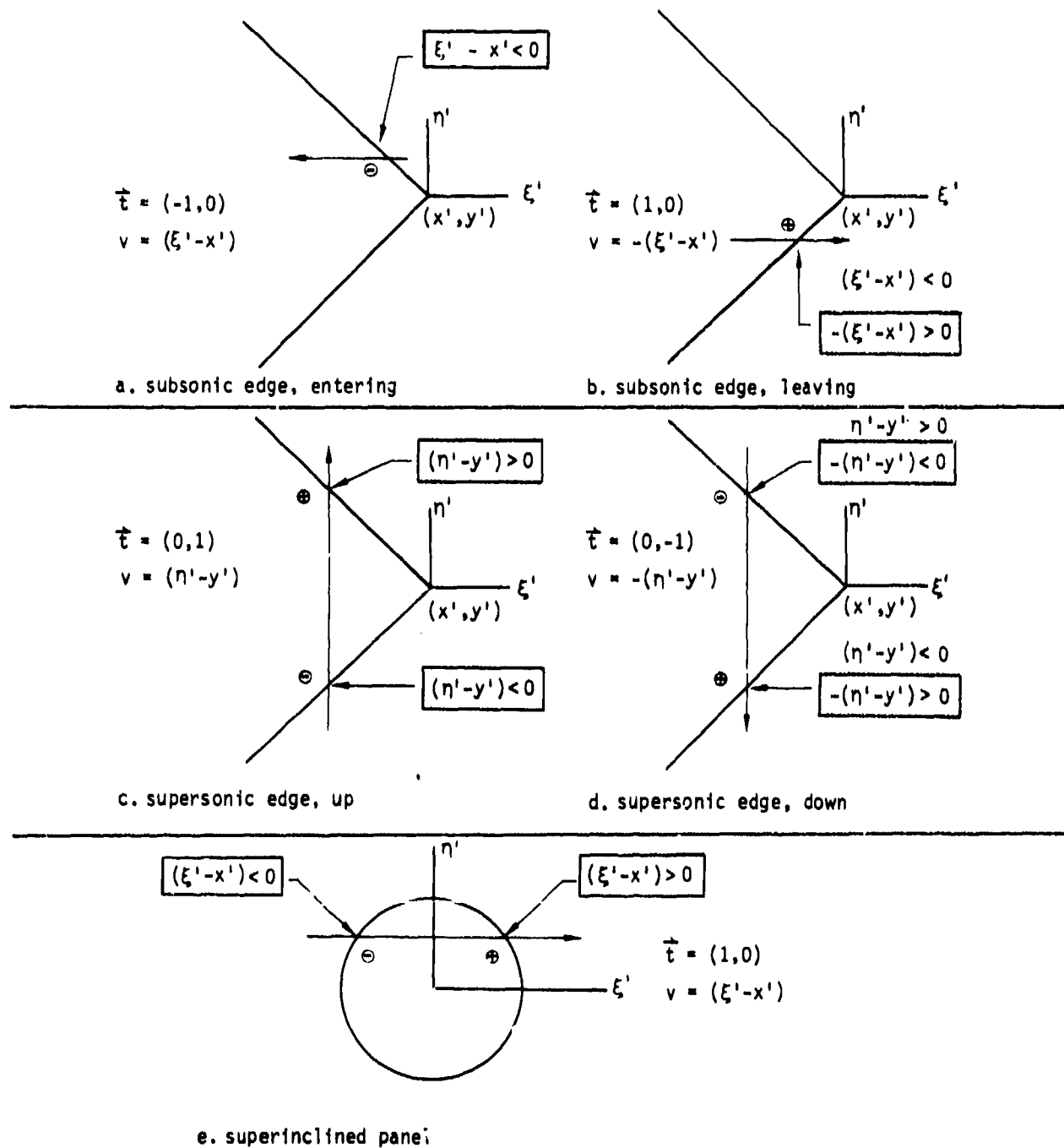
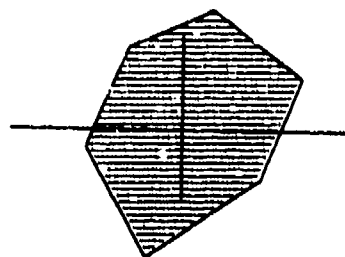
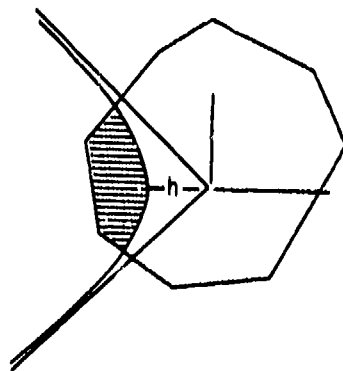


Figure J.29 - Evaluating  $v$  on the boundary of  $D_p$  : the various special cases



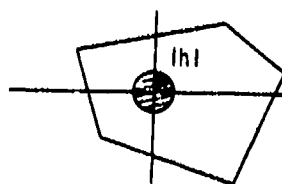
$$c_0 = 1 \quad J' \big|_{|h|=0} = 2\pi$$

a.  $s = +1$



$$c_0 = 0 \quad J' \big|_{|h|=0} = -\pi$$

b.  $rs = -1$



$$c_0 = 1 \quad J' \big|_{|h|=0} = 2\pi$$

c.  $r = -1$

Figure J.30 - The value of  $J'$  for some special configurations

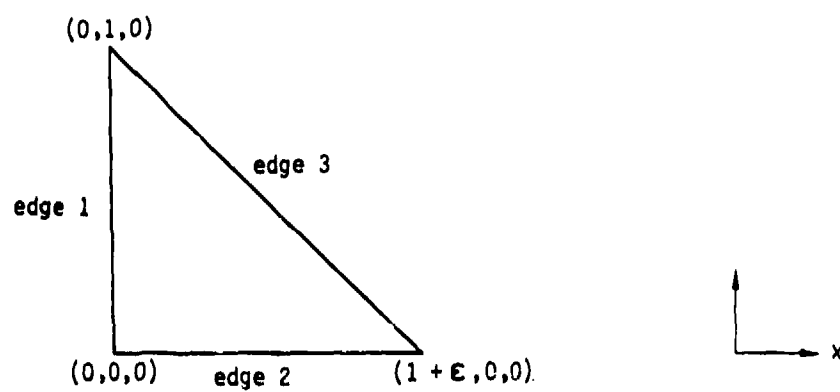
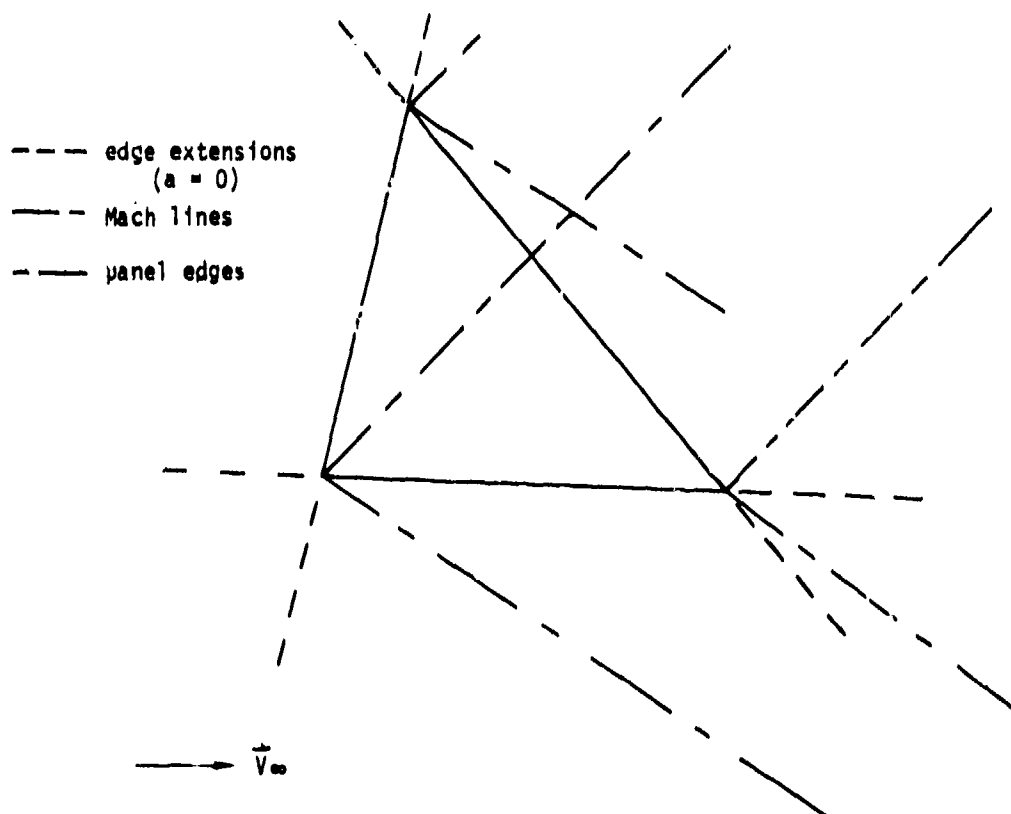


Figure J.31 - Region with nearly sonic edge



J.12-22

Figure J.32 - Potential lines of discontinuity in  $J^*$

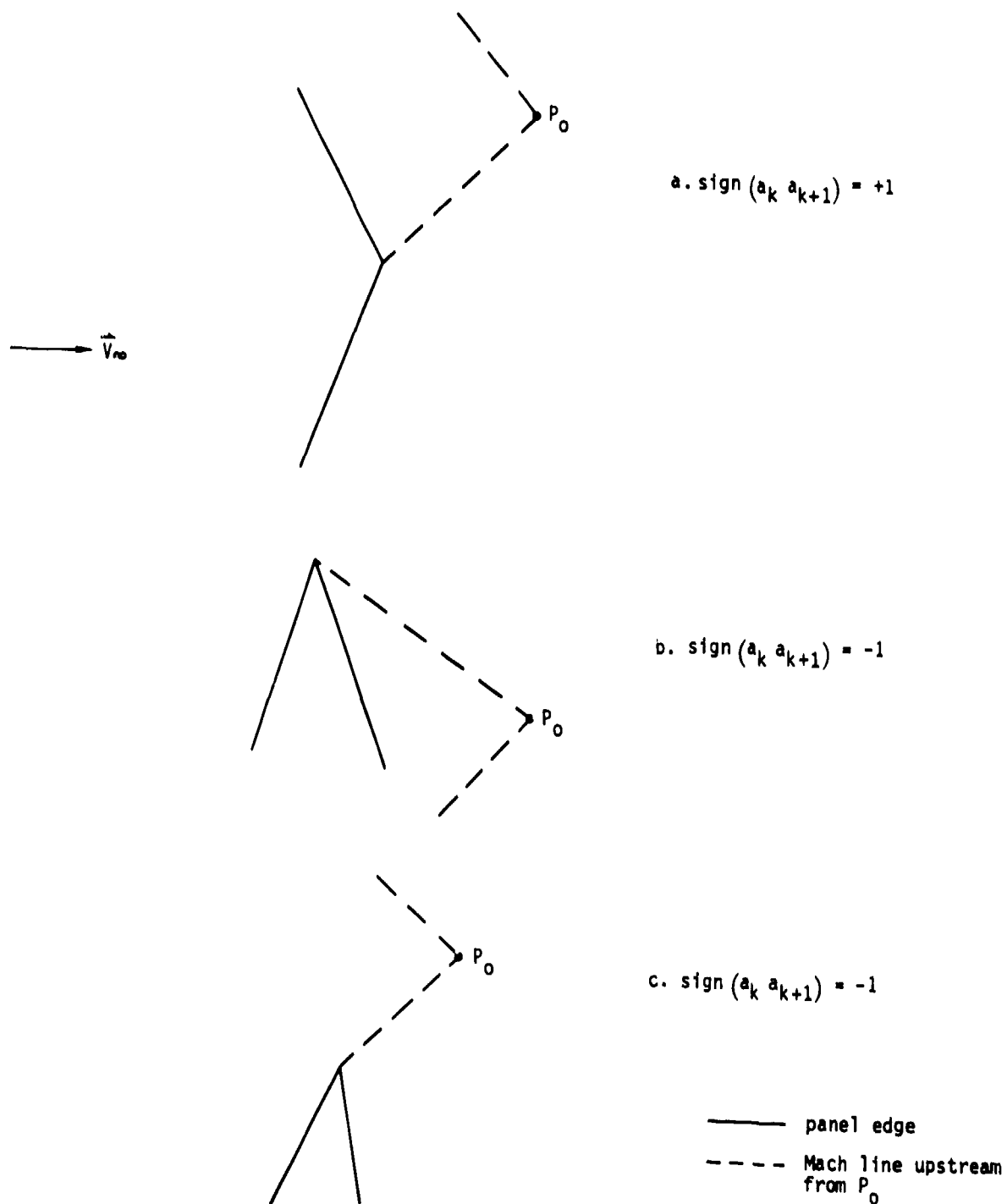


Figure J.33 - Panel corners on Mach lines

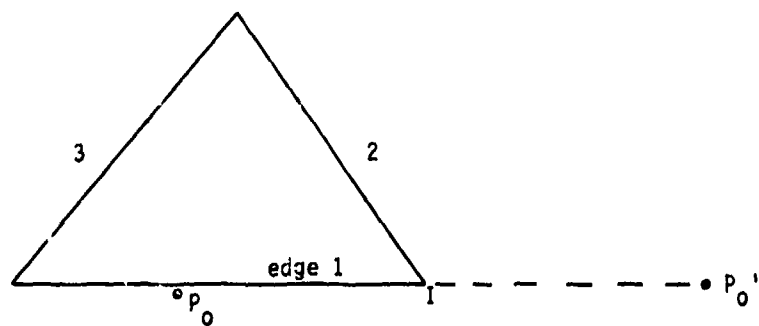
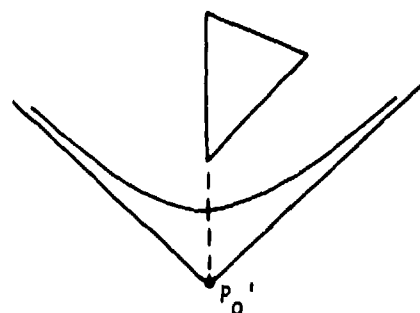
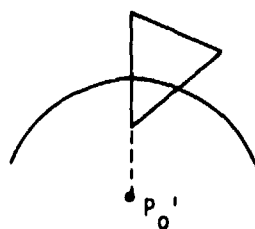


Figure J.34 - A point lies on the extension of an edge  
(subsonic flow)



a. subinclined panel



b. superinclined panel

Figure J.35 - A point lies on the extension of an edge  
(supersonic flow)

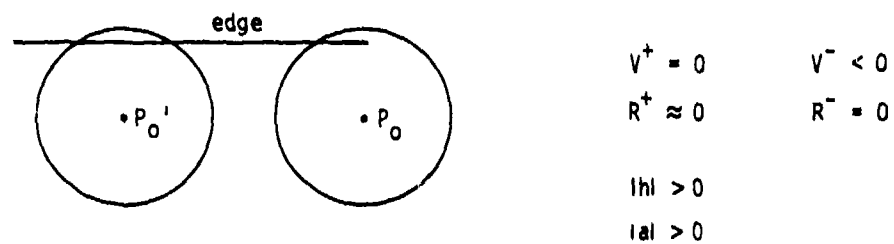


Figure J.36 - Edge barely intersects  $D_p$

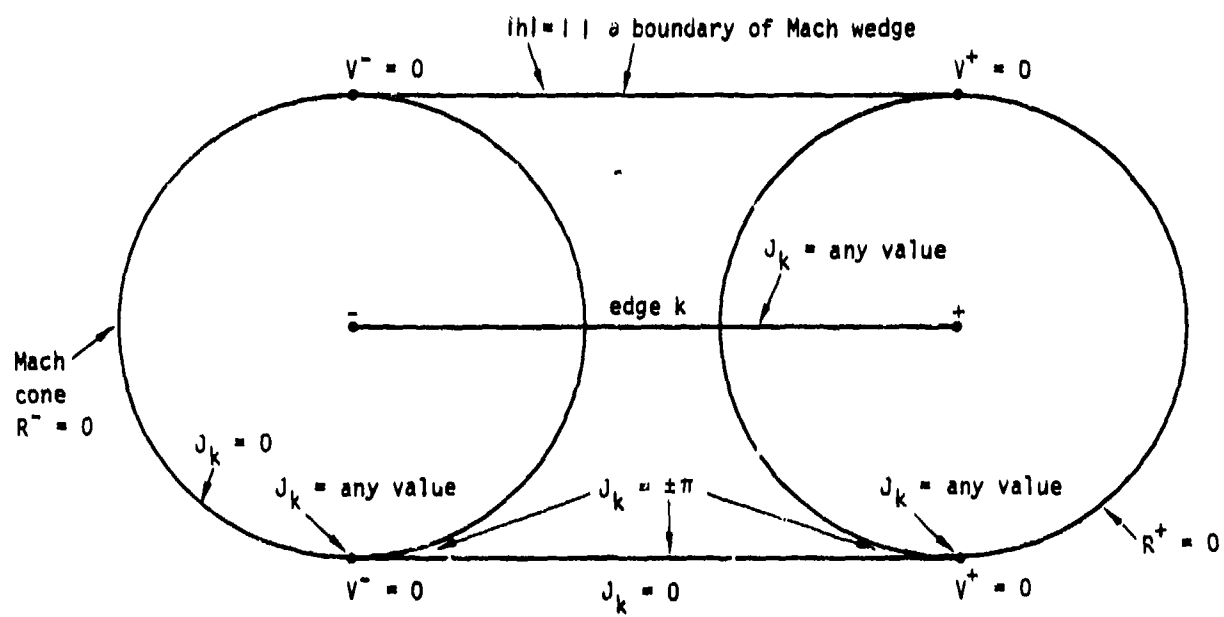


Figure J.37a - The Mach wedge in cross-section

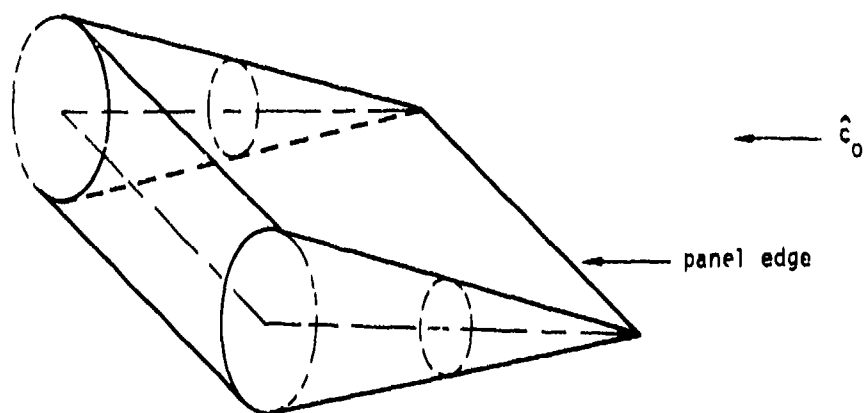


Figure J.37b - Mach wedge behind supersonic panel edge

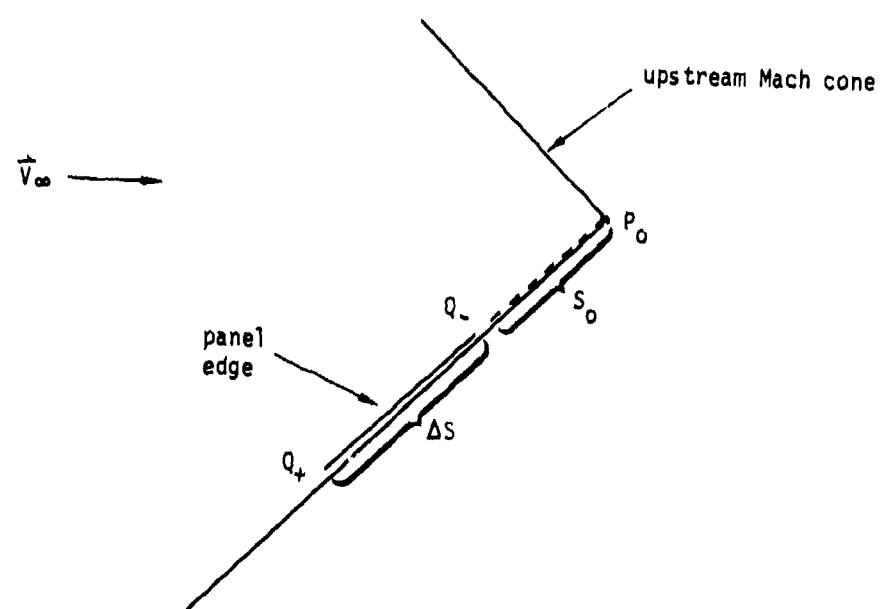
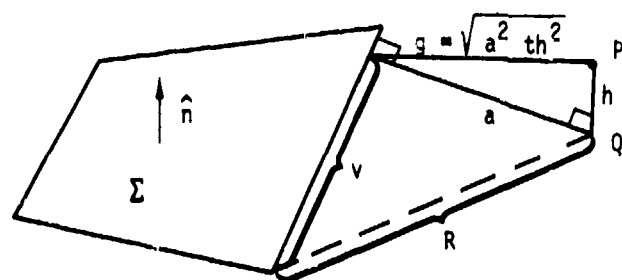


Figure J.38 - Subsonic nearly sonic edge





Note:  $\vec{P} - \vec{Q}$  is perpendicular to the plane of  $\Sigma$

Figure J.39 - The distances  $h$ ,  $v$ ,  $a$ ,  $g$ , and  $R$  in subsonic flow

## K.0 Matrix Assembly

The assembly of panel influence coefficient matrices to obtain an aerodynamic influence coefficient matrix is discussed briefly in Section 5.7. The primary purpose of this appendix is to discuss those details of the matrix assembly procedure which were omitted in section 5.7.

One item of complexity dealt with briefly in section 5.7 is that of symmetry planes. While the principle of symmetry is simple, implementation pervades almost the entire PAN AIR program. We will discuss symmetry in section K.1.

The identification of known singularity parameters is another measure undertaken for efficiency purposes. Implementation of this measure, however, is quite straightforward, and affects very little of the PAN AIR program. In section K.2 we will briefly identify the conditions under which a singularity parameter becomes "known."

The transformation of panel influence coefficient matrices  $[PIC^S]$  and  $[PIC^D]$  into a row of the aerodynamic influence coefficient matrix is straightforward to describe in engineering terms (see equation (5.7.1)), but poses considerable data manipulation problems. We outline briefly a solution to these problems in section K.3. In addition, we elaborate briefly on (5.7.1).

In appendices C and H we discussed the purpose and formulation of the closure boundary condition. In section K.4, we discuss the implementation of this boundary condition as a row of the aerodynamic influence coefficient matrix.

In appendix F, we discussed the assignment of matching boundary conditions at control points. The implementation of these boundary conditions is straightforward, except when the control point is located at a plane of symmetry. This special case is discussed in section K.5.

Finally, the implementation of the update capability in the construction of the AIC matrix is discussed in section K.6. This capability permits a program user to perturb the geometry of a portion of a configuration and thereupon analyze the perturbed configuration, without the program recomputing the entire influence coefficient matrix for the second analysis.

## K.1 Symmetry Planes

### K.1.1 One Plane of Geometric Symmetry

The basic principle of symmetry is that the perturbation potential induced by a panel on a control point is equal to the potential induced by the reflected image of the panel on the reflected image of the control point (see figure 5.20). It is this principle which permits the partition of the AIC matrix into portions which are identical.

For, using primes to designate the singularity parameters and right hand side entries of the image portion of the configuration, the fundamental system of linear equations (5.7.4) becomes

$$\begin{bmatrix} \text{AIC}_{11} & \text{AIC}_{12} \\ \text{AIC}_{21} & \text{AIC}_{22} \end{bmatrix} \begin{Bmatrix} \lambda_1 \\ \vdots \\ \lambda_N \end{Bmatrix} = \begin{Bmatrix} b_1 \\ \vdots \\ b_N \end{Bmatrix} \quad (\text{K.1.1})$$

Now, it follows from the basic symmetry principle that

$$\begin{aligned} [\text{AIC}_{11}] &= [\text{AIC}_{22}] \\ [\text{AIC}_{21}] &= [\text{AIC}_{12}] \end{aligned} \quad (\text{K.1.2})$$

and thus the program need only compute those matrices which are distinct. This means that the user need only define the "real" half of the configuration, from which the program may compute the matrices  $[\text{AIC}_{11}]$  and  $[\text{AIC}_{12}]$ , which we will henceforth label  $[\text{AIC}_1]$  and  $[\text{AIC}_2]$  (cf. equation (5.7.5)).

We now show that the basic symmetry principle is true under certain restrictions. Let  $\hat{v}$  be the unit normal to the plane of symmetry. Then, for a point P (see figure K.1), its reflected image P' is

$$\vec{P}' = \vec{P} - 2(\hat{v} \cdot (\vec{P} - \vec{P}_0))\hat{v} \quad (\text{K.1.3})$$

where  $P_0$  is any point on the plane. If we assume that the plane passes through the origin of the coordinate system, and take  $P_0$  to be the origin, we obtain

$$\vec{P}' = \vec{P} - 2\hat{v}(\hat{v} \cdot \vec{P}) = [I - 2\hat{v}\hat{v}^T]\vec{P} \quad (\text{K.1.4})$$

Next we recall the fundamental integral equation (5.2.8)

$$\phi(P) = \frac{1}{\kappa} \iint_{S \cup D_p} \left( -\frac{\sigma}{R} + \mu \hat{n} \cdot \tilde{\nabla} \left( \frac{1}{R} \right) \right) dS \quad (K.1.5)$$

We first investigate the conditions under which

$$\vec{R} = (\vec{P} - \vec{Q})^T [C_0] (\vec{P} - \vec{Q}) \quad (K.1.6)$$

is invariant under reflection. Equation (K.1.4) follows from (E.2.2) and (E.2.3), through these equations assumed that all vectors were written in compressibility coordinates. In transforming to reference coordinates,  $[C]$  is replaced by  $[C_0]$ . We note here that all vectors in this appendix are written in reference coordinates, and except for  $[C_0]$  we delete the subscript 0, used in appendix E to denote reference coordinates for reasons of clarity.

Here, we define any position-dependent quantity (vector or scalar) as being invariant or preserved under reflection if it remains unchanged when position vectors are replaced by their primed counterparts. For instance,  $R$  is invariant under reflection if it remains unchanged when  $P$  and  $Q$  in (K.1.6) are replaced by  $P'$  and  $Q'$ .

Clearly both  $R$  and  $1/R$  will remain unchanged under reflection exactly when  $R^2$  does, and so we will consider  $R^2$ . Writing  $\vec{V}$  for  $(P-Q)$  and  $\vec{V}'$  for its image, we wish to determine the conditions under which

$$\vec{V}^T [C_0] \vec{V} = \vec{V}'^T [C_0] \vec{V}' \quad (K.1.7)$$

for all possible vectors  $\vec{V}$ .

Now, by (K.1.2),

$$\vec{V}'^T [C_0] \vec{V}' = \vec{V}^T [I - 2\hat{\sigma}\hat{\sigma}^T] [C_0] [I - 2\hat{\sigma}\hat{\sigma}^T] \vec{V} \quad (K.1.8)$$

and thus (K.1.7) holds for all vectors  $V$  whenever

$$[C_0] = [I - 2\hat{\sigma}\hat{\sigma}^T] [C_0] [I - 2\hat{\sigma}\hat{\sigma}^T] \quad (K.1.9)$$

or, simplifying, whenever

$$[-2\hat{\sigma}\hat{\sigma}^T] [C_0] [-2\hat{\sigma}\hat{\sigma}^T] - [2\hat{\sigma}\hat{\sigma}^T] [C_0] - [C_0] [2\hat{\sigma}\hat{\sigma}^T] = 0 \quad (K.1.10)$$

Recalling from section 5.2 or (E.3.9) that

$$[C_0] = s\beta^2 I + (1 - s\beta^2) \hat{e}_0 \hat{e}_0^T \quad (K.1.11)$$

and noting that  $\hat{\sigma}^T \hat{\sigma} = 1$ , we can easily see that (K.1.10) is equivalent to

$$\begin{aligned}
0 &= 4 s_B^2 \hat{v} \hat{v}^T + [2\hat{v}\hat{v}^T] (1 - s_B^2) [\hat{e}_0 \hat{e}_0^T] [2\hat{v}\hat{v}^T] \\
&- [2\hat{v}\hat{v}^T] (s_B^2) - [2\hat{v}\hat{v}^T] (1 - s_B^2) [\hat{e}_0 \hat{e}_0^T] \\
&- s_B^2 [2\hat{v}\hat{v}^T] - (1 - s_B^2) [\hat{e}_0 \hat{e}_0^T] [2\hat{v}\hat{v}^T]
\end{aligned} \tag{K.1.12a}$$

$$\begin{aligned}
&= 4(1 - s_B^2) [\hat{v}\hat{v}^T \hat{e}_0 \hat{e}_0^T \hat{v}\hat{v}^T] \\
&- 2(1 - s_B^2) [\hat{v}\hat{v}^T \hat{e}_0 \hat{e}_0^T] - 2(1 - s_B^2) [\hat{e}_0 \hat{e}_0^T \hat{v}\hat{v}^T]
\end{aligned} \tag{K.1.12b}$$

$$\begin{aligned}
&= 4(1 - s_B^2) (\hat{e}_0, \hat{v})^2 [\hat{v} \hat{v}^T] \\
&- 2(1 - s_B^2) (\hat{e}_0, \hat{v}) [\hat{e}_0 \hat{v}^T + \hat{v} \hat{e}_0^T]
\end{aligned} \tag{K.1.12c}$$

Now, the matrix in (K.1.12) is zero whenever  $(\hat{e}_0, \hat{v})$  or  $(1 - s_B^2)$  is zero. Further, every column of  $[\hat{v} \hat{v}^T]$  and every column of  $[\hat{v} \hat{e}_0^T]$  are multiples of  $\hat{v}$ , while every column of  $[\hat{e}_0 \hat{v}^T]$  is a multiple of  $\hat{e}_0$ . Thus  $[\hat{v} \hat{v}^T]$  is a constant multiple of the matrix  $[\hat{e}_0 \hat{v}^T + \hat{v} \hat{e}_0^T]$  only if  $\hat{v}$  and  $\hat{e}_0$  are multiples (where the multiple is  $\pm 1$  since  $\hat{v}$  and  $\hat{e}_0$  are unit vectors) of each other.

Now, if  $\hat{v} = \pm \hat{e}_0$ , one may show that the expression in (K.1.12) is zero. So, we conclude that (K.1.12) is zero (or, equivalently,  $R^2$  is preserved under reflection) whenever

$$\begin{aligned}
s_B^2 &= 1 \iff M_{\infty} = 0 \\
\text{or} \quad \hat{e}_0 \cdot \hat{v} &= 0 \\
\text{or} \quad \hat{e}_0 \cdot \hat{v} &= \pm 1
\end{aligned} \tag{K.1.13}$$

Next let us consider the  $\hat{n} \cdot \tilde{\nabla}(1/R)$  term of (K.1.5). For any vector or dual vector  $\tilde{V}$ , such as a normal vector, tangent vector, or gradient, which remains fixed under a translation of the coordinate system, its reflection  $\tilde{V}'$  in the plane defined by  $\hat{v}$  is given by

$$\tilde{V}' = [1 - 2\hat{v}\hat{v}^T] \tilde{V} \tag{K.1.14}$$

Note that, because  $\tilde{V}$  remains fixed under coordinate translation, (K.1.14) holds for any coordinate system, whereas (K.1.2) only holds if the origin lies on the plane of symmetry.

$$\begin{aligned} \text{So, } \hat{n}' \cdot \vec{v}' &= \{[I - 2\hat{v}\hat{v}^T] \hat{n}\} \cdot [I - 2\hat{v}\hat{v}^T] \vec{v} = \\ \hat{n}^T [I - 4\hat{v}\hat{v}^T + 4\hat{v}\hat{v}^T \hat{v}\hat{v}^T] \vec{v} &= \hat{n} \cdot \vec{v} \end{aligned} \quad (\text{K.1.15})$$

Thus all the quantities in (K.1.5) are preserved under reflection, and so  $\phi(P)$  is preserved also. It follows from (K.1.14-15) that  $\hat{n} \cdot \vec{v}$  and  $\vec{t} \cdot \vec{v}$  (for any tangent vector  $\vec{v}$ ) are also preserved under reflection. Thus the quantities

$$\begin{aligned} \vec{w} \cdot \hat{n} &= \hat{n} \cdot \vec{w} \\ \vec{v} \cdot \hat{n} &= \hat{n} \cdot \vec{v} \\ \text{and} \quad \vec{t} \cdot \vec{v} &= \vec{t} \cdot \vec{v} \end{aligned}$$

are all preserved under reflection. Thus the left hand side of arbitrary boundary condition equation

$$a_A w_A n + c_A \phi_A + \vec{t}_A \cdot \vec{v}_A + a_D \sigma + c_D u + \vec{t}_D \cdot \vec{v}_D = b \quad (\text{K.1.17})$$

is also preserved.

To be precise, the row vector defining the dependence of (K.1.17) on the set of singularity parameters is preserved under reflection. That is, let us define  $\text{AIC}$  to be the row vector defined by specifying the left hand side of (K.1.17) at a control point, and partition  $\text{AIC}$  into portions corresponding to real and image singularity parameters:

$$[\text{AIC}] \vec{x} = [\text{AIC}_1 \quad \text{AIC}_2] \begin{Bmatrix} x_1 \\ x_2 \end{Bmatrix} \quad (\text{K.1.18})$$

Then  $[\text{AIC}']$ , defining the left hand side of (K.1.17) at the image of the real control point, is partitioned as

$$[\text{AIC}'] = [\text{AIC}_2 \quad \text{AIC}_1] \quad (\text{K.1.19})$$

We now apply (K.1.18) to each "real" control point, and (K.1.19) to each image control point, and thus obtain the partition (5.7.5) of the AIC matrix. We have thus shown that the basic symmetry principle, given by (K.1.1-2) or (5.7.5), follows from the conditions (K.1.13). This concludes our discussion of the case of one plane of symmetry.

#### K.1.2 Two Planes of Symmetry

We now determine the restrictions under which  $R^2$  and related quantities are preserved under reflection in two planes of symmetry. We see immediately that there are two ways to reflect a point  $P$  in two planes of symmetry. We

may reflect the point in the first plane and then in the second plane, or vice versa. Assuming the origin lies on both planes, we obtain two reflected points (see figure K.2):

$$\begin{aligned}\vec{p}(3) &= [I - 2 \hat{v}_2 \hat{v}_2^T] [I - 2 \hat{v}_1 \hat{v}_1^T] \vec{p} \\ \vec{p}(3)' &= [I - 2 \hat{v}_1 \hat{v}_1^T] [I - 2 \hat{v}_2 \hat{v}_2^T] \vec{p}\end{aligned}\quad (K.1.20)$$

For reflection in two planes of symmetry to make sense,  $\vec{p}(3)$  and  $\vec{p}(3)'$  must be the same point. That is, the two matrix products in (K.1.20) must be identical, or

$$\begin{aligned}I - 2[\hat{v}_2 \hat{v}_2^T] - 2[\hat{v}_1 \hat{v}_1^T] + 4[\hat{v}_2 \hat{v}_2^T \hat{v}_1 \hat{v}_1^T] \\ = I - 2[\hat{v}_1 \hat{v}_1^T] - 2[\hat{v}_2 \hat{v}_2^T] + 4[\hat{v}_1 \hat{v}_1^T] [\hat{v}_2 \hat{v}_2^T]\end{aligned}\quad (K.1.21)$$

Equation (K.1.21) holds when

$$(\hat{v}_1, \hat{v}_2) [\hat{v}_1 \hat{v}_2^T] = (\hat{v}_1, \hat{v}_2) [\hat{v}_2 \hat{v}_1^T] \quad (K.1.22)$$

Since every column of the first matrix is a multiple of  $\hat{v}_1$ , and every column of the second matrix is a multiple of  $\hat{v}_2$ , equation (K.1.22) holds when

$$\hat{v}_1 \cdot \hat{v}_2 = 0$$

or

$$\hat{v}_1 = \pm \hat{v}_2 \quad (K.1.23)$$

The second equation above corresponds to two identical planes of symmetry, and thus can be neglected. So, applying the first equation to (K.1.20), we have

$$\begin{aligned}[I - 2\hat{v}_1 \hat{v}_1^T] [I - 2\hat{v}_2 \hat{v}_2^T] &= \\ [I - 2\hat{v}_1 \hat{v}_1^T - 2\hat{v}_2 \hat{v}_2^T]\end{aligned}\quad (K.1.24)$$

$$\text{or} \quad \vec{p}(3) = \vec{p}(3)' = [I - 2\hat{v}_1 \hat{v}_1^T - 2\hat{v}_2 \hat{v}_2^T] \vec{p} \quad (K.1.25)$$

Now, in analogy to (K.1.7),  $R^2$  is preserved under reflection in both planes of symmetry if

$$[C_0] = [I - 2\hat{v}_1 \hat{v}_1^T - 2\hat{v}_2 \hat{v}_2^T] [C_0] [I - 2\hat{v}_1 \hat{v}_1^T - 2\hat{v}_2 \hat{v}_2^T] \quad (K.1.26)$$

Now just as (K.1.7) holds whenever (K.1.13) does, (K.1.26) also holds whenever (K.1.13) holds for both  $\hat{v}_1$  and  $\hat{v}_2$ . Applying (K.1.9) and (K.1.24) to (K.1.26), one can also show that (K.1.13) follows, for both  $\hat{v}_1$  and  $\hat{v}_2$ , from (K.1.26).

Summarizing,  $R^2$  is preserved under reflection in both planes of symmetry if

$$\hat{c}_1 \cdot \hat{c}_2 = 0 \quad (K.1.27a)$$

$$\text{and} \quad \hat{c}_i \cdot \hat{c}_0 = 0 \text{ or } \pm 1 \quad i = 1, 2 \quad (K.1.27b)$$

$$\text{or} \quad M_\infty = 0$$

It is now completely straightforward, following the arguments of section K.1.1, to show that the arbitrary boundary condition expression (K.1.17) is preserved under two reflections.

The requirements imposed on a program user are somewhat more stringent than indicated by (K.1.27). They are:

$$(\hat{c}_1, \hat{c}_2) = 0$$

$$\text{and} \quad (\hat{c}_i, \hat{c}_0) = 0 \quad i = 1, 2 \quad (K.1.28)$$

regardless of Mach number. That is, the normals and compressibility vector are mutually perpendicular. This is not actually a restriction at Mach zero, since all "compressibility directions" are equivalent and  $\hat{c}_0$  is only defined to avoid making  $M_\infty = 0$  a special case in the operation of the program. The angles of attack and sideslip used to define the freestream direction ( $\alpha$  and  $\beta$  in section B.2 of the User's Manual) may thus be different from the angles ( $\alpha_c$  and  $\beta_c$ ) defining the compressibility direction. In the special case of Mach zero, this involves no loss of accuracy.

### K.1.3 Application

We partition a configuration with two planes of symmetry into four quadrants as shown in figure K.2, also referring to the real configuration as the "first image." We partition a row  $\underline{AIC}^{(1)}$  of the AIC matrix pertaining to a real control point as

$$\underline{AIC}^{(1)} = \underline{AIC}_1 \quad AIC_2 \quad AIC_3 \quad AIC_4 \quad (K.1.29)$$

where the  $i$ th partition defines the dependence on the singularities in the  $i$ th image.

Now, applying the results of section K.1.1 to the first plane, the row vector  $\underline{AIC}^{(2)}$  pertaining to the reflection of the control point in the first plane, is given by

$$\underline{AIC}^{(2)} = \underline{AIC}_2 \quad AIC_1 \quad AIC_4 \quad AIC_3 \quad (K.1.30)$$



Similarly,  $\underline{AIC}^{(A)}_1$ , pertaining to the reflection of the control point in the second plane, is given by

$$\underline{AIC}^{(A)}_1 = \underline{AIC}_4 \ AIC_3 \ AIC_2 \ AIC_1 \quad (K.1.31)$$

Finally, applying the results of section (K.1.2) we compute the row vector  $\underline{AIC}^{(3)}_1$  pertaining to the reflection of the control point in both planes:

$$\underline{AIC}^{(3)}_1 = \underline{AIC}_3 \ AIC_4 \ AIC_1 \ AIC_2 \quad (K.1.32)$$

Now, applying (K.1.29-K.1.32) to every real and image control point, the fundamental system (5.7.4) of linear equations can be partitioned as

$$\begin{bmatrix} AIC_1 & AIC_2 & AIC_3 & AIC_4 \\ AIC_2 & AIC_1 & AIC_4 & AIC_3 \\ AIC_3 & AIC_4 & AIC_1 & AIC_2 \\ AIC_4 & AIC_3 & AIC_2 & AIC_1 \end{bmatrix} \begin{bmatrix} \vec{\lambda}(1) \\ \vec{\lambda}(2) \\ \vec{\lambda}(3) \\ \vec{\lambda}(4) \end{bmatrix} = \begin{bmatrix} \vec{b}(1) \\ \vec{b}(2) \\ \vec{b}(3) \\ \vec{b}(4) \end{bmatrix} \quad (K.1.33)$$

where  $\vec{\lambda}(i)$  and  $\vec{b}(i)$  are, respectively, the vector of singularity parameters and the vector of constraints for the  $i$ th image, where the first ( $i = 1$ ) image corresponds to the real configuration.

Now, adding the four systems of equations given by (K.1.33) yields

$$[AIC_1 + AIC_2 + AIC_3 + AIC_4] \begin{bmatrix} \vec{\lambda}(1) + \vec{\lambda}(2) \\ \vec{\lambda}(3) + \vec{\lambda}(4) \end{bmatrix} = \begin{bmatrix} \vec{b}(1) + \vec{b}(2) \\ \vec{b}(3) + \vec{b}(4) \end{bmatrix} \quad (K.1.34)$$

Adding the first and fourth, subtracting the second and third, we get

$$[AIC_1 - AIC_2 - AIC_3 + AIC_4] \begin{bmatrix} \vec{\lambda}(1) - \vec{\lambda}(2) \\ -\vec{\lambda}(3) + \vec{\lambda}(4) \end{bmatrix} = \begin{bmatrix} \vec{b}(1) - \vec{b}(2) \\ -\vec{b}(3) + \vec{b}(4) \end{bmatrix} \quad (K.1.35)$$

Adding the first and third, subtracting the second and fourth, gives

$$[AIC_1 - AIC_2 + AIC_3 - AIC_4] \begin{bmatrix} \vec{\lambda}(1) - \vec{\lambda}(2) \\ \vec{\lambda}(3) - \vec{\lambda}(4) \end{bmatrix} = \begin{bmatrix} \vec{b}(1) - \vec{b}(2) \\ \vec{b}(3) - \vec{b}(4) \end{bmatrix} \quad (K.1.36)$$

Finally, adding the first and second, subtracting the third and fourth, gives

$$[AIC_1 + AIC_2 - AIC_3 - AIC_4] \begin{Bmatrix} \vec{\lambda}(1) + \vec{\lambda}(2) \\ -\vec{\lambda}(3) - \vec{\lambda}(4) \end{Bmatrix} = \begin{Bmatrix} \vec{b}(1) + \vec{b}(2) \\ -\vec{b}(3) - \vec{b}(4) \end{Bmatrix} \quad (K.1.37)$$

Thus we have split the system (K.1.33) of  $4N$  equations in  $4N$  variables into 4 individual systems of  $N$  equations in  $N$  variables. The resulting benefits in efficiency are quite clear. First, we need only compute one fourth as many entries of the AIC matrix. Second, each system of equations costs approximately  $1/64$  as much to solve (since  $4^3 = 64$ ), though there are now four of them. Thus the equation solution cost is cut by a factor of 16.

When flow symmetry occurs, simplification may be made. For instance, if the flow is symmetric about the second plane of symmetry,  $\vec{b}^{(1)} = \vec{b}^{(4)}$  and  $\vec{b}^{(2)} = \vec{b}^{(3)}$ . Thus the right hand sides of (K.1.36) and (K.1.37) are zero, and so we need not compute the combinations on the left to see that

$$\begin{aligned} \vec{\lambda}(3) &= \vec{\lambda}(2) \\ \vec{\lambda}(4) &= \vec{\lambda}(1) \end{aligned} \quad (K.1.38)$$

Solving (K.1.34) and (K.1.35) yields solutions for  $\vec{\lambda}(1) + \vec{\lambda}(4)$  and  $\vec{\lambda}(2) + \vec{\lambda}(3)$ , and then (K.1.38) may be used to compute all four  $\vec{\lambda}(i)$  individually.

#### K.1.4 Networks Lying on a Plane of Symmetry

Under certain circumstances it may be of use to place a network on a plane of symmetry. Consider for example the case of a thick vertical tail, illustrated in cross-section in figure K.3. One may wish to represent this as a thin tail, in which case a special procedure must be undertaken.

The reason for this procedure is the following. Let us consider the configuration in figure K.3 in the limiting case as the space between the vertical tail network and its reflected image becomes smaller and smaller. We see that along the horizontal line, the potential approaches values  $\phi$  and  $\phi'$  on the two exterior surfaces. But as the surface and its image approach each other, the interior potential  $\phi_0$  may take on any value.

We know that, by definition

$$\begin{aligned}\mu &= \phi - \phi_0 \\ \mu' &= \phi' - \phi_0\end{aligned}\quad (K.1.39)$$

where  $\mu$  and  $\mu'$  are the limiting values of doublet strength on the two approaching surfaces. Thus we have

$$\mu - \mu' = \phi - \phi' \quad (K.1.40)$$

But there are infinitely many solutions of the potential flow problem which satisfy (K.1.40), since  $\phi_0$  may take on any value without changing the character of the flow. Thus in the limit as the two surfaces approach each other, there are infinitely many solutions to the potential flow problem. It is therefore necessary to make the problem unique by specifying another relation between  $\mu$  and  $\mu'$ . We consider the formulation of the AIC matrix in the presence of a symmetry plane in determining this relation.

So far, our recombined boundary condition equations always relate to the vectors  $\lambda \neq \lambda'$  in the case of one plane of symmetry (see equations (5.7.7-8)). Thus it is convenient to specify a relation between  $\mu$  and  $\mu'$  on a network which is also of this form. That relation is

$$\mu + \mu' = 0 \quad (K.1.41)$$

Next let us consider the behavior of the source strength as the network in figure K.3 approaches its image. We have

$$\begin{aligned}\sigma &= \hat{n} \cdot \vec{\nabla} \phi - \hat{n}' \cdot \vec{\nabla} \phi_0 \\ \sigma' &= \hat{n}' \cdot \vec{\nabla} \phi' - \hat{n} \cdot \vec{\nabla} \phi_0\end{aligned}\quad (K.1.42)$$

$$= -\hat{n} \cdot \vec{\nabla} \phi' + \hat{n} \cdot \vec{\nabla} \phi_0 \quad (K.1.43)$$

Thus

$$\sigma + \sigma' = \hat{n} \cdot \vec{\nabla} \phi - \hat{n} \cdot \vec{\nabla} \phi' \quad (K.1.44)$$

while the quantity  $\sigma - \sigma'$  is free to take on any value without changing the flow solution since  $\sigma - \sigma'$  can be varied by changing the flow solely in the infinitely small region between the network and its image. So, analogously to the case of doublets, the boundary condition

$$\sigma - \sigma' = 0 \quad (K.1.45)$$

is imposed on networks which lie on a plane of symmetry.

The imposition of (K.1.41) or (K.1.45) is a case for which a row of the matrix  $AIC_1 + AIC_2$  is computed differently from the corresponding row of  $AIC_1 - AIC_2$ . That is, a user-specified boundary condition equation of the standard form (5.6.1) is overridden by the imposition of the equation (K.1.41) or (K.1.45). The other case in which the corresponding rows of the two matrices are computed differently matching boundary condition at a plane of symmetry, is discussed in section K.5.

The discussion above notes the special procedures which must be undertaken if a network lies infinitely close to (that is, on) a plane of symmetry. The same situation would occur if two distinct networks, both of which have a non-zero doublet distribution, or both of which have a non-zero source distribution, lie infinitely close to each other (that is, are superimposed). This is because a plane of symmetry in effect produces a second, or image, network.

The difference between the two cases is that the superposition of two user-defined networks (except of source-alone superposed on doublet alone) is impermissible. No attempt is made by the program to determine that such a superposition has occurred, so if it does occur, the only error diagnostic given the user is that the AIC matrix is singular.

## K.2 Known Singularity Parameters

If the boundary condition at a control point is

$$a_D \sigma = b$$

or  $c_D \mu = b$  (K.2.1)

as in equation (5.7.14), the source strength or doublet strength at the "hypothetical location" of the control point (the grid point from which the control point has been receded slightly) is specified. This does not necessarily define a known singularity parameter, however.

In order for specification of the source or doublet strength at a point to define a known singularity parameter, two conditions must be satisfied. First, a source or doublet parameter must be located at the point. Second, the value of the parameter must be the source or doublet strength at the point.

For simplicity, known singularity parameters are defined by the program in only two cases. A known source or doublet parameter is defined when source strength or doublet strength is specified at a panel center control point of a source or doublet analysis network. Reference to figures D.1 and D.2 shows that these are always source or doublet parameter locations.

Next, known doublet parameters are defined whenever a portion of a network edge forms an "abutment with empty space," that is, an abutment containing no other network edges. In the case of a corner point, the corresponding singularity parameter is always located at the end point of an edge spline, and thus (see section 1.1.2) has a value equal to the doublet strength at the point. If a segment of a network edge belongs to an empty space abutment, the doublet strength is zero on the entire segment, and so all the doublet parameters on the edge are zero, and are thus set to zero by the program.

Known singularity parameters could conceivably be defined in one or two other special cases (for example, source strength specification at a corner point of a source design network). This is not done because of the rarity with which such measures would be used.

### K.3 Aerodynamic Boundary Conditions

Appendix J was devoted to the computation of the panel influence coefficient matrices  $[PIC^S]$  and  $[PIC^D]$ . We now outline the assembly of the aerodynamic influence coefficient matrix from the PIC matrices. This process is discussed in considerably more detail in the Maintenance Document (section 5).

#### K.3.1 Combining for Symmetry

The program ultimately deals with combinations of portions of the AIC matrix of the form

$$AIC_1 \pm AIC_2 \pm AIC_3 \pm AIC_4 \quad (K.3.1)$$

as discussed in section K.1.3. When flow symmetry occurs, not all these combinations are needed. Thus it is advisable to put influence coefficients in their combined form as early as possible. For example, we may multiply PIC matrices by outer spline matrices (see section K.3.2) first, assemble the products into partitions of the AIC matrix, and then recombine the partitions as in (K.3.1). On the other hand, we can recombine the PIC matrices, and assemble the recombined AIC matrices from those.

The latter method is more efficient in cases of flow symmetry (since there are fewer recombined partitions than there were original partitions) and is implemented in PAN AIR. For more details, see the discussion in the Maintenance Document of SUBROUTINE IC of the MAG module. Thus the program computes the influences  $[PIC_i]$  of a panel and its images on a control point, and hence computes recombined matrices

$$PIC_1 \pm PIC_2 \pm PIC_3 \pm PIC_4 \quad (K.3.2)$$

All the remaining manipulations involved in assembling the AIC partitions are performed on the recombined matrices.

#### K.3.2 Computing Influences of Image Panels

Given the geometry data for a panel and for a control point, there are two ways to measure the influence of an image of the panel on the control point. One is to reflect the panel geometry in the plane of symmetry. But since there are hundreds of precomputed panel geometry quantities, this would be quite inefficient. Thus PAN AIR measures the influence of the original panel on the reflected image of the control point.

But while  $\phi$ ,  $\vec{r} \cdot \vec{v}$ , and  $\vec{v} \cdot \hat{n}$  are preserved under reflection, (cf., section K.1), it follows from (K.1.14) that the velocity vector  $\vec{v}$  is not. For,

$$\vec{v} = \vec{v}_\phi \quad (K.3.3)$$

and thus its image  $\vec{v}'$  in one plane of symmetry is given by

$$\vec{v}' = \vec{v} \phi = [I - 2\hat{v}\hat{v}^T] \vec{v} \phi = [I - 2\hat{v}\hat{v}^T] \vec{v} \quad (\text{K.3.4})$$

where  $\vec{v}'$  is the image of  $\vec{v}$  under reflection, and since  $[I - 2\hat{v}\hat{v}^T]$  is not the identity,  $\vec{v}'$  need not equal  $\vec{v}$ .

We recall (cf., (5.6.8)) the definition of the PIC matrices:

$$\begin{bmatrix} \phi \\ v_x \\ v_y \\ v_z \end{bmatrix} = [\text{PIC}^S] \begin{bmatrix} \sigma_1 \\ \vdots \\ \sigma_4 \\ \sigma_9 \end{bmatrix} + [\text{PIC}^D] \begin{bmatrix} \mu_1 \\ \vdots \\ \mu_9 \end{bmatrix} \quad (\text{K.3.5})$$

Now suppose that the influence of a panel on the image of a control point is given by a matrix PIC. Then by (K.3.4-5), the influence PIC' of the reflected image of the panel on the control point is given by

$$[\text{PIC}'] = [Y] [\text{PIC}] \quad (\text{K.3.6})$$

where

$$[Y]_{4 \times 4} = \begin{bmatrix} 1 & 0 & 0 & 0 \\ 0 & \vdots & & \\ 0 & I - 2\hat{v}\hat{v}^T & & \\ 0 & & & \end{bmatrix} \quad (\text{K.3.7})$$

where  $v$  is the unit normal to the plane of symmetry.

It is straightforward to show that if the panel is reflected in both planes of symmetry, (K.3.6) holds with

$$[Y] = \begin{bmatrix} 1 & 0 & 0 & 0 \\ 0 & \vdots & & \\ 0 & I & -2\hat{v}_1 & \hat{v}_1^T \\ 0 & & -2\hat{v}_2 & \hat{v}_2^T \end{bmatrix} \quad (\text{K.3.8})$$

### K.3.3 Partial Rows

Recall from section 5.5 the outer spline matrices  $[B^S]$  and  $[B^D]$  which give the dependence of the panel source and doublet parameters on singularity parameters located in the neighborhood of the panel. Combining (5.5.8) and (K.3.5) we get the perturbation potential and velocity induced by a panel on a control point  $P$  as

$$\begin{Bmatrix} \phi(P) \\ \vec{V}(P) \end{Bmatrix} = [PRW]^{4 \times (k_s + k_d)} \begin{Bmatrix} \lambda_1^S \\ \vdots \\ \lambda_{k_s}^S \\ \lambda_1^D \\ \vdots \\ \lambda_{k_d}^D \end{Bmatrix} \quad (K.3.9)$$

where  $k_s$  and  $k_d$  are the number of source and doublet parameters on which the panel depends, and  $PRW$  is the "partial row" matrix defined by

$$[PRW] = \begin{bmatrix} [PICS \ B^S]^{4 \times k_s} & [PICD \ B^D]^{4 \times k_d} \end{bmatrix} \quad (K.3.10)$$

That is, the partial row matrix defines the contribution which a single panel makes to the rows of the  $\phi IC$  and  $VIC$  matrices corresponding to the control point. Thus the number of columns in the partial row matrix equals the number of singularity parameters on which the panel depends. This contrasts with the rows of the  $\phi IC$  and  $VIC$  matrices corresponding to the control point. These rows describe the influence of the entire configuration, and thus have as many columns as there are singularity parameters in the configuration. In writing (K.3.10) we have assumed no configuration symmetry. In the presence of symmetry (K.3.10) holds with recombined  $PIC$  matrices and recombined partial row matrices replacing  $PICS$ ,  $PICD$ , and  $PRW$ .

### K.3.4 Data Manipulation Problems

The assembly of partial row matrices  $PRW$  into  $\phi IC$  and  $VIC$  matrices poses data manipulation problems which are not truly within the scope of this document. We will, however, briefly outline the problems here.

First, approximately 1700 numbers (spline matrices, geometry data, etc) are precomputed and stored for each panel, in order to make  $PIC$  computation as efficient as possible. These quantities are stored on a disk, and must be retrieved when the influence of the panel on a control point must be measured. Thus it is advantageous to compute the influence of one panel on a sequence of control points.

On the other hand, the entire  $\phi IC$  and  $VIC$  matrices for the entire set of control points on the configuration can not be kept in core at once. Thus portions of these matrices must be retrieved from and stored on a disk as



well. One may reach the conclusion that both a "row-wise" method of computing influence coefficients, in which the influence of every panel on a control point is measured before passing to the next control point, and a "column-wise" method, in which the influence of a panel on every control point is measured before moving to the next panel, are inefficient.

An intermediate "partitioned column" method can be seen to be more efficient for all but the smallest cases. In this method, a block of control points, to which correspond several rows of the  $\phi$ IC and VIC matrices, is chosen, the influence of a panel is measured and accumulated to the  $\phi$ IC and VIC matrices for every control point in the block, then another panel is considered, until the influence of all panels has been measured, and the rows of  $\phi$ IC and VIC corresponding to all the control points in the block has been computed. The program thereupon proceeds to the next block of control points.

The value of the partitioned column method can be seen when estimating the volume of data transferred for large cases. For the row-wise and column-wise methods, this volume is proportional to the cube of the number of panels, while for the partitioned column method it is proportional to the number of panels squared. More details of the methods are provided in the discussion of the MAG module in the Maintenance Document.

#### K.3.5 Imposition of the Boundary Conditions

Given the  $(1 \times N)$   $\phi$ IC and  $(3 \times N)$  VIC matrix for a control point P, a row of the  $A$  matrix is obtained from an arbitrary boundary condition expression of the form (K.1.17) as specified in section 5.7. The first three  $(1 \times N)$  row vectors in equation (5.7.1) clearly express  $a_A \bar{w}_A \cdot \hat{n}$ ,  $c_A \phi_A$  and  $t_A \cdot \bar{v}_A$  at the control point in terms of the set of singularity parameters. That the fourth and fifth terms of (5.7.1) express  $a_D \sigma$  and  $c_D \mu$  follows from (5.6.2) and the analogous equation for doublet strength.

$$\mu(P) = \begin{bmatrix} 1 & \xi' & \eta' & 1/2 \xi'^2 & \xi' \eta' & 1/2 \eta'^2 \end{bmatrix} [\text{SPSPLD}] [BD] \cdot \begin{Bmatrix} D \\ \lambda_1 \\ \vdots \\ D \\ \lambda_{21} \end{Bmatrix} \quad (K.3.11)$$

Finally, we must show that the last term in (5.7.1) expresses  $\bar{t}_D \cdot \bar{\nabla} \mu$ . Since

$$[\text{SPSPLD}]^{6 \times 9} [BD]^{9 \times N} \bar{\lambda}^{N \times 1} = \begin{Bmatrix} \mu_0 \\ \mu_\xi \\ \vdots \\ \mu_{\eta\eta} \end{Bmatrix} \quad (K.3.12)$$

we need only show that

$$\vec{\nabla}_u = [A^T] \begin{bmatrix} 0 & 1 & 0 & \xi' & \eta' & 0 \\ 0 & 0 & 1 & 0 & \xi' & \eta' \\ 0 & 0 & 0 & 0 & 0 & 0 \end{bmatrix} \begin{Bmatrix} \mu_0 \\ \mu_\xi \\ \mu_\eta \\ \mu_{\eta\eta} \end{Bmatrix} \quad (K.3.13)$$

But by definition,

$$\vec{\nabla}_u = \begin{Bmatrix} \partial u / \partial x_0 \\ \partial u / \partial y_0 \\ \partial u / \partial z_0 \end{Bmatrix} \quad (K.3.14)$$

where  $(x_0, y_0, z_0)$  are reference coordinates.

According to appendix E, the gradient operator in reference coordinates is a dual vector, and transforms by

$$\vec{\nabla} = A^T \begin{Bmatrix} \partial / \partial \xi' \\ \partial / \partial \eta' \\ \partial / \partial \zeta' \end{Bmatrix} \quad (K.3.15)$$

where A transforms reference coordinates to local coordinates. For completeness, we prove (K.3.15) here. Let  $f(\xi', \eta', \zeta')$  be an arbitrary function. Then

$$\frac{\partial f}{\partial x_0} = \frac{\partial f}{\partial \xi'} \frac{\partial \xi'}{\partial x_0} + \frac{\partial f}{\partial \eta'} \frac{\partial \eta'}{\partial x_0} + \frac{\partial f}{\partial \zeta'} \frac{\partial \zeta'}{\partial x_0} \quad (K.3.16)$$

$$\text{But } \begin{Bmatrix} \xi' \\ \eta' \\ \zeta' \end{Bmatrix} = [A] \begin{Bmatrix} x_0 - x_c \\ y_0 - y_c \\ z_0 - z_c \end{Bmatrix} \quad (K.3.17)$$

where  $\begin{Bmatrix} x_c \\ y_c \\ z_c \end{Bmatrix}$  is the origin of the local coordinate system

$$\text{So, } \frac{\partial f}{\partial x_0} = [A_{11} \ A_{21} \ A_{31}] \begin{Bmatrix} \partial f / \partial \xi' \\ \partial f / \partial \eta' \\ \partial f / \partial \zeta' \end{Bmatrix} \quad (K.3.18)$$

We obtain similar equations for the y and z derivatives. Combining,

$$\vec{\nabla} f = \begin{Bmatrix} \partial f / \partial x_0 \\ \partial f / \partial y_0 \\ \partial f / \partial z_0 \end{Bmatrix} = [A^T] \begin{Bmatrix} \partial f / \partial \xi' \\ \partial f / \partial \eta' \\ \partial f / \partial \zeta' \end{Bmatrix} \quad (\text{K.3.19})$$

which is equivalent to (K.3.15)

Now, by definition,

$$\mu(\xi', \eta') = \mu_0 + \mu_\xi \xi' + \mu_\eta \eta' + 1/2 \mu_{\xi\xi} \xi'^2 + \mu_{\xi\eta} \xi' \eta' + 1/2 \mu_{\eta\eta} \eta'^2 \quad (\text{K.3.20})$$

Thus

$$\begin{aligned} \frac{\partial \mu}{\partial \xi'} &= \mu_\xi + \mu_{\xi\xi} \xi' + \mu_{\xi\eta} \eta' \\ \frac{\partial \mu}{\partial \eta'} &= \mu_\eta + \mu_{\xi\eta} \xi' + \mu_{\eta\eta} \eta' \\ \frac{\partial \mu}{\partial \zeta'} &= 0 \end{aligned} \quad (\text{K.3.21})$$

Equivalently,

$$\begin{Bmatrix} \partial \mu / \partial \xi' \\ \partial \mu / \partial \eta' \\ \partial \mu / \partial \zeta' \end{Bmatrix} = \begin{bmatrix} 0 & 1 & 0 & \xi' & \eta' & 0 \\ 0 & 0 & 1 & 0 & \xi' & \eta' \\ 0 & 0 & 0 & 0 & 0 & 0 \end{bmatrix} \begin{Bmatrix} \mu_0 \\ \mu_\xi \\ \mu_\eta \\ \mu_{\xi\xi} \\ \mu_{\xi\eta} \\ \mu_{\eta\eta} \end{Bmatrix} \quad (\text{K.3.22})$$

Combining (K.3.15) and (K.3.22) yields (K.3.13).

#### K.4 Closure

The closure boundary condition (see (5.7.3) or (H.2.4)) may be imposed in place of a source or doublet matching boundary condition at the control points on a matching edge of a source or doublet design network. The boundary condition is

$$\iint (a_A \hat{w}_A \cdot \hat{n} + a_D \sigma) dS = b$$

(K.4.1)

column  
or row

where the column or row of panels is that one which is headed by the edge control point.

The row vector which defines the integral above in terms of the singularity parameters is computed by approximating the average normal mass flux and source strength on a panel by their values at the panel center. That is, we assume

$$\iint (a_A \hat{w}_A \cdot \hat{n} + a_D \sigma) dS = \sum_{\text{panels}} A_i (a_A \tilde{n}_i^T [\text{VIC}_i] + [1 \ \xi_i' \ n_i'] [\text{SPSPL}_i^S] [B_i^S]) \vec{\lambda}$$

(K.4.2)

Here  $A_i$  is the area of the  $i$ th subpanel,  $\text{VIC}_i$  is the VIC matrix for the control point at its center,  $(\xi_i', n_i')$  are its local coordinates,  $[\text{SPSPL}_i^S]$  the source subpanel spline matrix for the subpanel in which the control point lies, and  $B_i^S$  the  $5 \times N$  matrix ( $N$  the total number of singularity parameters) which is the extension of the panel's outer spline matrix from 9 columns to  $N$  columns. Thus the row of the AIC matrix corresponding to the closure boundary condition is given by the row vector multiplying  $\vec{\lambda}$  on the right side of (K.4.2).

## K.5 Matching

The conversion of a doublet matching boundary condition

$$\sum s_j \mu_j = 0 \quad (K.5.1)$$

into a row of the aerodynamic influence coefficient matrix is straightforward in light of (K.3.11). Further, if there is one plane of symmetry, and the abutment is located away from the plane of symmetry (as illustrated in cross-section by abutment  $A_1$  in figure K.4), one also wishes to impose the boundary condition

$$\sum s_j \mu_j' = 0 \quad (K.5.2)$$

where the  $\mu_j$  are the values of doublet strength at the reflected images of the original points. Equation (K.5.2) insures doublet matching at the abutment  $A_1$  which is the image of  $A_1$ .

In fact, (K.5.1-2) are imposed in the recombined form in consideration of symmetry:

$$\sum s_j (\mu_j + \mu_j') = 0 \quad (K.5.3a)$$

$$\sum s_j (\mu_j - \mu_j') = 0 \quad (K.5.3b)$$

analogously to (5.7.7-8) or (K.1.34-37).

But now consider the abutment  $A_2$  in figure K.4. If the boundary condition

$$\mu_4 - \mu_4' + \mu_5 - \mu_5' = 0 \quad (K.5.4)$$

is imposed there, doublet matching is correctly imposed, and there is no need for another doublet matching boundary condition. So, we have a boundary condition of the form (K.5.3a), but none of the form (K.5.3b). Instead, the row of the matrix  $AIC_1 + AIC_2$  corresponding to this matching boundary condition is generated from a standard user-specified boundary condition of the form (5.6.1).

Finally we consider the case of an abutment which lies in both planes of symmetry, as illustrated in figure K.5. The single boundary condition

$$\mu(1) - \mu(2) + \mu(3) - \mu(4) = 0 \quad (K.5.5)$$

results in doublet matching along the entire abutment A. Thus a row of  $AIC_1 - AIC_2 + AIC_3 - AIC_4$  is constructed which specifies (K.5.5). Here, the corresponding rows of the three matrices  $AIC_1 + AIC_2 + AIC_3 + AIC_4$ , etc, are computed by implementing the standard user-specified boundary condition (5.6.1).

## K.6 The Update Capability

The purpose of the influence coefficient update capability is to permit a program user to make changes in the geometry (or, occasionally, the left hand side of the boundary condition equation (5.6.1)) of a portion of a configuration, and to solve the resulting potential flow problem more economically by making use of the previous solution.

The program user specifies certain networks as "updateable", that is, subject to future modification, when specifying the original potential flow problem. The program then identifies each control point and each singularity parameter as either "updateable" or "non-updateable", and resequences them so that the updateable ones occur last. The resulting AIC matrix can then be partitioned

$$[AIC] = \begin{bmatrix} AIC_{NU} & AIC_{U,1} \\ \hline AIC_{U,2} & AIC_{U,3} \end{bmatrix} \quad (K.6.1)$$

When the modified flow problem is solved, the matrix  $AIC_{NU}$  remains unchanged, and need not be recomputed. Only the matrices  $AIC_{U,i}$ ,  $i = 1, 2, 3$ , defining the influence of the updateable portion of the configuration, and the influence on the updateable portion, need to be computed. Thus, if  $r$  is the fraction of the configuration which is non-updateable, a proportion of the AIC computation of size  $r^2$  is saved.

The imposition of doublet matching causes the specification of updateable control points and singularity parameters to be non-trivial. Clearly every control point and singularity parameter on an updateable network is itself updateable. In addition, though, control points on an edge of a non-updateable network which abuts an updateable network must be made updateable. This arises from the possibility that the abutment in question may change by the addition, deletion, or change in panel density, of the updateable network. As a result, the boundary conditions on the edge of the non-updateable network may change from matching to a standard aerodynamic boundary condition (5.6.1) or vice versa.

In addition, the modification of the updateable network may cause the definition or deletion of extra singularity parameters on the edge of the non-updateable network (see figure K.6). Thus the edge spline on this edge may change, and so the singularity parameters on this edge must be specified as updateable.

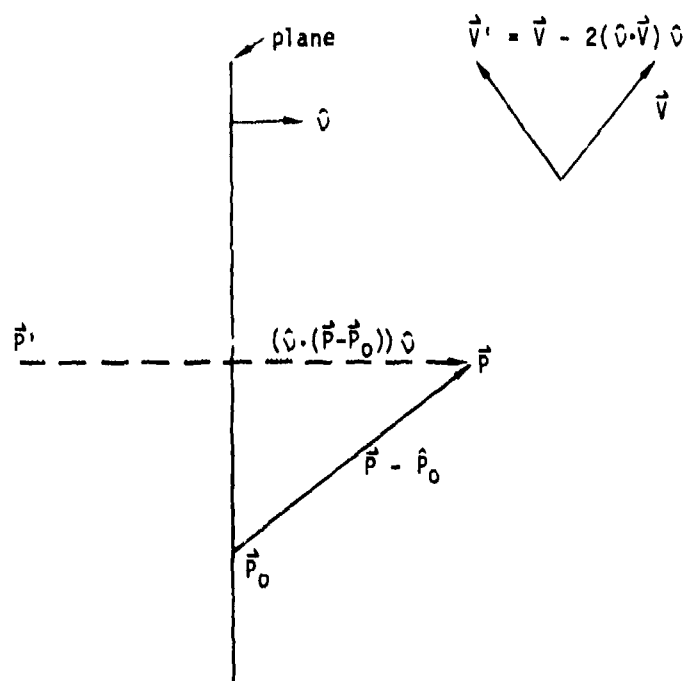


Figure K.1 - Reflection of point or velocity vector in plane of symmetry

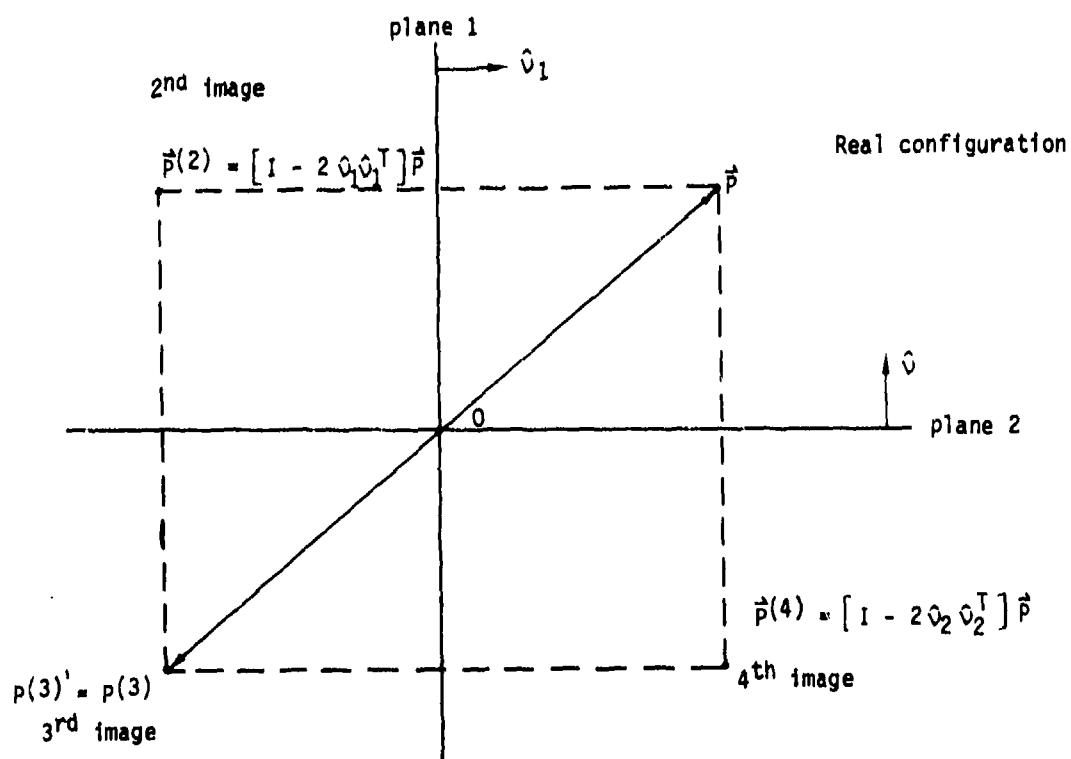


Figure K.2 - Reflection of point in 2 planes of symmetry

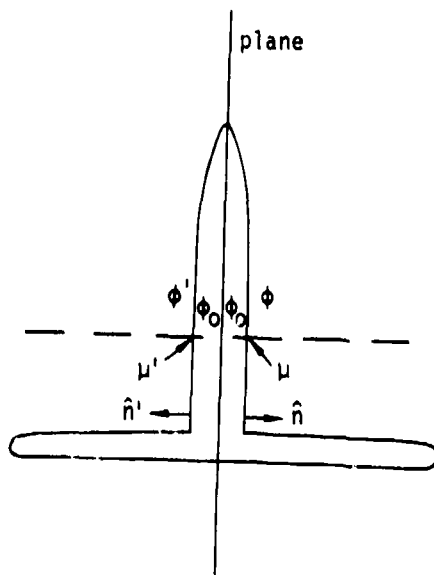


Figure K.3 - Vertical tail on a plane of symmetry

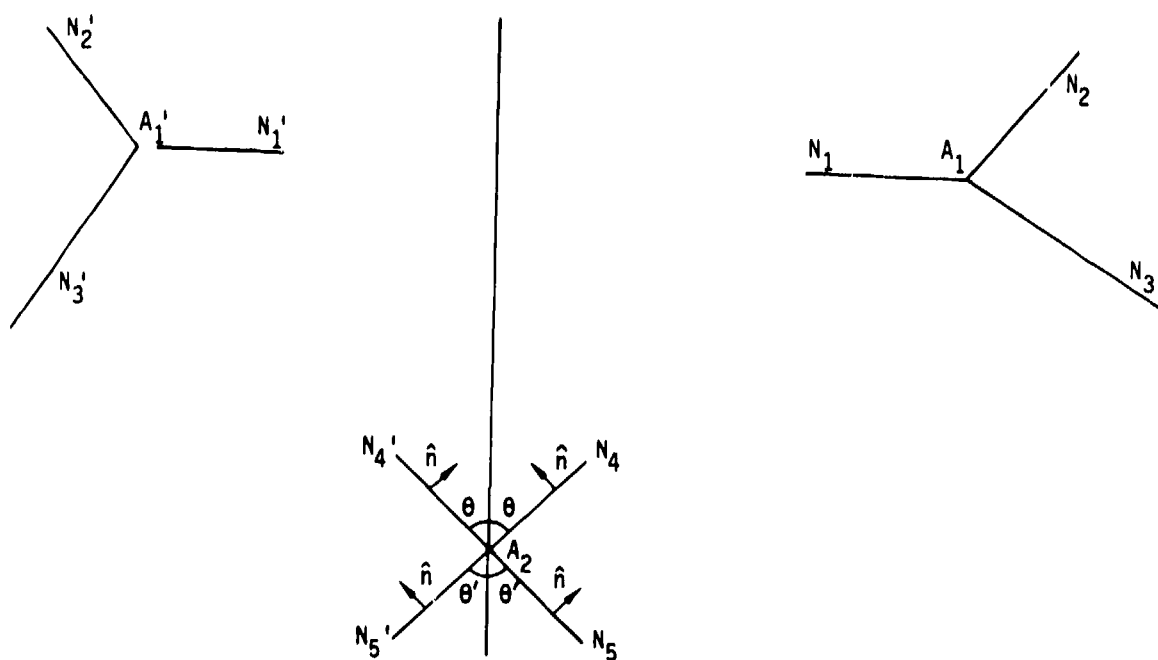


Figure K.4 - Reflections of abutments at and away from a plane of symmetry



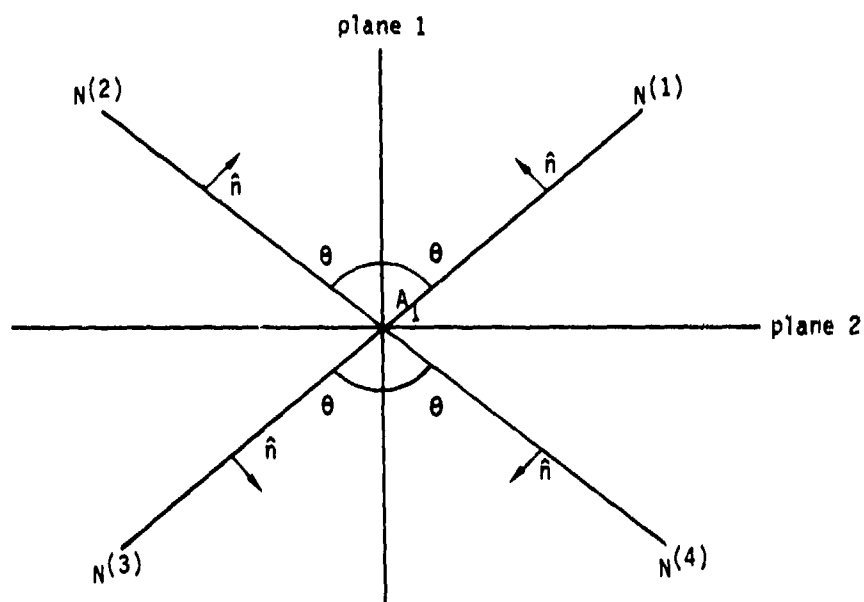


Figure K.5 - Abutment on two planes of symmetry

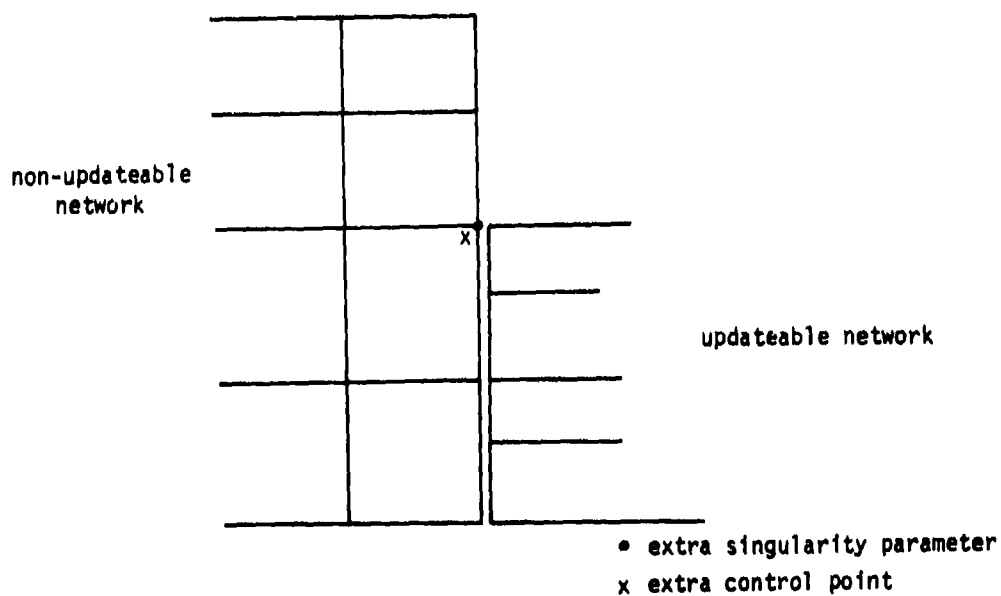


Figure K.6 - Extra singularity parameter and control point dependent on existence of updateable network

## L.0 The Constraint Matrix

The fundamental system of linear equations solved by PAN AIR is of the form (cf. (5.6.19))

$$[AIC] [A] = [B] \quad (L.0.1)$$

where each column of  $[B]$  is a constraint vector  $b_i$ , and each column of  $[A]$  is the corresponding vector of singularity parameters  $\lambda_i$ , and  $i$  is the index of the solution.

The construction of the constraint matrix has already been discussed in other portions of the document. In section 5.7, the reorganization of the constraint vector resulting from the definition of known singularity parameters is illustrated (cf. (5.7.12)). Also in section 5.7, and in section K.1, the recombination of constraint vectors in consideration of symmetry is discussed (cf. equations (5.7.7-8) and (K.1.34-37)).

In section H.3 the automatic options available in PAN AIR to compute entries of a particular constraint vector were discussed. Summarizing, for a given control point  $P$ , the entry of the constraint vector corresponding to a boundary condition imposed at  $P$  may be of the form (cf. (H.3.25))

$$b(P) = b_0 - b_n \vec{U}_0 \cdot \hat{n} - b_T \vec{t}_T \cdot \vec{U}_0 - \frac{b_p}{s_B^2} [\vec{U}_\infty, \vec{P}] \quad (L.0.2)$$

where  $b_0$ ,  $b_n$ ,  $b_T$ ,  $\vec{t}_T$ , and  $b_p$  are user-specified,  $\vec{U}_\infty$  is the "uniform onset flow," and  $\vec{U}_0$  is the "total onset flow" (cf. H.3.22):

$$\vec{U}_0(P) = \vec{U}_\infty + \vec{\Delta U}(P) + \vec{\omega} \times (\vec{P} - \vec{P}_0) \quad (L.0.3)$$

where  $\omega$ ,  $P_0$ , and the "incremental onset flow"  $\vec{\Delta U}(P)$  are user-specified.

Finally, in section 5.8 the "solution update" capability was discussed. If the program user expects in the future to be interested in additional "right hand sides" (such as additional angles of attack or sideslip, but with the compressibility axis and Mach number unchanged), he may request the factorization (5.8.2) of the AIC matrix to be stored. Future solutions may then be obtained very economically, since the main users of computer time in the operation of PAN AIR are the construction of the AIC matrix and its factorization. A more detailed discussion of the AIC matrix factorization procedure is given in the portion of the Maintenance Document which discusses the Real Matrix Solver (RMS) module.

#### M.O Computation of the Minimal Data Set

It is desirable that the solution of the potential flow problem (that is, the combination of the Prandtl-Glauert equation with a set of boundary conditions) be distilled into the smallest possible amount of data, yet still be readily convertible to data of aerodynamic interest. This smallest amount of data is called the minimal data set, and consists of the average potential and normal component of mass flux, source strength, and doublet strength at each control point and each grid point on the configuration. Each of these items exists for each solution, that is, for each column  $\vec{A}_j$  of the solution matrix  $[A]$  (cf. (L.O.1)). In our discussion here, we will assume we are dealing with only one solution, even though the program deals with blocks of solutions.

Under certain circumstances, an additional vector is added to the minimal data set. This vector is the average velocity, as computed from the velocity influence coefficient matrix. This occurs when the standard spline method of velocity computation (called the "boundary condition method" for simplicity; see section B.4.1 of the User's Manual), which computes the velocity from the potential and normal mass flux, is of insufficient accuracy for the purposes of the program user.

### M.1 Recovery of the Singularity Parameters

Solution of the systems of equations (K.1.33-37) produces not the vectors  $\vec{\lambda}^{(i)}$ ,  $i = 1, \dots, 4$ , but rather the vectors

$$\begin{aligned}\vec{\lambda}_1 &= \vec{\lambda}^{(1)} + \vec{\lambda}^{(2)} + \vec{\lambda}^{(3)} + \vec{\lambda}^{(4)} \\ \vec{\lambda}_2 &= \vec{\lambda}^{(1)} - \vec{\lambda}^{(2)} - \vec{\lambda}^{(3)} + \vec{\lambda}^{(4)} \\ \vec{\lambda}_3 &= \vec{\lambda}^{(1)} - \vec{\lambda}^{(2)} + \vec{\lambda}^{(3)} - \vec{\lambda}^{(4)} \\ \vec{\lambda}_4 &= \vec{\lambda}^{(1)} + \vec{\lambda}^{(2)} - \vec{\lambda}^{(3)} - \vec{\lambda}^{(4)}\end{aligned}\tag{M.1.1}$$

Since we are actually interested in the vectors  $\lambda^{(i)}$ , which define the singularity strengths on the  $i$ th image, we must extract these from the combination vectors  $\vec{\lambda}_i$ . Now, it is straightforward to verify that

$$\begin{aligned}\vec{\lambda}^{(1)} &= 1/4 (\vec{\lambda}_1 + \vec{\lambda}_2 + \vec{\lambda}_3 + \vec{\lambda}_4) \\ \vec{\lambda}^{(2)} &= 1/4 (\vec{\lambda}_1 - \vec{\lambda}_2 - \vec{\lambda}_3 + \vec{\lambda}_4) \\ \vec{\lambda}^{(3)} &= 1/4 (\vec{\lambda}_1 - \vec{\lambda}_2 + \vec{\lambda}_3 - \vec{\lambda}_4) \\ \vec{\lambda}^{(4)} &= 1/4 (\vec{\lambda}_1 + \vec{\lambda}_2 - \vec{\lambda}_3 - \vec{\lambda}_4)\end{aligned}\tag{M.1.2}$$

Thus we can separate out the singularity parameters pertaining to each image. So, from now on, we will deal with a single vector  $\vec{\lambda}$  of singularity parameters on a single image.

## M.2 Singularity Strength Calculation

Obtaining the source and doublet strength at a control point or grid point P, with local coordinates  $(\xi', n')$ , from the vector of singularity parameters, has in fact already been described. If the source and doublet subpanel spline and outer spline matrices for the subpanel and panel on which the control point lies are  $SPSPLS$ ,  $SPSPLD$ ,  $BS$ , and  $BD$  respectively, then by (5.6.2) and (K.3.11)

$$\sigma(P) = [1 \quad \xi' \quad n'] [SPSPLS] [BS] \begin{Bmatrix} \lambda_1^S \\ \vdots \\ \lambda_9^S \end{Bmatrix} \quad (M.2.1)$$

and

$$\mu(P) = [1 \quad \xi' \quad n' \quad 1/2 \xi'^2 \quad \xi' n' \quad 1/2 n'^2] [SPSPLD] [BD] \begin{Bmatrix} \lambda_1^D \\ \vdots \\ \lambda_{21}^D \end{Bmatrix} \quad (M.2.2)$$

Here,  $\lambda_i^S$  and  $\lambda_i^D$  are the source and doublet parameters in the neighborhood of the panel, and are entries of  $\vec{\lambda}$ .

### M.3 Computation of Potential and Normal Mass Flux

Three approaches to the computation of potential and normal mass flux at control points are described in section 5.9. One is the multiplication of the influence coefficient matrices by the vector of singularity parameters (cf. (5.9.1)). The second makes use of the boundary conditions to obtain  $\phi_A$  from  $u$  and  $w_A \cdot n$  from  $\sigma$ . For instance, suppose the boundary conditions

$$\phi_L = 0 \quad (M.3.1)$$

$$\sigma = -\vec{V}_\infty \cdot \hat{n} \quad (M.3.2)$$

are imposed.

The specification of (M.3.1) insures perturbation stagnation in the configuration interior. Thus

$$\phi_L = 0 \quad (M.3.3)$$

So,

$$\vec{\nabla} \phi_L \cdot \hat{n} = \vec{w}_L \cdot \hat{n} = 0 \quad (M.3.4)$$

Combining (M.3.2) and (M.3.4),

$$\begin{aligned} \vec{w}_A \cdot \hat{n} &= 1/2 (\vec{w}_U \cdot \hat{n} + \vec{w}_L \cdot \hat{n}) = 1/2 \vec{w}_U \cdot \hat{n} \\ &= 1/2 (\vec{w}_U \cdot \hat{n} - \vec{w}_L \cdot \hat{n}) = 1/2 \sigma \end{aligned} \quad (M.3.5)$$

Similarly,

$$\phi_A = 1/2 u \quad (M.3.6)$$

Thus both average normal mass flux and average potential may be obtained directly from the singularity strength.

We note that (M.3.6) follows directly from (M.3.1), while (M.3.5) only holds when both (M.3.1) and (M.3.2) are imposed. The average normal mass flux can however be computed directly from the boundary conditions in other circumstances as well. For instance, if the boundary condition

$$\vec{w}_U \cdot \hat{n} = b \quad (M.3.7)$$

is imposed, then it follows from the definitions of source strength and average normal mass flux that

$$\begin{aligned} \vec{w}_A \cdot \hat{n} &= 1/2 (\vec{w}_U \cdot \hat{n} + \vec{w}_L \cdot \hat{n}) = \vec{w}_U \cdot \hat{n} - 1/2 (\vec{w}_U \cdot \hat{n} - \vec{w}_L \cdot \hat{n}) \\ &= b - 1/2 \sigma \end{aligned} \quad (M.3.8)$$

Once average potential and normal mass flux have been computed at control points, they may be computed at grid points by a splining method virtually identical to the method used to construct the doublet spline vector  $SPD$  which defines the doublet strength at a grid point as a linear combination of

surrounding doublet parameters. The spline vector  $SP^D$  consists of a row of an outer spline matrix  $B^D$  (cf., section I.1). That is, if  $P$  is one of the nine "panel defining points", then the spline vector  $SP^D$  corresponding to  $P$  is defined by

$$u(P) = [SP^D]_{1 \times k} \begin{bmatrix} \lambda_1^D \\ \vdots \\ \lambda_k^D \end{bmatrix} \quad k \leq 12 \quad (M.3.9)$$

where the  $\lambda_i^D$  are the doublet parameters located in the neighborhood of the grid point.

Similarly, a "potential spline" row vector  $[SP^P]$  is computed such that

$$[\phi_A(P) \quad \vec{w}_A(P) \cdot \hat{n}] = [SP^P]_{1 \times k} \begin{bmatrix} \phi_1 & (\vec{w}_A \cdot \hat{n})_1 \\ \vdots & \vdots \\ \phi_k & (\vec{w}_A \cdot \hat{n})_k \end{bmatrix}_{k \times 2} \quad (M.3.10)$$

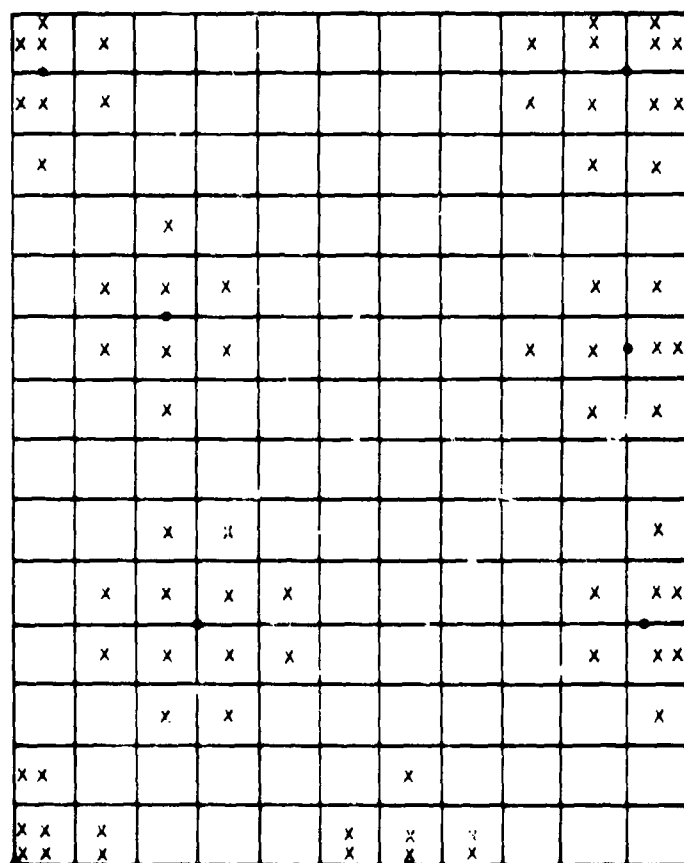
where  $\phi_i$  and  $(\vec{w}_A \cdot \hat{n})_i$  are average potential and normal mass flux at the neighboring control points, rather than singularity parameter locations. The row vector  $SP^P$  is computed by the same least squares method as the row vector  $SP^D$ , but the choice of the set of surrounding control points is slightly different from the choice of surrounding singularity parameters, as illustrated in figure M.1.

In particular, the potential at grid points on a network edge depends on control points in the interior of the network. An "edge spline" can not be used because the edge control points are receded from the network edge, while singularity parameters are not.

Whenever the program computes the velocity at control points by the influence coefficient method, the same potential spline vectors may be used to define an average velocity vector at each grid point  $P$  by

$$[\vec{v}_A(P)]_i = [SP^P]_{1 \times k} \cdot \begin{bmatrix} \vec{v}_{A,1}^T \\ \vdots \\ \vec{v}_{A,k}^T \end{bmatrix}_{k \times 3} \quad (M.3.11)$$

where  $\vec{v}_{A,i}$  is the average velocity, computed by the influence coefficient method, at the  $i$ th control point in the neighborhood of  $P$ .



- grid point
- x neighboring control points

Figure M.1 - Neighboring control points for potential spline computation



## N.0 Surface and Wake Flow Properties

With the construction of the minimal data set, the potential flow solution is complete. The items in the minimal data set, however, are not generally of great aerodynamic interest. Of more interest are the velocity and pressure at points in the configuration. In section N.1, the computation of velocity from the elements of the minimal data set is discussed. In section N.2 the computation of pressure from velocity is discussed. In section N.3, two semi-empirical velocity correction formulas are discussed. These are of use where the magnitude of the total velocity is significantly less than freestream. In section N.4, the effect of a non-uniform onset flow on pressure coefficient formulas is considered. Finally, in section N.5, we define the additional quantities computed by PAN AIR at points on the configuration surface.

## N.1 Velocity Computation

The splining method defines a distribution of potential on the configuration surface, with this distribution being defined by a single quadratic function on each subpanel. This distribution, when differentiated, defines the tangential component of the velocity. On the other hand, the normal mass flux, equal to the conormal component of the velocity, is also known. From these two components, we may reconstruct the entire velocity vector.

First, assume the distribution of potential on a subpanel is given by

$$\phi = \phi_S (\xi', n') \quad (N.1.1)$$

where  $(\xi', n')$  are the subpanel local coordinates, and the subscript emphasizes that this is a distribution on the configuration surface.

Now, applying (K.3.15)

$$\begin{aligned} \begin{Bmatrix} \partial \phi_S / \partial x_0 \\ \partial \phi_S / \partial x_0 \\ \partial \phi_S / \partial z_0 \end{Bmatrix} &= \vec{\nabla} \phi_S = [A^T] \begin{Bmatrix} \partial \phi_S / \partial \xi' \\ \partial \phi_S / \partial n' \\ \partial \phi_S / \partial \xi' \end{Bmatrix} \\ &= [A^T] \begin{Bmatrix} \partial \phi_S / \partial \xi' \\ \partial \phi_S / \partial n' \\ 0 \end{Bmatrix} \end{aligned} \quad (N.1.2)$$

where A (cf., equations (E.0.1) and (E.1.1)) sends reference coordinates to local coordinates.

Next, the tangential component of the velocity  $\vec{v}$  is clearly equal to that of  $\vec{\nabla} \phi$ ; that is; for any tangent vector  $\vec{t}$ ,

$$\vec{t} \cdot \vec{v} = \vec{t} \cdot \vec{\nabla} \phi_S \quad (N.1.3)$$

On the other hand,

$$\vec{n} \cdot \vec{v} = \vec{w} \cdot \hat{n} \quad (N.1.4)$$

where  $\vec{n}$  is the conormal to the surface.

Since any two linearly independent tangent vectors, along with  $\vec{n}$ , form a set of three independent vectors, there is a unique vector  $\vec{v}$  which satisfies

(N.1.4), and also (N.1.3) for all tangent vectors  $\vec{t}$ . Now, consider the expression

$$\vec{v}_0 = (\vec{\nabla} \phi)_T - \frac{\vec{n} \cdot (\vec{\nabla} \phi)_T}{\vec{n} \cdot \hat{n}} \hat{n} + \frac{\vec{w} \cdot \hat{n}}{\vec{n} \cdot \hat{n}} \hat{n} \quad (N.1.5)$$

where  $(\vec{\nabla} \phi)_T$  is the tangential component of the gradient of the potential.

We see that for any tangent vector  $\vec{t}$ ,

$$\vec{t} \cdot \vec{v}_0 = \vec{t} \cdot (\vec{\nabla} \phi)_T \quad (N.1.6)$$

and that

$$\vec{n} \cdot \vec{v}_0 = \vec{w} \cdot \hat{n} \quad (N.1.7)$$

Thus,  $\vec{v}_0$  satisfies (N.1.3-4) and so

$$\vec{v} = \vec{v}_0 \quad (N.1.8)$$

Equations (N.1.5) and (N.1.8) apply equally well to average and difference velocity. That is, applying (N.1.2),

$$v_A = [A^T] \vec{\nabla}' \phi_A - \frac{\vec{n} \cdot \{A^T \vec{\nabla}' \phi_A\}}{\vec{n} \cdot \hat{n}} \hat{n} + \frac{\vec{w}_A \cdot \hat{n}}{\vec{n} \cdot \hat{n}} \hat{n} \quad (N.1.8a)$$

$$v_D = [A^T] \vec{\nabla}' \mu - \frac{\vec{n} \cdot \{A^T \vec{\nabla}' \mu\}}{\vec{n} \cdot \hat{n}} \hat{n} + \frac{\sigma}{\vec{n} \cdot \hat{n}} \hat{n} \quad (N.1.8b)$$

where

$$\vec{\nabla}' = \begin{Bmatrix} \partial/\partial \xi' \\ \partial/\partial \eta' \\ \eta \end{Bmatrix} \quad (N.1.9)$$

We note from (E.3.70) that  $\vec{n}$  is a multiple of  $A^{-1}$

$$\begin{Bmatrix} 0 \\ 0 \\ 1 \end{Bmatrix}$$

Thus

$$\vec{n} \cdot (A^T \vec{\nabla}') = (A\vec{n}) \cdot \vec{\nabla}'$$

$$= \begin{Bmatrix} 0 \\ 0 \\ \alpha \end{Bmatrix} \cdot \begin{Bmatrix} \partial/\partial x'_1 \\ \partial/\partial x'_2 \\ 0 \end{Bmatrix} = 0 \quad (N.1.10)$$

N.1-2

where  $\alpha$  is some real number.  
 Substituting (N.1.10) in (N.1.9)

$$\vec{v}_A = A^T(\vec{\nabla}\phi_A) + \frac{\vec{w}_A \cdot \hat{n}}{\hat{n} \cdot \hat{n}} \hat{n} \quad (\text{N.1.11a})$$

$$\vec{v}_D = A^T(\vec{\nabla}\mu) + \frac{\sigma}{\hat{n} \cdot \hat{n}} \hat{n} \quad (\text{N.1.11b})$$

We have thus decomposed the average and difference velocity at a surface point into tangential and normal components. In addition, we see that they can be computed from the "minimal data set" consisting of  $\phi_A$ ,  $w_A$ ,  $n$ ,  $\sigma$ , and  $\mu$ .

Finally, upper surface and lower surface velocities may be computed from average and difference quantities:

$$\begin{aligned} \vec{v}_U &= \vec{v}_A + 1/2 \vec{v}_D \\ \vec{v}_L &= \vec{v}_A - 1/2 \vec{v}_D \end{aligned} \quad (\text{N.1.12})$$

## N.2 Pressure Formulas

In this section, we assume the existence of a uniform freestream velocity  $\vec{V}_\infty$ , aligned with the x-direction of the compressibility coordinate system, and a perturbation velocity at a point P:

$$\vec{V}(P) = \begin{pmatrix} u \\ v \\ w \end{pmatrix} \quad (N.2.1)$$

In this section, we derive the pressure coefficient  $C_p$  at P under a variety of simplifying assumptions, thus obtaining a collection of pressure coefficient formulas.

The assumption that the freestream and compressibility directions are identical is a necessary one in order to derive the results of this section (except when the Mach number is zero). In practice, however, Pan Air does not require these directions to be identical. If the user chooses the "uniform onset flow method" of pressure computation, then all the equations of this section are applied with  $\vec{V}_\infty$  replaced by the uniform onset flow  $\vec{U}_\infty$  defined in Appendix H, and with the compressibility coordinate system replaced by a "wind-axis system" whose x-axis is parallel to  $\vec{U}_\infty$ .

In addition, Pan Air makes available a "total onset flow" method of pressure computation. This will be discussed in section N.4.

### N.2.1 Preliminary Results

First, let us define the pressure coefficient as

$$C_p = \frac{p - p_\infty}{\frac{1}{2} \rho_\infty \cdot |\vec{V}_\infty|^2} \quad (N.2.2)$$

where  $p$  is pressure and  $\rho$  is density. In order to compute  $C_p$  from velocity, we need some basic results which hold for "one-dimensional" flows from Liepmann and Roshko (Ref. 1.4). A precise definition of one-dimensional flows is given there on p. 39. A tube of streamlines in a uniform fluid flow in three dimensional space, perturbed by an object of finite size, is such a flow.

The results we use are:

(a) Bernoulli's equation (2.18b in Liepmann and Roshko)

$$\frac{|\vec{V}|^2}{2} + \int \frac{dP}{\rho} = \text{constant} \quad (N.2.3)$$

where the path of integration is a streamline, and  $\vec{V}$  is velocity at a point,

(b) The integrated form of Bernoulli's equation for a perfect gas (see p. 55 of Liepmann and Roshko):

$$\frac{\gamma}{\gamma - 1} \frac{P}{\rho} + \frac{1}{2} |\vec{V}|^2 = \frac{\gamma}{\gamma - 1} \frac{P_\infty}{\rho_\infty} + \frac{1}{2} |\vec{V}_\infty|^2 \quad (\text{N.2.4})$$

where  $\gamma$  is the ratio of specific heats (7/5 for a diatomic gas), and

(c) an expression for the local speed of sound (equation 2.23)

$$a^2 = \frac{\gamma P}{\rho} \quad (\text{N.2.5})$$

We also define the local Mach number

$$M = \frac{|\vec{V}|}{a} \quad (\text{N.2.6})$$

Finally, for isentropic flow in a perfect gas (cf., Liepmann and Roshko, 2.21a)

$$\frac{P}{P_\infty} = \left( \frac{\rho}{\rho_\infty} \right)^\gamma \quad (\text{N.2.7})$$

#### N.2.2 Constant Density Flow

If the density  $\rho$  may be assumed to be a constant  $\rho_\infty$  (for instance, for an incompressible fluid or at zero Mach number), then (N.2.3) reduces to

$$\frac{|\vec{V}|^2}{2} + \frac{P}{\rho_\infty} = \frac{|\vec{V}_\infty|^2}{2} + \frac{P_\infty}{\rho_\infty} \quad (\text{N.2.8})$$

Solving for  $P$ ,

$$P = \frac{1}{2} \rho_\infty (|\vec{V}_\infty|^2 - |\vec{V}|^2) + P_\infty \quad (\text{N.2.9})$$

and so, by (N.2.2),

$$C_p = 1 - \frac{|\vec{V}|^2}{|\vec{V}_\infty|^2} \quad (\text{N.2.10})$$

### N.2.3 Compressible Flow

We first apply (N.2.7) to (N.2.4) in order to eliminate  $\rho$  from the equation. It follows from (N.2.7) that

$$\rho^{-1} = \rho_{\infty}^{-1} \left( \frac{P}{P_{\infty}} \right)^{\frac{\gamma}{\gamma-1}} \quad (\text{N.2.11})$$

Thus

$$\frac{\gamma}{\gamma-1} \left( \frac{P}{\rho} \right) = \frac{\gamma}{\gamma-1} \left( \frac{P_{\infty}}{\rho_{\infty}} \right) \left( \frac{P}{P_{\infty}} \right)^{\frac{\gamma-1}{\gamma}} \quad (\text{N.2.12})$$

and so (N.2.4) becomes

$$\frac{1}{2} |\vec{V}|^2 + \frac{\gamma}{\gamma-1} \left( \frac{P}{\rho} \right)^{\frac{\gamma-1}{\gamma}} \left( \frac{P_{\infty}}{\rho_{\infty}} \right)^{\frac{\gamma-1}{\gamma}} = \frac{\gamma}{\gamma-1} \left( \frac{P_{\infty}}{\rho_{\infty}} \right)^{\frac{\gamma-1}{\gamma}} + \frac{1}{2} |\vec{V}_{\infty}|^2 \quad (\text{N.2.13})$$

Next, we apply (N.2.5-6) to the freestream to obtain

$$a_{\infty}^2 = \frac{\gamma P_{\infty}}{\rho_{\infty}} = \frac{|\vec{V}_{\infty}|^2}{M_{\infty}^2} \quad (\text{N.2.14})$$

Thus

$$\frac{1}{2} \rho_{\infty} |\vec{V}_{\infty}|^2 = \frac{\gamma M_{\infty}^2 P_{\infty}}{2} \quad (\text{N.2.15})$$

Substituting this into (N.2.2),

$$C_p = \frac{2}{\gamma M_{\infty}^2 P_{\infty}} (P - P_{\infty}) = \frac{2}{\gamma M_{\infty}^2} \left( \frac{P}{P_{\infty}} - 1 \right) \quad (\text{N.2.16})$$

The quantity  $P/P_\infty$  may be calculated by rearranging (N.2.13):

$$\left(\frac{P}{P_\infty}\right)^{\frac{\gamma-1}{\gamma}} = 1 - \frac{1}{2} \left( \frac{|\vec{V}|^2}{|\vec{V}_\infty|^2} \right) \left(\frac{\gamma-1}{\gamma}\right) \frac{P_\infty}{P_\infty} \quad (\text{N.2.17})$$

= (substituting (N.2.15))

$$1 - \frac{\gamma-1}{2} M_\infty^2 \frac{|\vec{V}|^2 - |\vec{V}_\infty|^2}{|\vec{V}_\infty|^2} \quad (\text{N.2.18})$$

Thus

$$\frac{P}{P_\infty} = \left[ 1 - \left( \frac{|\vec{V}|^2}{|\vec{V}_\infty|^2} - 1 \right) \cdot \left( \frac{\gamma-1}{2} \right) \cdot M_\infty^2 \right]^{\frac{\gamma}{\gamma-1}} \quad (\text{N.2.19})$$

Substituting this expression in (N.2.16),

$$C_p = \frac{2}{\gamma M_\infty^2} \left[ 1 + \frac{\gamma-1}{2} \left( 1 - \frac{|\vec{V}|^2}{|\vec{V}_\infty|^2} \right) M_\infty^2 \right]^{\frac{\gamma}{\gamma-1}} - 1 \quad (\text{N.2.20})$$

This is often called the isentropic pressure coefficient formula. In section N.2.5, we will consider certain simplifying assumptions, and the behavior of the pressure coefficient formula under these assumptions.

#### N.2.4 Limitations of the Formula

Under certain circumstances the velocity computed by the potential flow solution is so unrealistic that the resulting pressure coefficient is meaningless. One such case is a velocity for which the corresponding pressure coefficient is more negative than the "vacuum pressure." A second case is that of a local flow exceeding the speed of sound while the freestream flow is subsonic.



#### N.2.4.1 The Vacuum Pressure Coefficient

The isentropic pressure coefficient may only be evaluated if the expression in (N.2.20) which is raised to the power  $\gamma/(\gamma-1)$  is non-negative. Thus the isentropic pressure coefficient reaches its minimum, or vacuum, value when this expression equals zero. So, we write

$$C_{p,vac} = \frac{-2}{\gamma M_{\infty}^2} \quad (N.2.21)$$

The velocity  $V_m$  for which  $C_{p,vac}$  is attained is therefore given by

$$1 + \frac{\gamma-1}{2} \cdot \left(1 - \frac{|\vec{V}_m|^2}{|\vec{V}_{\infty}|^2}\right) M_{\infty}^2 = 0 \quad (N.2.22)$$

Solving,

$$\frac{|\vec{V}_m|^2}{|\vec{V}_{\infty}|^2} = 1 + \frac{2}{(\gamma-1) M_{\infty}^2} \quad (N.2.23)$$

Thus the speed

$$V_m = |\vec{V}_{\infty}| \left[1 + \frac{2}{(\gamma-1) M_{\infty}^2}\right]^{1/2} \quad (N.2.24)$$

is called the maximum speed, since for any speed in excess of  $V_m$  the vacuum pressure is exceeded.

#### N.2.4.2 The Critical Speed

In subsonic flow, if the magnitude of the velocity exceeds the local speed of sound, the Prandtl-Glauert equation is clearly invalid. Thus a program user may be interested to know if the "critical speed," that is, the local speed of sound, has been exceeded.

To compute the local speed of sound, we substitute (N.2.11) in (N.2.5) to

obtain

$$a^2 = \gamma p \rho_{\infty}^{-1} \cdot \left( \frac{p}{p_{\infty}} \right)^{\frac{-1}{\gamma}} \quad (\text{N.2.25})$$

$$= \gamma \left( \frac{p}{p_{\infty}} \right)^{\frac{\gamma-1}{\gamma}} \frac{p_{\infty}}{\rho_{\infty}} \quad (\text{N.2.26})$$

= (applying (N.2.5))

$$\left( \frac{p}{p_{\infty}} \right)^{\frac{\gamma-1}{\gamma}} \cdot a_{\infty}^2 \quad (\text{N.2.27})$$

Thus by (N.2.19)

$$\frac{a^2}{a_{\infty}^2} = 1 - \frac{(\gamma-1)}{2} M_{\infty}^2 \left( \frac{|\vec{V}|^2}{|\vec{V}_{\infty}|^2} - 1 \right) \quad (\text{N.2.28})$$

So,

$$\begin{aligned} \text{So } \frac{|\vec{V}|^2}{a^2} &= \frac{|\vec{V}|^2}{|\vec{V}_{\infty}|^2} \cdot \frac{|\vec{V}_{\infty}|^2}{a_{\infty}^2} \cdot \frac{a_{\infty}^2}{a^2} = \\ &= \frac{|\vec{V}|^2 \cdot M_{\infty}^2}{\left[ 1 + \frac{\gamma-1}{2} \cdot M_{\infty}^2 \left( 1 - \frac{|\vec{V}|^2}{|\vec{V}_{\infty}|^2} \right) \right] |\vec{V}_{\infty}|^2} \end{aligned} \quad (\text{N.2.29})$$

Defining the local Mach number

$$M_1 = \frac{|\vec{V}|}{a} \quad (\text{N.2.30})$$

we see that the speed attains its critical value  $V_c$  if the local Mach number is 1, or if

$$(V_c)^2 M_\infty^2 = \left[ 1 + \frac{\gamma-1}{2} \cdot M_\infty^2 \left( 1 - \frac{(V_c)^2}{|\vec{V}_\infty|^2} \right) \right] |\vec{V}_c|^2 \quad (\text{N.2.31})$$

Solving,

$$\frac{(V_c)^2}{|\vec{V}_\infty|^2} = \frac{\gamma-1}{\gamma+1} + \frac{2}{(\gamma+1)M_\infty^2} \quad (\text{N.2.32})$$

Applying (N.2.24),

$$V_c = \left( \frac{\gamma-1}{\gamma+1} \right)^{1/2} \cdot V_m \quad (\text{N.2.33})$$

The Pan Air user may request the program to compute the critical and maximum speeds, and the corresponding pressure coefficients.

#### N.2.4.3 Pressure Coefficient at the Critical Speed

Substituting (N.2.32) in (N.2.20) yields, after some algebraic manipulation, the value of the isentropic pressure coefficient at the critical speed. It is

$$C_{p,c} = \frac{2}{\gamma M^2} \left[ \frac{2}{\gamma+1} + \frac{\gamma-1}{\gamma+1} \cdot M_\infty^2 \right]^{\frac{\gamma}{\gamma-1}} - 1 \quad (\text{N.2.34})$$

#### N.2.5 The Isentropic Formula under Simplifying Assumptions

For complete generality, we have avoided the assumption that  $|\vec{V}_\infty| = 1$ . Thus we can write, in compressibility coordinates,

$$\vec{V} = \begin{pmatrix} |\vec{V}| \\ 0 \\ 0 \end{pmatrix} \quad (\text{N.2.35})$$

$$\vec{V} = \begin{pmatrix} |\vec{V}| + u \\ v \\ w \end{pmatrix} \quad (\text{N.2.36})$$

Thus  $c_p$  is a function of  $u$ ,  $v$ , and  $w$ , the components of the perturbation velocity. We now look at (N.2.20) under a variety of small perturbation assumptions.

#### N.2.5.1 Second Order Theory

First, let us make the assumption that cubic and higher order terms in  $u$ ,  $v$ , and  $w$  may be ignored. This is called second order theory.

According to the binomial theorem,

$$(1 + \epsilon)^{\frac{\gamma}{\gamma-1}} = 1 + \frac{\gamma}{\gamma-1} \cdot \epsilon + \frac{1}{2} \left( \frac{\gamma}{\gamma-1} \right) \cdot \epsilon^2 + \text{cubic and higher terms in } \epsilon \quad (\text{N.2.37})$$

We will substitute (N.2.37) in (N.2.20) with

$$\epsilon = \frac{\gamma-1}{2} \cdot \left( 1 - \frac{|\vec{V}|^2}{|\vec{V}_\infty|^2} \right) M_\infty^2 \quad (\text{N.2.38})$$

$$= \frac{\gamma-1}{2} \cdot \frac{(1 - (|\vec{V}_\infty|^2 + u^2 + v^2 + w^2) M_\infty^2)}{|\vec{V}_\infty|^2} M_\infty^2 \quad (\text{N.2.39})$$

$$= \frac{\gamma-1}{2} \cdot M_\infty^2 \cdot \left( \frac{-2u}{|\vec{V}_\infty|} - \frac{u^2 + v^2 + w^2}{|\vec{V}_\infty|^2} \right) \quad (\text{N.2.40})$$

We see that, neglecting cubic and higher order terms

$$\epsilon^2 = \frac{(\gamma-1)^2 M_\infty^4 u^2}{|\vec{V}_\infty|^2} \quad (\text{N.2.41})$$

and

$$(1 + \epsilon) \frac{\gamma}{\gamma-1} = 1 + \frac{\gamma}{2} M_\infty^2 \left( \frac{-2u}{|\vec{V}_\infty|} - \frac{(1-M_\infty^2)u^2 + v^2 + w^2}{|\vec{V}_\infty|^2} \right) \quad (\text{N.2.42})$$

So, neglecting cubic and higher order terms in (N.2.20),

$$C_p = \frac{2}{\gamma M_\infty^2} \left( (1 + \epsilon) \frac{\gamma}{\gamma-1} - 1 \right) = \frac{-2u}{|\vec{V}_\infty|} - \frac{(1-M_\infty^2)u^2 + v^2 + w^2}{|\vec{V}_\infty|^2} \quad (\text{N.2.43})$$

$$= \text{(alternatively)} \quad 1 - \frac{|\vec{V}|^2}{|\vec{V}_\infty|^2} + M_\infty^2 \frac{u^2}{|\vec{V}_\infty|^2} \quad (\text{N.2.44})$$

This is the second order pressure coefficient formula.

Now we consider the evaluation of a number of other quantities under the assumption of neglect of cubic and higher terms. First, we see that (N.2.28) remains unchanged under the assumption, and so (N.2.29) still holds. That is, the local Mach number is still

$$M_1 = \frac{|\vec{V}|}{|\vec{V}_\infty|} \frac{M_\infty}{\left[ 1 + \frac{\gamma-1}{2} M_\infty^2 \left( 1 - \frac{|\vec{V}|^2}{|\vec{V}_\infty|^2} \right) \right]^{1/2}} \quad (\text{N.2.45})$$

Similarly, equation (N.2.24) for the maximum speed  $V_m$  and equation (N.2.33) for the critical speed still hold. To obtain  $c_{p,c}$ , the pressure coefficient at the critical speed, it does not suffice to substitute (N.2.32) in (N.2.44). In addition, a second order expression for  $u^2/|\vec{V}_\infty|^2$  at the sonic speed must be computed.

$$\text{Noting that } \frac{|\vec{V}|^2}{|\vec{V}_\infty|^2} = 1 + \frac{2u}{|\vec{V}_\infty|} + \text{second order terms} \quad (\text{N.2.46})$$

and substituting in (N.2.32), we see that at the critical speed

$$1 + \frac{2u}{|\vec{V}_\infty|} + \text{higher terms} = \frac{\gamma-1}{\gamma+1} + \frac{2}{(\gamma+1)M_\infty^2} \quad (\text{N.2.47})$$

Thus to second order

$$\frac{u^2}{|\vec{V}_\infty|^2} = 1/4 \left[ \frac{\gamma-1}{\gamma+1} + \frac{2}{(\gamma+1)M_\infty^2} - 1 \right]^2 \quad (\text{N.2.48})$$

at the critical speed. Substituting (N.2.32) and (N.2.48) in (N.2.44) we obtain a second order expression for the critical pressure coefficient

$$C_{p,c} = 1 - \frac{\gamma-1}{\gamma+1} - \frac{2}{(\gamma+1)M_\infty^2} + \frac{1}{(\gamma+1)^2} \left[ M_\infty^2 - 2 + \frac{1}{M_\infty^2} \right] \quad (\text{N.2.49})$$

$$= \frac{1}{(\gamma^2 + 1)} (2\gamma + M_\infty^2) - \frac{(2\gamma + 1)}{M_\infty^2} \quad (\text{N.2.50})$$

#### N.2.5 The Second Order Theory under Additional Assumptions

It may under certain circumstances be of interest to calculate the pressure coefficient under the additional assumption that the freestream Mach number is nearly zero, and thus terms with coefficient  $M$  may be neglected. Combining this and the second order assumption yields the "reduced second order" pressure formula (cf., (N.2.44))

$$C_p = 1 - \frac{|\vec{V}|^2}{|\vec{V}_\infty|^2} \quad (\text{N.2.51})$$

Note that this is equivalent to the constant density or incompressible pressure formula (N.2.10). Further, if the Mach number is zero, they are both equivalent to the second order pressure formula. Finally, the reader may verify that, in the limit as Mach number approaches zero, the isentropic pressure formula (N.2.20) becomes equivalent to (N.2.51) also.

Another possible simplifying assumption is that the configuration is sufficiently slender that quadratic expressions in  $u$  may be ignored. This results in the slender body pressure formula:

$$C_p = \frac{-2u}{|\vec{V}_\infty|} - \frac{v^2 + w^2}{|\vec{V}_\infty|^2} \quad (\text{N.2.52})$$

Finally, one may neglect all quadratic expressions in components of the perturbation, and thus obtain the linear pressure formula

$$C_p = \frac{-2u}{|V_\infty|} \quad (N.2.53)$$

The local Mach number, the critical speed, and the pressure coefficient at the critical speed may be computed under each of these simplifying assumptions. The validity of these expressions is questionable, since the existence of a point at which the local Mach number equals 1 is evidence that the particular assumption is not valid.

### N.3 Velocity Corrections

The empirical observation on which the two velocity corrections are based is that the linearized mass flux computed by a panel method under some circumstances more accurately represents the true mass flux than the computed velocity represents the true velocity. Thus a corrected velocity  $V'$  may be calculated from the computed mass flux by the equations below.

$$\frac{\rho}{\rho_\infty} V'_x = W_x \quad (N.3.1a)$$

$$V'_y = W_y \quad (N.3.1b)$$

$$V'_z = W_z \quad (N.3.1c)$$

or by

$$\frac{\rho}{\rho_\infty} \vec{V}' = \vec{W} \quad (N.3.2)$$

That is, to arrive at the first velocity correction formula, the exact relation for isentropic flow

$$\frac{\rho}{\rho_\infty} \vec{V} = \vec{W} \quad (N.3.3)$$

is applied to obtain a corrected value of the freestream or x-component of velocity. To arrive at the second velocity correction formula, equation (N.3.3) is used to obtain a corrected velocity vector which is a multiple of the mass flux vector.

#### N.3.1 The First Velocity Correction

This velocity correction is only applied, and in fact is only well-defined if the local flow is slower than freestream, that is, if

$$u = \frac{\vec{v} \cdot \vec{t}}{|\vec{t}|} < 0 \quad (N.3.4)$$

In that case, (N.3.1) is applied.



Now, substituting (N.2.7) in (N.2.19) we see that

$$\frac{\rho}{\rho_{\infty}} = \left[ 1 + \frac{(\gamma-1)}{2} M_{\infty}^2 \left( 1 - \frac{|\vec{V}|^2}{|\vec{V}_{\infty}|^2} \right) \right]^{\frac{1}{\gamma-1}} \quad (\text{N.3.5})$$

Thus (N.3.1a) becomes

$$W_x = \left[ 1 + \frac{(\gamma-1)}{2} M_{\infty}^2 \left( 1 - \frac{|\vec{V}|^2}{|\vec{V}_{\infty}|^2} \right) \right]^{\frac{1}{\gamma-1}} V'_x \quad (\text{N.3.6})$$

It follows easily from (N.3.6) that  $W_x$  is a monotonic function of  $V_x$ . That is, as  $V_x$  increases, so does  $W_x$ . Thus a simple iterative method (Newton's method) is available for numerically computing  $V'_x$  as a function of  $W_x$  while  $V'_y$  and  $V'_z$  are obtained from (N.3.1).

### N.3.2 The Second Velocity Correction

Under the second correction, the corrected velocity is some multiple of the mass flux. This correction is divided into two cases.

In the first case, we assume the local flow is again slower than freestream; that is, that (N.3.4) holds. Then (N.3.2) is applied, but using the linear density relationship

$$\frac{\rho}{\rho_{\infty}} = 1 + (s\beta^2 - 1) \frac{\vec{V} \cdot \vec{V}_{\infty}}{|\vec{V}_{\infty}|^2} \quad (\text{N.3.7})$$

To see that (N.3.7) follows from (N.3.5) to first order, we apply the binomial theorem to (N.3.5), to obtain

$$\begin{aligned} \frac{\rho}{\rho_{\infty}} &= 1 - \frac{M_{\infty}^2}{2} \left( \frac{|\vec{V}|^2}{|\vec{V}_{\infty}|^2} - 1 \right) + \text{higher terms} \\ &= 1 - \frac{M_{\infty}^2}{2} \left( \frac{2 \vec{V} \cdot \vec{V}_{\infty}}{|\vec{V}_{\infty}|^2} \right) + \text{higher terms} \end{aligned} \quad (\text{N.3.8})$$

and then (N.3.7) follows from the definition  $s\beta^2 = 1 - M_{\infty}^2$ .

Thus for slower than freestream flow, the correction which is applied is

$$\vec{V}' = \frac{\vec{W}}{1 + (se^2 - 1) \frac{\vec{V} \cdot \vec{V}_\infty}{|\vec{V}_\infty|^2}} \quad (N.3.9)$$

In the second case, the local flow is faster than freestream. That is

$$u = \frac{\vec{V} \cdot \vec{V}_\infty}{|\vec{V}_\infty|^2} > 0 \quad (N.3.10)$$

Under these circumstances, the magnitude of the velocity is left unchanged, while its direction is changed so that it is proportional to the mass flux. That is

$$\vec{V}' = \frac{|\vec{V}|}{|\vec{W}|} \vec{W} \quad (N.3.11)$$

where  $\vec{V}$  is the uncorrected velocity computed by the program. This concludes our discussion of the velocity corrections.

#### N.4 Onset Flow Calculations

We now consider the effect of a non-uniform onset flow on the pressure formulas. That is, we assume that the velocity is

$$\vec{V} = \vec{V} + \vec{U}_\infty + \Delta\vec{V} \quad (\text{N.4.1})$$

where  $\Delta\vec{V}$  is the "incremental onset flow" and includes both rotational onset flow and a local incremental onset flow. In the notation of appendix H,

$$\Delta\vec{V} = \vec{U}_0 - \vec{U}_\infty \quad (\text{N.4.2})$$

Our final equations will be based on a number of simplifying assumptions, which will be discussed as they come up. The first assumption is that

$$\vec{U}_0 = \vec{V}_\infty \quad (\text{N.4.2b})$$

That is, the uniform onset flow must be aligned with the compressibility direction for our formulas to hold. For the remainder of this section, we will assume that (N.4.2b) holds. When the pressures are computed by the program, however, the vector  $\vec{U}_\infty$  is used in place of  $\vec{V}_\infty$  whether or not (N.4.2b) holds. Thus if the program user violates (N.4.2b), the resulting pressures may not be correct, nor does any correct method for computing the effect of the incremental onset flow on the pressures exist. A user may violate (N.4.2b) by setting  $\alpha \neq \alpha_c$ ,  $\beta \neq \beta_c$  (see section (B.2.2) of the User's Manual for definitions of these quantities).

##### N.4.1 Bernoulli's Equation

We now need to revise Bernoulli's equation (N.2.4) to account for the incremental onset flow  $\Delta\vec{V}$ . Both (N.2.3) and its integrated form (N.2.4) state that the total energy per unit mass (kinetic energy in the form  $1/2 |\vec{V}_\infty|^2$  plus potential energy  $\gamma p / (\gamma - 1)$ ) is constant at any point on a streamline. Thus to correct (N.2.4) to account for the incremental onset flow we must add to the right hand side the energy per unit mass  $\Delta E$  added to the system by the incremental onset flow:

$$\frac{\gamma}{\gamma-1} \cdot \frac{p}{\rho} + 1/2 |\vec{V}|^2 = \frac{\gamma}{\gamma-1} \cdot \frac{p_\infty}{\rho_\infty} + 1/2 |\vec{V}_\infty|^2 + \Delta E \quad (\text{N.4.3})$$

Now, this added energy speeds up the fluid at infinity. Writing  $\Delta\vec{V}_\infty$  for the incremental onset flow along the streamline infinitely far from the configuration, we have

$$1/2 |\vec{V}_\infty|^2 + \Delta E = 1/2 |\vec{V}_\infty + \Delta\vec{V}|^2 \quad (\text{N.4.4})$$

Thus

$$\Delta E = \vec{V}_{\infty} \cdot \Delta \vec{V}_{\infty} + 1/2 |\Delta \vec{V}_{\infty}|^2 \quad (N.4.5)$$

At present there is no mechanism for the program user to specify either  $\Delta E$  or, equivalently,  $\Delta \vec{V}$ . For many problems involving onset flow, it will be quite reasonable to make the assumption

$$\Delta \vec{V}_{\infty} \approx \Delta \vec{V} \quad (N.4.6)$$

This is especially true if the control point at which the incremental onset flow is defined lies far from the source of the added energy. An example would be the analysis of an airplane flying in the onset flow generated by a second airplane. On the other hand, (N.4.6) would be highly inaccurate for a control point on an airplane wing directly behind the propeller.

Nevertheless, at present, the program assumes that (N.4.6) holds. That is, it computes  $\Delta E$  by

$$2 \cdot \Delta E = 2 \vec{V}_{\infty} \cdot \Delta \vec{V} + |\Delta \vec{V}|^2 \quad (N.4.7)$$

We may now recompute all the equations in section N.2 using (N.4.3) in place of (N.2.4). Following the algebra of section N.2, (N.2.17) becomes

$$\left( \frac{P}{P_{\infty}} \right)^{\frac{\gamma-1}{\gamma}} = 1 - 1/2 \left( |\vec{V}|^2 - |\vec{V}_{\infty}|^2 - 2\Delta E \right) \frac{(\gamma-1)}{\gamma} \cdot \frac{\rho_{\infty}}{P_{\infty}} \quad (N.4.8)$$

#### N.4.2 Pressure Formulas

Similarly (N.2.20) becomes

$$C_p, \text{ isentropic} = \frac{2}{\gamma M_{\infty}^2} \cdot \left[ 1 + \frac{\gamma-1}{2} \left( 1 - \frac{|\vec{V}|^2 - 2\Delta E}{|\vec{V}_{\infty}|^2} \right) M_{\infty}^2 \right]^{\frac{\gamma}{\gamma-1} - 1} \quad (N.4.9)$$

The vacuum pressure is still given by

$$C_{p, \text{vac}} = \frac{-2}{\gamma M_{\infty}^2} \quad (N.4.10)$$

but now (N.2.22) becomes

$$1 + \frac{\gamma-1}{2} \left( 1 - \frac{(V_m)^2 - 2 \Delta E}{|\vec{V}_\infty|^2} \right) M_\infty^2 = 0 \quad (\text{N.4.11})$$

and (N.2.24) becomes

$$V_m = |\vec{V}_\infty| \left[ 1 + \frac{2}{(\gamma-1)M_\infty^2} + \frac{2 \Delta E}{|\vec{V}_\infty|^2} \right]^{1/2} \quad (\text{N.4.12})$$

Next, (N.2.29) becomes

$$M_1^2 = \frac{|\vec{V}|^2}{a^2} = \frac{|\vec{V}|^2}{|\vec{V}_\infty|^2} \frac{M_\infty^2}{1 + \frac{(\gamma-1)}{2} M_\infty^2 \left( 1 - \frac{|\vec{V}|^2 - 2 \Delta E}{|\vec{V}_\infty|^2} \right)} \quad (\text{N.4.13})$$

Setting  $M_1 = 1$ , the critical velocity becomes

$$\frac{V_c}{|\vec{V}_\infty|} = \frac{\gamma-1}{\gamma+1} + \frac{2}{(\gamma+1)M_\infty^2} + \frac{\gamma-1}{\gamma+1} \left( \frac{2 \Delta E}{|\vec{V}_\infty|^2} \right) \quad (\text{N.4.14})$$

or (from (N.4.12))

$$V_c = \frac{(\gamma-1)}{\gamma+1} V_m \quad (\text{N.4.15})$$

Now, substituting (N.4.14) into (N.4.9),

$$C_{p,c} = \frac{2}{\gamma M_\infty^2} \left[ \frac{2}{\gamma+1} + \frac{\gamma-1}{\gamma+1} M_\infty^2 \left( 1 + \frac{2 \Delta E}{|\vec{V}_\infty|^2} \right) \right]^{\frac{\gamma}{\gamma-1}} - 1 \quad (\text{N.4.16})$$

### N.4.3 Simplifying Assumptions

Next, we may apply second order theory to (N.4.2), and thus we obtain

$$C_{p,2nd\ order} = 1 - \frac{|\vec{V}|^2}{|\vec{V}_{\infty}|^2} + \frac{2\Delta E}{|\vec{V}_{\infty}|^2} + M_{\infty}^2 \frac{(u + \Delta U)^2}{|\vec{V}_{\infty}|^2} \quad (N.4.17a)$$

where  $\Delta U$  is the x-component of  $\Delta\vec{V}$ .

Applying equation (N.4.5-6), we then obtain

$$C_{p,2nd} = 1 - \frac{|\vec{V}|^2}{|\vec{V}_{\infty}|^2} + \frac{2\Delta U}{|\vec{V}_{\infty}|} + \frac{|\Delta\vec{V}|^2}{|\vec{V}_{\infty}|^2} + M_{\infty}^2 \cdot \frac{u^2}{|\vec{V}_{\infty}|^2} \quad (N.4.17b)$$

Note from equation (N.4.5) that  $\Delta E$  is the sum of a first order and a second order quantity. Thus if  $2\Delta E$  is user-specified, it is no longer clear how to evaluate a second order expression for the pressure coefficient. One possible solution may be to use the user-specified value of  $2\Delta E$  only for the computation of the isentropic pressure coefficient formula. We will not address this problem at the present time; rather, we will assume that (N.4.6) holds.

Now, to obtain a second order expression for  $C_{p,c}$ , we first note that by (N.4.1)

$$|\vec{V}|^2 = |\vec{V}|^2 + |\vec{V}_{\infty}|^2 + |\Delta\vec{V}|^2 + 2\vec{V} \cdot \Delta\vec{V} + 2\vec{V} \cdot \vec{V}_{\infty} + 2\Delta\vec{V} \cdot \vec{V}_{\infty} \quad (N.4.18)$$

$$\text{Thus } |\vec{V}|^2 =$$

$$\frac{|\vec{V}|^2}{|\vec{V}_{\infty}|^2} + \frac{2u}{|\vec{V}_{\infty}|} + 2\Delta E + \text{second order terms} \quad (N.4.19)$$

Substituting into (N.4.14) we see that at the critical speed

$$1 + \frac{2u}{|\vec{V}_{\infty}|} + \frac{2\Delta E}{|\vec{V}_{\infty}|^2} = \frac{\gamma-1}{\gamma+1} + \frac{2}{(\gamma+1)M^2} + \frac{\gamma-1}{\gamma+1} \left( \frac{2\Delta E}{|\vec{V}_{\infty}|^2} \right) + \text{second order terms} \quad (N.4.20)$$

or

$$\frac{2u}{|\vec{V}_\infty|^2} = \frac{2}{(\gamma+1)} \left( 1 + \frac{2\Delta E}{|\vec{V}_\infty|^2} \right) + \frac{2}{(\gamma+1)M_\infty^2} \quad (\text{N.4.21})$$

+ 2nd order terms

or

$$\frac{u^2}{|\vec{V}_\infty|^2} = \frac{1}{(\gamma+1)^2} \left( 1 + \frac{2\Delta E}{|\vec{V}_\infty|^2} - \frac{1}{M_\infty^2} \right)^2 \quad (\text{N.4.22})$$

at the critical speed, to second order.

Substituting (N.4.14) and (N.4.22) into (N.4.17)

$$C_{p,c,2nd \text{ order}} = \frac{1}{(\gamma+1)^2} \cdot 2(\gamma + M_\infty^2) \cdot \left( 1 + \frac{2\Delta E}{|\vec{V}_\infty|^2} - M_\infty^2 - \frac{(2\gamma+1)}{M^2} \right) \quad (\text{N.4.23})$$

Further simplifying assumptions may be applied to (N.4.17). The "reduced second order" or small Mach number assumption yields

$$C_p = 1 - \frac{|\vec{V}|^2 - 2\Delta E}{|\vec{V}_\infty|^2} \quad (\text{N.4.24})$$

We note from (N.4.18) that

$$1 - \frac{|\vec{V}|^2 - 2\Delta E}{|\vec{V}_\infty|^2} = \frac{-2u}{|\vec{V}_\infty|} - \frac{2\vec{V} \cdot \Delta \vec{V}}{|\vec{V}_\infty|^2} + \frac{|\vec{V}|^2}{|\vec{V}_\infty|^2} \quad (\text{N.4.25})$$

and thus the slender body assumption, applied to (N.4.17b), yields

$$C_p = \frac{-2u}{|\vec{V}_\infty|} - \frac{2(v\Delta v + w\Delta w) + v^2 + w^2}{|\vec{V}_\infty|^2} \quad (\text{N.4.26})$$

where we again make use of (N.4.5-6), and  $\Delta v$  and  $\Delta w$  are y and z-components of  $\Delta \vec{V}$ .

Finally, the linear assumption yields

$$C_p = \frac{-2u}{|\vec{V}_\infty|} \quad (\text{N.4.27})$$

#### N.4.4 Velocity Corrections

In the presence of an onset flow, (N.3.6) becomes

$$W_x = \left[ 1 + \frac{(\gamma-1)M^2}{2} \left( 1 - \frac{|\vec{V}'|^2}{|\vec{V}_\infty|^2} + \frac{2\Delta E}{|\vec{V}_\infty|^2} \right) \right]^{\frac{1}{\gamma-1}} V'_x \quad (N.4.28)$$

and is used to solve for  $V'_x$  to obtain the first velocity correction. Also, (N.3.8) becomes

$$\frac{\rho}{\rho_\infty} = 1 + \frac{M_\infty^2}{2} \left( 1 - \frac{|\vec{V}'|^2}{|\vec{V}_\infty|^2} + \frac{2\Delta E}{|\vec{V}_\infty|^2} \right) + \text{higher terms} \quad (N.4.29)$$

Applying (N.4.19),

$$\frac{\rho}{\rho_\infty} = 1 - M^2 \cdot \frac{u}{|\vec{V}_\infty|} + \text{higher terms} \quad (N.4.30)$$

and thus (N.3.7) still holds. Thus equations (N.3.9) and (N.3.11), which define the second velocity correction, remain valid in the presence of an incremental onset flow.

This concludes our discussion of the computation of pressure coefficients in the presence of an onset flow.

It should always be remembered, however, that the presence of an onset flow violates the basic assumptions from which the Prandtl-Glauert equation was derived. In addition, the inability of the user to specify  $2\Delta E$  means that even if the potential flow solution represents the true flow well, the effect of the onset flow on the pressure may be incorrectly calculated.



## N.5 Associated Data

The PAN AIR program user has a large number of options available to instruct the program in calculating flow properties at a point on the configuration surface. We discuss here the effect that certain of these options have. Some options, such as choosing a value for  $\gamma$  other than 7/5, are implemented in such an obvious manner that they require no discussion. Some options, such as the choice of velocity corrections, have already been discussed in detail.

One user option is a reference speed  $U_r$  for pressure calculations. This speed is then used in place of  $|\vec{U}_\infty|$  whenever that quantity occurs in pressure computation formulas. This speed must be specified in the rare case that  $|\vec{U}_\infty|$  is zero, that is, when there is no freestream. Otherwise the appearance of  $|\vec{U}_\infty|$  in the denominator of various expressions will cause the program to terminate. The value the user chooses for  $U_r$  depends very heavily on the physics of the problem, and will not be discussed in this document.

Another user option is the "computation option for pressures." The user may choose to compute pressure using the uniform onset flow  $\vec{U}_\infty$ , in which case, the formulas of the previous sections are applied with  $\vec{U}_\infty$  substituted for  $\vec{U}$ . Second, he may choose to compute pressures using the compressibility vector, in which case  $\vec{U}_\infty$  is replaced by  $U_r \vec{C}_0$  where  $U_r$  is the reference speed for pressure calculation defined above. In both of these cases, the incremental onset flow is assumed to be zero, that is, the vector  $\Delta \vec{V}$  is set to zero for all the equations in section N.4. Finally, if the user requests that the local onset flow be used to calculate pressures, then  $\vec{U}_\infty$  is replaced by  $\vec{U}_0$  and  $\Delta \vec{V}$  is included in all equations in section N.4. No guidelines are given to the user on the appropriate option to use, since under practically all circumstances, the uniform onset flow option, which is the default, is appropriate.

Next, the user may request the computation of the angle between the surface vorticity  $\vec{\gamma}$  and the velocity  $\vec{V}$ , where  $\vec{\gamma}$  is defined by

$$\vec{\gamma} = \hat{n} \times \vec{\nabla}_u \quad (N.5.1)$$

(see section 5.6 following equation (5.6.11)). The program also prints the components of  $\vec{\nabla}_u$  in reference coordinates.

## 0.0 Forces and Moments

In this appendix we describe the computation of forces and moments in the PAN AIR system. In section 0.1 we comment briefly on the defining equations. In section 0.2 we describe the method by which PAN AIR performs the required integration. In section 0.3, we discuss edge forces, which must be calculated separately because the true potential flow solution for velocity at a subsonic edge of a thin configuration is infinite, while that calculated by a panel method is finite. In section 0.4 we compute the properties of force and moment vectors under a coordinate transformation.

## 0.1 Basic Formulas

A force is defined as a time rate of change of momentum. Ward (reference 1.5, equation 4.6.3) shows that for potential flow, equation (5.9.9) holds. PAN AIR actually computes a coefficient of force defined analogously to the pressure coefficient (cf., (N.2.2)):

$$\vec{C}_F = -\frac{1}{S_R} \iint \left[ \frac{\vec{V}(\rho \vec{V} \cdot \hat{n})}{1/2 \rho_\infty |\vec{V}_\infty|^2} + C_p \hat{n} \right] dS \quad (0.1.1)$$

where  $S_R$  is a user-specified "reference area" available for normalization of the force coefficient.

Applying the relation (N.3.3) between velocity and mass flux, we have, for either the upper or lower surface of a network,

$$\vec{C}_F = -\frac{1}{S_R} \iint \left[ \frac{2\vec{V}(\vec{W} \cdot \hat{n})}{|\vec{V}_\infty|^2} + C_p \hat{n} \right] dS \quad (0.1.2)$$

We note that the first term, called the "momentum transfer" term, is zero for impermeable surfaces. This term makes a contribution to the force on the surface, however, when the normal mass flux is non-zero. Note that the net force on a network of panels is the difference between upper and lower surface forces. Thus the net force on a fully permeable nacelle face is zero, though both the upper and lower surface forces are non-zero. The momentum transfer term is only computed in Pan Air when requested by the user.

The coefficient of moment  $\vec{C}_M$  is similarly derived from (5.9.10) and is defined by

$$\vec{C}_M = -\frac{1}{L_R} \iint \left[ \{ \vec{Q} - \vec{R}_O \} \times \vec{V} \left( \frac{2\vec{W} \cdot \hat{n}}{|\vec{V}_\infty|^2} \right) + C_p \{ \vec{Q} - \vec{R}_O \} \times \hat{n} \right] dS \quad (0.1.3)$$

Here  $L_R$  is a user-specified reference length,  $Q$  is a point of integration and  $R_O$  is the point about which the moment is calculated. Once again the first term is the momentum transfer term. If the surface is impermeable, this term makes no contribution to the angular force exerted by the fluid on the body.

## 0.2 Integration Procedure

The integrand in (0.1.2) may be evaluated from the velocity (see Appendix N). The velocity, in turn, may be computed at any point on the configuration by the splining methods (see section N.1). In fact, a velocity distribution may be computed on each subpanel, and so it is theoretically possible to integrate this distribution exactly over the entire configuration to obtain the resulting force distribution. In fact, the integrals are precomputed (in the DQG module) for an arbitrary piecewise quadratic pressure distribution, so that the integral over a panel may be obtained by the CDP module during post-processing by matrix multiplications.

This procedure makes use of the far field moments already required for far field influence coefficient calculation. Recall from section I.4.1.3 the row vector FFM and the matrix FFM defined by

$$\frac{sb^2}{\kappa} \iint_{\Sigma} \mu \, dS = \begin{bmatrix} \text{FFMD} \\ 0 \end{bmatrix} \begin{Bmatrix} u_1 \\ \vdots \\ u_9 \end{Bmatrix} \quad (0.2.1)$$

$$\frac{sb^2}{\kappa} \iint_{\Sigma} \hat{\mu} \, \hat{n} \, dS = \begin{bmatrix} \text{FFMD} \\ 1 \end{bmatrix}^{3 \times 9} \begin{Bmatrix} u_1 \\ \vdots \\ u_9 \end{Bmatrix} \quad (0.2.2)$$

But now, if we assume that the pressure varies in a piecewise quadratic manner (as  $\mu$  does) on each panel we may apply (0.2.2). This is actually a fairly reasonable assumption. Since we approximate the doublet strength by a quadratic function and the source strength by a linear function, (N.1.11b) shows that the velocity is of linear accuracy. Thus by (N.2.43) and (N.2.51-53), the second order, reduced second order, slender body, and linear pressure coefficient formulas can be adequately represented by quadratically varying functions. Further, the small perturbation assumptions on which the Prandtl-Glauert equation is based insure that differences between the isentropic and the second order formula should be negligible anyway.

So, we may compute the pressure coefficient  $C_{p,q}$  at the nine panel defining points, and obtain

$$\frac{sb^2}{\kappa} \iint_{\Sigma} C_p \, \hat{n} \, dS = \begin{bmatrix} \text{FFMD} \\ 1 \end{bmatrix} \vec{C}_p \quad (0.2.3)$$

where  $\vec{C}_p$  is the vector of length 9 whose qth entry is  $C_{p,q}$ .

Similarly, since the velocity on a panel is of linear accuracy,  $\vec{V} (\vec{W} \cdot \hat{n})$  also may be described by a piecewise quadratic, and so, writing  $\{\vec{V}_q\}_i$  for the ith entry of  $\vec{V}_q$ , the 3x1 column vector giving the velocity at the qth

panel defining point, the first term in (0.1.2) may be computed by,

$$\begin{aligned} \frac{s\beta^2}{\kappa} \iint_{\Sigma} \{\vec{V}\}_i (2\vec{W} \cdot \hat{n}) dS &= \text{FFM}_0^D \begin{Bmatrix} (\vec{V}_1)_i \cdot (\vec{W} \cdot \hat{n})_1 \\ \vdots \\ (\vec{V}_9)_i \cdot (\vec{W} \cdot \hat{n})_9 \end{Bmatrix} \\ &= 2[VWN]_{i, \cdot} \text{FFM}_0^9 \end{aligned} \quad (0.2.4)$$

where VWN is the 3x9 matrix whose i,q entry is the ith component of  $V_q$  times the normal mass flux at the qth defining point.

Thus, equation (0.1.2) becomes

$$\begin{aligned} S_R \{\vec{C}_F\}_i &= \frac{-\kappa}{s\beta^2} \sum_{\text{all panels}} \sum_{q=1}^9 \left\{ \frac{2}{|\vec{V}_q|^2} [VWN]_{iq} [\text{FFM}_0^D]_q \right. \\ &\quad \left. + [\text{FFM}_1^D]_{iq} C_{p,q} \right\} \end{aligned} \quad (0.2.5)$$

Next we consider the calculation of the moment coefficient. Assume that we have computed the 3x9 matrix  $\text{NCPM}_1$  ("normal cross-product moment") defined by

$$\iint_{\Sigma} (\vec{Q} - \vec{P}_q) \times \hat{n} dS = [\text{NCPM}_1] \vec{u} \quad (0.2.6)$$

where  $P_q$  is the panel center.

This matrix is precomputed in the same manner as the remaining far field moments. Similarly, let us define a 3x9 matrix  $[\text{NCPM}_2]$  by

$$\iint_{\Sigma} \mu (\vec{Q} - \vec{P}_q) \times \hat{n} dS = [\text{NCPM}_2] \vec{u} \quad (0.2.7)$$

The computation of  $\text{NCPM}_1$  and  $\text{NCPM}_2$  is described shortly. We may then compute (0.1.3) using the above two matrices.

First, we easily see that  $\iint_{\Sigma} [C_p (\vec{Q} - \vec{R}_0) \times \hat{n}] dS =$

$$\iint_{\Sigma} C_p (\vec{Q} - \vec{P}_q) \times \hat{n} dS + (\vec{P}_q - \vec{R}_0) \times \iint_{\Sigma} C_p \hat{n} dS \quad (0.2.8)$$

$$= [\text{NCPM}_2] \vec{c}_p + (\vec{P}_q - \vec{R}_0) \times \frac{\kappa}{s\beta^2} [\text{FFM}_1^D] \vec{c}_p \quad (0.2.9)$$

Next we recall from appendix E the permutation symbol

$$\begin{aligned} \epsilon_{ijk}: \quad & 1 \leq i, j, k \leq 3 \\ & = 1 \text{ if } i, j, k \text{ are distinct and cyclic} \\ \epsilon_{ijk} \quad & = -1 \text{ if } i, j, k \text{ are distinct and in reverse cyclic order} \\ & = 0 \text{ otherwise} \end{aligned} \quad (0.2.10)$$

which has the property that for vectors  $\vec{v}$  and  $\vec{w}$ ,

$$(\vec{v} \times \vec{w})_k = \sum_{i,j} \epsilon_{ijk} v_i w_j \quad (0.2.11)$$

$$\text{Thus} \quad \iint [(\vec{Q} - \vec{R}_0) \times \vec{V} (\vec{W} \cdot \hat{n})] dS =$$

$$\begin{aligned} & \sum_{i,j} (\vec{Q} - \vec{R}_0)_i V_j (\vec{W} \cdot \hat{n}) \epsilon_{ijk} dS + \\ & [(\vec{P}_g - \vec{R}_0) \times \iint \vec{V} (\vec{W} \cdot \hat{n}) dS]_k \end{aligned} \quad (0.2.12)$$

$$\text{Then} \quad \iint [(\vec{Q} - \vec{R}_0) \times \vec{V} (\vec{W} \cdot \hat{n})]_k dS =$$

$$\begin{aligned} & \sum_{i,j,q} [\text{NCPM}_2]_{iq} [\text{VWN}]_{jq} \epsilon_{ijk} \\ & + \sum_{i,j,q} (\vec{P}_g - \vec{R}_0)_i \frac{\kappa}{s_B^2} [\text{VWN}]_{jq} [\text{FFM}_0^D]_q \epsilon_{ijk} \end{aligned} \quad (0.2.13)$$

Combining (0.1.3), (0.2.9), and (0.2.13),

$$\begin{aligned} L_R \vec{C}_M &= \sum_{\text{panels}} -[\text{NCPM}_2] \vec{C}_p - (\vec{P}_g - \vec{R}_0) \times \left\{ \frac{\kappa}{s_B^2} [\text{FFM}_1^D] \vec{C}_p \right\} \\ &- \frac{2}{|\vec{V}_0|^2} \sum_{q=1}^9 \left\{ [\text{NCPM}_1]_{.,q} + \frac{\kappa}{s_B^2} (\vec{P}_q - \vec{R}_0) [\text{FFM}_0^D]_q \right\} \times [\text{VWN}]_{.,q} \end{aligned} \quad (0.2.14)$$

This completes our discussion of the integration of (0.1.3), except for the computation of  $[NCPM_1]$ . We use the notation of section I.4. We see that  $[NCPM_1]$  is constructed very similarly to  $[FFM_2^S]$ . The only differences are the replacement of  $\vec{Q}$  by  $\vec{Q} - \vec{P}_g$  and the substitution of  $\mu$  for  $\sigma$ . Thus (cf. (I.4.42))

$$[NCPM_1] = \sum_{i=1}^8 [SPNCPM_{1,i}] \quad (0.2.15)$$

where  $[SPNCPM_{1,i}] =$

$$J_i [A_i]^{-1} [K^D, i] + \frac{\kappa}{s\beta^2} \left\{ \vec{C}_i - \vec{P}_q \right\} [SPFFMD_{0,i}] \quad (0.2.16)$$

Next, we have

$$[NCPM_2] = \sum_{i=1}^8 [SPNCPM_{2,i}] \quad (0.2.17)$$

where  $[SPNCPM_{2,i}]_{.,q} =$

$$[SPNCPM_{1,i}]_{.,q} \times \hat{n}_i \quad (0.2.18)$$

### 0.3 Leading and Side Edge Force

#### 0.3.1 Thin Airfoil Theory

Consider a flat plate at an angle of attack, as illustrated in figure 0.1. It is known that such a configuration experiences zero drag in subsonic two-dimensional potential flow, where drag is the component of force in the freestream or x-direction. Yet the surface normal has an x-component and the surface is impermeable, and thus equation (0.1.1) indicates non-zero drag.

The resolution of this contradiction is found in the existence of a leading edge force resulting from an infinite leading edge velocity (see Ashley and Landahl, Ref. 0.1, section 5.3, or, for more detail, Sears, Ref. 0.2, section D). This leading edge force exactly cancels out the drag computed by integrating the pressure over the configuration surface. Since the surface is impermeable, the momentum transfer term gives no contribution to the force on the surface.

In linearized thin airfoil theory (see Section D of Sears) it may be shown that the x-component  $u$  of the perturbation velocity behaves according to

$$\frac{u(x)}{|\bar{V}_\infty|} = \frac{G}{\beta} (x)^{-1/2} \quad (0.3.1)$$

where the leading edge of the airfoil is at the origin and  $G$  is a constant. Further, the resulting leading edge force is in the freestream or x-direction, with

$$\bar{C}_{F,x} = - \frac{2\pi G^2}{\beta \cdot C_R} \quad (0.3.2)$$

where  $C_R$  is a reference chord length. Recall that  $\beta^2 = |1 - M_\infty^2|$ .

#### 0.3.2 Linearized Three-Dimensional Theory

These results are extended by Sears to the linearized theory of a thin three-dimensional wing by the assumption that the leading edge force per unit length at a point on the leading edge depends only on the velocity there. The result Sears obtains may be described by referring to the wing swept at an angle  $\Lambda$  illustrated in figure 0.2.

First, the leading edge force is zero if the edge is supersonic, that is, if it is swept ahead of the Mach cone. Otherwise, let  $\beta_n$  be the value of  $\beta$  for the component of  $\bar{V}_\infty$  in the x-direction. That is

$$\beta_n^2 = 1 - M_\infty^2 \cos^2 \Lambda \quad (0.3.3)$$

where the fact that the edge is not supersonic insures that  $\beta_n^2 > 0$ .



Then Sears find that the force  $\vec{C}_F$  is in the  $x_n$ -direction (see figure 0.2) with

$$\frac{d}{dy_n} |\vec{C}_F| = \frac{-2\pi}{\beta_n} \frac{G_n^2}{S_R} \quad (0.3.4)$$

where  $S_R$  is the reference area and  $G_n$  is a constant which describes the limiting behavior of the velocity in the vicinity of the leading edge. Writing  $v_n$  for the component of the perturbation velocity in the  $x_n$ -direction, Sears finds that near the leading edge

$$\frac{v_n}{|\vec{V}_\infty|} = \frac{G_n}{\beta_n} (x_n)^{-1/2} \quad (0.3.5)$$

where  $x_n$  is the distance along the  $x_n$ -axis from the leading edge.

Thus

$$G_n = \frac{\beta_n}{|\vec{V}_\infty|} \lim_{x_n \rightarrow 0} v_n (x_n)^{-1/2} \quad (0.3.6)$$

and

$$\vec{C}_F = \frac{-2\pi\beta_n}{S_R |\vec{V}_\infty|^2} \int_{\text{span}} \lim_{x_n \rightarrow 0} (v_n^2 x_n) dy_n \quad (0.3.7)$$

Sears does not actually assume that the leading edge of the wing is straight. and so (0.3.4) and (0.3.6) may be generalized to a curved leading edge, in which case  $\beta_n$  and thus  $G_n$  now become functions of  $y$ . So, letting  $\hat{e}_n$  be a unit vector normal to the leading edge, and lying in the  $(x,y)$  plane

$$G_n = \frac{\beta_n}{|\vec{V}_\infty|} \lim_{P \rightarrow P_0} (\vec{V}(P) \cdot \hat{e}_n) ((\vec{P} - \vec{P}_0) \cdot \hat{e}_n)^{1/2} \quad (0.3.8)$$

where  $P_0$  is a point on the leading edge, and so

$$\vec{C}_F = \frac{-2\pi}{S_R |\vec{U}_\infty|^2} \int_{\text{span}} \hat{e}_n (1 - M_\infty^2 \cos \Lambda) \lim_{P \rightarrow P_0} (\vec{V}(P) \cdot \hat{e}_n)^2 ((\vec{P} - \vec{P}_0) \cdot \hat{e}_n) dy_n \quad (0.3.9)$$

### 0.3.3 Application in PAN AIR

Equation (0.3.9) is implemented in PAN AIR at user request even where its theoretical validity is dubious, such as for highly cambered wings or wings at a high angle of attack. In fact, the PAN AIR user may request the computation of edge forces for any network edge in the configuration. Unless it is the leading or side edge of a thin configuration such as a mean surface of a wing, however, the limit in (0.3.8) will be zero and no edge force will result.

The principal problem resulting from attempting to apply (0.3.9) to a network of panels is the question of generalizing  $\hat{e}_n$ . In linearized theory, it is assumed that the flow direction lies in the plane of wing, and thus  $\hat{e}_n$  is clearly the normal vector to the leading edge lying in the plane of wing. The direction vector  $\hat{e}_F$  chosen for the edge force should clearly lie in the plane normal to the edge tangent  $\hat{t}$ . On the other hand, it should lie as nearly parallel to  $\vec{U}_\infty$  (the uniform onset flow) as possible, subject to the previous constraint.

The resulting vector is that vector which lies perpendicular to the edge, while still in the plane spanned by  $\vec{U}_\infty$  and  $\hat{n} \times \vec{U}_\infty$ .

Thus

$$\hat{e}_F = a \vec{U}_\infty + b(\hat{n} \times \vec{U}_\infty) \quad (0.3.10)$$

$$\text{where } \hat{e}_F \cdot \hat{t} = 0$$

$$\text{or } a \vec{U}_\infty \cdot \hat{t} + b(\hat{n} \times \vec{U}_\infty) \cdot \hat{t} = 0 \quad (0.3.11)$$

Further,  $\hat{e}_F$  is a unit vector, and so

$$a^2 |\vec{U}_\infty|^2 + b^2 |\hat{n} \times \vec{U}_\infty|^2 = 1 \quad (0.3.12)$$

Solving (0.3.11) for  $b$  and substituting in (0.3.12) yields

$$a = \frac{\pm |\hat{t} \cdot (\hat{n} \times \vec{U}_\infty)|}{[|\vec{U}_\infty|^2 (\hat{n} \times \vec{U}_\infty) \cdot \hat{t} + |\hat{n} \times \vec{U}_\infty|^2 |\vec{U}_\infty \cdot \hat{t}|]^{1/2}} \quad (0.3.13)$$

where the minus sign is chosen to give the correct solution in linearized theory.

Then solving for  $b$  yields

$$b = \frac{\vec{U}_\infty \cdot \hat{t}}{[|\vec{U}_\infty|^2 |(\hat{n} \times \vec{U}_\infty) \cdot \hat{t}|^2 + |\hat{n} \times \vec{U}_\infty|^2 |\vec{U}_\infty \cdot \hat{t}|^2]^{1/2}} \quad (0.3.14)$$

Thus

$$\begin{aligned} e_F = & - \frac{1}{\sqrt{1 + \frac{|\hat{n} \times \vec{U}_\infty|^2 |\vec{U}_\infty \cdot \hat{t}|^2}{|\vec{U}_\infty|^2 |(\hat{n} \times \vec{U}_\infty) \cdot \hat{t}|^2}}} \frac{\vec{U}_\infty}{|\vec{U}_\infty|} \\ & + \frac{1}{\sqrt{1 + \frac{|(\hat{n} \times \vec{U}_\infty) \cdot \hat{t}|^2}{|\vec{U}_\infty \cdot \hat{t}|^2}}} \frac{\hat{n} \times \vec{U}_\infty}{|\hat{n} \times \vec{U}_\infty|} \end{aligned} \quad (0.3.15)$$

So, for any edge, specified by the user, the edge force is computed by PAN AIR as (cf. (0.3.9))

$$C_F = \frac{-2}{S_R |\vec{U}_\infty|^2} \sum_{\substack{\text{panel} \\ \text{edges}}} \hat{c}_F (1 - M_\infty^2 \cos^2 \Lambda) \lim_{P \rightarrow P_0} (\vec{v}(P) \cdot \hat{e}_n)^2 (\vec{P} - \vec{P}_0) \cdot \hat{e}_F L \quad (0.3.16)$$

where  $L$  is the length of the panel edge.

Finally, in order to compute the limit in (0.3.16), at a panel edge, PAN AIR computes the required expression at a sequence of control points in the column or row of control points perpendicular to the panel edge. The limiting value is then computed by a standard numerical method known as Lagrange's formula. It has been found experimentally that a small number of control points (such as three) is sufficient; that is, the limiting value does not change when more control points are chosen.

## 0.4 Coordinate Transformations

In this section we examine the behavior of force and moment vectors under an orthogonal transformation of coordinates

$$\Gamma : \begin{Bmatrix} x \\ y \\ z \end{Bmatrix} \rightarrow \begin{Bmatrix} x' \\ y' \\ z' \end{Bmatrix} \quad (0.4.1)$$

This is necessary because the program permits force and moment computation in a multiplicity of axis systems. These axis systems are defined in section B.2.1 of the User's Manual.

We know from appendix E that velocity and normal vectors are dual vectors w transforming according to

$$\vec{w} = \Gamma^T \vec{w}' \quad (0.4.2)$$

But since we assume  $\Gamma$  is orthogonal, its inverse is its transpose, and so

$$\vec{w}' = \Gamma \vec{w} \quad (0.4.3)$$

Further, if  $\vec{w}$  is a vector rather than a dual vector, it also obeys (0.4.3), according to appendix E, because  $\det \Gamma = 1$ . In fact, because  $\Gamma$  is orthogonal, vectors and dual vectors behave identically all cases, and so we make no further distinction between them.

Applying (0.4.3) in (0.1.1) we obtain

$$\vec{c}'_F = \Gamma \vec{c}_F \quad (0.4.4)$$

since

$$\{\rho \Gamma V\} \cdot \hat{n} = \rho \vec{V}^T \Gamma^T \Gamma \hat{n} = \rho \vec{V} \cdot \hat{n} \quad (0.4.5)$$

and  $\Gamma$ , being a matrix of constants, may be taken out of the integral (0.1.1).

Next, we consider the transformation of the moment coefficient. Let us assume we have computed the moment vector  $\vec{c}_M$  about the origin in reference coordinates. That is,

$$\vec{c}_M = - \frac{1}{LRS_R} \iint \Gamma \vec{Q} \times \vec{V} \left( \frac{2\vec{W} \cdot \hat{n}}{|\vec{Q}|^2} \right) + c_p \vec{Q} \times \hat{n} dS \quad (0.4.6)$$

We now wish to compute the moment coefficient  $\vec{c}'_M$  in the primed coordinate system about a point  $R_0$ . That is,  $\vec{c}'_M$  is defined by (0.1.3) with  $\vec{Q}$ ,  $\vec{R}_0$ ,  $\vec{V}$ ,  $\vec{W}$ , and  $\hat{n}$  replaced by primed counterparts.

So,

$$\vec{C}_M = - \frac{1}{L_R S_R} [ \{ \Gamma \vec{Q} - \Gamma \vec{R}_0 \} \times \Gamma \vec{V} (2 \frac{\Gamma \vec{W} \cdot \Gamma \hat{n}}{|\vec{V}_\infty|^2}) + C_p \{ \Gamma \vec{Q} - \Gamma \vec{R}_0 \} \times \Gamma \hat{n} ] dS \quad (0.4.7)$$

But for vectors  $\vec{w}_1$  and  $\vec{w}_2$ , we have (cf. (E.1.12-13)):

$$\Gamma \vec{w}_1 \times \Gamma \vec{w}_2 = \Gamma \{ \vec{w}_1 \times \vec{w}_2 \} \quad (0.4.8)$$

Thus

$$\begin{aligned} \vec{C}_M &= - \frac{1}{L_R S_R} [ \Gamma \{ \vec{Q} \times \vec{V} \} (2 \frac{\vec{W} \cdot \hat{n}}{|\vec{V}_\infty|^2}) + C_p \Gamma \{ \vec{Q} \times \hat{n} \} ] dS \\ &+ \frac{1}{L_R S_R} [ \Gamma \{ \vec{R}_0 \times \vec{V} \} (2 \frac{\vec{W} \cdot \hat{n}}{|\vec{V}_\infty|^2}) + C_p \Gamma \{ \vec{R}_0 \times \hat{n} \} ] dS \end{aligned} \quad (0.4.9)$$

Noting that both  $\Gamma$  and  $R_0$  may be removed from the integral,

$$\vec{C}_M = \Gamma \vec{C}_M + \frac{1}{L_R S_R} \Gamma \{ \vec{R}_0 \times \iint [ \vec{V} (2 \frac{\vec{W} \cdot \hat{n}}{|\vec{V}_\infty|^2}) + C_p \hat{n} ] dS \} \quad (0.4.10)$$

So, substituting (0.1.2) in (0.4.10),

$$\vec{C}_M = \Gamma \vec{C}_M - \frac{1}{L_R} \Gamma \{ \vec{R}_0 \times \vec{C}_F \} \quad (0.4.11)$$

Thus moment vectors transform like force vectors, except with an extra term which results from a shift in the point about which the moment is calculated.

An additional minor complication is caused by the use of separate scaling factors for different components of the moment coefficient vector. The effect of separate scaling factors on (0.4.11) can easily be computed and is given by the code in SUBROUTINE TRNSFM of the CDP module.

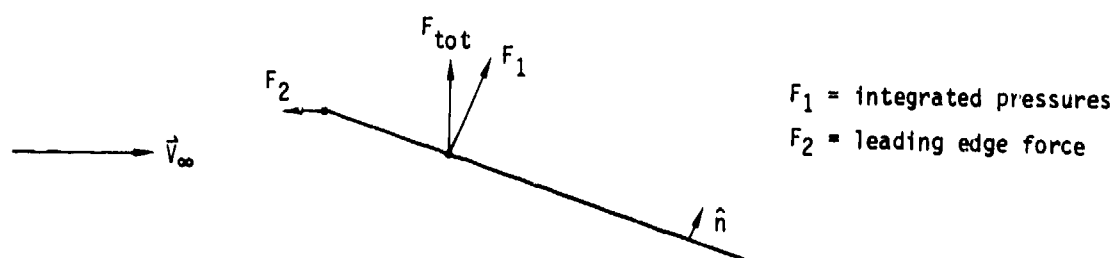


Figure 0.1 - Effect of leading edge force

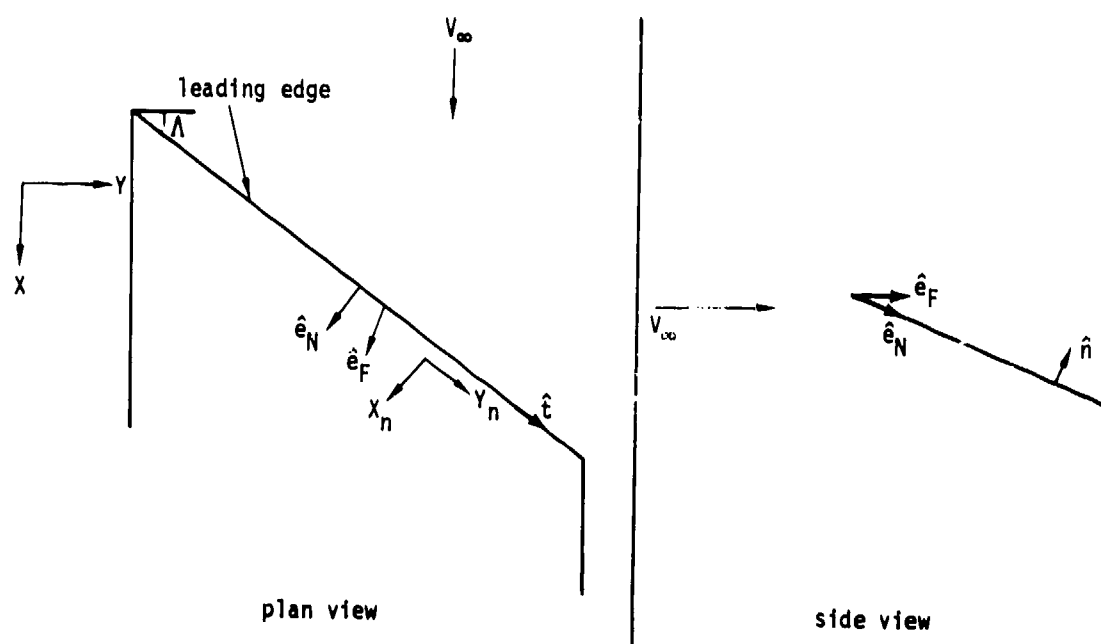


Figure 0.2 - Vectors associated with leading edge force